1127-21

146

JOURNAL OF
COLLOID SCIENCE

Editor-in-Chief
Victor K. La Mer, Columbia University, New York

Advisory Board

C. O. Beckmann
J. A. Christiansen
P. J. W. Debye
John T. Edsall
I. Fankuchen
John D. Ferry
Wilfried Heller
J. J. Hermans
John G. Kirkwood
E. C. Lingafelter
L. G. Longsworth
S. G. Mason
J. Th. G. Overbeek
R. Ruyssen
J. H. Schulman
Leo Shedlovsky
Theodore Shedlovsky
Robert Simha
R. H. Smellie
Jacinto Steinhardt
The Svedberg
Hugh S. Taylor
Arne Tiselius
Robert D. Vold
Bernard Vonnegut
Ralph W. G. Wyckoff
Bruno H. Zimm

VOLUME 13

1958

ACADEMIC PRESS INC.—PUBLISHERS
NEW YORK, N. Y.

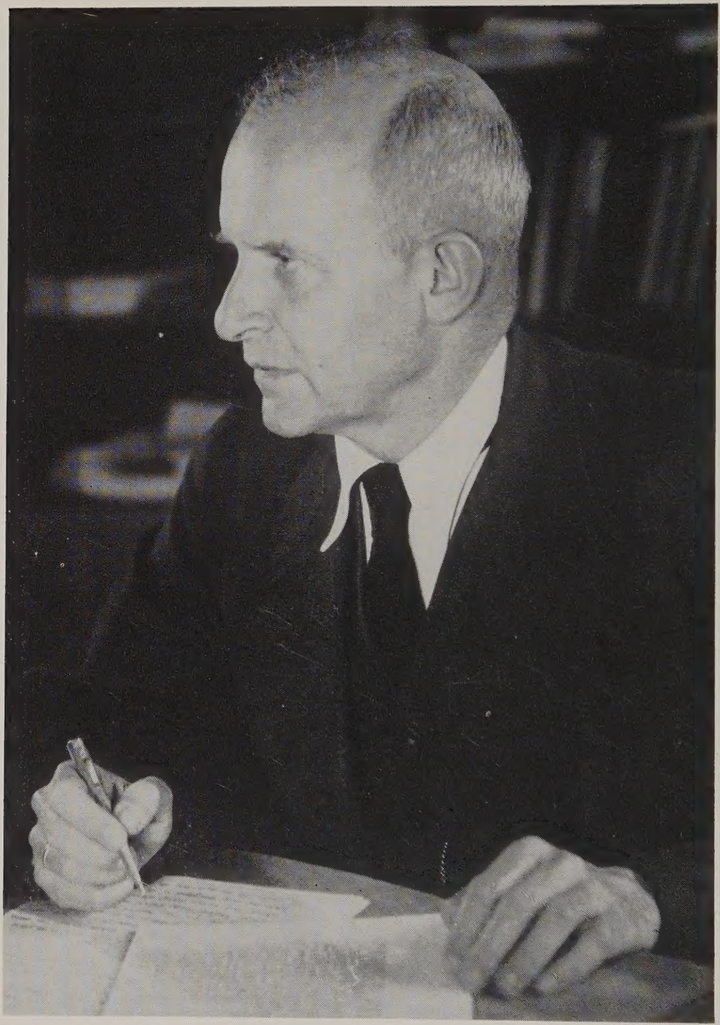

Karl Friedrich Bonhoeffer
1899–1957

IN MEMORIAM:

KARL FRIEDRICH BONHOEFFER

MAY 15, 1957

On the 15th of May 1957, Karl Friedrich Bonhoeffer passed away, the victim of a heart disease. He was taken away in the prime of his life and work. His death was an unexpected misfortune for his family, friends, and pupils. Bonhoeffer was regarded in Germany as the most outstanding man in the field of physical chemistry, and his dignity and pleasant personality were esteemed at home and abroad.

My association with him began 30 years ago as his pupil and then continued as his colleague and friend. He was born in Breslau in 1899, but grew up in Berlin as a member of a distinguished family of high cultural background. Geheimrat Bonhoeffer, his father, was Professor of Psychiatry at the University of Berlin. Since Berlin was one of the leading centers for physics and physical chemistry in the years following World War I, Bonhoeffer was influenced by such men as Walter Nernst, Max Planck, and Albert Einstein. However, the man who influenced him the most was Fritz Haber. It was in Haber's Institute, where he worked as a young man through the years 1923 to 1930, that Bonhoeffer made what was perhaps his most beautiful work. Some of his most important works are as follows: "The Behavior of Active Hydrogen"; "The Chemiluminescence of Active Hydrogen"; "Works on Active Nitrogen"; "Investigation of the Absorption Spectra of Hydrogen Iodide" and also of ammonia which led to the understanding of the predissociation; with Haber, a fundamental paper concerning band spectroscopy and flame processes, experimental evidence for the existence of SiO and the OH Radical; and with this writer, experiments on ortho- and para-hydrogen.

In 1930 he went to the University of Frankfurt, where he accepted the chair in physical chemistry. Since the duties of a director of an Institute for Physical Chemistry included not only the burden of administration, teaching, and examination but also responsibility for all the research undertaken at the institute, Bonhoeffer was a very hard working man from this time right up until his death. During this period in Frankfurt, he did pioneering work in the field of labeling organic chemical reactions with heavy hydrogen. This work led him to problems in physiological chemistry and biological physics which more and more through the years became his field of dominant interest.

From Frankfurt, Bonhoeffer went to Leipzig to accept the chair of physical chemistry founded by Wilhelm Ostwald, who is regarded in Germany as the founder of physical chemistry as a special field of science. He succeeded M. LeBlanc, who is considered one of the classicists in electrochemistry. However, the decision to go to Leipzig proved to be unfortunate in the light of later events, since the war years there were very hard and the city ultimately became part of the Eastern Zone of Germany. Bonhoeffer managed to go to the University of Berlin and succeeded to the chair of Nernst and Bodenstein in 1947. From there he became the director of the newly founded Institute of Physical Chemistry of the Max Planck Society and was able once again to turn his attention to pure research. This institute was regarded as the legal successor to Haber's institute in Berlin-Dahlem.

Starting with practically nothing in Göttingen, Bonhoeffer brought his institute to the forefront of electrochemistry in a few years. Just one year ago he was telling groups in the United States what he had completed in these few years. He had, in his lifetime, published over 120 articles and scientific papers on different fields of physical chemistry, of which a large part must be called classic or pioneering. He also coauthored a textbook on photochemistry in 1933. The papers which were inspired personally by him in his institute exceeded the number of his own publications. He was a member of several academies and received the Bunsen Medal in 1955 and the Palladium Medal of the American Electrochemical Society in 1957.

Bonhoeffer was married to Greta von Dohnany. His father-in-law is the famous composer and conductor, who lives in this country. He is survived by his wife, three sons, and one daughter, who brought him much joy during his lifetime. However, the entire Bonhoeffer family had to pass through difficult times. Several members were lost to the Third Reich after the 20th of July, 1944. All who saw Bonhoeffer one year ago did not expect such an abrupt end to his brilliant career. Obviously, his intensive scientific investigations and the strain of the war and postwar hardships had been too much for him.

Paul Harteck

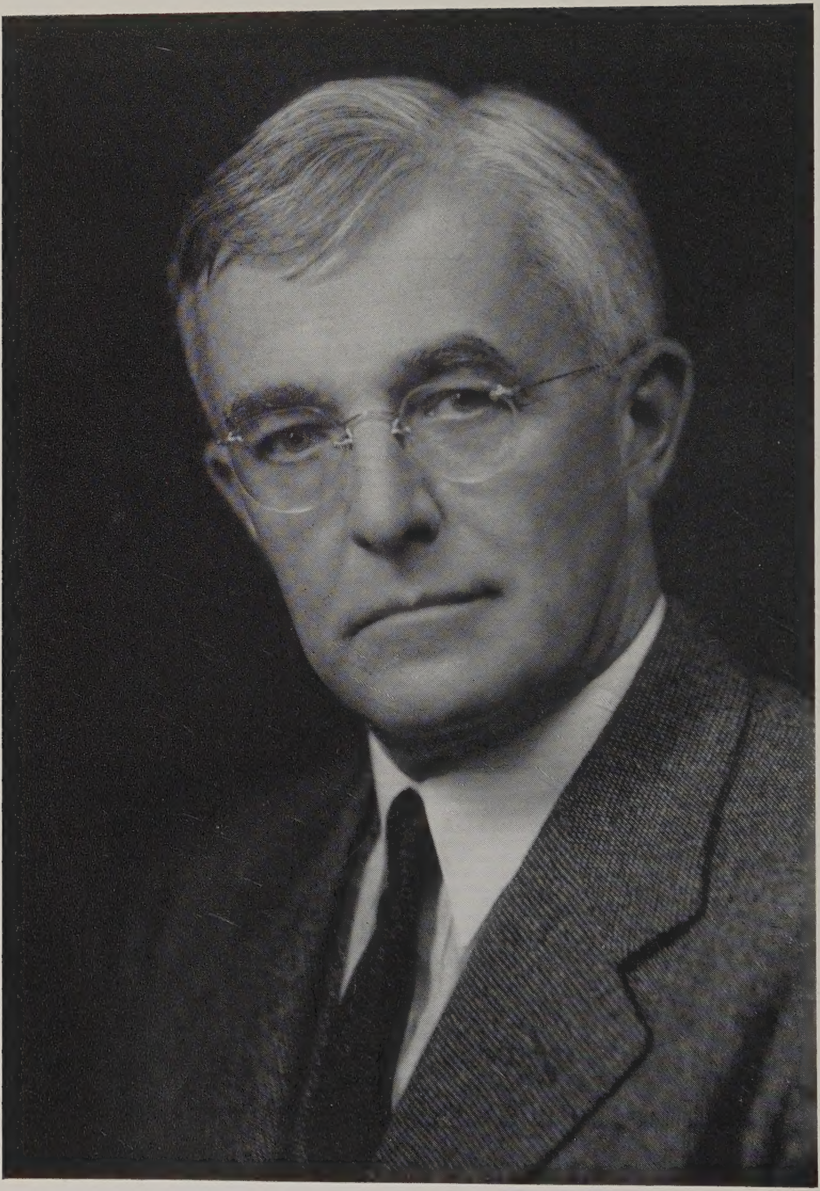

Irving Langmuir
1881–1957

IN MEMORIAM:

IRVING LANGMUIR—SCIENTIST

Irving Langmuir was one of that fast disappearing breed of scientists having the ability to enter a new field of research and within a very short time contribute such stimulating ideas, revolutionary concepts, and new experimental evidence that his impress on the field thereafter represents a reference point of major importance in the field.

The reason for this ability was not hard to find. A combination of broad basic training in physical, chemical, and mathematical concepts, an insatiable curiosity, a burning enthusiasm, and a tremendous capacity for work was part of the picture. The rest included a wide interest in the natural sciences, a fabulous memory, a meticulous method of making observations, and the ability to get others around him as enthusiastic as he was about the subject of his current interest.

He was a great believer in the need for complete freedom of movement for the investigator so that if by unexpected occurrence or fortunate accident a new discovery occurred, he had no reason to hold back from pursuing the new lead—so long as the trail looked promising.

His ability to move quickly to the heart of a problem was the result of his broad basic training as well as his technique of conducting experiments. This consisted of making a quick survey of the problem, designing a few simple and rough experiments directed at what seemed to be the heart of the problem as well as its periphery. Those on the borderline often yielded the greatest "pay dirt," as witness the importance of his discovery of the gas-filled lamp.

There is a fallacy at present that the day of the string, sealing wax, and paper clip type of experimenter has passed. I am sure Langmuir would challenge that statement. Many of his important basic contributions to science used the simplest of experimental apparatus—sometimes only a pair of intelligent eyes! He would often return to the laboratory, after spending a few days at home or camp at Lake George, with a notebook full of data gathered with the crudest type of makeshift apparatus. Subsequent work with nicely machined instruments, more exact timing, and other experimental procedures rarely altered his initial findings to an significant degree.

His work in the field of surface chemistry, for which he received the 1932 Nobel award in Chemistry, was based on the broad concepts he introduced into this important area of physical chemistry. His work in this field, with that of his staff consisting of Katharine Blodgett and the writer, typifies the complete freedom to follow research problems enjoyed in the G. E. Research Laboratory between 1930 and World War II under Directors Whitney and Coolidge. Studies based on single layers of molecules on water included surface reactions, the thickness of monolayers, cross sections of molecules, viscosity of films, evaporation of water through monolayers, force-area curves, conditioning of deposited films, expansion patterns, reactions of antibodies, properties of protein monolayers and mixed layers, characteristics of built-up multilayers, photochemical decomposition, properties of chlorophyll, nonreflecting coatings on glass, and the use of piston oils and indicator oils. Two new and highly important fields on which research had just started when World War II intervened were "line" and "point" chemistry—fields which involved the study of small aggregates and single isolated molecules. Work in this field was never resumed by our group beyond the discussion and early experimental stage.

Langmuir's interests in the period from 1940 till the end of the war introduced to us a number of new and challenging problems, all of which combined to alter the course of our research activities. It was the culmination of these wartime defense efforts which led us into weather research, experimental meteorology, and atmospheric physics and chemistry—subjects which fascinated Langmuir until his recent death.

Throughout all of this subsequent research work the familiarity with surface chemistry gained prior to 1940 was of immeasurable value in providing a proper perspective and understanding of the problems encountered. This background pattern is discernible throughout the fundamental research which was done with the development of filters for intercepting poison smokes; the development of the artificial fog generator used so successfully during the war for screening troops, cities, and naval operations; studies of precipitation static, aircraft icing, and then—after the war had ended—the study of atmospheric clouds, the formation of rain by chain reaction, the modification of clouds by seeding, the growth rates of snow crystals, and motions in the atmosphere.

Just a few months before his death Langmuir had returned from an extended auto trip with his wife, Marion, which took them to the California coast. Adventuring on back roads and in out-of-the-way places, recording his impressions in highly artistic color photographs, he returned as usual with a wealth of new ideas. Shortly before his death we conducted a series of experiments to test some new theories he was developing on the motion of air over the ocean in the subtropics and the role which "whisker" crystals play in the production of fragmentation ice nuclei in clouds.

Men like Langmuir leave a legacy of elegant experiments, a scientific tradition constituting a way of life, and a group of devoted followers dedicated to perpetuating the ideals.

Langmuir will be greatly missed by those who knew him, who respected his remarkable scientific abilities and who loved him for his kindliness, simplicity, and unpretentious way of life. His elegant scientific experiments, his uncompromising attitude toward those who were careless with scientific facts and his boldness in espousing causes which he believed to be right are some of the attributes which will mark him as one of the great scientists of history.

VINCENT J. SCHAFFER

JOURNAL OF COLLOID SCIENCE 13, 6–23 (1958)

EXPERIMENTAL INVESTIGATIONS ON THE LIGHT SCATTERING OF COLLOIDAL SPHERES[1]

III. THE SPECIFIC SCATTERING AT 90°

Richard M. Tabibian[2] and Wilfried Heller

Chemistry Department, Wayne State University, Detroit, Michigan

Received July 5, 1957

Abstract

An experimental arrangement for precise light-scattering measurements from colloidal solutions at an angle of 90° with respect to the primary beam is described. The results obtained from sixteen polystyrene and polyvinyltoluene latices with particle diameters ranging from 46 to 824 mμ provide an additional verification of the Mie theory of light scattering. The effect of multiple scattering and of the solid angle are studied and methods for excluding their interference with particle size determinations are described which should be useful also for molecular weight determinations in polymer solutions. The problem of the instrument constant is analyzed, and a principle is pointed out whereby quasi-absolute lateral scattering data can be obtained by suitable internal compensation within a properly constructed apparatus. The advantages and disadvantages of lateral measurements as compared to turbidity measurements are pointed out.

Introduction

Two preceding papers dealt with size determinations of colloidal dielectric spheres in a liquid medium by means of turbidity measurements (1, 2). The present paper is concerned with size determinations by means of light-scattering measurements carried out at 90° with respect to the incident beam, using again theoretical data derived from the Mie theory as the basis and electron microscopy as a check.

Compared to direct turbidity measurements, those of lateral scattering have the following advantages: (*a*) Provided the intensity of the primary beam is large enough, particle size determinations can be carried far into the range of small α values[3] not accessible to the former method. (*b*) At

---

[1] The exploratory first part of this work, the numerical results of which are not considered here, was carried out by J. N. Epel and was supported by a grant from the Research Corporation; the present investigations were supported by the U. S. Office of Naval Research.

[2] Present address: E. I. duPont de Nemours and Co., Jackson Laboratory, Wilmington, Delaware.

[3] Here $\alpha = \pi D/\lambda$, D being the diameter of the scattering spheres and λ the wavelength of the incident light in the medium.

those α values where the first, quite broad maximum of the specific turbidity is approached, turbidity measurements are not very sensitive to differences in particle size. Whereas lateral scattering also exhibits maxima and minima, they are comparatively narrow so that the sensitivity of lateral measurements is, on the whole, much larger at the same α-values. Considering, for example, scattering particles with a relative refractive index m[4] of 1.20—which is pertinent to the experiments described below—the range of comparative insensitivity of the specific turbidity extends from an α of about 6 to 9 which on the use of visible light corresponds to diameters of approximately 0.8 to 1.2 μ. (*c*) The presence of colored solutes of negligible scattering power does not interfere with particle size determinations from lateral scattering, but it seriously impairs turbidity measurements. These three items define the conditions under which lateral scattering measurements are preferable to direct turbidity measurements.

Obviously, lateral measurements have also disadvantages as compared to turbidity measurements. Foremost among them is the fact that lateral measurements cannot directly yield absolute data, as will become apparent from the discussion of this aspect below. Second, turbidity measurements are experimentally somewhat simpler. Finally, the first narrow maximum of lateral scattering followed by lesser maxima occurs at a relatively low α value ($\alpha = 1.6$, if $m = 1.20$) so that bivalued or multivalued answers are obtained for particle size unless the spectral change of scattering is considered also. In contradistinction, the theoretical turbidity curve is monotonic over a much wider range of α values (first maximum at $\alpha = 7.75$ if $m = 1.20$).

A combination of both turbidity and lateral measurements, whenever possible will obviously serve to eliminate some of the uncertainties arising in the unfavorable α ranges for either one or the other method. Of particular interest is the combination of both types of measurements in the case of heterodisperse systems which can yield information not obtainable by either one alone: since lateral scattering is generally more sensitive to α than the turbidity if $\alpha > 0.4$ the particle size obtained from either will generally not be the same in heterodisperse systems. This may allow a rough evaluation of the degree of heterodispersion in a given system using the discrepancy of particle size obtained from the two individual quantities as a criterion. (Extensive investigations of this possibility are under way at the present time in this laboratory.) Also, within the range of symmetrical radiation diagrams, which is roughly defined by an α value of 0.4 or less ($m = 1.20$), the ratio of turbidity to laterally scattered intensity should be constant, thus providing a rapid check in a given case as to whether or not the light-scattering particles have dimensions within or above this range.

---

[4] The value of $m = \mu_2/\mu_1$ where μ_2 and μ_1 are the refractive indices of the scattering particles and surrounding medium, respectively.

1. Definition of Light-Scattering Quantities Considered

The Mie equations furnish the quantities $i_\perp$ and $i_\parallel$(3) which represent the basic angular scattering functions of a particle irradiated by linearly polarized light vibrating perpendicular and parallel, respectively, to the plane of observation. Their numerical values depend on α, m, and γ, where γ is the angle of observation with respect to the reverse direction of the primary beam. The quantities

$$\begin{aligned} (J_\perp)_\gamma &= (\lambda^2/4\pi^2r^2)(i_\perp)_\gamma \\ (J_\parallel)_\gamma &= (\lambda^2/4\pi^2r^2)(i_\parallel)_\gamma \end{aligned} \qquad [1]$$

represent the total radiant energy—per unit area and unit time and per unit intensity of the incident beam—which passes at γ through a differential surface area of a sphere of radius r, where r is equivalent to the photometric distance and λ is the wavelength in the medium[5]. On using natural incident light—the case to be considered here—the total intensity of the scattered wave per unit intensity of incident light is ½ of the sum of the two quantities defined in Eqs. [1]:

$$J_\gamma = \tfrac{1}{2}\,(J_\perp + J_\parallel)_\gamma = (\lambda^2/8\pi^2r^2)(i_\perp + i_\parallel)_\gamma. \qquad [2]$$

More interesting for practical purposes is the quantity $J_\gamma r^2$, i.e. the radiant energy, per unit solid angle, scattered by one particle along a differential cone in the γ-direction (per unit time and unit intensity of the incident beam).[5] For a given α- and m-value the intensity of light scattered, per unit solid angle, from an incident beam of intensity, I_0, by a unit volume containing N particles is

$$I_\gamma = NJ_\gamma r^2 I_0 \text{ cm.}^{-3}. \qquad [3]$$

On evaluating $i_\perp$ and $i_\parallel$ for $\gamma = 90°$, which is the lateral direction to be considered in the present investigation,

$$I_{90}/I_0 = NJ_{90}r^2 \text{ cm.}^{-3}. \qquad [4]$$

For practical purposes it is convenient to consider the specific scattered intensity, i.e., either the relative intensity scattered per unit volume fraction, $I_{90}/I_0\phi$, or per unit weight concentration, I_{90}/I_0c. In the latter instance

$$N = (6c/\pi D^3)(\rho_{12}/\rho_2) \times 10^{-2} \qquad [5]$$

where c is given as grams of scattering material per 100 g. of total system, D is the diameter of the scattering spheres, and ρ_{12} and ρ_2 are the densities of the total system and the scattering particles, respectively. Substituting this into [4] gives

---

[5] The quantity J is often referred to as the differential cross section.

$$I_{90}/I_0c = (6 \times 10^{-2}/\pi D^3)(\rho_{12}/\rho_2)J_{90}r^2 \text{ cm.}^{-3}. \qquad [6]$$

In order to compare experimental and theoretical results it is necessary to eliminate complications in the experimental data arising from multiple scattering by extrapolating them to zero concentration. The limiting quantity

$$(I_{90}/I_0c)_0 = \lim_{c \to 0} I_{90}/I_0c \qquad [7]$$

thus obtained, after applying the proper instrument constant to the actual experimental data, can be compared with the theoretical value calculated from Eq. [6].

2. Apparatus and Experimental Procedure

The apparatus used for the present work has been described previously (1) to the extent necessary in connection with turbidity measurements. The section of the apparatus pertinent to measurements at 90°, not shown previously, is shown in Fig. 1.

An AH_4 mercury vapor lamp is again used as a light source and all measurements are made at 5461 A. A Sorensen voltage regulator, Model 500-S, serves to keep the intensity of the air-cooled light source constant within ±0.25%. While the monochromator prevents the other mercury lines from entering the scattering apparatus directly, a faint background superimposed upon the mercury green line leads to the presence of con-

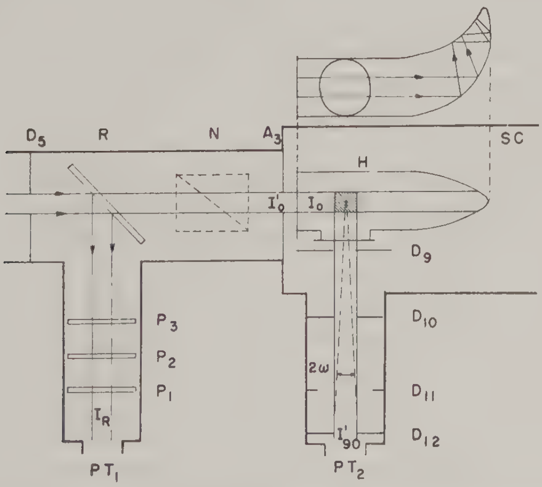

FIG. 1. Section of apparatus for light-scattering measurements at 90°. *A:* variable aperture; *D:* diaphragms; *H:* Rayleigh horn; *N:* Glan-Thompson prism; *PT:* positions of photomultiplier tube; *P:* polaroids; *R:* reflecting glassplate; *SC:* scattering cell assembly. For rest of apparatus, see Fig. 1 in refs. (1) or (2).

taminating radiation. Most of this is removed by replacing the water in the tank F (Fig. 1, ref. (1)) by a solution of $NdCl_3$ and by inserting, in addition, a yellow glass filter in front of the monochromator itself. The interchangeable circular entrance slit A_2 (Fig. 1, ref. (1)) has for the present work an opening of 3 mm. and the diaphragm A_3 one of 4 mm.

The light-scattering solution is contained in a Rayleigh horn, H. The Rayleigh horn, painted black throughout except for the entrance and observation windows, has the well-known advantage of eliminating completely back reflection of the primary beam by absorption in the tail. The specially designed mount holding the horn is screwed into the metal tube SC. The shaded rectangular area in Fig. 1 represents a cut through the mid-section of the cylindrical volume from which scattered light reaches the phototube at PT_2. Four diaphragms are housed in the respective sidearm. The diaphragm D_9 is 4.0 mm. in diameter and is placed 3 mm. from the lateral window of the Rayleigh horn. The aperture of this diaphragm is the same as the diameter of the primary light beam and serves to define the observed volume. Diaphragms D_{10} and D_{11} which are 4.5 mm. and 12.9 mm. in diameter, respectively, serve to eliminate stray light. Diaphragm D_{12} preceding the phototube is 5.1 mm. The resulting solid angle ω_0 of the scattered beam is—after correction for refraction by the exit window of the Rayleigh horn—4.1×10^{-4} steradian ($\omega = 0.66°$; see Fig. 1). An IP21 photomultiplier tube housed in a rectangular box fastens to a light tight carriage which enables one to slide the tube back and forth between the PT_2 and PT_1 positions. Thus, consecutive measurements of the light intensity at each position, I'_{90} and I_R, respectively, can be made, the former being related to I_{90} and the latter, i.e., the reference intensity, being related to I_0. In the actual experiments, the individual readings of the two quantities rarely varied by more than $\pm 1\%$. Several readings were taken in each position and averaged.

The reference beam is obviously necessary for precise measurements. It differs from I_0', the intensity of the light incident upon the Rayleigh horn, by a constant factor. In turn, I_0', differs from I_0 by a nearly constant factor which varies very slightly with the refractive index of the scattering system. The reference beam is obtained by inserting a plane parallel glass plate R into the path of the primary beam and carries approximately 11% of the light flux incident upon R. The intensity of the reference beam is 10^6 to 10^8 times larger than that of the scattered light observed at PT_2. Precise measurements require that the intensity of the two beams be of approximately the same order of magnitude. Since the scattered intensity varies with the scattering system, not only a drastic reduction but a precise and reproducible variation of the reference intensity within several orders of magnitude is desirable. This is accomplished by the insertion of three polaroids P_1, P_2, and P_3. Each polaroid can be rotated through six stops to a maximum of 90°. The use of three polaroids instead of two has an advantage in that the intensity at PT_1 can be varied in very little steps to a high degree of reproducibility between its maximum value and zero. Taking into account the polarizing effect of R itself[6], the total number of definite steps is 216. A Glan-Thompson prism, N, not needed for the present experiments can be inserted into the housing between the glass plate and the A_3 diaphragm. The prism can be rotated through 90° and was used in light-scattering measurements to be reported in a subsequent publication.

3. The Instrument Constant

As already pointed out, the intensity measured at PT_1, I_R, is an unknown fraction of the intensity I_0' incident upon the entrance window of the Rayleigh horn. Similarly, the intensity measured at PT_2, I'_{90}, is related to but not identical with I_{90}, the intensity of light scattered by 1 c.c. of the scattering solution per unit solid angle. Consequently, the ratio of the actual intensity readings at PT_2 and PT_1 per unit concentration, I'_{90}/I_Rc, differs from the theoretical I_{90}/I_0c values. In order to obtain the latter value from the actual measurements, $(I'_{90}/I_Rc)_0$ values must be converted into I_{90}/I_0c values by means of an instrument constant K, which will depend, of course, on the particular combination of the three polaroid settings and on the wavelength used. (It would, in addition, change if the photometrically active volume of the scattering solution and the effective solid angle of the scattered beam were changed. A comparatively minor, but not always negligible, change would also result from a change of the liquid in the scattering cell, if the calibration was carried out with a liquid, solution or dispersion of different refractive index. None of these changes entered in the present work except for changes in solid angle discussed in Section 4D.)

Several methods can be used for the evaluation of K. The one most extensively used at the present time for light-scattering studies on solutions of macromolecular substances is the calibration of a given apparatus with a standard solution of polystyrene of known molecular weight and known turbidity. An alternate, far better, but more delicate, method also frequently used is the calibration of an apparatus by means of the light scattering exhibited by pure liquids, taking advantage of Einstein's equation (4). Experience has shown that standardization of instruments with either of these two methods easily leads to errors if dust is not rigorously excluded from the calibrating substance. More secure data can be expected on using colloidal solutions of scattering spheres small enough so that the symmetry of the radiation diagram is assured. Thus, Maron (5) has used colloidal silica (ludox) as a calibrating material. If these particles are sufficiently small to exhibit Rayleigh scattering, the theoretical value of the ratio $\tau I_0/I_{90}$ for the units specified earlier is obtained from τ/c and I_{90}/I_0c as

---

[6] In order to have completely unpolarized light incident upon the Rayleigh horn, the partial polarization of the primary beam due to the polarizing effect of R and of the monochromator prism was eliminated by means of a compensator (1).

$$\tau I_0/I_{90} = 16\pi/3 = 16.75. \tag{8}$$

The instrument constant K is readily obtained by comparing this to the experimental ratio

$$(\tau/c)_0/(I'_{90}/I_Rc)_0 \quad = \quad (\tau I_R/I'_{90})_0, \tag{9}$$

the latter having been obtained by extrapolations to zero concentration, i.e.,

$$K = 16.75/(\tau I_R/I'_{90})_0. \tag{10}$$

According to our calculations based on the Mie theory the theoretical value of the ratio $\tau I_0/I_{90}$ is—to within four figures—identical to that given by Eq. [8] as long as $\alpha \leqslant 0.2$ and $m \leqslant 1.25$. This means that the diameter of the scattering particles should not exceed approximately 30 mμ if Eq. [10] is to be used for obtaining K. However, on using sufficiently small colloidal spheres for calibration purposes, the specific turbidity is so small that rather high concentrations must be used (5) which introduces uncertainties of extrapolation to $(\tau/c)_0$. The following related method used in the present investigation appears, therefore, preferable.

Granting that light-scattering quantities derived from the Mie theory are quantitatively correct—which has definitely been proved by the turbidity experiments (1) and, therefore, implicitly for any other data obtained from the basic equations—one can lift any restriction as to particle size for the calibrating experiments provided the system is monodisperse. By using larger particles, more accurate $(\tau/c)_0$-values can therefore be obtained. If their diameter and refractive index are known, K can—for a given wavelength—be evaluated very accurately from Eqn. [10] on replacing 16.75 by the proper numerical factor. The system used as a calibrating standard was a polyvinyltoluene latex containing spherical particles with a diameter of 120 mμ and a standard deviation of only 4 mμ. The theoretical values of $(\tau/c)_0$ and $(I_{90}/I_0c)_0$ were calculated for the pertinent α- and m-values and the green Hg-line (λ_0 = 5461 A.) using the Mie theory (6). From them, one obtains

$$K = 17.14/(\tau I_R/I'_{90})_0. \tag{11}$$

Since the experimental $(\tau/c)_0$-values reproduced the theoretical Mie values very satisfactorily (1), no real need existed for $(\tau/c)_0$-measurements during the periodic determinations and redeterminations of the instrument constants; i.e., the calibration procedure could be abbreviated considerably by deriving K from a comparison of $(I'_{90}/I_Rc)_0$ with the theoretical value of

I_{90}/I_0c. Thus, for 5461 A. and the latex used

$$K(I'_{90}/I_Rc) = (I_{90}/I_0c)_0 = 1.60, \qquad [12]$$

which resulted in a K-value of 0.138 for the polaroid setting selected for the experiments described below.[7] The absolute value $(I_{90}/I_0c)_0$, was obtained for all other samples by multiplying their $(I'_{90}/I_Rc)_0$-values by this constant. Operating with this instrument constant irrespective of the particle size presupposes, besides extrapolation of the experimental data to zero concentration, that the solid angle used is small enough. Otherwise, K would vary with particle size. This applies also to the use of Eq. [11] (see Section 4D).

It is apparent from Eq. [12] that any change in I_R, by varying the polaroid setting, will alter K. Thus, by selecting the proper polaroid setting, K can be made to equal 1.00 so that the apparatus will then furnish, by internal compensation, absolute I_{90}/I_0 measurements. This possibility was not taken advantage of in the present investigation.

It should in principle be possible to dispense with an empirical calibration constant and to substitute for it an absolute constant calculated for the apparatus and scattering cell used. An attempt was made to test this possibility which would open the way for transforming the method of lateral measurements into an absolute method. The attempt to convert the I'_{90}/I_R data by calculation into I_{90}/I_0 data requires that two relationships be known, that between I_R and I_0, the intensity of the incident light beam after passage through the window of the Rayleigh horn, and, second, that between I'_{90} and I_{90}. We shall first discuss the former.

Calibration of the reflecting glass plate, R, and of the polaroids for any one of the mutual positions of their planes of polarization desirable for a given series of measurements allows one to express the intensity of the beam emerging from PT_1 in terms of the intensity I'_0 in front of the entrance window of the Rayleigh horn. The constant factor k_1 by which I_R differs from I'_0, can be evaluated most simply by alternating the position of the phototube between PT_1 and A_3[8] making sure that the phototube is placed both times into a position of maximum response. On taking into account the width of the primary beam at the latter position (0.13 cm.^{2}) one obtains for the polaroid setting selected for the following experiments the value of 0.95×10^{-6} for the ratio $k_1 = I_R/I_0'$. Multiplication of the experimental quantity I_{90}'/I_R by this ratio yields directly I_{90}'/I_0'.

---

[7] Both Eqs. [11] and [12] yield obviously the same apparatus constant except for minor numerical differences due to the uncertainty inherent in turbidity measurements. Preference was given to the value derived from [12].

[8] Alternate, more rigorous, but more time-consuming methods for obtaining k_1 were also tried out. One of these methods consists of replacing the Rayleigh horn by a second plane parallel glass plate like R, placed at 45° with respect to the primary beam. On using the apparatus as was done for the purpose of turbidity measurements (1), the intensity change in the forward direction, on bringing this plate into the light path, gives the fraction of the total intensity reflected in the PT_2 direction. This, combined with a subsequent measurement of the reflected intensity at PT_1 relative to that at PT_2, yields the desired ratio I_R/I_0'. Whatever the method used, frequent recalibrations are necessary.

(Further conversion of this quantity to I_{90}'/I_0 is achieved below by means of the constant k_4 which takes care of the reflections.)

The problem of the relationship between I_{90}' and I_{90} is more difficult and involves several considerations. The theoretical values calculated from the Mie theory (with which the experimental data will be compared) refer to a scattering volume of 1 c.c. The illuminated volume defined by the aperture A_3 can be determined quite well because of the nearly parallel character of the primary beam. Diaphragm D_9 in conjunction with the subsequent diaphragms in the sidearm cuts out a very definite fraction of this illuminated volume. With the apertures of both A_3 and D_9 equal to 4 mm., the photometrically active volume amounts to 0.043 c.c.[9] This yields a partial instrument constant, k_2, of 23.2 by which the values of I_{90}'/I_0 have to be multiplied.

An additional factor to be considered is the solid angle. The theoretical values pertain to the intensity of light scattered through unit solid angle. The geometry of the apparatus as used for these experiments (photometric distance = 16.2 cm.; aperture of D_{12} = 5.1 mm.) results in an *apparent* solid angle ω_0' of 7.2×10^{-4} steradian. Translating this into a quantity which can be more easily visualized, the vertex of the planar projection of the light cone has an apparent half-angle ω' of 0.9°. Consideration of the fact that the solid angle is somewhat smaller than assumed owing to refraction of the secondary beam at the exit window, leads to an actual ω_0-value of 4.1×10^{-4} steradian ($\omega = 0.66°$; Fig. 1). Conversion of the data to unit solid angle gives, therefore, a third partial apparatus constant $k_3 = 1/\omega_0 = 2.4 \times 10^3$.

If, in addition, the intensity losses by the reflections of the primary beam at the entrance window of the Rayleigh horn and of the secondary beam at its exit window are taken account of, a fourth constant k_4 is obtained. It has the value of 1.10 for the Rayleigh horn filled with water or a dilute aqueous solution or dispersion.

The overall instrument constant K_0 is then defined as

$$K_0 = k_1k_2k_3k_4 = 0.058. \qquad [13]$$

This value applies to the particular polaroid setting and solid angle selected. It is of interest to note that the orders of magnitude of the ratios $I_R/I_0' = k_1$ and $I_{90}/I_{90}' = k_2k_3$ are nearly the same but of opposite sign. This is the basis for the interesting possibility already mentioned of selecting a combination of polaroid settings such that $K_0 = K = 1.00$.

The value of 0.058 differs from that of the empirical instrument constant K by a factor of 2.4. Considering that the intensity of the primary beam is, as stated, 10^6 times stronger than that of the reference beam, the discrepancy between K and K_0 must be considered as minor. There exists, therefore, the very definite possibility that a sufficient refinement of the absolute calibration method might yield an absolute instrument constant which can be relied upon. This can most likely be achieved by further refining the following: (*1*) the relative measurement of I_0', (*2*) the definition of the scattering volume, and (*3*) the definition of the solid angle.

4. Experimental Data and Discussion

A. The Systems Investigated. Most of the model systems used in this investigation were the same monodisperse Dow polystyrene and polyvinyltoluene latices used for the turbidity measurements (1). Two additional polyvinyltoluene latices characterized by average diameters of 46 and 315 mμ with standard deviations of 8 and 4 mμ, respectively, were included. A third polystyrene latex kindly given to us by Dr. McCartney of DuPont had an average diameter of 47 mμ. The manner of preparation of the diluted suspensions, the precautions taken in doing so, and the other experimental details are adequately treated in the previous paper (1).

---

[9] The photometrically active volume was calculated by considering the volume of intersection of two equal cylinders at right angles.

B. Variation of Lateral Scattering with Particle Size. The primary data needed, i.e., the values of $(I'_{90}/I_Rc)_0$ may be obtained directly from the limiting slopes of I'_{90}/I_R vs. c curves. These curves are shown in Figs. 2 and 3 for half of the samples investigated, data for the other half having been omitted to avoid overcrowding. Although, in general, the slopes are simple in nature (Fig. 2), they may in some instances (Fig. 3) show inflection points at rather small concentrations. The collection of data was therefore extended to concentrations smaller than 0.002 g./100 g. in order to obtain secure limiting slopes. These initial slopes are seen to increase with particle size until a maximum is reached for the 249 mμ sample. Beyond this maximum, the slopes begin to decrease until the particle size reaches 381 mμ. At still larger sizes, the behavior is unclear at first sight, but it will follow from Fig. 7 that the increase and subsequent decrease in slope periodically repeats itself with further increase in particle size.

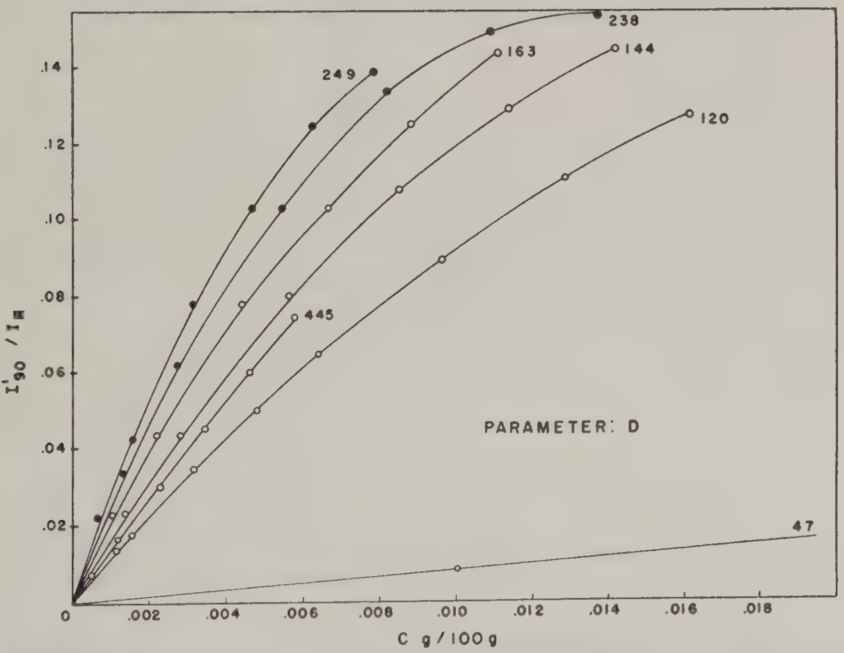

FIG. 2. Concentration dependence of light scattering at 90°. I. ●: Polystyrene; ○: Polyvinyltoluene; Parameter: particle diameter in millimicrons.

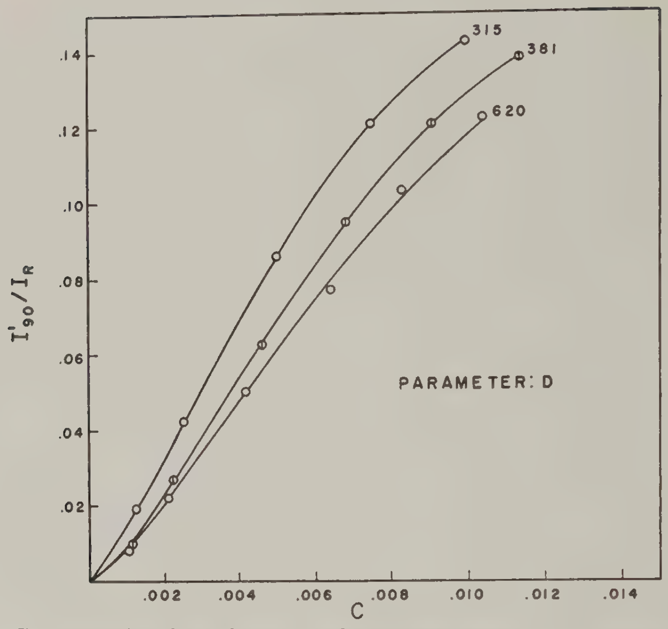

Fig. 3. Concentration dependence of light scattering at 90°. II. Polyvinyltoluene.

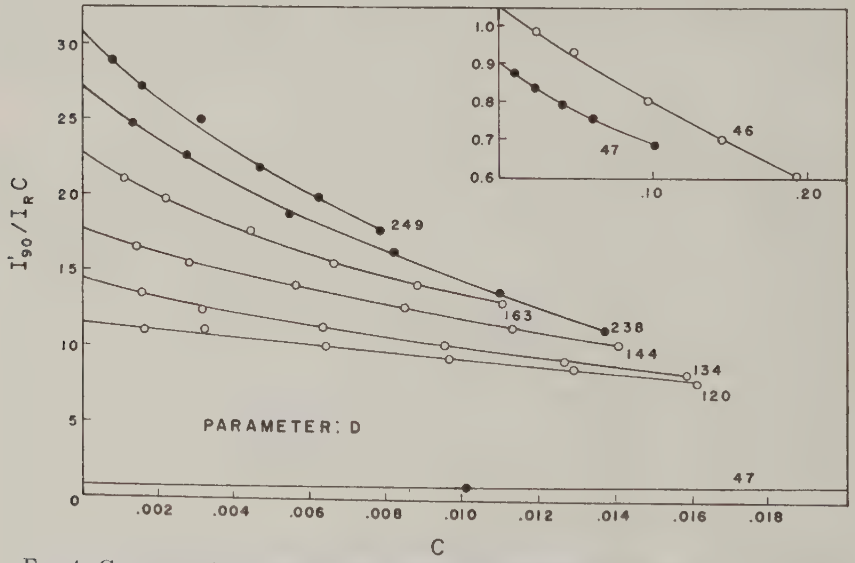

Fig. 4. Concentration dependence of specific light scattering at 90°. I. ● : Polystyrene; ○ : polyvinyltoluene.

To find the initial slopes of these curves, i.e., $(I'_{90}/I_Rc)_0$, more accurately, one merely plots I'_{90}/I_Rc as a function of concentration and extrapolates to infinite dilution. This is done in Figs. 4, 5, and 6. Results for the latices with the smallest particles are shown in the insert to Fig. 4. The latter systems scattered too weakly over the concentration ranges ordinarily employed and, hence, higher concentrations were used. Even more clearly than seen from the slopes in Figs. 2 and 3, the $(I'_{90}/I_Rc)_0$-values, here the intercepts, increase at first as a function of particle size (Fig. 4) and then decrease (Fig. 5). The subsequent behavior (Fig. 6) is not clear at first sight, but it will follow from Fig. 7 that this pattern, an increase followed by a decrease, is being repeated periodically.

A plot of these intercepts as a function of the electron microscopic diameter yields the dotted curve III in Fig. 7, which immediately clarifies the intricate variation of slope and intercept in Figs. 2 and 3, and in Figs. 4, 5, and 6, respectively. On applying the empirical instrument constant $K = 0.138$ the $(I_{90}/I_0c)_0$ values are obtained. These data are represented by

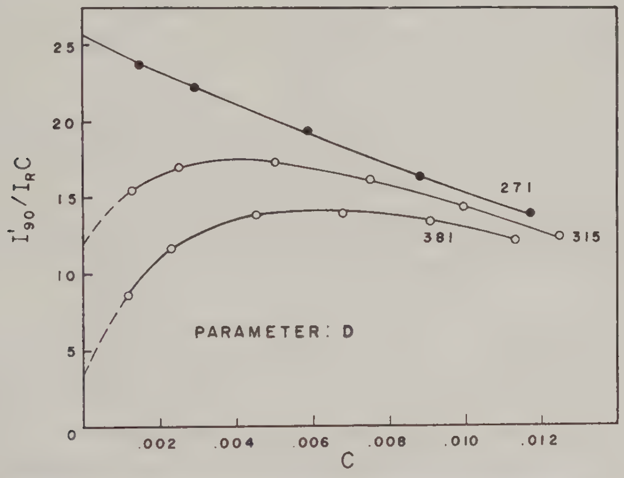

FIG. 5. Concentration dependence of specific light scattering at 90°. II. ●: Polystyrene; ○: polyvinyltoluene.

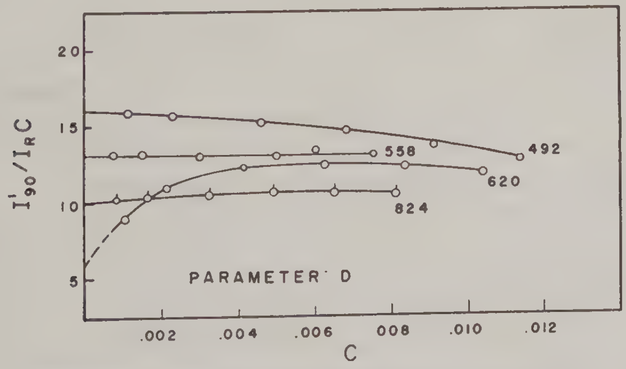

FIG. 6. Concentration dependence of specific light scattering at 90°. III. Polyvinyltoluene.

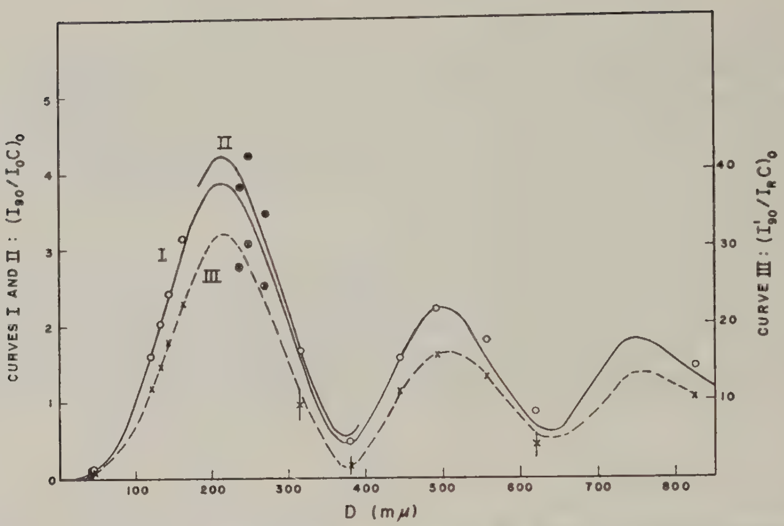

FIG. 7. Variation of specific light scattering at 90° with the particle diameter. I. Theoretical curve for polyvinyltoluene ($m = 1.188$). II. Section of theoretical curve for polystyrene ($m = 1.199$). III. Curve for primary experimental data $(I'_{90}/I_Rc)_0$.

⊗ : polystyrene

✕ : polyvinyltoluene

✱ vertical range of uncertainty (see dotted extrapolations in Figs. 5 and 6)

Application of the instrument constant to the primary data yields $(I_{90}/I_0c)_0$ symbolized by:

● for polystyrene;

○ for polyvinyltoluene.

open and full circles for polyvinyltoluene and polystyrene, respectively. The solid curve I and curve section II show the theoretical variation of I_{90}/I_0c with particle size for polyvinyltoluene and polystyrene, respectively. These curves were obtained by interpolating theoretical data (6) to the proper relative refractive indices, m, and densities ρ_2.[10]

The converted experimental data are seen to agree very satisfactorily with the theoretical data within the entire range considered, i.e., up to 0.82 μ. This furnishes additional proof (1) for the validity of the Mie theory, since the agreement between theory and experiment is obvious only for the sample used as a standard for $K(D = 120\ m\mu)$. A more detailed comparison between the particle sizes thus obtained and the electron microscopic particle sizes is given in Table I.

An additional implicit result of the very satisfactory agreement is that the instrument constant does not vary detectably with the particle size within

---

[10] A separate study carried out in this laboratory by Pugh (7, 8) furnished those data. The densities, ρ_2, for polystyrene and polyvinyltoluene are 1.057 and 1.026 g./cc., respectively, at 25.0° C. The relative refractive index, m, against water for $\lambda_0 = 5461$ A. is 1.199 and 1.188, respectively.

TABLE I

Comparison of Particle Diameters Obtained from Specific Light Scattering at 90° (D_0) and Electron Microscopy (D_e)

Sample no.	$(I_{90}/I_0c)_0$	D_0 ($m\mu$)	D_e ($m\mu$)	% Deviation
116	0.146	51	46	10.9
61*	0.124	45	47	−4.3
41	1.60	120	120	0**
39	2.01	132	134	−1.5
40	2.44	144	144	0
42	3.14	167	163	2.5
7065*	3.81	246	238	3.4
2023*	4.23	218	249	−12.4
7194*	3.48	258	271	−4.8
23	~1.0	311–332	315	−(1–5)
2012	~0.2	375–377	381	−(1–2)
43B	1.56	445	445	0
44A	2.21	447	492	1.0
43C	1.81	543	558	−2.7
44B	~0.4	602–620	620	0 to −3
44C	1.41	812	824	−1.5

* Starred samples are polystyrene; others are polyvinyltoluene.

** Standard used for obtaining instrument constant k.

the range investigated. There is no doubt that this is valid only for the solid angle used or for any other smaller angles. At sufficiently larger angles an equally good agreement cannot be expected.

C. Variation of I'_{90}/I_Rc with Concentration. In general, the values of I'_{90}/I_Rc decrease with increasing concentration (Fig. 4). At certain particle sizes, however (Figs. 5 and 6), an initial increase with a subsequent decrease after passage through a maximum is observed. In these cases, the I'_{90}/I_R vs. c curves show an inflection point (Fig. 3).

Considering first the "normal" curves, i.e., those which exhibit a decrease of I'_{90}/I_Rc with increasing concentration, the primary beam incident upon the observed volume is being weakened because of the turbidity of the suspension, the more the higher the concentration. The intensity of the scattered light I'_{90} suffers a similar attenuation. Consequently, even though I'_{90}/I_R will increase with concentration, it will do so at a decreasing rate since the losses due to turbidity increase more rapidly (exponentially). It can be expected that eventually the I'_{90}/I_R vs. c curve will pass through a maximum not reached as yet at the highest concentrations investigated (Fig. 2). As a result of the foregoing, the I'_{90}/I_Rc vs. c curves must continually decrease. In accordance with this explanation the negative slopes of the latter curves increase, at constant c, appreciably with increasing particle size since the turbidity losses increase faster over a given concentration range the larger the particles.

In order to explain those curves which show an initial increase in I_{90}/I_Rc

with c (an inflection point in the (I'_{90}/I_R) vs. c curves), it must be borne in mind that a third effect, the lateral radiation of multiply scattered light, also is bound to affect the concentration dependence of this quantity. It is therefore interesting to note that this more complex behavior is limited to those diameters which lie at or near the minima of Fig. 7. The multiply scattered light reaching the phototube is not representative of the angle of 90° in the radiation diagram of a single particle but, obviously, represents all angles. The decrease of $(I_{90}/I_0c)_0$ to a minimum at about 375 and 650 mμ indicates that for these particle sizes the intensity scattered at 90° is much smaller relative to the total scattered intensity than for other particle sizes since the total scattering increases continuously with particle size within the range of particle sizes covered by the experiments. Multiple scattering will, therefore, make at those particle sizes the largest contribution to the total intensity received by the phototube at 90° no matter whether the minima in Fig. 7 represent absolute minima in the radiation diagram or not. Since multiple scattering increases with concentration, I'_{90}/I_Rc can be expected to increase with c until the turbidity losses begin to predominate.

D. Effect of Solid Angle. Measurements carried out at 90° are in reality of light scattered by each particle over a cone of finite surface area defined by a solid angle ω_0.[11] Strictly speaking such measurements (and measurements made at other angles of observation likewise) should be carried out at various solid angles and the data to be used for comparison with the theoretical data should be expressed in terms of $(I'_{90}/I_Rc)_0/\omega_0$ and the latter quantity extrapolated to zero solid angle. Such an elaborate procedure can be dispensed with only if a single solid angle is used which is small enough to make $(I'_{90}/I_Rc)_0/\omega_0$ independent of ω_0.

It is of general interest to point out the manner in which the data vary with the solid angle and the manner in which the largest permissible solid angle is to be selected. The solid angle of 4.1×10^{-4} steradian used in the preceding experiments was obtained with the diaphragm D_{12} at the distal end of the sidearm PT_2. Larger solid angles were obtained by moving D_{12} along the sidearm towards the Rayleigh horn. A solid angle of 0.95×10^{-4} steradian was obtained by attaching extension tubes 18 cm. long—not shown in Fig. 1—to both sidearms and placing D_{12} at the distal end of this. Plots of I'_{90}/I_Rc against concentration with the solid angle as the parameter are shown in Fig. 8*A* and *B* for two particle sizes. In addition to the strong decrease in the numerical value of the specific scattering with decreasing solid angle there is also a general flattening out of the curves. Figure 9 gives the variation of $(I'_{90}/I_Rc)_0$ with the solid angle for three particle sizes. Each of the respective points had been obtained by extrapolation, at constant solid angle, of $I'_{90}/I_R c$ vs. c curves to zero concentration as shown in Fig. 8. The curves are or approach a straight line up to solid angles of about 5×10^{-4} steradian which corresponds to a planar angle, as defined earlier, of slightly more than 0.7°. At still larger solid angles the specific lateral scattering increases less than proportionally with an increase of the solid angle. It follows from this graph that the scattering per unit solid angle will be essentially independent of the solid angle selected as long as it is not larger in terms of ω than about 0.7°. The angle selected for the systematic work reported in the preceding sections pertained to 0.66° (4.1×10^{-4} steradian).

---

[11] All the numerical values given for ω_0 have been corrected to account for refraction at the lateral exit window of the Rayleigh horn. This is an indispensable correction. It amounted in our case to 43%.

The fact that the curves in Fig. 9 represent straight lines in their initial portions means that the section of the three-dimensional radiation diagram operative in the light cone received by the photocell approximates fairly

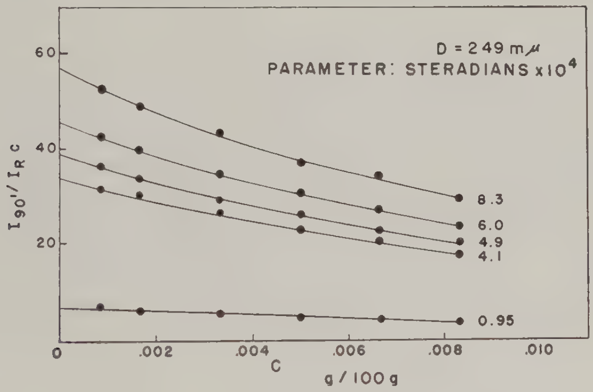

FIG. A

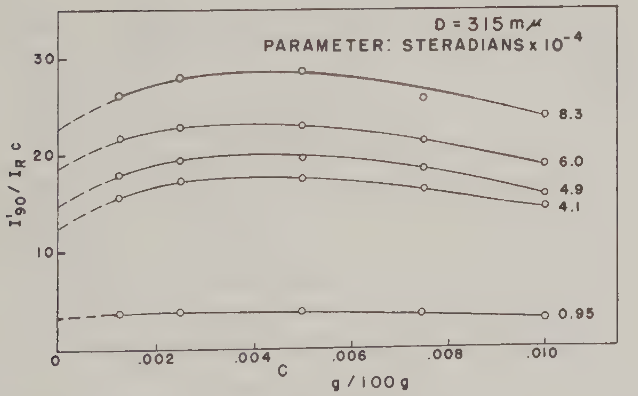

FIG. B

FIG. 8. Concentration dependence of specific light scattering at 90° at various solid angles. *A:* Polystyrene; *B:* Polyvinyltoluene.

well a section of the surface of a sphere. Obviously this can no longer be true if a larger section of the radiation diagram is operative and it is therefore easy to understand why these plots eventually degenerate into curves. Consequently a replot of the curves in Fig. 9, in terms of $(I_{90}/I_Rc)_0/\omega_0$ vs. ω_0, would yield a practically straight line of nearly zero slope degenerating into a curve of increasingly negative slope at ω_0-values $>5 \times 10^{-4}$ steradian, as shown for two examples in Fig. 10. The scattering of the points is obviously somewhat larger in this type of plot.

The empirical instrument constant by which $(I'_{90}/I_Rc)_0$ data have to be multiplied in order to get absolute $(I_{90}/I_0c)_0$ data, at a given solid angle

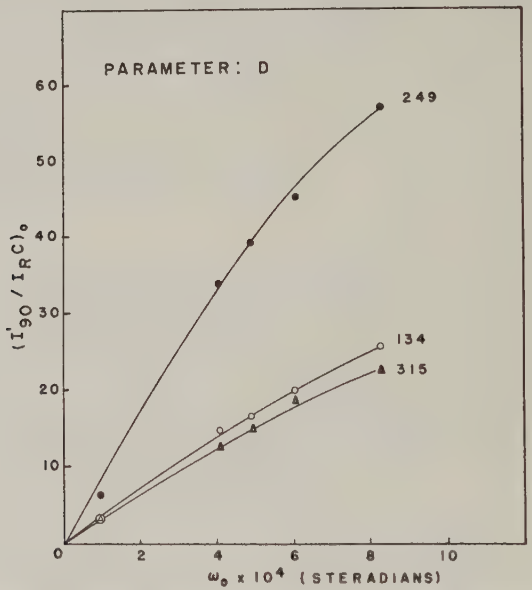

FIG. 9. Variation of specific scattering with solid angle. ●: Polystyrene; ○, △: Polyvinyltoluene.

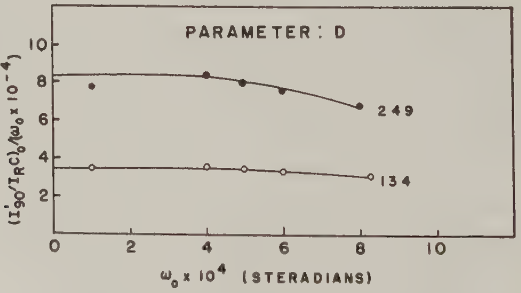

FIG. 10. Variation of specific light scattering per unit solid angle with the solid angle.

●: Polystyrene; ○: Polyvinyltoluene.

will obviously be independent of particle size as long as the particular angle used is within the linear section of the plot given in Fig. 9. The fact that Fig. 7 gave very good agreement between experiment and theory gave additional assurance that the solid angle generally used in these experiments, i.e., 4.1×10^{-4} steradian, was small enough. On the other hand, it is clear that the choice of appreciably larger solid angles would lead to incorrect particle sizes (particle weights) if derived from light-scattering data by means of a single instrument constant.

In conclusion, it may be noted that the information given here on the effect of the solid angle may usefully be applied also to those cases where molecular weights in polymer solutions are obtained by extrapolation of scattering data to the forward direction or where approximate molecular shapes are derived from the variation of scattering with the angle of observation.

REFERENCES

1. TABIBIAN, R., HELLER, W., AND EPEL, J. N., *J. Colloid Sci.* **11**, 195 (1956).
2. HELLER, W., AND TABIBIAN, R., *J. Colloid Sci.* **12**, 25 (1957).
3. HELLER, W., AND PANGONIS, W. J., *J. Chem. Phys.* **26**, 498 (1957).
4. EINSTEIN, A., *Ann. Phys.* **33**, 1275 (1910).
5. MARON, S. H., AND LOU, R., *J. Polymer Sci.* **14**, 29 (1954).
6. Data to be published shortly elsewhere.
7. PUGH, T. L., AND HELLER, W., *J. Colloid Sci.* **12**, 173 (1957).
8. HELLER, W., AND PUGH, T. L., *J. Colloid Sci.* **12**, 294 (1957).

JOURNAL OF COLLOID SCIENCE **13**, 24–31 (1958)

DIFFUSION IN INHOMOGENEOUS MEDIA. CAPILLARY DIFFUSION IN BEDS OF GLASS BEADS

Kurt H. Stern and Harold Shniad

Department of Chemistry and Department of Mathematics, University of Arkansas, Fayetteville, Arkansas

Received May 6, 1957; revised October 7, 1957

ABSTRACT

The diffusion of $AgNO_3$ into K_2CrO_4 and that of HCl into H_2O have been studied as a function of the size of glass beads filling the system. The diffusion constant decreases with decreasing bead size below 200 μ. Diffusion of electrolyte into the beads occurs also.

INTRODUCTION

In some previous work on Liesegang ring formation (1, 2) in media made inhomogeneous by (*a*) partial coagulation of the gelatin and (*b*) addition of glass powder to the medium, it was shown that the diffusion velocity decreases linearly with increasing inhomogeneity, i.e., with the increasing fraction of the total volume which becomes unavailable for diffusion.

In the present study we examine the effect of inhomogeneities on diffusion in greater detail, in particular the effect of differences in the size of the glass beads constituting the inhomogeneity. Our system then consists of a tube (described in the previous papers) filled with a close-packed array of glass beads. The space between the beads is filled with a solution of the medium into which diffusion is to take place. Two separate sets of reactions were studied: (*1*) the diffusion of $AgNO_3$ into K_2CrO_4, and (*2*) the diffusion of HCl into phenol red indicator solution. In the latter case the complication of precipitate formation is avoided and the boundary forms at the "end point" of the indicator. In each set of experiments ten different sizes of glass beads were used. One property of these systems of interest is that the fraction of the total available volume occupied by the beads is independent of bead size and equal to $\pi/3\sqrt{2}$ = 0.74, assuming only close-packing and uniform bead size. Previous work in this field is rather scarce. McBain and Liu (3) studied the diffusion of HCl through various kinds of porous filters and found the diffusion constant unaffected. In this case the size of the pores was about 10^4 times as great as that of the diffusing ions. On the other hand, Cady and Williams

(4) found that diffusion into wood decreased with decreasing pore size. Piret and co-workers (5) studied the diffusion of various electrolytes out of capillaries. They found that the diffusion rate was decreased when the capillaries were packed with glass beads of 150 μ diameter. Diffusion constants were determined, but no systematic study of the effect of pore size was made. Aten and Dreve (6) and Wall, Grieger, and Childs (7) used diffusion out of thin frits for the determination of diffusion constants, but did not study the effect of pore size. Moreover, the solution of the diffusion equation for thin frits is not applicable to our system, since the frits constitute a very short diffusion path, whereas our conditions correspond to a semi-infinite path.

Davtyan (8) analyzed capillary diffusion and concluded that diffusion increases with decreasing size because of an electroosmotic effect. His results show that the diffusion constant of KCl is increased by about 70% in 0.012 mm. slits over its value in large tubes.

Thus it appears that several effects influence the diffusion rate even in a simple system such as the present one. It resembles both porous solids and small capillaries.

EXPERIMENTAL PART

A. Diffusion Experiment

1. Procedure. Measurements were carried out in the tubes described previously. The 3M "Superbrite" glass beads (Minnesota Mining and Manufacturing Company) used are made of a sodium glass. The following sizes were used (diameter in microns): 470, 390, 290, 200, 150, 100, 70, 44, 28. Within each grade the size varies to ±5%. Many of the particles appear not to be spherical under a magnifying glass or microscope, but the "average particle" can be assumed to be a sphere.

Each tube was filled with a slurry of the glass beads and the diffusion medium, a 0.5% K_2CrO_4 solution in one series and aqueous phenol red in the other. The beads were allowed to settle freely. At intervals the tubes were tapped to promote the formation of a close-packed structure and the supernatant liquid was removed. When the beads had settled, a small wad of glass wool was placed on top to break the force of the diffusing solution to be added from a pipet. In one series the diffusing solution was 25 ml. of a 12% by weight $AgNO_3$, in the other 20 ml. of $0.1N$ HCl. The tubes were thermostated in a refrigerator at 5°C.

2. Observations. In the $AgNO_3$ series diffusion could not be studied when the beads were larger than 150 μ because the crystals of Ag_2CrO_4 fell down between the beads, i.e., the interstices were larger than the crystals. With the 150, 100, 70, 44, and 28 μ beads diffusion occurred as shown by the linearity of the $x/\sqrt{t}$ plot (Fig. 1). None of the straight lines intersects the origin, however, because initially the crystals fell some distance before diffusion occurred, i.e., some of the interstices were first plugged with Ag_2CrO_4 crystals before diffusion occurred in the remainder of the tube. This effect was particularly striking with the 150 μ beads where diffusion began only after 150 mm. of tube was filled with crystals.

In the diffusion of HCl into phenol red sharp diffusion boundaries were obtained for all bead sizes of 200 μ or less, with the x vs. $\sqrt{t}$ plots (Fig. 2) extending from the origin. For larger size beads the boundary was uneven because of convections currents, but even in these cases the plots are approximately linear.

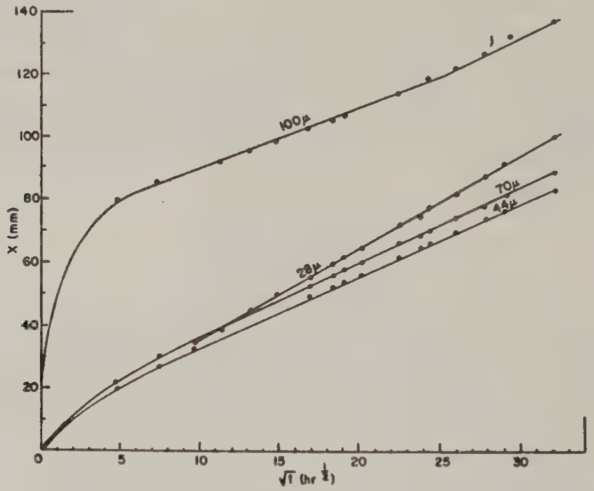

Fig. 1. Diffusion of $AgNO_3$ in K_2CrO_4 for various sizes of beads.

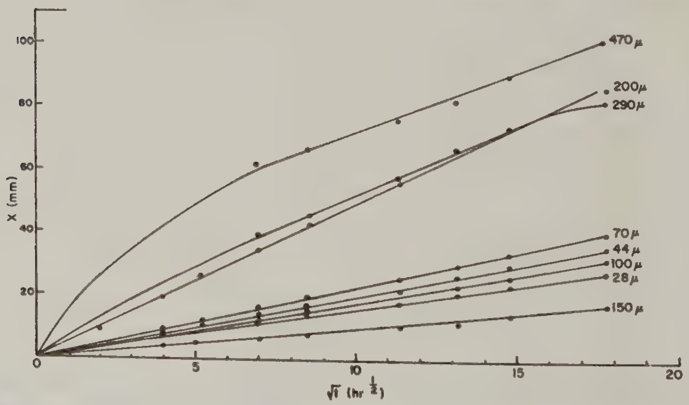

Fig. 2. Diffusion of 0.1N HCl into phenol red indicator for various sizes of beads.

Several duplicate experiments in both series showed that values of $x/\sqrt{t}$ were reproducible to within 5%.

A plot of bead size vs. $x/\sqrt{t}$ for both sets of experiments is shown in Fig. 3. In general, diffusion is highest with the largest beads, $x/\sqrt{t}$ reaching a nearly constant value for beads above 200 μ.

The minimum for the 150 μ seemed particularly disturbing and led to the experiment described below. The agreement for the two sets of diffusion experiments is fairly good.

B. Titration Experiment

It had been assumed initially that diffusion would occur only between the beads, which were considered inert. The results in Fig. 3 throw considerable doubt on this. Moreover, the observations that the addition

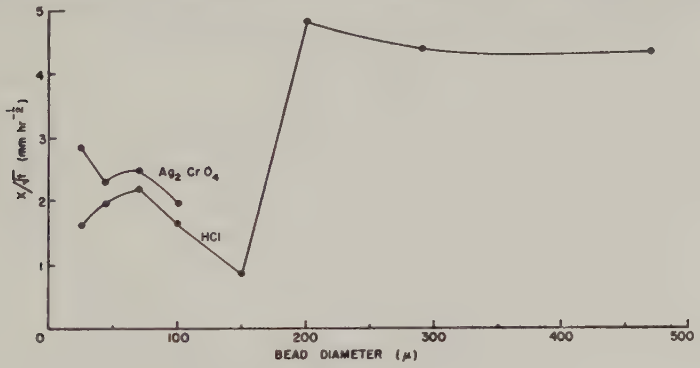

FIG. 3. $x/\sqrt{t}$ vs. bead diameter for the systems in Figs. 1 and 2.

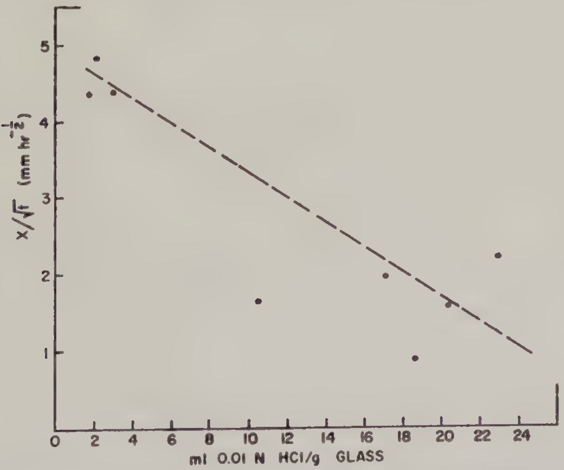

FIG. 4. HCl absorbed by glass beads over a three-month period related to the diffusion velocities in Fig. 2.

of glass causes an aqueous phenol red solution to change from its acid to its basic color (pH 6.8–8.4) indicates that at least the surface of the beads is not inert. Some recent work by Beattie (9) on the reaction between water and vitreous silicates shows that Na^+ ions diffuse out of the glass and H^+ ions diffuse into it. This was confirmed by titrating about 1 g. of 44 μ beads with 0.01N HCl. The titration was carried out by adding the acid to a phenol red solution over the glass intermittently over a period of 400 hours. A plot of (ml. acid/g. glass) vs. $\sqrt{t}$ is linear, indicating that diffusion was responsible.

A similar experiment was then carried out for all the different size beads, the total amount of acid/g. consumed after two months being recorded (this does not represent the end of the titration). A plot of ml. 0.01N HCl/g. glass vs. $x/\sqrt{t}$ is shown in Fig 4. No obvious correlation exists, but there is a general trend for diffusion to be most rapid in the systems where the beads take up the least amount of acid.

Discussion

The gross features of the system, i.e., the progress of the indicating boundary along the tubes, can be described in terms of the one-dimensional diffusion equation

$$D\frac{\partial^2 C}{\partial x^2} = \frac{\partial C}{\partial t}. \qquad [1]$$

The usual boundary conditions are

$$C = 0 \text{ at } t = 0 \text{ and } 0 < x < \infty;$$

$$C = C_0 \text{ for all } t \text{ and } x < 0.$$

Then the solution is

$$C(x, t) = \frac{2C_0}{\sqrt{\pi}}\int_{\frac{x}{2\sqrt{Dt}}}^{\infty} \exp(-\zeta^2)\, d\zeta, \qquad [2]$$

where ζ is a variable of integration.

From this it follows that $x/\sqrt{t}$ is constant. This situation represents diffusion from a semi-infinite reservoir into a space initially containing none of the diffusing substance. From measured values of x and t at the boundary we can calculate the diffusion coefficient of 0.1N HCl in these systems in the following way. From the end point of phenol red we know the hydrogen ion concentration at the diffusion front is near 10^{-7}. Since the reservoir concentration is 10^{-1} we get for the ratio $C/C_0 = 10^{-6}$. Darken and Gurry (10) give a table of $x/\sqrt{Dt}$ for various values of C/C_0. For all our tubes $x/\sqrt{Dt} \simeq 6.0$. From Fig. 3 we obtain values of $x/\sqrt{t}$. For beads above 200 μ, $x/\sqrt{t} = 0.45$ cm. hr.$^{-1/2}$ and $D = 5.6 \times 10^{-3}$ cm.^{2}

hr.$^{-1}$. This is considerably smaller than the values usually cited (11) for the diffusion coefficient of 0.1 N HCl at 5°C., 7×10^{-2} cm.^{2} hr.$^{-1}$. However, we also obtained the smaller value for the open capillaries. No explanation is evident for the discrepancy.

If the diffusion of HCl into the beads occurred with velocities comparable to that between them one would expect the x vs. $\sqrt{t}$ curves to curve convexly downward, particularly for larger values of t. Since this is not appreciably the case, this effect is evidently not great, at least for low values of t. It may be that the curves would show the expected slope had the experiment been carried out longer. This was not possible because the end point of the indicator eventually smears out as the concentration gradient becomes less steep. However, the similar diffusion velocities obtained for $AgNO_3$ into K_2CrO_4 indicate that diffusion of electrolyte into the beads cannot be very important in influencing the rate, since it is unlikely that silver ions will diffuse into glass to the same extent as hydrogen ions. This is true at least for concentrations of diffusing electrolyte above 0.1N.

Any diffusion into the beads should become more important as the concentration of the diffusing solution is decreased. There should then exist a lower concentration limit below which the diffusion front does not advance at all, because diffusion into the beads uses up all the diffusing solution. A check of this idea, using the 150 μ beads (which most strongly absorb acid), bears this out. When the HCl concentration is lowered to 0.01N the diffusion front becomes stationary after advancing about 6 mm. For this case it seems reasonable to write the diffusion equation in the form

$$D\frac{\partial^2 C}{\partial x^2} = \frac{\partial C}{\partial t} + BC, \qquad [3]$$

where B is a constant. The assumption made here is that the diffusion rate into the beads is proportional to the concentration outside them. The solution of this equation under the same boundary conditions as before is

$$C(x, t) = \frac{2C_0}{\sqrt{\pi}} \int_{\frac{x}{2\sqrt{Dt}}}^{\infty} e^{-\frac{Bx^2}{4\zeta^2}} e^{-\zeta^2}\, d\zeta. \qquad [4]$$

A solution of [3] for the steady-state case yields

$$C = C_0 e^{-\sqrt{B}x}. \qquad [5]$$

Substituting our experimental values we can calculate B. Using $C_0 = 10^{-2}$, $C = 10^{-7}$, $x = 0.6$ cm. we obtain $B = 366$ cm.$^{-2}$. To assess the importance of B it would be necessary to compare the relative magnitude of the two terms on the right side of Eq. [3]. Unfortunately this is impossible since our experiment does not yield dC/dt.

An assembly of close-packed beads resembles both a porous solid and a suspension of fine solid in a solution. As the bead size decreases, the total surface area of the beads is increased and the size of the capillary channels between the beads is decreased. The following factors should then be considered: (*1*) With decreasing capillary size the diffusion constant increases because of differences in ionic mobilities and diffusion potential over the bulk case (8). On this basis alone one would predict an increasing diffusion rate with decreasing bead size. (*2*) Adsorption of electrolyte on, and diffusion into, the beads both increase with decreasing bead size. As has already been shown above the importance of both is relatively small in decreasing electrolyte concentration in the solution between the beads. An estimate of the adsorption capacity can be made from the initial titration of the beads with acid. For the smallest size beads this amounts to a few tenths of a milliliter $0.1N$ HCl per gram of glass. Unfortunately, since the porosity of glass beads may differ considerably from one batch to the next, titration curves of one type of beads are of limited applicability to others. (*3*) Mechanical blocking is responsible for the decreased diffusion rate in porous solids. To the extent that close-packed beads approach this type of structure, the degree of porosity decreasing with bead size, similar arguments apply to both. Certainly our results are in accord with those of Piret and co-workers (5) on glass-bead-filled capillaries and those of Cady and Williams (4) on wood. In this context the work of McBain and Liu (3) seems anomalous.

The relative complexity of the curves in Fig. 3 also suggests that more than one factor is responsible for the observed diffusion rate in these systems. This rate will increase with decreasing bead size because of the capillary effect (8) and decrease because of mechanical blocking, adsorption, and absorption. The divergence of the Ag_2CrO_4 and HCl curves for the smallest beads indicates that for the former the capillary effect prepredominates over that of electrolyte adsorption. This is reasonable since silver ions would not be expected to diffuse as readily into glass as hydrogen ions. The similarity of the curves over the next three sizes suggests competition between the capillary and blocking effects. The increase in diffusion rate in going from 150 μ to 70 μ is evidence for the capillary effect, whereas the sharp decrease from 200 μ to 150 μ may be caused by mechanical blocking.

The increase of diffusion rate with decreasing capillary size is a consequence of the electrical charges on the diffusing particles; i.e., the mobility of the particles is enhanced by an electroosmotic potential. This effect should be absent for uncharged molecules. The diffusion rate of these into beds of glass beads should either be independent of bead size, if the only factor is the total volume of channels available for diffusion, or decrease with bead size, if mechanical blocking is a factor. However, no data on this are yet available.

REFERENCES

1. STERN, K. H., *J. Colloid Sci.* **9,** 329 (1954).
2. STERN, K. H., *J. Colloid Sci.* **10,** 409 (1955).
3. McBAIN, J. W., AND LIU, T. H., *J. Am. Chem. Soc.* **53,** 59 (1951).
4. CADY, L. C., AND WILLIAMS, J. W., *J. Phys. Chem.* **39,** 87 (1935).
5. PIRET, E. L., EBEL, A., KIANG, C. T., AND ARMSTRONG, W. P., *Chem. Eng. Prog.* **47,** 405 (1951).
6. ATEN, A. H. W., AND DREVE, J. v., *Trans. Faraday Soc.* **44,** 202 (1948).
7. WALL, F. T., GRIEGER, P. F., AND CHILDS, C. W., *J. Am. Chem. Soc.* **74,** 3562 (1952).
8. DAVTYAN, O. K., *Zhur. Fiz. Khim.* **20,** No. 9, 1043 (1946).
9. BEATTIE, I. R., *Trans. Faraday Soc.* **49,** 1059 (1953).
10. DARKEN, S. D., AND GURRY, R. W., "Physical Chemistry of Metals," p. 444. McGraw-Hill, New York, 1953.
11. "International Critical Tables," Vol. 5, p. 63. McGraw-Hill, New York, 1929.

JOURNAL OF COLLOID SCIENCE **13,** 32–50 (1958)

THE SPREADING OF LOW VAPOR PRESSURE LIQUIDS IN PAPER

T. Gillespie[1]

Suffield Experimental Station, Ralston, Aberta, Canada

Received November 5, 1956; revised July 19, 1957

Abstract

A study has been made of the spreading of the stains produced by low vapor pressure liquids in various types of filter paper and in printflex card. Both the rate of spreading and the distribution of the liquid in the stains have been measured. Semiempirical equations describing the data have been developed.

The spreading studies have led to a theoretical stain size drop size relation for low vapor pressure liquids, which may be used for estimating the drop size distribution of a liquid spray. A short time after collection, the stain diameter, D, will be proportional to the drop diameter, d. With such liquids there is no "final stain size." The spreading factor, D/d, should be proportional to $t^{1/6}$, where t is the time after collection. These conclusions have been verified in subsidiary experiments.

Introduction

For many years the stain method for estimating the size distribution of drops (1–3) has been used to assess the aerosols resulting from spray devices. In this technique the drops are collected on a paper and their sizes determined by measuring the stains and comparing with stains produced in an appropriate calibration. Because the process by which a drop spreads in paper is not understood completely, it has been found necessary to calibrate repeatedly in order to ensure reliable assessment. As a first step toward improving this situation, a study has been made of the spreading of non-volatile drops in various papers.

The problem of a drop spreading in paper is closely related to the behavior of liquids in other fibrous materials such as cloth or in granular materials such as sand or soil. These related phenomena are of considerable interest. In consequence, the spreading in paper has been treated in some detail in order that the results may be of use in future studies of these other problems.

In the past, studies of the spreading of drops in paper have been confined to a measurement of "the final stain size" produced by drops of

---

[1] Present address: The Physical Research Laboratory, The Dow Chemical Company, Midland, Michigan.

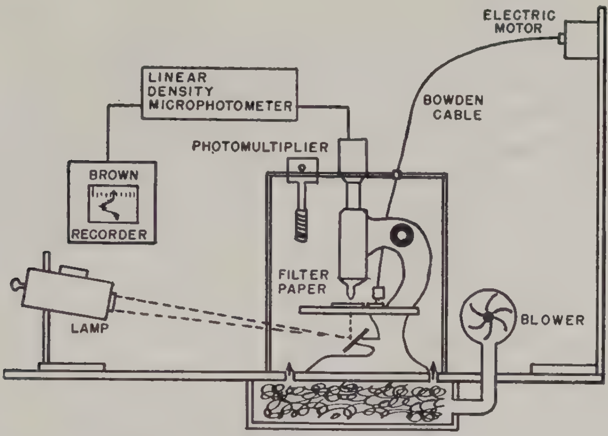

FIG. 1. Schematic diagram of the drop spreading apparatus.

various sizes (1–3). Theoretical work has been limited to an attempt to find an empirical drop size-stain size relation (3).

In the present work the change of stain size with time and the distribution of the liquid in the paper at various times have been examined. This has led to a satisfactory semiempirical description of spreading which includes, among other things, a drop size-stain size relation when evaporation is negligible.

EXPERIMENTAL

The apparatus used in the spreading studies is shown in Fig. 1. The microscope (40 × objective, 15 × eyepiece) used to assess the stains was mounted in a plastic box with two wooden sides. The air temperature in the microscope chamber was controlled by feeding the output of a hair dryer through the false bottom of the box, which was filled with steel wool, and allowing the heated air to seep through a number of uniformly distributed holes bored in the box floor.

Strips of the filter paper or printflex paper card[2] chosen for assessment were mounted on large microscope slides using adhesive tape at both ends and were then placed face up in the mechanical stage of the microscope. Provision was made for driving the stage automatically at a constant speed by means of a Bowden cable connected to a gear box and a small electric motor. The drops of undyed liquid to be tested were released from a syringe mounted with the needle tip 1 cm. above the filter paper and positioned so that when the paper was carried across the microscope stage the center of the drop passed through the axis of the microscope.

[2] This card is sized with casein and the finish is described as "satin white"; it consists of a mixture of calcium sulfate and calcium carbonate.

The main experiment consisted of two parts. In the first, the diameters of the stains were measured at various times using a graticule in the eyepiece of the microscope. In the second, the distribution of the liquid in the stains was measured in terms of the attenuation of a narrow beam of light, 1.5 mm. in diameter; light intensity being determined with a photomultiplier tube connected to a linear density microphotometer unit, the readings of which were found to be directly proportional to the liquid concentration. The microphotometer was attached to a Brown recorder so that permanent records of the distribution of the liquid in the stain could be quickly obtained. To eliminate spurious effects from extraneous light the microscope chamber was covered with opaque cardboard.

This optical method of assessing liquid concentration was checked by comparing the microphotometer readings on a series of strips of filter paper which contained a known amount of liquid (previously determined by weighing). The result of a typical calibration is illustrated in Fig. 2.

As might be expected, it was found with some of the papers that there was a tendency for the liquid to spread more easily in one direction than in others. In these cases the stain diameters and liquid concentrations were assessed in two directions, one parallel and one normal to the preferred direction. Since the difference was in no case very large (<10%), the average of the results would be expected to give a sufficiently accurate picture of drop spreading.

In a subsidiary set of experiments the rate of one-dimensional spreading and the distribution of liquid in one dimension were determined. This was done by placing a drop at the center of thin horizontal strips of various types of filter paper (7.3 mm. wide), and assessing the stains as above.

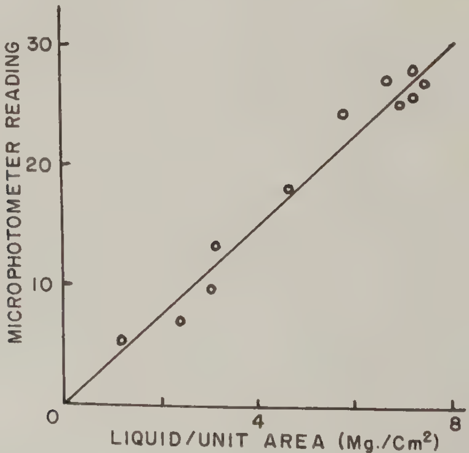

FIG. 2. A typical calibration of the microphotometer (D.B.P. on Whatman No. 1 filter paper).

Experimental Results

In Fig. 3, the variation of the stain radius, denoted by R, is illustrated for various liquids at 28°C. in Whatman No. 1 filter paper. In Fig. 4, similar data for dibutyl phthalate in various grades of filter paper and in printflex cards are plotted. In Fig. 5 the effect of temperature on the spreading of dibutyl phthalate in printflex cards is shown.

Figure 6 illustrates typical results of the determination of liquid dis-

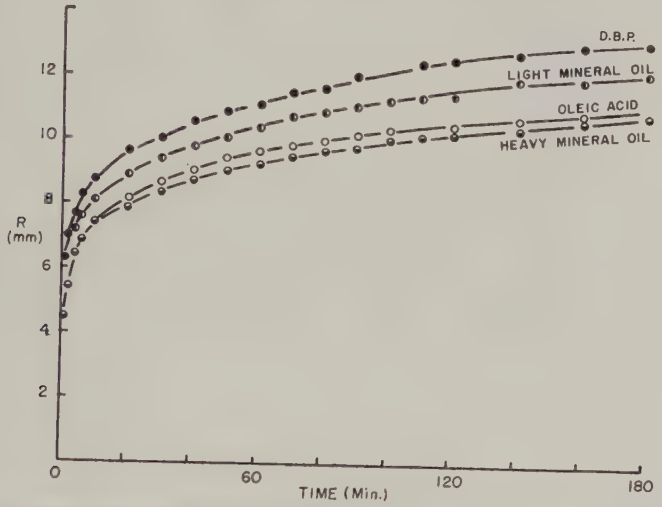

Fig. 3. Variation of stain radius with time for various liquids on Whatman No. 1 paper.

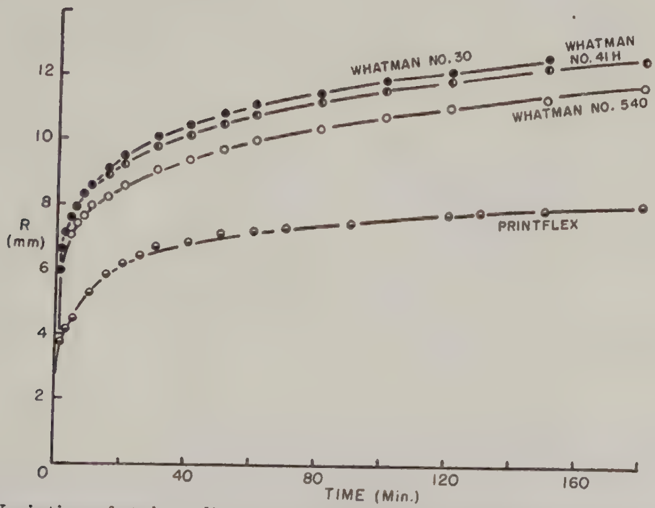

Fig. 4. Variation of stain radius with time for dibutyl phthalate on various papers and printflex card.

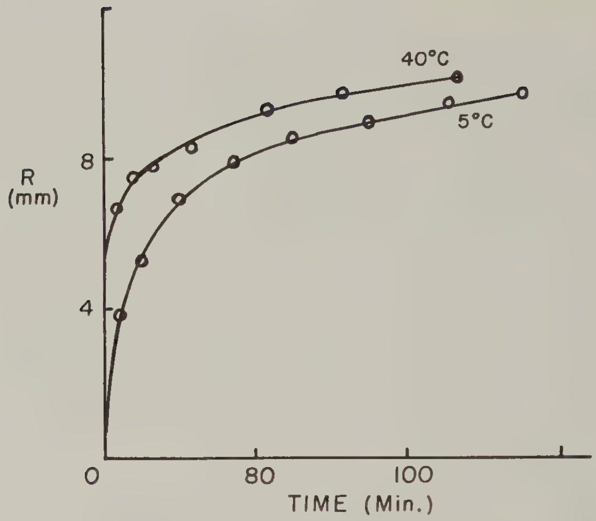

FIG. 5. Illustration of the effect of temperature on the stain produced in printflex card by dibutyl phthalate. (The arrows indicate the times of disappearance of the residual drop.)

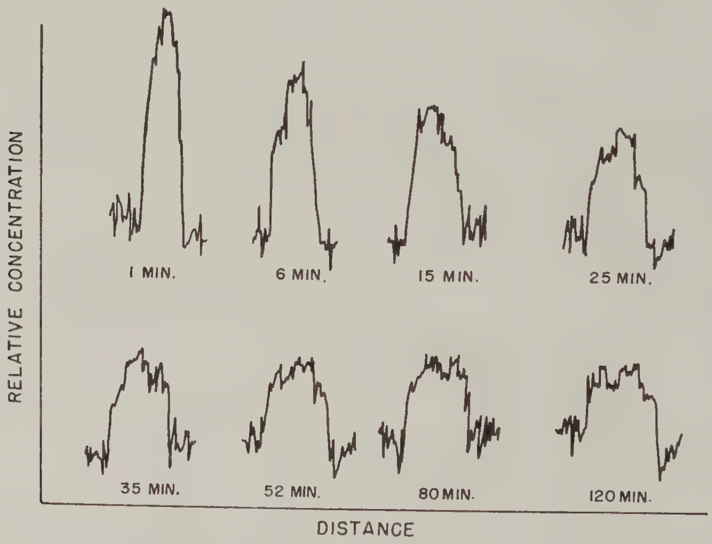

FIG. 6. Typical liquid distribution curves for dibutyl phthalate on Whatman No 1 filter paper.

tribution in stains as obtained with the microphotometer-recorder arrangement. The irregularities in the traces are due to the nonuniformity of the paper and are accentuated by the necessity of using a finite light spot (1.5 mm. diameter) in concentration assessment. As the light spot arrived at the edge of the stain the microphotometer readings would not give a correct indication of the liquid concentration. The position of zero concentration can, however, be located by referring to the results of the visual stain diameter determination.

Once the liquid had all entered the paper the liquid concentration curves were all of the same general form, even when the time of spreading was as long as three weeks. Furthermore, the stains were still spreading after such long times although the rate was very small.

The results of the one-dimensional experiments with the thin strips of paper were qualitatively similar. There were, however, some important quantitative differences which are discussed more appropriately in the following section.

THEORETICAL CONSIDERATIONS

When a drop of liquid is placed on a filter paper it will spread through the paper if the contact angle is less than 90°. Although for very small drops or very thick paper the drops may all soak into the paper before any of the liquid reaches the other side, in the present experiments the stain had the same diameter when viewed from either side even before all the liquid had entered the paper. The spreading process may be split conveniently into two phases. In the first there will be some of the liquid remaining on the surface of the paper in the form of a flattened drop. In the second the liquid will all be contained "within" the paper. These two stages are illustrated in Figs. 7*a* and 7*b*. Since the first stage was completed, in most cases, in a relatively short time, it may be considered of secondary importance in a first treatment of drop spreading.

At the beginning of the second stage the center of the stain is saturated, meaning that all the pores are filled with liquid. The stain spreads owing to capillary forces pulling the liquid preferentially into the fine pores at

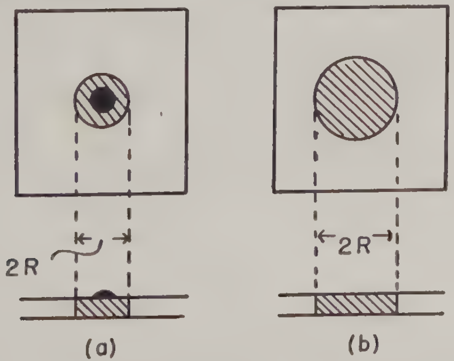

FIG. 7. Illustration of the two stages in drop spreading (not drawn to scale).

the edge and out of the larger pores at the center of the stain. The problem is to determine the distribution of liquid at any time t, measured from the beginning of the second stage, and also the rate of spreading of the boundary.

a). *One-Dimensional Spreading*

When one measures the velocity at which a liquid is forced through a porous material by a given pressure gradient, spurious effects often occur which are caused by air trapped either in the material or at the entrance to it. With the use of correct techniques these difficulties may be minimized, and it is generally agreed (4) that, provided the Reynolds number is less than 1, D'Arcy's law holds, i.e.,

$$\frac{dQ}{dt} = -\frac{k}{\eta}\nabla p, \qquad [1]$$

where dQ/dt is the volume of liquid passing through unit area per second, η is the viscosity of the fluid, and ∇p is the gradient of the pressure. The constant, k, is called the permeability and may be defined as the volume of liquid of unit viscosity passing through unit cross section of the medium under the action of a unit pressure gradient.

Combining D'Arcy's law with the equation of continuity Muskat and Meres (5) have shown that when a gas-liquid mixture flows through a porous medium the liquid flow satisfies the following equation

$$\nabla\cdot(k_1\nabla p) = \eta\frac{\partial C}{\partial t}, \qquad [2]$$

when k_1 is the liquid permeability of the porous medium when the liquid concentration is C measured in cubic centimeters of liquid per cubic centimeter of paper.

The possibility of extending Eq. [2] to cover the case of a liquid spreading under capillary forces alone depends entirely upon the question of whether D'Arcy's law holds. This empirical law effectively states that the resistance to flow is proportional to the viscosity and velocity of the liquid which one would expect if the inertia of the fluid was negligible. In capillary spreading the flow velocities are very small, and it is quite reasonable therefore to expect that D'Arcy's law would hold and hence one could apply Eq. [2].

In the one-dimensional case Eq. [2] becomes

$$\frac{\partial C}{\partial t} = -\frac{1}{\eta}\frac{\partial}{\partial x}\left(k_1\frac{dp}{dx}\right). \qquad [3]$$

If the manner in which the permeability, k_1, and the pressure gradient varied with changes in C, x, and t were known it would be possible to solve Eq. [3].

The pressure in the liquid at any point would depend upon the two principal radii of curvature of the free liquid surface. These in turn would be determined by the concentration and the concentration gradient. Using Haines' technique for measuring the suction due to unsaturated porous media (6) it can be shown that the pressure drop between the center and the boundary of a one-dimensional stain is proportional to the length of the stain if the center of the stain is kept saturated. (See the Appendix.) This suggests the possibility that the pressure gradient is a constant, presumably because concentration and concentration gradient effects cancel out. Hence it is not unreasonable to assume

$$\frac{dp}{dx} = a\gamma \cos \theta \qquad [4]$$

where a is a constant descriptive of the paper, γ is the surface tension of the liquid, and θ is the contact angle between the fibers and the liquid.

The other factor required to solve Eq. [3], namely, the permeability k_1, would be expected to increase with liquid concentration, but it would be very difficult to calculate the precise manner in which it would vary. Even in the relatively simple case of flow through a saturated porous body there is no generally accepted procedure for calculating permeability (4, 7). The permeability of a sample of paper can be determined using air, and reproducible results are obtained. Measurements with liquids are far more difficult, and the results are not very reproducible (8). This is presumably due to the air which one would expect to be trapped in the smaller pores as the liquid was forced through.

In some subsidiary experiments it was found that small bubbles introduced into a saturated paper plug reduced the permeability and furthermore the permeability was time-dependent.

In view of these difficulties the most convenient way to solve the present problem is to find the relation between permeability and concentration which when substituted in Eq. [3] yields a result consistent with the experimental data. The correct relation appears to be

$$k_1 = k_0 \left(\frac{C}{C_s}\right)^3, \qquad [5]$$

when k_0 denotes the permeability of the paper when all the voids in the paper are carrying liquid and C_s is the saturation concentration.

There is some experimental evidence in the literature which lends support to Eq. [5]. In Fig. 8 some of the data of Wyckoff and Botset (9) obtained in their study of the flow of gas-liquid mixtures through unconsolidated sands are plotted. They agree with Eq. [5]. These data were obtained over a considerable range of experimental conditions (9), and it is therefore reasonable to suggest that paper would act the same.

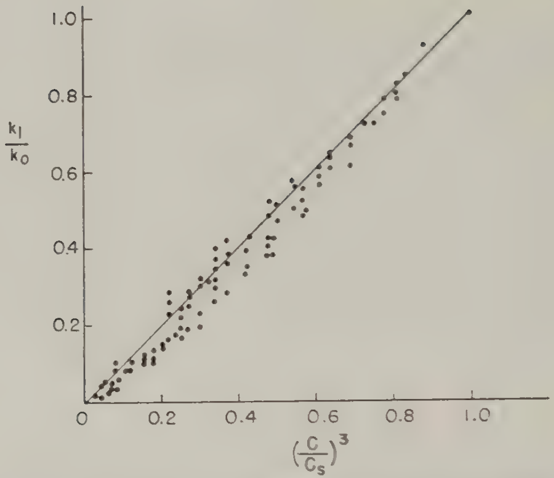

FIG. 8. Illustration of the proportionality between liquid permeability and the cube of the liquid concentration for the flow of gas-liquid mixtures through unconsolidated sand (Wyckoff and Botset (9)).

Combining Eqs. [3], [4], and [5]

$$\frac{\partial C}{\partial t} = -\alpha \frac{\partial C^3}{\partial x} \qquad [6]$$

where

$$\alpha = \frac{ak_s \gamma \cos \theta}{C_s^3 \eta}. \qquad [7]$$

The distribution of the liquid in the experiments with thin strips of filter paper should be given by the solution of Eq. [6] with the following boundary conditions:

$$C = C_s \quad \text{at } x = 0 \quad \text{and} \quad t = 0; \qquad [8]$$

$$C = 0 \quad \text{at } x = L \text{ for all } t. \qquad [9]$$

L denotes one half the length of the stain or the position of the boundary as measured from an origin at the center of the stain.

The solution is

$$C = C_0 \left[1 - \frac{x}{L}\right]^{1/2}, \qquad [10]$$

where

$$C_0 = C_s \left[1 + \frac{3\alpha C_s^2 t}{L}\right]^{-1/2}. \qquad [11]$$

C_0 is the concentration at the center of the stain.

Because the total volume of liquid in the stain, denoted by M, remains a constant,

$$V = 2wh \int_0^L C\,dx; \qquad [12]$$

hence

$$L(L^2 - L_0^2) = \frac{27}{16}\,\alpha \left(\frac{V}{wh}\right)^2 t, \qquad [13]$$

where w and h refer to the width and thickness of the paper strip, respectively. L_0 is the position of the boundary at $t = 0$. α is descriptive of the rate of spreading in one dimension. According to Eq. [7], for a given paper α should be proportional to $\gamma/\eta \cos\theta$.

b). *Two-Dimensional Spreading*

For a drop spreading in two dimensions to form a circular stain, Eq. [2] becomes

$$\frac{\partial C}{\partial t} = -\frac{1}{\eta r}\,\frac{\partial\left(rk_1\,\dfrac{dp}{dr}\right)}{\partial r}. \qquad [14]$$

Unfortunately it was not possible to measure the suction at the boundary of a circular unsaturated fibrous system as it was in the linear case (see the Appendix for details). As in the one-dimensional case, the pressure in a circular stain will depend upon both the concentration and the concentration gradient.

A number of attempts were made to determine the relation between C, $\delta C/\delta r$, and the pressure, but none of these were convincing enough to reproduce here. It has been suggested in the linear case treated above that

$$\nabla^2 p = 0; \qquad \frac{\partial p}{\partial t} = 0. \qquad [15]$$

It has been found that if we assume that liquid spreading in fibrous media adjusts itself so that Eq. [15] holds in two dimensions as well as in the one-dimensional case, equations for the liquid distribution and rate of spreading can be derived which are in agreement with experiment.

For radial spreading Eq. [15] leads to

$$\frac{dp}{dr} = \frac{b\gamma\cos\theta}{r}, \qquad [16]$$

where b is a constant.

Combining Eqs. [5], [14], and [16]

$$\frac{\partial C}{\partial t} = -\frac{\beta \partial C^3}{r \partial r}, \tag{17}$$

where

$$\beta = \frac{b k_s \gamma \cos \theta}{C_s^3 \eta}. \tag{18}$$

For a drop spreading in stage 2 as illustrated in Fig. 7b, the boundary conditions are

$$C = C_s \quad \text{at } t = 0 \quad \text{and} \quad r = 0, \tag{19}$$

$$C = 0 \quad \text{at } r = R \text{ for all } t, \tag{20}$$

where R denotes the stain radius.

The liquid distribution in a circular stain is therefore

$$C = \left[1 - \left(\frac{r}{R}\right)^2\right]^{+1/2}; \tag{21}$$

$$C_0 = \left[1 + \frac{6\beta C_s^2 t}{R^2}\right]^{-1/2}. \tag{22}$$

The volume of liquid in the stain being a constant, denoted by V,

$$V = 2\pi C_0 h \int_0^R \left[1 - \left(\frac{r^2}{R^2}\right)\right]^{+1/2} r\,dr. \tag{23}$$

Hence

$$R^2[R^4 - R_0^4] = \frac{3\beta}{2}\left(\frac{3V}{2\pi h}\right)^2 t \tag{24}$$

where R_0 is the radius of the stain at time zero. Here β is descriptive of the rate of radial spreading and for a given paper should be proportional to $\gamma/\eta \cos \theta$; see Eq. [18].

Equation [23] leads to the useful relation

$$R_0^2 = \frac{3V}{4\pi C_s h}. \tag{25}$$

This is similar to the empirical expression Fournier D'Albe *et al.* obtained for raindrops (10).

COMPARISON OF THEORY WITH EXPERIMENT

Equations [10], [11], and [13] should describe all the features of one-dimensional flow measured in the experiments with the thin strips of paper. According to these equations plots of $L/(L^2 - L_0^2)$ vs. t and $1/C_0^2$

vs. t/L should be linear. Figures 9 and 10 indicate that this is the case. In Fig. 11 some of the liquid distribution experimental results are compared with data calculated from Eq. [10]. Apart from the uncertainty of the concentration at the boundary the agreement is satisfactory.

Equations [21], [22], and [24] should describe all the data obtained in the circular stain experiments. Plots of $R^2(R^4 - R_0^4)$ vs. t were linear as suggested by Eq. [24]. (See Fig. 12.)

Plots of $1/C_0^2$ vs. t/R^2 were found to be linear as required by Eq. [22]. (See Fig. 13.) In addition, the calculated liquid distribution curves determined by using Eq. [21] were in agreement with the experimental results as illustrated in Fig. 14.

Application to the Stain Technique for Sizing Drops

Equation [24] should be the correct stain size-drop size relation for low vapor pressure liquids. Since it is usual to work with diameters rather

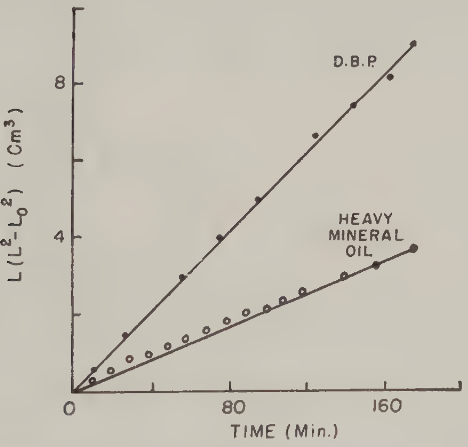

FIG. 9. Illustration of the proportionality between $L(L^2 - L_0^2)$ and time for one-dimensional spreading.

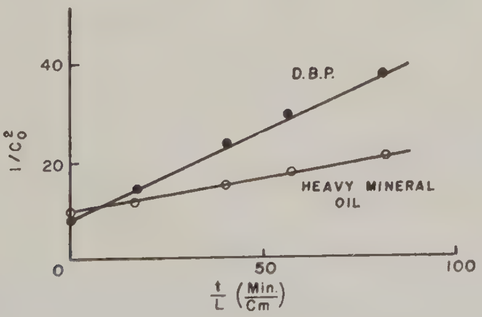

FIG. 10. Illustration of the proportionality between $1/C_0^2$ and t/L.

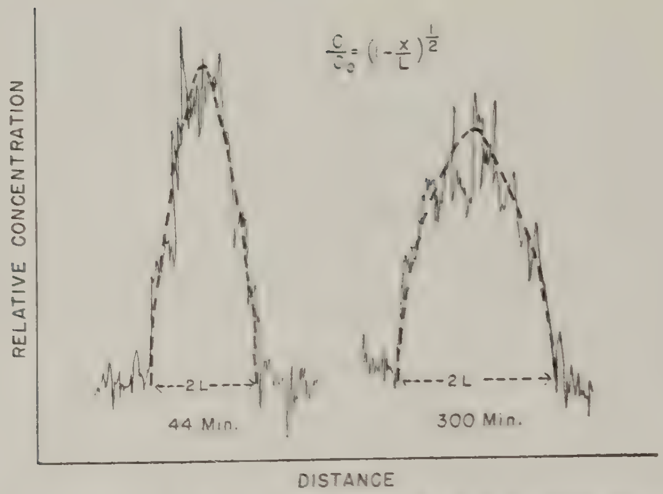

FIG. 11. A comparison of theory and experiment for one-dimensional liquid distribution curves (D.B.P. stains on Whatman No. 1 paper).

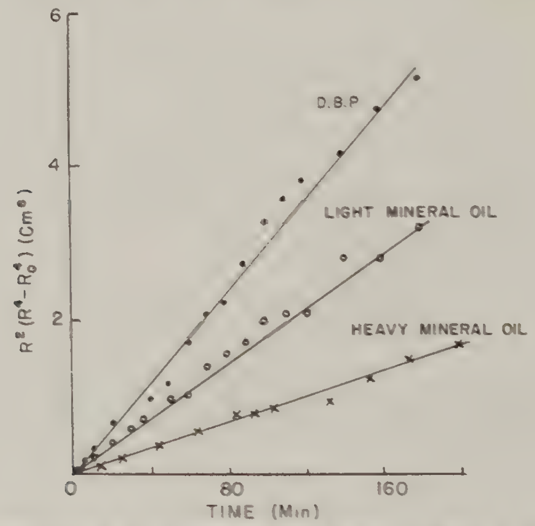

FIG. 12. Illustration of the proportionality between $R^2(R^4 - R_0^4)$ and time for two-dimensional spreading (Whatman No. 1; 28°C.).

than radii, this equation is more usefully expressed in the form

$$\left(\frac{D}{d}\right)^6 = \left(\frac{D}{C_s h}\right)^2 + \frac{6\beta t}{h^2}, \tag{26}$$

where D and d are the stain and drop diameter, respectively.

Provided $t \gg D^2/6\beta C_s^2$ the stain diameter would be proportional to the

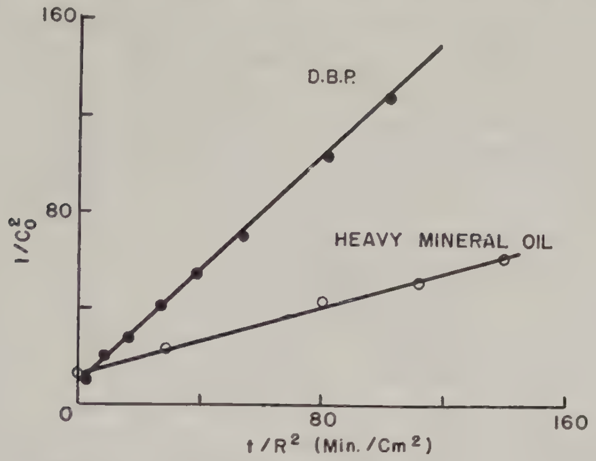

FIG. 13. Illustration of the proportionality between $1/C_0^2$ and t/R^2.

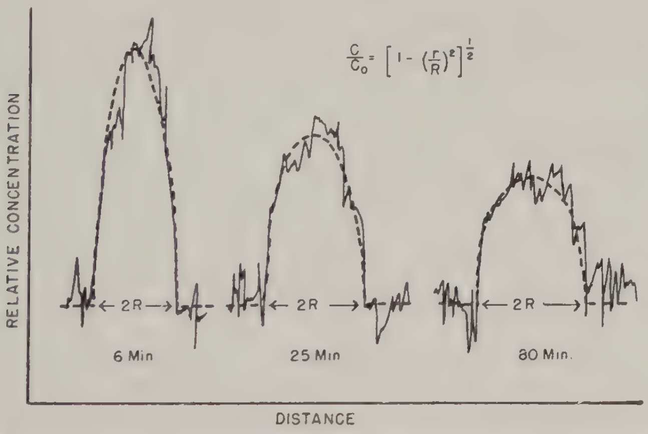

FIG. 14. A comparison of experimental and theoretical liquid distribution curves for dibutyl phthalate circular stains on Whatman No. 1 filter paper.

drop diameter. The spreading factor, defined as the ratio of D/d, should be equal to

$$\left[\left(\frac{6\beta}{h^2}\right) t\right]^{1/6}$$

Figures 15 and 16 illustrate data obtained in this laboratory. They indicate that Eq. [26] is the correct stain size-drop size relation for liquids with low vapor pressure.

With such liquids there is no "final stain size," and erroneous results may be obtained if this is not taken into account. This means that it is essential to record both the time of sampling and the time of assessing the stains.

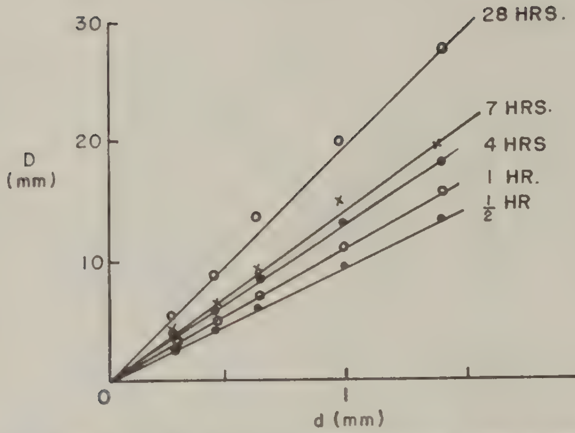

Fig. 15. Illustration of the proportionality between stain diameter (D) and drop diameter (d) for D.B.P. stains which have spread for more than ½ hour on Whatman No. 1 filter paper.

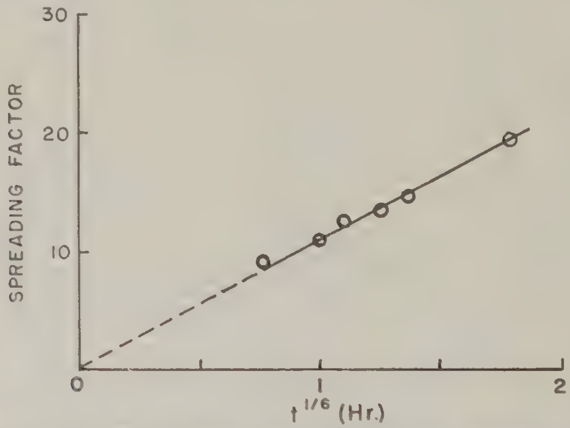

Fig. 16. Illustration of the proportionality between the spreading factor (D/d) and $t^{1/6}$ per D.B.P. drops which have spread for more than ½ hour on Whatman No. 1 filter paper.

Equation [25] is applicable to drops which are large enough to penetrate from one side of the paper to the other and to have the same diameter when viewed from either side at the moment when all the liquid has entered the paper. The size limit will of course depend upon the thickness and porosity of the paper.

In using the stain technique with liquids which evaporate readily, a dye is added either to the paper or to the drops so that it will be left behind after evaporation of the liquid. There is in this case a final stain size. For a liquid-paper combination such that the second stage of spreading does not proceed very far, Eq. [25] or Eq. [26] indicates that D should be proportional to $d^{3/2}$ instead of the linear relation found with low vapor pressure liquids. Many of the data obtained in routine calibrations are in agreement with this.

If the second stage in spreading is significant, then one would expect D to be proportional to d^q where $1 \leq q \leq 1.5$. Log D vs. log d plots would be linear with slopes ranging between 1 and 1.5. This is generally the case (3).

DISCUSSION

The constant descriptive of the rate of spreading, i.e., β, can be determined from the slopes of plots such as those in Fig. 12. If cos θ can be taken equal to unity, plots of β against γ/η should be straight lines going through the origin. As illustrated in Fig. 17 this seems to be the case, except perhaps for the data at 5°C.

This first treatment of spreading leaves much to be desired. For example, it has not been possible to derive quantitatively the relation between permeability and concentration. There will be little hope of doing this until the easier problem of the flow through a saturated plug is understood more completely.

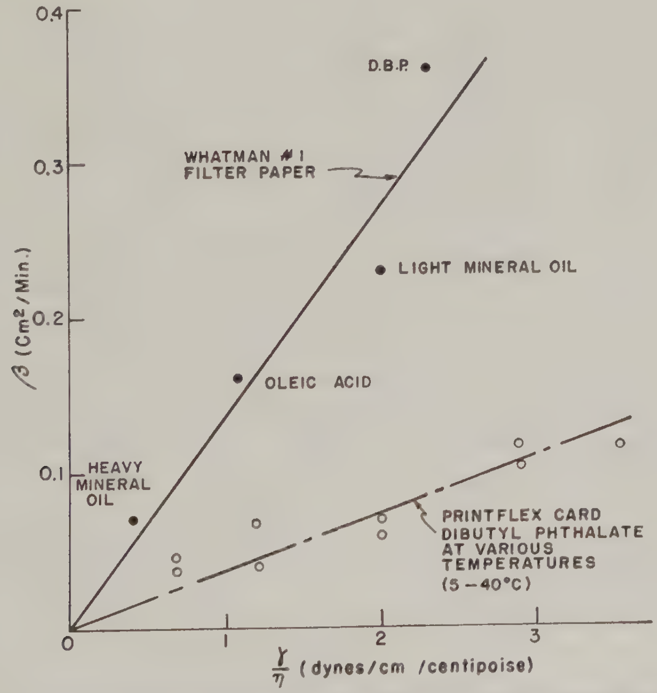

FIG. 17. Illustration of the proportionality between the constant descriptive of the rate of spreading and the ratio γ/η.

In this connection it would be interesting to know what part electric double layers play in determining the flow. Calculations based on Elton's theory of electroviscosity (11, 12) indicate that for a circular tube of diameter 2 μ the viscosity of water would be effectively doubled if the conductivity were 10^{-6} ohm^{-1} cm.$^{-1}$ and the zeta potential were 150 millivolts. For smaller tubes the increase in viscosity would be greater, so that in some cases electroviscosity might affect the concentration-permeability relation.

At a paper-water interface the zeta potential is believed to be of the order of 20 to 30 millivolts (8). Taking the conductivity equal to 10^{-6} ohm^{-1} cm.$^{-1}$ the increase in viscosity due to electric double layers would be negligible for circular tubes of 2 μ diameter, about 7% for 1 μ diameter, and 118% for 0.25 μ diameter. One would therefore suspect that electroviscous effects are small in a relatively loose structure such as filter paper.

Because of the difficulties encountered in measuring the permeability of paper (8) it is not possible to be completely sure of this. In a subsidiary set of experiments a piece of filter paper was placed in a permeability system. Water was drawn up and through the paper by suction. The permeability was not dependent upon time when the paper was filled in this way. Sodium chloride was gradually added to the water during a set of permeability measurements. There was no detectable change in permeability, indicating that electroviscosity effects were negligible.

Whether the present approach to capillary phenomena can be applied to other porous media is an important question. It depends upon whether the liquid adjusts itself so that the pressure is independent of time and $\nabla^2 p = 0$; see Eq. [15]. Spreading experiments using a variety of porous media would be worth while.

At first sight it might seem that Fujita's analysis of the distribution of liquid ascending in a vertical strip of filter paper (13) would be applicable to the horizontal spreading of liquids. Fujita's analysis, however, is based on an unrealistic mechanism and leads to the improbable conclusion that the rate of spreading is proportional to the atmospheric pressure and is independent of surface tension effects (see Eq. [9], reference 13).

The present approach has been applied to the ascent of liquid into a vertical strip of filter paper which is of importance in paper chromatography.

It has led to a satisfactory description of both the rate of ascent and the distribution of the liquid. The results should be in appropriate form for publication in the near future.

Appendix

Measurement of Suction Due to Unsaturated Paper

Figure 18 illustrates the apparatus used to measure the suction exerted by paper containing various amounts of liquid on a liquid column below it. It is essentially the same as used by Haines (6) to measure the suction due to granular materials.

Known amounts of liquid were drawn off into a beaker by turning the stopcock to the appropriate position. When the stopcock was put in its

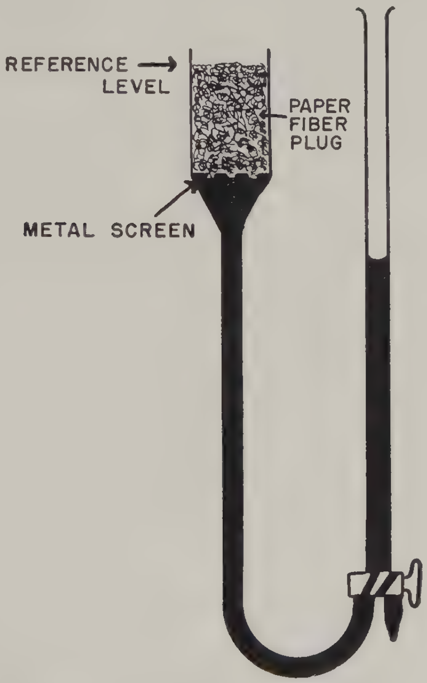

FIG. 18. Apparatus used to measure the suction due to an unsaturated paper plug.

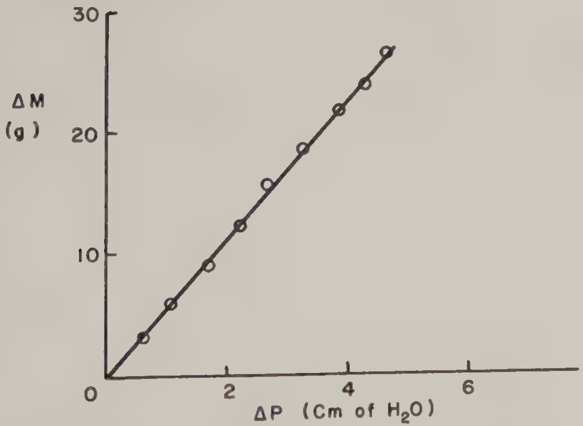

FIG. 19. Illustration of the proportionality between the suction and loss of water in a paper plug.

other position, liquid was drawn out of the paper until the pressure difference measured with the top of the paper as reference level was just equal to the suction of the paper. The relation between the amount of liquid drawn out of the paper ΔM and the change in the pressure ΔP is illustrated in Fig. 19.

As liquid is drawn out of the paper there will be a concentration gradient leading up to saturation concentration at some point below the top of the paper. This concentration gradient should be of the same form as given by Eq. [10]. The amount of liquid of density pulled out of the paper will be

$$M = wC_sh \int_0^L \left[1 - \left\{1 - \frac{x}{L}\right\}^{1/2}\right] dx = \frac{1}{3} wC_shL. \qquad [27]$$

Since ΔP was found to be proportional to ΔM, it will also be proportional to L.

The simplest pressure distribution which can lead to this result is that in which the pressure gradient is a constant. This was the pressure distribution assumed in the analysis of spreading.

REFERENCES

1. Richardson, E. G., "Flow Properties of Disperse Systems," Ch. 6. Interscience, New York, 1953.
2. Niederdorfer, E., *Met. Z.* **49,** 1, 278 (1932).
3. Armstrong, G. R., Unpublished Suffield Expt. Station Tech. Minute No. 34 (1943).
4. Muskat, M., "The Flow of Homogeneous Fluids Through Porous Media," McGraw-Hill, New York, 1938.
5. Muskat, M., and Meres, M. W., *J. Appl. Phys.* **7,** 346 (1936).
6. Haines, W. B., *J. Agr. Sci.* **20,** 97 (1930).
7. Childs, E. C., and Collis-George, N., *Proc. Roy. Soc.* (*London*) **A201,** 392 (1950).
8. Goring, D. A., and Mason, S. G., *Can. J. Research* **B28,** 307–323 (1950).
9. Wyckoff, R. D., and Botset, H. G., *J. Appl. Phys.* **7,** 325 (1936).
10. Fournier D'Albe, E. M., Lateef, A. M. A., Rasool, S. I., and Zaidi, I. H., *Quart. J. Roy. Meteorol. Soc.* **81,** 574 (1956).
11. Elton, G. A. H., *Proc. Roy. Soc.* (*London*) **A194,** 259 (1948).
12. Elton, G. A. H., and Hinschler, F. G., *Proc. Roy. Soc.* (*London*) **A198,** 581 (1949).
13. Fujita, H., *J. Phys. Chem.* **56,** 625 (1952).

JOURNAL OF COLLOID SCIENCE **13**, 51–60 (1958)

THE FLOCCULATION OF SODIUM MONTMORILLONITE BY ELECTROLYTES[1]

Allan Kahn

Shell Development Company, Emeryville, California

Received April 26, 1957; revised August 12, 1957

Abstract

The flocculation of sodium montmorillonite by four electrolytes, NaCl, $CaCl_2$, $AlCl_3$, and $La(NO_3)_3$, has been studied by means of viscometry and optical transmission. The clay concentrations used varied from 0.025% to 0.83%. The concentration of sodium chloride necessary for flocculation of the clay was found to be independent of the particle size and the concentration of the clay, in agreement with the predictions of the Verwey-Overbeek theory. For the other electrolytes, the concentration of electrolyte necessary for flocculation was found to be a function of the clay concentration. This latter phenomenon indicates that ion exchange occurs rapidly between the sodium montmorillonite and the added electrolyte.

Introduction

The flocculation of clay suspensions has been studied extensively from both a technical (1) and a scientific (2) standpoint. The research reported here was begun to determine the effect on the flocculation of montmorillonite of (*a*) the particle size and (*b*) the concentration of montmorillonite, about which no information was available. In addition it was desired to determine the role which ion exchange played in flocculation.

Preparation of Sodium Montmorillonite Samples

The sodium montmorillonite samples were prepared from a batch of Wyoming bentonite in the manner described in a previous paper (3). Five size fractions were obtained and were labeled in order of decreasing size, Cl-1, Cl-2, Cl-3, Cl-4, and Cl-5.

General Remarks on Flocculation

There is, to the knowledge of the author, no adequate general definition of the term "flocculation"; however, the operational concept of flocculation is well understood. In the flocculation of clay by electrolytes there are generally two factors of importance:

---

[1] Publication No. 73, Shell Development Company, Exploration and Production Research Division, Houston, Texas. Presented at the Symposium on Chemistry in the Exploration and Production of Petroleum, of the Division of Petroleum Chemistry, of the American Chemical Society, held in Dallas, Texas, April 8–13, 1956.

a). The concentration of electrolyte at which a given clay suspension just begins to flocculate. This will be known as the "flocculation value."

b). The change in physical properties of the clay suspension after flocculation.

We shall be concerned mostly with (*a*) but we shall make use of (*b*) to determine (*a*).

The primary criterion for the determination of flocculation depends on visual observation. However, a number of other criteria are used which depend on the rapid change in physical properties of the clay suspension near the flocculation value (4). The viscosity of the suspension has been used in our flocculation value studies. The general behavior of the viscosity of the suspensions that we have observed is as follows:

On the addition of small amounts of electrolyte, there is a slight decrease in the viscosity of the suspension. This decreased viscosity remains fairly constant on addition of more electrolyte until there is a sudden very large increase in the viscosity of the suspension, a phenomenon noted by other workers also (5). The electrolyte concentration at which this increase occurs is taken to be the flocculation value.

EXPERIMENTAL

Viscosity Determinations

The method of preparing the samples for viscosity determinations was very simple. To prepare a sample containing a final concentration of x% clay and y equivalents/l. of electrolyte, 10 ml. of $2x$% clay was pipetted into a bottle and 10 ml. of $2y$ equivalents/l. electrolyte was then added slowly with constant stirring. By this means, high local concentrations of electrolyte were avoided during preparation of the samples.

The viscosity was generally determined in A.S.T.M. size 50 modified Ostwald viscometers. In early experiments, the viscosity was determined as a function of the time after preparation of the sample. It was measured as soon as possible after the sample was prepared and at various intervals thereafter up to a maximum time of 24 hours. No change of viscosity with time was found in the unflocculated samples. With the flocculated samples, although the viscosity obtained changed slightly with time (generally decreased), the basic characteristics of the flocculation curve did not change with time. Eventually, the viscosities were determined directly after preparation of the sample, and these initial viscosities are the only ones presented in this report.

Optical Density Determinations

Optical densities were determined with the Beckman DU spectrophotometer using 1 ml. path length calibrated quartz cells. The optical density was determined relative to water in all cases.

RESULTS

Flocculation Value as a Function of Clay Concentration and Particle Size

The effect of sodium chloride on the reduced viscosity, $(\eta_r - 1)/\text{concn.}$ where

$$\eta_r = \frac{\text{viscosity of suspension}}{\text{viscosity of solvent}}$$

is shown in Fig. 1. The two extreme size fractions Cl-1 and Cl-5 were used each at final concentrations of 0.025% and 0.125%. It may be seen that the flocculation behavior is the same in all cases. With small amounts of added electrolyte, there is a decrease in reduced viscosity probably due to the electroviscous effect. There is a sharp increase in reduced viscosity at about 3 meq/l. NaCl, which indicates the onset of flocculation in all four systems.

In Fig. 2, the effect of sodium chloride on sample Cl-4 is presented for the three concentrations (of Cl-4), 0.025%, 0.125%, and 0.83%. For Cl-4, the sharp increase in reduced viscosity occurs at about 2.5 meq./l. NaCl, in close agreement with the values for Cl-1 and Cl-5. The dotted line between the two points at 3 meq./l. NaCl for the 0.83% suspension indicates that the reduced viscosity of the suspension varied in this range during the course of the measurements. At 3.5 meq./l. NaCl the 0.83% suspension would not flow through the viscometer.

The results of Figs. 1 and 2, which encompassed both the largest and smallest size fractions of the montmorillonite, indicated that the flocculation characteristics of sodium montmorillonite-sodium chloride systems did

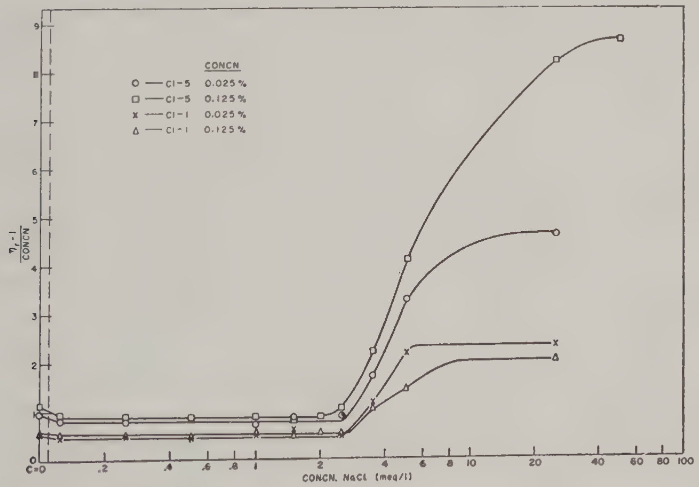

FIG. 1. Variation of reduced viscosity with sodium chloride concentration for two concentrations of Fractions Cl-1 and Cl-5.

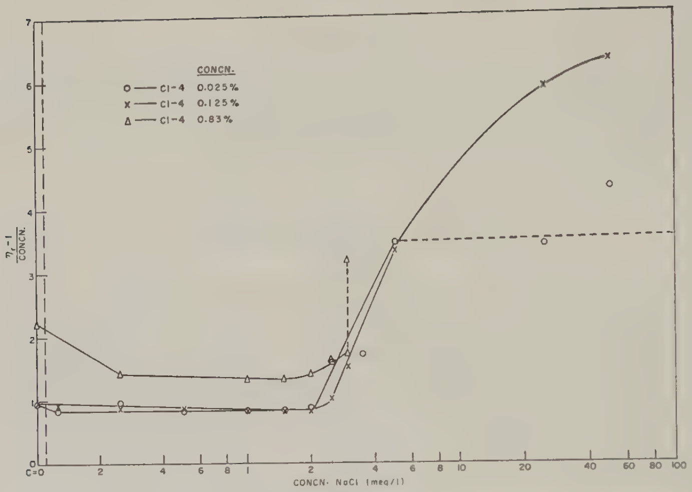

FIG. 2. Variation of reduced viscosity with sodium chloride concentration for two concentrations of Fraction Cl-4.

not depend greatly on the particle size of the montmorillonite or on the clay concentration up to a concentration of 0.83%.

Optical Density Data for Sodium Montmorillonite-Sodium Chloride Systems

The optical density data for samples Cl-1 and Cl-5 containing no NaCl, 2.5 meq./l. NaCl (below flocculation value), and 25 meq./l. NaCl (above flocculation value) are presented in Fig. 3. It can be seen that there is no marked change in the optical density for the flocculated suspension. The difference in optical density between Cl-1 and Cl-5, without added salt, is greater than the difference between the flocculated and unflocculated states of either sample. This behavior contrasts markedly with the viscosity behavior, which is extremely sensitive to flocculation.

Comparison of Flocculation Behavior Produced by Various Electrolytes

In Fig. 4, data are presented on the flocculation of sample Cl-3 at 0.025% concentration by NaCl, $CaCl_2$, $AlCl_3$, and $La(NO_3)_3$. As might ordinarily be expected for a colloidal material, the multivalent ions were much more effective than the monovalent in producing flocculation. There was, however, little difference between the di- and trivalent ions.

At a clay concentration of 0.50%, the data presented in Fig. 5 were obtained. In this case, there is only a small difference between the concentrations of the mono- and multivalent electrolytes necessary for flocculation. This seemed at first a rather surprising result, but it led to the idea that in the flocculation of sodium montmorillonite by a multivalent

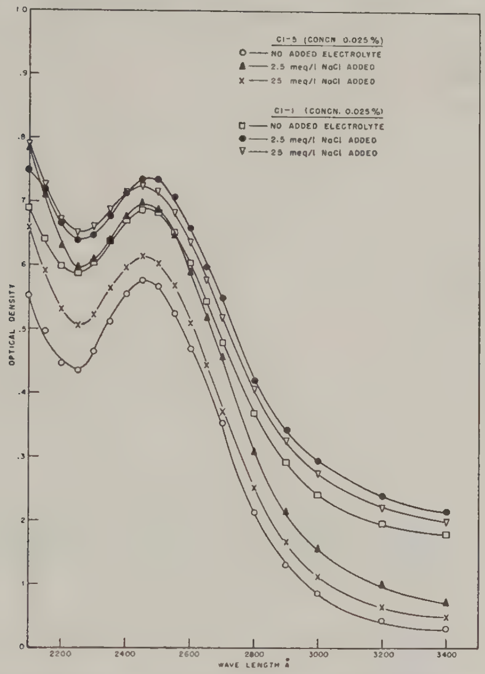

FIG. 3. Variation of optical density with wavelength for Fractions Cl-1 and Cl-5 with various concentrations of electrolytes.

electrolyte the primary process before flocculation occurs is the replacement of the sodium by the multivalent ion. Thus, for example, when $AlCl_3$ is added to sodium montmorillonite, one forms aluminum montmorillonite and NaCl. There is most likely an equilibrium of the form

$$AlCl_3 + 3\text{ Na Mont.} \leftrightarrows \text{Al Mont.} + 3\text{ NaCl}$$

with the montmorillonite tending to be predominantly in the aluminum form. This equilibrium is attained very rapidly (6). Therefore, one might expect that as $AlCl_3$ is added the Al^{3+} exchanges with the Na^+ of the clay, until an amount of Al^{3+} in excess of the base-exchange capacity is added. The excess aluminum ions act, together with the liberated sodium ions, to flocculate the clay.

For the clay that we have used, a base-exchange capacity of 80 meq./100 g. has been obtained. Therefore in 20 ml. of a 0.025% clay suspension there would be 0.0040 meq. of Na^+. The number of milliequivalents of Al^{3+} in the solution required to flocculate this (20 ml. of 0.2 meq./l. $AlCl_3$ from Fig. 4) is 0.0040 meq. This quantitative agreement is of no significance except to show that at low concentrations of clay the amount of Al^{3+} necessary for flocculation is numerically very close to the amount of exchangeable Na^+.

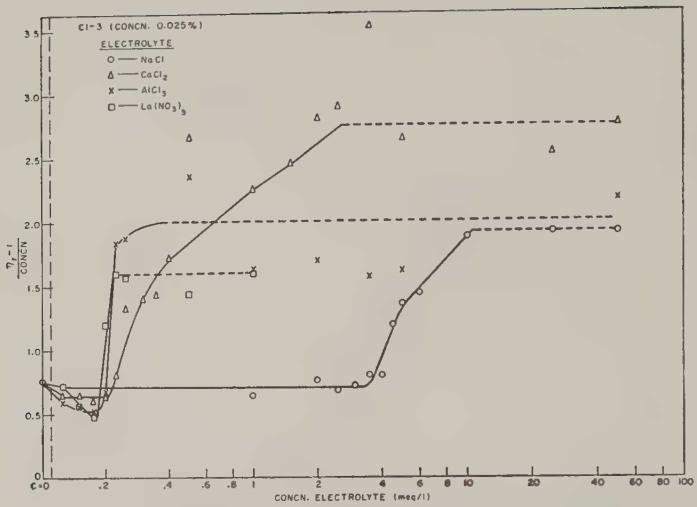

FIG. 4. Variation of reduced viscosity with electrolyte concentration for Fraction Cl-3 (0.025%) with various added electrolytes.

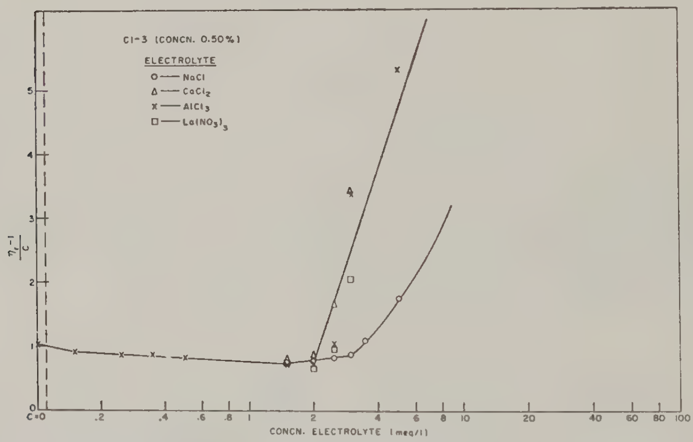

FIG. 5. Variation of reduced viscosity with electrolyte concentration for Fraction Cl-3 (0.50%) with various added electrolytes.

The concentration of $AlCl_3$ required for flocculation was also determined at two other concentrations, 0.0625% and 0.125%. The total results are presented in Figs. 6 and 7. In Fig. 7, there is for the first three points a linear relationship between the amount of $AlCl_3$ required for flocculation and the concentration of the clay. This linear relationship indicates that the Al^{3+} must be almost completely exchanged for the Na^+ before any is available to act as a flocculating agent. At the higher concentrations, the sodium which is released on base exchange becomes effective as a flocculating agent, so that the linear relationship breaks down.

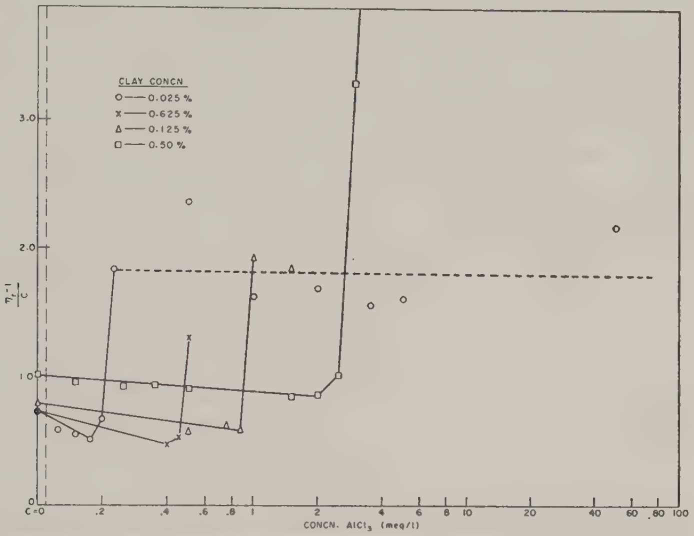

FIG. 6. Variation of reduced viscosity with aluminum chloride concentration for various clay concentrations.

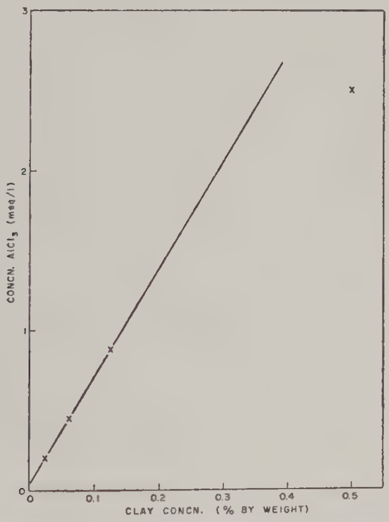

FIG. 7. Variation of aluminum chloride *flocculation value* with clay concentration.

Optical Density Data for Sodium Montmorillonite with Various Added Electrolytes

The variation of optical density at one wavelength with electrolyte concentration for NaCl, $CaCl_2$, $AlCl_3$, and $La(NO_3)_3$ is presented in Figs. 8 and 9 for the two clay concentrations, 0.025 % and 0.50 %. The optical density of the sodium montmorillonite-sodium chloride system changes very little

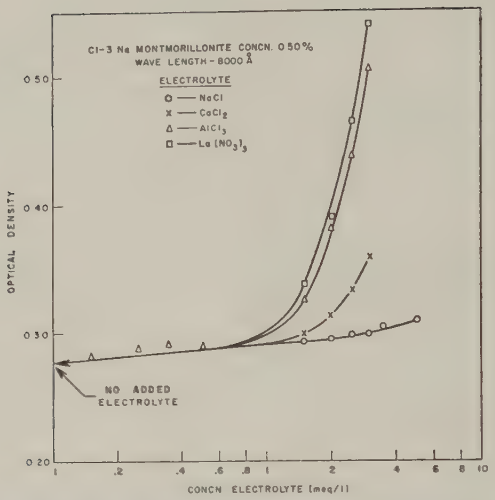

FIG. 8. Variation of optical density with electrolyte concentration for Fraction Cl-3 (0.50%) with various added electrolytes.

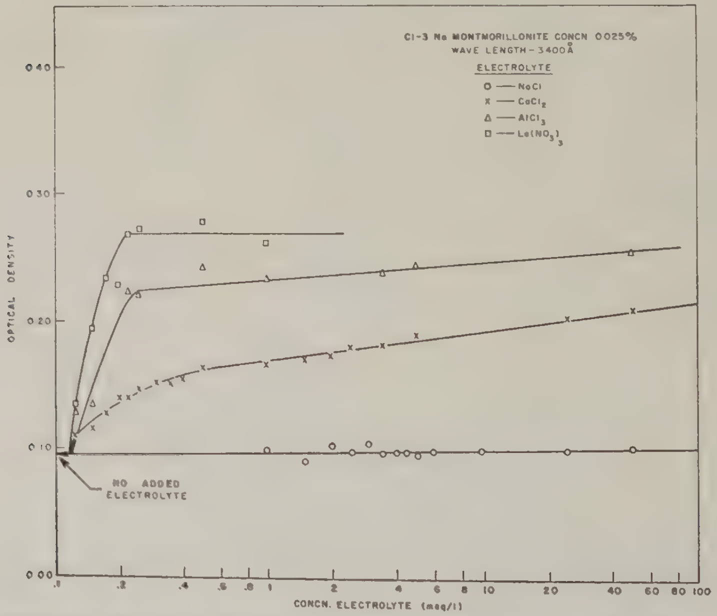

FIG. 9. Variation of optical density with electrolyte concentration for Fraction Cl-3 (0.025%) with various added electrolytes.

with sodium chloride concentration (even well past the flocculation value). However, for the other systems, there is a marked change in optical properties as the flocculation value is approached. The observations may be explained by the assumption that on addition of multivalent cations the number of structural unit layers per clay particle is increased and so the light-scattering properties are enhanced.

Discussion and Conclusions

Two major conclusions arise from this work:

a). The flocculation value of sodium chloride for sodium montmorillonite is relatively independent of the particle size and concentration of the sodium montmorillonite.

b). In the flocculation of sodium montmorillonite by polyvalent cations, ion exchange plays a dominant role.

The first conclusion would be expected from a colloidal material which may be described in terms of the Verwey-Overbeek theory (7). If particles of different size maintain the same surface potential, then the concentration of electrolyte necessary for flocculation does not depend on the particle size. In the Verwey-Overbeek theory, concentration of the sol does not enter, for the theory is developed on the basis of the interaction of two particles at any given time without considering the presence of other particles. In terms of our results, this seems feasible up to a concentration of close to 1%, although from other considerations considerable particle interaction is known to exist at such a concentration.

The results of the flocculation of sodium montmorillonite by polyvalent cations do not at first glance fit into the Verwey-Overbeek theory, which predicts flocculation values in the ratio of $1 : (1/2)^6 : (1/3)^6$ for mono-, di-, and trivalent cations. However, the theory does not take into account the complicating effects of ion exchange.

It seems possible to eliminate the effect of ion exchange in the following manner:

In the flocculation of sodium montmorillonite the flocculation value of sodium chloride is independent of the clay concentration. However, the flocculation value of aluminum chloride is a function of the clay concentration. If the aluminum chloride flocculation value is extrapolated to zero clay concentration, the flocculation value when no ion exchange occurs is obtained. This may then be compared with the sodium chloride flocculation value.

There is one complicating factor in this procedure. When aluminum chloride is added to sodium montmorillonite the final material which is flocculated is predominantly aluminum montmorillonite, and it is not to be expected that the electrolyte concentrations necessary for the flocculation of aluminum and sodium montmorillonite, even when ion exchange considerations are eliminated, should be equal.

However, from the data in Fig. 5, which show that at a clay concentration of 0.50% the concentration of $AlCl_3$ required for flocculation is 2.5 meq./l. as compared to 3.5 meq./l. for NaCl, it seems reasonable to assume that the concentrations of a given electrolyte necessary for the flocculation of sodium and aluminum montmorillonite are not substantially different, when ion exchange considerations are eliminated.

On this assumption, and using the flocculation value of 3.5 meq./l. for sodium chloride, the ratio of the flocculation values of sodium chloride and aluminum chloride is 175: 1,[2] the order of magnitude that would be expected from the Verwey-Overbeek theory (and the Schulze-Hardy rule).

Thus it seems that the flocculation of sodium montmorillonite by electrolytes may be considered to a first approximation in terms of the Verwey-Overbeek theory if allowance is made for ion exchange between the clay and the flocculating electrolyte.

References

1. Rogers, Walter F., "Composition and Properties of Oil Well Drilling Fluids." Gulf Publishing Company, Houston, Texas, 1953.
2. Marshall, C. E., "The Colloid Chemistry of the Silicate Minerals." Academic Press, New York, 1949.
3. Kahn, A., and Lewis, D. R., "The size of sodium montmorillonite particles in suspension from electro-optical birefringence studies." *J. Phys. Chem.* **58**, 801 (1954)
4. Kruyt, H. R., "Colloid Science," pp. 292–301. Elsevier, Amsterdam, 1952.
5. Slabaugh, W. H., and Culbertson, J. L., "The effect of certain reagents upon the properties of bentonite colloids. I." *J. Phys. Chem.* **55**, 744 (1951)
6. Kelley, W. P., "Cation Exchange in Soils," p. 51. Reinhold, New York, 1948.
7. Verwey, E. J. W., and Overbeek, J. Th. G., "Theory of the Stability of Lyophobic Colloids." Elsevier, Amsterdam, 1948.

[2] The extrapolated value of the aluminum chloride flocculation value at zero concentration of clay cannot be obtained very accurately, but a variation in this value even within a factor of two would not alter the conclusions.

JOURNAL OF COLLOID SCIENCE **13**, 61-66 (1958)

ON THE STRUCTURE OF TUNGSTIC OXIDE IN THE COLLOIDAL STATE

S. N. Chatterjee

Institute of Nuclear Physics, Calcutta 9, India

Received August 30, 1957

Abstract

Tungstic oxide crystals in the colloidal state were seen under the electron microscope. Three different types of particles were found: (1) Very small particles the shapes of which were not resolved, (2) rectangular plates, (3) large hexagonal plates. Electron diffraction from the fine particles gave rings consistent with a cubic structure. The other two types gave diffraction patterns consistent with the orthorhombic structure of tungstic oxide obtained by X-ray analysis. It was interpreted that in the process of growth in the colloidal state, the tungstic oxide crystals occur in a metastable cubic structure which ultimately changes into the stable orthorhombic form.

I. Introduction

It is known that the colloidal solutions are metastable systems that are prone to undergo various changes after no or apparently little change in conditions. The principal change in aggregation occurring within colloid particles is the crystallization of amorphous particles or the transformation from a metastable to a stable crystalline form. The electron microscope has been applied to the study of the aging of such colloidal solutions as vanadium pentoxide, ferric oxide (8), tungstic oxide (1, 7, 10).

The electron microscope, however, does not reveal the nature of very small crystals, and often it is difficult to identify the structure of a gross crystal from its electron micrograph. Hence from the electron microscopic studies alone it is difficult to follow the changes in structure, if any, that take place in a colloidal state. In the present work, electron microscopy and electron diffraction techniques have been combined in the study of the structure of tungstic oxide in the colloidal state.

II. Experimental Methods

The specimen was prepared by adding hydrochloric acid to an alkaline sodium tungstate solution. The sodium chloride was removed by dialysis and the tungstic acid left in the aqueous medium in a state of colloidal suspension. The particles were studied by three different methods, electron microscopy, normal electron diffraction, and fine spot diffraction.

a). Direct Electron Microscopy: For this purpose, a small drop of this solution was deposited on the collodion film spread over the steel wire mesh and dried in a desiccator. This was then inserted in the electron microscope and micrographed in the usual way by a Siemens Elmiscope I.

b). Normal Diffraction Studies: In this case the aqueous suspension of the specimen was kept undisturbed for a few weeks when the bigger particles settled down. A drop from the supernatant was deposited on the collodion-covered mesh and the diffraction picture taken. Under this condition the diffraction was due to particles present in an area approximately 40μ in diameter and the diffraction length was 587 mm.

c). Fine-Spot Diffraction: As the electron micrograph revealed the presence of well-formed crystals together with fine particles, diffraction patterns due to individual big crystals were also obtained by the method of fine-spot diffraction. In this case, the specimen area giving rise to the diffraction was limited approximately to $2\mu \times 2\mu$ and the diffraction length was 545 mm.

III. RESULTS

Figure 1 shows the electron micrograph (15,000 ×) of the specimen. This picture reveals the presence of three different types of particles. (*1*) Rect-

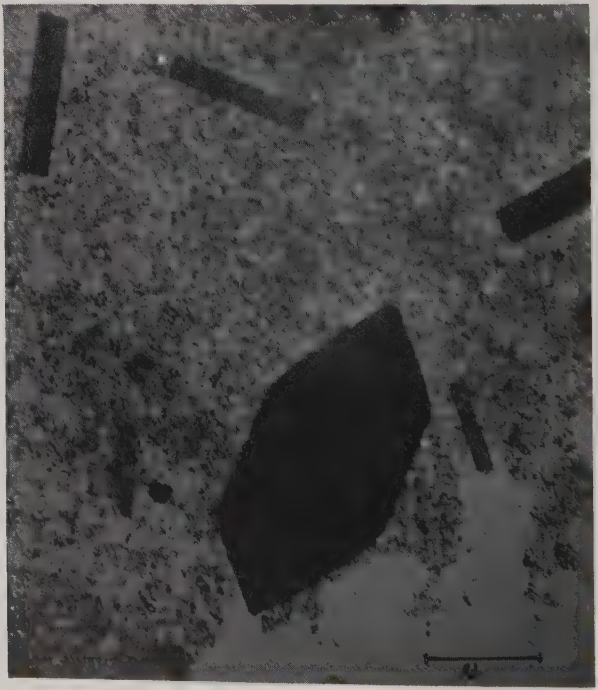

FIG. 1. Electron micrograph of tungstic oxide sol. (15,000 ×).

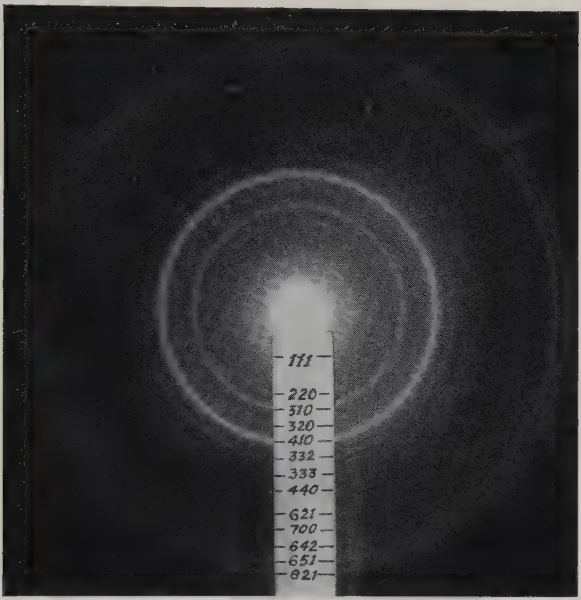

FIG. 2. Normal diffraction from the fine particles present in a drop of the sol.

angular platelike particles of size $1.4\mu \times 0.26\mu$ approximately. (*2*) Big hexagonal particles the tip to tip distance of which is 3μ and the width of which at the central region is 1.4μ. A number of such particles were present in the whole field of view. Some of them, as observed by Watson (11), had toothed edges. (*3*) Scattered fine particles of approximate size 0.04μ.

Figure 2, the normal diffraction pattern due to fine colloidal particles, shows the presence of rings only. Measurements on these rings indicate that these fine particles are simple cubes with unit cell dimension (a) 14.2 A. The indexing of the rings has been indicated on the figure.

Figure 3 is the fine-spot diffraction from a specimen region (not shown) comprising a number of the platelike particles. This figure is interesting in that it reveals not only the type of the crystals but also their peculiar disposition. The spots were indexed. It was found that only hko spots (for $h = 2n$ and $k = 2n$) appeared. Thus all such crystals were formed with one particular plane (001) parallel to the substrate. The indexing also revealed that the basal plane of such a crystal has the periods 7.26 A. and 7.50 A., respectively. These correspond well with the X-ray data (6) of pseudo-orthorhombic structure of WO_3 having the space group $P2_1/_a$.

Figure 4 is the fine-spot diffraction pattern from the big apparently hexagonal crystal shown in the micrograph (Fig. 1). The pattern was found to be precisely the same as that from a single rectangular platelike crystal. These apparently hexagonal particles are the result of incomplete development of rectangular platelike crystals.

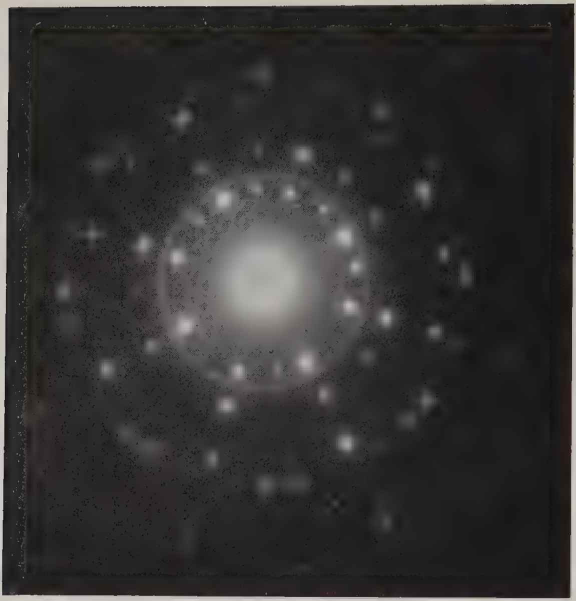

Fig. 3. Fine spot diffraction from a group of the plate-like crystals.

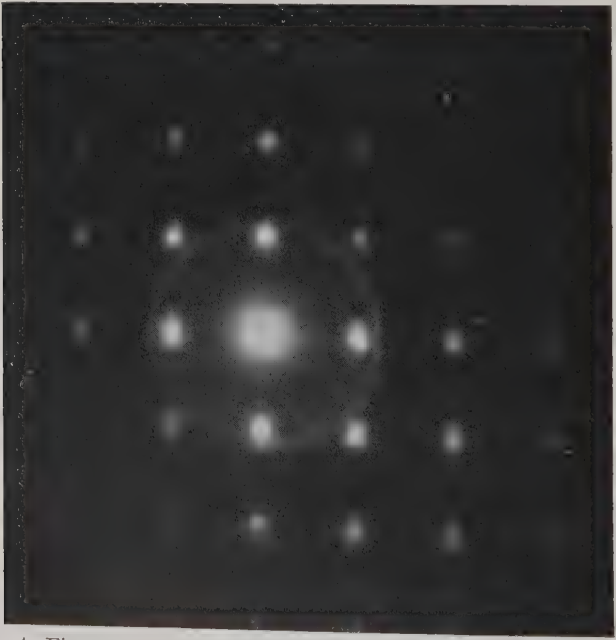

Fig. 4. Fine spot diffraction from the big crystal seen in Fig. 1.

IV. DISCUSSION

Attempts were first made to fit the ring pattern (Fig. 2) with the orthorhombic tungstic oxide polycrystals. The pattern did not correspond to such a structure. In order to identify the structure (4) of the crystals contributing to this pattern, Hesse's method of analysis (2) was followed. It was shown there that for the cubic system, the $\sin^2 \theta$ values could be expressed as the product of a factor which is common for all the rings and an integer which is different for different rings. Table I shows the details of the analysis. It was found that the pattern corresponded to the simple cubic crystals. The unit cell dimension, a, calculated from the formula, $a = \lambda/2\sqrt{K}$, where K is the common factor of the $\sin^2 \theta$ values, is 14.2 A.

Some very big apparently hexagonal crystals were seen in the whole field of view. Electron diffraction evidence (Fig. 4) does not show any hexagonal symmetry. It rather identifies them with the rectangular plates. Further, various crystals of this apparently hexagonal type were found attaining various degrees of closeness to the rectangular forms. This shows that the rectangular plate crystals grow in size while retaining their internal symmetry. On the other hand, not a single big cubic crystal was found, which proved that the cubic structure was unstable and that this state possibly represented a metastable phase. In the process of growth internal rearrangement within the very small cubic crystals takes place with the final attainment of the stable orthorhombic symmetry. The results obtained by Kehl, Hay, and Wahl (3), Sawada (5) and Ueda and Ichinokawa (9, 10) are relevant in this connection. These authors found that when tungstic oxide in the solid state was heated to very high temperature, a transition took place from the orthorhombic form at room temperature to the tetragonal form at a temperature between 700° and 750°C. The

TABLE I

Analysis of the Ring Pattern

Diameter of rings (*mm.*)	$10^5 \sin^2 \theta$	Factors of $10^5 \sin^2 \theta$	*hkl*
7.00	0.897	0.3007 × 2.99	111
11.40	2.382	0.3007 × 7.94	220
12.50	3.026	0.3007 × 10.08	310
14.70	3.917	0.3007 × 13.03	320
16.75	5.089	0.3007 × 16.92	410
19.30	6.637	0.3007 × 22.10	332
21.20	8.147	0.3007 × 27.10	333
23.00	9.596	0.3007 × 31.91	440
26.10	12.359	0.3007 × 41.10	621
28.50	14.723	0.3007 × 48.99	700
30.50	16.866	0.3007 × 56.10	642
32.10	18.664	0.3007 × 62.08	651
33.80	20.701	0.3007 × 68.93	821

present study therefore indicates that transitions between different states of symmetry in colloidal WO_3 sol may take place at room temperature.

Acknowledgments

The author wishes to express his indebtedness to Professor N. N. Das Gupta and Mr. M. L. De for helpful criticisms. He is also indebted to Prof. B. N. Ghosh for the supply of colloidal sols from his laboratory. Thanks are also due to Mr. A. K. Ghosh and to Mr. N. N. Gupta for valuable discussions.

References

1. Heller, W., Wojlowicz, W., and Watson, J. H. L., *J. Chem. Phys.* **16**, 10, 998 (1948).
2. Henry, N. F. M., Lipson, H., and Wooster, W. A., "The Interpretation of X-ray Diffraction Photographs," p. 178. Macmillan & Co., London, 1953.
3. Kehl, W. L., Hay, R. G., and Wahl, D., *J. Appl. Phys*, **23**, 212 (1951).
4. Pinsker, Z. G., "Electron Diffraction." Butterworth, London, 1953.
5. Sawada, S., *Phys. Rev.* **91**, 1010 (1953).
6. *Structurbericht II*, *Leipzig* **32**, 298 (1931–1943).
7. Studer, H., *Int. Cong. Elect. Micro.*, Paris, 1950, 545.
8. Tamamushi Bun-ichi and Todano Bunya, *Int. Cong. Elect. Micro.* Paris, 1950, 537.
9. Ueda, R., and Ichinokawa, T., *Phys. Rev.* **82**, 563 (1951).
10. Ueda, R., and Kobayashi, T., *Phys. Rev.* **91**, 1565 (1953).
11. Watson, J. H. L., *J. Chem. Phys.* **16**, 10, 997 (1948).

JOURNAL OF COLLOID SCIENCE **13**, 67–85 (1958)

INTERACTION OF WATER VAPOR WITH SILICA SURFACES

G. J. Young[1]

Contribution from the Multiple Fellowship Maintained at Mellon Institute by the Corning Glass Works and Dow Corning Corporation

Received August 20, 1957; revised October 17, 1957

Abstract

The interaction of water vapor and other surface properties were studied for silicas prepared by the flame hydrolysis of silicon tetrachloride. Surface areas, heats of adsorption, water vapor adsorption, surface structure, and infrared spectra were measured as a function of temperature up to 1200°C. Sintering, which occurred sharply at the quartz-tridymite transformation temperature, appeared to proceed by viscous flow. By correlation of water vapor adsorption and infrared data it is shown that water vapor physically adsorbs only on the silanol sites of the silica surface and not on the remainder of the surface. These results suggest that the surface silicon-oxygen bonds are nearly homopolar in character. The dehydration of silanol sites and subsequent rehydration by chemisorption of water vapor was quantitatively evaluated as a function of heat treatment temperature. Rehydration from the vapor phase was completely reversible up to 400°C. Above 400°C. the rehydration of silanol sites by water vapor was not reversible. This observation suggests that a change in the nature of the dehydrated silica surface occurs above 400°C.

Introduction

Literature pertaining to the surface chemistry of silica is extensive, as illustrated, for example, by the numerous references dealing with this subject in the recent books of Iler (1), Marshall (2), Hauser (3), and Eitel (4). This large amount of research reflects the interest silica has attracted, ranging from early studies of silica gel as a colloid system to present-day applications as a drying agent, catalyst component and support, refractory, finely divided filler and reinforcing agent, etc. Despite the considerable work on silica surface chemistry, our knowledge of the silica surface is still limited. For example, little quantitative information is available on the nature of the silanol (hydroxyl) groups that are present on most silica surfaces, and the role of the surface in chemical and physical adsorption of water vapor has yet to be clearly defined.

The present investigation had two primary objectives: (*1*) to study the general nature of the interaction of silica surfaces with water vapor and

---

[1] Present address: College of Mineral Industries, Pennsylvania State University.

(*2*) to characterize silicas produced by the flame hydrolysis of silicon tetrachloride. The flame hydrolysis silicas are unique in possessing a high surface area with little internal porosity. They are currently becoming of considerable industrial importance, but their surface properties have not been previously studied.

Experimental

Nitrogen adsorption determinations were made with a conventional volumetric adsorption apparatus. The same apparatus was used for argon adsorption except that equilibrium pressures were read from a wide-bore manometer with a traveling microscope (sensitivity ca. ±0.001 cm.). The nitrogen, argon, and helium (for dead space determinations) were obtained from the Matheson Company and were of 99.9% purity. Nitrogen and argon were dried over activated silica gel, condensed, and fractionated into storage bulbs. Helium was passed over activated silica gel at −195°C. before storage.

Water vapor adsorption determinations were made with a gravimetric apparatus employing a quartz spring to index the weight adsorbed. Extensions of the quartz spring were read to ±0.0005 cm. with a Gaertner precision traveling microscope. The springs could support 1-g. loads and had constants of 0.18 and 0.21 mm. per milligram. An Apiezon B oil manometer, which could be read to 0.02 cm., was used to measure equilibrium pressures. Sample buckets were blown from very thin-walled tubing and weighed about 0.1 g. Several much lighter sample buckets were also made by winding strands of Pyrex wool on a suitable form and brushing them carefully with a flame until the Pyrex wool started to sinter.[2] This was continued until sufficient Pyrex wool was built up to form a rigid shape that would hold the sample. Sample buckets prepared in this manner were very light and porous to the adsorbate. However, they were also very fragile and, of course, could not be activated at high temperatures.

Three samples of silica were investigated that varied in particle size and surface characteristics. These samples were prepared by the Dow Corning Corp. by burning silicon tetrachloride in a stream of hydrogen and air; the particle size and surface characteristics being controlled by the ratios of the three components in the flame. Concentrated aqueous slurries of these silicas gave no detectable evidence of chloride ion. Spectrographic analysis showed less than 1 p.p.m. of metallic impurities.

Results

The surface areas, helium densities, bulk densities, and particle sizes of the three silica samples are given in Table I. The surface areas were calculated from nitrogen adsorption data at −195°C. by use of the BET

[2] Suggested by F. M. Ernsberger, Mellon Institute.

TABLE I

Characteristics of Silica Samples

Sample	Surface area (*m.*^{2}/*g.*)	Particle diam. (*Angstroms*)	Helium density (*g./cm.*^{3})	Bulk density (*g./cm.*^{3})
Silica A	420	65	2.2	0.038
Silica B	220	124	2.2	0.032
Silica C	76	360	2.2	0.092

equation. Particle sizes, which were calculated from the surface area and density data, corresponded closely to those estimated from electron micrographs. The electron micrographs showed the particles as discrete irregular grains approximating spheroid shape. The bulk density represents the density of the silicas in the "as received" state and corresponds to a very open packing of the particles with each particle touching only three others on the average.

Complete nitrogen adsorption-desorption isotherms were determined for the three silica samples. The isotherms showed no evidence of hysteresis. This fact coupled with the observation that particle sizes calculated from surface areas and from electron micrographs were in reasonable agreement indicates that the silica particles are nonporous. Also, the lack of regular particle clusters in the electron photomicrographs, the absence of any interparticle porous structure, and the very low bulk densities suggest that the ultimate particles are not permanently agglomerated. Thus, the silica particles are to be pictured as discrete, nonporous grains roughly spherical in shape.

Water Vapor Adsorption

Water vapor adsorption isotherms at 25°C. were determined for each of the three silicas. The samples were evacuated for various times up to 72 hours at room temperature and 10^{-6} mm. Hg pressure. Isotherms determined after each evacuation time showed that, as far as water vapor adsorption was concerned, 8 hours evacuation was as effective as 72 hours. Data, presented later in the paper, suggest that essentially all the truly physically adsorbed water is removed by evacuation at room temperature.

The adsorption isotherms were unusual in that they were intermediate between Type II and Type III. Surface areas, given in Table II, were estimated from the water vapor isotherms by using the BET equation (using 10.6 A.^{2} per molecule) and by picking "B" points in the relative pressure range where Vm values for Type II water vapor isotherms generally occur. Both methods, although open to objections for isotherms of this nature, gave Vm values in reasonable agreement. These surface areas are only $\frac{1}{4}$ to $\frac{1}{8}$ of the area calculated from the nitrogen adsorption data, and a statistical monolayer of water, based on the nitrogen area, is not reached until 0.85 to 0.95 relative pressure. Since the water vapor adsorption isotherms

TABLE II

Water Vapor Adsorption Results

Sample	Surface area calculated from H_2O isotherm (*m.²/g.*)	Surface covered by H_2O vapor (%)
Silica A	104	25
Silica B	30	13
Silica C	12	16

are partially of Type III character and surface areas calculated from these isotherms are considerably less than the nitrogen surface areas, it can be concluded that a major portion of the silica surface is hydrophobic and does not adsorb water vapor.

The water vapor adsorption isotherms were completely reversible below relative pressures of 0.5. Equilibrium times in this region were of the order of 15 minutes, which can be accounted for by the time required for dissipation of the heat evolved on adsorption and for diffusion of the water vapor to all portions of the sample. Thus, the actual rate of adsorption is probably nearly instantaneous. The rapid attainment of equilibrium supports the contention that no fine-pore or capillary structure is present. Studies made over periods of several hours indicate that no further adsorption of water vapor occurs. Since the water vapor adsorption isotherms are completely reversible and reproducible, no chemisorption appears to occur.

At higher relative pressures the equilibrium times increased to 1 or 2 hours, and hysteresis was observed on desorption. Not only was hysteresis observed but, with subsequent adsorption-desorption cycles, the area of the hysteresis loop decreased with the adsorption isotherm approaching the desorption curve. Also, the volume of gas adsorbed at saturation increased. After five adsorption-desorption cycles a stable situation was achieved and the curves could be reproduced. This behavior is illustrated in Fig. 1 for data on Silica A. The effect on the other two samples was similar but not as pronounced.

The shifting of the adsorption-desorption isotherms in the higher relative pressure region and the increase in total volume adsorbed at saturation appear to be due to changes in the interstitial spacing between particles resulting from vapor tension effects on desorption. Carman (5, 6) has discussed such phenomena in detail. That these effects are due to particle packing is experimentally substantiated. The isotherm up to 0.4 relative pressure showed no change nor did the silica samples permanently gain weight; hence there was no increase in the number of adsorption sites or chemisorption of water after the adsorption-desorption cycles. Further, disturbing the packing of the sample, after the desorption experiments, returned it to its initial state.

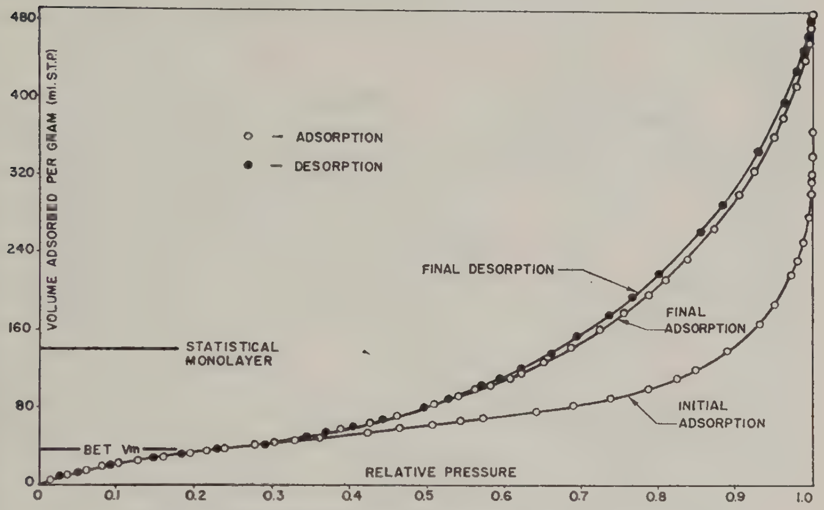

FIG. 1. Adsorption-desorption water vapor isotherms.

Effect of Heat Treatment

The water vapor adsorption results presented so far were obtained on silica samples evacuated at room temperature. It was now pertinent to examine adsorption on samples heated to various temperatures. Before proceeding to this, however, it was first necessary to study sintering and surface changes that occur on heating.

Nitrogen adsorption isotherms were determined for each of the silica samples after the following treatments: evacuation at 10^{-6} mm. Hg at room temperature for 8, 24, and 72 hours; evacuation at 10^{-6} mm. Hg for 4 hours at temperatures of 150, 250, 350, 450, 550, 650, 750, 850, 950, 1050, and 1150°C. As was the case for water vapor, the length of time of evacuation at room temperature over 8 hours had no effect on the nitrogen isotherms. The isotherms in the region of Vm and the surface areas for silica B are shown in Figs. 2 and 3 for the various heat treatment temperatures. The results for silica B are representative of those obtained for the other samples.

A slight decrease in surface area is shown by Figs. 2 and 3 in the range 550–650°C. and a general loss in surface area due to sintering above 850°C. The temperatures where these changes in the surface area occur are fixed more precisely by the differential thermal analysis curve shown in Fig. 4. Here the surface area changes show up as inflections in the differential thermal analysis curve due to changes in the thermal conductivty of the sample. The other two silicas gave inflections at the same temperatures. This suggests that the surface area changes may be related, in part, to volume changes of the silica.

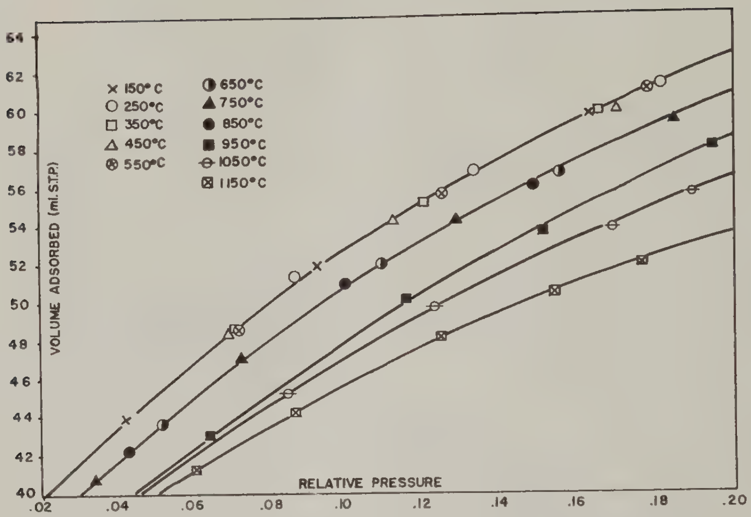

FIG. 2. Nitrogen isotherms as a function of sample heat treatment.

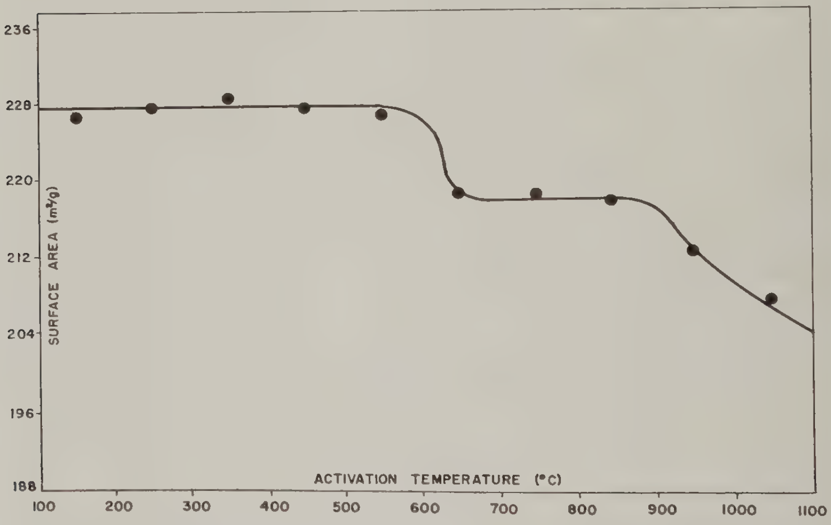

FIG. 3. Change in surface area with heat treatment of sample.

It seems more than fortuitous that both sintering and the area change at 575°C. occur exactly at points of transition in the quartz system for all three silicas. β-Quartz transforms into tridymite at 870°C. and α-quartz into the β modification at 575°C. It is suggested that the silica particles, though amorphous, have small quasi-crystallites tending toward a quartz-like structure. When taken through the α to β transition temperature and recooled, these quasi-crystallites are able to extend their orientation so that the silica particles in effect would assume a more compact structure.

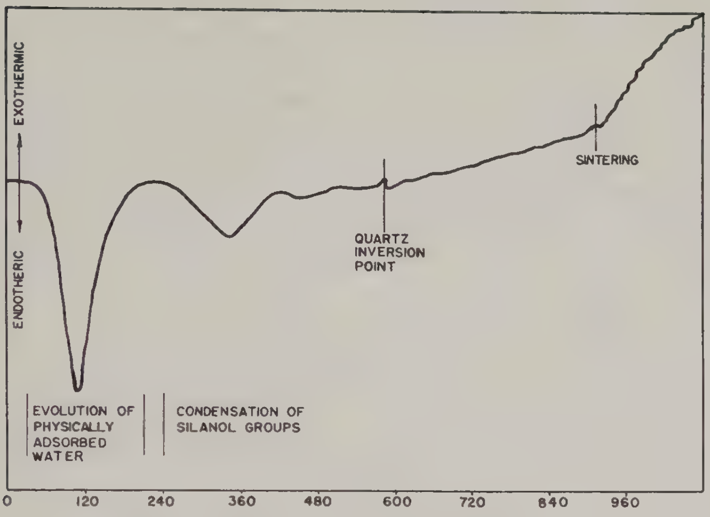

FIG. 4. Differential thermal analysis curve.

Thus, the particles would decrease in volume with a corresponding decrease in surface area. The surface area change at 575°C. was ca. 2.3% for the silica samples, which would correspond to a 4.5% decrease in volume. If it is assumed that this volume change results from a change in density from 2.2 g./cm.^{3} for amorphous silica to 2.6 g./cm.^{3} for α-quartz, then approximately 25% of the structure would be reoriented to the more dense modification. It is not inferred that the amorphous silica reorients to α-quartz but only that a change in density toward a more compact structure occurs.

The extent of the surface area change above 900°C. is quite dependent on the time of heating as would be expected for sintering. For example, at 950°C. the area decrease is nearly a linear function of the time of heating (up to 20 hours) and is of the order of 6.3 m.^{2}/g./hour. However, the temperature where sintering started to occur did not appear to vary with time (up to 4 hours). If a partially oriented structure does exist in the silica particles, the tendency for the lattice to open up at the tridymite transition temperature would provide greater mobility for the surface atoms. This would result in a fixed sintering temperature for all three silicas regardless of particle characteristics or heating times.

In addition to area changes, the evolution products on heating also were studied. A curve for the differential thermal evolution of gases from silica A is shown in Fig. 5. In these experiments the sample was evacuated at room temperature and the volume of gas evolved at a given heating rate was measured. Essentially the same curve was obtained for heating rates of 0.6 and 1.2°C. per minute; thus it was assumed that the curve given in

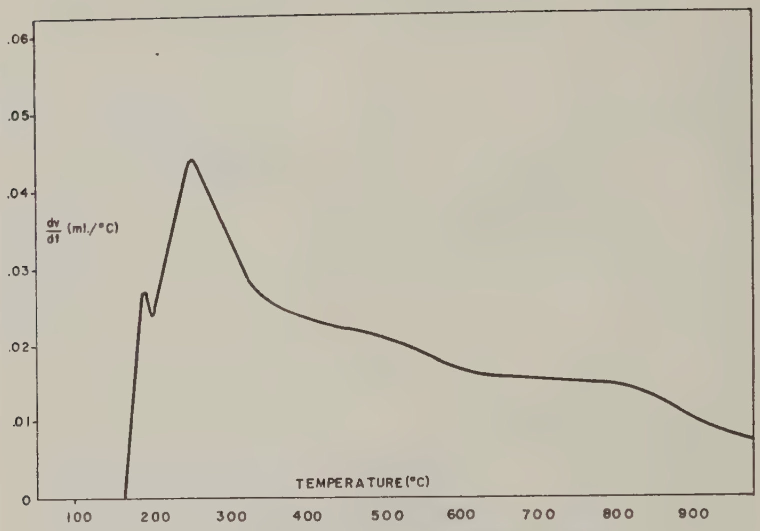

FIG. 5. Differential thermal evolution curve.

Fig. 5 represents approximately equilibrium data. The evolution of gas commenced rather sharply at ca. 180 C.° (*in vacuo*), passed through a maximum rate at about 260°C., and continued until 1100°C., although the rate decreased rapidly after 800°C. Experiments were also carried out where the evolution products were frozen out, weighed, and analyzed. These data were in general agreement at lower temperatures with values obtained by integrating the differential curve in Fig. 5. Water vapor was the only detectable product evolved up to 1200°C. This water results from the condensation of surface silanol (≡Si—OH) groups as shown later by infrared studies. Stober (7) has reported that small amounts of hydrogen were given off on heating quartz and Aerosil[3] at temperatures above ca. 600°C. No evidence of hydrogen evolution was found in the present work.

The differential thermal analysis curve (Fig. 4) shows the evolution of water from the condensation of silanol group as a broad endothermic band occurring after the removal of physically adsorbed water vapor from the surface. The differential thermal analysis determinations were conducted under atmospheric conditions; hence physically adsorbed water vapor was present at the start of the experiments.

In order to determine if changes in the physical heterogeneity of the silica surface occurred on activation, argon isosteric heat of adsorption curves were determined on samples of silica A evacuated at room temperature and heated to 850°C. (just below the sintering temperature) for 4 hours. These enthalpy curves, shown in Fig. 6, were calculated in the usual manner from a Clausius-Clapeyron equation at constant volume adsorbed. When the volume axis is normalized with respect to Vm the two curves are nearly identical. Both are indicative of a heterogeneous surface. The removal of silanol groups from the silica surface (which amounted to removing them from approximately 20% of the surface for silica A at 850°C.) seemed to have little effect on the interaction of argon with the surface. Further, surface defects and physical heterogeneities apparently are not removed below the sintering temperature.

---

[3] A silica produced by Degussa in the same manner as the silicas used in this investigation.

Water Vapor Adsorption on Heat-Treated Samples

It has been shown that water vapor adsorbs only on a portion of the silica surface. The sites of adsorption are generally thought to be surface silanol groups (1). During heating to high temperatures water is evolved from the silica owing to condensation of these silanol groups. Thus, if the silanol groups are not reversibly rehydrated on exposure to water vapor, a decrease in water vapor adsorption should be observed for activated silica samples.

Water vapor adsorption isotherms were determined on the silica samples heated for 4 hours at various temperatures up to 850°C. Since these measurements were made gravimetrically it was possible to determine not only physical adsorption but also the weight loss on activation and the amount of chemisorption. No weight loss or change in isotherm characteristics was observed on heating samples below 150°C. However, after heating at 250°C. the silicas lost weight and the water vapor adsorption isotherms showed a pronounced change. The isotherm behavior is illustrated in Fig. 7, which shows initial water vapor adsorption isotherms on a sample of silica B after room temperature evacuation and after heating for 4 hours at 250°C. and 450°C. The initial isotherms on the activated samples were more pronounced Type III than the isotherm for the original sample and showed less adsorption. On desorption after exposure to relative pressures below saturation, it was found that water vapor was chemisorbed by the heat-treated samples. For silica B the weight loss on activation to 250°C. was equivalent to 1.6 ml. of water vapor STP per gram. The chemisorption of water, which could be divided into a rapid and a slow process, was exactly equivalent to 1.6 ml. of water vapor STP per gram. Thus, those surface hydroxyl groups which had condensed during heating could be reversibly rehydrated by exposure to water vapor at 25°C. The adsorption isotherm on this rehydrated sample was identical to that for the original unheated sample.

Silica samples heated at higher temperatures gave initial water vapor isotherms that showed progressively more Type III character and less adsorption. Above 400°C. the rehydration of the surface was no longer completely reversible. This irreversibility is illustrated in Fig. 8 for silica

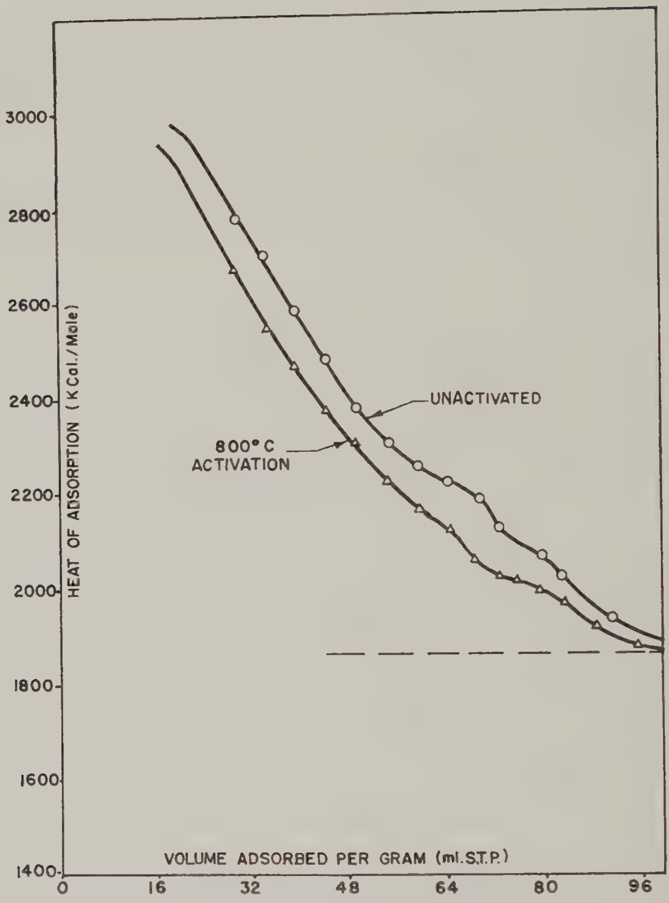

FIG. 6. Argon isosteric heat curves.

A. Here the number of surface silanol groups (or number of adsorption sites) is plotted against the activation temperature of the sample. The total number of hydroxyl sites originally present on the surface, as given by water vapor adsorption, is shown at the top of the graph. The curve showing the number of these silanol groups removed by activation at various temperatures was determined from weight loss data and also independently by measuring the amount of water vapor evolved. It was assumed that each molecule of water removed from the sample was equivalent to condensation of two silanol sites (i.e., $2{\equiv}Si{-}OH \rightarrow {\equiv}Si{-}O{-}Si{\equiv} + H_2O$). The curve giving the number of hydroxyl sites that could be rehydrated by water vapor after once being removed from the surface was determined from the amount of water vapor chemisorption and independently by measuring the number of adsorption sites by physical adsorption of water vapor after chemisorption. This graph shows that (*1*) condensation of the

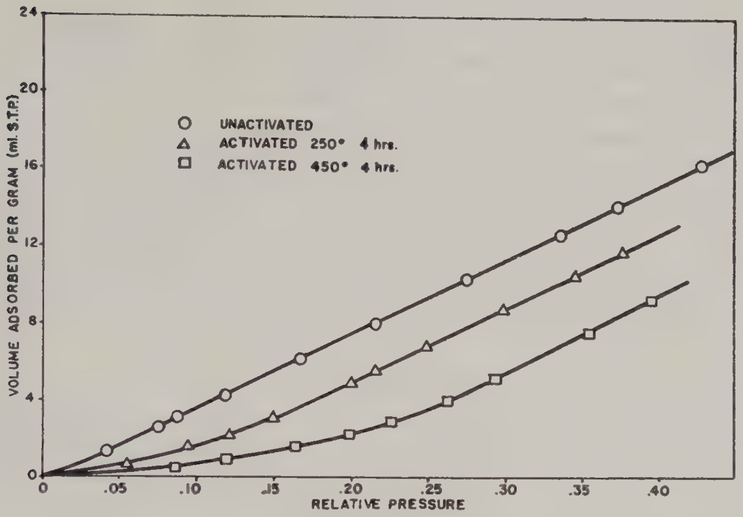

FIG. 7. Water vapor isotherms for different sample heat treatments.

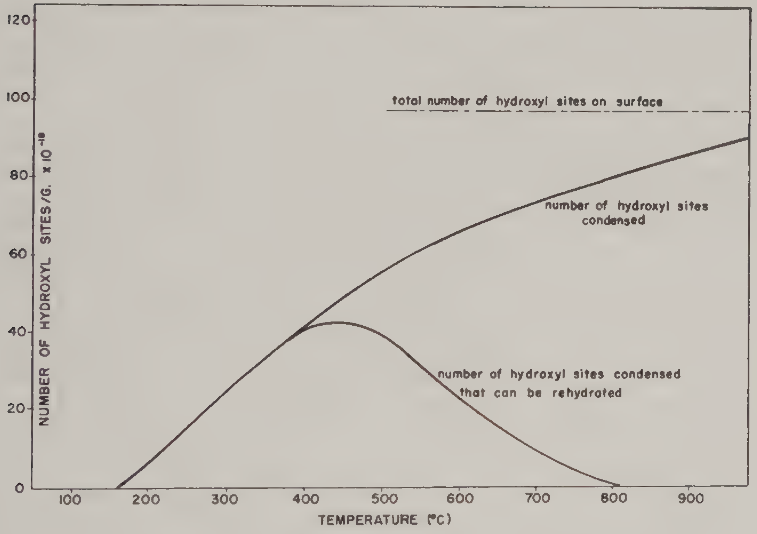

FIG. 8. Change in surface silanol sites with sample heat treatment.

surface silanol does not start to occur until ca. 170°C.; (*2*) the rehydration by water vapor of sites previously occupied by the silanol groups is reversible to 400°C.; (*3*) after 400°C. the number of dehydrated sites that could be reversibly rehydrated by water vapor below saturation decreased until after heating at 850°C. no chemisorption of water vapor occurred; and (*4*) not all the surface silanol groups are removed even at the temperature where sintering starts to occur.

The number of sites remaining on the silica surface that either exist per se as adsorption sites for water vapor or can be rehydrated to give silanol sites is shown as a function of the temperature of heat treatment in Fig. 9. This curve, which was determined directly by water vapor adsorption isotherms, represents the difference between the two curves in Fig. 8 subtracted from the total number of adsorption sites originally present. Here it is seen that, whereas silanol sites may be removed by heating, they are reversibly rehydrated below 400°C. so that the surface area given by water vapor after chemisorption remains constant up to this temperature. Above 400°C., a progressively larger number of the dehydrated sites could not be rehydrated; hence the water vapor surface area decreases.

Infrared Absorption Studies

Changes in the nature of the silica surface can also be observed by infrared studies. For this purpose, the silicas were compressed under high pressure to form flat disks from 0.2 to 0.8 mm. thick. These disks, although fragile, were sufficiently cohesive so that they could be handled and heated. They were mounted in a stainless steel infrared cell for activation, the same sample being used throughout a given series of heatings. The most prominent feature of the infrared spectra of these silica disks was a broad absorption peak at ca. 3 microns wavelength due to oxygen-hydrogen stretching vibrations.

The change in the infrared spectrum of silica A with activation is shown in Fig. 10. These data were determined after the silica had been heated at the designated temperatures for 4 hours, then cooled and scanned at 0.4

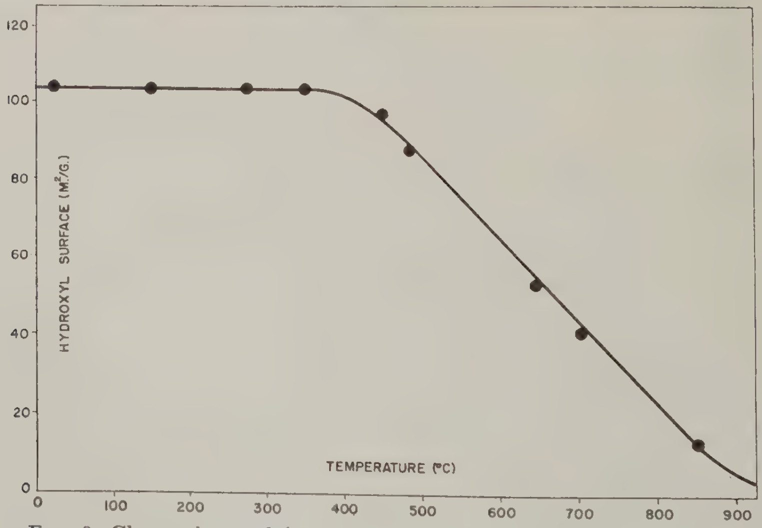

Fig. 9. Change in total (rehydrated and per se) surface silanol sites with sample heat treatment.

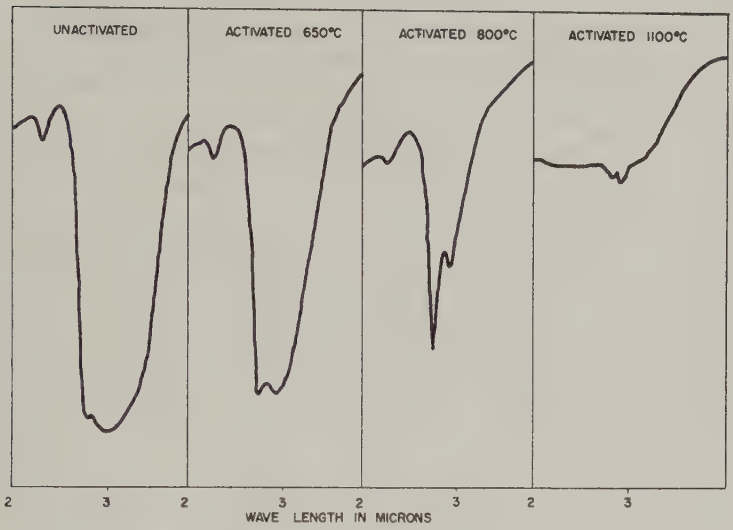

FIG. 10. Change in infrared spectra with sample heat treatment.

relative pressure of water vapor; hence physically adsorbed water is present on the surface. It is seen that the initial broad absorption band at 3 microns narrows with increasing temperature of activation, and after heating at 650°C., splits into two well-defined absorption peaks. On further heating, these peaks sharpen considerably and diminish in intensity until at 1100°C. they have nearly vanished. The peak at the lower wavelength (ca. 2.8 microns) results from an oxygen-hydrogen stretching vibration in the silanol groups, and the peak at the higher wavelength (ca. 3.0 microns) corresponds to the oxygen-hydrogen stretching vibration in the physically adsorbed water. Thus, the infrared studies show that heat treatment results in a decrease of both the number of silanol groups and the amount of water vapor that can physically adsorb on the silica surface.

The change in the infrared spectra on removal of physically adsorbed water from the silica surface is shown in Fig. 11. Here two samples with different activations are compared under anhydrous conditions and at 0.4 relative pressures of water vapor. The absorption peak at 3.0 microns disappears completely when the physically adsorbed water is removed. Indeed, the physical adsorption of water vapor can be followed quantitatively by measuring the intensity of the 3.0 micron peak.

On activation, the decrease in the number of silanol groups as determined by infrared studies was proportional to the decrease in silanol sites as measured by water vapor adsorption. Indeed, the infrared studies show that the amount of water vapor that can be physically adsorbed at a given relative pressure is directly related to the number of silanol groups. Thus, the infrared data in conjunction with the adsorption results constitute direct evidence that water vapor adsorption occurs only on silanol sites on the silica surface. However, the infrared work also shows that there are more silanol groups initially present in the silica than are accounted for by only those on the surface. Thus, there must be a small number of silanol groups in the bulk structure of the silica that are not exposed to the surface. These internal silanols are not readily condensed and do not start to disappear until the onset of sintering (900°C.).

The frequency of the silanol oxygen-hydrogen stretching vibration is dependent to some extent on sample activation. The wave numbers corresponding to this vibration for different activations are given in Table III. The frequency is also influenced by adsorbed species. Physically adsorbed water vapor tends to shift the frequency to lower wave numbers, and this may explain, in part, the change in frequency on activation. It was not possible to study the unactivated sample completely free of physically ad-

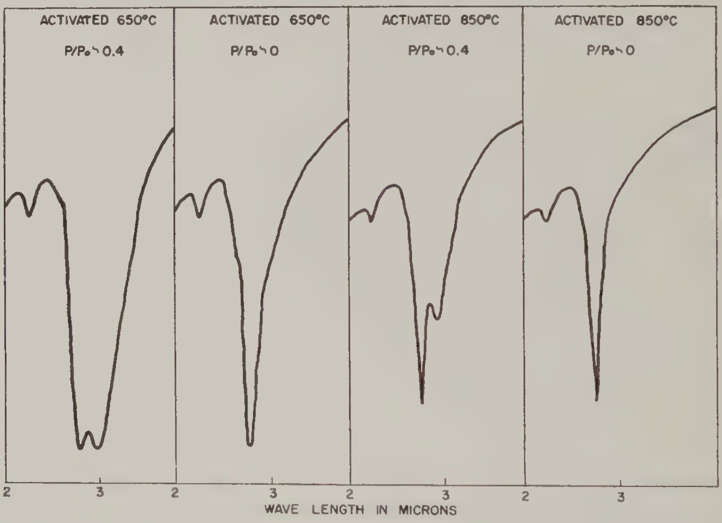

Fig. 11. Changes in infrared spectra on removal of physically adsorbed water.

TABLE III

Wave Numbers of Oxygen-Hydrogen Stretching Vibrations

Activation (4 hrs.)	Wave number (*cm.*$^{-1}$) Silanol	 Adsorbed water
Unactivated	Ca. 3731	Ca. 3530
450°C.	3740	
550°C.	3741	
650°C.	3741	
850°C.	3750	
1100°C.	3750	3678

sorbed water; hence the change in wave number from 3731 cm.$^{-1}$ to 3740 cm.$^{-1}$ may represent perturbation by physically adsorbed water.

Discussion

Silicon-Oxygen Surface Bonds

Experimental evidence presented in this paper establishes that water vapor adsorption is restricted to silanol sites on the silica surface. This finding, which appears valid for silica surfaces in general, is suggested by certain results of other investigators (i.e., references 7–9) and has been discussed by Iler (1). Presumably, the remainder of the silica surface, which does not adsorb water vapor, is composed only of silicon and oxygen atoms in more-or-less the general arrangement of the bulk structure but subject to displacements normally expected in a surface layer. The fact that water vapor does not adsorb on a silica surface which is void of silanol groups implies that the silicon-oxygen surface bonds are essentially homopolar in character.

Only such surfaces as graphite and hydrocarbons that are homopolar, or nearly so, and thus exhibit practically no electrostatic force field, are found experimentally to be hydrophobic and to give rise to Type III isotherm behavior with water vapor. In these cases there is no contribution to adsorption forces from dipole attractions or polarization of the adsorbate, and the only major attraction arises from dispersion forces. Dispersion forces alone are not sufficient to give rise to a normal monolayer, with subsequent multilayer formation, in the case of water vapor at room temperature on homopolar surfaces. A similar situation must exist for the interaction between water vapor and the silica surface as for the graphite type surface. That is, the silica surface when void of silanol groups can exhibit only a weak electrostatic force field; otherwise normal Type II water vapor adsorption would occur. A weak electrostatic force field implies that the silicon-oxygen surface bonds are nearly homopolar in character.

The exact nature of the tetrahedral silicon-oxygen bond in bulk silica is not known. Pauling (10) assigns 50% ionic character to this bond on the basis of empirical calculations from electronegativities. However, values up to 80% covalent may be obtained by selecting different heat of formation data. Brill (11) has determined electron density contours for the bulk quartz structure. Although these data do not lead directly to a quantitative measure of the character of the silicon-oxygen bond, they do indicate that the bond is intermediate between homopolar and heteropolar classification. It is quite reasonable that such a bond, which may be largely covalent in nature in the bulk structure, could give rise to a nearly homopolar surface bond through deformation of the electron distribution due to the unbalance of bonding forces at the surface. It is also possible that the nature of the silicon-oxygen bond at the surface differs considerably from the type of bonding in the interior, perhaps approaching a two-dimensional structure of bonds similar to the silicon monoxide type.

Water Vapor Adsorption

Physical adsorption of water vapor on the silica surface is restricted to the vicinity of silanol sites even at high relative pressures. Adsorption is initiated on the surface hydroxyl sites and probably proceeds by the build-up of clusters of adsorbed molecules around these sites. Thus, even at pressures approaching saturation, those portions of the silica surface that are devoid of silanol sites would be bare of adsorbed water molecules. This view is supported by the fact that sufficient water vapor for complete monolayer coverage cannot be adsorbed, even at relative pressures close to saturation, on silica surfaces with few silanol sites. The slight amount of hysteresis observed in the water vapor adsorption-desorption isotherms after the manifestation of interstitial effects (Fig. 1) may result partly from this cluster-wise adsorption. Cassie (12) has pointed out that adsorption in clusters can give rise to isotherm hysteresis due to configurational changes resulting from the merging of clusters.

The amount of water vapor that could be adsorbed and the isotherm character were found not to change upon heating the silica samples to ca. 180°C. Further, no additional water was removed from the sample over that obtained by evacuation for 8 hours at room temperature. Heating above 180°C. removed additional water from the silica, but a change in the character of the water vapor isotherm as well as chemisorption of water vapor were noted upon carrying out adsorption measurements. Thus it appears that all of the truly physically adsorbed water is removed from the silica surface by evacuation at room temperature.

On activation above ca. 180°C. silanol groups on the silica surface start to condense to form silica-oxygen bonds and water. In this low-temperature region the dehydrated silanol sites can be reversibly rehydrated by chemisorption of water vapor to regenerate the original surface. However, at higher temperatures the dehydration of hydroxyl groups is irreversible and water vapor cannot be chemisorbed (Fig. 8). These facts suggest that the resultant surface formed by dehydration of silanol sites at low temperatures differs from the surface formed at higher temperatures. After dehydration of silanol sites the surface initially formed is susceptible to rehydration, but at higher temperatures it transforms into a state that cannot be rehydrated by water vapor below saturation pressures. Two possible mechanisms are proposed to explain this behavior.

The condensation of two neighboring silanol groups might result in a $\equiv\mathrm{Si-O-Si}\equiv$ linkage that was under considerable strain if the two silicon atoms were not the appropriate distance apart. Mills and Hinden (13) and Weyl (14) have noted that dehydration of oxide catalysts leaves the surface in a strained condition. Presumably such a bond could first physically adsorb water because of the strain itself or because the close proximity of neighboring silanol sites and then be readily rehydrated because of the strain. However, on heating to higher temperatures, surface mobility might be sufficient to relieve the strain, perhaps by forming a different type of surface bond, and thus the site would no longer be susceptible to rehydration. It is possible that at higher temperatures the surface bonds could rearrange to form a two-dimensional structure with both tetrahedral and silicon monoxide type bonds.

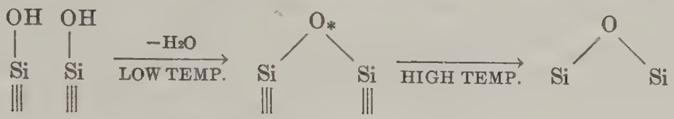

Alternatively, there may be more than one hydroxyl group attached to surface silicon atoms. In this case, the splitting out of a single molecule of water at lower temperatures would leave a site that could still physically adsorb water and thus initiate rehydration. On removal of the second hydroxyl group at higher temperatures, the site would no longer physically adsorb water and this portion of the surface would not be rehydrated. An unsuccessful attempt was made to determine if this second proposed mechanism was responsible for the chemisorption behavior of water vapor. Goates and Anderson (15) have reported that mono- and diprotic silanol groups (one and two hydroxyl groups per silicon atom) can be distinguished by titration in ethyl alcohol with $NaOC_2H_5$. Titration of the silicas employed in this study by their method gave only a single end point for both activated and unactivated silicas. This implies either that the method is not applicable or that no diprotic groups are present.

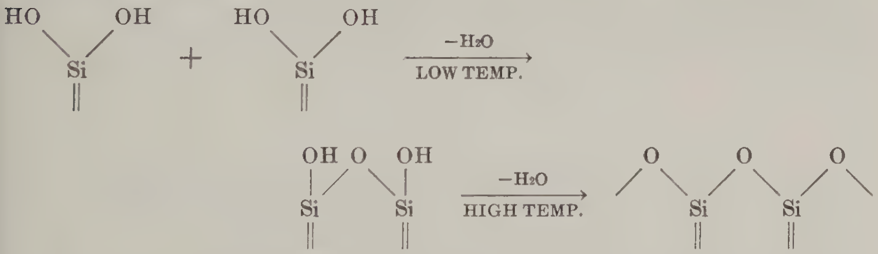

The chemisorption behavior of water vapor brings out an important point in the activation of silicas used for drying purposes. Regeneration of the silica requires moderate heating to remove physically adsorbed water which may be tenaciously held because of the porous nature of most silica adsorbents. However, heating to temperatures above 400–500°C. should be avoided since this removes silanol sites from the surface which cannot be rehydrated by water vapor and thus actually decreases the drying capacity of the silica. Former silanol sites which have been dehydrated by heating to high temperatures cannot be rehydrated because they cannot physically adsorb water vapor to initiate the rehydration. However, if a silica surface which has been made hydrophobic to water vapor by the removal of silanol groups from the surface is exposed to bulk water, silanol sites are readily reformed.

Sintering

The rate of sintering of the silicas at temperatures above 900°C., as indexed by the decrease in surface area, was unusual in that the loss in surface area was a linear function of the time of heating. For example, at 950°C. the rate of surface area decrease for silica A was ca. 6.3 $m.^2/g./hr.$ for heating times up to 20 hours. Since there is no internal porosity, the decrease in surface area presumably results from the smoothing out of surface roughness and the cementing together of silica particles by the formation of "necks" between adjacent particles.

Kuczynski (16) has shown, from measurements of the rate of growth of necks formed between glass spheres, that the sintering of glass proceeds by viscous flow. The equation used by Kuczynski for a specified temperature is:

$$\chi^n = A(t)$$

where χ is the radius of the neck between particles, t is the time, and n and A are constants. A value of 2 for n is indicative that plastic or viscous flow is the predominant mechanism of sintering.

Both the smoothing out of micro-surface roughness and the growth of small necks between particles would have approximately the same effect in decreasing the surface area, since in both cases the rate of material transport is similarly related to the change in surface area. Thus, for purposes of calculation, the decrease in surface area may be considered as resulting entirely from the formation of necks between adjacent particles. As a first approximation, this decrease in surface area would be proportional to the square of the neck radius (for small necks). Thus, the square of the neck radius would be proportional to the time for heating. The value of n in Kuczynski's equation therefore is 2, which indicates that viscous flow is the major mechanism of sintering rather than surface diffusion, volume diffusion, or other effects.

REFERENCES

1. ILER, R. K., "The Colloid Chemistry of Silica and Silicates." Cornell University Press, Ithaca, New York, 1955.
2. MARSHALL, C. E., "The Colloid Chemistry of the Silicate Minerals." Academic Press, New York, 1949.

3. Hauser, E. A., "Silicic Science." Van Nostrand, Princeton, New Jersey, 1955.
4. Eitel, W., "The Physical Chemistry of the Silicates." University of Chicago Press, Chicago, Illinois, 1954.
5. Carman, P. C., *J. Phys. Chem.* **57**, 56 (1953).
6. Carman, P. C., and Raal, F. A., *Nature* **167**, 112 (1951).
7. Stober, W., *Kolloid-Z.* **145**, 17 (1956).
8. Shapiro, I., and Kolthoff, I. M., *J. Am. Chem. Soc.* **72**, 776 (1950).
9. Shapiro, I., and Weiss, H. G., *J. Phys. Chem.* **57**, 219 (1953).
10. Pauling, L., "Nature of the Chemical Bond." Cornell University Press, Ithaca, New York, 1948.
11. Brill, R., Hermann, C., and Peters, C., *Naturwissenschaften* **27**, 676 (1939).
12. Cassie, A. B. D., *Discussions Faraday Soc. No.* **3**, 11 (1948).
13. Mills, G. A., and Hinden, S. G., *J. Am. Chem. Soc.* **72**, 5549 (1950).
14. Weyl, W. A., *Trans. N. Y. Acad. Sci.* **12**, 245 (1950).
15. Goates, J. R., and Anderson, K., *Soil Sci.* **81**, 227 (1956).
16. Kuczynski, G. C., *J. Appl. Phys.* **20**, 1160 (1949).

JOURNAL OF COLLOID SCIENCE **13**, 86–98 (1958)

MICELLAR DISPERSION OF α-MONOGLYCERIDES IN BENZENE AND CHLOROBENZENE[1]

P. Debye and W. Prins[2]

Department of Chemistry, Cornell University, Ithaca, New York

Received October 1, 1957

ABSTRACT

Hardly any data are available on the behavior of oil-soluble, pure, nonionic detergents in solution. In view of this, a series of α-monoesters of glycerol and normal fatty acids (C_{10}, C_{12}, C_{14}, C_{16}, C_{18}) have been prepared.

These compounds are surface-active in benzene and chlorobenzene. By means of light scattering, it is shown that they form small micelles in these solvents. In a better solvent, like chloroform, they exhibit molecular dispersion.

It is found that small amounts of impurities, like free fatty acid and free glycerol, enhance the scattering considerably. The systems are not sensitive to traces of water.

From the infrared spectra evidence is gained for the existence of *inter*molecular hydrogen bonding in the micelles in benzene, whereas only *intra*molecular hydrogen bonds are found to exist in chloroform.

The experimental decrease in micellar size with increasing C-number, and the decrease in size when passing from benzene to chlorobenzene as a solvent, can be explained by existing theories.

I. INTRODUCTION

An important feature of detergents is the combination in one molecule of a polar (or ionic) and a nonpolar part. This structure of the detergent molecule is significant in explaining the existence of micelles, i.e., clusters of molecules in true solution, in aqueous as well as nonaqueous solvents.

It is well known that in aqueous solvents the nonpolar hydrocarbon tails form the interior of the micelle and the polar parts form the outer layer in contact with the water. In nonaqueous, nonpolar solvents, like benzene, the situation is very likely the inverse: the polar parts form the interior and the nonpolar parts form the outside of the micelle. The balance of polar to nonpolar part determines whether the detergent will be water- or oil-soluble.

---

[1] Presented during the Symposium on the Structure of Micellar Solutions, Division of Colloid Chemistry, 131st Meeting of the American Chemical Society (April 7–12, 1957, Miami, Florida).

[2] Cellulose Research Institute, State University College of Forestry at Syracuse University, Syracuse, New York.

A review of the data on oil-soluble detergents (ionic as well as nonionic) has been given by Singleterry (1). He compiled experimental data giving evidence for the existence of micelles ranging in size from a few to a few thousand molecules, depending on the type of detergent used and, quite often, on the presence of traces of water in the solvent.

It appears that very little information is available on *pure nonionic* detergents. Ross (2) studied some commercial samples like "Glaurin" (commercial glycerol monolaurate, Glyco Product Company, New York) and various "Span" products (like sorbitan monolaurate, Atlas Powder Company, Wilmington, Delaware). He found some indication of a critical micelle concentration (CMC) by means of a dye solubilization technique. Addition of a polyoxyethylene chain onto the "Glaurin" or "Span" molecules gives a longer polar part and, therefore, less oil solubility, but better emulsifying properties in an oil-water system. Compounds like these have been studied by Marsden and McBain (3), Schulman, Matalon, and Cohen (4), and Gonick (5); all these authors found evidence for micelles only if some water was present in the solvent.

To get an idea of the fundamental forces governing micellization, it seems advisable to start from pure products rather than from commercial samples, the more so since per se a detergent system is greatly influenced by small amounts of impurity. In view of this, we decided to synthesize a series of pure nonionic detergents of the "Glaurin" type, viz., the α-monoglycerides with C_{10}, C_{12}, C_{14}, C_{16}, and C_{18} fatty acid chains, and to study their physicochemical behavior in nonaqueous solvents, dry and moistened.

In this communication, we wish to present some results obtained mainly from light scattering measurements. Additional information about micellization was obtained by studying the infrared OH stretching frequency. Other lines of research have been initiated but do not yet warrant publication.

II. PREPARATION OF THE α-MONOGLYCERIDES

The α-esters of glycerol and fatty acids with 10, 12, 14, 16, and 18 carbon atoms were prepared following the procedure described by Averill, Roche, and King (6). In this procedure the pure fatty acid chloride (redistilled products from Fisher Scientific Company, Matheson Fine Chemical Company, and Fluka, Chemische Fabrik, Buchs, Switzerland) is slowly added to acetone glycerol (Aldrich Chemical Company, Milwaukee, Wisconsin) dissolved in quinoline or pyridine. The α-ester is isolated by ether extraction and either distilled or crystallized. Subsequently, the protecting acetone group is removed by cold acid hydrolysis in ether. Pouring out the mixture into cold water yields the α-monoglycerides as a white precipitate. The products obtained in this way can be recrystallized from CCl_4 or petroleum ether. Crystallization from absolute alcohol may cause a shift of the ester link to the β position (7), as happened with part of our monopalmitin product.

All α-esters were obtained in the form of white flaky crystals with melting points slightly below the literature values (Table I). X-ray reflection diagrams show the existence of a long spacing due to double layer packing as in most detergents[3] (8). Measurements of the capillary rise, as a function of concentration on the C_{12} and C_{14} products in benzene, indicate a definite surface activity of these compounds. First, there is a 10% reduction of the benzene surface tension, then a leveling off to an almost constant value at higher concentrations. The type of curve is similar to that found by McBain and Perry (9) for lauroyl sulfonic acid in benzene.

In view of some discrepancies in the light scattering results (see below), it was thought that small amounts of impurity might still be present in some of the products. During the synthesis, it was observed that not all of the acid chloride reacted. Unless this is removed very carefully, this may end up in the final product as free fatty acid (F.F.A.). Furthermore, it is conceivable that some hydrolysis of the ester occurs, giving rise to some free fatty acid and glycerol.

In order to determine the F.F.A. content, 500 mg. samples in 20 ml. 95% alcohol were titrated with 0.00964 N alcoholic NaOH, using phenolphthalein as an indicator. Blank titrations on 20 ml. alcohol were always performed and subtracted. The results are shown in Table I.

In an attempt to remove the F.F.A. and its possible counterpart of glycerol, a sample of the monomyristrin, which had the highest impurity, was suspended in cold saturated aqueous $NaHCO_3$ solution and shaken vigorously. After filtering, washing, and drying, the F.F.A. content was determined again and found to be much smaller than before (Table I). The consequences of this partly successful treatment on the light scattering will be discussed below.

III. Light Scattering

The monoglycerides are insoluble in water, but can be dissolved to approximately 2% at room temperature in nonaqueous solvents like benzene, chlorobenzene, and toluene. Chloroform is a very good solvent. Light scattering is a convenient technique for gaining information about the extent of micellization in these solvents, since the light scattered by a micelle is proportional to the square of its weight (this rule is valid if the micelles are smaller than $1/10$ of the wavelength).

---

[3] Complete unit cell determinations of the products have been performed by the staff of the X-ray Department in the Physics Laboratory (Director, J. A. Prins), T. H. Delft, the Netherlands. The long spacings found, coincide with those of reference 8.

TABLE I

Melting Points and Free Fatty Acid (F.F.A.) Contents of the Monoglycerides

Values in brackets are taken from reference 8.

Compound	Fatty acid	M.P. (°C.)	W% F.F.A.
α-Monocaprin	C_{10}	51 (53)	~0.1
α-Monolaurin	C_{12}	62 (63)	0.2
α-Monomyristin	C_{14}	66.5 (70.5)	1.3
α-Monopalmitin	C_{16}	76.5 (77)	~0.1
α-Monostearin	C_{18}	80.2 (81)	~0.0
β-Monopalmitin	C_{16}	69.5 (69.5)	
α-Monomyristin			
After treatment	C_{14}	66.5 (70.5)	0.22
Second batch	C_{14}	67 (70.5)	0.17

Usually a detergent solution of concentration c g./ml. is considered to consist of monomers of concentration c_0(CMC) and micelles of an average weight $\overline{M}_W$ and concentration $(c - c_0)$. Since only the micelles give a measurable scattering, we have the following well-known expression for the light scattered, R_{90}, by the (micellar) solute (10)

$$K(c - c_0)/R_{90} = 1\sqrt{\overline{M}_w} + 2A(c - c_0), \qquad [1]$$

where

$$K = 2\pi^2 n^2(\Delta n/\Delta c)^2/\lambda_0^4 N_A$$

with n the refractive index of the solution, $\Delta n/\Delta c$ the refractive index increment, λ_0 the wavelength of the light *in vacuo*, and N_A Avogadro's number. Rayleigh's ratio, R_{90}, is a measure of the light scattered by the solute at 90° with the incident beam. The second virial coefficient A accounts to a first approximation for deviations from ideal behavior.

Measurements were performed at room temperature and $\lambda_0 = 436$ mμ on solutions of the α-monoglycerides, β-monopalmitin, and recrystallized "Myverol" (commercial monostearin) in benzene, chlorobenzene, and chloroform. The A.R. solvents were dried, carefully distilled, and kept in a drybox. Solutions and solvents were always filtered through fine (or medium fine) sintered glass filters to remove dust particles.

The necessary refractive index differences between solvent and solution were measured at $\lambda_0 = 436$ mμ in the differential refractometer, designed by P. P. Debye (11). The temperature was kept at 30° or 28°C. Results are given in Table II.

The light scattering instrument has been described by Debye and Bueche (12). One of the main features of this instrument is a small prism outside the cell which reflects the scattered light downwards onto the photo-multiplier. The prism and multiplier can be moved around the cell from 30° to 150° to measure the angular dependence of the scattering. The prism device eliminates stray light effectively. The cell was made of 41 mm. Pyrex tubing, with a flat bottom sealed on and equipped with a

TABLE II

Summary of Light Scattering Results

$\Delta n/\Delta c$ in ml./g., c_0 in g./100 ml.

Compound	Monomer weight	Fatty acid	In benzene			In chlorobenzene		
			$\Delta n/\Delta c$	c_0	$\overline{M}_W$	$\Delta n/\Delta c$	c_0	$\overline{M}_W$
α-Monocaprin	246	C_{10}	−0.0626	0.02	10000	−0.849	0.025	4000
α-Monolaurin	274	C_{12}	−0.0705	0.02	20000	−0.0747	0.10	13000
α-Monomyristin 1.3% F.F.A.	302	C_{14}	−0.0631	0.02	58000	−0.0911	0.03	32000
α-Monomyristin 0.22%	302	C_{14}	−0.0631	0.02	28000	−0.0911	—	—
α-Monomyristin 0.17%	302	C_{14}	−0.0631	0.02^5	26000	−0.0911	—	—
α-Monopalmitin (β same)	330	C_{16}	−0.0655	0.05	5000	−0.0874	0.06	3000
α-Monostearin	358	C_{18}	−0.0628	0.14	4000	−0.0890	0.16	1200

Rayleigh horn to trap the primary beam after it had passed through the solution. The cell was painted black, except where the primary beam enters and the scattered light leaves. To calibrate the instrument, we compared the scattering of pure benzene with the scattering of a 0.5% "Styron" solution ("Cornell Standard"). Its turbidity has been determined by a number of authors (13), as well as by the National Bureau of Standards. Using the former value, we find for benzene $R_{90} = 48.5\ 10^{-6}$ cm.$^{-1}$, whereas the NBS value leads to $R_{90} = 45.7\ 10^{-6}$ cm.$^{-1}$. Because of the good correspondence between 48.5 and the value 48.7 obtained by an independent calibration with Ludox suspensions (14), this value was adopted instead of the NBS value as the basis for the interpretation of the results on the detergent solutions.

In none of these solutions did we observe a dissymmetry of more than 1% or 2%, which we attributed to remnants of dust left behind after filtration. In view of the reported influence of traces of water on solutions of oil-soluble detergents, we made up a number of solutions in a drybox filled with nitrogen and dried with P_2O_5. Solvent, solute, and cell were stored in the drybox for at least 48 hours and the solutions were filtered into the cell in the drybox. After measuring the scattering of such a solution in a closed cell, a strip of wet filter paper was suspended in the cell above the level of the solution. No significant changes in scattering were observed over a period of several days.

The scattering of the monoglycerides in benzene, as well as chlorobenzene, is rather small. A typical value for a 1% solution is 10% above the solvent scattering. In chloroform almost no solute scattering was found at all, indicating that in this (good) solvent micellization does not occur.

The scattering of monocaprin (C_{10}), monopalmitin (C_{16}), and monostearin (C_{18}) in benzene and chlorobenzene was quite low, whereas the

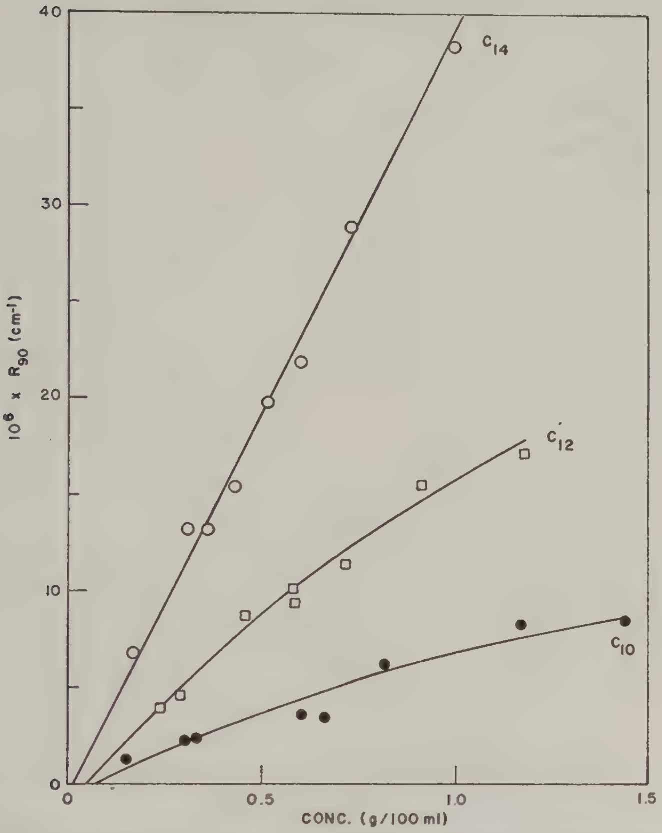

FIG. 1. Light scattering by C_{14}, C_{12}, and C_{10} monoglycerides in benzene.

monolaurin (C_{12}) and monomyristin (C_{14}) scattering was much larger. It was found that this large scattering intensity of C_{12} and C_{14} was reproducible even after recrystallizing the detergents. In Figs. 1 and 2, R_{90} values are plotted as a function of concentration for C_{14}, C_{12}, and C_{10}. In view of the fact that the C_{16} and C_{18} scattering was again of the same order of magnitude as the scattering by C_{10} (Figs. 3 and 4), this high scattering power of the C_{12} and C_{14} solutions made us suspicious with respect to the purity of the compounds C_{12} and C_{14}. Several experiments were conducted to clarify this matter.

In Fig. 3, the scattering of monopalmitin (C_{16}) in benzene is given. The open circles are measurements made on an impure product (lower m.p.). Some of the open circles are points found after adding about 5% F.F.A. to the solution. It can be seen that the effect of the F.F.A. is appreciable, although the same amount of F.F.A. in benzene without detergent has barely any effect on the benzene scattering. After these experiments, titrations to determine the F.F.A. contents of our products

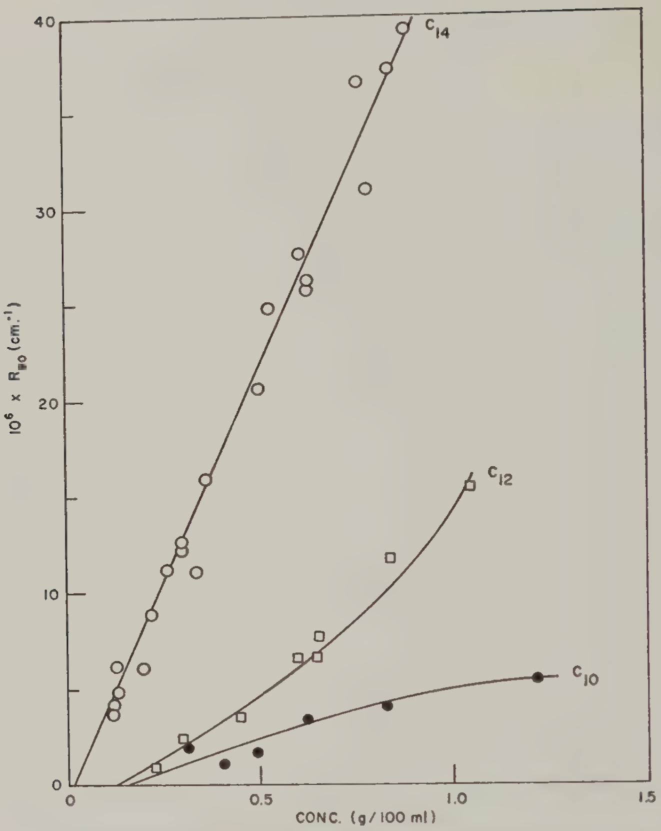

FIG. 2. Light scattering by C_{14}, C_{12}, and C_{10} monoglycerides in chlorobenzene.

were performed. They are described in the preceding section, and the results given there indicate that the C_{12} and C_{14} products do contain some F.F.A., whereas the C_{10}, C_{16}, and C_{18} do not.

It is conceivable that the F.F.A. is present as a result of partial hydrolysis of the monoglycerides. In that case, an equivalent amount of glycerol should be present in the material. This glycerol may very well be the cause of the larger scattering found in the impure C_{12} and C_{14} samples. If we measure the scattering of the pure C_{16} product in benzene, saturated with glycerol, we find that the solute scattering is indeed enhanced in about the same amount as the enhancement due to 5% F.F.A.

The impurities—F.F.A. and possibly glycerol—can be removed, at least partly, by washing with bicarbonate solution as described in the previous section. The effect of this treatment on the C_{14} scattering is shown in Fig. 5. Corresponding with the decrease in F.F.A. content, the scattering has decreased significantly.

From these experiments we can conclude that small amounts of im-

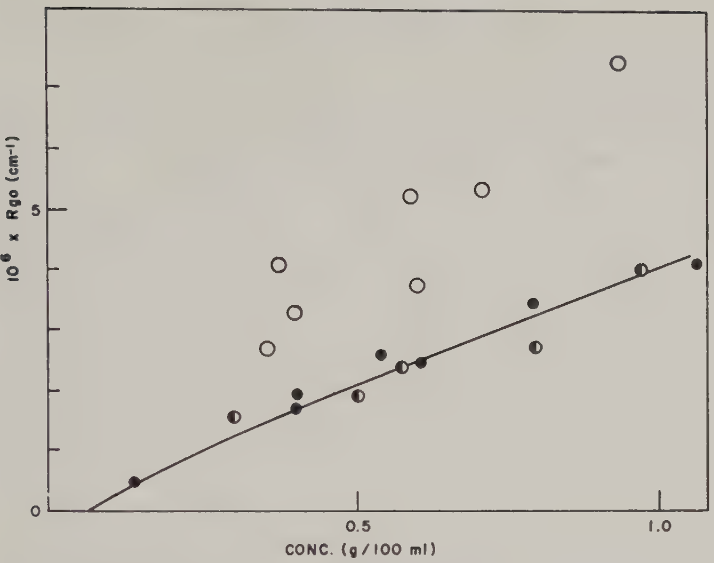

FIG. 3. Light scattering by monopalmitin (C_{16}) in benzene. ● = αC_{16} m.p. 76.5°C. ◐ = βC_{16} m.p. 69.5°C. ○ = deliberately or accidentally impure C_{16}.

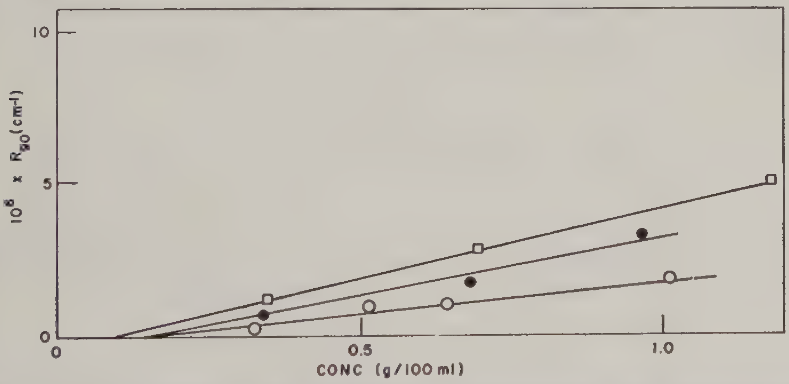

FIG. 4. Light scattering by monostearin (C_{18}) in benzene and chlorobenzene. ● = αC_{18}, m.p. 80–80.5°C. in benzene. ○ = same in chlorobenzene. □ = recrystallized commercial C_{18} (Myverol 18-06 D.P.I.), m.p. 79.5–81°C. in benzene.

purities do have a large effect on the scattering and, therefore, on the calculated micellar weight. The insoluble glycerol particularly may conceivably be solubilized in the micelle, thereby causing the anomalous size of the micelle found in the C_{12} and C_{14} systems.

In Table II, we have summarized the light scattering results by calculating the average micellar weight $\bar{M}_W$, using Eq. [1]. In most cases, there is hardly any reason for extrapolation to infinite dilution, because of the inaccuracy of the measurement, due to the low level of solute scattering.

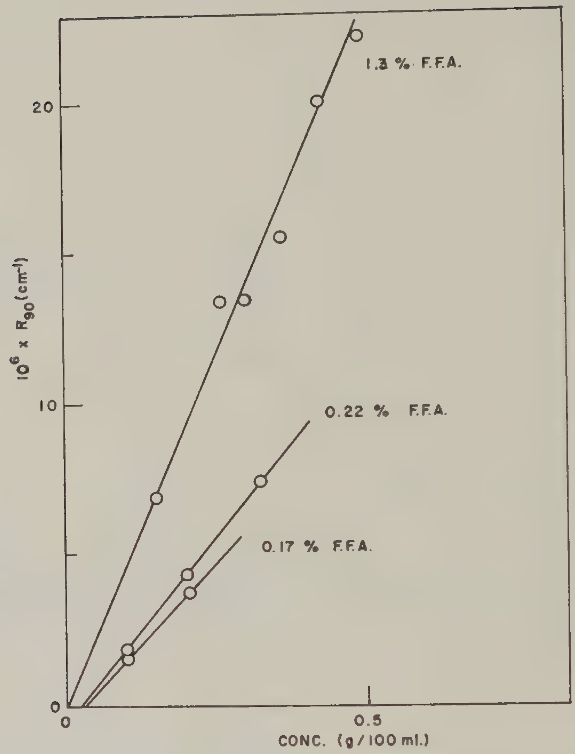

FIG. 5. Decrease of monomyristin (C_{14}) scattering in benzene after partial removal of impurities.

A second virial coefficient is, therefore, not given. The CMC (c_0) values given in Table II again are very inaccurate. It even seems barely justified to conclude from the measurements that a CMC exists.

IV. HYDROGEN BONDING IN THE MICELLE

The polar part of the monoglyceride molecule contains two OH groups and one ester link. In our picture of the micelle, these polar parts form the interior of the micelle. It is, therefore, conceivable that intermolecular hydrogen bonds are formed in this core, which may be detected by studying the infrared absorption spectra of the solutions.

It is well known (15) that the free OH stretching frequency is located at 2.74–2.79μ. If this OH group is hydrogen bonded in a single bridge, the absorption peak shifts to 2.82–2.90μ. This bridge may be intra- as well as intermolecular. The intramolecular peak should be independent of concentration (or rather, follow Beer's law), whereas the intermolecular peak should show deviations from Beer's law. Polymeric hydrogen bonding, as, for example, in the liquid or solid normal alcohols, shows a broad band at 2.94–3.12μ.

The OH region of monolaurin was studied in the solid state (in a KBr pellet) and in solution, using a Perkin-Elmer Type 21 double beam recording spectrophotometer. For the work on solutions, two matched cells of 0.508 mm. thickness were used, one filled with solvent, the other with solution, so as to obtain the differential spectrum of the solute only. Figure 6 shows the OH region of the solid material, as well as that of a monolaurin solution in benzene. In the solid state, we have polymeric hydrogen bonding (2.92–3.10μ), whereas in solution the broad band is split up in two peaks both shifted to a shorter wavelength. The 2.79μ peak is the free OH frequency; the 2.89μ is the hydrogen-bonded one. In Fig. 6, we have also plotted the logarithm of the intensity of these two peaks as a function of concentration for benzene as well as chloroform solutions. We know from Section III that monolaurin forms micelles in benzene and exhibits monomeric dispersion in chloroform. In accordance with this, we find that Beer's law is obeyed in chloroform, since only the proportionally increasing *intra*-molecular hydrogen bonds are present. In benzene, Beer's law is not followed: here the 2.89μ peak grows stronger at higher concentrations at the expense of the 2.79μ peak. This more than proportional increase in the number of hydrogen bonds in benzene indicates that they must be at least partly *inter*molecular.

From this we conclude once more that benzene is a micelle-forming

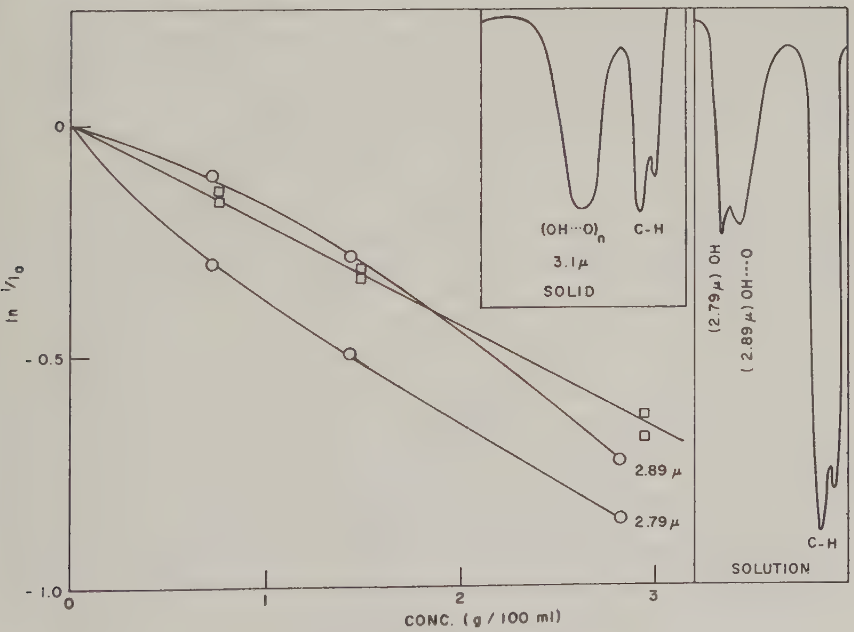

FIG. 6. Hydrogen bonding in monolaurin solutions as derived from the infrared absorption. ○ in benzene; □ in chloroform.

solvent and chloroform is not. Also, intermolecular hydrogen bonds make the existence of clusters of polar parts in the inside of the micelle all the more probable.

V. DISCUSSION

If we first confine our attention to the micellar weights of the three presumably pure compounds (C_{10}, C_{16}, and C_{18}), the results given in Table II allow two definite conclusions:

a). The micellar weight decreases with increasing number of carbon atoms in the hydrocarbon part of the detergent molecules, in benzene as well as chlorobenzene.

b). The micellar weights are smaller in chlorobenzene than in benzene.

The first conclusion can be explained qualitatively by adapting to our case the theory of micellization of nonionic detergents as put forward by Reich (16). Micellization is, at least partly, induced by the fact that there is a gain in interfacial free energy on clustering a number of detergent molecules in such a way that the polar parts stick together in the interior, and the nonpolar hydrocarbon parts form the outside of the micelle, in contact with the equally nonpolar solvent. Representing the polar ends (glycerol in our case) by little spheres of radius r, it is easily seen that the surface of the spherical aggregate of the polar parts is given by

$$A = 4\pi r^2 m^{2/3}. \qquad [2]$$

If we assume now, with Reich, that a portion a of the surface of each polar end is *screened* against solvent contact by the hydrocarbon tail, we have for the *exposed* surface of a cluster of m monomers

$$F(m) = 4\pi r^2 m^{2/3} - am. \qquad [3]$$

Reich identifies that m value at which there is no exposed surface left with the maximum in the size distribution and calls that cluster then a "complete micelle." Putting $F(m) = 0$ in Eq. [3] gives the size m_0 of this complete micelle:

$$m_0^{1/3} = 4\pi r^2/a. \qquad [4]$$

It is reasonable now to assume that 18 carbon atoms screen a larger portion a of the glycerol ends than 10 carbon atoms. Accordingly, m_0 will be smaller, the longer the hydrocarbon chain, as indeed was found experimentally.

The change in micellar size with the length of the screening portion of the detergents has also been found by Kushner, Hubbard, and Doan (17). They measured two fractions of the commercial nonionic detergent, Triton X-100, in water. The two fractions had a polar chain length (polyoxyethylene) of 8 and 12 units, respectively. Since they were measured in water, the polar parts form the outside of the micelle and perform the screening function for the hydrocarbon core of the micelle. The authors found the micelles with the 8-unit polar chain to be much larger than the micelles with the 12-unit polar chain. This again is qualitatively explained by assuming that a in Eq. [4] has increased significantly, with a corresponding decrease in m_0.

Since, in Reich's theory, the maximum in the micellar size distribution is completely determined by the geometrical factor $4\pi r^2/a$, it fails to predict the second of our conclusions, viz., the decrease in micellar weight in changing the solvent from benzene to the more polar chlorobenzene. The reason for the observed decrease is quite obvious in general terms: the more "polar" the solvent, the less "reason" there is for micellization (less interfacial energy gain, for example), until finally in chloroform there are no micelles at all. Hoeve and Benson (18) have recently written down very carefully all factors that in principle play a role in micellization. These authors derive the free energy of micellization as a function of m, in which the screening function is introduced in a different way. They also point out that the micellar weight distribution is a function of the concentration. From their equations, again adapted of course to our inverse type of micelles, it is indeed possible to see that the maximum in the distribution should be smaller in chlorobenzene than in benzene. The usefulness of their theory beyond the point of qualitative predictions is very limited, however, because there are too many numerically unknown factors involved.

Finally, we mention the striking effects of small impurities on the micelle formation, as found in the C_{12} and C_{14} products and summarized in Table II. This should make us wary in drawing conclusions about micellar structure from measurements on ill-defined products.

ACKNOWLEDGMENTS

We wish to thank Mrs. P. Dreyfuss and Dr. D. D. Phillips, Department of Chemistry, Cornell University, for the preparation of the α-monoglycerides. The refractive index increments were partly measured by Mrs. G. McConkey, to whom our gratitude is due.

This investigation was supported in part by the Office of Naval Research, under Contract Nonr-401(17), Task No. NR 051-360.

REFERENCES

1. SINGLETERRY, C. R., *J. Am. Oil Chemists' Soc.* **32,** 446 (1955).
2. ROSS, S., *J. Colloid. Sci.* **6,** 497 (1951).
3. MARSDEN, S. S., AND MCBAIN, J. W., *J. Phys. Chem.* **52,** 110 (1948).
4. SCHULMAN, J. H., MATALON, R., AND COHEN, M. *Discussions Faraday Soc.* **11,** 117 (1951).
5. GONICK, E., *J. Colloid Sci.* **1,** 393 (1946).

6. Averill, H. P., Roche, J. N., and King, C. G., *J. Am. Chem. Soc.* **51,** 866 (1929).
7. Clarke, T. H., and Stegemann, C., *J. Am. Chem. Soc.* **62,** 1815 (1940).
8. Filer, L. J., Sidlin, S. S., Daubert, B. F., and Longenecker, H. E., *J. Am. Chem. Soc.* **66,** 1333 (1944).
9. McBain, M. E. L., and Perry, L. H., *J. Am. Chem. Soc.* **62,** 989 (1940).
10. See, for example, Stacey, K. A., "Light Scattering in Physical Chemistry," p. 19. T. Butterworth, London.
11. Debye, P. P., *J. Appl. Phys.* **17,** 392 (1946).
12. Debye, P., and Bueche, A. M., Technical Report 2242 (1949), Reconstruction Finance Corporation, Office of Rubber Reserve, Polymer Research Branch.
13. See, e.g., Carr, C. I., and Zimm, B. H., *J. Chem. Phys.* **18,** 1616 (1950).
14. Prins, W., and Hermans, J. J., *Koninkl. Ned. Akad. Wetenschap. Proc.* **B59,** 302 (1956).
15. Bellamy, L. J., "Infrared Spectra of Complex Molecules." Wiley, New York, 1954.
16. Reich, I., *J. Phys. Chem.* **60,** 257 (1956).
17. Kushner, L. M., Hubbard, W. D., and Doan, A. S., *J. Phys. Chem.* **61,** 371 (1957).
18. Hoeve, C. A. J., and Benson, G. C., paper presented at the Miami Meeting of the American Chemical Society, Division of Colloid Chemistry, April 1957 (to be published).

JOURNAL OF COLLOID SCIENCE **13**, 99–102 (1958)

LETTER TO THE EDITOR

BEHAVIOR OF AMMONIUM AURINTRICARBOXYLATE AS A COLLOIDAL ELECTROLYTE

Ammonium aurintricarboxylate (Aac), which is well known as a chelating agent, has the structure:

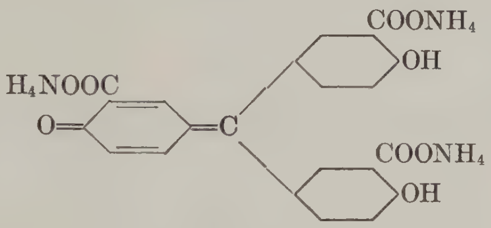

This dye, commonly known as Aluminon, has found wide applications in the colorimetric determination of aluminum and other metal ions (2, 4).

During our studies with metal chelates involving Aluminon (5), we observed that in cases where the concentrations employed were high, the compositions of the chelates were often found to be in nonstoichiometric ratios. This suggests that the behavior of the reagent, unlike that of true solutions, when concentrated, is responsible for such anomalous compositions.

EXPERIMENTAL

The electrical conductance of solutions of Aac was determined at different dilutions at a temperature of 20°C. The measurements were carried out using a measuring cell of the dip type, having a cell constant of 0.132. The bridge used was L&N Kohlrausch Slidewire, with an audio-frequency oscillator. The solutions were freshly prepared in conductivity water, using reagent grade chemical, and were kept immersed in a thermostat before and during measurements. In Fig. 1, the variation of equivalent conductivity with $\sqrt{c}$ (square root of concentration) has been plotted. It is obvious that the compound does not behave as a simple electrolyte.

The conductance, determined at five different temperatures, is shown in Table I and plotted in Fig. 2.

All the data extrapolate to a common temperature of zero conductance of about − 36°C.

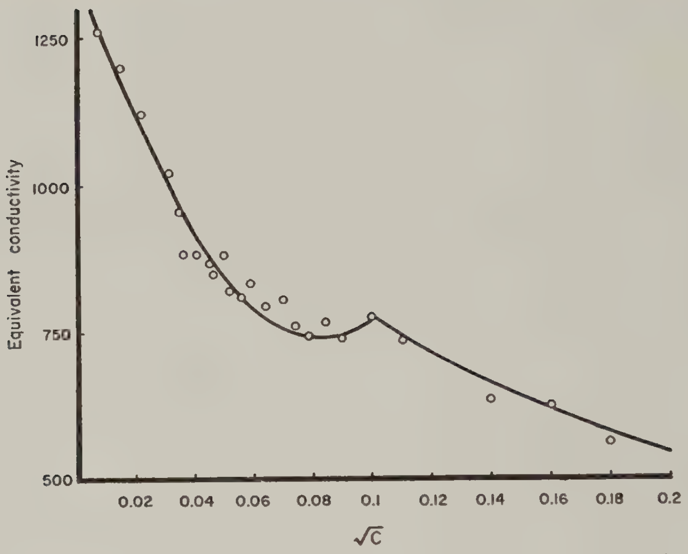

Fig. 1. Ammonium aurintricarboxylate. Variation of Λ with $\sqrt{c}$.

TABLE I

Concentration (M)	10^3 specific conductance (mhos)				
	23°C.	28°C.	33°C.	38°C.	43°C.
0.0100	1.95	2.10	2.27	2.45	2.59
0.0050	1.02	1.12	1.19	1.27	1.36
0.0025	0.53	0.59	0.64	0.69	0.74

The temperature coefficient of specific conductance per degree Centigrade has been calculated and shown in Table II.

Summary and Conclusion

The nature of Fig. 1 resembles that of colloidal electrolytes recorded by McBain (3), for this class of substances. In Fig. 2, the temperature at which the solutions would have zero conductance have been found by linear extrapolation to be −36°C. The temperature coefficient per degree Centigrade is 2.6%–2.8% of the conductance at 35°C. Ordinarily, it has been recorded that the conductivity of electrolytes becomes zero at about −40°C, and that of colloidal solutions at −15° to −35°C. (6, 7). In the case of certain dyes (8), this temperature ranges from −20° to −25°C. It is evident, therefore, that the collodial nature of dyes is responsible for the temperature of zero conductance being higher than that of electrolytes. In the case of Aac the temperature of zero conductance

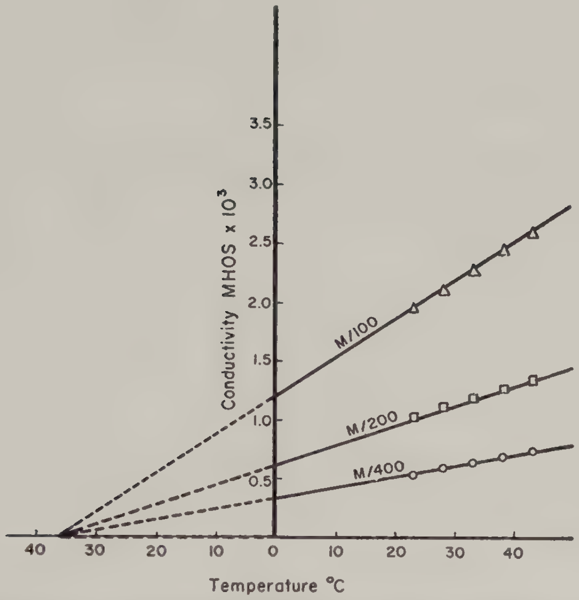

FIG. 2. Conductivity of ammonium aurintricarboxylate at different temperatures.

TABLE II

Concentration (M)	Temperature coefficient per °C.	Temperature coefficient per 100 of conductance
0.0100	0.032	2.6
0.0050	0.017	2.7
0.0025	0.009	2.8

shows the solution of the reagent to have characteristics intermediate between those of colloidal solutions and of true electrolytes. Thus, it is concluded that the compound behaves as a colloidal electrolyte, and it is only in extremely dilute solutions that the solution is apt to behave as a true solution (1).

REFERENCES

1. DEY, A. K., *J. Colloid Sci.* **3,** 473 (1948).
2. JOHNSON, W. C., "Organic Reagents for Metals." Chemical Publishing Co., New York, 1955.
3. McBAIN, J. W., "Colloid Science." Heath, Boston, 1950.
4. MUKHERJI, A. K., AND DEY, A. K., *Z. anal. Chem.*, **152,** 424 (1956).
5. MUKHERJI, A. K., AND DEY, A. K., *Anal. Chim. Acta* **18,** (1958).
6. MUSHRAN, S. P., AND PRAKASH, S., *J. Phys. Chem.* **50,** 251 (1946).
7. PRAKASH, S., *J. Phys. Chem.* **37,** 907 (1933).

8. SHIVAPURI, T. N., AND PRAKASH, S., *Current Sci. (India)* **18**, 403 (1949).

Chemical Laboratories,
University of Allahabad,
Allahabad, India.

ANIL K. MUKHERJI[1]
ARUN K. DEY

Received July 18, 1957; revised November 4, 1957.

---

[1] Present address: Coates Chemical Laboratory, Louisiana State University, Baton Rouge 3, Louisiana.

JOURNAL OF COLLOID SCIENCE **13**, 103–113 (1958)

DYNAMIC MECHANICAL PROPERTIES OF POLY-*n*-OCTYL METHACRYLATE[1]

Walter Dannhauser,[2] William C. Child,[3] Jr., and John D. Ferry

Department of Chemistry, University of Wisconsin, Madison, Wisconsin

Received November 27, 1957

INTRODUCTION

Following previous reports on the dynamic mechanical properties of several methacrylate polymers—the ethyl (1), *n*-butyl (2), and *n*-hexyl (3)—we now present similar data for the *n*-octyl polymer. These measurements were part of a cooperative investigation with the Samuel Feltman Ammunition Laboratories, Picatinny Arsenal.

MATERIALS AND METHOD

The synthesis and fractionation of the polymer have been described elsewhere by Chinai (4). The fraction used in this study, with a weight-average molecular weight of 3.62×10^6, had been dried from frozen benzene solution and stored over silica gel desiccant.

Measurements of the complex shear compliance ($J^* = J' - iJ''$) were made between 15 and 3600 cycles/sec. with the Fitzgerald Apparatus manufactured by Atlantic Research Corporation, Alexandria, Virginia. Three pairs of disc-shaped samples were employed, molded at 150°F. The samples were quite clear and almost colorless, and they adhered very readily to the driving surfaces in the apparatus. The sample coefficients were calculated from the weights and thicknesses as usual (1). The density of the polymer at 25°C. and the thermal expansion coefficient above the glass transition temperature were taken as 0.98 g./cm.^{3} and 6.5×10^{-4} deg.$^{-1}$, respectively, sufficiently close to the values since reported by Rogers and Mandelkern (5). Detailed descriptions of the samples follow.

Samples 90, approximate dimensions $1\frac{1}{16}$ in. diameter by $\frac{3}{32}$ in. thickness, were compressed slightly in the apparatus and the sample coefficient was 15.4 cm. at 25°C. Measurements were made at approximately 5° intervals from 25° down to 10°, then from 30° up to 45°, followed by a check run at 25° which agreed with the initial results. (The exact temperatures are given in the legend of Fig. 1.)

---

[1] Part XXVIII of a series on Mechanical Properties of Substances of High Molecular Weight.

[2] Present address: University of Buffalo, Buffalo, New York.

[3] Present address: Carleton College, Northfield, Minnesota.

Samples 91, approximate dimensions 1⅟16 in. by 1⁄32 in., were mounted at the same time as samples 90 and experienced the same temperature sequence. Their nominal sample coefficient was 58.9 cm. at 25°C. Measurements were made at approximately 5° intervals from 25° to 70° and then at 10° intervals to 130°, followed by a check run at 30° which agreed with the initial results. At overlapping temperatures, the values of J' and J'' were lower than those of samples 90 by about 18%; the discrepancy was assumed to be due to an error in thickness measurement of these very thin samples, and an empirical correction factor of 1.18 was applied to these data.

Samples 94, approximate dimensions 5⁄16 in. by ⅛ in., were compressed about 4%, and the nominal sample coefficient was 2.69 cm. at 25°C. Measurements were made at approximately 5° intervals from 25° down to 10° and then at −14°, 0°, −5°, 5°, 25°, −10°, and 25°. The check runs at 25° agreed satisfactorily with the initial results. The values of J' and J'' were about 18% higher than those for samples 90, attributable to bulging, and so an empirical correction factor of 0.82 was applied to these data.

RESULTS

The data for J' and J'', measured at 24 temperatures from −14° to 130°C., are shown plotted logarithmically in Fig. 1. Where data on different samples were taken at the same frequencies and temperatures, the values have been averaged after applying the empirical corrections.

For reduction to a standard temperature, 100°C. was chosen for conformity with other members of the series; J'_p and J''_p were calculated by the usual formulas (6), using the thermal expansion coefficient given above. The value of J_∞, the limiting high-frequency compliance, was taken as 10^{-10} cm.²/dyne, but the choice was not critical.

Logarithmic plots of the reduced functions could be superposed quite well by the usual arbitrary shift factors a_T, identical for both real and imaginary components, except for J'' at the very lowest temperatures. The empirical a_T values followed very closely an equation of the WLF form (7):

$$\log a_T = -c_1^0(T - T_0)/(c_2^0 + T - T_0) \qquad [1]$$

with $c_1^0 = 7.60$ and $c_2^0 = 227.3$ for $T_0 = 373.2$°K. Values of a_T calculated from this equation were actually used for the final logarithmic plots against reduced frequency (ωa_T) shown in Figs. 2 and 3.

With knowledge of the glass transition temperature, $T_g = 253$°K. (5), the values of c_1' and c_2' appropriate to T_g as reference temperature may be calculated from formulas previously given (7), and from these the parameters f_g and α_f. For f_g, interpreted as the fractional free volume at T_g, we obtain 0.027, close to the average "universal" value of 0.025. For α_f, interpreted as the thermal expansion coefficient of the free volume relative to the total volume, we obtain 2.5×10^{-4} deg.$^{-1}$; this is reasonable in

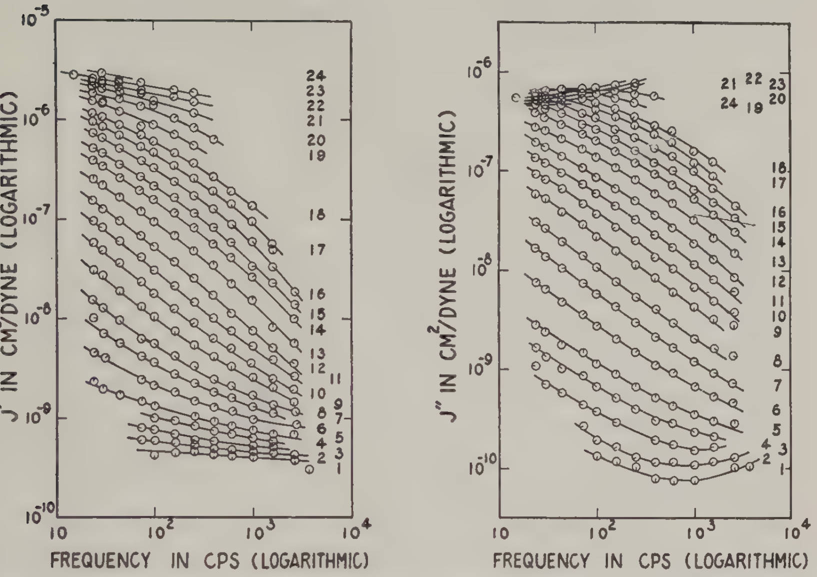

FIG. 1. Variation of the real part of the dynamic shear compliance, J' (left) and the imaginary part, J'' (right) with frequency for poly-n-octyl methacrylate at 24 temperatures; numbers correspond to the sequence (with 45° or 90° clockwise rotations of pips corresponding to increments of approximately 5°C. or 10°C., respectively) −14.3°, −9.6°, −5.0°, −0.1°, 4.0°, 9.9°, 15.1°, 19.8°, 25.3°, 30.0°, 34.2°, 38.8°, 44.4°, 50.2°, 54.4°, 59.8°, 65.8°, 70.9°, 80.2°, 89.4°, 99.8°, 109.4°, 120.3°, and 129.5°C.

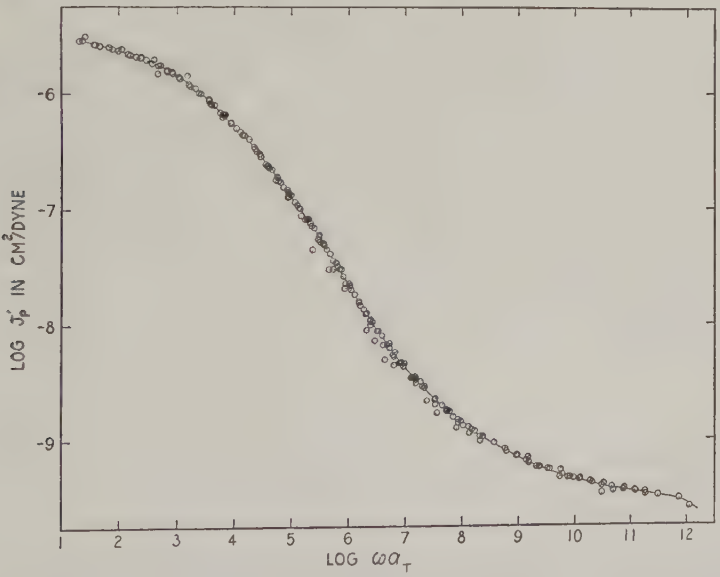

FIG. 2. Real part of the complex compliance, J', reduced to 100°C. and plotted logarithmically against reduced frequency with reduction factors calculated from the WLF equation. Temperature key by pips same as in Fig. 1.

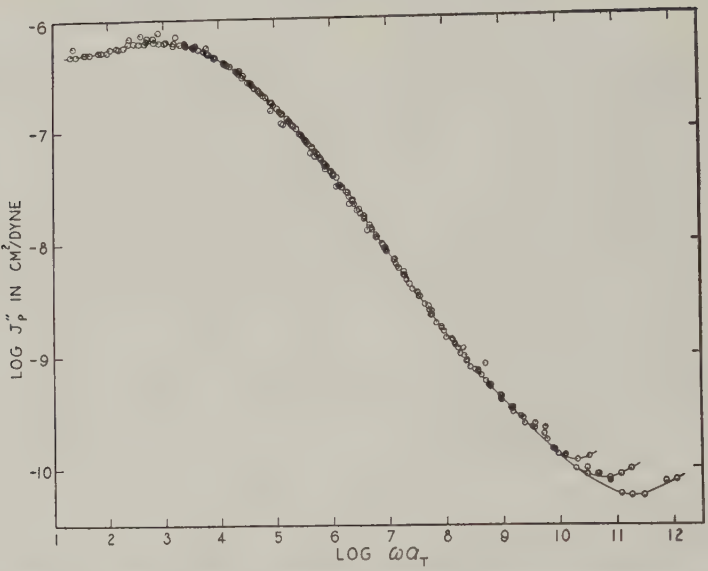

FIG. 3. Imaginary part of the complex compliance, J'', reduced and plotted in Fig. 2.

magnitude, though rather small as the corresponding values for the other methacrylate polymers have been.

DISCUSSION

Low-Temperature Reduction Anomaly

The anomalies in temperature reduction which appeared in poly-*n*-butyl and poly-*n*-hexyl methacrylate are absent here. However, at very high reduced frequencies J'' fails to superpose, and it passes through a minimum as though entering a new high-frequency dispersion region. This is probably what has previously been termed a β mechanism (1–3), attributable to motions of the side chains, but the data are not adequate here to analyze for its contribution as was done for the lower members of the homologous series. The measurements extended to a temperature only 6° above T_g. Further study over a wider frequency range near T_g would be of considerable interest.

Distribution Functions

The retardation spectrum, L, was calculated by the second approximation formulas of Williams and Ferry (8) from the data of Figs. 2 and 3. (At high reduced frequencies, the lowest values of J'' were chosen for the calculation.) The compliance data were also converted to the real and imaginary components of the complex shear modulus, G' and G'', and from these the relaxation spectrum, H, was calculated by the second approxi-

TABLE I

Retardation and Relaxation Spectra Reduced to 100°C.

	Log L_p (cm.^{2}/dyne)		Log H_p (dynes/cm.^{2})	
Log τ_p (*sec.*)	from J'	from J''	from G'	from G''
−12.0	—	−10.29	—	8.48
−11.5	−10.59	−10.39	8.13	8.45
−11.0	−10.57	−10.48	8.38	8.46
−10.5	−10.36	−10.35	8.47	8.47
−10.0	−10.22	−10.23	8.59	8.50
−9.5	−10.02	−10.01	8.65	8.61
−9.0	−9.79	−9.78	8.62	8.61
−8.5	−9.61	−9.53	8.53	8.51
−8.0	−9.35	−9.33	8.29	8.28
−7.5	−9.02	−9.00	7.85	7.87
−7.0	−8.71	−8.66	7.44	7.38
−6.5	−8.34	−8.22	7.05	7.05
−6.0	−7.89	−7.82	6.68	6.71
−5.5	−7.47	−7.42	6.31	6.39
−5.0	−7.12	−7.13	6.05	6.07
−4.5	−6.82	−6.83	5.75	5.76
−4.0	−6.60	−6.58	5.52	5.55
−3.5	−6.42	−6.40	5.29	5.28
−3.0	−6.36	−6.38	5.04	5.06
−2.5	−6.43	−6.40	4.85	4.86
−2.0	−6.47	−6.46	4.62	4.70
−1.5	−6.51	−6.47	4.34	4.61

mation formulas. Both spectra are given in Table I; the agreement between calculations from the real and imaginary components is in most cases excellent.

The relaxation spectrum is plotted logarithmically in Fig. 4, together with those for the α mechanisms of the n-hexyl, n-butyl, and ethyl polymers. Its shape is rather similar to the others' except for a new feature at short times, where there is a suggestion of a minimum to the left of the usual maximum, again indicative of a well-separated β mechanism in contrast to the overlapping β mechanism which has complicated the analysis of data for the previous polymers. The height of the maximum is $\log H = 8.64$, the lowest thus far found in the methacrylate series. The height of the maximum in the retardation spectrum is $\log L = -6.35$; the shape of this function and its relation to those of the other polymers will be discussed below.

Monomeric Friction Coefficient

By fitting the lower portion of the logarithmic relaxation spectrum, $\log H(\log \tau)$, to the theoretical slope of $-\frac{1}{2}$, the monomeric friction coefficient ζ_0 can be calculated from the equation (9)

$$\log \zeta_0 = 2 \log H + \log \tau + \log (6/kT) + 2 \log (2\pi M_0/a\rho N_0), \quad [2]$$

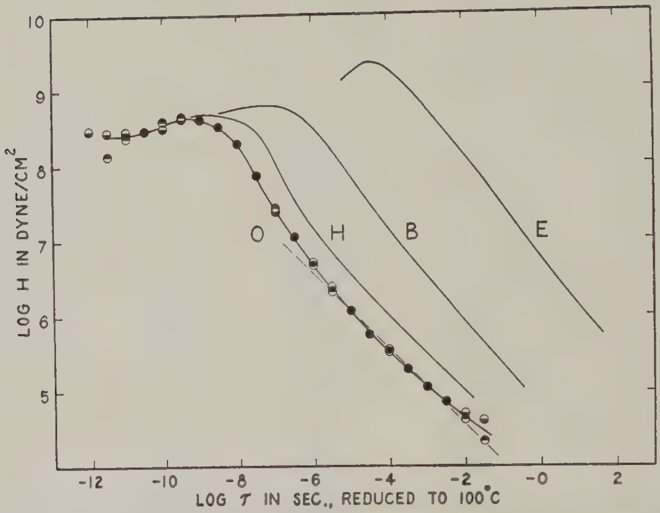

FIG. 4. Relaxation spectrum reduced to 100° (Curve O); points top black, from G'; bottom black, from G''. Curves H, B, and E are the relaxation spectra of the α mechanisms of n-hexyl, n-butyl, and ethyl methacrylate polymers reduced to 100°C.

where M_0 is the molecular weight of a monomer unit, ρ the density, N_0 Avogadro's number, and a the root-mean-square end-to-end distance per square root of the number of monomer units. For this purpose, a is taken as 7.0 A, derived from light-scattering measurements in a Θ-solvent (4). At 100°, log ζ_0 (in dynes-sec./cm.) is -5.78. Reduced to T_g, log $\zeta_0 = 2.54$. This is a very small value, but only slightly smaller than that for poly-n-hexyl methacrylate (3).

Comparisons of Four Methacrylate Polymers at 100°C.

Although further studies of the methacrylate series are planned, it is of interest to summarize now certain characteristics of the four polymers studied to date. First, a comparison at 100°, well above T_g for each polymer, reveals the effect of side chain length on mechanical properties at constant temperature. The spacings of the relaxation spectra in Fig. 4, as well as the values of log ζ_0 in Table II, show that with increasing side chain length the time scale shifts progressively but at a diminishing rate to shorter times. Moreover, the maximum in H progressively diminishes.

To compare the detailed shape of the spectra, the n-butyl polymer has been chosen as a reference and the others have been converted to corresponding states in the following way. Equation [2] shows that the position of H on the logarithmic time scale at the right where the theoretical slope is followed depends on the values of ζ_0, a, and ρ/M_0. The first two of these are concerned with microscopic properties of the monomer unit which influence the time scale of motions; while the ratio ρ/M_0 is a measure of the number of monomer units per cubic centimeter, which determines the magnitude of contributions to the spectrum. Equation [2] can be rearranged as

$$\log H - \log(\rho/M_0) = -\tfrac{1}{2}(\log \tau - \log a^2\zeta_0) + \text{constant}.$$

Thus a plot of the left side of the above against $\log \tau - \log a^2\zeta_0$ should be the same for all polymers in the region of the theoretical slope, and outside that region should provide a critical comparison of differences in shapes. In practice, for the present homologous series, it is more convenient to plot $\log H - \Delta \log (\rho/M_0)$ against $\log \tau - \Delta \log a^2\zeta_0$, where Δ refers to the difference between a given polymer and the n-butyl reference; then the curve for each polymer should correspond with that for the n-butyl. Values of the Δ shifts are given in Table II, and the plot is shown in Fig. 5.

It is particularly notable that the maxima of the n-butyl, n-hexyl, and n-octyl polymers are now practically identical, showing that their heights in Fig. 4 differ only because of "dilution" of the backbones by the side chains in accordance with the factor ρ/M_0. The maximum for the ethyl is somewhat in doubt because the original data were dominated by the β mechanism in this region and the separation of mechanisms was not certain. The four spectra in the transition region lie quite near together, although that for n-butyl most closely resembles ethyl and that for n-octyl most closely resembles n-hexyl.

It may be remarked that the product $a^2\zeta_0$, unlike ζ_0 itself, is independent of the choice of the value of a. The procedure we have followed, taking a from dilute solution measurements at room temperature and assuming it to be the same for the undiluted polymer at 100°, may introduce some uncertainty into $\Delta \log \zeta_0$ but not into $\Delta \log a^2\zeta_0$.

Perhaps the most interesting feature of this treatment is that the time scale shift, $\Delta \log a^2\zeta_0$, can be attributed to differences in free volume at constant temperature just as in a single polymer the temperature-dependent factor a_T can be related to changes in free volume. The WLF equation (7)

TABLE II

Comparison of Four Methacrylate Polymers

	Ethyl	n-Butyl	n-Hexyl	n-Octyl
Log ζ_0 at 100°C. (in dynes-sec./cm.)	−0.21	−3.51	−5.21	−5.78
a in A	5.9	6.4	7.5	7.0
Δ log ($a^2\ \zeta_0$) referred to n-butyl	3.23	0	−1.56	−2.19
Δ log (ρ/M_0) referred to n-butyl	0.13	0	−0.10	−0.18
f at 100°C. from data of Ref. (5)	0.033	0.042	0.047	0.050
f at 100°C. from Eq. [3]	0.032	(0.042)	0.049	0.053
Log ζ_0 at T_g (in dynes-sec./cm.)	6.22	3.74	2.63	2.54
f_g from WLF analysis	0.025	0.026	0.025	0.027

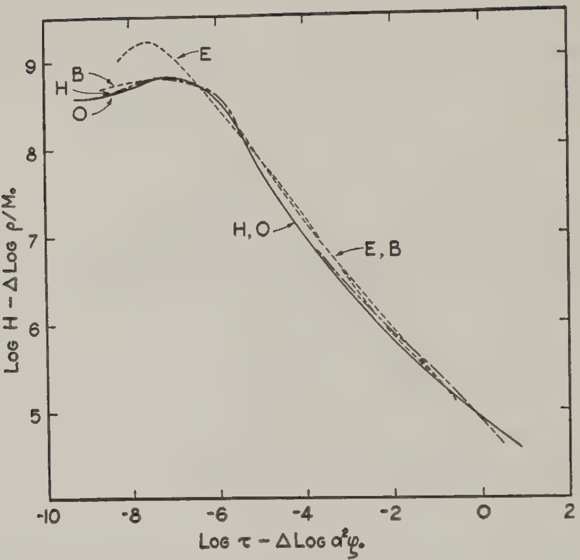

FIG. 5. Relaxation spectra of the ethyl (*E*), *n*-butyl (*B*), *n*-hexyl (*H*), and *n*-octyl (*O*) polymers at 100°C. reduced to the reference state of the *n*-butyl by the procedure described in the text. (Except for octyl, the spectra refer to the α mechanism only.)

is derived from the relation modified from Doolittle (10)

$$\log a_T = (1/2.303)(1/f - 1/f_g),$$

where a_T is the ratio of any relaxation time at temperature T to that at T_g, and f and f_g are the fractional free volumes at T and T_g. If the differences in relaxation times between individual polymers in the series are similarly related to free volume, the corresponding relation is

$$\Delta \log a^2\zeta_0 = (1/2.303)(1/f_i - 1/f_B), \qquad [3]$$

where f_B and f_i are the fractional free volumes of the reference (*n*-butyl) polymer and the other polymer compared with it.

Rogers and Mandelkern (5) have concluded that in the methacrylate polymer series 15% of the added specific volume associated with increasing side chain length can be attributed to free volume. From their data, the specific volumes per g. at 100°C. can be compared and the differences in free volume per g. estimated to be −0.012, 0, 0.007, and 0.012 c.c./g. for the ethyl, *n*-butyl, *n*-hexyl, and *n*-octyl polymers at this temperature. The value of f (free volume per cubic centimeter) is obtained for the *n*-butyl from the "universal" estimate of 0.025 at T_g (7) with the difference in thermal expansion coefficients $\Delta\alpha$ (5); it is 0.042 at 100°, and the values for the other polymers are obtained by difference. Finally, using the same value of 0.042 for f_B in Eq. [3], the values of f for the other polymers are calculated from $\Delta \log a^2\zeta_0$, and as shown in Table II they are in moderately good agreement.

Next, the retardation spectra are plotted in corresponding states with the n-butyl polymer as reference, as shown in Fig. 6. The curves lie very near each other except at the long-time end where the maxima still differ considerably in height. This suggests that the disposition of the Bueche entanglements is altered by increasing side chain length, over and above the "dilution" in accordance with the factor ρ/M_0 as previously considered by Bueche (11). In fact, $L_{\max}$ is approximately proportional to $(\rho/M_0)^{-3}$ instead of to $(\rho/M_0)^{-1}$. A similar dependence on plasticizer concentration has been noted in studies which will be reported subsequently (12). (For the n-butyl and n-hexyl polymers, $L_{\max}$ also depends on temperature to some extent; the curves in Fig. 6, taken from the original composite plots, reflect measurements at 130° and 125°C., respectively. Strict comparison at 100° would exaggerate slightly the differences seen in Fig. 6 without changing the above conclusions.)

Comparisons of Four Methacrylate Polymers at T_g

When each polymer is compared at its own T_g, the friction coefficients still differ considerably, as shown in the next to last line of Table II, though those for the n-hexyl and n-octyl are nearly equal. But the fractional free volume (as derived by WLF analysis of the temperature dependence of relaxation times) is substantially the same for all. Thus it is clear that, un-

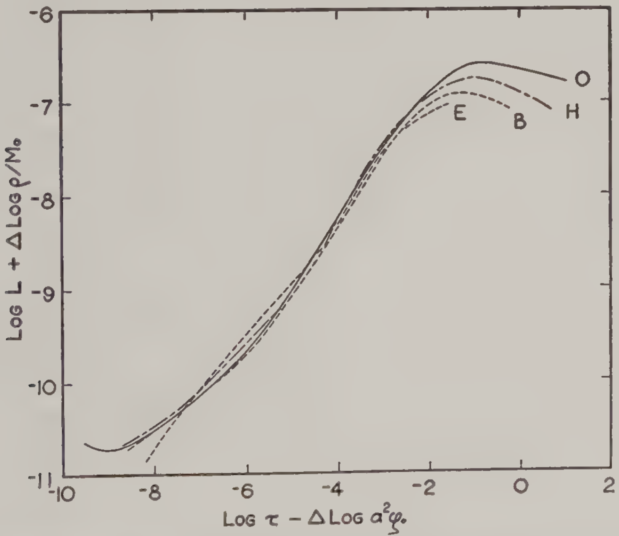

FIG. 6. Retardation spectra of the four polymers, identified as in Fig. 5, reduced to the reference state of the n-butyl by the procedure described in the text. (Except for octyl, the spectra refer to the α mechanism only.)

like the situation far above T_g, the relative friction coefficients are not determined by free volume alone. At T_g where there is very little free volume to spare, steric effects of specific local geometry are important, and the shorter the side chain, the more firmly the backbone can become interlocked with its neighbors. Well above T_g where the structure is expanded, the local steric relationships are less important and the mobility is primarily determined by the average free volume alone. Actually, the discrepancies in the calculated values of f in Table II would correspond to a small residual steric effect. Similar suggestions have been made to explain the differences between viscoelastic mobility and the mobility of small foreign molecules in diffusion (9).

Acknowledgments

This work was supported in part by Picatinny Arsenal, Ordnance Corps, Department of the Army, and in part by a grant from Esso Research and Engineering Corporation to the Department of Chemistry, University of Wisconsin. We are indebted to Mrs. Garrett Droppers and Mrs. William C. Frazier for making most of the calculations.

Summary

The real (J') and imaginary (J'') components of the complex compliance have been measured between 15 and 3600 cycles/sec. in the temperature range from −14° to 130°C. for a fractionated poly-*n*-octyl methacrylate with molecular weight 3.62×10^6. The method of reduced variables gave superposed curves for J' and J'' except for an anomaly at the lowest temperatures where J'' passes through a minimum and fails to superpose, suggesting the onset of a β mechanism. The temperature dependence of relaxation times follows the WLF form with f_g (relative free volume at the glass transition temperature, T_g) = 0.027 and α_f (thermal expansion coefficient of free volume) = 2.5×10^{-4} deg.$^{-1}$. The relaxation and retardation spectra, reduced to 100°C., resemble in shape those for the other methacrylates studied except for minor features. The logarithm of the monomeric friction coefficient (in dynes-sec./cm.) is −5.78 at 100°C. and 2.54 at −20°C. (T_g). The relaxation and retardation spectra for the ethyl, *n*-butyl, *n*-hexyl, and *n*-octyl polymers at 100°C. can be brought into corresponding states (choosing the butyl as reference) by adjusting the magnitudes with a dilution factor representing the number of monomoles per unit volume and the time scales with a factor derived from the friction coefficients. Their positions then agree very closely at short times and moderately well in the transition zone, but near the maximum of the retardation spectrum there are residual differences, probably associated with the Bueche entanglements. The time scale adjustments can be fairly well accounted for by the differences in free volume at 100°C. as deduced by Rogers and Mandelkern.

References

1. Ferry, J. D., Child, W. C., Jr., Zand, R., Stern, D. M., Williams, M. L., and Landel, R. F., *J. Colloid Sci.* **12,** 53 (1957).
2. Child, W. C., Jr., and Ferry, J. D., *J. Colloid Sci.* **12,** 327 (1957).
3. Child, W. C., Jr., and Ferry, J. D., *J. Colloid Sci.* **12,** 389 (1957).
4. Chinai, S. N., Resnick, A. L., and Lee, H. T., to be published.
5. Rogers, S. S., and Mandelkern, L., *J. Phys. Chem.* **61,** 985 (1957).
6. Ferry, J. D., and Fitzgerald, E. R., *J. Colloid Sci.* **8,** 224 (1953).
7. Williams, M. L., Landel, R. F., and Ferry, J. D., *J. Am. Chem. Soc.* **77,** 3701 (1955).
8. Williams, M. L., and Ferry, J. D., *J. Polymer Sci.* **11,** 169 (1953).
9. Ferry, J. D., and Landel, R. F., *Kolloid-Z.* **148,** 1 (1956).
10. Doolittle, A. K., *J. Appl. Phys.* **23,** 236 (1952).
11. Bueche, F., *J. Appl. Phys.* **26,** 738 (1955).
12. Stern, D. M., Ph.D. Thesis, University of Wisconsin, Madison, 1957.

JOURNAL OF COLLOID SCIENCE **13,** 114–124 (1958)

THEORY OF TURBULENT EVAPORATING CLOUDS

Richard H. Milburn[1]

Chemical Corps, Fort Detrick, Frederick, Maryland

Received November 18, 1957

Abstract

A theory is deduced to describe the evaporation dynamics of turbulent clouds of water droplets. The formulation of the macroscopic transfer processes is in terms of the "eddy diffusivities" familiar to meteorologists. It is shown that the effects characteristic of evaporation arise from a nonlinear source term which is appended to the diffusion equation describing the behavior of nonvolatile particles and gases under similar conditions. A form of psychrometric equation is found to relate the temperatures and vapor concentrations throughout the cloud.

I. Introduction

In a previous article the author has described a mathematical theory of evaporating water clouds (1). It was there assumed that the water droplets were fixed in space and were initially all of the same size.

This paper extends the previous work in a logical manner to turbulent clouds, in which occurs a continual mixing of droplets in various stages of evaporation. The formulation of the basic heat, vapor, and particulate transfer processes is given in terms of the "eddy diffusivities" familiar to meteorologists (*cf.* Sutton (2), Chapters 3, 4, and 8; also Sutton (3) and U. S. Weather Bureau (4)). These diffusivities enter as more or less empirical quantities in the study of the lower atmosphere, and have been applied extensively to examinations of the behavior of clouds of nonvolatile materials. The essential contribution of the following paper is to show that the primary effects of the heat and vapor transfer involved in evaporation processes may be described by the addition of a nonlinear source term to the homogeneous differential diffusion equation which is the basis of existing cloud travel studies (Sutton (3), pp. 35 ff.).

The numerical solution of the resulting cloud equation is considered beyond the scope of this paper. The effect of the evaporating cloud, acting as a heat sink, upon the atmospheric motions themselves also is not discussed. Some aspects of the latter very complicated problem are considered in the literature (Sutton (2), pp. 295 ff. ; Hewson (5)).

---

[1] Now at Department of Physics, Harvard University, Cambridge, Massachusetts.

II. The Physical Model

The present study utilizes the two physical assumptions applied earlier (Milburn (1), Sections II*a* and III*b*). These permit the vapor concentrations and temperatures to be described by continuous functions of space and time. In addition, the evaporation of individual droplets is assumed to be describable by "quasistatic" or equilibrium-flow equations. This means that the usual transient terms are already damped out—a very rapid process relative to normal cloud lifetimes—for aerosol-sized particles. It also is assumed to mean that the cloud droplets are able to attain their equilibrium temperatures before saturation is reached. This requires that a certain minimum evaporation of each droplet be allowed to occur.

It was found earlier that both of the conditions will hold for an initially homogeneous cloud provided the starting concentration of water in droplet form is suitably restricted—a situation found to exist in most practical cases (*cf.* Milburn (1), Sections III*b* and V*a*). Even in a turbulent and initially heterogeneous cloud the local flow and temperature equilibria required by the second assumption would be expected to occur rapidly under the same concentration restrictions.

The description of the physical transport processes resulting from atmospheric molecular properties and turbulent motions will be based upon differential *operators* having the general form (Sutton (2), Chapters 3, 4, and 8; Sutton (3); and U. S. Weather Bureau (4)):

$$\mathfrak{D} = \partial_t + \nabla\cdot\mathbf{v} - \nabla\cdot[\mathbf{K}\cdot\nabla]. \qquad [1]$$

Here the vector $\mathbf{v}$ represents the local mean velocity of the atmosphere relative to a fixed coordinate system, while the dyadic $\mathbf{K}$ describes the transfer arising from processes such as molecular diffusion, heat conduction and convection, and turbulent mixing. In general the coefficients $\mathbf{v}$ and $\mathbf{K}$ will depend in a complicated way upon the detailed motions of the atmosphere and will be functions of position. Let $\chi(\mathbf{r}, t)$ be a density function representing some physical property of the atmosphere such as the vapor concentration or particle density at $(\mathbf{r}, t)$. Application of the divergence theorem to an equation of the form $\mathfrak{D}\chi(\mathbf{r}, t) = \eta(\mathrm{r}, t)$ shows that the function $\eta(\mathrm{r}, t)$ represents an instantaneous source density of the quantity described by $\chi(\mathbf{r}, t)$.

Deductions based upon the detailed forms of the operator $\mathfrak{D}$ in Eq. [1] will not be made in the present study. Indeed, it will be assumed that all equations of the form $\mathfrak{D}\chi = 0$, with boundary conditions specified, may be solved in detail for $\chi(\mathbf{r}, t)$. It is upon the equation $\mathfrak{D}\chi = 0$, in various forms, that most existing mathematical studies of cloud travel have been based. It is not intended here to minimize the difficulty of obtaining such solutions for particular meteorological environments. For homogeneous isotropic diffusion $\mathbf{v} = 0$, $\mathbf{K}$ is a constant multiple of the unit dyadic, and $\mathfrak{D} = \partial_t - K\nabla^2$, an operator leading to exact solutions in a variety of cases. More complicated dependences of $\mathbf{v}$ and $\mathbf{K}$ upon position have been studied as well (Sutton (2), Chapters 4, 6, and 8; and Sutton (6)). It is evident that the additional consideration of evaporation processes cannot simplify a physical situation already very complicated.

III. THE TRANSPORT EQUATIONS

The notation used will be that of the earlier paper, with suitable augmentation (*cf.* Milburn (1), Table I). The fields $c(\mathbf{r}, t)$ and $T(\mathbf{r}, t)$ are defined as functions of position and time representing the mean vapor concentration and temperature, respectively, at points distant from the surfaces of the individual droplets making up the cloud. Let $C_0(\mathbf{r}, t)$ and $T_0(\mathbf{r}, t)$ similarly refer to quantities immediately over the surfaces of droplets at $(\mathbf{r}, t)$. Thus the empirical relationship determining the saturated vapor pressure over a water surface may be expressed as the equation $C_0 = C_0(T_0)$. Define $n(m, \mathbf{r}, t)$ as the number density (per cm.^{3}) of droplets in a unit mass interval at $(\mathbf{r}, t)$. Similarly let $W(m, \mathbf{r}, t)$ be the time rate with which a particle of mass m at $(\mathbf{r}, t)$ increases its mass.

Under the assumptions of Section II, the evaporation of the individual droplets will be governed by the quasistatic equation appropriate to spheres,

$$W(m, \mathbf{r}, t) = (3/2)\alpha m^{1/3}[c(\mathbf{r}, t) - C_0(\mathbf{r}, t)], \qquad [2]$$

where $\alpha = (8\pi D/3)(3/4\pi\rho_W)^{1/3}$, D is the molecular diffusivity of water vapor in air, and ρ_W is the density of water. Equation (2) neglects the effect of atmospheric turbulence upon the rate of evaporation from individual droplets. It has been estimated that for such turbulence the boundary layer inside of which molecular diffusion takes place is of the order of millimeters thick (7). Since the usual cloud droplet has a radius less than 1% of this, the spatial integration across the boundary layer may be replaced by one out to infinity, giving Eq. [2] directly.

The evaporation of a droplet requires that heat be conducted in from the surroundings to supply the latent heat of vaporization, L. Again local turbulence effects may be neglected, giving an equation similar to [2],

$$LW(m, \mathbf{r}, t) = -(k/D)(3\alpha/2)m^{1/3}[T(\mathbf{r}, t) - T_0(\mathbf{r}, t)]. \qquad [3]$$

Here k is the thermal conductivity of air.

It may be argued in connection with Eqs. [2] and [3] that diffusion in a temperature gradient is more accurately represented by an equation in partial vapor pressures than by one in vapor concentration. At practical temperatures there is but little difference, however. The use of vapor concentrations in the present work yields relations having direct physical interpretation and is, moreover, not an essential feature of the development. Stefan's correction is also of negligible interest in this discussion (8).

The mass-rate per unit volume with which vapor is condensed into droplet form is given by the product $W(m, \mathbf{r}, t)n(m, \mathbf{r}, t)$ integrated over all masses from zero to infinity. Letting $\mathfrak{D}_c$ be a transport operator of the general form Eq. [1], characteristic of vapor transfer, the function $c(\mathbf{r}, t)$ will be described by

$$\mathfrak{D}_c c(\mathbf{r}, t) = -\int_0^\infty dm W(m, \mathbf{r}, t)n(m, \mathbf{r}, t). \qquad [4]$$

The temperature field throughout the cloud will be governed by an equation similar to [4], involving, however, perhaps a different operator $\mathfrak{D}_T$. It is of greater meteorological significance to use, instead of the mean air temperature $T(\mathbf{r}, t)$, rather the "potential temperature" $\vartheta(\mathbf{r}, t)$. Customarily $\vartheta(\mathbf{r}, t)$ is defined as the temperature that an element of air would have were it transported adiabatically to some standard altitude, usually the earth's surface (Sutton (2), p. 10). Thus in a perfectly mixed atmosphere $\vartheta(\mathbf{r}, t)$ would be a constant at all altitudes. In an isobaric environment ϑ and T may be identified. Atmospheric heat transfer may be described by an equation of the form $\mathfrak{D}_T\vartheta = 0$ (Sutton (2), pp. 145 ff.). Nonlinear modifications to $\mathfrak{D}_T$ are also described in this reference to represent the influence of free thermal convection in preventing the occurrence in practice of the equilibrium state $\vartheta = constant$. Such effects will be omitted in the following discussion. Inclusion of the heat sinks provided by the evaporating droplets gives the equation

$$\mathfrak{D}_T\vartheta(\mathbf{r}, t) = (L/\rho_a c_p)\int_0^\infty dm W(m, \mathbf{r}, t)n(m, \mathbf{r}, t). \qquad [5]$$

Here ρ_a is the density of air and c_p is the specific heat of air at constant pressure, both assumed constant. In this equation the effects of radiation are neglected. Over a long time period these can be important for certain types of meteorological clouds (5).

One additional equation is required to govern the changes in the particle mass distribution effected by the evaporation process. The number of droplets in a small mass interval Δm located at $\mathbf{r}$ at time t is given by $n(m, \mathbf{r}, t)\Delta m$. Let $\mathfrak{D}_n$ be the transport operator characteristic of the turbulent diffusion of the droplets themselves. Then, were there no evaporation occurring, the conservation of particles in the mass interval Δm yields the usual equation $\mathfrak{D}_n n(m, \mathbf{r}, t) = 0$. However, in the present case droplets may enter the interval $m \to m + \Delta m$ by evaporating down from larger masses, and may leave by evaporating further into smaller masses. The net rate of increase of particle number in the interval Δm is then given by

$$n(m, \mathbf{r}, t)W(m, \mathbf{r}, t) - n(m + \Delta m, \mathbf{r}, t)W(m + \Delta m, \mathbf{r}, t). \qquad [6]$$

Proceeding to the limit $\Delta m \to 0$, the equation for the particle density distribution function becomes

$$\mathfrak{D}_n n(m, \mathbf{r}, t) = -\partial_m[n(m, \mathbf{r}, t)W(m, \mathbf{r}, t)]. \qquad [7]$$

The five equations [2], [3], [4], [5], and [7], together with the equations for the saturated vapor pressure as a function of temperature and for ϑ as a function of T and position, provide, with suitable boundary conditions, a defining system for the seven variables c, C_0, ϑ, T, T_0, W, and n.

IV. THE PSYCHROMETRIC EQUATION

A number of the dependent variables may be conveniently eliminated at once. From Eqs. [2] and [3] the variable W can be removed to give the equation

$$[c(\mathbf{r}, t) + (k/LD)T(\mathbf{r}, t)] = [C_0(\mathbf{r}, t) + (k/LD)T_0(\mathbf{r}, t)]. \qquad [8]$$

It is now assumed that the operators $\mathfrak{D}_c$ and $\mathfrak{D}_T$ are essentially identical. This is approximately the case for strictly molecular transport processes, and would appear to be physically reasonable for turbulent transfer also. Empirically this seems to be true for stable atmospheres, but not for large lapse rates (Sutton (2), p. 318). However, $\mathfrak{D}_c = \mathfrak{D}_T \equiv \mathfrak{D}$ will be assumed in all that follows. By this means the source terms in Eqs. [4] and [5] may be eliminated to give

$$\mathfrak{D}[c(\mathbf{r}, t) + (\rho_a c_p/L)\vartheta(\mathbf{r}, t)] = 0. \qquad [9]$$

Define the variable

$$\phi(\mathbf{r}, t) = c(\mathbf{r}, t) + (\rho_a c_p/L)\vartheta(\mathbf{r}, t). \qquad [10]$$

Physical requirements restrict $\phi(\mathbf{r}, t)$ to being continuous and differentiable for all points and times $(\mathbf{r}, t)$. Moreover the initial values of $c(\mathbf{r}, t)$ and $\vartheta(\mathbf{r}, t)$ are presumed to be given, so that $\phi(\mathbf{r}, 0)$ is known. Spatial boundary conditions on $\phi(\mathbf{r}, t)$ will also be known. Since it was assumed in Section II that all equations of the form $\mathfrak{D}\phi = 0$, with boundary conditions, can be solved in detail, the function $\phi(\mathbf{r}, t)$ of Eq. [10] will henceforth be considered to be completely known. It should be noticed that $L\phi(\mathbf{r}, t)$ corresponds essentially to the available heat energy per unit volume of space, and that $\mathfrak{D}\phi = 0$ represents the overall conservation of this energy during the cloud dissipation process.

Over moderate ranges of altitude $\vartheta(\mathbf{r}, t) = T(\mathbf{r}, t) + f(\mathbf{r})$, where $f(\mathbf{r})$ is a known function of altitude (Sutton (2), p. 11). Moreover, $\rho_a c_p = k/\kappa$, where κ is the molecular heat diffusivity of air. With these substitutions

Eqs. [8] and [10] may be combined and written in the form

$$[C_0(\mathbf{r}, t) + (k/L\kappa)T_0(\mathbf{r}, t)] = \phi(\mathbf{r}, t) - (k/L\kappa)f(\mathbf{r}) - (k/L)(\kappa^{-1} - D^{-1})[T(\mathbf{r}, t) - T_0(\mathbf{r}, t)]. \quad [11]$$

Empirically D and κ are of similar magnitude for water vapor at normal temperatures. (At 20°C. D is about 0.225 cm.^{2} sec.$^{-1}$ and κ about 0.200 cm.^{2} sec.$^{-1}$, using values of D and k quoted by Ranz and Marshall (9)). If D and κ are taken to be essentially equal, the third term on the right of Eq. [11] is removed leaving the psychrometric equation

$$[C_0(\mathbf{r}, t) + (k/L\kappa)T_0(\mathbf{r}, t)] = \phi(\mathbf{r}, t) - (k/L\kappa)f(\mathbf{r}). \quad [12]$$

The right-hand side of Eq. [12] is a known function of $(\mathbf{r}, t)$. Since C_0 is also a known empirical function of T_0, Eq. [12] may be solved numerically for $C_0(\mathbf{r}, t)$ and $T_0(\mathbf{r}, t)$.

The interpretation of Eq. [12] is simplified by considering the case of an atmosphere having an initially constant vapor concentration and potential temperature (corresponding to an adiabatic lapse rate). Providing $\mathfrak{D}$ has the linear homogeneous form of Eq. [1], Eq. [9] has the solution

$$\phi(\mathbf{r}, t) = C_i + (k/L\kappa)\vartheta_i, \quad [13]$$

where C_i and ϑ_i are the initial concentration and potential temperature values, respectively. Substitution of Eq. [13] into Eq. [12] yields

$$[C_0(\mathbf{r}, t) - C_i] = -(k/L\kappa)[T_0(\mathbf{r}, t) - T_i(\mathbf{r})], \quad [14]$$

where $T_i(\mathbf{r})$ is the actual initial temperature at the altitude corresponding to $\mathbf{r}$. Equation [14] is just a form of the familiar wet-bulb psychrometer equation (10), and shows that all droplets in the cloud will attain the constant wet-bulb temperature appropriate to the initial properties of the air at the same altitude. This constancy is true only for the special case considered.

It is interesting to observe that although an equation very similar to Eq. [11] can be derived for the evaporation of a single droplet in an otherwise free atmosphere, it is Eq. [14], based upon the assumption that $D = \kappa$, which seems to give the truest representation of empirical wet-bulb temperatures. This anomaly, in view of the apparent measured disparity of D and κ, does not seem to be fully understood (11).

Henceforth it will be assumed that the fields $C_0(\mathbf{r}, t)$ and $T_0(\mathbf{r}, t)$ have been calculated from Eq. [12]. Also, once $c(\mathbf{r}, t)$ has been determined, the temperatures $\vartheta(\mathbf{r}, t)$ and $T(\mathbf{r}, t)$ may be found directly from Eq. [10] and $\vartheta(\mathbf{r}, t) = T(\mathbf{r}, t) + f(\mathbf{r})$. In view of these simple relations, the temperature fields will not enter further into this discussion.

V. Mass Conservation

Using Eq. [2], in which $C_0(\mathbf{r}, t)$ is a known function, $W(m, \mathbf{r}, t)$ may be eliminated from Eqs. [4] and [7]. Thus

$$\mathfrak{D}c(\mathbf{r}, t) = -(3\alpha/2)[c(\mathbf{r}, t) - C_0(\mathbf{r}, t)] \int_0^\infty dm m^{1/3} n(m, \mathbf{r}, t), \qquad [15]$$

and

$$\mathfrak{D}_n n(m, \mathbf{r}, t) = -(3\alpha/2)[c(\mathbf{r}, t) - C_0(\mathbf{r}, t)]\{\partial_m[m^{1/3} n(m, \mathbf{r}, t)]\}. \qquad [16]$$

These two equations are to be solved for $c(\mathbf{r}, t)$ and $n(m, \mathbf{r}, t)$ with boundary conditions such as

$$\begin{gathered} n(m, \mathbf{r}, 0) \text{ given} \\ c(\mathbf{r}, 0) = c(\infty, t) = C_i \\ n(m, \infty, t) = n(\infty, \mathbf{r}, t) = 0 \end{gathered} \qquad [17]$$

along with suitable spatial symmetry conditions.

Equation [16] may be multiplied by m and integrated over m from zero to infinity. If the right-hand side of the resulting equation is integrated by parts, the integrated term will vanish as a result of the conditions in Eq. [17] and because the integral in Eq. [15] must converge at the origin. The remainder, combined with Eq. [16], yields the equation

$$\mathfrak{D}c(\mathbf{r}, t) + \mathfrak{D}_n \int_0^\infty dm m n(m, \mathbf{r}, t) = 0. \qquad [18]$$

If Eq. [18] is integrated over all space the result is just a statement that the total mass of water in vapor and condensed forms is conserved, as is to be expected from a physically consistent set of transfer equations [2]–[7]. It may similarly be verified from Eq. [16] that the total number of droplets is conserved except for those which evaporate away to nothingness or otherwise leave the system at the boundaries.

VI. Special Case of Static Clouds

It is of interest to show that the system of Eqs. [15] and [16] reduces under appropriate conditions to the special case of static clouds studied earlier (1). The assumption that the droplets remain fixed in space may be satisfied by taking the droplet transfer operator to be of the form $\mathfrak{D}_n = \partial_t$. It was also assumed in the earlier paper that the initial droplets were all of the same mass. Since the droplets do not move around in space, all droplets at a given position and time will have the same mass. Thus the droplet distribution function may be replaced by

$$n(m, \mathbf{r}, t) = \begin{cases} n_0 \delta[m - m(\mathbf{r}, t)], & m(\mathbf{r}, t) \geq 0 \\ 0, & m(\mathbf{r}, t) < 0 \end{cases} \qquad [19]$$

where n_0 is the constant droplet density within the cloud, $\delta(m)$ is the unit impulse (or delta) function, and $m(\mathbf{r}, t)$ is the mass of each of the individual droplets at $(\mathbf{r}, t)$. Substituting for $\mathfrak{D}_n$ and $n(m, \mathbf{r}, t)$ in Eqs. [16] and [18] leads to the equations

$$\partial_t m^{2/3}(\mathbf{r}, t) = \alpha[c(\mathbf{r}, t) - C_0(\mathbf{r}, t)], \qquad [20]$$

and

$$\mathfrak{D}c(\mathbf{r}, t) + n_0\partial_t m(\mathbf{r}, t) = 0, \qquad [21]$$

respectively. To achieve Eq. [20], Eq. [16] is multiplied by m and integrated over m from zero to infinity, as in Section V. Elimination of $c(\mathbf{r}, t)$, and the assumption of isobaric conditions so that C_0 is constant (Eq. [14]), yields

$$\mathfrak{D}\partial_t m^{2/3}(\mathbf{r}, t) + \alpha n_0\partial_t m(\mathbf{r}, t) = 0. \qquad [22]$$

The transport operator $\mathfrak{D} = \partial_t - D\nabla^2$ in the absence of turbulence or convection. Also Eq. [22] may be integrated with respect to time, assuming all particles have the initial mass m_0. This leads to

$$\mathfrak{D}m^{2/3}(\mathbf{r}, t) + \alpha n_0 m(\mathbf{r}, t) = \alpha[n_0 m_0 - (C_0 - C_i)], \qquad [23]$$

which is equivalent to the fundamental nonlinear equation found earlier (Milburn (1), Eq. [13]).

VII. Turbulent Clouds

It is now assumed that sufficient turbulence is present for the eddy diffusion processes to dominate completely all other forms of heat, vapor, and particle transfer. Mathematically this is taken to mean that $\mathfrak{D}_n = \mathfrak{D}$. This assumption clearly limits consideration to droplets small enough for the maximum gravitational fall-out velocity to be negligible relative to the eddy and convective velocities making up the bulk of $\mathfrak{D}_n$. In addition, particle loss at the spatial boundaries should be small. If these conditions do not hold, the pair of equations [15] and [16] must be solved simultaneously as they stand. Even for droplets of negligible size the identification of the particle and vapor transport operators is subject to some dispute (Sutton (2), p. 318). Nonetheless setting $\mathfrak{D}_n = \mathfrak{D}$ should form a limiting case which will represent fairly well the major features of the turbulent mixing process.

Defining the function

$$\psi(\mathbf{r}, t) = c(\mathbf{r}, t) + \int_0^\infty dm\, m n(m, \mathbf{r}, t), \qquad [24]$$

Eq. [18] becomes

$$\mathfrak{D}\psi(\mathbf{r}, t) = 0. \qquad [25]$$

Since the initial values and spatial boundary conditions for $c(\mathbf{r}, t)$ and $n(m, \mathbf{r}, t)$ are known, the same will be the case for $\psi(\mathbf{r}, t)$. Thus, as was earlier assumed for $\phi(\mathbf{r}, t)$ of Eq. [10], $\psi(\mathbf{r}, t)$ will henceforth be considered a completely determined function.

Equation [24] may now be used to eliminate $c(\mathbf{r}, t)$ from Eq. [16]. Thus

$$\mathfrak{D}n(m, \mathbf{r}, t) = (3\alpha/2)\{\partial_m[m^{1/3}n(m, \mathbf{r}, t)]\} \cdot \left\{\int_0^\infty dm\,mn(m, \mathbf{r}, t) + C_0(\mathbf{r}, t) - \psi(\mathbf{r}, t)\right\}. \qquad [26]$$

This is the basic nonlinear integro-differential equation for the determination of the droplet mass distribution $n(m, \mathbf{r}, t)$. It is seen that all the effects of evaporation are contained in the right-hand side of Eq. [26], and that the apparent source term provided by these effects vanishes for nonvolatile droplets. The remaining equation, $\mathfrak{D}n(m, \mathbf{r}, t) = 0$, is just that for the propagation of clouds of gas, dust, or smoke (Sutton (3), pp. 35 ff.). The boundary conditions of Eq. [17] are to be applied to the solution of Eq. [26].

VIII. Dimensionless Equation

It may be desirable for computational purposes to put Eq. [26] into a simplified, dimensionless form. Let R be a distance characteristic of the size of the cloud, and define the dimensionless spatial vector $\mathbf{x} = \mathbf{r}/R$. Also let K_0 be the characteristic scalar magnitude of the eddy diffusivity dyadic $\mathbf{K}$, and define $\mathbf{\Lambda} = \mathbf{K}/K_0$. Thus the transport operator Eq. [1] becomes $\mathfrak{D} = (K_0\pi^2/R^2)\mathfrak{D}_s$, where

$$\mathfrak{D}_s = \partial_s + \nabla_x \cdot \mathbf{u} - \frac{1}{\pi^2}\nabla_x \cdot [\mathbf{\Lambda} \cdot \nabla_x], \qquad [27]$$

dimensionless times are defined by $s = (K_0\pi^2/R^2)t$, and $\mathbf{u} = (R/\pi^2K_0)\mathbf{v}$ is a dimensionless convection velocity.

Let m_0 be a characteristic droplet mass, and define $\zeta = m^{2/3}/m_0^{2/3}$. Let n_0 be a measure of the droplet density,

$$\nu(\zeta, \mathbf{x}, s) = \zeta^{1/2}n_0^{-1}m_0n(m, \mathbf{r}, t), \qquad [28]$$

and

$$\delta^2 = (4/\pi)(D/K_0)n_0R^3(r_0/R), \qquad [29]$$

where $r_0 = (3m_0/4\pi\rho_W)^{1/3}$. Then the cloud equation [26] becomes

$$\mathfrak{D}_s\nu(\zeta, \mathbf{x}, s) = \delta^2[\partial_\zeta\nu(\zeta, \mathbf{x}, s)]\left\{\int_0^\infty d\zeta\,\zeta^{3/2}\nu(\zeta, \mathbf{x}, s) + \gamma(\mathbf{x}, s)\right\}, \qquad [30]$$

where

$$\gamma(\mathbf{x}, s) = \frac{2}{3}\left[\frac{C_0(\mathbf{x}, s) - \psi(\mathbf{x}, s)}{m_0 n_0}\right] \qquad [31]$$

is a previously computed known function of $(\mathbf{x}, s)$, from Eqs. [12] and [25]. It is Eq. [30] which, with known conditions initially and at the spatial boundary, must be solved for the variable $\nu(\zeta, \mathbf{x}, s)$ to describe the detailed history of the cloud.

It is worth while noting that δ^2 defined by Eq. [29] is a simple generalization to turbulent clouds of the "cloudiness" defined earlier for static clouds (Milburn (1), Eq. [16]). Other conditions being equal, it may be inferred crudely that a turbulent cloud is less "cloudy" than a static one (within the sense of reference (1)) in the ratio D/K_0. The time scale of the turbulent dissipation process will be shorter in the same ratio.

IX. Conclusion

It will be observed that the theory developed in this paper depends upon a variety of assumptions to make the physical phenomena tractable to analysis. One of these appears to be indispensable for the use of continuous functions to describe the behavior of a collection of evaporating droplets. Both this and the "quasistatic" assumption of Section II are fundamental to the theory. Other assumptions, typified by the equating of $\mathfrak{D}_n$ and $\mathfrak{D}$ in Section VII, are used only to effect a simplification in the mathematics. Indeed, the pair of equations [15] and [16] are, in principle, as determinate as the single combined equation [26]. However, Eq. [26] has a much more auspicious form for the purpose of numerical analysis.

In summary, it has been demonstrated that the turbulent cloud equations [2]–[7] lead to physically reasonable conservation laws which enable the total mass and heat energy densities, $\psi(\mathbf{r}, t)$ and $\phi(\mathbf{r}, t)$, respectively, to be calculated by the standard micrometeorological analysis used for diffusing nonvolatile clouds. With $\phi(\mathbf{r}, t)$ so calculated a generalized psychrometric equation has been derived to determine the drop temperature in the various regions of the cloud. This turned out to be, Eq. [12], essentially the wet-bulb temperature appropriate to the initial temperature and humidity at the altitude in question, suitably modified to allow for the turbulent diffusion of the total heat energy $\phi(\mathbf{r}, t)$.

As a result of these considerations the description of the dissipation process is reduced to a pair of nonlinear equations, [15] and [16], for the vapor concentration and the particle-size distribution. These are shown to yield the correct conservation law for the total mass. Identification of the vapor and particulate transport operators, approximating a strongly turbulent atmosphere containing only small droplets, effects the further reduction of the problem to the solution of a single equation in the droplet mass distribution, Eq. [26]. Solution of this nonlinear integro-differential equation is not attempted in the present work. The mathematical complexity of the equation, even with the simplest forms of transport operator, Eq. [1], is such as would suggest the use of automatic computational methods. Numerical procedures appropriate to such calculations are available (*cf.* Crank and Nicolson (12) and Douglas (13)).

The material in the present article clearly does not lead directly to quantitative data. It is believed, however, that the essential physical relationships have been established herein, and that primarily numerical analysis is now needed to predict the behavior of evaporating water clouds in a variety of micrometeorological environments.

ACKNOWLEDGMENT

The author is indebted to Mr. Kenneth L. Calder for critical advice and encouragement.

REFERENCES

1. MILBURN, R. H., *J. Colloid Sci.* **12,** 378 (1957).
2. SUTTON, O. G., "Micrometeorology." McGraw-Hill, New York, 1953.
3. SUTTON, O. G., "Atmospheric Turbulence." Wiley, New York, 1955.
4. U. S. Weather Bureau, "Meteorology and Atomic Energy," Chapters 4, 7, and 9. U. S. Govt. Printing Office, Washington, 1955.
5. HEWSON, E. W., *Quart. J. Roy. Meteorol. Soc.* **74,** 321 (1948).
6. SUTTON, W. G. L., *Proc. Roy. Soc.* (*London*) **A182,** 48 (1943).
7. TUNICKI, N. N., *J. Phys. Chem.* (*U. S. S. R.*) **20,** 1137 (1946).
8. JOST, W., "Diffusion in Solids, Liquids, Gases," pp. 8–10. Academic Press, New York, 1952.
9. RANZ, W. E., AND MARSHALL, W. R., JR., *Chem. Eng. Progr.* **48,** 145 (1952).
10. HEWSON, E. W., AND LONGLEY, R. W., "Meteorology Theoretical and Applied," p. 59. Wiley, New York, 1944.
11. BRUNT, D., "Physical and Dynamical Meteorology," p. 87, pp. 269 ff. Cambridge University Press, Cambridge, 1941.
12. CRANK, J., AND NICOLSON, P., *Proc. Cambridge Phil. Soc.* **43,** 50 (1947).
13. DOUGLAS, JIM, JR., *J. Soc. Ind. Appl. Math.* **3,** 42 (1955).

JOURNAL OF COLLOID SCIENCE **13**, 125–133 (1958)

DISTANCE BETWEEN EMULSIFIED OIL GLOBULES UPON COALESCENCE

M. Van den Tempel

Unilever Research Laboratory, Vlaardingen, Netherlands

Received September 20, 1957

The rate-determining process in the coagulation of concentrated oil-in-water emulsions is the coalescence of contacting oil globules (1). Coalescence occurs immediately upon rupture of the thin water film separating the oil globules "in contact." The thickness of this water film, at the moment of coalescence, will affect the probability of rupture. In the present investigation, the minimum distance between oil drops in an aqueous detergent solution has been measured directly. The results of these measurements are discussed in terms of van der Waals-London and electrostatic interaction.

The thickness of the water layer between oil-water interfaces, immediately before coalescence occurred, has been estimated by Gillespie and Rideal (2) from the time used for drainage of film liquid from between the approaching surfaces. Values of the order of 10^{-4} cm. were found for the minimum distance between hydrocarbon drops in pure water. Direct measurement of the thickness of the water film between two air bubbles in an aqueous soap solution was carried out by Derjaguin (3). It was demonstrated that this thickness is influenced by the electrostatic repulsion between the charged interfaces, which explains the effect of the electrolyte concentration on the thickness of the water film.

EXPERIMENTAL

The distance between two interfaces was measured by means of a microphotometer, as used by Derjaguin and others (3, 4). A light beam with intensity I_0 passes through the interfaces, and the amount of light reflected is measured. With normal incidence, each of the interfaces reflects a fraction $e^2 = (n_2 - n_1)^2/(n_2 + n_1)^2$ of the incident light, where n_1 and n_2 are the refractive indices of the media at both sides of the interface. A phase reversal occurs at only one of the interfaces. The beams reflected from the interfaces will have nearly equal intensity, and a phase difference equal to π plus or minus the difference caused by one of the beams having passed twice the distance separating the interfaces. Interference of both light beams results in an intensity depending upon this interfacial distance.

The phenomenon has been investigated more quantitatively by Lord Rayleigh (1888), who found for the intensity of the reflected light:

$$I = I_0 \frac{4e^2 \sin^2 (2\pi\delta/\lambda)}{1 - 2e^2 \cos (4\pi\delta/\lambda) + e^4}, \qquad [1]$$

where δ is the interfacial distance and λ is the wavelength in the medium separating the two interfaces.

In the present case, both e^2 and $\delta/\lambda \ll 1$, and [1] may be approximated by:

$$I = I_0\, 4e^2 \sin^2 (2\pi\delta/\lambda). \qquad [2]$$

The reflected light beam was observed in a microscope, and its intensity was compared with that of a beam obtained from the same light source, the intensity of which could be varied by means of a gray wedge (Fig. 1). The position of the wedge was calibrated by observing the light reflected from one single interface between pairs of liquids having known refractive indices.

The 16 mm. Zeiss objective, with n.a. 0.30, had to be immersed in the upper liquid layer. This also prevented the reflection from the uppermost liquid surface from interfering with the measurement. A yellow filter was

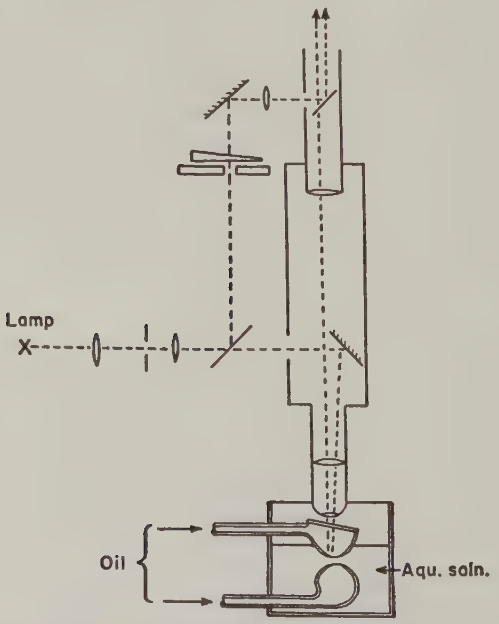

Fig. 1. Microphotometer used for measuring distance between oil drops.

used in the measurements; the wavelength in water was taken as 4500 A. The diameter of the light beam near the interfaces was less than 0.2 mm.

Drops of paraffin oil were produced by pressing the oil through circular holes in spherical glass vessels, submerged in the aqueous detergent solution. Drop volumes could be controlled by means of Agla micrometer syringes. The glass spheres could be moved in three mutually perpendicular directions, to ensure a horizontal "plane of contact" between the oil drops. The diameter of the drops could be varied between about 1 and 3 mm.

In several experiments only one drop was produced from the lower glass sphere, and this drop was pressed against the plane interface produced by a layer of paraffin floating on the aqueous solution.

The aqueous phase consisted of a 0.010 *M* solution of sodium dodecyl sulfate, with varying amounts of sodium chloride. This is well above the critical micellar concentration, and ensures a high stability against coalescence even in the presence of electrolyte. In several cases 0.5% of the nonionic stabilizing agent Emulphor O (a polyethylene oxide ether of a fatty alcohol, produced by Badische Anilin- und Soda Fabrik) was added to the aqueous solution. This increased the time during which the drops would remain stable at the minimum distance, without otherwise affecting the results. Paraffin oil was a water-white medical grade devoid of surface-active impurities; refractive index 1.4771, density 0.875 g./cm.^{3}, both at 20°C.

RESULTS

a). Drainage

Interference colors, and alternating light and dark rings, could be observed in a freshly formed water film. These subsided in a time of up to about 1 hour, depending on drop size. After that time, the drops remained stable for up to many hours, with no detectable change in the intensity or color of the reflected light. Coalescence occurred without prior change, in most cases after several hours.

The colors appearing in the reflected light in the case of one oil droplet approaching a plane interface, could be used to measure the thickness of the interfacial layer in the region between about 800 and 1200 A. This thickness was always obtained in much less than 1 hour.

The rate of drainage of the water film between a single drop and a plane interface has generally been described (5, 6) by means of an equation due to Reynolds, valid for drainage between two parallel flat surfaces. It is hereby assumed that the droplet and the interface deform in such a way that they present parallel interfaces over a considerable area. The results, however, show that a layer thickness of about 1000 A. was obtained much more rapidly than would follow from Reynolds' equation, if it is assumed (2, 5) that this equation may be used at a film thickness of the same order of magnitude as the drop radius. Evidently, the width of the gap separating the interfaces is much larger at the periphery than at the center, during a considerable portion of the drainage period. This results in an enormously increased rate of drainage. At distances of about 1000 A. the thickness δ was found to decrease with time t according to the relation: $t\delta^2$ = constant, showing that in this case the model of two parallel flat surfaces becomes applicable.

In the emulsions used, the interfacial tension is of the order of 1 dyne/cm. Even at this low value, flattening of the oil drop at the interface is insufficient to allow the model of two parallel flat plates to be used for a description of the rate of drainage, at distances in excess of 1000 A. It must be assumed that the values of the layer thickness upon coalescence as estimated by Gillespie and Rideal (2) are, for this reason, much too high.

Another factor increasing the rate of drainage consists of the presence of a force in excess of gravity, pressing the interfaces together. It was found necessary to keep the oil droplet attached to the glass sphere, because it had to remain in a fixed position with respect to the light beam for many hours. Contact with the plane interface was made by moving the glass sphere, with attached droplet, upward until a slight distortion of the interface became visible to the naked eye. This will introduce a force pressing the interfaces together, which can not easily be controlled and which renders application of the equation for the rate of drainage as a function of drop size meaningless.

The contribution of the van der Waals-London attractive forces can be neglected with respect to gravity, at distances in excess of about 500 A.

b). *Equilibrium Distance*

After the drainage period a constant intensity of light was measured during several hours. The thickness of the water film calculated from the light intensity has been plotted in Fig. 2, as a function of the electrolyte concentration. The results obtained by Derjaguin (3) for the distance between two air bubbles in water have also been indicated; they are substantially in agreement with the results of the present investigation.

Variation of the drop size between about 1 and 3 mm. had no measurable effect on the equilibrium distance.

Discussion

If two charged interfaces, of identical composition, are pressed together in an aqueous solution the distance between the interfaces will decrease until the repulsive forces are in equilibrium with the force pressing the interfaces together. The repulsive force is of electrostatic origin. Its mag-

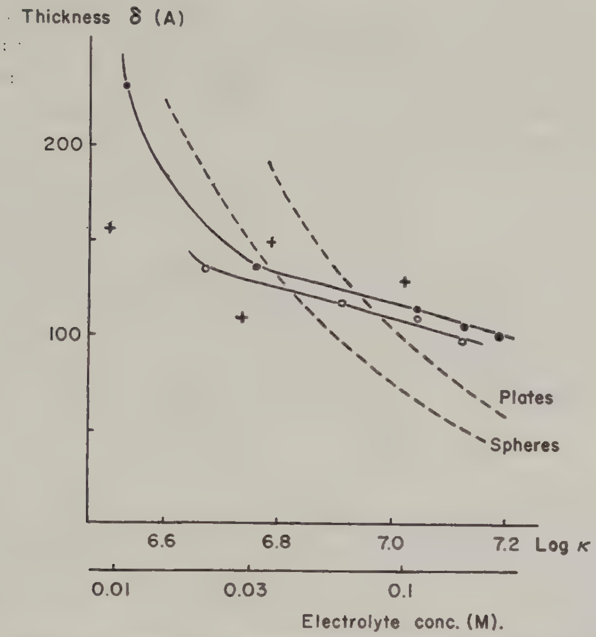

FIG. 2. Equilibrium thickness of water layer between interfaces, as a function of electrolyte concentration. ○—2 drops. ●—single drop at plane interface. +—results of Derjaguin (3). ------theory (Eqs. [8] and [9]).

nitude as a function of the distance between the interfaces has been investigated in considerable detail (7). The attractive force is generally assumed to be a van der Waals-London type of interaction, about which still less quantitative information is available.

The anions of the emulsifying agent are adsorbed at the oil-water interface, causing a potential drop in a diffuse double layer at the aqueous side of the interface. The thickness of this diffuse double layer ($1/\kappa$) is mainly determined by the ionic concentration in the aqueous phase. With 1–1 valent electrolytes:

$$1/\kappa = (DkT/8\pi n\epsilon^2)^{1/2} \qquad [3]$$

where D is the dielectric constant, n the ionic concentration, and ϵ the elementary charge. The other symbols have their usual meaning. In the presence of a completely dissociated emulsifying agent the ionic concentration is always sufficiently high to ensure a double layer thickness of less than 10^{-6} cm.

The extension of the double layer is, then, always small compared with the dimensions of the oil globules in an emulsion. In that case a method indicated by Derjaguin (8) may be used for calculating the electrostatic repulsion between oil globules. A general expression giving the repulsive energy V_R as a function of interparticle distance δ is not known, but an approximation may be used which is valid for fairly large distances between the particles ($\kappa\delta > 3$). This gives for the repulsive energy between two droplets of equal radius a:

$$V_R = \frac{8Dk^2T^2}{\epsilon^2}\gamma^2 a \exp(-\kappa\delta) \tag{4}$$

This equation expresses that the electrostatic interaction energy decreases exponentially with increasing distance δ, where the distance should be measured in the appropriate units $1/\kappa$. Moreover, the interaction energy is proportional to the particle radius, and depends upon the potential drop in the double layer (ψ_0) by the term containing γ:

$$\gamma = (e^{z/2} - 1)/(e^{z/2} + 1)$$

where $z = \epsilon\psi_0/kT$.

In the region where Eq. [4] may be used, the interaction energy is not very sensitive to changes in the double layer potential ψ_0. A value of $z = 4$, corresponding with a double layer potential of about 100 mv., will be used throughout (9).

The water film between a single oil drop and a plane interface behaves as a layer of uniform thickness over a considerable area, if the thickness is less than about 1000 A. The electrostatic repulsion in this case should be calculated for a model consisting of two parallel flat plates. This gives for the repulsive energy per cm.^{2}, in the approximation valid if $\kappa\delta > 3$:

$$V_R = \frac{64nkT}{\kappa}\gamma^2 \exp(-\kappa\delta) \tag{5}$$

Calculation of the repulsive potential between oil droplets in a typical emulsion shows that a potential barrier having a height of several thousand times kT is present between the approaching interfaces. It is evident that the energy of Brownian motion is insufficient to cause direct contact between the surfaces of oil drops.

The height of the potential barrier between two approaching oil droplets is somewhat decreased by taking into account the van der Waals-London attraction between the globules. Using the most probable values for the magnitude of this attraction (10) still results in a barrier height of many thousand times kT, in emulsions showing a reasonable stability caused by the presence of an ionized detergent.

The energy of the van der Waals-London attraction between two spheres of radius a, at a distance $\delta \ll a$ apart, is (11):

$$V_A = -\frac{Aa}{12\delta}, \tag{6}$$

where A is a constant depending on the polarizability of the atoms present in both phases. In the case of two flat plates, the attraction energy is given by:

$$V_A = -\frac{A}{12\pi\delta^2}. \qquad [7]$$

The attractive and repulsive forces are in equilibrium in a minimum of the total interaction energy, $V = V_A + V_R$. The interfacial distance δ_m in this minimum is determined by, in the case of two spheres:

$$\delta_m^2 \exp(-\kappa\delta_m) = \frac{A\epsilon^2}{96Dk^2T^2} \cdot \frac{1}{\kappa_\gamma^2} \qquad [8]$$

and in the case of two parallel flat plates:

$$\delta_m^3 \exp(-\kappa\delta_m) = \frac{A}{384nkT\gamma^2\pi} \qquad [9]$$

The relation between δ_m and the electrolyte concentration, which results from the Eqs. [8] and [9], has also been plotted in Fig. 2. The constant A has been given a value of 10^{-13} erg (9). It should be noticed that, in the approximation used, the equilibrium distance between two spheres does not depend upon their size.

The presence of a minimum in the potential energy of interaction of two colloidal particles has been discussed earlier (12). Such a "secondary minimum" will always be present if the attractive forces decrease less rapidly with increasing distance, than the repulsive forces. The experimental evidence for the existence of an equilibrium distance between two approaching interfaces proves the presence of a secondary minimum in the potential energy. This minimum is situated between about 100 and 200 A. at the electrolyte concentrations used in the present investigation, in accordance with the theory resulting in Eqs. [8] and [9]. Moreover, the equilibrium distance between a single drop and a flat interface is slightly larger than between two spherical drops, as required by theory. The experimental results show, however, that the equilibrium distance decreases less rapidly with increasing electrolyte concentration than the theory predicts.

The effect of gravity and other external forces can be neglected compared with that of the molecular forces, at the small interfacial distance measured. The introduction of a relativity correction in the van der Waals-London attraction (13) has no appreciable effect on its magnitude at distances smaller than about 1000 A.

Calculation of the electrostatic repulsive energy, at the distances measured, results in the values plotted in Fig. 3. The repulsive energy increases with decreasing distance, i.e., with increasing electrolyte content, up to

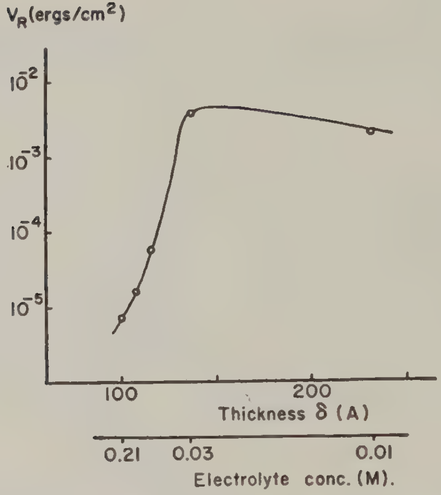

FIG. 3. Energy of electrostatic repulsion (Eq. [5]) at measured values of film thickness.

concentrations of about 0.1 *M*. At higher electrolyte concentrations the interfacial distance is further decreased, but the electrostatic repulsion in the secondary minimum is now also decreasing! An interpretation of the results in terms of electrostatic repulsion and van der Waals-London attraction *only* would require an attraction *decreasing* with decreasing distance, at distances smaller than about 125 A. It is suggested that other repulsive forces become operative at such small distances; these forces might be of a steric nature.

SUMMARY

Flocculated oil globules in an emulsion are still separated by a water film having a thickness of at least 100 A. A high potential barrier of electrostatic origin prevents closer contact between the particle surfaces. Coalescence occurs immediately upon rupture of this water film.

The thickness of the water film decreases with increasing electrolyte concentration. A theory in which electrostatic repulsion and van der Waals-London attraction are the only kinds of interaction taken into account, predicts a much more rapid decrease of the film thickness with increasing electrolyte concentration. The experimental results suggest the presence of still other repulsive forces which become operative at distances between the interfaces smaller than about 125 A.

ACKNOWLEDGMENTS

The author is indebted to the Management of Unilever N.V. for their permission to publish this paper. He further wishes to thank Miss M. Vermeulen for her skilful experimental work.

REFERENCES

1. VAN DEN TEMPEL, M., *2nd Intern. Congr. Surface Activity, London, 1957*, Vol. 1, p. 40.
2. GILLESPIE, T., AND RIDEAL, E. K., *Trans. Faraday Soc.* **52,** 173 (1956).
3. DERJAGUIN, B. V., AND TITJEVSKAJA, A. S., *Discussions Faraday Soc.* **18,** 27 (1954); *2nd Intern. Congr. Surface Activity, London, 1957*, Vol. 1, p. 536.
4. WELLS, P. V., *Ann. phys.* **16,** 69 (1921).
5. ELTON, G. A. H., AND PICKNETT, R. G., *2nd Intern. Congr. Surface Activity, London, 1957*, Vol. 1, p. 287.
6. LINTON, M., AND SUTHERLAND, K. L., *J. Colloid Sci.* **11,** 391 (1956).
7. VERWEY, E. J. W., AND OVERBEEK, J. TH. G., "Theory of the Stability of Lyophobic Colloids." Elsevier, New York, 1948.
8. DERJAGUIN, B. V., *Kolloid-Z.* **69,** 155 (1934); *Acta physicochim. U.R.S.S.* **10,** 333 (1939).
9. VAN DEN TEMPEL, M., *Rec. trav. chim.* **72,** 419 (1953).
10. ABRIKOSSOVA, I. I., AND DERJAGUIN, B. V., *2nd Intern. Congr. Surface Activity, London, 1957*, Vol. II, p. 587.
11. HAMAKER, H. A., *Physica* **4,** 1058 (1937).
12. VERWEY, E. J. W., AND OVERBEEK, J. TH. G., "Theory of the Stability of Lyophobic Colloids," p. 124. Elsevier, New York, 1948.
13. OVERBEEK, J. TH. G., *in* H. R. Kruyt's "Colloid Science," Elsevier, New York, 1952. Vol. 1, p. 266.

JOURNAL OF COLLOID SCIENCE **13**, 134–139 (1958)

THE INTERACTION OF SOME NAPHTHALENE DERIVATIVES WITH A CATIONIC SOAP BELOW THE CRITICAL MICELLE CONCENTRATION

T. Nash

Air Hygiene Laboratory, Central Public Health Laboratory, Colindale Avenue, London, N.W.9, England

Received April 26, 1957; revised September 23, 1957

Abstract

Cetyl trimethyl ammonium bromide, at and considerably below the cmc, becomes viscoelastic in the presence of many kinds of naphthalene derivative. The effect of salt and of concentration is investigated, using an arbitrary but quantitative parameter. The results show certain regularities which are related to previous work and ideas on the structure responsible for viscoelasticity.

Introduction

Solutions of many soaps well above the critical micelle concentration (cmc) become viscoelastic in the presence of sufficient salt (1). With some cationic soaps all or part of the salt can be replaced by benzene derivatives (2, 3). The pure salt effect is generally agreed to be due to the formation of linear micelles, according to fairly well understood principles (4). With benzene derivatives the situation is more complicated, and a variety of structures has been proposed (3, 5, 6). The importance of aromatic character has been demonstrated (3).

Binuclear aromatic compounds such as the naphthols give viscoelastic solutions with cetyl trimethyl ammonium bromide (CTAB) even below the cmc (7); salts now have a secondary influence, but their effect is detectable at much lower concentrations, e.g., less than 10 μM for sulfate (7). In the present series of experiments it was planned to follow viscoelasticity down to the lowest detectable limit for a number of naphthalene derivatives and CTAB. It was hoped that these experiments would clarify the function of aromatic character because of the lack of "pure" salt effect and also because of the fact that at very low concentrations, any detectable viscoelasticity would mean that at least one of the components had undergone fairly complete reaction.

Experimental

The method used to give a quantitative estimate of the viscoelasticity was to take 50 ml. of solution in a standard bottle and to give it a rapid swirl by hand. The time was then taken for the swirl to be destroyed, before motion in the reverse sense set in. The viscoelastic parameter is then the "swirl decay time" or SDT, in seconds. Reproducibility is better than might be expected (7), and the method is adequate for mapping the viscoelastic regions. It had been hoped to obtain more accurate results with a Couette-type viscometer, but large and apparently random fluctuations in reading made any such increase impossible. Similar irregularities were noted by others, both in the Couette viscometer (8) and in the rheogoniometer (1).

The bottle used was of uniform circular section, 4.3 cm. internal diameter and 7.5 cm. parallel height. Timings were with a stop clock; with water only movement was still visible after 60 sec., the working range being 3 to 30 sec. CTAB was purified by extracting twice with ligroin and crystallizing from acetone containing 5% water. Solid naphthalene derivatives were crystallized from alcohol or water. Stock solutions were $M/2$, $M/20$, and $M/200$ in water or alcohol, as convenient; using these it was at no time necessary to introduce more than 1% of alcohol into the experimental solution. This amount was known to have a negligible effect on viscoelasticity. To avoid adding other anions only one salt was used, sodium bromide in stock solutions of $5M$, $M/2$, and $M/20$ strength. The experiments were done in a room the temperature of which was thermostatically controlled at 20° ± 0.2° C. The viscoelasticity was known to depend, under some conditions at least, on the order of addition of the components; an extreme case of this was recently described (9). The order of addition was therefore standardized, first the CTAB, then the aromatic component, and finally the salt, if any.

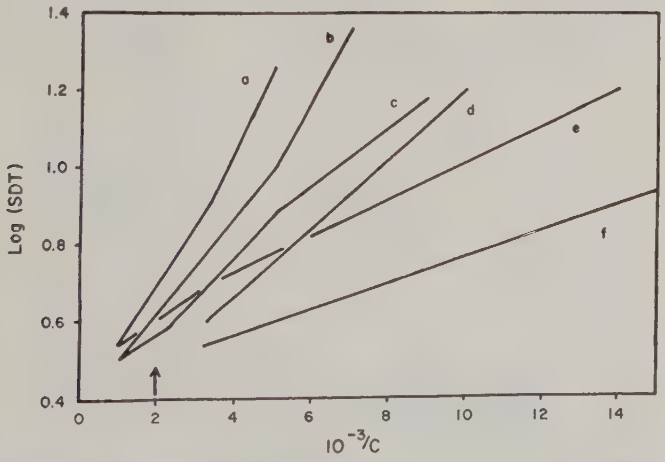

FIG. 1. Change in viscoelastic parameter with concentration C for equimolar CTAB and the following naphthalene derivatives: (*a*) 1-CHO, (*b*) 1-nitro, (*c*) 2-CHO, (*d*) 1-COOH, (*e*) 2-SH, and (*f*) 2-COOH, with mM NaBr throughout.

Results

In the first series of experiments the SDT was found for different concentrations of equimolar CTAB/naphthalene derivative with m*M* NaBr. The range of concentration was from twice the expected cmc down to $\frac{1}{25}$th of it, or 1.0 to 0.02 m*M*. With four of the five acidic derivatives, solutions were perceptibly viscoelastic down to the lower end of this range, but the technique was correspondingly insensitive at the higher end. Solutions at limitingly low concentrations of CTAB are better treated another way (see below); some of the results obtained at the higher end of the range are shown in Fig. 1. Log (SDT) is plotted against the reciprocal of the concentration, as this gave a linear relation with the naphthols (7). In the course of these experiments it was noticed that most of the less soluble compounds were strongly solubilized, especially after the addition of the salt.

In the second series of experiments the CTAB concentration was always 50 μM, while the salt and derivative concentrations were varied. This

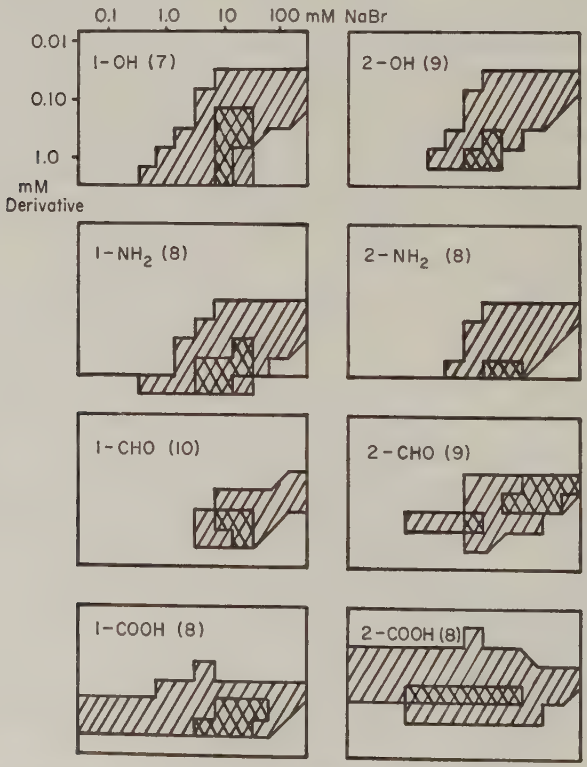

FIG. 2. Concentration of NaBr and of naphthalene derivative showing viscoelastic region with 50 μM CTAB. Minimum value of viscoelastic parameter in seconds, for example, (7).

concentration was chosen because it gave a measurable effect with all seventeen compounds used, while still keeping the SDT in the sensitive region. The range of salt concentration was zero to 0.2 M, that of the aromatic compound 0.01 to 5 mM, increments being 1, 2, 5, 10, etc., for both. The viscoelastic region for each derivative is shown (Fig. 2) in the form of a rectangular diagram with contour lines. The blank portions of each diagram correspond to solutions without detectable viscoelasticity, while the first contour represents the limit of detectability, with a SDT of about 30 sec. The inner cross-hatched region represents compositions having maximum viscoelasticity, with a SDT within 1 sec. of the minimum value. This minimum value is shown in brackets somewhere on each diagram, together with the substituent group or groups to identify the compound. A diagonal boundary line represents viscosity without viscoelasticity, i.e., the swirl was noticed to decay faster than with water but there was no sharp end-point owing to the absence of motion in the reverse sense; this was always a marginal effect, at the higher salt concentrations. Solutions with much salt or aromatic compound, or both, were sometimes turbid, and timing was difficult. The lower edge of some of the diagrams is there-

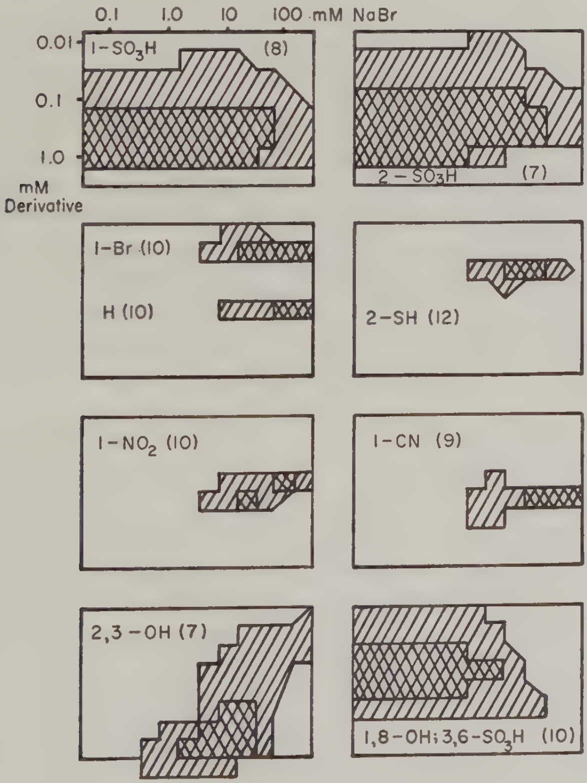

FIG. 2.—*Continued*

fore finished off in a rather arbitrary manner, without invalidating the general picture.

Secondary Nature of Salt Effect

Some 50 μM CTAB was made up in $2M$ NaBr, 10 times the maximum salt concentration used in the experiments. The solution was not detectably viscoelastic, so more CTAB was added. A transient effect arose at 1.5 mM (30 times the concentration used in the second series) which disappeared as the solution became turbid.

Dyelike Behavior of Aromatic Compounds

The pK shifts observed with mono- and dihydroxy-naphthalenes in mM CTAB (7) recall those found with dyes (10). To check this point with one of the insoluble (but solubilized) derivatives, the first UV absorption peak of l-nitronaphthalene was determined, both in ligroin and in mM aqueous CTAB. The shift in CTAB was 15 mμ to the red, typical of an anionic dye.

Discussion

Possible Presence of Micelles below the cmc

The arrow in Fig. 1 indicates the cmc to be expected in the absence of aromatic compound. Micelles are presumably present above this, but there is no sign of a break in the plots on passing through it, only a gradual increase in the viscoelastic parameter. The dyelike behavior of some of the compounds suggests that the considerations of Mukerjee and Mysels (11) apply. They showed that dyes can cause soaps to aggregate below the cmc, the stoichiometric salt formed at very low concentrations sometimes merging with true micelles. A "blurring" of the cmc in this manner readily accounts for the results shown in Fig. 1. Organic salt formation should not however, be as strong as with the true dyes.

Disposition of the Aromatic Compound in the Complex

Two features of Fig. 2 should be noted. The first is the small range covered by the minimum SDT for the different compounds, having widely different properties. It is reasonable to deduce that the structure responsible for viscoelasticity is based on the common component, CTAB, aggregated fairly completely and in much the same way, around those particular concentrations of the other two components. The second is the fact that the least soluble compounds required the most salt, the opposite being expected if the aromatic component were simply dissolved in some hydrocarbon region of the complex. The experimental results are not inconsistent with the presence of linear micelles having the polarized aromatic compound radially adsorbed on the outside (7, 9). This view elaborates an earlier suggestion on phenol-containing aggregates (5) and is related to the idea of oriented penetration (12).

The incorrect discussion of fluorescence quenching in the 1956 paper (7) should be disregarded; the experimental results described there are typical of dye-induced aggregation (11).

The cmc of CTAB in mM NaBr was found in this laboratory by a new method depending on the accurate measurement of foam density, and was sharply defined at 0.5 mM (2 units on the reciprocal scale of Fig. 1). A parallel determination without salt gave a value of 0.9 mM, in complete agreement with that of Hartley and Runnicles (13).

REFERENCES

1. PILPEL, N., *Trans. Faraday Soc.* **50,** 1369 (1954).
2. STAINSBY, G., AND ALEXANDER, A. E., *Australian J. Chem.* **6,** 123 (1953).
3. SMITH, M. B., AND ALEXANDER, A. E., *Proc. 2nd Intern. Congr. Surface Activity,* 1957 (to be published).
4. STAINSBY, G., AND ALEXANDER, A. E., *"The size and shape factor in colloidal systems," Discussions Faraday Soc.* **11,** 150 (1951).
5. ANGELESCU, E., AND MANOLESCU, T., *Kolloid-Z.* **94,** 319 (1941).
6. GOOD, W., AND MILLOY, M. H., *Chemistry & Industry* **1956,** p. 872.
7. NASH, T., *J. Appl. Chem.* **6,** 539 (1956).
8. HATSCHEK, E., AND JANE, R. S., *Kolloid-Z.* **38,** 32 (1926).
9. NASH, T., *Nature* **180,** 188 (1957).
10. HARTLEY, G. S., *Trans. Faraday Soc.* **30,** 444 (1934).
11. MUKERJEE, P., AND MYSELS, K. J., *J. Am. Chem. Soc.* **77,** 2937 (1955).
12. HARKINS, W. D., AND OPPENHEIMER, H., *J. Chem. Phys.* **16,** 1000 (1948).
13. HARTLEY, G. S., AND RUNNICLES, D. F., *Proc. Roy. Soc.* (*London*) **A168,** 240 (1938).

JOURNAL OF COLLOID SCIENCE **13,** 140–147 (1958)

STRUCTURE OF THE DOUBLE LAYER SURROUNDING THE PARTICLES OF THE SOL OF SILVER IODIDE

A. J. Rutgers and P. Nagels

University of Ghent, Ghent, Belgium

Received September 27, 1957

ABSTRACT

ζ-potentials have been measured in H-sols, K-sols, and Ba-sols of AgI, to which 0–10 millimoles/l. of KNO_3, of KI, and 0–1 meq./l. of $Ba(NO_3)_2$, and 0–50 μeq./l. of $AgNO_3$ had been added. The ζ-curves are of the form predicted by Overbeek. Their interpretation is possible only if we assume a new layer of counter-ions, the lattice-layer; the ions of this layer are mobilized by the addition of 3 millimoles/l. of electrolyte; this causes the considerable drop in ζ-potential between 0 and 3 millimoles/l of indifferent electrolyte.

Some years ago we gave values of the ζ-potential as a function of the concentration of indifferent electrolyte for a sol of silver iodide (1). This curve showed a strong drop of $|\zeta|$ between 0 and 3 millimoles of added electrolyte, followed by a slightly rising part. In order to verify this striking behavior, we now have repeated and extended these researches; this has verified the earlier results and has also led to an interpretation.

The sols were prepared by adding a solution of 75 millimoles $AgNO_3$/l. to a solution containing 82 millimoles KI/l.; the colloidal solution was electrodialyzed, decanted, and dialyzed again. Thus a sol containing 200 millimoles/l. of AgI was obtained, conductivity $\sigma = 7.0 \times 10^{-5}$ ohm^{-1} cm.$^{-1}$. This sol contained a considerable quantity of polyvalent ions, from the water used in the dialysis; these were completely removed (as shown by spectrographic analysis) by passing the sol over a cation-exchanger, saturated with H-ions. The sol obtained in this way had a pH value of 3.15; $a_{H^+} = 7.08 \times 10^{-4}$.

We have taken no special measures to obtain a homogeneously dispersed sol; pictures taken with the electron microscope, however, showed that a remarkable degree of homogeneity had been obtained (Fig. 1*a*, 1*b*). Many of the bigger spots are seen to be caused by two or more particles, which have come together in the process of preparing the pellicule; the diameter of the smallest particles is about 600 A.

The surface area of one particle is then 1.1×10^{-10} cm.^{2}, the volume 1.13×10^{-16} cm.^{3}. The surface of the particles per millimole is 41.5×10^3 cm.^{2} (the density of silver iodide is 5.67). The pictures were taken by Dr. Van der Meerssche.

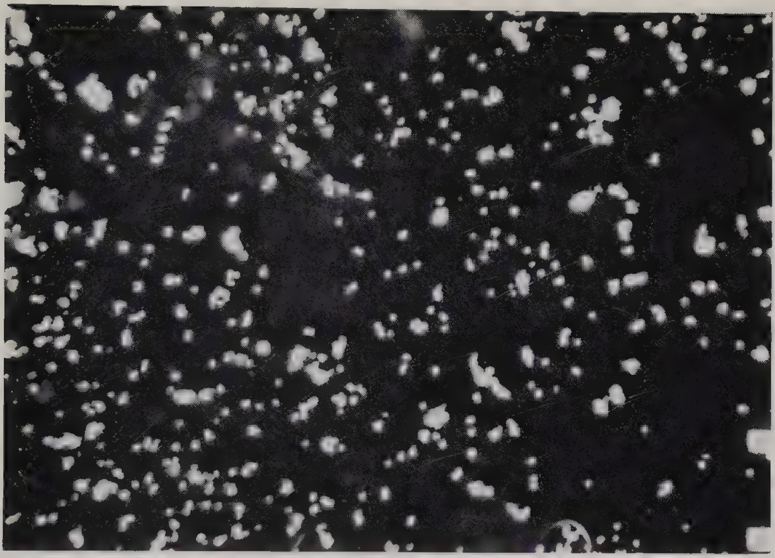

FIG. 1*a*. Electron microscopic photograph of particles of sol of silver iodide; shadowed with Pd; ×8000.

The acid sol just described will be called a H-sol. If such a sol is passed over a cation-exchanger, saturated with K-ions, all the H-ions are exchanged and we get a K-sol. In a similar way we prepared a Ba-sol.

The various electrolytes added to these various sols are given in Table I.

In the case of HNO_3, KNO_3, and KI, the amount added was limited by the increase in conductivity, which hampers the measurement of centrifugation potentials; in the case of $AgNO_3$ (potential determining electrolyte) and $Ba(NO_3)_2$ (divalent indifferent electrolyte) the flocculation of the sol determined the maximum amount to be added.

As a first step, ζ-values were calculated from centrifugation potentials by the formula

$$V_{C.P.} = \frac{D\zeta}{6\pi\eta} \frac{m'n}{\sigma} \frac{\omega^2}{2} (R_2^2 - R_1^2). \tag{1}$$

Here D is the dielectric constant of the solution, σ its conductivity, η its viscosity, $m'n$ the (apparent) mass of AgI/cm.^{3}, ω the angular speed of centrifugation, and R_2, R_1 the distances from the axis of rotation of the two points, between which the value of the centrifugation potential $V_{C.P.}$ is measured. The ζ-c curve, obtained in this way, showed a steep descent between 0 and 3 millimoles/l. of electrolyte, a minimum at $c = 3$ millimoles/l., and a slow rise between 3 and 10 millimoles/l. Now it has been proved from irreversible thermodynamics (2), by Mazur, Overbeek, and De Groot (3), that all corrections which have to be applied to electrophoresis must also be applied to centrifugation potentials; hence we de-

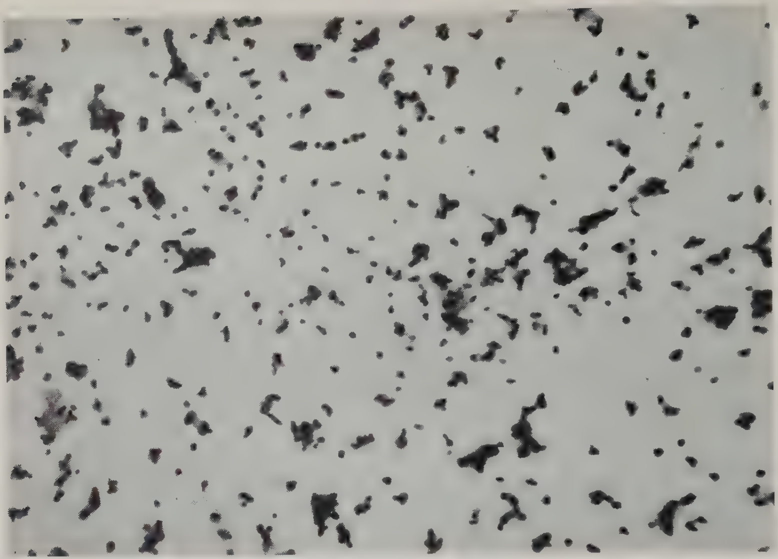

FIG. 1*b*. Electron microscopic photograph of particles of sol of silver iodide; no shadowing; ×8000.

cided to apply Henry's correction (4), the well-known $f_1(\kappa a)$ for an isolating particle, and Overbeek's correction (5) for the relaxation effect. This results in the formula

$$V_{C.P.} = \frac{D\zeta}{6\pi\eta} \frac{m'n}{\sigma} \frac{\omega^2}{2} (R_2^2 - R_1^2) f(\kappa a), \qquad [2]$$

where

$$f(\kappa a) = f_1(\kappa a) - z^2 \left(\frac{\epsilon\zeta}{kT}\right)^2 f_3(\kappa a) - \frac{\rho_+ + \rho_-}{2\epsilon} \frac{DkT}{6\pi\eta\epsilon} \left(\frac{\epsilon\zeta}{kT}\right)^2 f_4(\kappa a) \qquad [3]$$

for a symmetric z-z-valent electrolyte, and a similar formula for an asymmetric electrolyte. The various functions have been taken from the drawings in Henry's and Overbeek's works.

Since the correction term contains ζ, the calculation was carried out twice, first with the uncorrected value of ζ, then with the corrected value. Further repetitions proved to give no change of results.

The value of κ (which occurs in κa) was found from the capacity C_{diff} of the diffuse part of the double layer, which was found as the quotient of the charge/cm.^{2} (q_{diff}) and the potential drop ζ over the double layer; q_{diff} was calculated from Gouy's formula; hence

$$q_{\text{diff}} = \sqrt{\frac{n_0 DkT}{2\pi}} \left[\exp\left(-\frac{e\zeta}{2kT}\right) - \exp\left(\frac{e\zeta}{2kT}\right)\right] \qquad [4]$$

$$C_{\text{diff}} = \frac{D}{4\pi\delta} = \frac{-q_{\text{diff}}}{\zeta}; \qquad \kappa = \frac{1}{\delta}$$

TABLE I

Concentration range	H-sol	K-sol	Ba-sol
0–10 millimoles/l.	KNO_3	KNO_3	—
0–3 millimoles/l.	HNO_3	HNO_3	—
0–10 millimoles/l.	KI		
0–50 micromoles/l.	$AgNO_3$		
0–1000 micromoles/l.			$Ba(NO_3)_2$

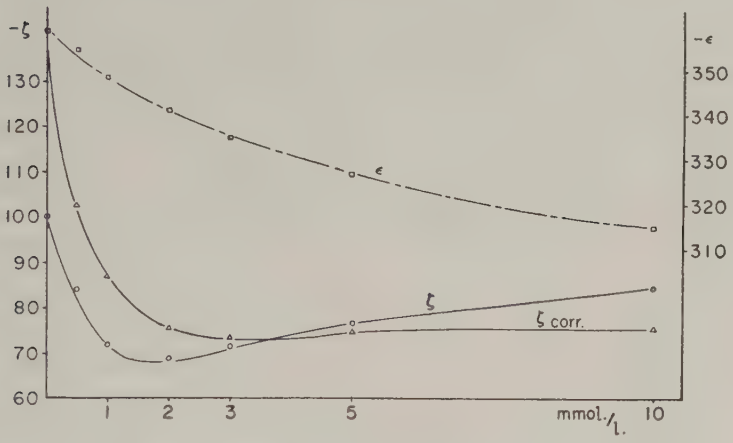

FIG. 2. Values of ζ_{corr} for a H-sol + KNO_3.

Equations [2], [3], and [4] were solved by a process of successive approximation. A first value of ζ was obtained from Eq. [2] by putting $f(\kappa a) = 1$; with this value for ζ, a value for κ, and therefore of (κa), was calculated from Eq. [4]. Now $f(\kappa a)$ could be obtained from the graphs representing Eq. [3]; Eq. [2] now yielded a corrected ζ-value. This process was repeated once more. A third repetition gave only a negligible change in the value of ζ.

The results for a H-sol [containing 32.8 g./l. of AgI, or 139.5 mole/l.] are given in Fig. 2; the added electrolyte being KNO_3. The values of ϵ were measured by means of a AgI-electrode together with a calomel-electrode; the ϵ-values thus obtained were converted to absolute values by assuming the zero point of charge for AgI at $p_I = 10.4$, according to Verwey and Kruyt (6), Kolthoff and Lingane (7), and Van Laar (8).

At the same time we measured the pH values of the sol with a glass electrode,[1] and also the total amount of H-ions in the sol by an electrometric titration. Thus we found the electrometric activity of the H-ions rose from about 50 % at $c = 0$ to 100 % at $c = 5$ millimoles/l. of indifferent electrolyte.

---

[1] By measuring pH after consecutive additions of known amounts of HNO_3 to one of our sols we verified the reliability of our pH measurements. The same holds for our p_I measurements.

TABLE II

H-Sol + KNO₃

$C(KNO_3)$ (1)	σ (2)	$-\zeta$ (3)	a_{H^+} (4)	a_{I^-} (4)	q_{diff} (5)	C_{diff} (6)	$\delta_{\text{d·ff}}$ (7)	κa	$f_i(\kappa a)$	$f(\kappa a)$	$-\zeta_{\text{corr}}$ (3)	z (8)
0	0.80	103.0	347	59.7	0.70	5.1	140	2.0	1.07	0.73	137	3270
0.5	2.02	84.6	507	51.0	1.04	10.1	70.5	4.25	1.15	0.825	103	5170
1	2.90	72.6	575	40.3	1.04	11.9	59.5	5.05	1.16	0.84	87	5920
2	4.37	69.1	660	29.8	1.12	14.7	49.3	6.1	1.18	0.905	76	7140
3	5.60	72	692	23.65	1.32	17.6	40.5	7.4	1.21	0.97	74	7550
5	6.92	77	692	17.1	1.74	23	31.0	9.7	1.25	1.02	75.5	7650
10	13.7	82	692	11.1	2.50	33	21.5	14	1.30	1.115	76	7750

(1) In millimoles/l.

(2) In 10^{-4} ohm^{-1} cm.$^{-1}$

(3) In millivolts

(4) In microequivalents/l.

(5) In microcoulombs/cm.^{2}

(6) In microfarads/cm.^{2}

(7) In Angstrom units

(8) In electr. charges

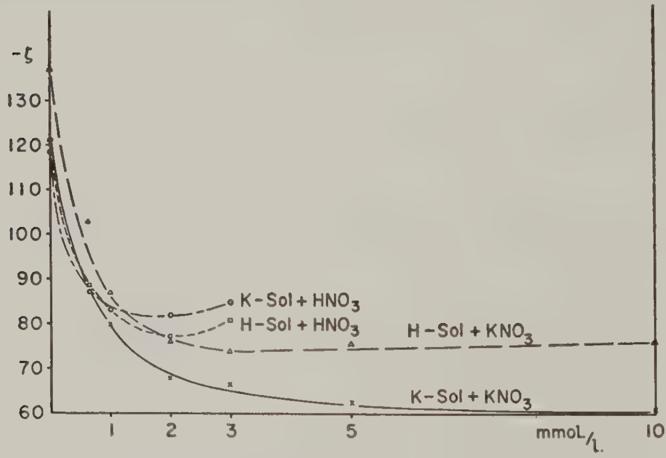

FIG. 3. Values of ϵ, ζ, and ζ_{corr} for H-sol + KNO_3; H-sol + HNO_3; K-sol + KNO_3; K-sol + KNO_3.

In Table II we give the relevant data for a H-sol, containing 32.8 g./l. or 139.5 millimoles/l. of AgI; surface area = 5.8×10^6 cm.^{2}/l.

Looking at the curves of Fig. 2, we find it worth while to quote Overbeek's words (5) of 1943.

"At increasing κa the electrophoretic speed decreases first, passes through a minimum and increases then; at still higher values of κa it will decrease again; however, such a complete curve is not often found."

In the ζ-curve of Fig. 2 only the last part is missing; but it should be remembered that we were limited in the concentration of added electrolyte.

The results for the K-sol + KNO_3 were very similar to those for the H-sol + KNO_3 ; the same holds for the addition of HNO_3 to a H-sol and a K-sol; we therefore give the curves for ζ_{corr} in one figure (Fig. 3).

In Fig. 4 we give the results for a H-sol + KI, in Fig. 5 for a H-sol + $AgNO_3$, and in Fig. 6 for a Ba-sol + $Ba(NO_3)_2$.

Of these results the most remarkable thing is the fact that the ζ-curve for H-sol + KI is not at all influenced by the increasing values of ϵ.

In this case the behavior of the H-ions is exactly similar to that in the H-sol + KNO_3 ; on the other hand, the concentration of the I-ions increases from 36 to 9530 microequivalents/l., when 0, 1, 2, 3, 5, 10 millimoles/l. of KI is added.

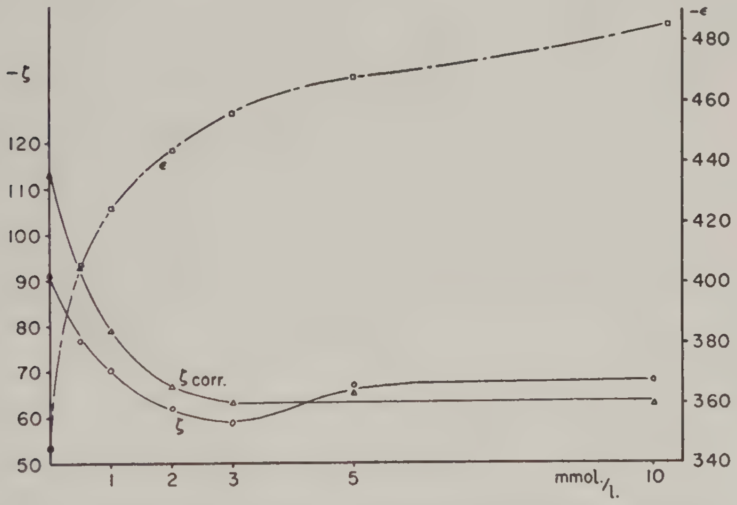

FIG. 4. Values of ϵ, ζ, and ζ_{corr} for H-sol + KI (0-10 millimoles/l.)

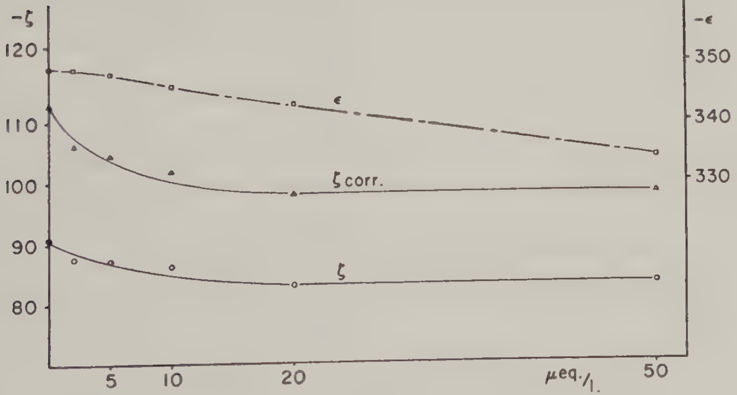

FIG. 5. Values of ϵ, ζ, and ζ_{corr} for H-sol + $AgNO_3$ (0-50 microequivalents/l.)

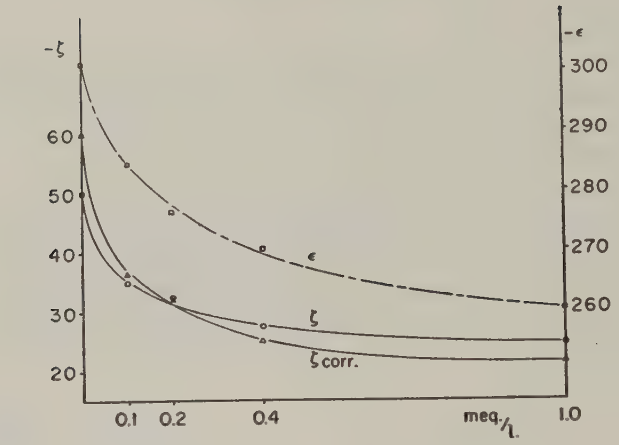

FIG. 6. Values of ϵ, ζ, and ζ_{corr} for Ba-sol + $Ba(NO_3)_2$ (0–1 meq./l.)

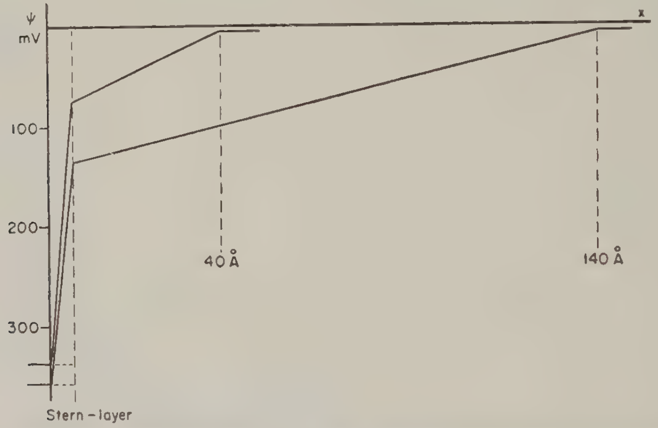

FIG. 7. Schematic representation of the counter-charge distribution at $c = 0$ and $c = 3$ millimoles/l. of KNO_3 added to a H-sol; the most important change is the increase of the particle charge, owing to the mobilization of the inactive H-ions.

We think that these results allow only one interpretation: If we look to Table II, we discover a parallelism between the values of ζ_{corr} and those of a_{H^+}; there is no parallelism between the values of ζ_{corr} and any of the other columns. The same behavior is apparent from the results for the H-sol + KI. Further, the similarity of behavior of the four cases represented in Fig. 3 suggests that this behavior is general.

We conclude, therefore, that the addition of indifferent electrolyte results in a compression of the diffuse part of the double layer, and that this causes the conversion of the inactive H-ions to active H-ions; in the pure H-sol, the inactive H-ions form a layer quite close to the lattice of the AgI-particles, a *lattice*-layer. At $c = 3$ millimoles/l., all these H-ions have been transferred to the Stern-layer; at still higher concentrations, they are partly transferred to the Gouy layer (Table II, Column 6).

The same conclusion about the state of the H-ions at $c = 0$ follows from our conductivity data (Table II, Column 2). In fact, an increase of 1 millimole/l. of KNO_3 in water gives only an increase of 1.36×10^{-4} ohm^{-1} cm.$^{-1}$ in σ; however, in our sols the first millimole gives an increase in σ of 2.1×10^{-4} ohm^{-1} cm.$^{-1}$; we ascribe the difference of 0.74×10^{-4} ohm^{-1} cm.$^{-1}$ to the mobilization of $575–347 = 228$ microequivalents/l. of H-ions; if we use the value 315 for the mobility of the H-ions, the agreement is quantitative.

The behavior of the charges, upon and near the wall, is schematically represented in Fig. 7.

REFERENCES

1. RUTGERS, A. J., AND NAGELS, P., *Nature* **171,** 568 (1953).
2. ONSAGER, L., *Phys. Rev.* **37,** 405 (1931); *ibid.* **38,** 2265 (1931).
3. MAZUR, P., AND OVERBEEK, J. TH., *Rec. trav. chim.* **70,** 83 (1953).
   OVERBEEK, J. TH., *J. Colloid Sci.* **8,** 4 (1953).
   DE GROOT, S., MAZUR, P., AND OVERBEEK, J. TH., *J. Chim. Phys.* **20,** 1825 (1952).
4. HENRY, D. C., *Proc. Roy. Soc. (London)* **133,** 106 (1931).
5. OVERBEEK, J. TH., *Kolloid. Beihefte* **54,** 320 (1943).
6. VERWEY, E. J., AND KRUYT, H., *Z. physik. chem.* **A167,** 149 (1933).
7. KOLTHOFF, I. M., AND LINGANE, J. J., *J. Am. Chem. Soc.* **58,** 2457 (1936).
8. VAN LAAR, J. A., Thesis, Utrecht, 1952.

JOURNAL OF COLLOID SCIENCE **13,** 148–150 (1958)

THE ELECTROVISCOUS EFFECT IN SOLS OF SILVER IODIDE

A. J. Rutgers and P. Nagels

University of Ghent, Ghent, Belgium

Received September 27, 1957

Abstract

The electroviscous effect has been measured in a H-sol of AgI to which 0–10 mmole/l. of KNO_3 had been added. The results are interpreted with the theory of Booth, which gives satisfactory results.

The relative change in viscosity caused by the presence of charged solid spherical particles in the liquid is given by the Einstein-Smoluchowski equation:

$$\frac{\eta - \eta_0}{\eta_0} = 2.5\varphi\left[1 + \frac{1}{\sigma\eta_0 a^2}\left(\frac{D\zeta}{2\pi}\right)^2\right] \qquad [1]$$

Here φ is the volume fraction of the solid, σ the conductivity, η the viscosity of the solution, a the radius, and ζ the electrokinetic potential of the particles.

A derivation of this formula was given by Krasny-Ergen (1) resulting in a factor 3.75 instead of 2.5.

In the derivation it is assumed that the thickness of the double layer is small compared to the radius of the particles ($ka \ll 1$).

In 1950 Booth (2) published a theory of the electroviscous effect, leading to the result, valid for all values of ka,

$$\frac{\eta - \eta_0}{\eta_0} = 2.5\varphi\left[1 + \frac{1}{\sigma\eta_0 a^2}\left(\frac{D\zeta}{2\pi}\right)^2 \pi(ka)^2 Z(ka)(1 + ka)^2\right]. \qquad [2]$$

The functions $Z\ (ka)$ (curve 2) and $Z\ (ka)\ (1 + ka)^2$ (curve 1) are given in Fig. 1.

The equations of Smoluchowski and Booth could not yet be tested, since no reliable ζ-values were available. However, our centrifugation potentials measurements have given us the necessary ζ-values.

The measurements were carried out with a $\mathrm{AgII}^- ¦ \mathrm{H}^+$ sol containing 32.76 g./l. of AgI.

$$\varphi = \frac{5.78}{994} = 0.00581.$$

The electrolyte added was KNO_3 (0–10 mmole/l.). The viscosities were measured in an Ostwald viscosimeter at 20.5°C; the temperature was kept constant to 0.01°C.; the times of flow out were about 320 sec., measured with an accuracy of 0.1 sec.

We write Eq. [2] as

$$A = f\,(1 + BC)$$

where

$$A = \frac{\eta - \eta_0}{\eta_0 \varphi}\;; \qquad B = \frac{1}{\sigma \eta_0\, a^2}\left(\frac{D\zeta}{2\pi}\right)^2; \qquad C = \pi(ka)^2 Z(ka)(1 + ka)^2. \quad [3]$$

The test will be carried out in such a way that A and B are calculated from

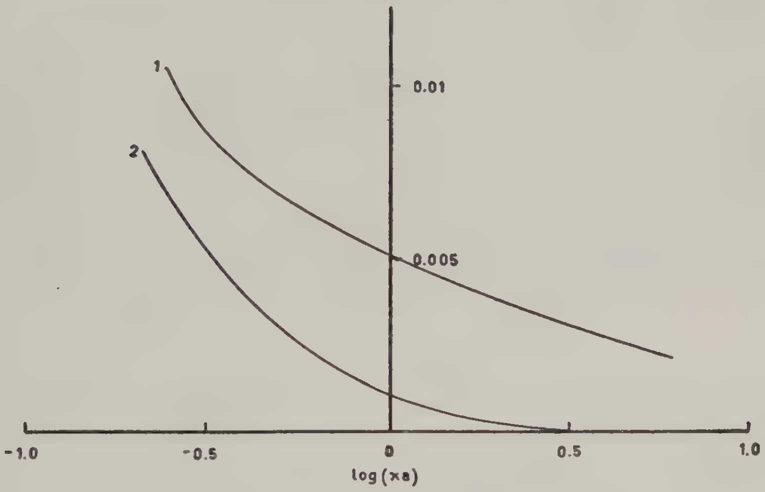

FIG. 1. The functions $Z\ (ka)$ and $Z\ (ka)\ (1 + ka)^2$.

TABLE I

Electroviscous Effect for a H-sol of AgI + KNO_3

C (1)	η (2)	A	$-\zeta$ (3)	σ (4)	B	ka	C	D	f	$1+B$
0	1.0319	6.73	137	0.68	6.15	2.0	0.0478	1.294	5.2	7.15
0.5	1.0198	4.64	103	1.75	1.35	4.25	0.153	1.207	3.85	2.35
1	1.0176	4.26	87	2.59	0.650	5.05	0.202	1.131	3.76	1.65
2	1.0167	4.10	76	3.98	0.323	6.1	0.258	1.083	3.78	1.323
3	1.0154	3.88	74	5.32	0.229	7.4	0.327	1.075	3.62	1.229
5	1.0154	3.88	75.5	7.97	0.159	9.7	0.473	1.075	3.62	1.159
10	1.0154	3.88	76	14.02	0.092	14.0	0.678	1.062	3.65	1.092

(1) in mmol e/l. (3) in millivolts.
(2) in 10^{-2} poise. (4) in 10^{-4} ohm^{-1} cm.$^{-1}$.

the experimental values of η, η_0, σ, ζ, and a; C is calculated from the relevant values of ka; finally

$$f = \frac{A}{1 + BC} = \frac{A}{D} \qquad [4]$$

is calculated, so that we can answer the questions: Is f a constant? What is its numerical value?

The results of the measurements and the calculations are given in Table I.

We see from the columns for f that the values for f are constant at about $f = 3.75$, with an exception only for the first point; this strongly supports Booth's theory, although the numerical factor is not 2.5; the last column was added to show that the Smoluchowski theory

$$f = \frac{A}{1 + B} \qquad [5]$$

would *not* lead to constant f-values and would lead to far too big correction terms.

REFERENCES

1. KRASNY-ERGEN, W., *Kolloid-Z.* **74,** 172 (1936).
2. BOOTH, F., *Proc. Roy. Soc.* (*London*) **A203,** 533 (1950).

JOURNAL OF COLLOID SCIENCE 13, 151–158 (1958)

EYRING'S MODEL OF FLOW APPLIED TO THIXOTROPIC EQUILIBRIUM[1]

Sven-Eric Dahlgren

AB Gustavsbergs Fabriker, Gustavsberg, Sweden. Present address: AB Förenade Superfosfatfabriker, Landskrona, Sweden

Received October 7, 1957

INTRODUCTION

In the last few years a number of investigations on thixotropic materials have been carried out, some in order to try to explain the mechanism and some to obtain formal relationships of thixotropic behavior. Some years ago the author made an analysis of the formal relationships found by Green and Weltmann (1). Further studies showed, however, that the validity was limited to certain types of thixotropic materials. The author came to the conclusion that when studying thixotropic materials one should start with the equilibrium conditions to get a suitable base for further penetration.

THE TERM THIXOTROPY

Different investigators have given thixotropy varying meanings. Pryce-Jones (2), for instance, characterizes a substance as thixotropic if the structure reversibly breaks down under the influence of shear stresses and afterwards behaves as a true liquid, with a linear relationship between shear rate and shear stress. If the properties of a solid of the substance disappear only to some extent, he calls it a false-body. As we shall see later, the real difference between the two types is only quantitative. Therefore this classification cannot be considered adequate.

To make a definition which covers all possible reaction mechanisms of thixotropic changes would be extremely difficult. Until more basic facts are known one is left to fit the definition to the assumptions with which one works and thus allow some looseness in the conception of thixotropy. Here we define thixotropy in the following manner:

Thixotropy—a phenomenon including an isothermal reversible process, in which bonds in a substance are broken down under the influence of shear stress and the mean lifetime of the broken bonds (the activated states) is longer than what is stipulated for a place change between two neighboring equilibrium positions of the same kind and where the number of broken bonds of each kind per unit of volume and their mean lifetime depends on shear rate and time; the equilibrium is attained in both directions of the process more or less delayed depending, among other things, on the strength of the attracting forces, the size of the shear acceleration, and the prehistory of the substance.

---

[1] Presented at the Rheological Conference in Stockholm, September, 1956, arranged by the Rheological Section of the Swedish National Committee for Mechanics.

The word bond is used here in its widest sense, meaning any force tending to keep atoms, molecules, or particles together.

The definition is a little more extended than those stated before. This does not require the delaying phenomenon to be of such an order of magnitude that it may be observed by common rheological equipment. Examples of thixotropic substances are suspensions of attracting particles and gels.

EYRING'S MODEL OF FLOW

The following treatment is based on Eyring's model of flow. Eyring (3, 4) has treated the viscosity as a case of absolute reaction rates. Through a place-exchange mechanism the unit of flow moves via an energy barrier from one equilibrium position to the nearest in the direction of flow. In its simplest form the following expression of viscosity is obtained.

$$\eta = \frac{\tau}{a \sinh (b\tau)}, \qquad [1]$$

where η = coefficient of viscosity; τ = shear stress; and a and b are constants, if the dimensions of the flow unit and the temperature are not changed. For sufficiently small values of $b\tau$ the expression approximates to the Newtonian case

$$\eta_0 = \frac{1}{ab}. \qquad [2]$$

The index "0" indicates the limiting value when τ approaches zero.

For sufficiently large values of $b\tau$ Eq. [1] changes into

$$\eta = \frac{2\tau}{a} e^{-b\tau}. \qquad [3]$$

But

$$\eta \equiv \frac{\tau}{R}, \qquad [4]$$

where R = shear rate = [time^{-1}].

Thus we obtain

$$R = a \sinh (b\tau) \qquad [5]$$

$$\tau = \frac{1}{b} \operatorname{arsinh} \frac{R}{a} = \frac{1}{b} \ln \left(\frac{R}{a} + \sqrt{\frac{R^2}{a^2} + 1} \right) \qquad [6]$$

(or where arsinh is the inverse sinh); for small values of R/a Eq. [6] gives

$$\tau = \frac{R}{ab} \tag{7}$$

and for large values of R/a

$$\tau = \frac{1}{b} \ln \frac{2R}{a}. \tag{8}$$

The above is applicable to simple substances. In complex systems the relationships are somewhat more complicated. Powell and Eyring (5, 6) have suggested that in these systems two or more place-exchange mechanisms (types of bond) occur simultaneously. We assume here that the homogeneity of the system is maintained, that is, no unmixing occurs, and thus the different components of the system have the same shear rate. The different types of bond are allowed to take up shear stresses of different magnitude. The total shear stress in the system is the sum of the partial shear stresses for each single type of bond. From Eq. [6] we obtain the following general expression

$$\tau = \sum^{i} \frac{1}{b_i} \operatorname{arsinh} \frac{R}{a_i}. \tag{9}$$

The place-exchange mechanism which first shows nonlinearity is given $i = 1$, the next $i = 2$, and so on.

If we are within an interval where n place-exchange mechanisms are nonlinear and the others are approximately linear, Eq. [9] after insertion of Eq. [2] changes into

$$\tau = \sum_{n+1}^{i} \eta_{0_i} \cdot R + \sum^{n} \frac{1}{b_i} \cdot \operatorname{arsinh} \frac{R}{a_i}. \tag{10}$$

THIXOTROPIC EQUILIBRIUM

A place-exchange reaction may in some cases occur very rapidly, but not momentarily. All substances therefore can show elastoviscous relaxation. In addition to this some substances show relaxation by destruction of bonds. The magnitude of the ultimate load of a single bond depends, however, on how rapidly the load has been applied and also here we get a delaying phenomenon. If this destruction is reversible and the mean lifetime of the broken bonds is longer than stipulated for a place change between two neighboring equilibrium positions of the same kind, then it follows from the given definition that we have to do with a thixotropic substance. If a and b in the equations above are to be treated as constants, then there must be equilibrium between the activated and the nonactivated states, that is, the delaying and relaxation phenomena should be released. If equilibrium is not on hand the "constants" become time-dependent. Another condition mentioned is that to each place-exchange reaction (type of bond) belongs a flow unit of fixed dimensions. Equations [9] and [10] are thus valid for thixotropic substances under equilibrium conditions.

A third type of relaxation of interest in this connection is that molecules or particles on increasing shear stress to a higher degree orient themselves in such a way that they store potential energy. Here also there are delaying phenomena and equilibria. Substances showing such orienting phenomena are said to be rheopexic. Rheopexic relaxation could be superpositioned on the thixotropic; it does not exist in the absence of thixotropy. The given relations are valid also for rheopexy, but a and b for such a process are dependent on shear rate as well as time (7). The analysis of the equilibrium curve becomes much more difficult.

On several suspensions at high shear rates one has determined a limiting viscosity of the same order of magnitude as that of the suspension medium. The viscosity obtained correlates well with that theoretically calculated for a suspension of nonattracting spheres with the same volume concentration (8). This indicates that when all intermicellar bonds are broken, the suspension behaves as if it consisted of nonattracting particles in a liquid.

A SPECIAL CASE

We will now treat the special case of Eq. [10] when $n = 1$ and a_1 and the product a_1b_1 are small quantities. The first part of the flow curve nearly coincides with the τ-axis, and the substance can approximately be treated as stiff. After an inconsiderable transition region the flow curve becomes a nearly straight line with a different slope than before. Such a substance is thus approximately a Bingham body. This means further that the yield value concept is only an approximation and theoretically is without physical meaning. Depending on the size of a_1 the transition region is more or less pronounced and the substance loses more or less rapidly on increasing shear stress its character of a solid. Any boundary between what Pryce-Jones (2) names "false-body" and a thixotropic substance thus does not exist.

CALCULATION EXAMPLE

As an example of how to determine the occurring constants from experimental data we shall apply the equations on an 8% bentonite suspension, the thixotropic equilibrium curve of which has been determined by Roller and Stoddard (9). Complications in the form of variable constants are not present in this case. The experimental data are plotted in an R–τ diagram, and the most likely curve is drawn. See Fig. 1. First we apply Eq. [10] for $n = 1$. By suitable selection of axis functions we now try to obtain a linear relationship. With values from the curve in a new diagram therefore we put τ/R as ordinate and R^{-1} arsinh R/a_1 as abscissa. With the correct

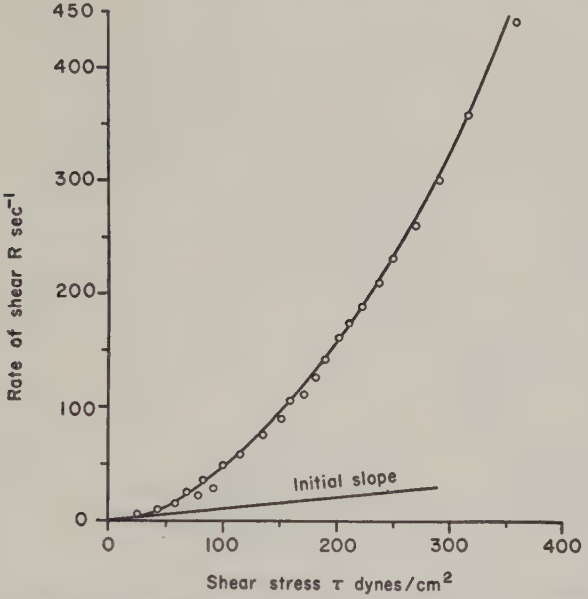

FIG. 1. Flow curve at equilibrium state of an 8% bentonite suspension after experimental data by Roller and Stoddard. The continuous curve corresponds to the equation

$$\tau_E = 0.04R + \frac{\operatorname{arsinh}\dfrac{R}{200}}{0.0067} + \frac{\operatorname{arsinh}\dfrac{R}{2.0}}{0.060}\ \text{dynes/cm.}^2.$$

value of a_1 we shall obtain a straight line within the region in which the approximation is valid. The value of a_1 is obtained by trial-and-error solution. In Fig. 2 curves for three values of a_1 are shown. At the same time the derivative of the straight line gives us b_1, and the ordinate at zero abscissa gives $\sum_2^i \eta_{0_i}$ from which $\sum^i \eta_{0_i}$ can be calculated.

For high values of R, the data deviate from the straight line. With knowledge of a_1 and b_1 we can make a second approximation and put $n = 2$. As ordinate we now choose

$$R^{-1}\left(\tau - b_1^{-1} \operatorname{arsinh} \frac{R}{a_1}\right)$$

and as abscissa

$$R^{-1} \operatorname{arsinh} \frac{R}{a_2}.$$

For the correct value of a_2 we get a straight line within the region where the approximation is valid. See Fig. 3. The derivative of the line gives us

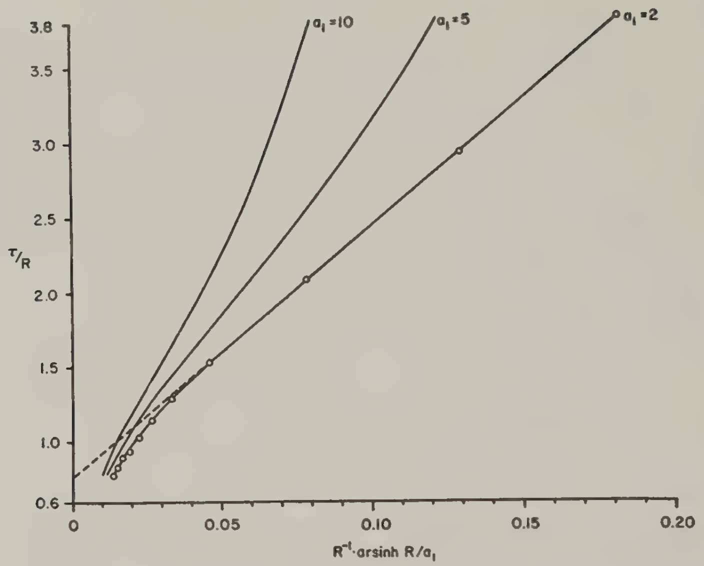

FIG. 2. Graphic determination of the constants in the first approximation.

$$a_1 = 2{,}0 \text{ sec}^{-1}$$

$$b_1 = 0{,}060 \text{ cm}^2/\text{dyne}$$

$$\sum_{\mathrm{II}}^{i} \eta_{0_i} = 0{,}78 \text{ dyne sec/cm}^2$$

$$\eta_{0_1} = \frac{1}{a_1 b_1} = 8{,}35 \text{ dyne sec/cm}^2$$

b_2 and the ordinate at zero abscissa gives $\sum_3^i \eta_{0_i}$. The latter could also be calculated from $\sum_2^i \eta_{0_i}$ and a_2 and b_2. Thus we have determined the equation of the equilibrium curve of the bentonite suspension

$$\tau_E = 0.04 \cdot R + \frac{\text{arsinh}\,\frac{R}{200}}{0.0067} + \frac{\text{arsinh}\,\frac{R}{2.0}}{0.060} \text{ dynes/cm.}^2.$$

Index E indicates equilibrium.

The inverse derivative at the origin of the curve in Fig. 1 gives the viscosity of the undisturbed state, which is 9.13 dynes sec./cm.^{2}

If data are available further approximations can be made as to the principle indicated, provided that more types of bonds are present. However, each further approximation step makes the calculations still more extensive. In most cases two steps are sufficient.

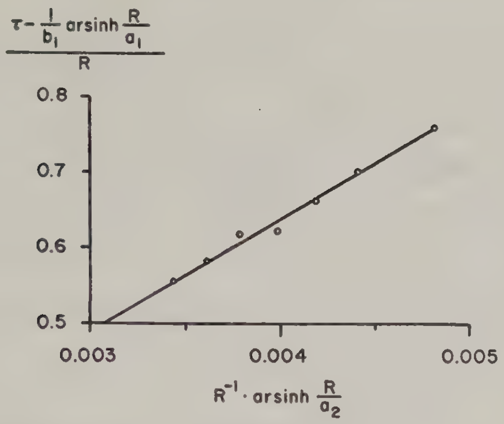

FIG. 3. Graphic determination of the constants in the second approximation.

$$a_2 = 200 \text{ sec.}^{-1}.$$

$$b_2 = 0.0067 \text{ cm.}^2/\text{dyne.}$$

$$\sum_3^i \eta_{0i} = 0.04 \text{ dyne sec./cm.}^2.$$

$$\eta_{02} = \frac{1}{a_2 b_2} = 0.74 \text{ dyne sec./cm.}^2.$$

CONCLUSIONS

The purpose of this investigation was to find formal relationships for the thixotropic equilibrium curve to facilitate the study of thixotropic materials. I have not formed an opinion as to whether Eyring's conception about the flow mechanism is correct. Water is a thixotropic substance; here, however, it is not a transport of flow units, but a sliding of dislocations in a fairly stable lattice. We know from other contexts that different proposed mechanisms can give the same net result. This could also be the case concerning thixotropy. That certain experimental data agree with a supposed mechanism is no guarantee for the correctness of the mechanism. Therefore it should be of great interest to have the treated problem elucidated by the dislocation theory with several coexistent types of dislocations.

SUMMARY

The conception of thixotropy is discussed and a definition presented. It is shown that Eyring's model of flow can describe the equilibrium curve of thixotropic substances with two or more coexistent place-exchange mechanisms. A numerical example of determination of the equilibrium equation of a thixotropic substance is given.

REFERENCES

1. DAHLGREN, S.-E., "On the break-down of thixotropic materials," *Acta Polytech.* **No. 171** (1955). Also *Trans. Chalmers Univ. Technol. Gothenburg* **No. 159** (1955).
2. PRYCE-JONES, J., "Studies in thixotropy," *Kolloid-Z.* **129,** 96–122 (1952).
3. EYRING, H., "Viscosity, plasticity, and diffusion as examples of absolute reaction rates," *J. Chem. Phys.* **4,** 283–291 (1936).
4. GLASSTONE, S., LAIDLER, K. J., AND EYRING, H., "The Theory of Rate Processes," Chapter 9. McGraw-Hill, New York, 1941.
5. POWELL, R. E., "The theory of flow processes." Dissertation, Princeton Univ., Princeton, New Jersey, 1943.
6. POWELL, R. E., AND EYRING, H., "Mechanisms for the relaxation theory of viscosity," *Nature* **154,** 427–428 (1944).
7. KAUZMANN, W., AND EYRING, H., "The viscous flow of large molecules," *J. Am. Chem. Soc.* **62,** 3113–3125 (1940).
8. HERMANS, J. J., "Flow Properties of Disperse Systems," Chapter 1. North Holland Publ. Co., Amsterdam, 1953.
9. ROLLER, P. S., AND STODDARD, C. K., "Viscosity and rigidity of structural suspensions," *J. Phys. Chem.* **48,** 410–425 (1944).

Recommended tables:

LÖSCH, F., "Siebenstellige Tafeln der elementaren transzendenten Funktionen." Springer-Verlag, Berlin, 1954.

JOURNAL OF COLLOID SCIENCE **13**, 159–162 (1958)

EQUATIONS OF STATE FOR IONIZED MONOLAYERS AT THE OIL-WATER INTERFACE

D. A. Haydon

I.C.I. Fellow, Department of Chemistry, Imperial College of Science and Technology, London S.W.7.

Received March 25, 1957; revised September 26, 1957

Abstract

Two equations of state for ionized monolayers at the oil-water interface have recently been proposed which differ by a factor of 2 in the term representing the kinetic energy of the molecules. Both equations have here been derived, and it has been shown that whereas one equation (with the factor of 2) should apply to detergents at relatively high concentrations in aqueous solution, the other applies at very low concentrations, and also when excess of a non-surface-active electrolyte is added to the substrate.

Introduction

The behavior of ionized monolayers at the oil-water interface has been studied by a number of investigators, and various equations have been derived to account quantitatively for their pressure-area (π-A) relationships. Assuming the monolayer to be completely ionized and to be in equilibrium with the bulk phase, two different equations have recently been proposed, the first by Davies (1),

$$\pi = \frac{kT}{A - A_0} + 6.1\sqrt{c}\left\{\sqrt{1 + \left(\frac{134}{A\sqrt{c}}\right)^2} - 1\right\}, \qquad [1]$$

and the second by Phillips and Rideal (2),

$$\pi = \frac{2kT}{A - A_0} + 6.1\sqrt{c}\left\{\sqrt{1 + \left(\frac{134}{A\sqrt{c}}\right)^2} - 1\right\}. \qquad [2]$$

Here π is the surface pressure, A is the area per molecule in the interface, A_0 is the limiting area per molecule, and c is the substrate concentration in gram moles/liter. The temperature has been taken as 20°C.

Both equations were intended to apply to completely ionized uni-univalent detergents both in presence and absence of other non-surface-active electrolytes, and the discrepancy has not yet been explained. The experimental evidence published so far is inconclusive, and attempts to explain theoretically the difference between the two equations have revealed some disagreement (3, 4). The latter aspect is considered here.

DISCUSSION

In deriving a monolayer equation of state it is convenient to consider that no electrolyte other than the detergent is present or that there is present in excess a non-surface-active electrolyte having one ion common with the detergent. We shall first consider the former case.

For a detergent R^+X^-, which is a strong electrolyte (R^+ being surface-active), adsorbed at the oil-water interface, the adsorbed film being in equilibrium with the bulk phase, the Gibbs' equation may be written (5)

$$d\pi = kT\Gamma'_{\mathrm{RX}} d\ln c_{\mathrm{R}^+}^{B} c_{\mathrm{X}^-}^{B} f_{\mathrm{R}^+} f_{\mathrm{X}^-}. \qquad [3]$$

Γ'_{RX} is the surface excess of RX and for RX in dilute solution $c_{\mathrm{R}^+}^{B}$ and $c_{\mathrm{X}^-}^{B}$ are the bulk concentrations in gram ions/liter. If we now consider RX to be at infinite dilution we have

$$d\pi = kT\Gamma'_{\mathrm{RX}} d\ln c_{\mathrm{R}^+}^{B} c_{\mathrm{X}^-}^{B}. \qquad [4]$$

We may also write

$$\mu_{\mathrm{RX}}^{B} = \mu_{\mathrm{ORX}}^{B} + kT\ln c_{\mathrm{R}^+}^{B} c_{\mathrm{X}^-}^{B}, \qquad [5]$$

$$\mu_{\mathrm{RX}}^{s} = \mu_{\mathrm{ORX}}^{s} + kT\ln c_{\mathrm{R}^+}^{s} c_{\mathrm{X}^-}^{s}, \qquad [6]$$

where the superscript *s* refers to the surface phase. At equilibrium

$$\mu_{\mathrm{RX}}^{B} = \mu_{\mathrm{RX}}^{s}; \qquad [7]$$

and at constant temperature

$$\exp\left(\frac{\mu_{0RX}^{B} - \mu_{0RX}^{s}}{kT}\right) = \frac{c_{RX}^{s}}{c_{RX}^{B}} = \text{constant}. \qquad [8]$$

For a small change in c_{RX}^{B} Eq. [8] becomes

$$dc_{\mathrm{RX}}^{B} \times \text{constant} = dc_{\mathrm{RX}}^{s}, \qquad [9]$$

and from Eqs. [4], [8], and [9],

$$d\pi = kT\Gamma'_{RX} \frac{d(c_{R^+}^{s} + c_{X^-}^{s})}{c_{R^+}^{s} + c_{X^-}^{s}}. \qquad [10]$$

If the surface phase is to be electrically neutral $c_{\mathrm{R}^+}^{s} = c_{\mathrm{X}^-}^{s}$, and if we are to have a double layer,

$$c_{R^+}^{s} = c_{X^-}^{s} = c_{RX}^{s} \,\alpha\, \frac{1}{A}. \qquad [11]$$

This step has been criticized (4), but it is merely an extension to the surface phase of the treatment of a strong electrolyte in the bulk. Substituting for Γ'_{RX}, $c_{\mathrm{R}^{+}}{}^{s}$, and $c_{\mathrm{X}^{-}}{}^{s}$ in Eq. [10],

$$d\pi = \frac{-2kT}{A^2}\,dA \qquad [12]$$

and

$$\pi = \frac{2kT}{A} + \text{constant}. \qquad [13]$$

When $A \rightarrow \infty$, $\pi \rightarrow 0$ and, allowing for the finite size of the molecules,

$$\pi = \frac{2kT}{A - A_0}. \qquad [14]$$

For the case of excess added electrolyte, MX (where M^+ is non-surface-active) the Gibbs equation for RX at infinite dilution approximates to

$$d\pi = kT\Gamma'_{\mathrm{R}^+} d\ln c^{B}_{\mathrm{R}^+}. \qquad [15]$$

Following the reasoning outlined above we find

$$\pi = \frac{kT}{A - A_0}. \qquad [16]$$

From Eqs. [14] and [16] we see that at the limit of dilution the π-A relationships should differ according to the presence or absence of added electrolyte. It is very unlikely, however, that the conditions under which Eq. [14] should be obeyed would be found experimentally, since at concentrations low enough for the activity coefficients to be taken as unity the hydrogen and hydroxyl ions in the water would constitute excess electrolyte. The π-A relationship would then be given by Eq. [16].

For finite areas and concentrations, where the hydrogen and hydroxyl ions can be neglected, we should on theoretical grounds expect a difference in behavior between the two cases. In order to obtain the complete equations for finite areas we shall consider detergent to be added to the bulk phase, equilibrium with the surface being maintained. This process of transforming an infinitely attenuated film to finite areas is equivalent to a method described by Overbeek (6) for calculating the free energy (or surface pressure) of the double layer, i.e., charging the diffuse layer from infinity. The surface pressure change during this process is therefore (1), after numerical substitution (at 20°C.)

$$\Delta\pi = 6.1\sqrt{c}\left\{\sqrt{1 + \left(\frac{134}{A\sqrt{c}}\right)^2} - 1\right\}. \qquad [17]$$

The complete equations for presence of excess and absence of added electrolyte are thus derived from Eqs. [14], [16], and [17] and are found to be those of Davies (Eq. [1]) and Phillips and Rideal (Eq. [2]), respectively.

In conclusion it may be said that although the physical picture of the surface phase may be rather obscure, the factor of 2, if present in the Gibbs equation, must also occur in the corresponding equation of state.

The author wishes to thank Professor E. A. Guggenheim and Sir Eric Rideal for helpful discussions.

References

1. Davies, J. T., *Proc. Roy. Soc. (London)* **208*A*,** 224 (1951).
2. Phillips, J. N., and Rideal, E. K., *Proc. Roy. Soc. (London)* **232*A*,** 159 (1955).
3. Ter Minassian-Saraga, L., *Proc 2nd Inter. Congr. of Surface Activity, London. 1957.*
4. Payens, T. A. J., *Kolloid-Z.* **153,** 57 (1957).
5. Cockbain, E. G., *Trans. Faraday Soc.* **50,** 874 (1954).
6. Verwey, E. J. W., and Overbeek, J. T. G., "Theory of the Stability of Lyophobic Colloids." Amsterdam, 1948.

JOURNAL OF COLLOID SCIENCE **13**, 163–169 (1958)

THE EFFECT OF SOAPS AND DETERGENTS ON THE CRITICAL SOLUTION TEMPERATURE OF TRIETHYLAMINE AND WATER

Robert J. Kline[1] and Aaron J. Ihde

Department of Chemistry, University of Wisconsin, Madison, Wisconsin

Received August 20, 1956, revised November 25, 1957

ABSTRACT

Soaps and detergents cause an elevation of the critical solution temperature of the system triethylamine-water. This is probably due to the greatly increased mutual solubilities of the liquids in the presence of the soap and detergent ions. Cationic detergents, anionic soaps and detergents, and mixtures of the two types produce changes of the critical solution temperature which may be explained by the principle that "like dissolves like."

INTRODUCTION

Triethylamine and water are partially miscible liquids which exhibit a lower critical solution temperature.[2] A mixture which contains 26 weight % amine is completely miscible below 18.33°C. but breaks into two layers once that temperature is exceeded. Added salts change the c.s.t. of the system. Some salts lower the c.s.t., whereas other salts, the colloidal electrolytes included, elevate it (1). Soap and detergent ions cause an abnormally large temperature change compared to the simple inorganic ions.

Bailey (2) found that sodium oleate in phenol-water solution caused a large depression of the c.s.t. Since this system has an upper c.s.t., the behavior is consistent with the supposition that the mutual solubilities of phenol and water are increased in the presence of the soap ions.

Palit (3, 4) has found that large amounts of soap can be made to dissolve in certain solvent mixtures. The liquid components, which ordinarily, may not be very soluble in each other, become mutually miscible in the process. To account for this behavior, it was assumed that the hydrocarbon portions of the soap ions interacted with and dissolved the oil-soluble liquid while the polar head groups of the soap ions became hydrogen bonded to the water-soluble component. Thus the peculiar effects noted were a result of the favorable structure of the soap ions.

It was felt that the abnormal influence of soaps and detergents on the

---

[1] Present address: Department of Chemistry, Ohio University, Athens, Ohio.

[2] The initials c.s.t. will be used henceforth to designate critical solution temperature.

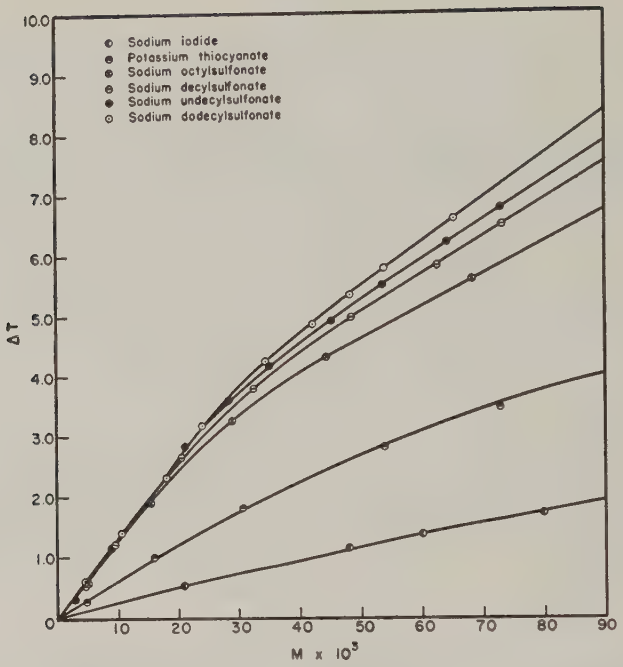

FIG. 1. Variation of miscibility temperature of the system salt-triethylamine-water as a function of salt molality.

c.s.t. of partially miscible liquids might also be a result of the favorable structure of the ions. Further, it was hoped that a systematic study would shed more light on the solution process in these systems.

Triethylamine and water were chosen as the partially miscible liquid pair for several reasons: (*1*) hydrolysis of the soap and detergent ions was expected to be minimized in the basic media, (*2*) pure soaps could be made *in situ* by simply adding the purified fatty acids to the amine-water mixtures, and (*3*) the c.s.t. of the system is relatively insensitive to small changes in composition.

EXPERIMENTAL

Solutions were made up by weight to contain 26% amine, which composition is very nearly the critical (1). These were contained in a conventional jacketed tube equipped with stirrer and thermometer. The average of five ascending and five descending temperature readings were recorded when the solutions were just cloudy enough to obscure the scale on the immersed thermometer. The thermometer was calibrated to the ice point and could be read with an accuracy of ±0.02°C.

Methyl esters of the fatty acids were fractionated in a Todd type column which gave a performance equivalent to 60 theoretical plates. After saponification, the recovered acids were recrystallized several times from aqueous ethanol.

The sulfonate salts were prepared from purified alkyl bromides by a procedure described by Jensen and Lingafelter (5). Sodium dodecylsulfate was prepared from purified dodecanol by the method of Shedlovsky (6). Dodecyl bromide, made from dodecanol by the method of Kamm and Marvel (7), was used to prepare both cationic detergents using methods developed by Shelton (8).

The triethylamine was carefully distilled. The middle-third fraction was retained for passage through an alumina-filled adsorption column. Inorganic salts were reagent grade materials which were dried in an oven at 110°C. before use.

RESULTS

Figures 1, 2, and 3 show the elevations of the c.s.t. plotted against the molalities of the third components.

Soaps and detergents give families of similar curves which consist of two essentially linear sections joined by an intermediate curved portion.

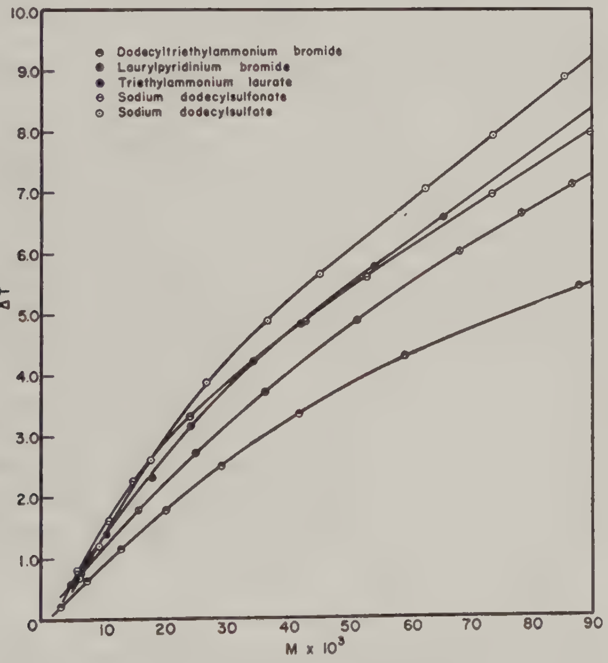

FIG. 2. Variation of miscibility temperature of the system salt-triethylamine-water as a function of salt molality.

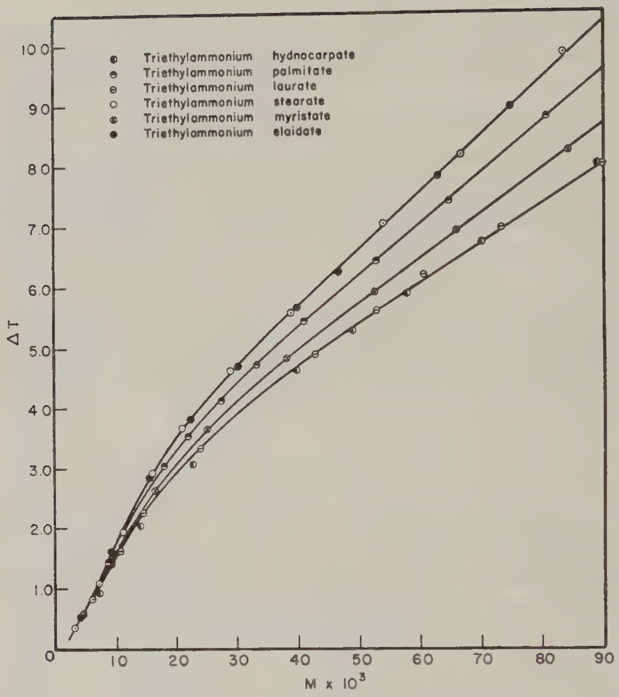

FIG. 3. Variation of miscibility temperature of the system salt-triethylamine-water as a function of salt molality.

The two inorganic salts are seen to be much less effective than the soaps or detergents. Also, cationic detergents are seen to be less effective than anionic soaps and detergents.

In solutions of concentration 0.05 molal or higher, the order of decreasing elevative effect is: sodium dodecylsulfate, sodium dodecylsulfonate, triethylammonium laurate, dodecylpyridinium bromide, dodecyltriethylammonium bromide. This order changes slightly in more dilute solutions, as can be seen in Fig. 2.

The effect of chain length may be seen by comparing the carboxylates in Fig. 3 and the sulfonates in Fig. 1. The elevative power is greater the longer the carbon chain. However, the hydnocarpate with 16 carbons is only about as effective as the 12-carbon straight-chain soap. The stearate and elaidate appear to have identical elevative powers.

Table I contains data which show the effect of mixing certain of the compounds in amine-water solutions.[3]

These results may be summarized as follows: (*1*) Mixtures of inorganic

---

[3] The ΔT versus M curve for KI follows that of NaI very closely.

TABLE I

Effect of Salt Mixtures on the Critical Solution Temperature

Mixture	Molality of each addendum	Elevation °C.	
		Observed	Calculated[a]
1. Sodium iodide Potassium iodide	0.148	3.64	3.65
2. Triethylammonium stearate Triethylammonium myristate	0.0372	8.55	8.57
3. Triethylammonium stearate Potassium iodide	0.0372	5.67	5.25
4. Sodium dodecylsulfate Sodium iodide	0.0308	4.10	3.80
5. Sodium palmitate Sodium iodide	0.0440	5.85	5.63
6. Sodium decylsulfonate Laurylpyridinium bromide	0.0303	2.73	5.57
7. Sodium dodecylsulfonate Laurylpyridinium bromide	0.0304	2.58	5.95
8. Sodium palmitate Lauryltriethylammonium bromide	0.0277	2.83	5.14

[a] Assuming complete additivity.

salts or of two anionic soaps were found to be additive in their effects on the c.s.t. (*2*) The effects of mixtures of inorganic salts and anionic soaps were slightly greater than calculated. (*3*) The effects of mixtures of anionic soaps and cationic detergents were much less than additive.

DISCUSSION

The explanation usually given for an increase in c.s.t. with added salts is that the third component distributes itself approximately equally between the two liquids (9). Evaporation of samples of the amine-rich layer at the end of some of the runs established the fact that the third component was concentrated in the water-rich layer, however.

In a c.s.t. study of the system propylene glycol-benzene (10), Palit and McBain explained their results with the help of a mechanism involving polar head group-glycol and hydrocarbon tail-benzene interactions. Presumably the soap was molecularly dispersed in the ternary system. This is cosolvency.

Although it is probably not possible to account for all the effects noted here by means of a single mechanism, there is some evidence that points towards the applicability of the Palit-McBain mechanism in the amine-water system also. Accordingly, one supposes the hydrocarbon portion of the soap or detergent ions to interact with the hydrocarbon portion of the amine while the polar head groups of the soaps or detergents and the nitrogen atom of the amine are expected to hydrogen bond with the water.

Examination of molecular models shows that a twelve-carbon chain in its extended form has enough surface area to accommodate about seven amine molecules. The amine molecules are essentially disc-shaped with the nitrogen atom on one side. This would lead to a small aggregate bearing about eight polar sites that could interact with the water.

The increased c.s.t. with increasing chain length would be expected since increasing hydrocarbon chain length should increase the surface with which amine may interact. Further evidence may be found in comparing the elevative powers of the hydnocarpate soap with the normal chain soaps. Hydnocarpate ions, which contain 16 carbon atoms, terminating in a five-membered ring containing one double bond, were about as effective as 12-carbon normal chain soap ions. Molecular models show that the effective length of hydrocarbon chain in the hydnocarpate is about the same as in the laurate. The unsaturation in the hydnocarpate probably is not a factor since elaidate ions show identical elevative powers to stearate ions.

The antagonism of the cationic and anionic soaps may also be consistent with this mechanism. Ion pairing in which the oppositely charged long-chain ions are oriented "head to head" and "tail to tail" may be expected to occur when cationics are mixed with anionics. Several probable consequences of such behavior may be pointed out. They are: (*1*) There occurs a reduction of hydrocarbon surface with which the amine may interact. (*2*) Triethylammonium ions which were ion-paired to the anionic soap would be liberated into the solution. A shift of the equilibria

$$\mathrm{Et_3N + H_2O \rightleftharpoons Et_3NHOH \rightleftharpoons Et_3NH^+ + OH^-}$$

toward the left would result. (*3*) A reduction of water binding capacity and a loss of charge would be expected to occur. The effect of loss of charge is not clear but all other consequences mentioned should lead to decreased miscibility of the major components and a lower c.s.t.

The differences in elevative powers of the 12-carbon anionics and cationics may be due to differences in the strength of interaction between the long-chain ions and triethylammonium ions (*vide supra*). Some difference may be attributed to the presence of different inorganic ions in the solutions also. The Palit-McBain mechanism calls for H-bonding between the polar groups and water. The highly electronegative and tetrahedral sulfate group would be expected to interact most strongly and the cationic detergents least strongly as is observed. This may explain the small differences in the elevative effects of the anionics.

It is not known what part conventional soap micelles play in these systems. If the change in slope of the curves is due to micellization, it takes place at about the same concentration no matter what the chain length.

Although the transition portions of the curves do not fall in or slightly above the general range for micellization in water alone, one would expect more significant differences between the various soaps and detergents used. Also, it may be concluded from the shapes of the curves that if micelles are responsible for the change in slope, they must be less effective in promoting the mutual solubility of water and triethylamine than is soap in "molecular" solution. A consideration of the behavior of the mixtures of anionic soaps and detergents with inorganic salts may shed some light on this question. It is well known that the proportion of soap in the micellar state in an aqueous solution of a soap is greatly increased when inorganic salts are added. Thus the elevative power of these mixtures would be expected to be less than additivity predicts. What is observed is a slight elevation in the three mixtures studied here (Table I). Finally it should be added that similar inflections have been observed in systems containing inorganic salts (11). For example, sodium chloride, sodium bromide, and sodium cyanide lower the c.s.t. of the triethylamine-water system and the depression versus concentration curves show an abrupt change in slope at about 0.15 molal. The system sodium acetate-ethanol-hexane shows a similar change in slope which has been attributed to solvolysis of the inorganic salt (12).

SUMMARY

1. The change of the c.s.t. of triethylamine and water solutions containing soap and detergent ions has been studied.

2. A probable mechanism for the action of these ions may involve association of the amine with the hydrocarbon portion of the soap giving small aggregates which are dissolved by the water. The principle that "like dissolves like" is probably applicable to these systems.

REFERENCES

1. TIMMERMANS, J., *Z. physik. Chem.* **58,** 197 (1907).
2. BAILEY, C. R., *J. Chem. Soc.* **123,** 2579 (1923).
3. PALIT, S. R., *J. Indian Chem. Soc.* **19,** 271 (1942).
4. PALIT, S. R., *J. Am. Chem. Soc.* **69,** 3120 (1947).
5. JENSEN, L. H., AND LINGAFELTER, E. C., *J. Am. Chem. Soc.* **66,** 1944 (1946).
6. SHEDLOVSKY, L., *Ann. N. Y. Acad. Sci.* **46,** 428 (1946).
7. KAMM, O., AND MARVEL, C. S., *Org. Syntheses* **1,** 25 (1932).
8. SHELTON, R. S., *et al.*, *J. Am. Chem. Soc.* **68,** 753 (1946).
9. FINDLAY, A., "The Phase Rule and Its Applications," p. 101. Dover, New York, 1938.
10. McBAIN, J. W., AND PALIT, S. R., *J. Am. Oil Chemists' Soc.* **24,** 190 (1947).
11. KLINE, R. J., Ph.D. Thesis, University of Wisconsin, Madison, 1953.
12. HOWARD, E. J., AND PATTERSON, W. H., *J. Chem. Soc.* **130,** 2787 (1926).

JOURNAL OF COLLOID SCIENCE **13**, 170–178 (1958)

ANOMALOUS BEHAVIOR OF POLYMER SOLUTIONS
II. VISCOSITY BEHAVIOR OF RUBBER SOLUTIONS AT HIGH DILUTIONS

S. L. Kapur and S. Gundiah

National Chemical Laboratory, Poona-8

Received May 6, 1957; Revised October 14, 1957

Abstract

Studies in the viscosity behavior of dilute solutions of crepe and deproteinized natural rubber in different solvents have shown that carbon tetrachloride and other chlorinated solvents are not suitable for viscosity determinations of rubber. Data are presented to show that the anomalous increase of viscosity at very high dilutions cannot be explained by Öhrn's adsorption hypothesis but could be attributed to the extension and disentangling of polymer chains at higher dilutions. The anomaly is also shown to disappear if the solutions are shaken for a minimum period of time before viscosity determinations.

Introduction

The viscosity behavior of polymer solutions at high dilutions has been the subject of intensive study in recent years. Since the viscosity at high dilutions is very close to that of the solvent, it requires precision viscometry. With improved techniques, however, it has been possible to obtain reliable data at considerable high dilutions, and various kinds of departures of viscosity-concentration graphs from linearity have been reported (1–5).

The viscosity-concentration plots for solutions of polyelectrolytes depart from linearity at lower concentrations owing to the uncoiling of the chains as a result of the electrostatic repulsive forces of the adjacent ionic groups on the chains (6). Similar anomalies have been reported for solutions of nonpolar polymers also. Betzer (1) attributed the nonlinearity of viscosity-concentration curves for polyvinyl chloride in tetrahydrofuran to branching of the polymer chains; this was, however, disputed by subsequent workers (7).

An anomalous increase followed by a decrease in relative viscosity of solutions of gel, sol, and whole rubber and chlorinated rubbers in carbon tetrachloride at lower concentrations has been reported (2). Umstatter (3) observed an anomalous increase in viscosity at high dilutions for polyisobutylenes in decalin. Streeter and Boyer (4), using a viscometer having a long flow time, observed a minimum and a maximum below a concentration of 0.1 g./dl. (i.e., 0.1 g./100 ml.) for polystyrene in toluene and methylethyl ketone and attributed the increase to the disentangling of the polymer chains and the decrease thereafter to their adsorption on the walls of the capillary. For solutions of polystyrene in benzene they reported an anomalous increase in viscosity. For dilute solutions of polystyrene in toluene Öhrn (5) failed to notice an upturn in the viscosity curve but observed only an anomalous decrease. Öhrn, though at first concluding that adsorption alone cannot completely account for the anomalies, later (8) explained both the anomalous increase observed by Streeter and Boyer (4) and the anomalous decrease observed by him (5) as being due to different degrees of adsorption. Kapadia (9) in his studies on solutions of rubber and chlorinated rubber concluded that adsorption is not the cause of the anomalies observed by him. Recently Öhrn's adsorption hypothesis has been supported by a few Japanese workers for the anomalous behavior of polyvinyl chloride in cyclohexanone (10). In the studies on dilute solutions of polystyrene the importance of shaking the solutions for a sufficiently long time before the viscosity measurements was emphasized by Streeter and Boyer (4). They further suggested (11) that this controversy could be settled by use of the light-scattering technique, but Frank (12) failed to notice any such anomaly in his light-scattering studies of polystyrene in methylethyl ketone and toluene.[1]

It is, therefore, seen that the viscosity behavior of highly dilute polymer solutions is a controversial issue and calls for more experimental work. In the National Chemical Laboratory, we have examined the viscosity behavior of dilute solutions of natural rubber, even though it presents more complications than a polymer synthesized in the laboratory. Such a study is likely to be useful in several applications of natural rubber.

A preliminary study of the effect of light on the solutions of rubber in different solvents showed a progressive decrease in viscosity with time for all solutions in diffused daylight. No change in viscosity was observed for solutions in benzene, *n*-hexane, and absolutely dry and pure carbon tetrachloride under red light. It was, however, noticed that the viscosity of the solutions in carbon tetrachloride changed considerably even in red light when the solvent contained traces of moisture. Similar phenomena were observed for solutions of rubber in other chlorinated solvents such as ethylene dichloride, tetrachloroethane, and chloroform. Our studies on the concentration dependence of the viscosity of rubber solutions were confined to benzene and *n*-hexane solutions in red light, and the behavior in benzene was studied exhaustively.

---

[1] Recently T. Kawai and K. Saito [*J. Polymer Sci.* **26,** 213 (1957)] have pointed out that the absence of the anomalous behavior in the light scattering studies (12) need not necessarily mean that changes in configuration of polymer chains do not take place with dilution.

EXPERIMENTAL

Material. Sixty per cent centrifuged latex was deproteinized according to the method of Nobel (13) and the sols of crepe and deproteinized rubbers were obtained (we are thankful to Mr. D. Raghunath for the above samples) by extracting with petroleum ether (b.p. 40°–60°C.) as described by Bloomfield (14). The solutions of sols were obtained by the following two different techniques carried out in a dark room with a 15-watt red lamp; the same dark room was used for viscosity measurements also. In the first method the petroleum ether extract was dried at room temperature at reduced pressure followed by thorough drying under high vacuum. A known weight of this dry sol was dissolved in the solvent to give a solution of known concentration. In the second method, the extract was concentrated under reduced pressure and when quite viscous, the solvent was added and the evaporation continued. The process was repeated five times to ensure complete replacement of petroleum ether by the solvent. A known volume of the final solution was evaporated to constant weight and concentration determined. The solutions prepared by both the methods were preserved in well-stoppered bottles in the dark.

Benzene, carbon tetrachloride, were C.P. grade and were purified according to the method of Vogel (15) and were fractionated twice before use. Benzene was stored over sodium wire and carbon tetrachloride over technical grade fused calcium chloride. The other solvents ethylene dichlo-

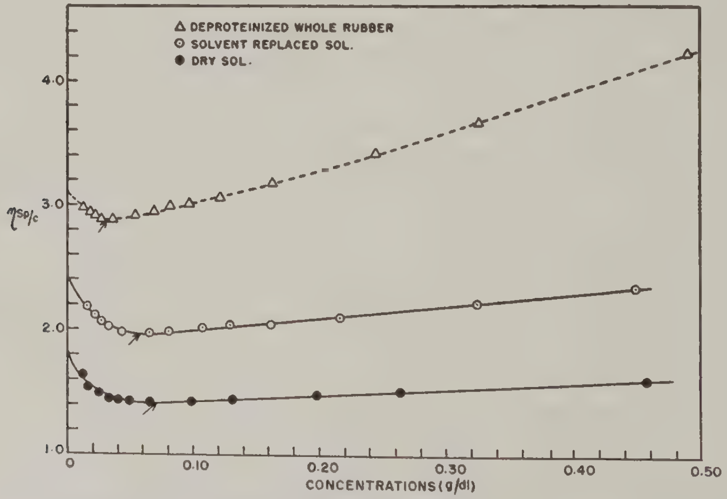

FIG. 1. Viscosities of deproteinized whole, sol rubbers in benzene at 30°C. in the dark.

ride, tetrachloroethane, tetrahydrofuran, *n*-hexane, and iso-octane (2,2,4-trimethyl pentane) were A.R. grade and only middle fractions with constant boiling points were used in viscosity measurements.

Apparatus. The viscosity measurements were carried out at 30°C. and 40°C. in the dark room in a thermostat controlled to ±0.01°C. An Ubbelohde suspended-level dilution viscometer obtained from M/S. Polymer Consultants Ltd., London, having a 10.2 cm. long capillary of 0.15 mm. radius, was used. It had a flow time of 616.6 ± 0.1 sec. for benzene at 30°C. and negligible kinetic energy correction.

RESULTS

The viscosity-concentration plots for dry sol, solvent-replaced sol, and deproteinized whole rubber in benzene are shown in Fig. 1. Up to a concentration of 0.07 g./dl. for dry sol, it follows a straight line and an anomalous increase in $\eta sp/c$ is observed at lower concentrations. In the case of solvent-replaced sol the minimum shifts towards a lower concentration, and this occurs at a still lower concentration for the deproteinized whole rubber. Similar behavior was observed for solutions of deproteinized whole rubber in *n*-hexane and crepe rubber in benzene and *n*-hexane.

Preliminary experiments on the effect of shaking the solutions prior to viscosity measurements showed that the viscosity is much influenced by this pretreatment. This observation called for an intensive investiga-

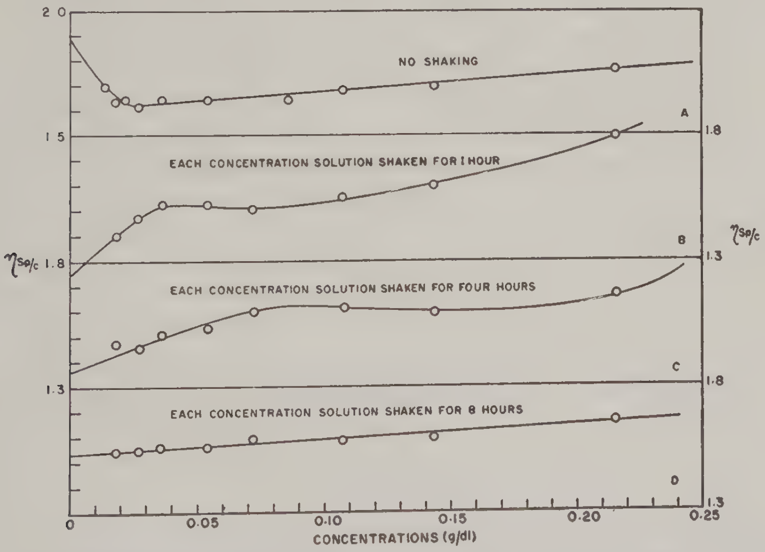

FIG. 2. Viscosities of dry sol of deproteinized rubber in benzene at 30°C. in the dark.

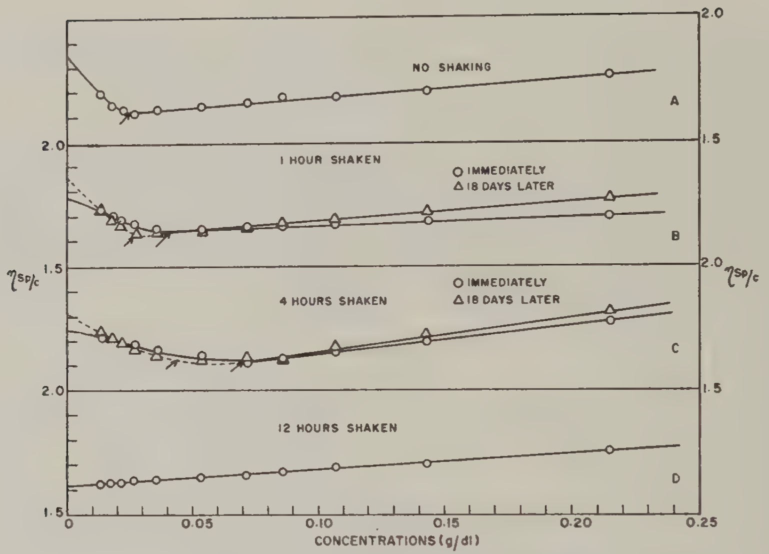

FIG. 3. Viscosities of dry sol of deproteinized rubber in benzene at 30°C. in the dark.

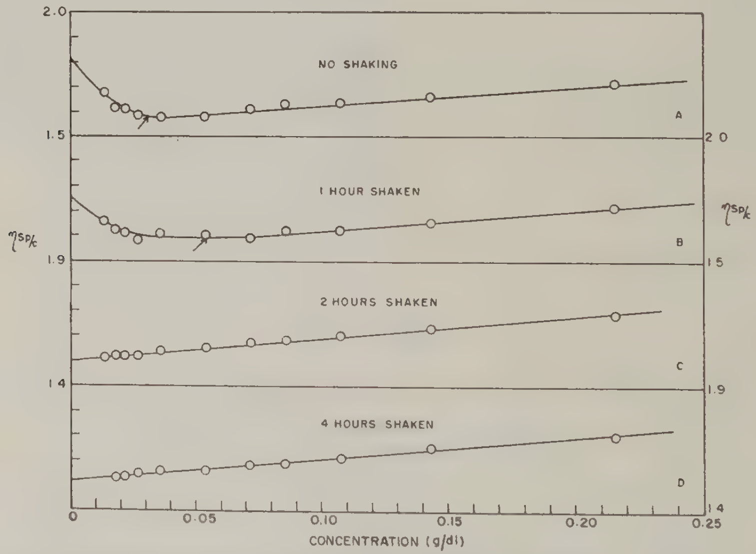

FIG. 4. Viscosities of dry sol of deproteinized rubber in benzene at 40°C. in the dark.

tion. The results of these studies on deproteinized dry sol in benzene are shown in Figs. 2, 3, and 4. Figure 2 represents the results of shaking each one of the several concentrations separately and carrying out the viscosity measurements thereafter. With increasing periods of shaking the minimum broadens and shifts towards higher concentrations, and the viscosity-concentration plot for solutions shaken for 8 hours or more is a straight line. These experiments were repeated by shaking only the initial concentrated solutions, 10 ml. of which was transferred to the viscometer, and the measurements were carried out at 30°C. (Fig. 3) and 40°C. (Fig. 4) by successive dilutions in the viscometer alone. With the increase in the period of initial shaking the minimum shifts towards higher concentrations. A straight line is obtained for solutions shaken for 12 hours if the measurements are made at 30°C. and for solutions shaken for 2 hours if the measurements are made at 40°C. It is pertinent to point out that in contrast to plots in Fig. 2, no maxima are observed in Figs. 3 and 4.

The viscosity falls slightly after shaking but slowly recovers when the solutions are allowed to rest and approaches that of the unshaken solutions. The recovery is slow for solutions shaken for longer times. The increase of temperature of the viscosity measurements reduces the minimum period of shaking necessary to observe a linear behavior of the viscosity-concentration plot. The interval of 12 hours at 30°C. is reduced to 2 hours at 40°C.

Discussion

The effect of shear on the viscosity of dilute solutions of rubber was estimated by the method used by us for polyvinyl acetate solutions (16). Since a maximum variation of only 1% in the $\eta sp/c$ was observed for zero shear and shear rate of about 1000 sec.$^{-1}$, the anomaly cannot be attributed to shear effects. The other possible explanations that may be advanced to explain this anomalous behavior are adsorption of the rubber on the capillary walls of the viscometer (8) and/or disentanglement of the polyisoprene chains at high dilutions (4). Kapadia's experiments (9) on the possibility of adsorption of the polymer molecules on the capillary walls were repeated by us by using glass beads (B.D.H. 0.3 to 0.4 cm. diameter) instead of glass wool since glass beads provide a surface more akin to that of the capillary walls. No change in viscosity was observed even after 40 hours, ruling out the possibility of adsorption being the cause of the anomaly.

A possible explanation for the anomalous behavior seems to be in the disentanglement of polyisoprene chains in solution. The fact that with shaking of the solutions, the nature of the viscosity-concentration curve slowly changes and tends to a straight line characteristic of the normal behavior, is sufficient evidence in support of this view. The reduction in minimum period of shaking with increase in temperature of viscosity measurements suggests that for every temperature there is a minimum period of shaking required to observe the normal behavior. By the increase of temperature the disentangling of the polymer chains is greatly facilitated and is achieved with a much shorter period of shaking.

The polyisoprene chains will get more entangled during the preparation of dry sol than in that of the solvent-replaced sol; this should impart a lower intrinsic viscosity to the solution of the former. This is in conformity with our observation (Fig. 1). Since mechanical shaking has helped to disentangle the polyisoprene chains they should return to their original state when the solutions are allowed to rest. The time required for this recovery should be more, the more they are disturbed from their original configuration, which is supported by Fig. 3. The decrease in viscosity of the solutions after the initial shaking may be attributed to the rupture of the intermolecular agglomeration of the polyisoprene chains. On resting they will regain their original configuration, owing to secondary valence forces, as shown by the viscosity recovery. It also shows that the behavior is purely a physical phenomenon.

Streeter and Boyer (4) observed an increase in the viscosity of polystyrene solutions after shaking which is contradictory to our observation. It may be stated that shaking solutions at high concentration involves the breaking of intermolecular clusters which leads to a decrease in viscosity, whereas in the case of sufficiently dilute solutions, shaking brings about disentangling of the individual macromolecular chains or the rupture of the intramolecular agglomeration which is responsible for the increase in viscosity. This also explains the presence of maxima in Fig. 2 and their absence in Figs. 3 and 4. Disentangling is affected both by shaking and by the availability of a relatively large volume of solvent. Under the influence of both these factors, the minima in the viscosity-concentration graph (or the start of the intramolecular disentanglement of the macromolecular chains) must be at a relatively high concentration; this is supported by Fig. 2. Once the chains are extended, a linear decrease of viscosity with subsequent dilution should result, and this accounts for the maxima in Fig. 2. The shift of minima towards higher concentrations with increase in the period of shaking may be attributed to increased disturbance of the macromolecular chains, disentanglement being facilitated earlier or at higher concentrations. The shift in minima with increase in intrinsic viscosity also suggests that with increase in molecular dimensions the availability of the excess of solvent is an important factor for the disentangling of the macromolecular chains.

The difference in slopes of the viscosity-concentration plots for the shaken and unshaken solutions is quite significant. On shaking, since the number of aggregates is much reduced, intramolecular disentanglement tends to occur on dilution resulting in a lesser slope—a further fact in favor of the disentanglement hypothesis.

It may be pointed out that Streeter and Boyer (4), although putting forward an explanation of the anomalous behavior of dilute solutions of polystyrene, did not fully attribute it to the disentangling of polymer chains and stressed the importance of shaking the solutions for a sufficiently long time before viscosity measurements. It is likely that if they had taken a quantitative effect of the time of shaking into consideration they might have arrived at a conclusion similar to ours. Very recently Cragg (19) has demonstrated the physical reality of the critical concentration by quite a different and indirect method. It may be stated that the critical concentrations reported by him are of the same order as in our studies. An inverse relation between [η] and critical concentration has been reported which is in conformity with our results (Fig. 1).

The decrease in viscosity of rubber solutions when they are exposed to light may be attributed to cyclization of the polyisoprene chains. The decrease in iodine value observed by Stevens (17) in the final products (which he calls photogels) is indicative of this. Solutions of rubber in absolutely dry carbon tetrachloride, benzene, *n*-hexane did not show any decrease in viscosity in red light, whereas all solutions showed an enormous decrease in viscosity when exposed to daylight (Fig. 5). In these experiments 0.4% to 0.5% solutions were used. Traces of moisture were sufficient to bring about decrease of viscosity with time for carbon tetrachloride solutions in red light. The aging effect cannot be ascribed to

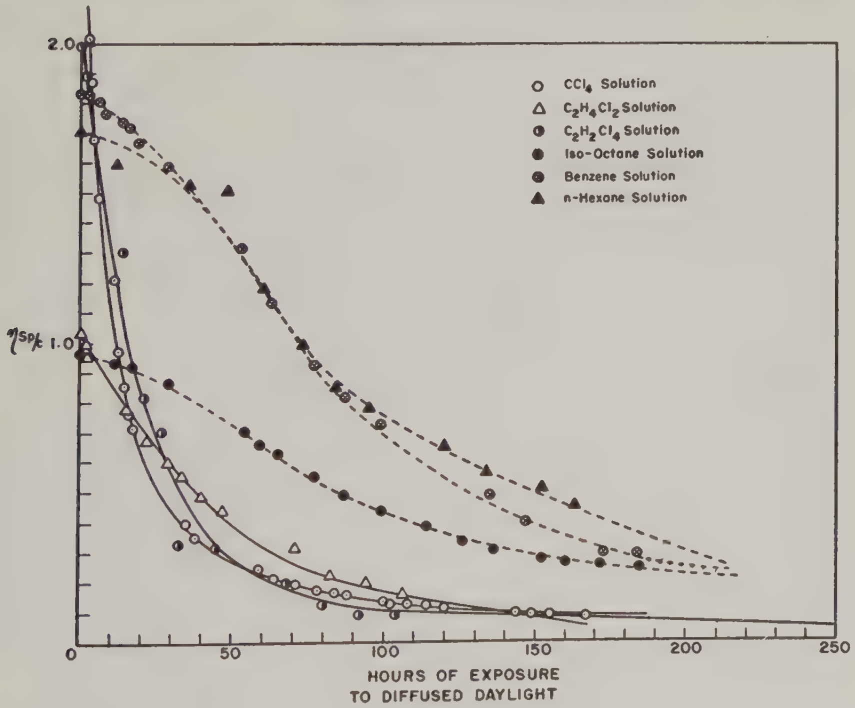

FIG. 5. Aging of solutions of dry sol of deproteinized rubber.

oxidation of rubber, since Stevens (17) observed that though traces of oxygen acted as catalyst, absence of air did not prevent gelling. In fact, in some of the cases presence of large excess of oxygen retarded the rate of gelling.

No doubt cyclization will lead to a decrease in viscosity, but this does not explain the fall in viscosity to almost that of the solvent (Fig. 5) when the solutions are exposed for a long time. The fall in viscosity to this level could be due to the physical separation of cyclized rubber from the liquid phase, as observed by us.

Cyclization alone cannot fully explain the aging of rubber in chlorinated solvents. Stevens (17) detected firmly bound chlorine in the final product, and it could not be removed even by acetone extraction of the dried product. This accounts for the increase in weight of the final product over that of the rubber in the original solution, thus establishing that chlorination also proceeds along with cyclization when rubber in chlorinated solvents is exposed to light. Some previous work (18) done in our Laboratory also lends support to this view.

It may be concluded that carbon tetrachloride and other chlorinated solvents are not suitable for the viscosity determination of natural rubber. Further work on these systems is in progress.

REFERENCES

1. BETZER, H. *Makromol. Chem.* **12,** 145 (1954).
2. KAPADIA, F. H., *Makromol. Chem.* **13,** 194 (1954).
3. *a.* UMSTATTER, H., *Makromol. Chem.* **12,** 94 (1954).
   b. UMSTATTER, H., *Makromol. Chem.* **16,** 65 (1955).
4. STREETER, D. J., AND BOYER, R. F., *J. Polymer Sci.* **14,** 5 (1954).
5. ÖHRN, O. E., *Acta Chem Scand.* **8,** 1303 (1954).
6. MATHIESON, A. P., AND PORTER, M. R., *J. Polymer Sci.* **21,** 495 (1956).
7. *a.* MANCIK, Z., AND LAUIKOVA, J., *Makromol. Chem.* **14,** 118 (1954).
   b. PATAT, R., AND ELLIAS, H. G., *Makromol. Chem.* **14,** 40 (1954).
8. ÖHRN, O. E., *J. Polymer Sci.* **17,** 137 (1955).
9. KAPADIA, F. H., *Makromol. Chem.* **16,** 238 (1955).
10. TAKEDA, M., AND ENDO, R., *J. Phys. Chem.* **60,** 1202 (1956).
11. STREETER, D. J., AND BOYER, R. F., *J. Polymer Sci.* **17,** 154 (1955).
12. FRANK, H. P., *J. Polymer Sci.* **17,** 130 (1955).
13. NOBEL, R. J., *Proc. Rubber Technol. Conf.*, 131(1938).
14. BLOOMFIELD, G. F., *J. Rubber Research Inst. Malaya,* Jan., 1953.
15. VOGEL, A. I., "Practical Organic Chemistry Including Qualitative Organic Analysis," 3rd ed., pp. 173 and 176. Longmans, London 1956.
16. KAPUR, S. L., AND GUNDIAH, S., *J. Polymer Sci.* **26,** 89 (1957).
17. STEVENS, H. P., *Trans. Inst. Rubber Ind.* **16,** 211 (1940).
18. PANDE, J. B., RAGHUNATH, D., AND RAMAKRISHNAN, C. S., *J. Indian Chem. Soc.* **33,** 430 (1956).
19. CRAGG, L. H., AND BIGELOW, C. C., *J. Polymer Sci.* **24,** 429 (1957).

JOURNAL OF COLLOID SCIENCE **13**, 179–187 (1958)

THE PREPARATION OF UNIFORM EMULSIONS BY ELECTRICAL DISPERSION

M. A. Nawab[1] and S. G. Mason

Pulp and Paper Research Institute of Canada and Department of Chemistry, McGill University, Montreal, Quebec, Canada

Received August 5, 1957, revised November 12, 1957

ABSTRACT

A method of preparing emulsions having narrow size distributions in which the disperse phase is first formed as an aerosol, is described. The method is of general applicability, is particularly suitable for preparations of accurately known concentration of disperse phase, and has a number of advantages over conventional methods of emulsification. The basic factors governing the process are considered, but no attempt is made to arrive at a quantitative explanation of the phenomena involved.

INTRODUCTION

In order to investigate the viscosity behavior of dilute emulsions, it became necessary to develop a convenient technique for preparing stable emulsions of accurately known concentration and of reasonably uniform particle size. Since none of the conventional methods of emulsification, e.g., mechanical shaking, colloid milling, and injection, was suitable, a new technique based on electrical dispersion of the discontinuous phase was developed.

A high electrical potential applied to water emerging from a fine capillary causes the water to break into fine threads which break into small globules. Zeleny (1) discovered the phenomenon and recently Vonnegut and Neubauer (2) extended the observations. Using glass capillaries and applying high positive potentials to water, ethanol, lubricating oil, and aqueous sugar solutions, they produced aerosols which exhibited higher order Tyndall phenomena, from which it was concluded (2) that the particles were of uniform size, about 1 μ diameter. In a subsequent study (3) of the effect of simple electrolytes on dispersion, it was found necessary to place a negative electrode near the capillary; when the conductance of the solution was much higher than that of water, only a single stream of large drops could be produced.

---

[1] Colombo Plan Scholar on leave from Chemistry Department, Dacca University, East Pakistan.

Vonnegut and Neubauer considered the breakup to result from the autorepulsion of the electrostatically charged surface which overcomes the cohesive forces of surface tension, and from elementary considerations derived the following relationship:

$$r^3 = \frac{9V^2K\gamma}{4\pi Q^2}, \qquad [1]$$

where r is the radius of the droplets formed, Q is the total electrostatic charge carried by a volume V of dispersed liquid, γ is the surface tension, and K is a constant.

Although Eq. [1] has not been confirmed quantitatively, it is of interest to note that, other conditions remaining the same, it predicts that r^3 is proportional to the surface tension.

Drozin (4) conducted a more elaborate study using a number of liquids and gave a systematic description of the various stages of dispersion as the applied field was varied. He tried, without success, to arrive at a quantitative treatment of the process.

The investigation described here was undertaken to use the technique to prepare monodisperse emulsions. The development of the method together with pertinent observations of dispersion phenomena is the subject of this paper.

EXPERIMENTAL PART

Electrical Dispersion

Preliminary experiments were made using glass capillaries of about 0.08 mm. diameter with the electrode dipped in the liquid. It was soon found that by substituting a metal capillary for the glass one, and directly connecting it to a high-voltage source, dispersion occurred at much lower voltages, particularly in the case of poorly conducting liquids.

Figure 1 shows the essential parts of the apparatus used. The steel hypodermic needle (N) was ground to a flat end and was connected to a 0 to 4 kv. d.-c. source. The graduated tube (L) contained the liquid to be dispersed. Depending upon the viscosity of the liquid used, the needle diameter was chosen so that a flow rate of about 20 to 30 drops per minute was maintained in absence of the field.

In some observations of dispersion of various liquids in air, the brass tube (M), which served as the ground, was replaced by flat metal strips kept parallel to the needle, or directly below the needle tip, in such a way that the distance between the ground and the needle could be varied. By proper choice of the needle diameter and the gap between the needle and the ground, various liquids could be dispersed at a potential of 4 kv. or less. The liquids used included benzene, carbon tetrachloride, 0.1 % aqueous

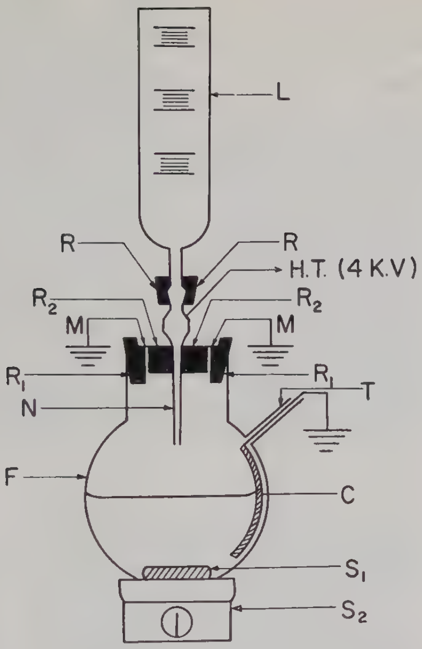

FIG. 1. Apparatus for preparation of emulsions.

L —graduated tube for the disperse phase.
R, R_1, R_2—rubber stoppers.
M —grounded brass tube.
N —hypodermic needle.
T —side tube.
C —grounded electrode in continuous medium.
S_1, S_2 —magnetic stirrer.
F —receiving flask.

caustic soda, solutions of different emulsifiers in water and in butyl benzoate, amyl benzoate, etc. There appeared in fact to be no limitation to the type of the liquid used, provided that the flow rate, ground-to-needle distance, and potential were suitably adjusted.

The successive stages of dispersion on slowly increasing the potential, which could be either positive or negative, were observed through a microscope having a magnification of 40×. The various stages are shown in the photographs in Fig. 2.

On increasing the potential (from i to ii Fig. 2), the drop size leaving the capillary decreased and the drop frequency increased. On further increase of the potential (to iii) the drops, elongated in the vertical direction, emerged very close together, possibly at times even touching one another, to give the appearance of a vibrating thread. This was a transition stage at which a slight increase in potential (to iv) of 20 volts or less caused the

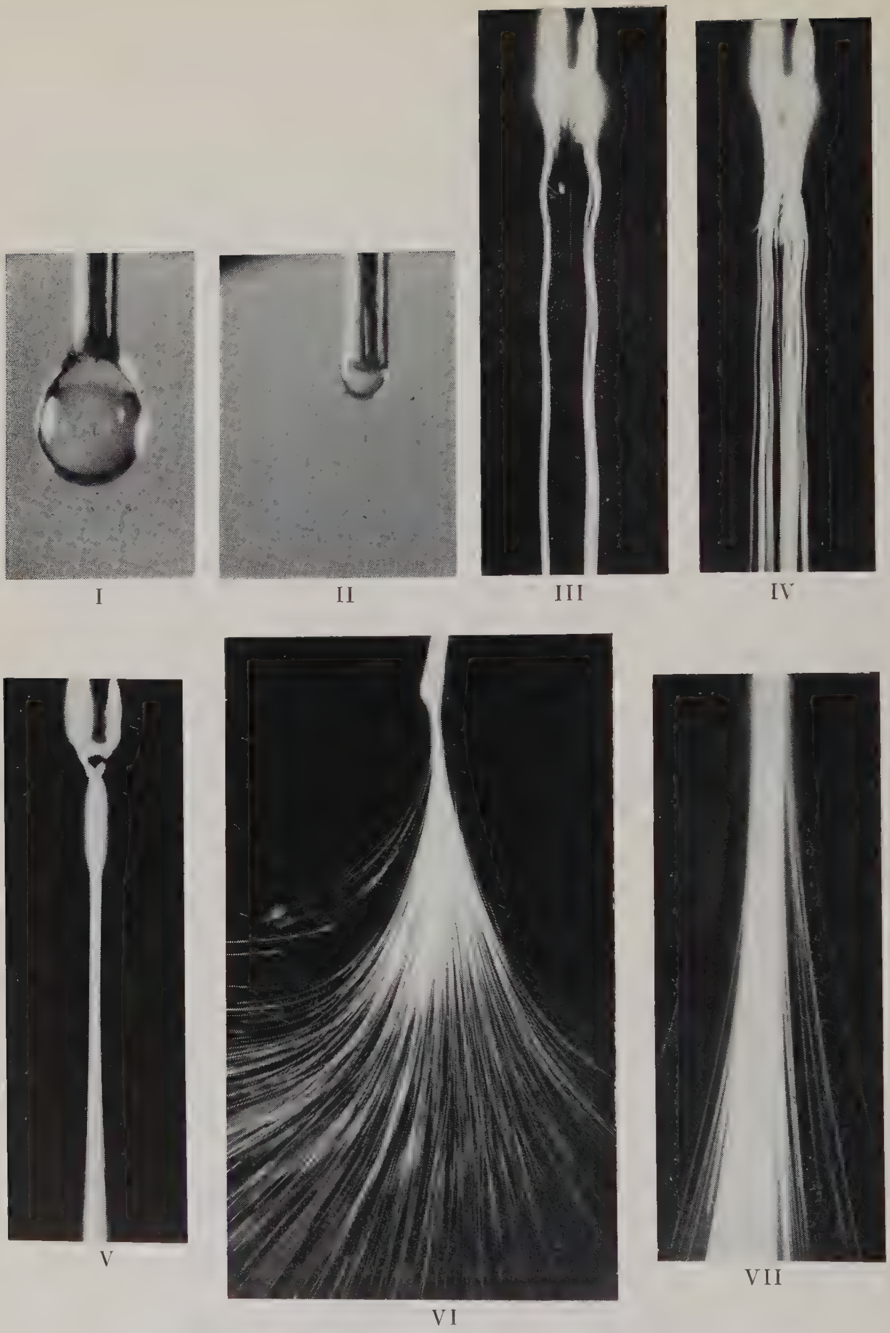

FIG. 2. Various stages of dispersion of water.

i. 0.0 kv. –normal drop.
ii. 1.8 kv.—drops becoming smaller.
iii. 2.56 kv.—continuous column.
iv. 2.60 kv. –critical potential; onset of dispersion.
v. 3.9 kv.—upper part of the dispersed column.
vi. 3.0 kv.—closeup view of the whole dispersed column. Owing to the finite exposure time and lack of resolution, the streams of discrete droplets appear as continuous threads.
vii. 3.9 kv.—middle part of the dispersed column.

single column of liquid to split into multiple "threads" (iv) each consisting of a succession of small drops. The "critical potential" at which threading of the single liquid column occurred (between iii and iv) was highly reproducible for a fixed geometry. After further increase of potential (to v, vi, and vii), the threads became more numerous and the drop size decreased further. It was observed for all liquids and under all circumstances studied, that the liquid jet emerging from the needle tip was conical and converged at a distance of about 0.5 mm. into a narrow column which then broke into several filaments about 6 mm. from the tip (vi). Increasing the potential above the critical value (iii to iv) caused the particle size to decrease gradually and the number of threads to increase, but otherwise did not change the general behavior.

The critical potential (V_c) was independent of the polarity and was highly reproducible for a fixed position of the ground relative to the metal capillary. When the distance between the ground and capillary was decreased, V_c decreased as shown in Table I, presumably because of the increase in field strength. In these experiments, a thin metal probe serving as ground was held at various distances directly below the needle opening. On replacing the metal needle with a glass capillary, V_c increased. A plot of log V_c/R vs. log R gave excellent linear relationships for all cases studied. Two of them are shown in Fig. 3.

It was found that reducing the surface tension by means of surface-active agents caused a reduction of the critical potential and, as predicted by Eq. [1], a reduction in drop diameter at a given potential. The effect of surface tension was not investigated quantitatively, although it would have been of interest to do so. It is considered that these observations are in qualiattive agreement with the mechanism proposed by Vonnegut and Nuebauer (2).

TABLE I

Effect of Field Strength on Critical Potential of Water

Metal capillary 0.11 mm. i.d.

R = distance between ground and capillary.

R (*cm.*)	Critical potential (V_c) (*volts*)
1.18	3876
1.03	3840
0.88	3766
0.73	3680
0.58	3560
0.43	3368
0.33	3192
0.23	2960
0.18	2810
0.13	2560

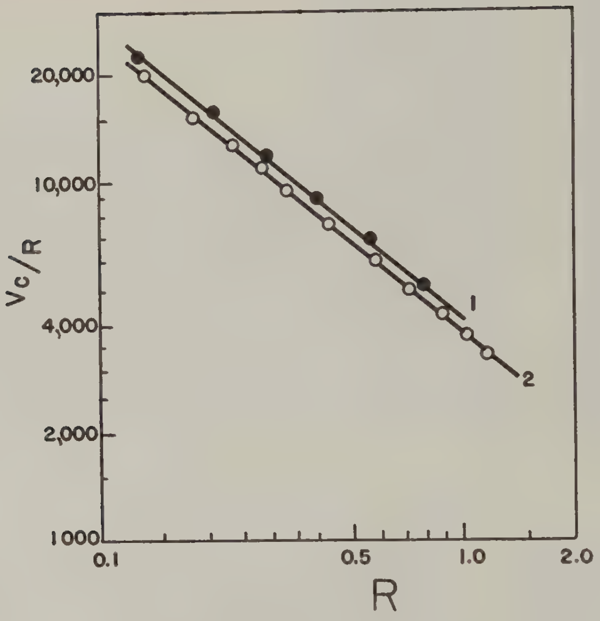

FIG. 3. Plot of log V_c/R versus log R.

Line 1—glass capillary (diameter = 0.08 mm.).
Line 2—metal capillary (diameter = 0.11 mm.).
Empirical relationship: $V_c = K.R^{0.2}$.

Drozin (4), who used glass capillaries, was unable to disperse carbon tetrachloride and benzene even at 30 kv. probably because of the low electrical conductivity which would tend to produce low field strengths at the needle tips in his experiments. In the present work both liquids could be dispersed at 4 kv. or less when a metal capillary directly connected to the high tension source was used. Moreover, in contrast to the experience of Vonnegut and Neubauer (2), the method was not affected by the polarity of the electrostatic charge in the liquid.

Preparation of Emulsions

In first applying the technique to the preparation of emulsions, the disperse phase was introduced directly into the continuous medium by immersing the charged hypodermic needle tip in the latter medium which also contained the ground. This method proved excellent for small concentrations of the disperse phase. When the emulsion concentration reached about 1%, however, it failed. Initial emulsification went on smoothly; but after several minutes elongated globules from 1 to 3 mm. in length with pointed ends were formed at the ground. These deformed globules, which appeared invariably to be multiple emulsions, moved to and fro with their major axes in the direction of the electric field. On continuing the process the emulsions broke. These observations appeared to be similar to those made by Dixon and Bennet-Clark (5) in a study of the electrical conductance of emulsions. This method was finally abandoned.

Instead, the disperse phase was dispersed into the air and then allowed to settle into the continuous phase. After a series of experiments the arrangement shown in Fig. 1 was adopted for preparing oil/water emulsions. The outermost rubber stopper (R_1) served as a stopper for the receiving flask (F). The ground (M) was a 1.5 cm. diameter brass tube whose bottom was about 2 cm. above the needle tip. At smaller separations the dispersed liquid tended to be attracted up towards the ground and deposited on it. The disperse phase in the graduated tube (L) was dispersed in air and collected as a finely divided spray on the continuous phase containing a suitable emulsifier. The continuous medium was stirred gently by a variable-speed magnetic stirrer (S_1, S_2) so as to entrain and distribute the atomized liquid immediately after the droplets met the surface. The rate of stirring was adjusted to avoid foaming.

The height of the needle-tip above the surface of the continuous medium was also important. If the needle was too close to the surface, electrical charge accumulated in the lower layer and caused the emulsion to break, presumably because travel through the air was too brief for dissipation of most of the charge; also the liquid column (Fig. 2, v) struck the surface before the dispersed filaments (Fig. 2, vi, lower part) could form, and thus caused coalescence at the surface. A distance of about 2 to 3 cm. was found suitable. It is possible that dissipation of the charge in the air could be assisted by introducing a small ionizing source such as polonium to increase the conductivity of the air. The continuous phase was also grounded by a metal strip (C) passing through a side arm (T). Without this additional ground dispersion soon stopped presumably owing to charge accumulation in the bulk liquid.

n-Butyl benzoate and solutions of castor oil and carbon tetrachloride in butyl benzoate, isoamyl benzoate, solutions of benzene and carbon tetrachloride were used as the disperse phases; water, aqueous solutions of sucrose, and glycerine of varying concentration containing both ionic and nonionic emulsifiers were employed as the continuous phases. The ionic and nonionic emulsifiers were propyl benzene (and naphthalene) amine sulfonate (G-3300), and sorbitan monolaurate (Tween 20), respectively, supplied by the Atlas Powder Co., Brantford, Canada. These emulsions were used in the investigation of viscosity behavior which is reported elsewhere (6). The highest concentration attempted was 37 % by volume, but doubtless this could have been exceeded.

To prepare an emulsion of known concentration the tared receiving flask (F) was filled half-way with a known weight of the continuous medium.

TABLE II

Size Distribution of a Typical O/W Emulsion

Butyl benzoate in water (plus 1% Tween 20); aged 3 days.

Diameter (*microns*)	Particles counted
0–2	2
2.5–3.5	712
4–5	3
6–7	2
7–8	2

After collecting the appropriate amount of the dispersed phase from the graduated tube (L), the stirring magnet was removed from the flask by means of another magnet and covered with a tared filter paper to soak up the liquid to the stirrer. The flask was then weighed on an analytical balance and after correcting for the liquid adhering to the magnet, the volume concentrations were calculated from the density values of the two phases. In this way the volume concentrations could readily be determined with a precision of at least ±0.02 volume %.

DISCUSSION

Emulsions so prepared were stable for periods of at least several months. The particles were reasonably uniform in size and were not agglomerated. It was observed that freshly prepared emulsions often contained about 5% of globules 5 to 10 μ diameter but on aging (preferably under very gentle agitation) the large globules became dispersed in about two days. After this period, 98% to 99% of the particles were in the diameter range from 2.5 to 3.5 μ for emulsions of butyl benzoate dispersed in water, and 3.5 to 4.5 μ for emulsions dispersed in aqueous glycerol. Table II gives a size count of a typical emulsion.

The dispersion of the large globules on standing is believed to have been due to a slight residual charge on the particles. Similar emulsions prepared by shaking, and having much larger particles, did not show any tendency to disperse further on standing; on the contrary, they slowly showed signs of breaking.

As a technique of preparing emulsions for research purposes, the method described has a number of advantages over conventional methods: it is simple and straightforward; it can be used equally well for oil/water or water/oil emulsions; there is no tendency to entrap air or to form multiple emulsions; the particles are of reasonably uniform size, and the disperse-phase concentration can be determined accurately. Finally, emulsions of high stability can be prepared with relatively low content of emulsifier (0.2% to 1%). In conventional methods of emulsification, emulsifier contents are kept high, 2% to 10% being common, to reduce the interfacial tension sufficiently to facilitate mechanical disruption of the liquid. In the present method lowering of interfacial tension is not necessary since dispersion is accomplished before the phases are mixed.

Two limitations should be mentioned. If the viscosity of the continuous medium is high, coalescence at the surface become pronounced and thus causes polydispersity. If, on the other hand, the viscosity of the disperse phase is high, the flow rate from the capillary becomes small and long preparation times are necessary. This might be overcome by using several capillaries or by using a pressure feed.

No attempt has been made to arrive at a quantitative explanation of the phenomena involved in the dispersion process. It is evident, however, that this is worthy of further study.

REFERENCES

1. ZELENY, J., *Phys. Rev.* **10**(2), 1 (1917).
2. VONNEGUT, B., AND NEUBAUER, R. L., *J. Colloid Sci.* **7**, 616 (1952).
3. VONNEGUT, B., AND NEUBAUER, R. L., *J. Colloid Sci.* **8**, 551 (1953).
4. DROZIN, V. G., *J. Colloid Sci.* **10**, 158 (1955).
5. DIXON, H. H., AND BENNET-CLARK, T. A., *Nature* **124**, 650 (1929).
6. NAWAB, M. A., AND MASON, S. G., Forthcoming publication.

JOURNAL OF COLLOID SCIENCE **13**, 188–191 (1958)

THE GELATION OF BILE SALT SOLUTIONS[1]

Harry Sobotka and Nina Czeczowiczka

Department of Chemistry, Mount Sinai Hospital, New York

Received November 7, 1957

Abstract

The gelation of aqueous bile salt solutions, accidentally observed in bacteriological media, has been studied. This property was observed with deoxycholic acid and lithocholic acid. It precedes or competes with crystalline precipitation. No gelation is observed with cholic acid, nor with conjugated bile acids. The maximum effect is found at pH 7, but at higher concentrations of bile acids gelation may be observed between pH 6.4 and 7.8. Under certain conditions spherical gel particles occur and may eventually form a gel within a gel.

The phenomenon and its specificity are explained on the basis of the specific molecular architecture of the bile acids. The analogy to the gelation of bromophenol blue solutions is pointed out.

Pneumococcus can be distinguished from other cocci by its dissolution in bile salt solutions, the so-called Neufeld phenomenon (1). The conditions for this reaction and the underlying mechanism have been reviewed elsewhere (2). The media used in such studies include a combination of bile salts with various buffers. One of the present authors has been consulted on several occasions by bacteriologists who were puzzled by formation of limpid gels during the preparation of such bile salt media. We therefore undertook a study of the conditions favoring gelation. We investigated the influence of the nature and concentration of the bile acid, of the pH, and of the nature of the buffer upon gelation, and the time requirements of the phenomenon.

Materials and Method

Bile acids were dissolved in a slight excess over the equivalent amount of aqueous sodium hydroxide to yield a final concentration of 5% bile salt (W/V). These alkaline solutions were diluted in various ratios with 1 *M* stock solutions of buffer and with water to give a series containing a constant concentration of bile acid and buffer.

We used phosphate, borate, and acetate buffers; the phosphate buffers

---

[1] This work was supported by U. S. Public Health Service Grant C-1791; it was presented at the semiannual meeting of the American Chemical Society, New York, September 1957, in the Division of Colloid Chemistry.

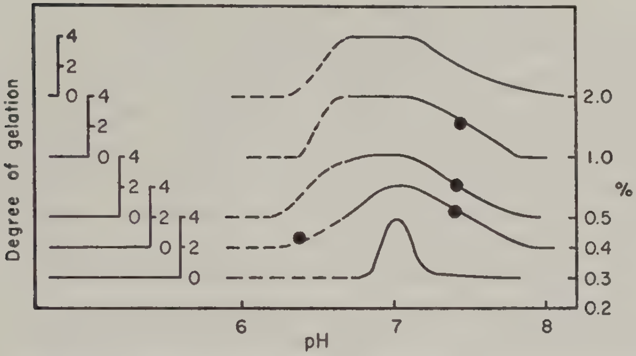

FIG. 1. Gelation of aqueous solutions of deoxycholic acid at 20° at various concentrations and acidities.

were applied in final concentrations of *M*/2, *M*/5, and *M*/10; the high concentrations were obtained by mixtures of KH_2PO_4 and K_2HPO_4. The acetate was diluted to *N*/2. The borate buffers were adjusted with *N*/10 hydrochloric acid to fall within the pH range where gelation takes place. The solutions were placed in covered 20 ml. beakers for observation. After addition of the bile salt solution the pH of the mixture was measured by a glass electrode with a Coleman pH-meter.

We compared the following acids: deoxycholic acid (purissimum) (3), cholic and glycocholic acid (Riedel de Haen), lithocholic acid (Schering Co.), and glycodeoxycholic acid (prepared according to Boissonas) (4).

RESULTS

Figure 1 gives a summary of the results for deoxycholic acid at room temperature (*ca.* 20°C.). The pH values are plotted as abscissa, the degree of gelation as ordinate. For the sake of convenience, the curves are staggered for the deoxycholic acid concentrations given, viz., 0.2, 0.3, 0.4, 0.5, 1.0, and 2.0%, and scales are indicated for each concentration on the left margin of the diagram. These scales give five semiquantitative steps, "0" meaning no gelation, "4" a firm gel, and "1, 2, 3" intermediate steps.

The curves combine the results of experiments with the various buffers and buffer concentrations used, since the nature and quantity of the buffer did not affect the results. In fact, identical points were observed when the pH was adjusted by adding *N*/10 hydrochloric acid to the bile salt solution without addition of buffer.

The essential factor for gelation is the hydrogen ion concentration. Its range narrows with decreasing concentrations of deoxycholic acid. No gelation is observed for 0.2%, but a sharp maximum is observed for 0.3%, at pH = 7.0. The maximum broadens with increasing concentrations of bile salt, so that for 0.5% the zone of gelation reaches from 6.4 to 7.8, with maximal gelation from 6.6 to 7.2. These values do not change further in higher concentrations up to 2.0% deoxycholic acid.

In general, the higher the degree of gelation, the faster its rate. Complete gelation is often reached within 1 hour. The figure represents observations after 16 hours standing. Since gelation is predicated upon the decreasing solubility of the bile acid towards acid pH values, it competes with crystalline precipitation and sometimes precedes it. In the dotted part of the curves, i.e., up to pH = 6.6 to 6.7, precipitation is observed to occur at once or to supersede gelation.

In pH regions where gelation is incomplete, there occurs a peculiar phenomenon, which we have indicated by circles wherever we have observed it. In these experiments gelation was slow and after a few hours transparent spherical bodies appeared in the solution, which was still liquid, although viscous. These balls, up to 2 mm. diameter, are slightly heavier than the surrounding fluid and settle slowly. On the alkaline side at pH 7.4 to 7.5 the surrounding medium also jells eventually and one then has a gel within a gel. Occasionally, a solution containing gel balls, would stay liquid for 16 hours and suddenly form a gel within a gel upon viewing and handling of the tube. All bile acid gels are thixotropic.

These observations are rather specific for deoxycholic acid. No gelation has been found in the case of cholic acid, which precipitates immediately in crystalline form upon acidification. Glycocholic acid does not jell and glycodeoxycholic acid jells just faintly after three weeks standing, evidently owing to incipient hydrolysis liberating deoxycholic acid.

Lithocholic acid has a strong tendency to form gels; with this acid it is difficult to prepare solutions of its sodium salt. The acid particles when treated with aqueous alkali surround themselves with a gelatinous layer of the sodium salt. If forced into solution with stirring and heat, it will form gels over a wide range of pH at 0.3% and even up to pH 12 at 0.4%. These gels become partly dehydrated and shrink. Higher concentrations could not be obtained.

It appears possible that the lithocholic acid network differs from the deoxycholic acid network by the absence of a certain degree of rigidity which is imposed on the deoxycholic acid gel by the presence of the OH-groups on C_{12} in the middle of the longitudinal extension of the molecule.

COMMENTS

If one compares the three unconjugated bile acids, lithocholic acid, deoxycholic acid, and cholic acid, one notices that polar groups are situated at both extremities of the molecules (positions 3, 24). In cholic acid both sides of the molecule are spiked, as it were, with methyl or hydroxyl groups. In deoxycholic acid the "lower" side of the molecule has an unbroken frontage of methylene groups, uninterrupted by methyl or hydroxyl groups.

This arrangement has been adduced to explain the outstanding affinity of deoxycholic acid for lipids and its particular aptitude for complex formation. It must also be responsible for the gelation phenomenon, for which the "lower" side of the molecule allows unhindered van der Waals attraction. This factor is enhanced in lithocholic acid, where neither side of the molecule is encumbered by polar groups.

The conjugated glycocholic and glycodeoxycholic acids lack the insolubility on which gelation as well as choleic acid formation is dependent.

Assuming that large surface-active molecules of this type form micellae in alkaline solution, it is plausible that the decrease in solubility towards lower pH values may lead to increased micellar size and eventual gelation. This trend is facilitated by the specific molecular architecture discussed above.

An analogous observation has been described by La Mer and Amis (5). Solutions of bromophenol blue become colorless in strong alkali. Upon acidification of the faded dye, a gel of the yellowish un-ionized acidic state of bromophenol blue is formed. This phenomenon is observed down to concentrations of 0.003 *M*, which corresponds to 0.2%, a figure of the same magnitude as the lower limit of concentration leading to gelation in our experiments.

REFERENCES

1. NEUFELD, F., *Z. Hyg. Infektionskrankh.* **34,** 454 (1900).
2. SOBOTKA, H. "Physiological Chemistry of the Bile," p. 127 f. Williams & Wilkins, Baltimore, 1937.
3. SOBOTKA, H., "The Chemistry of the Sterids," p. 77. Williams & Wilkins, Baltimore, 1938.
4. BERGSTROM, S., AND NORMAN, A., *Acta Chem. Scand.* **7,** 1126 (1953).
5. LA MER, V. K., AND AMIS, E. S., *Science* **90,** 90 (1939).

JOURNAL OF COLLOID SCIENCE **13,** 193–197 (1958)

LETTERS TO THE EDITOR

ANOMALOUS BEHAVIOR OF THE EXTINCTION ANGLE OF MODERATELY CONCENTRATED POLYVINYLALCOHOL–WATER SOLUTIONS

Anomalies in flow birefringence of macromolecular solutions have been discussed in some recent articles (1). Here we point out an anomalous behavior of the extinction angle in moderately concentrated polyvinylalcohol-water solutions. The unstable character of such solutions is well known; for instance their viscosities increase on aging. In studies of flow birefringence an unexpected phenomenon was noted in aged polyvinylalcohol-water solutions.

The polymers used were purified commercial polyvinylalcohol samples, with an average degree of polymerization about 2000. They were dissolved by mixing with distilled water for 4 hours at 100°C. The concentrations of the solutions used were 5 g. and 7 g. polymer per 100 ml. water, and they were filtered through No. 4 glass filter immediately after dissolving, then stored at about 20°C. To study the effects of aging, measurements were made on the fresh solution, and then 3 days and 7 days later. Almost all the determinations were carried out as a function of velocity gradient up to 5000 sec.$^{-1}$ at 20°C.

The results obtained are represented in Figs. 1 and 2, which show the existence of remarkable anomalous phenomena in the aged solutions. The extinction angle of the aged solutions (Fig. 1), is between 0° and 10° at low velocity gradients, near 300 sec.$^{-1}$, then rises with increasing velocity gradients, gradually approaching the curve for the fresh solutions at gradients near 5000 sec.$^{-1}$

The values of χ in the aged solutions are well-defined functions of the rate of shear, and are the same whether or not the solution has just been subjected to a higher rate of shear, before being studied at a given gradient.

Figure 2 represents the magnitude of the birefringence for the same solutions before and after aging. Notably it shows no such marked differences between the fresh and the aged solutions as are found in the curves for extinction angle in Fig. 1.

It is very difficult to interpret these phenomena in terms of the established theory of flow birefringence. However, the observed behavior suggests the existence of gelation or association processes of the polymers during aging in aqueous solutions.

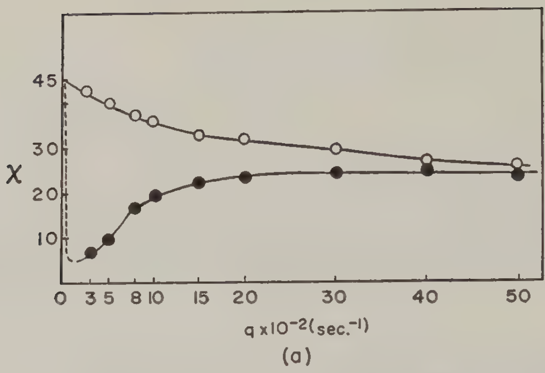

FIG. 1*a*. Extinction angle vs. velocity gradient curves of 7% polyvinylalcohol-water solutions determined before (—○—) and after (—●—) aging.

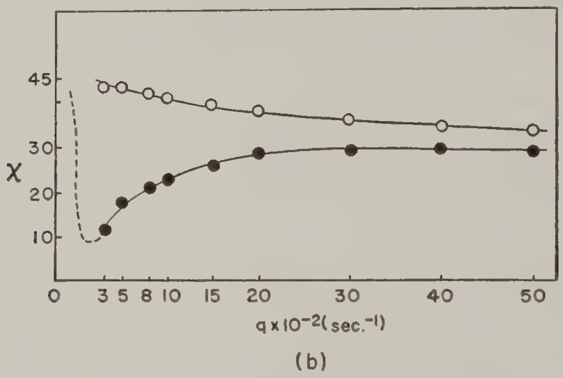

FIG. 1*b*. Extinction angle vs. velocity gradient curves of the 5% solutions determined before and after aging, respectively.

A plausible interpretation of the experimental facts is that when the molecularly dissolved polyvinylalcohol-water solutions are aged they form a loose gel system, composed of associated polymer molecules, with aggregates which are fairly large as compared with the dimensions of the molecularly dispersed macromolecular chains. These aggregates are oriented easily even at low rates of shear.

In view of the reversibility phenomena of the extinction angle values with the velocity gradient in a range of 300 to 5000 sec.$^{-1}$, it is suggested that owing to junctions, formed perhaps by hydrogen bonding, the molecular chains are cross-linked to form loose gels. These are broken up when further shear forces are applied to them, although they are oriented easily by very small external forces. Thus the extinction angle curves turn upward and approach those of the fresh solutions at higher velocity gradients.

To interpret the above-mentioned phenomena, notably the reversibility of the anomalous extinction angle curves as a function of the rate of shear,

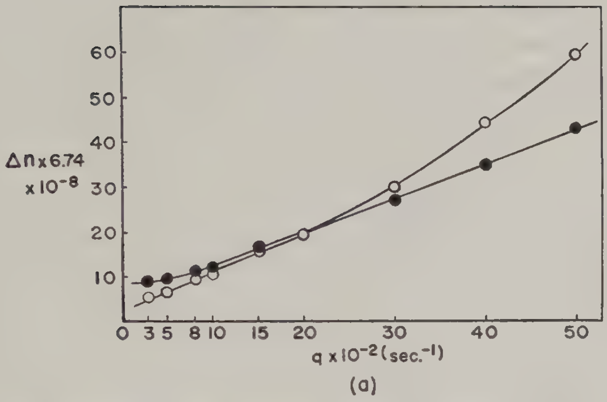

Fig. 2a. Degree of birefringence vs. velocity gradient curves of 7% polyvinylalcohol-water solutions determined before (—○—) and after (—●—) aging.

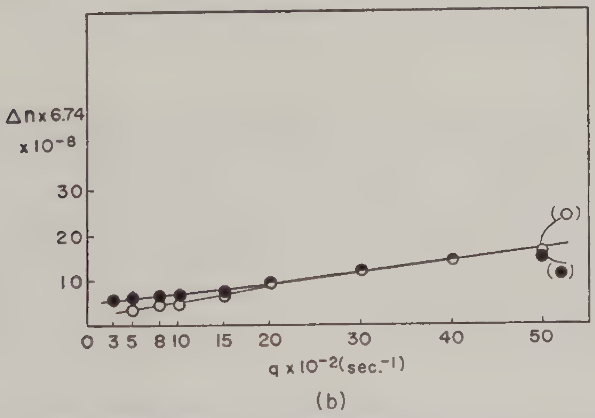

Fig. 2b. Degree of birefringence vs. velocity gradient curves of the 5% solutions determined before and after aging, respectively.

it appears necessary to assume that the gel structures reform almost instantly when the shearing stress is removed.

The fact that the birefringence data are not so affected by the aging process appears favorable to the above assumptions.

In conclusion, the anomalous behavior of the extinction angle in the aged polyvinylalcohol-water solutions suggests the existence of interesting gelation or association phenomena during aging in the solutions studied.

These findings may be compared with the excellent work on these polymer solutions reported by Maeda and Kawai (2).

The author wishes to thank Drs. T. Yurugi, a chief researcher in our laboratories, and H. Maeda and T. Kawai of the Textile Chemical Laboratory of Tokyo Institute of Technology, for valuable discussions and advice in the interpretation of experimental results contained in this article.

Also, I am greatly indebted to Dr. John T. Edsall for careful reading of the manuscript and for his kindness in informing me concerning experimental details of flow birefringence studies.

REFERENCES

1. SIGNER, R., LIECHTI, V., AND LIECHTI, H., *J. Chim. Phys.* **44,** 58 (1947). SNELLMAN, O., AND SAVERBORN, S. *Kolloid-Beih.* **52,** 467 (1941). TSVETKOV, V. N., AND PETROVA, A., *J. Tech. Phys. U.S.S.R.* **14,** 289 (1944); *Rubber Chem. and Technol.* **19,** 360 (1946).
2. MAEDA, H., AND KAWAI, T., *Chem. High Polymer, Japan* **13,** 193 (1956).

Textile Research Institute of
Japanese Government
4 Sawatari, Kanagawa,
Yokohama, Japan

SHOEI FUJISHIGE

Received January 16, 1958

MOLECULAR WEIGHT DISTRIBUTION BY STRESS RELAXATION

The stress relaxation properties of linear amorphous polymers in the region of rubbery flow have been shown to be dependent on molecular weight and molecular weight distribution (1). The new "living polymer" technique of M. Szwarc (2) affords a convenient way of obtaining nearly monodisperse samples of polymer, which were formerly available only by tedious fractionation procedures. It would appear that these "monodisperse" samples and mixtures thereof can be used in stress relaxation studies to develop a method for estimating polydispersity of unknown polymer samples. Such a method would be very rapid and very convenient.

As a first step in this direction we have compared the distribution of relaxation times $H(\log \tau)$ in the rubbery region for a "monodisperse" sample (A) supplied by Professor Szwarc and a polydisperse sample (B) prepared by polymerizing styrene with benzoyl peroxide.

As discussed by Baysal and Tobolsky (3), sample (B) is characterized by the molecular weight distribution where the mole fraction is given by: $X(n) = np^{n-1}(1 - p)^2$ and has a heterogeneity index $\bar{M}_w/\bar{M}_n = 1.5$. Experiments by Dr. N. Schneider have indicated that sample (A) is truly a fairly sharp fraction with a heterogeneity index of perhaps 1.1.

The intrinsic viscosities of samples (A) and (B) measured in benzene at 30°C. are 0.72 and 0.78, respectively. From equation (14) in reference (3), $\bar{M}_n$ of sample (B) is 1.17×10^5, and therefore $\bar{M}_w = 1.75 \times 10^5$. Assuming $K_u''/K = 1.32$ (see reference [3]) we can calculate that M_n of sample (A) is 1.54×10^5 and $\bar{M}_w$ is probably about 10% greater.

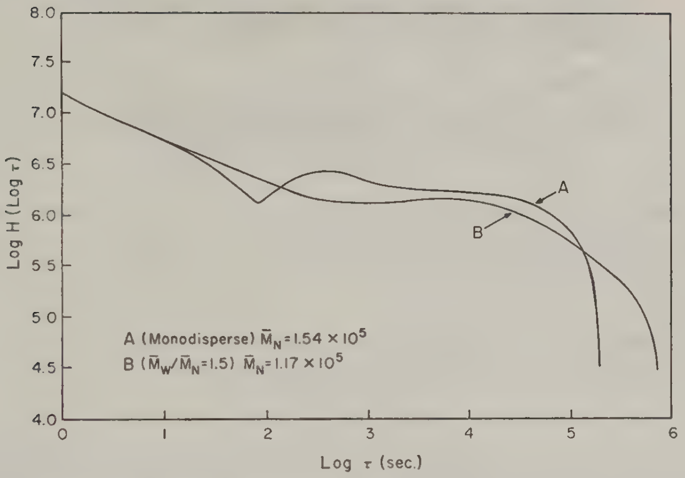

FIG. 1. Relaxation spectra of monodisperse and polydisperse polystyrene by the second approximation method reduced to 115°C.

Figure 1 shows $H(\log \tau)$ versus $(\log \tau)$ for samples (A) and (B) at 115°C. The definition of $H(\log \tau)$ and the methods for obtaining it are discussed in reference (1). It is clear that the monodisperse sample has a definitely narrower distribution of relaxation times than the polydisperse sample (*B*). Furthermore (A) has the character of the "box" distribution previously advanced (1). Apparently stress relaxation can easily distinguish between these two samples, as shown in the figure, even though a heterogeneity index of 1.5 for sample (B), though not monodisperse, is characteristic of a quite sharp continuous distribution.

REFERENCES

1. TOBOLSKY, A. V., *J. Appl. Phys.*, **27**: 673 (1956).
2. WAACK, R., REMBAUM, A., COOMBES, J. D., AND SZWARC, M., *J. Am. Chem. Soc.* **79**: 2026 (1957).
3. BAYSAL, B., AND TOBOLSKY, A. V., *J. Polymer Sci.* **9**, 171 (1952).

A. V. TOBOLSKY
A. MERCURIO
K. MURAKAMI

Frick Chemical Laboratory
Princeton University
Princeton, New Jersey
Received February 4, 1958

Just published—Volume 1

Biophysical Chemistry

By JOHN T. EDSALL, *Harvard University, Cambridge, Massachusetts*
and JEFFRIES WYMAN, *UNESCO, Cairo, Egypt*

Volume 1

Thermodynamics, Electrostatics, and the Biological Significance of the Properties of Matter

February 1958, 699 pp., illus., $14.00

Biophysical Chemistry is based on a course taught by the authors dealing with the physical chemistry of biochemical systems. Emphasis has been placed on broad general principles and fundamental concepts in order to provide the reader with the basic understanding of the quite difficult problems of current interest in the field of biophysical chemistry.

Volume 1 presents a lucid discussion and a detailed analysis of the biological significance of the properties of matter. The second volume will be devoted to the physical chemistry of biological macromolecules, and their study by such methods as osmotic pressure, light scattering, diffusion, sedimentation, viscosity and electrophoresis.

These volumes will be indispensable to graduate students and advanced undergraduates familiar with the fundamentals of differential and integral calculus. This work will be of basic interest to investigators in organic and physical chemistry, biology, and biochemistry.

CONTENTS OF VOLUME 1:

Biochemistry and Geochemistry. Water and Its Biological Significance. Problems of Protein Structure. Thermodynamics. Electrostatics: Its Application to Polar Molecules, and Ionic Solutions. Dielectric Constants and Their Significance. Conductivity of Electrolytes. Acid-Base Equilibria. Polybasic Acids, Bases, and Ampholytes, Including Proteins. Carbon Dioxide and Carbonic Acid. Some General Aspects of Molecular Interactions. AUTHOR INDEX—SUBJECT INDEX.

Volume 2, in preparation

Physical Chemistry of Macromolecules and of Blood

Descriptive leaflet available upon request

AP

ACADEMIC PRESS INC., ***Publishers***
111 FIFTH AVENUE, NEW YORK 3, NEW YORK

JOURNAL OF COLLOID SCIENCE **13**, 199–207 (1958)

THE DEFOAMING OF SYNTHETIC DETERGENT SOLUTIONS BY SOAPS AND FATTY ACIDS[1]

Henry Peper[2]

Lever Brothers Company, Research Center, Edgewater, New Jersey

Received January 8, 1958

ABSTRACT

The foam of sodium dodecylbenzenesulfonate solutions is rendered extremely unstable by small amounts of sodium palmitate or stearate and calcium ion except in strongly acid solutions. In the presence of sodium laurate or oleate under the same conditions the foam is more stable. Detergents having a straight hydrocarbon chain containing 14 or more carbon atoms give a stable foam in the presence of small amounts of calcium palmitate. A study of the penetration by detergents of monolayers of stearic acid spread on dilute solutions of calcium chloride shows that those detergents the foam of which is stable in the presence of calcium soap penetrate strongly the stearate film, converting it to a mixed, viscous, liquid film.

INTRODUCTION

In many cases the foam of synthetic detergent solutions is destroyed very quickly by the presence of soap.

In this investigation, the foam stabilities of many different systems were measured, and the character of the film at the air-water interface was studied under carefully controlled conditions.

Some of the conditions which are necessary for foam stability of detergents in the presence of fatty acids have been determined. In addition, the research on the penetration of calcium stearate films suggests a mechanism for the destruction of nonsoap detergent foam by soap and fatty acids.

EXPERIMENTAL

The foaming tests were performed by shaking 50 ml. of solution in a 250 ml. graduated cylinder. The volume of foam was observed with time.

The penetration experiments were performed by the techniques described by Matalon and Schulman (1, 2) in which the penetrated monolayer is studied at constant area and at constant pressure. For constant-area experiments, the change in surface pressure was measured by the Wilhelmy plate technique using a sand-blasted platinum plate to insure good wettability. The Wilhelmy plate was used to avoid the leaks around the floating barrier of the Langmuir balance caused by the high pressures developed. The detergent was injected with a special device consisting of a funnel attached to a long perforated tube lying on the bottom of the trough. Mixing was accomplished by repeated drawing of 100 ml. of the substrate into the funnel and allowing it to run back into the trough.

---

[1] Presented at the American Chemical Society meeting in Miami, Florida, April 1957.

[2] Present address: Harris Research Laboratories, 1246 Taylor St., N.W., Washington 11, D. C.

A different apparatus was used for the constant-pressure experiments. The insoluble film was contained by a paraffined, floating mica frame which was anchored by a glass rod at each end. The barrier bearing on the torsion balance was fixed to the mica frame by Vaseline-coated silk fibers. Use of the floating mica frame reduced the tendency for leakage of the film past the threads of the floating barrier (3). The Langmuir balance required the incorporation of a device for compensation of the adsorption of detergent at the free or reference side of the barrier (4). This consisted of a sandpapered mica plate dipping into the water and connected to the torsion wire by a lever arm. The plate and lever arm were constructed with dimensions that would, for a given lowering of surface tension, produce a decrease in torque equal and opposite to that caused by the pressure of the adsorbed film on the floating barrier. This assured that the reference pressure remained the same after the detergent had been injected.

After injecting the detergent, the pressure was maintained constant by expanding the area of the film to accommodate the penetrating detergent. This was accomplished automatically by a motor-driven movable barrier. The motor was controlled by a switch connected to the torsion wire in such a way that the motor was started by an increase in pressure and stopped when the pressure again dropped. The area of the film was observed with time.

Stearic acid was used as a barrier film because it gave stable pressures at pH 6. The force-area curve for stearic acid on 10^{-5} molar $CaCl_2$ (pH 5.8) was obtained.

The usual starting pressure for the penetration experiment was about 17 dynes/cm. for the stearic acid film, a value substantially below the collapse point of the film. The equilibrium surface pressure of the adsorbed detergent alone was always less than the pressure of the stearic acid film. The surface pressure-concentration curve for low concentrations for each of the detergents was determined in order to find the concentration which gave an equilibrium pressure of 15 dynes/cm. The penetrating powers of the different detergents were measured at this concentration.

The sodium alkyl sulfates used are special samples obtained from the research department of E. I. DuPont de Nemours. The sodium dodecylbenzenesulfonate is a commercial material from the Oronite Chemical Company. The distilled water used in these experiments was saturated with air to prevent a change in pH due to dissolution of CO_2.

RESULTS AND DISCUSSION

In the exploratory experiments, the defoaming of 0.1% sodium dodecylbenzenesulfonate solutions by soap in distilled water was irreproducible. When 2 p.p.m. of $CaCl_2$ were added to the system, however, the rapid foam decay could be readily reproduced. Polyvalent metal ion impurities in some samples of distilled water may have been responsible for the defoaming.

The foam stabilities of 0.1% sodium dodecylbenzenesulfonate solutions with 2 p.p.m. $CaCl_2$ and 0.002% of several soaps were measured. The results reported as foam volume vs. time are shown in Fig. 1. Sodium palmitate and stearate caused the foam to decay completely in less than a minute. The foam was, relatively, quite stable in the presence of laurate soap, and oleate had an intermediate effect.

The question of the effect of calcium ion on defoaming was examined in greater detail. It was found that solutions of sodium dodecylbenzenesulfonate in deionized water were not defoamed at such a great rate in the presence of sodium palmitate (Table I). Even greater stability was ob-

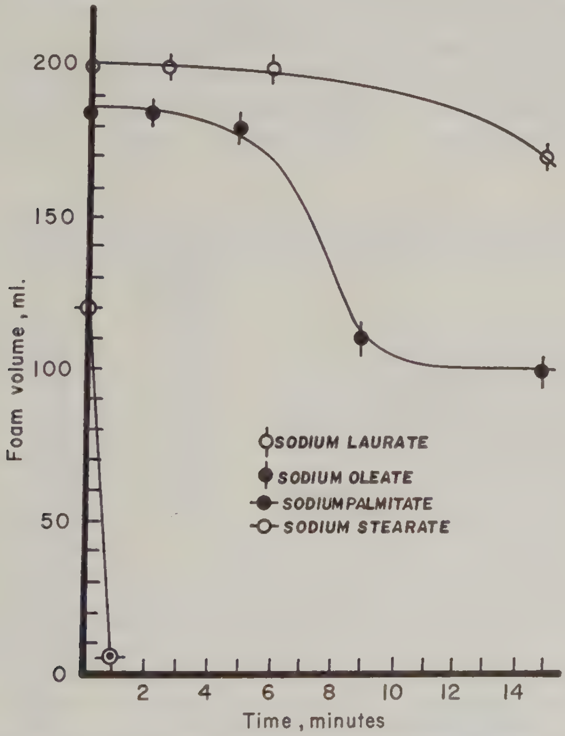

FIG. 1. Foam volume as a function of time of 0.1% sodium dodecylbenzenesulfonate solutions containing 2 p.p.m. of calcium chloride and 0.002% soap at 25°C. ϕ Sodium laurate; ● sodium oleate; -●- sodium palmitate; -○- sodium stearate.

tained in the presence of 0.1% Versene (tetrasodium ethylenediamine tetraacetate). Palmitic acid had an effect similar to that of sodium palmitate if the pH was sufficiently high (pH 6.5). However, at pH 3 palmitic acid was a much less effective defoamer. The loss of defoaming power at pH 3 is probably due to the inability of calcium to react with the unionized carboxyl group. This interpretation is substantiated by the finding with stearyl alcohol, for which the result was similar to that obtained with palmitic acid at pH 3. Since foaming is essentially a surface phenomenon, these results must be related to changes brought about in the air-water interface by the presence of long-chain soaps and calcium ion. Polyvalent metal ions, in general, are known to have a strong condensing effect on fatty acid films. This additional cohesive factor in some cases results in solidification of the fatty acid film. If the state or degree of condensation of the additive in the surface is greater in cases where there is defoaming and less where there is smaller defoaming, this difference should manifest itself in smaller surface pressure (surface tension lowering) when the additive is in a more condensed state. The surface tensions were measured of sodium dodecylbenzenesulfonate solutions in 2 p.p.m. $CaCl_2$ with 0.002% of different fatty acids. The lowering of the surface tension from the value of the solution (29.5 dynes/cm.) without the additive is given in Table II. The results show smaller surface tension lowering (surface film of the additive in a condensed state) for the additives which are strong defoamers.

The reason for the small surface tension lowering by the palmitic and

TABLE I

Foam Stability of 0.1% Sodium Dodecylbenzenesulfonate Solutions in the Presence of Various Additives

Additive	Initial foam volume (*ml.*)	Foam volume at time *t*	
No additive 2 p.p.m. $CaCl_2$	200+	200+	(10 min.)
Na palmitate (deionized water)	200	160	(5 min.)
Na palmitate 2 p.p.m. $CaCl_2$	120	5	(1 min.)
Na palmitate 0.1% Versene	180	180	(10 min.)
Palmitic acid 2 p.p.m. $CaCl_2$; pH 6.5	120	10	(1 min.)
Palmitic acid 2 p.p.m. $CaCl_2$; pH 3	150	150	(5 min.)
Stearyl alcohol 2 p.p.m. $CaCl_2$; pH 6.5	170	160	(5 min.)

TABLE II

Surface Tension Lowering by Fatty Acids in 0.1% Sodium Dodecylbenzenesulfonate Solutions in 2 p.p.m. $CaCl_2$

Additive	Dynes/cm.
Palmitic acid	0.9
Stearic acid	0.8
Oleic acid	1.6
Lauric acid	4.2

stearic acids is the presence of aggregates of molecules in the surface which because of their large size do not produce a substantial pressure.

It has been shown (5) by scanning a surface with an electrode that heterogeneity exists which is due to these islands of molecular aggregates. The expanded films show a greater surface tension lowering because each molecule is free to contribute its kinetic energy to the pressure. In this case, the molecules of additive form a homogeneous mixture or solution with the detergent molecules in the surface.

Next, the foam stability of several sulfated and sulfonated detergents was measured in the presence of sodium palmitate and 2 p.p.m. of calcium chloride. The results are plotted as foam volume vs. time (Fig. 2) where it will be seen that the alkylbenzene sulfonate gives unstable foam. In the alkyl sulfate series only the lauryl homolog has unstable foam. The myristyl and cetyl sulfate foams are not affected by the soap, the foam showing no decay.

The information obtained in the experiments described above shows that rapid defoaming of detergent solutions by soap or fatty acid occurs only when conditions are favorable for the formation of a solid or "tanned" film by the action of calcium ion. It was also shown that some detergents are not affected by the soap. The following hypothesis is advanced to ex-

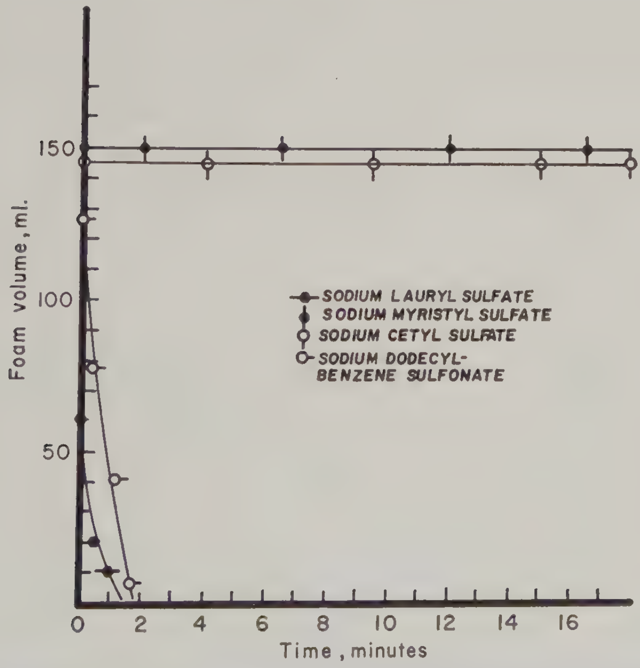

FIG. 2. Foam volume as a function of time for 0.1% solutions of various detergents containing 0.002% sodium palmitate and 2 p.p.m. of calcium chloride at 25°C.

plain these phenomena; the surfaces of the foam bubbles have a heterogeneity consisting of a continuous gaseous film of adsorbed detergent in which there are islands of solid calcium soap film. These islands make the film unstable because of their inflexible, brittle nature. The detergents the foam of which is unaffected by the calcium soap form a mixed film with it which is either gaseous or liquid and does not contain regions of solid film.

Experiments in which insoluble monolayers were penetrated by detergents were performed to test the validity of this hypothesis. A monolayer of stearic acid on a calcium chloride solution substrate was formed and a detergent solution injected beneath the film. Changes in the calcium stearate film due to penetration by the detergent were then observed.

Some results of penetration at constant pressure of stearic acid films on calcium chloride solution are shown in Fig. 3 as expansion of a stearic acid film vs. time. The insoluble film was expanded only slightly by the alkylaryl sulfonate. This indicates that only a relatively small number of these molecules have been able to force their way into the surface occupied by the insoluble film. In the case of cetyl sulfate, the stearic acid film has been greatly expanded, indicating that cetyl sulfate molecules are able to force their way into the insoluble film and consequently expand it. The results of the constant-area penetration experiments are shown in Fig. 4 plotted as surface pressure vs. time. In this case the effect of penetration of the insoluble film by the detergent is manifested by an increase in pressure of the film. The penetrating powers of three alkyl sulfates with respect to

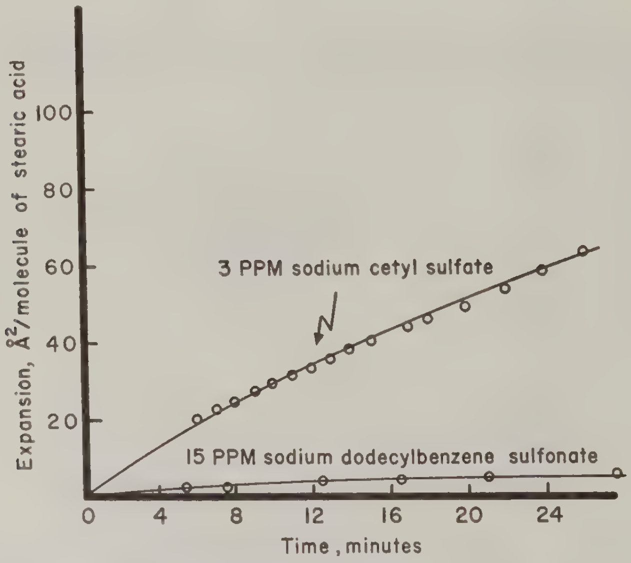

FIG. 3. Constant-pressure penetration of stearic acid on 10^{-5} m. calcium chloride at 17.5 dynes/cm. at 25.0°C.

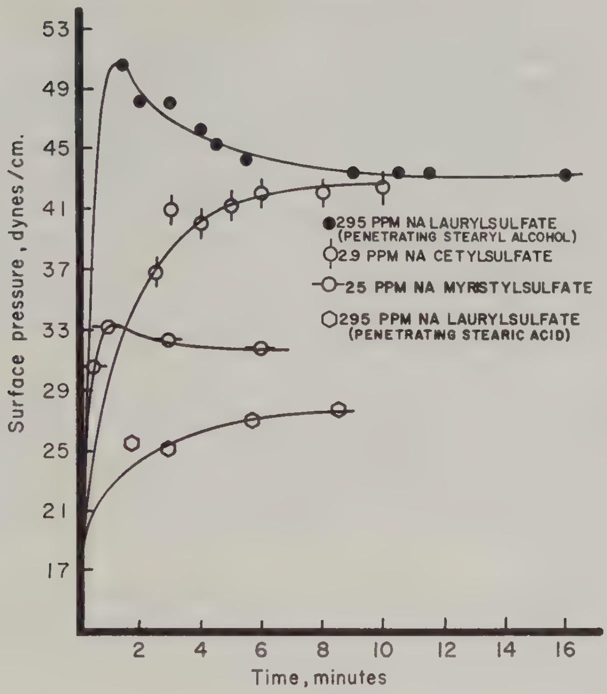

FIG. 4. Constant-area penetrations by alkyl sulfates.

stearic acid are compared and also the difference in resistance to penetration by lauryl sulfate of stearic acid and stearyl alcohol.

Lauryl sulfate has very small penetrating power toward stearic acid, whereas the myristyl sulfate and cetyl sulfate penetrate more strongly. A simple observation can be made on these films to show their nature. Sprinkling a few talc particles on the film and gently blowing on them shows, by the kind of motion of the particles, the state of the film. The mixed films formed between cetyl sulfate and stearic acid and myristyl sulfate and stearic acid are highly viscous liquids. With lauryl sulfate and stearic acid the film does not show this viscous, liquid character. In other words, strong penetration of the stearic acid film by a detergent results in a change in state of the film to liquid. Although there is only weak penetration of stearic acid by lauryl sulfate, when stearyl alcohol is used as a barrier film, it is strongly penetrated by lauryl sulfate.

Dodecylbenzenesulfonate (DDBS) produced only a weak penetration of stearic acid (Fig. 5). When stearyl alcohol is used, however, the penetration of DDBS is very strong; stearyl alcohol also was considerably less active than stearic acid as a defoamer in the presence of calcium chloride.

Evidently, the phenomenon of film penetration and consequent mixed film formation is strongly affected by the structure of the hydrophobic hydrocarbon chain as well as the polar groups of the surface-active materials involved.

The results of these studies show that the number of carbon atoms in the hydrophobic group and its configuration are important in mixed film formation between detergents and calcium soap films. These observations confirm, for the penetrating species, what Schulman (6) has shown for the insoluble penetrated film, namely, that penetration is, to a large extent, governed by the amount of van der Waals' interaction between the two components. A straight chain will afford more contact and consequently stronger van der Waals' attraction with the chains of the insoluble film than a branched chain and likewise a longer chain more than a shorter chain.

The importance of the polar group of the insoluble film in respect to penetrability has been strikingly demonstrated by the difference in resistance to penetration by stearyl alcohol and stearic acid. It is likely that this difference is due to the solidification of the fatty acid film by the calcium ions. This results in a more coherent film having a greater resistance to penetration.

Evidently, the surface activity of members of a homologous series is directly related to the ability to penetrate. However, in comparisons of detergents which do not have the same polar group this relation does not apply.

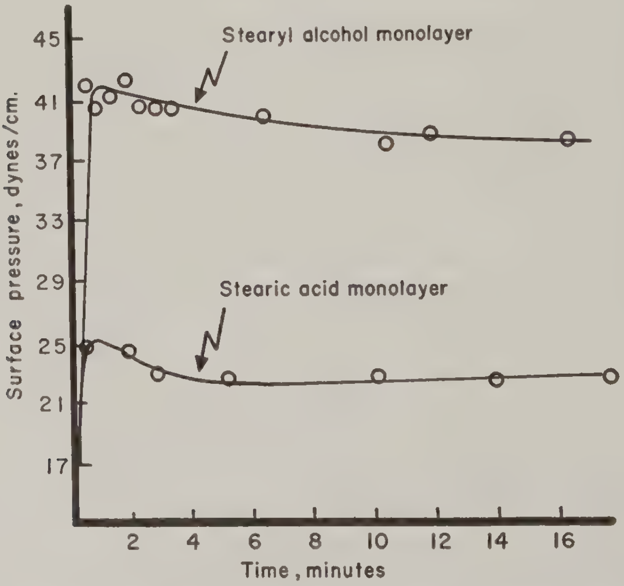

FIG. 5. Constant-area penetrations by 15 p.p.m. of sodium dodecylbenzenesulfonate.

The results of the penetration experiments substantiate the hypothesis of the necessity for formation of a mixed film between calcium soap and detergent in cases where the detergent foam is not destroyed by the presence of calcium soap. In every case where the foam remained stable in the presence of calcium soap, this detergent penetrated the stearic acid and formed a liquid-condensed film.

REFERENCES

1. Matalon, R., and Schulman, J. H., *Trans. Faraday Soc.* **43,** 479 (1947).
2. Matalon, R., *J. Colloid Sci.* **8,** 53 (1953).
3. Rosano, H. L., *J. Colloid Sci.* **10,** 362 (1955).
4. Matalon, R., and Schulman, J. H., *J. Colloid Sci.* **4,** 89 (1949).
5. Harkins, W. D., and Fischer, E. K., *J. Chem. Phys.* **1,** 852 (1933).
6. Goddard, E. D., and Schulman, J. H., *J. Colloid Sci.* **8,** 329 (1953).

JOURNAL OF COLLOID SCIENCE 13, 208–217 (1958)

THE ULTRAVIOLET ABSORPTION SPECTRUM AS A CRITERION OF THE TYPE OF SOLUBILIZATION

S. Riegelman, N. A. Allawala, M. K. Hrenoff, and L. A. Strait

University of California Medical Center, School of Pharmacy, San Francisco

Received April 25, 1957, revised November 19, 1957

INTRODUCTION

It is generally agreed that the mechanism of micellular solubilization is complex and requires more than one physical mode of incorporation of the solubilizate in the micelle. The natures of both the solubilizers and the solubilizates studied are too varied to fit any one pattern, and the inclusion of additives such as salts produces different influences on the solubilization of different compounds (1–4). However, up to this time no single method has revealed clearly experimental evidence of the existence of the postulated different modes of solubilization. The ultraviolet spectra of most compounds are sensitive to changes in the environment (5) and especially to the changes in the dielectric constant of the environment (6). Since the micelle is characterized by regions of different polarity, the ultraviolet spectrum of the solubilized agent affords a sensitive approach to a study of the mode of solubilization with respect to the placement of the solubilized agent in the micelles.

EXPERIMENTAL

The ultraviolet spectra of the selected compounds were determined on a Cary automatic recording spectrophotometer, model 11. The compounds measured were ethyl benzene, naphthalene, anthracene, trans-azobenzene, *o*-nitro aniline, *p*-nitro aniline, and dimethyl phthalate. The following solvent systems were used: water, water-ethanol, octane, cetane, and aqueous solutions of: potassium laurate, dodecylamine, and polyoxyethylene ether of lauryl alcohol.[1] The solvents were purified where necessary by recognized procedures, and were optically transparent in the wavelength ranges examined. The spectrum of the solvent system was eliminated by using it in the comparison cell in all cases.

Since the absorbing molecules were compared in the several solvent systems on the basis of the positions of the absorption maxima and the relative degree of fine structure, it was not necessary to duplicate exactly the same concentration of the absorbing species in each solvent system.

[1] Brij 35, Atlas Powder Co., Wilmington, Delaware.

This would have been exceedingly difficult in a number of cases because of solubility limitations. The experimental data are, therefore, presented in optical density units rather than as extinction coefficients. The concentrations of the absorbing species and the absorbing path lengths used in the various absorption measurements are listed below.

Ethyl Benzene. With the exception of water all solvents contained 0.86 g./100 ml. of ethyl benzene in solution and were measured in a path length of 1 mm. Water solutions were saturated with ethyl benzene and were measured in a path length of 50 mm.

Naphthalene. The solutions measured contained approximately 13 mg.% of naphthalene. The path lengths for the various absorption bands were 10 mm., 1 mm., and 0.1 mm. for the 320 mμ, 260 mμ, and 210 mμ absorption bands, respectively.

Anthracene. With the exception of the water-ethanol solvent system, all solutions contained 3 mg.% of anthracene. The water-ethanol (40% v/v) was saturated with anthracene. In all cases the path length was 10 mm.

Trans-azobenzene. With the exception of water, which was saturated, all solutions contained 20 mg.% of trans-azobenzene. They were measured in a path length of 10 mm. for the water solution and 1 mm. for all other solvent systems.

o-Nitro Aniline. Measurements were taken at a concentration of 92 mg.% of *o*-nitro aniline and at a 10 mm. path length for all solvent systems.

p-Nitro Aniline. With the exception of octane, which was saturated, all solutions contained 80 mg.% of *p*-nitro aniline. They were measured at a path length of 1 mm. and 0.1 mm., respectively.

Dimethyl Phthalate. Measurements were taken at a concentration of 500 mg.% of dimethyl phthalate and in a path length of 1 mm. for all solvent systems.

RESULTS

The absorption spectra of the various compounds in the various solvent systems are reproduced in Figs. 1 through 6 inclusive.

DISCUSSION

The changes in spectrum associated with changes in the solvent may be due to any of the following (6):

1. The changes which influence the polarizability of the valence electrons, e.g., changes in the dielectric constant of the environment (or its index of refraction).

2. The influence of the environment on permanent or induced dipoles through solvent-solute interaction.

3. Hydrogen bonding, dimerization, and similar molecular interaction.

4. The changes associated with variation in pH.

The first two effects are associated with small changes in the ultraviolet

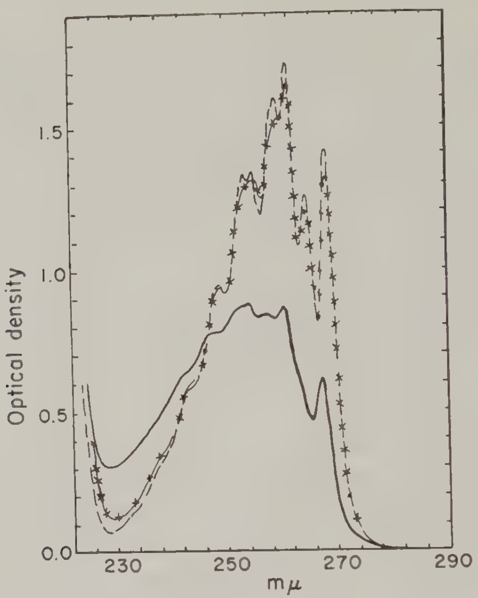

FIG. 1. The ultraviolet spectrum of ethyl benzene in water (——), octane (– – –) and 0.28 *M* potassium laurate (–x–x–x).

spectrum, whereas the last two may lead to relatively large changes in the spectrum. The effects due to the changes in the polarizability have been thoroughly studied for many compounds (7). The most common effect observed in the ultraviolet spectrum by changes in the polarity of the environment, particularly in aromatic compounds, is associated with the appearance of vibrational fine structure. In changing from a polar solvent to a nonpolar solvent, the spectrum approaches that of the free vapor state. Also, the absorption maxima are shifted slightly in wavelength with variation of the polarity of the environment. In fact, the change in absorption maxima ($\Delta\lambda$) has been observed (8) to be a function of the dielectric constant and in such cases can be used to estimate the polarity of the environment.

A comparison of the ultraviolet spectrum of ethyl benzene in water, in aqueous solution of potassium laurate, and in octane is presented in Fig. 1. As expected when ethyl benzene is dissolved in octane, it is seen to possess a high degree of fine structure in comparison with its spectrum in a polar solvent, namely, water. The spectrum of ethyl benzene in aqueous potassium laurate solution is strikingly similar to its spectrum in octane and dissimilar to that in water, indicating not only that the ethyl benzene molecules are in the micelles but that they are completely surrounded by the hydrocarbon environment of the micelles.[2]

---

[2] The gross difference in the heights of the curves is caused by differences in solution concentration and path length. Comparison is on a basis of fine structure and relative positions of absorption maxima.

The spectra of ethyl benzene in dodecylamine hydrochloride and Brij 35 are essentially identical to that represented in Fig. 1, indicating that the solubilized ethyl benzene molecules are surrounded by the hydrocarbon environment. It is a reasonable assumption, therefore, that ethyl benzene

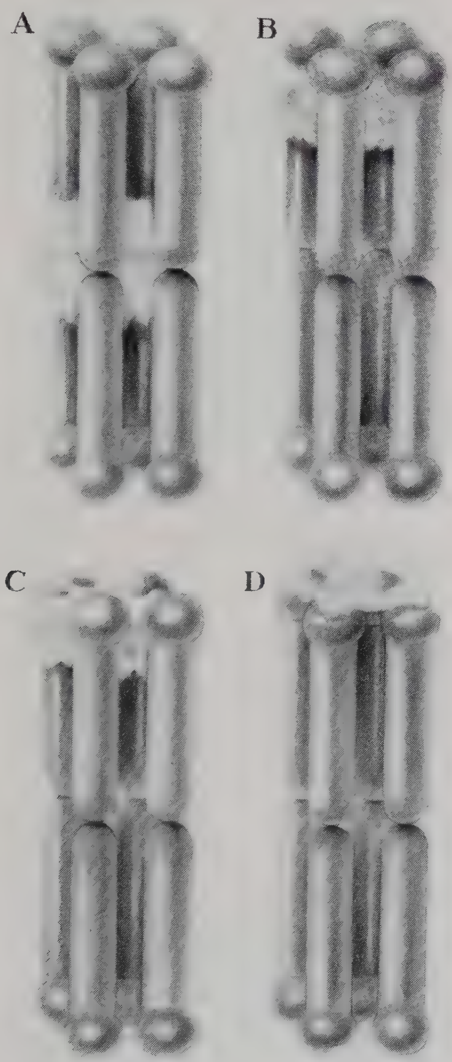

Fig. 2. A diagram of possible placements of a solubilized molecule within the structure of a surface-active agent micelle:

(*A*) Inclusion into the hydrocarbon interior of the micelles.
(*B*) Deep penetration of the palisade layer.
(*C*) Short penetration of the palisade layer.
(*D*) Adsorption on the surface of the micelles.

is located in the hydrocarbon interior of the micelles. This is in conformity with the conclusions arrived at from the X-ray studied (9–11); however, the spectral data offer no evidence as to the exact location of ethyl benzene inside the micellular hydrocarbon. Figure 2-*A* represents one possible placement of ethyl benzene in the micelle.

By analogy with the interpretations of X-ray data on the alkyl benzene series (9), it has been assumed (12) that the polycyclic hydrocarbons are also included in the micellular interior. As a matter of fact, this mode of solubilization is so well accepted that Klevens (2, 12) has suggested the existence of huge swollen micelles containing up to 3000 molecules each to accommodate one of these polycyclic molecules. Examination of the ultraviolet spectra of naphthalene in various solvent systems offers experimental evidence that polycyclic hydrocarbons are solubilized in a manner quite different from that shown for ethyl benzene.

The ultraviolet spectrum of naphthalene shows electronic absorption maxima in three different regions; namely, a strong, sharp absorption band around 220 mμ, a weak absorption band between 240 and 300 mμ, and a weaker transition band around 310 mμ.

The absorption bands between 240 and 300 mμ represented in Fig. 3 demonstrate the spectra in the three surface-active agents, water, and octane. Again, as expected, naphthalene in octane shows fine structure in

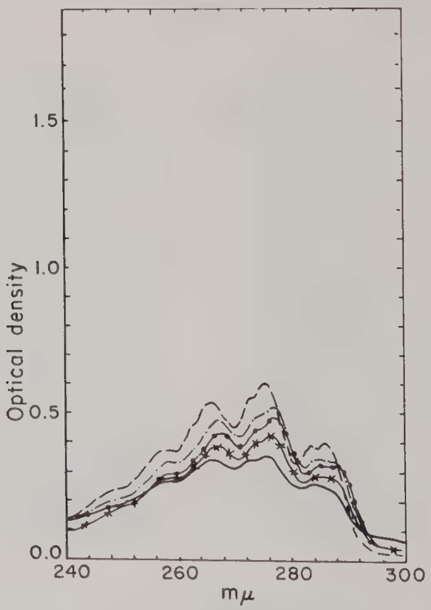

Fig. 3. The ultraviolet spectrum of naphthalene in water (——), octane (– – –), 0.22 *M* potassium laurate (-x-x-x), 0.175 *M* dodecylamine hydrochloride (–·–·–), and 10% Brij 35 (–o–o–o–o–).

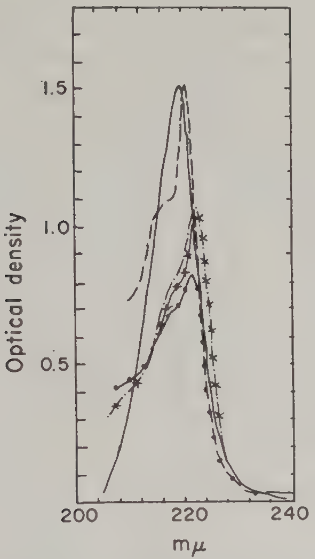

FIG. 4. The ultraviolet spectrum of naphthalene in water (——), octane (- - -)' 0.28 *M* potassium laurate (-x-x-), 0.175 *M* dodecylamine hydrochloride (-·-·-), and 10% Brij 35 (-o-o-o-).

greater detail than in water. Taking the spectrum in water as a comparison standard, it is noticed that the absorption maxima are shifted slightly towards shorter wavelengths in octane. The 240–300 mμ spectra of naphthalene in the three surface-active agents have characteristics of naphthalene in a polar solvent; the fine structure is notably less than in octane and the maxima are shifted in the same direction as in water as expected for polar solvents. Indeed the degree of shifts and the loss of fine structure is such that naphthalene in the three surface-active agents behaves as if it is in a slightly more polar environment than water.

The examination of the absorption band of naphthalene around 220 mμ reveals a picture which leads to a conclusion surprisingly opposite to that arrived at by the study of 240–300 mμ band. As shown in Fig. 4, the absorption maxima in the three-surface active agents are shifted in such a manner as to correspond with an environment for naphthalene molecules which is nonpolar—in fact, slightly more nonpolar than octane.[3]

---

[3] The hydrocarbon solvent of micelles of C_{12} surface-active agents should correspond to a saturated hydrocarbon with 12–24 carbons (19) and should be more nonpolar than octane. The values of the maxima of the 220 μ band of naphthalene in octane, cetane, Brij 35, dodecylamine hydrochloride, potassium laurate, and water are 221 mμ, 222 mμ, 223 mμ, 222.5 mμ, 222 mμ, and 220 mμ, respectively. From these values, it would seem that there is a difference between the lengths of the hydrocarbon solvent of the micelles of the three surface-active agents used. This is understandable since the organization of the micelles is known to vary with the type of surface-active agent (20).

Finally, from the comparison of the fine structure and the absorption maxima, it can be concluded that the first transition band of naphthalene at about 310 mμ like the 210 mμ band suggests a nonpolar environment for naphthalene molecules in the three surface-active agents.

Thus the naphthalene molecule in the three surface-active agents presents a paradox: the absorption bands between 240 and 300 mμ correspond with the naphthalene molecules in a polar environment, whereas 220 mμ and 310 mμ bands correspond with the molecules in a nonpolar environment. Experimental data (15, 16) and theoretical predictions (13, 14, 17, 18) lead to the assignment of the 310 mμ and the 210 mμ to the transition moment in the molecular plane and, more specifically, in the long axis. The 240–300 mμ band arises from a transition moment in the same plane but in the short axis. The spectroscopic paradox may be resolved by a postulate about the placement of the naphthalene molecules in the micelles based upon this accepted interpretation of naphthalene bands. Its position in the micelle has to be such that the 240–300 mμ transition, polarized along the short axis, is influenced by a polar environment whereas both the 210 and 310 mμ transition are influenced by a nonpolar environment. The only possibility to meet these restrictions is to place the compound in the palisade layer of the micelle. It is believed that the region of placement of naphthalene in the micelles may be represented as shown in Fig. 2*B*.

The spectra of anthracene in the surfactant solutions show shifts which can be interpreted in accordance with the postulate presented for naphthalene. Craig (18) has assigned the 380 mμ band of anthracene to the vibrational moment in the molecular plane in the short axis while the 250 mμ band is in the long axis. The 380 mμ band appears to confirm electron polarization in a polar environment while the 250 mμ band indicates an octane-like environment. Anthracene, like naphthalene, may be placed in the palisade layer of the micelles with its short axis exposed to the polar environment and the long axis in the nonpolar environment.

Figures 5 and 6 show the absorption spectra of trans-azobenzene in the region of 310 and 230 mμ in octane, water, and the three surface-active agents. Both of these bands in the three surface-active agents show nonpolar character; however, there is concomitant loss of some fine structure. Each band seems to be a hybrid of polar and nonpolar characteristics. If both bands are assumed to correspond to electron polarization in the same direction the azobenzene molecule may be oriented in the micelle so that one benzene ring is under the influence of a polar environment and the other under nonpolar influence. This would place the azobenzene in the palisade layer such that one benzene ring lies adjacent to the hydrocarbon portion of the surfactant molecule and the other benzene is near the polar surface of the micelle. Therefore, azobenzene appears to behave in the micelle much as naphthalene or anthracene rather than ethyl benzene as originally postulated by Hartley (21). Hutchinson and McBain (22) have cited this

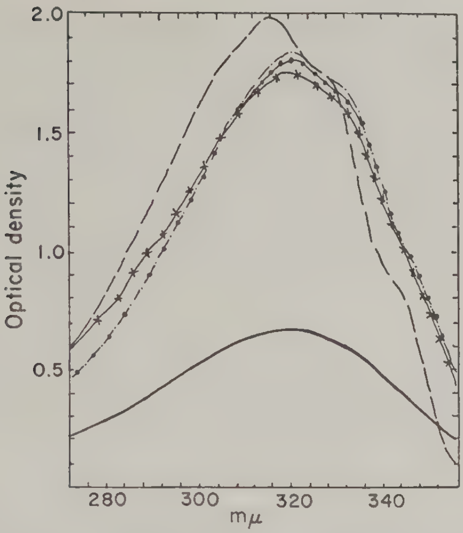

FIG. 5. The ultraviolet spectrum of trans-azobenzene in water (——), octane (- - -), 0.28 *M* potassium laurate (-x-x-), 0.11 *M* dodecylamine hydrochloride (-·∘·-), and 10% Brij 35 (-∘-).

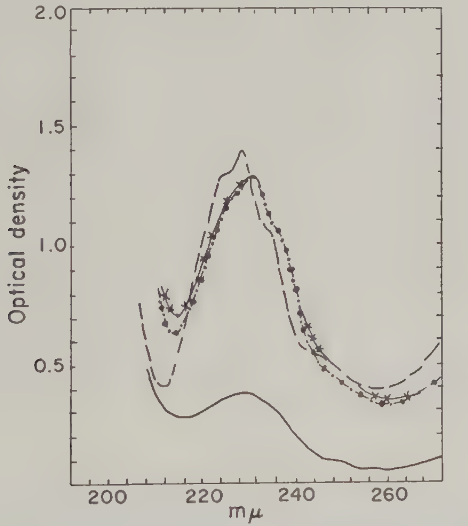

FIG. 6. The ultraviolet spectrum of trans-azobenzene in water (——), octane (- - -), 028 *M* potassium laurate (-x-x-), 0.11 *M* dodecylamine hydrochloride (-·-·-), and 10% Brij.35 (-∘-).

reference to be one of the most clear-cut pieces of research in support of the view that solubilization is a pseudo-two-phase distribution phenomenon.

The individual bands of *o*-nitro aniline cannot be assigned to the various portions of this molecule with the degree of certainty ascribed to anthracene and naphthalene (23); but on the basis of the comparison of its spectra in water, in octane, and in the three surface-active agents, it may be proposed that *o*-nitro aniline molecules are located in the micelles with their polar groups sticking out into the surrounding water. A location of *o*-nitro aniline molecules in the micelles is schematically represented in Fig. 2*C*.

The spectra of dimethyl phthalate in the three surface-active agents indicate that it is in a highly polar environment. This is consistent with adsorption as the mode of solubilization as was postulated by McBain (24). A probable region of location of dimethyl phthalate in the micelles is pictured in Fig. 2*D*.

That the observed solvent effects on the ultraviolet spectrum are not due to the changes in ionic strength, was confirmed by showing that 1.0 *M* sodium chloride had no influence on the position of the absorption maxima of *o*-nitro aniline or of naphthalene.

The discussion of the spectra so far has neglected any contribution to the total spectrum by the solubilizate which may be dissolved in the free water component of the surface-active solvent systems. One would expect that the solubilizate should be present both in the "water phase" and the "micelle phase," and the observed spectra should be a summation of the spectra in the two solvents. Actually, in the case of ethyl benzene, naphthalene, anthracene, and azobenzene the ratio of the solubility in the surface-active agents to that in water is so large (ratio of several hundred), that for all practical purposes all of the small amount of the solubilizate added may be assumed to be entirely associated with the micelle. In the cases of *o*-nitro aniline, *p*-nitro aniline, and dimethyl phthalate some corrections are needed. However, the magnitude of the corrections would not alter the conclusions drawn here.

The conclusions drawn in this paper are by no means final, nor entirely unambiguous. If more than one solubilized molecule occurs together in a cluster within a micelle the shifts of the individual band would resemble those found in crystals rather than in dissolved molecules. Additional studies on the absorption spectral characteristics of mixed solvent systems may contribute further clarification.

SUMMARY

The ultraviolet spectrum of the solubilizate affords a sensitive method for determining different modes of solubilization which have been interpreted to be (*a*) inclusion into the hydrocarbon interior of the micelles, (*b*) deep penetration of the palisade layer, (*c*) short penetration of the palisade layer, and (*d*) adsorption on the surface of the micelles.

REFERENCES

1. MERRILL, R. C., AND MCBAIN, J. W., *J. Phys. Chem.* **76**, 10 (1942).
2. KLEVENS, H. B., *Chem. Revs.* **47**, 1 (1950).

3. Kolthoff, I. M., and Strick, W., *J. Phys. & Colloid Chem.* **52,** 915 (1948); *ibid.* **53,** 424 (1949).
4. Klevens, H. B., *J. Am. Chem. Soc.* **72,** 3780 (1950).
5. Friedel, R. A., and Orchin, M., "Ultraviolet Spectra of Aromatic Compounds." Wiley, New York, 1951.
6. LeRosen, A. L., and Reid, C. E., *J. Chem. Phys.* **20,** 233 (1952).
7. Eucken, A., "Landolt-Börnstein-Zahlenwerte und Funktionen" Teil 3, Band 1, Springer, Berlin, 1951.
8. Brooker, L. G. S., and Sprague, R. H., *J. Am. Chem. Soc.* **63,** 3214 (1941). Abstract American Chemical Society, 115th Meeting, San Francisco, 1949, pp. 156, 166.
9. Philippoff, W., *J. Colloid Sci.* **5,** 183 (1950).
10. Krishnamurti, P., *Indian J. Phys.* **3,** 307 (1929).
11. Winsor, P. A., *J. Phys. & Colloid Chem.* **56,** 391 (1952).
12. Klevens, H. B. *J. Phys. & Colloid Chem.* **54,** 283 (1950).
13. Moffitt, W., *J. Chem. Phys.* **22,** 320 (1954).
14. Pariser, R., *J. Chem. Phys.* **24,** 250 (1956).
15. McClure, D. S., *J. Chem. Phys.* **22,** 1668 (1954).
16. Sidman, J. W., *J. Chem. Phys.* **25,** 115 (1956).
17. Platt, J. R., *J. Chem. Phys.* **17,** 484 (1949).
18. Craig, D. P., and Walsh, J. R., *J. Chem. Phys.* **24,** 471 (1956).
19. McBain, J. W., *in* "Frontiers in Colloid Chemistry" (Burk, R. E. and Grummett, O., eds.), Vol. 8. Interscience, New York, 1950.
20. Klevens, H. B., *J. chim. phys.* **49,** 615 (1952).
21. Hartley, G. S., *J. Chem. Soc.* **1938,** 1968.
22. Hutchinson, E., and McBain, M. E. L., "Solubilization and Related Phenomena," p. 99. Academic Press, New York, 1955.
23. Doub, L., and Vanderbilt, J. M., *J. Am. Chem. Soc.* **71,** 2414 (1949).
24. McBain, J. W., and McHan, H. J., *J. Am. Chem. Soc.* **70,** 3838 (1948).

JOURNAL OF COLLOID SCIENCE **13**, 218–231 (1958)

TACKY ADHESION

H. Strasburger

(Received June 5, 1957, revised December 2, 1957)

ABSTRACT

An instrument for the study of "tack" forces, which can split liquid films at speeds ranging from 6×10^{-2} cm./sec. to 6 cm./sec. coupled with electronic recording of the forces, is described.

Results are given of experiments with films of oils and printing inks ranging in thickness from 0.005 cm. to 0.008 cm. and in viscosity from 1.6 poises to 68.3 poises.

Forces observed at slow speeds of separation are in general agreement with Stefan's earlier results. Transition from viscous flow forces to rapid film rupture forces is quantitatively shown, and the latter are found to confirm generally the conclusions of Banks and Mill (20) on the function of cavitation in limiting the forces of separation of flat plates joined by a tacky liquid.

INTRODUCTION

The definition of tack and the measurement of tack forces is not as yet standardized, and a study of References (1)–(16) will readily show the differences of interpretation in the meaning of "tack" adopted by different branches of industry. Studies on the tackiness of fluid systems have been made both with roller systems (14) and with apparatus involving the separation of flat plates (2). It has also been recognized that a fundamental difference exists between tack forces measured at slow and fast speeds of separation of the surfaces. A quantitative analysis of the former characterized by viscous flow, was first made by Stefan with separating plates (17). Breakdown of viscous flow at higher speeds due to the formation of gaseous bubbles in regions of low pressure was originally observed on roller apparatus (23), and a quantitative study of cavitation was carried out by Banks and Mill on a plate system (20) and later on a roller system (22).

The purpose of the present study was to investigate under more precisely defined experimental conditions the observations of Banks and Mill.

For the total force to separate two circular plates joined by a liquid, Banks and Mill derived the expression

$$F = 3/2\, \pi \eta U \frac{R^4}{h^3}, \qquad [1]$$

where η = viscosity of liquid,
U = speed of separation,

R = radius of the plates,
h = distance between the plates,

which is Stefan's expression for constant velocity of separation.

With the present experimental method F could be studied at a controlled and constant velocity of separation and at a known h. The short duration of the forces necessitated oscillographic measurement in which the force was displayed as a function of time. Knowledge of instrumental constants allowed the conversion of time into distance.

Under ideal conditions of separation h at any time t measured from the start was given by

$$h = h_0 + Ut,$$

and hence from [1] we have

$$F = \frac{C\eta U}{(h_0 + Ut)^3}, \qquad [2]$$

where C is an apparatus constant. The experiments therefore required the time factor of the measurement to be short in comparison to the duration of the force and furthermore the strain in the system should be confined to that in the liquid.

APPARATUS AND MATERIALS

A cross section of the apparatus is shown in Fig. 1. It consists essentially of two circular brass plates D mounted face to face on a rectangular platform. The liquid is confined between the plates, and any excess is squeezed out into the trough formed by the beveled circumferences so that the working surfaces are initially submerged and conditions are analogous to those of Stefan's experiments. The micrometer thimble H controls the initial distance h_0 between the plates and hence the thickness of the liquid.

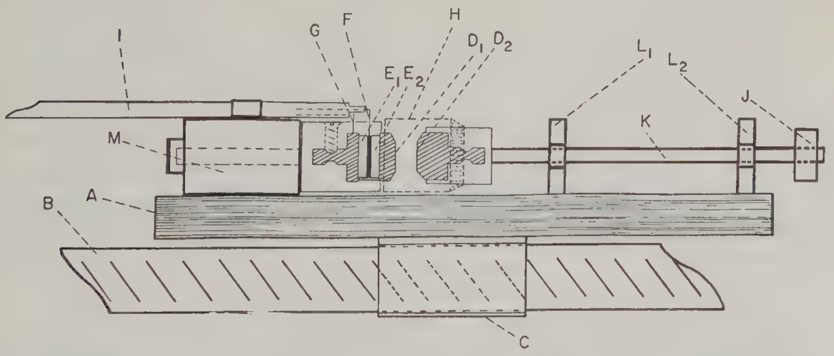

FIG. 1. Schematic diagram of trackmeter platform with piezoelectric strain gauge.

The platform *A* is driven along a track (not indicated in the figure) at a controlled speed. The bar *J* comes against a stop and the plates are pulled apart at the speed of the platform.

The tack forces on the plates were recorded by two types of strain gauges: (*1*) a wheatstone bridge type of transducer: an unbonded wire strain gauge; (*2*) the piezoelectric gauge shown in Fig. 1. The second unit consisted of two *X*-cut quartz crystal discs E_1 and E_2 bonded directly to one of the plates (D_1) and connected through an impedance converter to the grid of an oscilloscope (Fig. 2). The total leakage of the unit represented a resistance of 5000 megohms, which, with a capacitance of 13000 pF, provided a time constant of over 65 sec. The long time constant enabled calibration by direct loading of the plate *D* with weights.

Both the resistance and the piezoelectric gauges yield elastically in some degree to the applied forces, and this can affect measurements in two ways. It will modify the speed of separation of the plates, so that this is no longer equal to the speed of the platform except when the deflection of the strain gauge is passing through a maximum since

$$V = \frac{dl}{dt} + \frac{dh}{dt},$$

where V is the platform velocity, dl/dt is the rate of extension of the measuring unit, and dh/dt is the speed at which the plates are separating. (Most of the results discussed are in fact based on the maximum deflection point of the trace.) Secondly it can allow the mass of the yielding portion of the strain gauge to behave as an oscillatory system which may be a limiting factor in measuring very short transient forces. If we consider the brass plate and crystal unit as an oscillating system with a mass and stiffness it

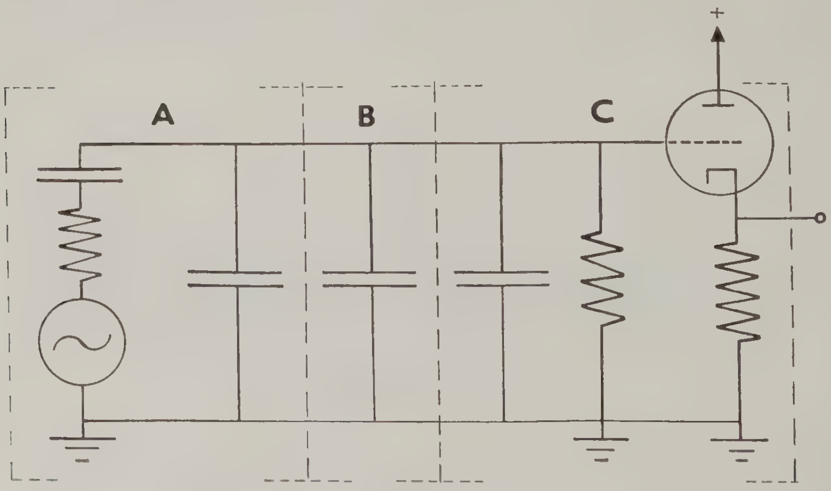

FIG. 2. Equivalent circuit of crystal—*A*, cable—*B*, and converter—*C*.

TABLE 1

Peak Cavitation Forces for Untreated and Aerated Samples in Relation to Instrumental Constant

Oil	(sec.)	Force (g.)	$F/\eta U$	$1/(h_m)^3 \times 10^{-6}$
Shell K20	0.0047	2620	432	2.824
	0.0012	873[a]	144	5.759
Castor oil	0.00206	1051	274	4.740
	0.00265	1508	392	4.179
	0.00147	950[a]	248	4.470
Shell Vitrea 71	0.00278	1290	539	4.082
	0.00235	1112	466	4.454
	0.00235	794[a]	331	4.454
Paraffin oil	0.00224	1170	1057	4.577
	0.00224	754[a]	683	4.579

[a] Aerated samples.

can be shown that allowing a maximum error of 5% in the recorded peak deflection (i.e., the semi-amplitude of the oscillation 5% of the peak force), the time to reach peak deflection should be at least 3.2 T_0, where T_0 is the natural period. The natural frequency of the resistance and the piezoelectric gauges were 250 cycles/sec. and 2 kc. It should be possible therefore to record forces with time intervals down to approximately 0.013 sec. and 0.0016 sec., respectively, within the 5% error limit. The failure of the resistance gauge to record forces with time intervals of the order shown in Table I was evident from the shape of the traces, and this necessitated the subsequent adoption of the piezoelectric method.

MATERIALS

The materials were selected to allow measurement of forces in the Stefan region at the lower end of the speed of separation scale as well as at the higher speeds. The liquids below had the requisite viscosity characteristics:

Medicinal Paraffin	1.66 poises at 21°C.
Shell Vitrea 71—Mineral Oil	5.60 poises at 21°C.
Castor Oil	9.06 poises at 21°C.
Shell K 20—Mineral Oil	14.30 poises at 21°C.

Separation forces were also recorded for liquids of higher viscosity:

Aqueous solution of carboxy-methyl cellulose (I.C.I. Cellofas)	
Lithographic printing inks	Plastic viscosity approximately 17 poises
Letterpress bag printing inks	Plastic viscosity approximately 29.6–68.3 poises.

EXPERIMENTAL RESULTS

Experimentally obtained force/time oscillograms were of three distinct types:

(*a*). Figure 3*a*—where the deflection rises from 0 at t_0 to a maximum in a finite time t and then decays in a continuous curve to 0. For all liquids forces up to 600 g. were recorded by this type of trace. When plotted (Figs. 5 and 6) against the speed of separation the peak forces fall on the straight lines.

b). Figure 3*b*—where the deflection rises to a maximum, falls to a certain

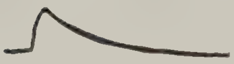
(a)

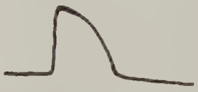
(c)

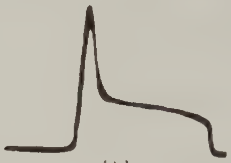
(b)

FIG. 3*a*. Trace typical of slow rates of separation characterized by flow of liquid between surfaces.

FIG. 3*b*. Trace typical of transition from separation by flow to separation with cavitation.

FIG. 3*c*. Trace typical of rapid rates of separation characterized by cavitation breakdown of liquid.

TABLE II

Peak Cavitation Forces and Hump Values Obtained With Resistance and Piezoelectric Gauges

Material	Viscosity (*poises*)	Initial separation (*cm.*)	Speed of separation (*cm./sec.*)	Peak force (*g.*)	Hump value (*g.*)
Castor oil[a]	9.06	0.00508	1.27×10^{-1}	1304	901
	9.06	0.00508	6.36×10^{-1}	2010	869
	9.06	0.00508	8.48×10^{-2}	1218	869
Cellofas D.M.	17	0.00508	1.48×10^{-1}	2360	901
	17	0.00508	2.12×10^{-1}	1720	869
Shell K20	14.29	0.00762	6.36×10^{-1}	1829	794
	19.4	0.00508	1.59×10^{-1}	1190	857
	14.29	0.00508	4.24×10^{-1}	2620	794
	14.29	0.00508	4.24×10^{-1}	853[b]	853
Shell Vitrea 71	5.65	0.00508	4.24×10^{-1}	1110	774
	5.65	0.00508	4.24×10^{-1}	794[b]	794
	5.1	0.00762	4.34	3415	913
Castor oil	9.06	0.00508	4.24×10^{-1}	1509	873
	9.06	0.00508	4.24×10^{-1}	952[b]	930
Liquid paraffin	2.61	0.00508	4.24×10^{-1}	1170	794
	2.61	0.00508	4.24×10^{-1}	754[b]	754
Letterpress bag blue	62.1	0.00762	2.12×10^{-1}	2750	932
	62.1	0.0117	2.12×10^{-1}	1412	932
Litho ink blue		0.00762	7.42×10^{-2}	2743	873
		0.00762	7.42×10^{-2}	913[b]	913
		0.00762	7.42×10^{-1}	1040[b]	1040
		0.00762	1.16	2755	1040
		0.00762	1.16×10^{-1}	1350[b]	957

[a] Resistance gauge. [b] Aerated samples.

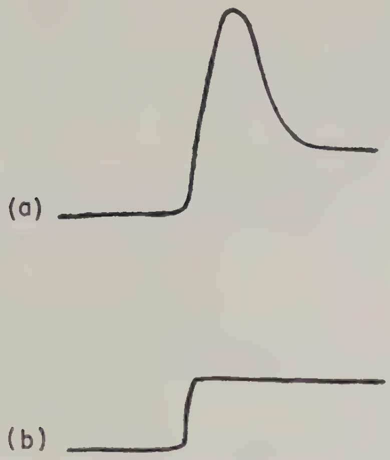

FIG. 4*a* and *b*. Traces showing reduction of peak force by seeding tacky film with air bubbles prior to splitting. (Piezoelectric gauge.) *a*. Untreated—2.62 kg.; *b*. Aerated—0.874 kg.

level (878 ± 150 gm. for all liquids tested), and turns sharply to follow a course almost parallel to the abscissa, until finally it decays to 0. It should be noted that over a limited, overlapping range of speeds, the occurrence of the horizontal discontinuity (subsequently referred to as the hump) was observed at the same level with both tension gauge systems which differed considerably in natural frequency. The peak forces do not fall on the same curve as for the (*a*) traces, but appear to rise irregularly with increasing speed while the level of the hump remains constant (Table II).

c). Figure 3*c*—where the peak and hump are not clearly differentiated and the decay portion of the trace tends to be convex. This type of trace occurs as an intermediate type between the (*a*) and (*b*) traces and when plotted, the peak forces fall at the end of the straight line obtained from the peaks of the (*a*) traces. (Figures 5 and 6.)

A smooth liquid surface on the plates after separation was characteristically related with traces of type (*a*). When traces of type (*b*) were in evidence, a thin circular pitted area of radius $r < R$ the radius of the plates, was observed, surrounded by a smooth, thicker annulus of unpitted liquid. This condition was particularly easy to observe in the case of stiff liquids where the pattern was more persistent. Furthermore it was found that the peaks in traces of type (*b*) could be reduced or completely eliminated to the level of the hump by seeding the liquid film with air bubbles prior to separation. Figures 4*a* and 4*b* and Table II.

DISCUSSION

It would appear that the two different types of traces are associated with two distinct mechanisms of liquid breakdown between the plates. Results are divided into two groups. In the first group (associated with traces of type (*a*)) an attempt is made to verify the reliability of the instrument according to the accepted theory of Stefan and hence, to establish the validity of subsequent deviation from Stefan's law in the second group (associated with traces of type (*b*)).

For the oscillogram of any one tack test the force recorded at a time t can be put as $F = k_1 \delta_x$, where k_1 is the calibration constant and δ_x the deflection of the trace. Substituting in Eq. [2] we obtain the equation of the trace

$$\delta_x = \frac{C\eta U}{k_1(h_0 + t_x U)^3}, \qquad [3]$$

where C is the instrumental constant. We can then plot δ_x against t.

Group 1 Results

As indicated earlier the movement of the platform is equal to the increase in separation between the plates and the displacement of the strain gauge used to measure the force. The latter is proportional to the force and thus at time t after starting, the gap between the plates is given by

$$h = h_0 + Ut - k_2F.$$

The stress takes a finite time to respond to the movement of the platform, and the distribution of velocites between the strain gauge and viscous element is unknown initially. At maximum stress, however, the velocity of displacement of the strain gauge is zero so the conditions for the plunger are known precisely if we substitute in the above expression for h the values

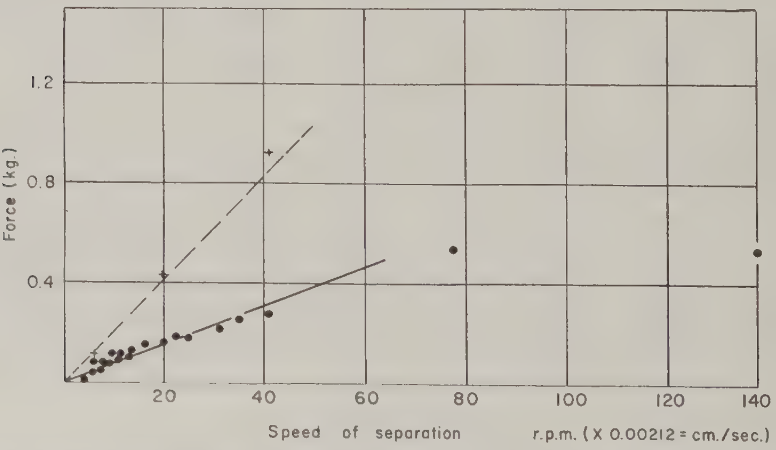

FIG. 5. Observed and theoretical peak forces of separation. Resistance strain gauge.

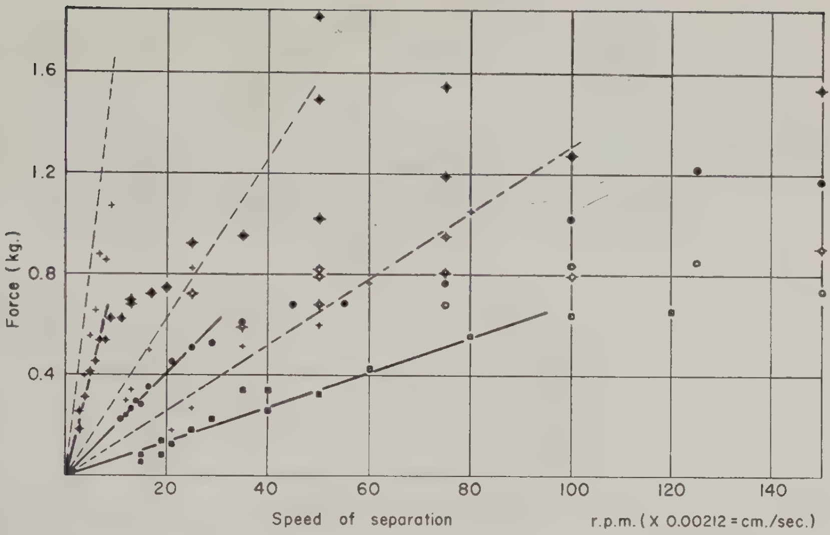

FIG. 6. Observed and theoretical peak forces of separation. Piezoelectric strain gauge. ----- Curve predicted by Stefan's equation; ◆ Shell K 20, $h_0 = 0.00508$ cm; -◇- Shell K 20, hump, $h_0 = 0.00508$ cm; ● Shell K 20, $h_0 = 0.00762$ cm; ○ Shell K 20, hump, $h_0 = 0.00762$ cm; □ Liquid paraffin, $h_0 = 0.00508$ cm; + F_m corrected for increase in separation according to $F_0 = F_m[(h_0 + t_m U)^3/h_0^3.]$

t_m, F_m of the oscillograph curve. The corrected value F_0 of the measured force F_m is then given by

$$F_0 = F_m\left(\frac{h_0 + t_m U - k_2 F_m}{h_0}\right)^3.$$

In the case of the piezoelectric gauge the value of k_2 is insignificant for the range of velocities used in these experiments, and the third term in the numerator vanishes. In Figs. 5 and 6 are shown the experimental points for a number of speeds of separation. A few of the points have been corrected in accordance with the above formula and are shown in relation to the theoretical (broken) line.

In Fig. 7*a* is shown a curve δ against t calculated from Eq. [3] compared with an experimental trace. The calculated curve was made to fit the experimental one at $t = 0.02$ sec. by applying a correction of 2.7 % to h_0 and the agreement over the remainder of the trace is satisfactory. The maximum force, attained at $t = 0.012$ sec., was 499 g. and was still well below the transition value.

A further test of the agreement with Stefan is afforded if we write

$$\frac{F}{\eta U} = (3/2\,\pi R^4)\,\frac{1}{h^3}$$

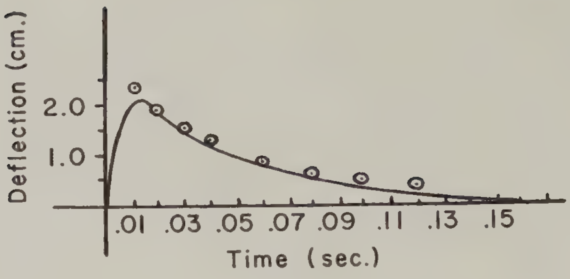

Fig. 7a.

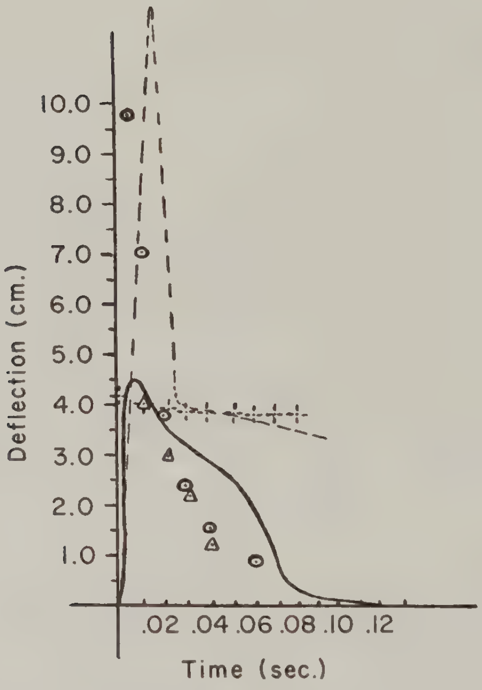

Fig. 7b.

Fig. 7. Comparison of experimentally obtained traces of force against time (× 2 magnified) with calculated curves (piezoelectric gauge). *a*. Shell Vitrea 71; $h_0 = 0.00762$; Speed 6.36×10^{-1} cm./sec.; Peak force 0.499 kg.; *b*. (Continuous curve)—Shell K 20; $h_0 = 0.00762$; speed $= 2.12 \times 10^{-1}$ cm./sec.; Peak force $= 1.02$ kg.; (Broken curve) Lithographic ink $h_0 = 0.00762$; Speed 2.12×10^{-1} cm./sec.; Peak force 2.75 kg.; Initial hump 0.79 kg.

Calculated: $\odot$ from Stefan; ·¦· Constant radius bubble; $\triangle$ Shrinking bubble.

By plotting $F/\eta U$ against $1/h^3$ we should obtain a slope equal to $\frac{3}{2}\pi R^4$ constant and dependent only on the instrumental dimensions. If F is measured in grams, then $C = 0.867 \times 10^{-4}$—the value used for the theoretical curve in Fig. 8. The lower group of points (Fig. 8) was derived from

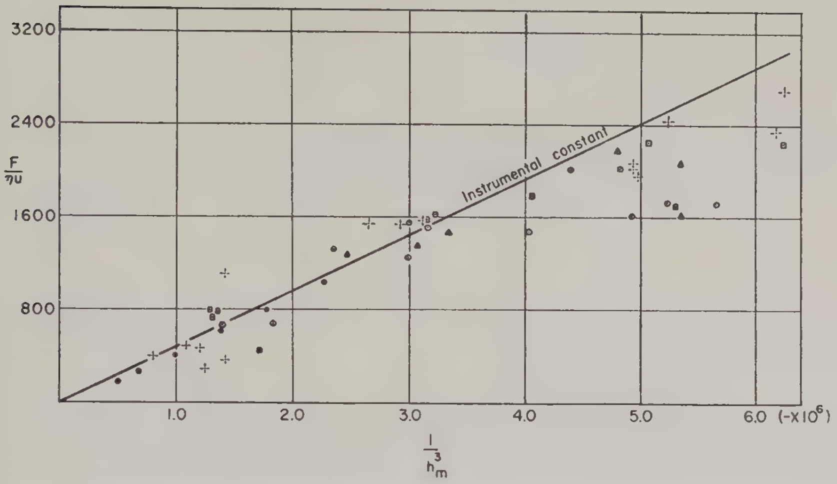

FIG. 8. Instrumental constant—actual and calculated from peak forces in the Stefan region.

the h_0 = 0.00762 cm. experiments; the middle and upper groups were derived from the h_0 = 0.00635 and h_0 = 0.00508 cm. experiments, respectively. The solid points were calculated from the single trace (Fig. 7*a*). Any experimental errors tending to increase the initial separation between the plates become more significant for smaller gaps, which may account for the tendency of the 0.00508 experiments to fall below the instrumental constant.

On the basis of the above evidence it was concluded that the force/time relationship obtained experimentally up to forces of 600 g./cm. ±50 g. can be expressed mathematically by the single curve derived from Eq. [1] and that this curve can be expressed physically by saying that throughout separation of the plungers there is a single, liquid phase in a streamline flow.

Group II Results

It now remains to discuss the traces (type (*b*)) obtained at forces of separation above 500 g. ± 50 g.

Plotting $F/\eta U$ for the peaks above this critical level, against $1/h^3_m$ there is no agreement with the instrumental constant, as can be verified from Table I for both the aerated and nonaerated results. Furthermore there is no agreement between the experimental traces and the distribution of forces according to Eq. [3]. Compare the calculated points with the experimental trace (unbroken) (Fig. 7*b*). It can also be verified from Fig. 6 that the peak forces are considerably scattered for any one speed of sepa-

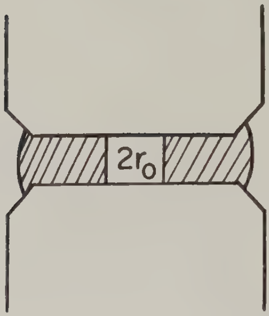

FIG. 9. Schematic formation of a cavity of radius r in liquid between the tackmeter plates.

ration. By drawing an analogy with the unstable state of superheated liquids it was postulated that the tension in the liquid between separating plates is released (at peak force) by the formation of a cavity from the expansion of bubbles around solid or gaseous nuclei present in the film. The observed horizontal discontinuity (hump) was said to record the expansion of the cavity with increasing distance of the plates up to the breaking point or collapse of the surrounding cylindrical fluid envelope.

If we consider the occurrence of a cavity in the liquid film (Fig. 9) and assume:

1. The velocity of separation sufficiently great to cause a cavity of radius r_0 to form immediately we have a pressure $(-A)$ relative to atmosphere.

2. Only a limited volume of material is available $= V$.

The pressure in the liquid (20) is given by

$$P_r = +\frac{3\eta U}{h^3}(r^2 + I),$$

where $P_r = 0$ at $r = r_m$.

$$\therefore\ P_r = -\frac{3\eta U}{h^3}(r_m^2 - r^2), \tag{4}$$

and since $P_r = -A$ for $r \leq r_0$ and $h = h_0$ (assumption (*1*)) we have

$$A = \frac{3\eta U}{h_0^3}(r_m^2 - r_0^2). \tag{5}$$

The force to separate the plates, assuming laminar flow between r_m, r_0, and constant pressure for $r \leq r_0$,

$$\begin{aligned} F &= \int_{r_0}^{r_m} 2\pi r P_r\, dr + \pi r_0^2 A \\ &= \pi r_0^2 A + \frac{3\pi\eta U}{2h^3}(r_m^2 - r_0^2)^2. \end{aligned} \tag{6}$$

From Eqs. [5] and [6] we have

$$F = \pi r_0^2 A + \frac{\pi A^2}{6\eta U} \cdot \frac{h_0^6}{h^3}. \qquad [7]$$

If the viscous forces in the beveled area surrounding the discs are neglected the effective value of r_m is R, the radius of the disc, and this will be true until the gap has widened and the relation

$$\pi(r_m^2 - r_0^2) = \pi(R_2 - r_0^2) = V \qquad [8]$$

is satisfied.

If the radius of the bubble remains constant throughout the separation, we obtain r_0 from Eqs. [5] and [8] and substitution in [7] gives

$$F = \pi a^2 A \left(1 - \frac{A h_0^3}{3R^2 \eta U} + \frac{A h_0^6}{6R^2 \eta U h^3}\right). \qquad [9]$$

Alternatively, if the bubble shrinks so that the relation

$$A = \frac{3\eta U}{h^3}(R^2 - r_0^2) \qquad [10]$$

always holds, then eliminating r_0 between [7] and [10] gives

$$F = \pi R^2 \left(1 - \frac{A h^3}{6\eta U R^2}\right). \qquad [11]$$

Equations [9] and [11] thus represent two possible relationships between force and separation after cavitation occurs.

For the experimental trace, Fig. 7 (*b*—unbroken curve), (Shell K 20 η = 14.29 poises) the constant radius bubble forces and the shrinking bubble forces were calculated from Eqs. [8] and [9], respectively, and plotted in terms of deflections. It is evident that for this particular case the experimental trace follows a course between the two possible theoretical curves. We can tentatively say that the expressions [8] and [9] account for the two extreme cases and that in practice neither one nor the other is entirely true, i.e., the bubble persisting at a constant radius for a finite time and then shrinking.

The initial hump values were found to be relatively constant over the range of speeds and liquids tested, with the higher values usually associated with the higher speeds of separation. The average hump value for over 80 measurements with both the piezoelectric and resistance gauges was equivalent to 38.6 mm. deflection on the same scale as used in Fig. 7*b* (average of values quoted in Table II is equivalent to 38.9 mm.), whilst the theoretical value calculated for Shell K 20 is 39 mm. (constant radius bubble, Fig. 7*b*—compare with broken curve, Fig. 7*b*).

On the basis of the above evidence it was concluded that the observed discontinuity of slope in the force/time distribution traces when the peak of the traces record a force above 600 g. ± 50 g. is due to the inception of a gaseous phase, and that this discontinuity tends with increasing speeds of separation towards the curve of Eq. [14], whilst the peak deflection tends towards a point on the curve obtained from Stefan's equation.

According to Banks and Mill, who took the limit of realizable pressure at the center of the liquid as 0 atmosphere, we should expect cavitation to occur in the present system at forces of separation of 517 g. It would, however, appear from the level of the hump and the peak forces recorded by transitional traces that cavitation occurs at a tension greater than 10^6 dynes cm.$^{-2}$.

It is interesting to note that Banks and Mill (22) working with a system of completely immersed rollers have found that both with liquid paraffin and with castor oil, cavitation occurred in the nip of the rollers when pressure reduction was of the order of 2×10^6 dynes cm.$^{-2}$.

How nearly the peak forces approach the Stefan value may be dependent on the relative rate of the growth of cavitation to the rate of application of stress and possibly at the same time on viscoelastic effects, but it is doubtful that forces could exceed the Stefan value.

ACKNOWLEDGMENTS

I would like to thank Dr. Banks for encouraging the work, Mr. Mill for his contributions to the theory, and Mr. Wall for technical assistance. Thanks are also due to the Council and Director of the Printing, Packaging and Allied Trades Research Association for permission to publish.

REFERENCES

1. GOLOVISTIKOV, J. J., *Prom. Org. Khim.* **6,** 461 (1939).
2. GREEN, H., *Ind. Eng. Chem.* **13,** 632 (1941).
3. DE BRUYNE, N. A., BOWLES, R. F., RIVLIN, R. S., AND OTHERS, *Paint Technol.* **9**(106), 211–221 (1944).
4. PHILIPSON, J. M., *Paint Technol.* **10**(117), 215 (1945).
5. BONNER, R. E., AND BREWSTER, M. D., *Offic. Gaz. U. S. Pat. Office* **590,** 119 (1946).
6. FULD, M., *Rev. Current Lit. Paint, Colour, Varnish and Allied Inds.* **20**(117), 212 (1947).
7. BIKERMAN, J. J., *J. Colloid Sci.* **2,** 163 (1947).
8. BIKERMAN, J. J., *Trans. N. Y. Acad. Sci.* **9,** 273–276 (1947).
9. LAMBERT, J. M., AND MCDONALD, R. A., *Rev. Sci. Instr.* **19,** 119 (1948).
10. BIKERMAN, J. J., *J. Colloid Sci.* **3,** 75 (1948).
11. BROLL, H. R., FULD, M., AND DUBREIS, A. S., *Soap Sanit. Chemicals* **23**(2), 151 (1948).
12. VOET, A., *Am. Ink Maker* **28**(6), 36 (1950).
13. VOET, A., *Chem. Weekblad* **46,** 801.
14. VOET, A., AND GEFFENKEN, C. A., *Ind. Eng. Chem.* **43,** 1614 (1951).
15. BOSTROM, S., *Kautschuk u Gummi* **4,** 207 (1951).
16. ZETTLEMOYER, A. C., MILLER, J. C., AND MYERS, R. R., Div. Paint Plastic and

Printing Ink Chem., Papers Presented at the Cincinnati Meeting **15,** 1 (1955).

17. Stefan, J., *Sitzber. Akad. Wiss. Wien. Math.-naturw. Kl. Abt. II* **69,** 713 (1874).
18. Reynolds, O., *Phil. Trans.* **177,** 157 (1886).
19. Purday, H. F. P., "Streamline Flow," p. 173. Constable, London, 1949.
20. Banks, W. H., and Mill, C. C., *J. Colloid Sci.* **8,** 53 (1953).
21. Myklestad, N. O., "Vibration Analysis," p. 105. McGraw-Hill, New York, 1944.
22. Banks, W. H., and Mill, C. C., *Proc. Roy. Soc. London*, **A223,** 414 (1954).
23. Sjodahl, S. J., Proceedings Tali April 15, 1949.

JOURNAL OF COLLOID SCIENCE **13**, 232–236 (1958)

STUDIES ON PERIODIC FORMATIONS

I. RADIAL RHYTHMICITY

A. C. Chatterji and Hari Bhagwan

Chemical Laboratory, The University, Lucknow, India

Received August 20, 1957, revised November 25, 1957

Introduction

In a previous communication (1), the authors described rhythmic patterns obtained by diffusing the reactant solution on strips of filter paper impregnated with the precipitating agent. It was reported that in the case of colloid-impregnated strips, the interspaces found in rhythmic patterns were along the direction of the diffusing solution. Detailed investigations of these patterns have been undertaken in this paper.

A very large number of workers have obtained periodic precipitates in columns of various materials set in test tubes and on material spread on flat plates, petri dishes, etc. Runge (2), Mikhalev (3), and Packter (4) have used impregnated filter papers. Ghosh (5) and Carey (6) have obtained the rings between microscope slides. But the interspaces described by these workers and others were observed to lie perpendicular to the direction of the diffusing reactant.

In addition to this usual type of interspaces, it has been observed here that interspaces exist along the direction of diffusion also. This leads to discontinuous periodic precipitation emerging radially (called hereafter radial rhythmicity). Both these types of rhythmicity have been studied in petri dishes microscopically as well as on filter paper with a view to elucidate the cause of radial rhythmicity. Ring rhythmicity has been explained by many workers (7–11).

Experimental Methods

Discs 7 inches in diameter of Whatman No. 1 filter paper were cut. These were dipped in the impregnating solution, which contained protective colloid, such as agar (1–3 %), gelatine (3–7 %), starch (4–8 %), and dextrin (4–8 %) and precipitating agents—1.0 % each of KI, K_2CrO_4, $K_3Fe(CN)_6$, and $K_4Fe(CN)_6$. After draining the extra solution, they were dried in an oven at 45° ± 1°C.

A petri dish, 6 inches in diameter was taken and a watch glass, 3 inches in diameter with the reactant solution was kept in it. Then a small hole was made in the center of the disc and a plug of filter paper was inserted in it. The disc was placed on the petri dish in such a manner that the other end dipped in the reactant solution contained in the watch glass. Above the disc was placed the cover of the petri dish.

Ten per cent reactant solution in the watch glass was allowed to diffuse for 1½ to 3 hours in the following way:

a). With KI-impregnated filter papers: lead nitrate, silver nitrate, and mercurous nitrate; and mercuric acetate.

b). With $K_3Fe(CN)_6$-impregnated filter papers: silver nitrate and uranyl nitrate; sulfates of copper and nickel and cobaltous chloride.

c). With $K_4Fe(CN)_6$-impregnated filter papers: silver nitrate, lead nitrate, and uranyl nitrate; sulfates of copper and nickel and cobaltous chloride.

d). With K_2CrO_4-impregnated filter papers: lead nitrate, silver nitrate, and mercurous nitrate; and mercuric acetate.

In a second series of experiments, agar (1–3%) along with the precipitating agent was set in petri dishes to study the rhythmicity of PbI_2. Rings start forming as soon as the crystal or solution of $Pb(NO_3)_2$ is kept in the center of the impregnated colloid set in the petri dish. Their formation could, therefore, be studied with the help of *camera lucida* under the microscope.

The rings can be obtained by reversing the process as well. Agar may be impregnated by $Pb(NO_3)_2$ and the reaction started by a crystal of KI. For obtaining better rings, electrolyte (5–10% $NaNO_3$ or KNO_3) may be added to the agar solution.

Results and Discussion

With circular discs of filter paper, 19 cases were studied. In all these cases periodic nonuniform precipitation occurred. The rhythmic patterns are of two types:

a). Type I patterns show either clear radial interspaces or zones of different densities of precipitate emerging out radially. Addition of the electrolyte, such as KNO_3 or $NaNO_3$ to the diffusing reactant was found to give clearer, empty interspaces. *See* Fig. 1.

b). Type II patterns show concentric rings with portions bulging out radially.

Of 19 cases studied, 14 show type I patterns. If a careful examination of the remaining 5 type II cases (ferricyanide of copper and silver; ferrocyanide of copper and uranyl; and mercuric chromate) is made, then faint traces of the type I pattern along with concentric rings are seen. The type I pattern persists even when the colloid is changed.

The nature and concentration of the impregnating colloid, the precipitating agent, and the diffusing electrolyte have an effect on rhythmicity.

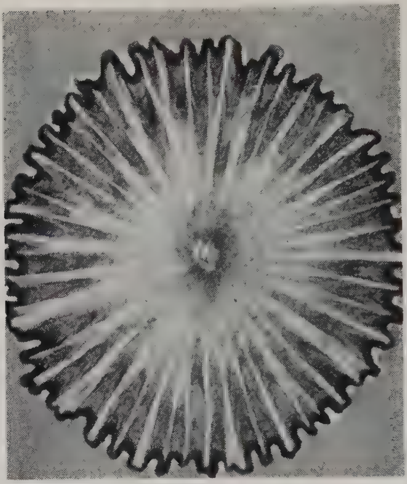

Fig. 1. Type I Radial pattern of Ag_2CrO_4 on filter paper (×1½).

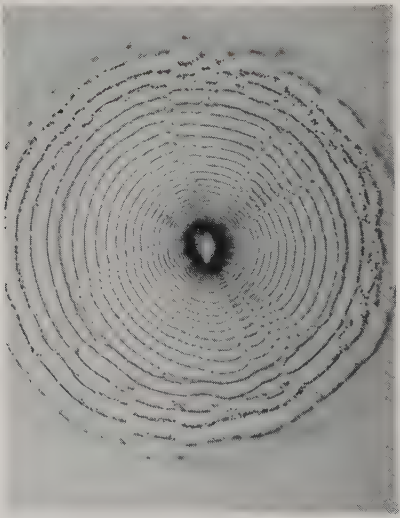

Fig. 2. Radial breaks of PbI_2 in concentric rings formed in a petri dish (×2).

The radial spaces may be due to: (*a*) rapid diffusion in the case of filter paper; and/or (*b*) unrestricted diffusion in the horizontal direction.

In ring experiments performed in the test tubes, greater vertical diffusion of the reactant is possible, because the horizontal diffusion is checked by the sides of the wall. Hence it was necessary to perform experiments with petri dishes, where unrestricted horizontal diffusion is possible. As expected, these experiments gave the usual concentric rings. But when the dish (Fig. 2) was examined in reflected light, the rings appeared to be broken.

The vertical part of the rings showed distinct concentrated zones of the precipitate along with clear radial interspaces, which became widely gapped in the subsequent rings. These breaks are sometimes visible in the test tube experiments also, but they are less in number and less distinct.

An obvious explanation of these breaks suggested itself when the origin of rings was studied under the microscope. The ring was found to originate in the form of small specks at different places in the concentric form. Specks gradually became bigger and larger in number to form zones in the same ring. In the beginning, when the rate of formation of these zones was fairly rapid, they fused immediately to give a complete ring. After a while the radial gaps increased and consequently it took some time for each ring to complete. In the last stages these radial gaps became so wide that they could not be filled up by the coalescence of radially originated zones, leaving thereby radial gaps, thus resulting in incomplete rings. The origin of rings may be imagined on the lines of Fig. 2, where the radial gaps tend to coalesce.

It is suggested that in the case of filter papers, the radial origins of rings coalesce in the same direction as that of the diffusing reactant because of rapid diffusion, to give rise to radial rhythmicity. In the case of petri dishes, the rate of diffusion is much slower. So the coalescence of radial zones may take place along the direction perpendicular to that of the diffusing reactant. This gives rise to ring rhythmicity.

In addition, the possibility that one of these two types is merely an aberration due to high molecular concentration and rapid rate of diffusion, thus affording a common basis for the occurrence of these two types, suggests itself readily. But a detailed variation of the various factors in the case of PbI_2 has not resulted in resolving both the types of rhythmicity on the filter paper.

Summary

Three important observations are:

1). Radial patterns on filter paper.

2). Radial gaps in the petri dish experiments.

3). Formation of radial origins of PbI_2 ring as revealed by microscopic study.

On the basis of these observations, it can be concluded that two types of rhythmicity occur:

a). Rhythmicity along the direction of the diffusing reactant.

b). Rhythmicity in a direction perpendicular to that of the diffusing reactant.

As (*a*) gives rise to radial patterns on filter paper, it has been called "Radial Rhythmicity." As (*b*) gives rings, it has been called "Ring Rhythmicity." Both these types can be operative simultaneously. In the case of

slow horizontal diffusion in petri dishes, concentric rings with wide radial gaps may be seen. In the case of test tube experiments, where slow vertical diffusion takes place, ring rhythmicity is chiefly operative; here small breaks or gaps are sometimes left in the rings. In the case of filter papers, patterns showing radial rhythmicity are more common.

REFERENCES

1. CHATTERJI, A. C., AND BHAGWAN, H., *Z. anal. Chem.* **156,** 7 (1957).
2. RUNGE, G., "Der Bildungstrieb der Stoffe." Oranienburg, 1855.
3. MIKHALEV, P. F., *Colloid J.* (*U. S. S. R.*) **4,** 725 (1938).
4. PACKTER, A., *J. Chem. Soc.,* **1955,** 1180.
5. GHOSH, D. N., *J. Indian Chem. Soc.* **7,** 509 (1932).
6. CAREY, E. J., *Biodynamica* **3,** 251 (1941).
7. OSTWALD, W., "Lehrbuch der allgemeinen Chemie," 2nd ed., vol. 2, p. 788. Engelmann, Leipzig, 1897.
8. DHAR, N. R., AND CHATTERJI, A. C., *J. Phys. Chem.* **28,** 41 (1924); *Kolloid-Z.* **37,** 2 (1925); *ibid.* **37,** 89 (1925).
9. HEDGES, E., "Liesegang and Other Periodic Structures." Chapman, London, 1932.
10. BRADFORD, S. C., *Kolloid-Z.* **30,** 364 (1922).
11. STERN, K. H., *Chem. Revs.* **54,** 79 (1954).

JOURNAL OF COLLOID SCIENCE **13**, 237–241 (1958)

STUDIES ON PERIODIC FORMATIONS

II. TIME AND DISTANCE RELATIONSHIPS OF PERIODIC PRECIPITATES

A. C. Chatterji and Hari Bhagwan

Chemical Laboratory, The University, Lucknow, India

Received August 20, 1957, revised November 25, 1957

INTRODUCTION

Jablczynski (1) pointed out that the position of Liesegang rings follows a geometric progression law, $X_n = aK^n$, where X_n is the distance of the nth ring from the origin of diffusion; a and K are constants, K being known as the spacing coefficient, and a is the first term. Mathur (2), on the basis of the observation that "the ring formation in the earlier stages of periodic precipitation is very fast and soon becomes very slow", has suggested a logarithmic relationship of times of ring formation also.

Morse and Pierce (3), by assuming the existence of a supersaturation product, formulated $X/\sqrt{T} = K$, where X is the distance to which the precipitate penetrates in time T. Van Hook (4) derived the same equation independent of Morse's assumption of supersaturation. Wagner (5) has found this equation a necessary consequence of the diffusion equations. Stern (6) in his review article has pointed out that Morse's equation is a necessary condition from which all the equations determining the criteria for the occurrence of the Liesegang ring phenomenon are derived. There have been many theoretical investigations of periodic structures. But Stern (6) points out that "while the qualitative and semi-quantitative agreement between theory and experiment is quite satisfactory, no rigorous comparison between the two e.g. ring distances and times of formation observed experimentally and derived theoretically, has been carried out." A method of their experimental determination corrected for the induction time and nonpoint source is given in this paper.

EXPERIMENTAL METHODS

Ten milliliters of agar solution along with KI (1 %) as the precipitating agent was poured in petri dishes 8 cm. in diameter. After keeping it overnight, when the thin gel was set, a crystal of $Pb(NO_3)_2$ was placed in the center of impregnated colloid set in the dish. The dish was brought under the focus of the microscope, and the formation of the rings of PbI_2 was studied at room temperature. With the help of *camera lucida*, a diagram of ring formation was drawn on paper. After determining the magnification with the slide, their actual distances were calculated. Times of formation were noted adjacent to the origin of rings. Four to five determinations of each set showed similarity of results within the range of experimental error, and the results tabulated here are the mean of several determinations.

For 0.01 to 0.05 g. of $Pb(NO_3)_2$, the rate of ring formation is constant for 30 minutes, because the same number of rings is formed in this time period. In all the cases studied, reaction was started by 0.02 g. of the reactant and was studied for 20 to 25 minutes continuously. The data were collected from about the 5th ring and onwards.

Similar experiments were done with Ag_2CrO_4 also.

RESULTS AND DISCUSSION

The process of formation of rings can be observed under the microscope. In the beginning, the rate of formation is very quick. The rings originate at different radial fronts. These fronts grow and coalesce (7). Since the boundary of the precipitate formation is different at different radial fronts, so the subsequent rings were drawn from the same radial front.

There is no displacement of rings and they originate one after another. Rings formed after 5 to 7 minutes showed small specks at a magnification of 72. The small specks of the same ring are not of uniform size. In the middle of the ring they are smaller and at the periphery they are 2 to 3 times bigger. Times of formation, distances, interspaces, and sizes of particles, all increase with the passage of time.

Since a number of rings is formed in 30 seconds, the induction period for the initiation of ring formation may be regarded as negligibly small. It is observed that ring formation does not start right from the boundary of the crystal. There is a continuous precipitation zone around it. The position of rings was drawn from the place of the first ring. If α be regarded as the zone of continuous precipitation and x_n, the distance of the nth ring from the first ring, then

$$X_n = x_n + \alpha \qquad [1]$$

and

$$X_{n+1} = x_{n+1} + \alpha, \qquad [2]$$

where X_n and X_{n+1} are the distances of nth and $(n + 1)$th rings from the boundary of the crystal. From the data of x and T, α can be calculated in the following way.

According to Morse's equation

$$\frac{X_n}{\sqrt{T_n}} = \frac{x_n + \alpha}{\sqrt{T_n}} = K \qquad [3]$$

and

$$\frac{X_{n+1}}{\sqrt{T_{n+1}}} = \frac{x_{n+1} + \alpha}{\sqrt{T_{n+1}}} = K, \qquad [4]$$

where T_n and T_{n+1} are the times of formation of the nth and $(n + 1)$th rings, respectively. It follows from the above equations that

$$\alpha = \frac{x_{n+1}\sqrt{T_n} - x_n\sqrt{T_{n+1}}}{\sqrt{T_{n+1}} - \sqrt{T_n}}. \qquad [5]$$

Equation [5] was used to estimate the best values of α from the experimental data. The mean values of α under different experimental conditions were 0.02 ± 0.005 cm. These were in approximate agreement with the experimental values found by actual observation. The values of α are more or less unchanged by the variation of the concentration of colloid and the precipitating agent in the gel solution and the quantities of $Pb(NO_3)_2$.

In the initial stages of ring formation, $Pb(NO_3)_2$ behaves as an electrolyte also, causing thereby the immediate coagulation of peptized particles. The presence of a continuous precipitation zone, therefore, is a direct proof of the coagulation theory of Dhar and Chatterji (8).

TABLE I

Values of x and T and the Relationship of X and T in the Case of 1% Agar + 1% KI with Crystal of $Pb(NO_3)_2$ as the Reactant

Serial No.	T Time of ring formation *(sec.)*	x Distance from the first ring *(cm.)*	$X/\sqrt{T}$ When α = 0.0020cm.	Diam. of particles constituting the ring *(cm.)*
1	—	0.0400	—	Below 0.00025
2	77	0.0486	0.0078	Below 0.00025
3	105	0.0590	0.0077	Below 0.00025
4	150	0.0715	0.0075	Below 0.00025
5	210	0.0860	0.0073	Below 0.00025
6	298	0.1035	0.0071	0.00025–0.00075
7	399	0.1243	0.0072	0.0005–0.0010
8	572	0.1500	0.0071	0.00075–0.00150
9	769	0.1806	0.0072	0.00075–0.00175
10	1058	0.2153	0.0073	0.001–0.002

Note: The size of the particles constituting the rings depends upon the type of agar used. Even two samples of agar obtained from the same company may give different results. The diameter of the particles seen in B.D.H. agar are, however, reported, as they give an idea of the extent of variation of their sizes in the same and subsequent rings with the same type of agar.

In Table I are listed the mean values of x and T. They are in geometrical progression. The values of space and time coefficients calculated by X_{n+1}/X_n and T_{n+1}/T_n are 1.21 ± 0.02 and 1.38 ± 0.05, respectively.

The observed effect of different experimental conditions is summarized below:

a). Concentration of the precipitating agent: By raising the concentration of KI from 1% to 3% in the gel solution, a marked decrease in rhythmicity is noted. The thickness of rings, the value of the time coefficient, and the size of particles increase. The clear interspace between the rings becomes narrower and their lines of demarcation are less sharp.

b). When $Pb(NO_3)_2$ is taken as the precipitating agent in the gel solution and KI crystal as the diffusing reactant, a marked difference is noticeable. KI crystal gets dissolved in the gel. Dissolution when completed leads to the formation of rings, which in this case is comparatively rapid. The value of the time coefficient shows a fall from 1.38 to 1.07.

c). The addition of electrolyte such as KNO_3, $NaNO_3$, or NH_4NO_3 to the gel solution showed in general an increase in the value of the time coefficient, i.e., a decrease in the rate of ring formation. The interspace generally decreased. The particles were of bigger size and the rings thicker.

SUMMARY

The time and distance relationship of periodic precipitates can be studied conveniently by following rhythmic precipitation in petri dishes under the microscope with the help of camera lucida. In substantiation detailed studies of PbI_2 and Ag_2CrO_4 were undertaken by the authors, and the following points emerged as a result of this study:

1). There is no displacement in the rings. Radial fronts (7) originate one after another and rings are formed by the coalescence of these zones.

2). There is a continuous precipitation zone around the reactant.

3). Each ring is found to originate not instantaneously but it takes some time for initiation and completion. Particles of the same ring are not of the same size.

4). Rings start appearing after clear interspaces. Times of Formation (T_n) are in geometrical progression. The coefficient of this series has been called the "Time Coefficient."

5). Distances of rings from the first ring (x_n) are also in geometrical progression, and this series gives the value of the Space Coefficient. Its values, as found by us, are between 1.15 to 1.20 for PbI_2 under different experimental conditions and 1.18 in the case of Ag_2CrO_4. These are in close agreement with Packter's values (8)—1.186 and 1.182 for PbI_2 and Ag_2CrO_4, respectively.

6). Total distance penetrated by the diffusing reactant (X_n) and Times of formation (T_n) are related to each other by a relationship $X_n/\sqrt{T_n} = K$. Morse's equation has, thus, been verified experimentally.

References

1 Jablczynski, K., *Bull. soc. chim. France* **33,** 1592 (1923).
2. Mathur, P. B., Thesis, p. 51. Allahabad University, Allahabad, India, 1956.
3. Morse, H. W., and Pierce, C. W., *Z. physik. Chem.* **45,** 589 (1903).
4. Van Hook, A., *J. Phys. Chem.* **45,** 879 (1941).
5. Wagner, C., *J. Colloid Sci.* **5,** 85 (1950).
6. Stern, K. H., *Chem. Revs.* **54,** 79 (1954).
7. Chatterji, A. C., and Bhagwan, H., *J. Colloid Sci.* **13,** 232 (1958).
8. Dhar, N. R., and Chatterji, A. C., *J. Phys. Chem.* **28,** 41 (1924).
9. Packter, A., *J. Chem. Soc.* **1955,** 1180.

JOURNAL OF COLLOID SCIENCE **13**, 242–256 (1958)

THE FORMATION OF SILVER HALIDE SOLS IN THE PRESENCE OF CATIONIC DETERGENTS

E. Matijević[1] and R. H. Ottewill

Department of Colloid Science, University of Cambridge, Cambridge, England

Received November 19, 1957

Abstract

The influence of cationic detergents on the formation of negative sols of silver chloride, silver bromide, and silver iodide has been studied by means of spectrophotometry, microelectrophoresis, and electron microscopy. As cationic detergents, dodecyltrimethylammonium bromide, dodecylpyridinium chloride, bromide, and iodide, and dodecylquinolinium bromide were employed; these were all pure compounds. All the detergents studied gave "sensitized" coagulation of the silver halide sols; critical coagulation concentrations of the order of 10^{-5} M were obtained with sol concentrations of 1×10^{-4} M and 5×10^{-4} M. With silver bromide, using dodecyltrimethylammonium bromide and dodecylpyridinium bromide periodic coagulation and stabilization of the sols was observed. A similar phenomenon was observed with dodecylpyridinium iodide and silver iodide, but with dodecylpyridinium chloride–silver chloride and dodecylquinolinium bromide–silver bromide only one coagulation region was found. The mechanism of sol formation in the presence of detergents is discussed and an interpretation is given of the results obtained.

The coagulation of lyophobic sols by neutral electrolytes is mainly dependent upon the valency of the counter ion, as expressed by the Schulze-Hardy rule. However, existing experimental evidence on coagulation by large organic counter ions does not follow the latter rule; coagulation values with such ions are much more akin to those obtained with four-valent inorganic ions. Generally, large organic ions cause a reversal of charge of the sol particle—a phenomenon which in the case of inorganic ions is a property only of those of high valency (e.g., Th^{++++}). Excluding macromolecules, large organic ions so far investigated include strychnine (1–5), morphine (3), aniline (3), guanidine (3), dodecylpyridinium (3, 6, 7), and dodecylamine (8); all these materials give low coagulation values and reverse the charge on the colloid.

The fact that the coagulation effects of large molecules are due mainly to specific adsorption seems to be well established (7), and the low coagulation values observed have led to a widespread use of the term "sensitization" for such processes. However, in view of the large number of processes for which this term is used, "adsorption coagulation" would seem a better description.

---

[1] On leave of absence from Faculty of Science, University of Zagreb.

Much of the earlier work on this phenomenon has been purely qualitative and unsystematic. In order to make a more quantitative approach we have selected as coagulating ions various cationic detergents of the same chain length and different head group; these are well-defined chemical compounds. As the colloid system the silver halide sols have been chosen, since their colloidal properties, particularly their behavior in coagulation, have been extensively investigated (9–11). In the present paper the behavior of silver halide sols prepared *in statu nascendi* in the presence of cationic detergents will be described, and in another publication the interaction of detergents and "preformed" sols will be discussed (12). The interaction has been investigated mainly by spectrophotometric and electrophoretic measurements, but preliminary results using electron microscopy and microdiffraction have also been obtained.

EXPERIMENTAL

Materials

The silver nitrate and potassium halides used were of Analar grade and were not further purified. Water was doubly distilled from Pyrex apparatus and then finally distilled from quartz. The detergents used were dodecylpyridinium chloride (DPyC), dodecylpyridinium bromide (DPyB), dodecylpyridinium iodide (DPyI), dodecyltrimethylammonium bromide (DTAB), and dodecylquinolinium bromide (DQuB). The preparation of these detergents will be described elsewhere (13); surface tension versus concentration curves of these materials in water did not exhibit any minima before the onset of micelle formation, suggesting that they were of a high standard of purity.

All glassware was thoroughly cleaned and steamed before use.

Preparation of Sols

In principle, the preparation of sols followed the method described by Težak *et al.* (9). Aliquots of a potassium halide stock solution were mixed with differing amounts of detergent stock solutions and then diluted to 5 ml. with distilled water. In this way a constant concentration of potassium halide was maintained and the concentration of detergent varied systematically. Three milliliters of the solution prepared in this way was used for each experiment, and to this was added 0.1 ml. of silver nitrate solution by an adder-mixer device. The concentration of silver nitrate was so chosen that final silver halide sol concentrations of either 1×10^{-4} M or 5×10^{-4} M were obtained. The potassium halide was kept constant and equal to 2×10^{-3} N, thus ensuring that initially a negative sol resulted. In the final solution a slight change of halide ion concentration occurred owing to the addition of halide ions from the detergent. However, this increase, within the coagulation range, amounted to only a p_{halide} change of 0.2

unit with maximum addition of detergent; a p_{halide} change of this magnitude does not in itself influence coagulation values (10, 11).

Turbidity Measurements

The formation of the solid phase from solution was followed by measuring the changes of turbidity with time, in a spectrophotometer. The turbidity, τ, is defined by the relation

$$I = I_0 e^{-\tau l} \qquad [1]$$

where I_0 and I are the intensities of the incident and transmitted radiation, respectively, and l is the optical path length of the cell employed. For small particles ($r < \lambda/20$) in the absence of consumptive light absorption τ is related to the number of particles per milliliter, N_0, and their individual volume V by Rayleigh's equation, viz.,

$$\tau = AN_0V^2. \qquad [2]$$

Here A is an optical constant which for small particles of refractive index, n, is given by:

$$A = \frac{24\pi^3 n_0^4}{\lambda^4}\left(\frac{n^2 - n_0^2}{n^2 + 2n_0^2}\right)^2, \qquad [3]$$

where n_0 is the refractive index of the solvent and λ is the wavelength of light used (*in vacuo*). There is a possibility in the present system that the value of n may be altered by the adsorption of detergent to the sol particles. This fact is recognized but will not alter the essential features of the data presented.

Measurements were carried out using a Unicam SP 600 spectrophotometer adapted for automatic recording of light transmission changes at constant wavelength. The response time of the recording system was of the order of 1 second; a full description of the apparatus and its application to coagulation measurements has appeared elsewhere (14). In order to achieve rapid mixing a device developed from that described by Boyer and Segal (15) was used to add 0.1 ml. aliquots of silver nitrate solution to 3 ml. quantities of the other components in the optical glass cells (1 cm. path length). All measurements were carried out at room temperature (18° ± 1°C.) and at a wavelength of 5460 A. Turbidity values were obtained continuously from the first second.

Electrophoretic Measurements

Micro-electrophoresis measurements were carried out using a glass cell of the type described by Mattson (16). Readings were always taken at the stationary level, after initial experiments had ascertained that the distribution of velocities throughout the tube was parabolic, even in the presence of detergent. Optical effects were corrected for by the use of the equation given by Henry (17). Although mobility determinations were often carried out at different time intervals, after the initial mixing of the reacting components no appreciable variation of mobility with time was detected. The systems in which coagulation occurred were sufficiently stable to enable mobility measurements to be made provided that these were carried out within 1 hour of mixing.

Electron Microscopy

Samples were taken 30–60 seconds after mixing and deposited onto grids covered with an evaporated carbon film. Electron microscopy was carried out using the Siemens-Elmiskop UM 100 microscope, which has been shown by earlier work on colloidal silver iodide (18) to have a resolving power of the order of 10 A.

RESULTS

Method of Expressing Data

When systems *in statu nascendi* are studied the initial state before mixing is an optically clear solution, and hence turbidity measurements can be used without ambiguity to follow the early stages of solid phase formation. The dependence of turbidity on time (t in seconds) is then given by the equation

$$\tau = AN_0V^2(1 + kt), \qquad [4]$$

where k is a rate constant (19, 20). While the particles are small enough to obey Rayleigh's equation [2] a linear relationship between turbidity and time is obtained, but as the particles become larger, deviations from linearity are observed. Figure 1 shows a number of turbidity versus time curves for the formation of silver bromide in the presence of different concentrations of DPyB; these are typical examples of the curves found in all the systems investigated in this paper. It can be observed from Fig. 1 that the rate of reaction differs considerably according to the detergent concentration. For the fastest reactions the curves become asymptotic after about 60 seconds, indicating that the observed coagulation is almost complete within the first minute. Two different types of curve were obtained, the "normal" type, which was always convex towards the time axis, and an S-shaped curve. A detailed kinetic analysis of these curves will be given in a later publication.

In the systems investigated the use of initial rates for comparative purposes (14) was complicated by the S-shaped nature of many of the curves. Therefore, we have plotted the turbidity against the logarithm of the molar detergent concentration for different time intervals; for convenience of representation decreasing values of concentration are plotted towards the

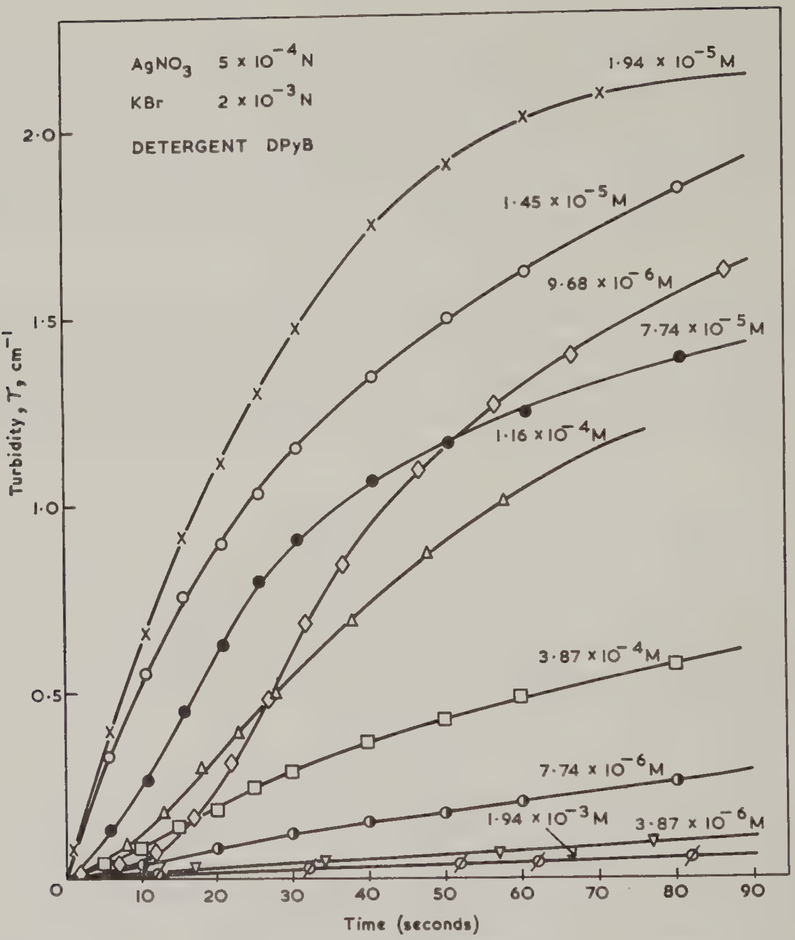

FIG. 1. Curves of turbidity versus time (seconds) for the formation of silver bromide in the presence of various concentrations of dodecylpyridinium bromide. Sol concentration 5 × 10^{-4} *M*.

right. Figure 2 shows such a diagram for the system, silver bromide—DPyB; for which some of the reaction curves have been given in Fig. 1. This method of presentation is very useful in giving a broad representation of regions of high and low sol stability. The main features of the curves are independent of time from 10 to 90 seconds. At all times a very sharp limit is observed between sol stability and the first coagulation region as represented by the boundary between *A* and *B*. Such a sharp division is also found in the case of coagulation by simple electrolytes, and leads to a definition of a critical coagulation concentration. Thus extrapolation of the steepest part of the boundary *A*–*B* to the concentration axis defines the value of this concentration (9). It will be noted that if this extrapolation is

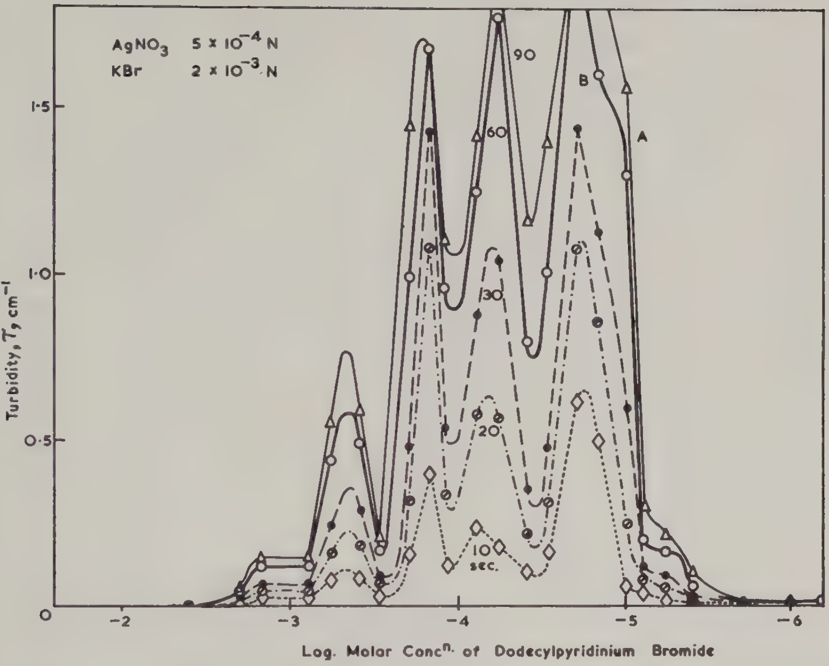

FIG. 2. Turbidity versus log molar concentration of dodecylpyridinium bromide at different time intervals: −◇− 10 sec.; −·⊘·− 20 sec.; −●− 30 sec.; −○− 60 sec.; −△− 90 sec. Sol concentration, silver bromide 5 × 10^{-4} M.

carried out at times between 30 and 90 seconds, exactly the same coagulation concentration is obtained; this value is only slightly higher if shorter times are taken. Therefore, as a method of representing the data the turbidity versus log concentration curves have been taken 1 minute after initiating the reaction.

Influence of Sol Concentration, Character of Sol, and Size of Detergent Ion

In Fig. 3 are plotted turbidities against log molar concentration of detergent for the formation of a silver iodide sol in the presence of DPyI at two different sol concentrations, viz., 1 × 10^{-4} M and 5 × 10^{-4} M. At the higher sol concentration the same number of maxima occur as in the formation of silver bromide in the presence of DPyB, but at the lower concentration the maximum at F has disappeared. Also the critical coagulation value is higher at the low sol concentration; a similar sol concentration effect has been observed in the coagulation of silver halide sols in the nascent state by simple inorganic ions (9).

The influence of the character of the sol has been investigated by forming different silver halides in the presence of the relevant detergent halides, keeping the potential determining ion and sol concentration identical. The

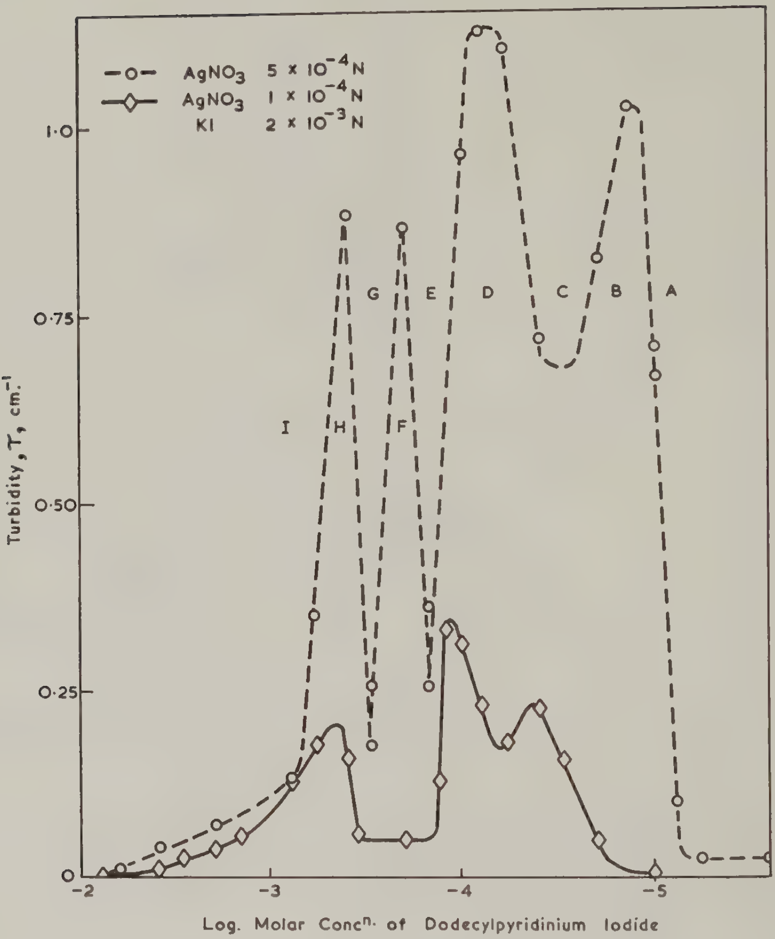

FIG. 3. Influence of sol concentration on the formation of silver iodide in the presence of dodecylpyridinium iodide. Sol concentration, –○– 5 × 10^{-4} M, –◇– 1 × 10^{-4} M. Turbidity values taken 1 min. after mixing.

results of these experiments are given in Fig. 4. Silver bromide and iodide show the same type of periodic maxima, with very close correspondence of the maxima, whereas silver chloride behaves differently, showing only one broad maximum. The critical coagulation values for the bromide and iodide sols at sol concentrations of 5×10^{-4} M are in very close agreement (7.5×10^{-6} M), whereas the value for chloride is markedly higher (2.5×10^{-5} M). In the case of the coagulation of silver halide sols (conc. 2×10^{-4} M) by strychnine nitrate (2) the critical coagulation concentrations are found to be in the order: silver chloride, 4×10^{-5} M, silver bromide, 1.8×10^{-5} M, and silver iodide, 3×10^{-5} M, values which are of the same

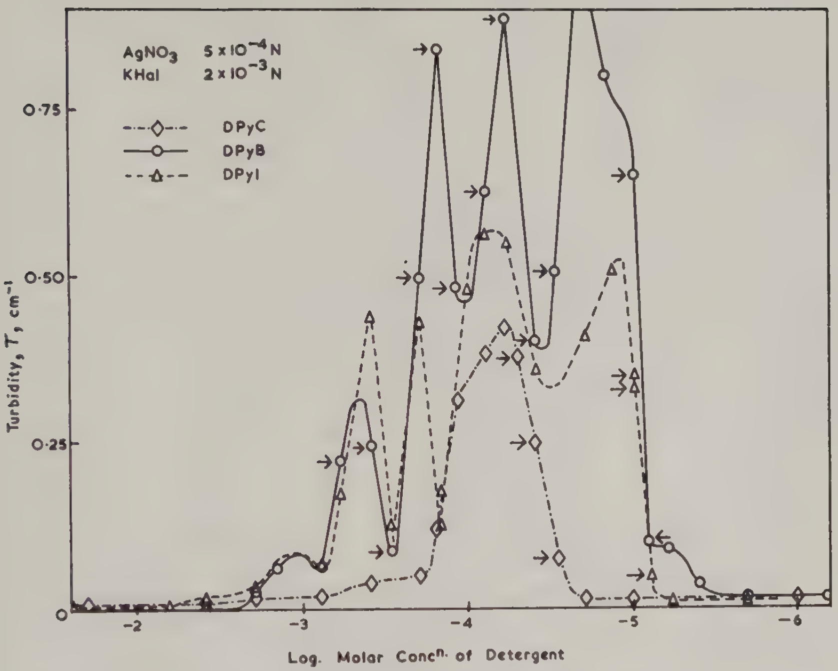

FIG. 4. Formation of silver chloride, silver bromide, and silver iodide in the presence of dodecylpyridinium chloride (-·◇-·), dodecylpyridinium bromide (-○-), and dodecylpyridinium iodide (-△-). Turbidity values taken 1 min. after mixing. → indicate S-shaped turbidity-time curves. Sol concentrations 5×10^{-4} *M*.

order of magnitude. The turbidity values reached at the maxima are very different for the three silver halides (Fig. 4), being in the order silver bromide > silver iodide > silver chloride. Since the sol concentration is identical and the refractive indices for the three halides differ by only a small amount, it would seem that this order must be an indication of the relative size of the aggregates. The arrows on Fig. 4 indicate those points obtained from **S**-shaped turbidity-time reaction curves.

The influence of the cationic head group of the detergent is shown in Fig. 5, in which curves are given for the formation of silver bromide in the presence of DTAB, DPyB, and DQuB. With DTAB a coagulation curve similar to that of DPyB, is obtained, although the maxima and minima are less pronounced. On the other hand, DQuB exhibits only one narrow coagulation region. The critical coagulation concentrations are in the order DTAB (1.4×10^{-5} *M*) > DPyB (7.5×10^{-6} *M*) > DQuB (2.9×10^{-6} *M*); the relative head group areas for vertically orientated molecules on a surface as calculated from models are found to be 26, 36, and 52 A^2., respectively.

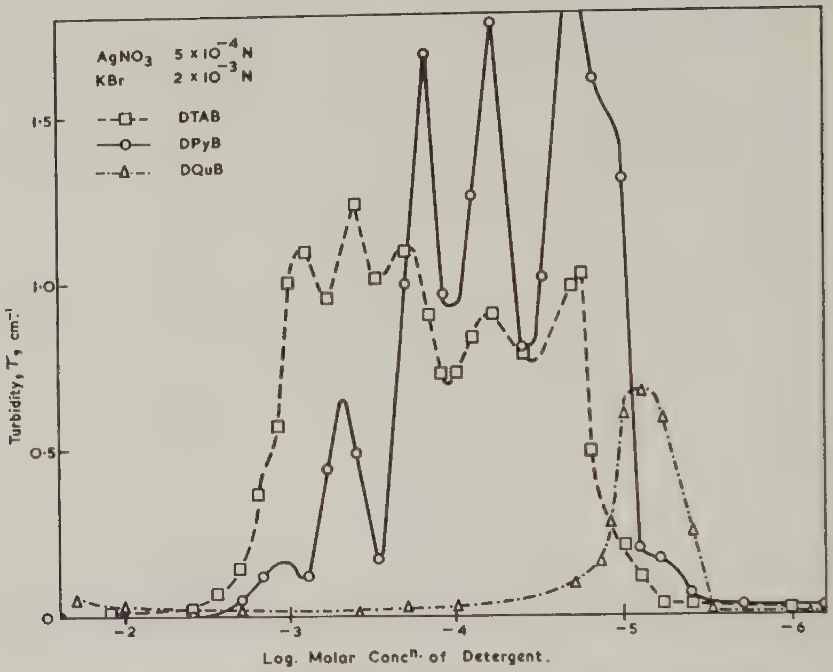

FIG. 5. Formation of silver bromide in the presence of dodecyltrimethylammonium bromide (-□-), dodecylpyridinium bromide (-○-), and dodecylquinolinium bromide (-△-). Turbidity values taken 1 min. after mixing. Sol concentration 5 × 10^{-4} *M*.

Electrophoretic Data

Microelectrophoretic measurements were carried out on the system silver iodide—DPyI at a sol concentration of 5 × 10^{-4} *M*. In Fig. 6 the results obtained are compared with the relevant turbidity curve. The mobility curve shows clearly that although the sol is strongly negatively charged in the absence of detergent, a reversal of charge occurs when the latter reaches a certain concentration. Moreover, the mobility values show a rhythmic rise and fall with increasing concentration of detergent. The regions of lowest mobility correspond with the maxima (*B*, *D*, *F*, *H*) in coagulation, as exhibited by the turbidity diagram. At the turbidity maxima *B*, *D*, and *H* the particles are virtually uncharged, whereas at the maximum *F* the particles are positively charged. It is of interest that it is the latter maximum which disappears when coagulation, in the same system, is carried out at a lower sol concentration (see Fig. 3). Electrophoretic measurements at higher detergent concentrations than those recorded on Fig. 6 were not possible since the particles became submicronic.

Electron Microscope Studies

An examination has been made using the electron microscope of mixtures having the composition given by the maxima and minima of the turbidity

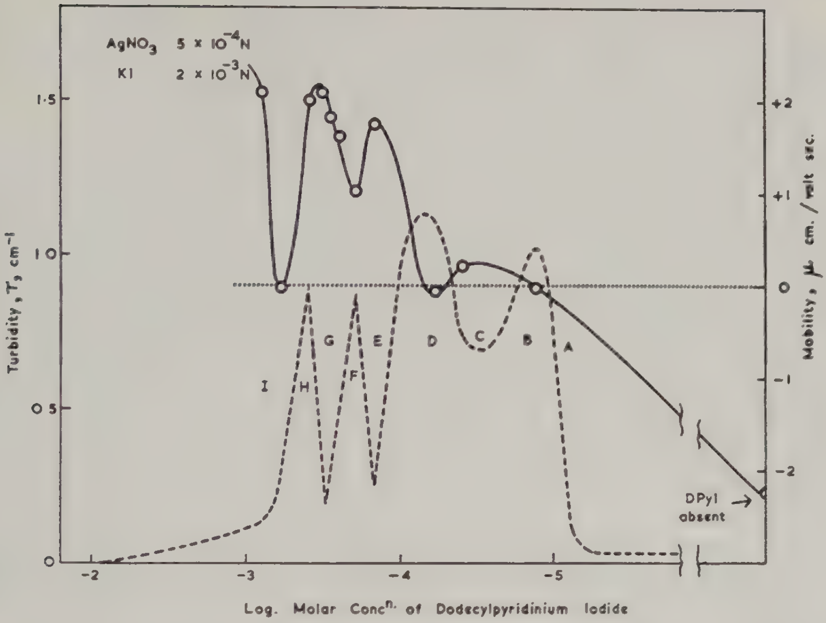

FIG. 6. Curves showing mobility (–O–) and turbidity (– – –) versus log molar concentration of dodecylpyridinium iodide. Turbidity values taken 1 min. after mixing. Sol concentration 5 × 10^{-4} *M*.

curve shown in Fig. 6, namely, those designated *B*, *C*, *D*, *E*, *F*, *G*, *H*, and *I*. It was found that a distinct subdivision into different particle size ranges was apparent. The mixtures *B* to *D* were composed of aggregates of discrete particles in which the average diameters of the particles ranged from 1000 A. in *B* to 600 A. in *D*. The size of the aggregates in *C* were smaller than in *B* and *D*. In mixtures *E* to *G* the particle size distribution covered a range of 60 to 400 A., but whereas *E* and *G* were composed of small diaphanous areas of detergent with a few silver iodide particles contained therein, the micrographs of *F* showed clearly clumps of particles surrounded by detergent. The mixture *H* showed filamentous aggregates, in which the average particle diameter was 125 A., and *I* was composed of well-dispersed particles having an average diameter of 50 A. Microdiffraction patterns were also obtained from each mixture in order to establish whether any change in crystal structure occurred in the various coagulation zones. A detailed account of these observations will appear elsewhere in due course (21).

DISCUSSION

In general, the formation of a solid phase from electrolytic solutions can be considered as a sequence of processes each of different rate constant; this may be schematically written (22, 23):

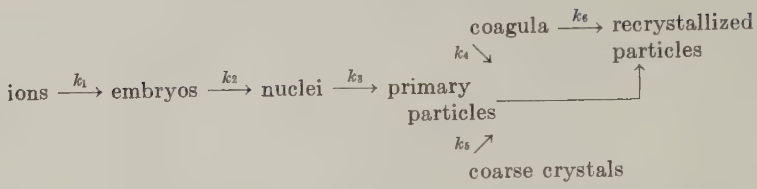

In the study of the coagulation of "preformed" sols the rate process represented by k_4 is the relevant one, whereas in the study of sols *in statu nascendi* a sequence of processes has to be considered. In the study of coagulation by simple ions in the nascent state k_4 is still much smaller than k_2 and k_3; in fact, the process k_4 is that normally measured. This would explain the good agreement obtained for coagulation values using both "preformed" sols and those formed *in statu nascendi* (11, 24). However, when nascent state processes are studied in the presence of other substances such as detergents, the influence of these on the different stages must be taken into account.

The evidence from previous work on the coagulation of inorganic sols by large organic ions suggests that coagulation is primarily due to strong adsorption of these compounds by the sol particles (3, 7, 8, 12). The amount of adsorption depends upon the specific properties of the sol, and the coagulating ion, as well as upon nonspecific properties such as sol concentration and particle size. When forming sols in the nascent state in the presence of detergents the processes of embryo formation and nucleation may well be influenced, especially at higher detergent concentrations, by factors other than adsorption. Hence, studies on the formation of a solid phase can offer possibilities for the detection of specific influences on different stages (25). It would appear unlikely, stereochemically, that detergent ions would be incorporated into the crystal lattice of silver halides. This is supported by preliminary microdiffraction observations (21).

In the systems studied in the present paper some of these influences can be recognized and interpreted. Strong adsorption of detergent ions is indicated by the low coagulation values, as well as by neutralization and reversal of charge (see Fig. 6). All the critical coagulation values obtained are in the region of 10^{-5}–10^{-6} M, values which correspond closely to those obtained for simple four-valent inorganic ions (e.g., Th^{++++}), indicating that in coagulation using detergents the valency of the ion is of minor importance.

Coagulation using detergents of the same chain length but different head groups gives a lowering of critical coagulation concentration with increase in size of the head group, which is the order expected on the basis of strong adsorption of the detergent cation. Now, in order for adsorption of a large detergent ion onto a particle to occur at all, the particle must first reach a certain minimum size. This would suggest that coagulation due to the adsorption of organic ions will begin to occur only after the sol particles formed in the nascent state have reached this minimum or critical size—an assumption which offers an explanation of the **S**-shaped turbidity curves shown in Fig. 1. The slow initial rise of turbidity with time is due to the formation of small particles of silver halide; however, when these have reached a certain size the detergent ions are instantly adsorbed (chemisorption) and coagulation occurs. If the particle growth rate is increased the delay period would be expected to become shorter. For silver halides the rate of particle growth is in the order silver chloride > silver bromide > silver iodide, and in Fig. 7 we have compared the turbidity

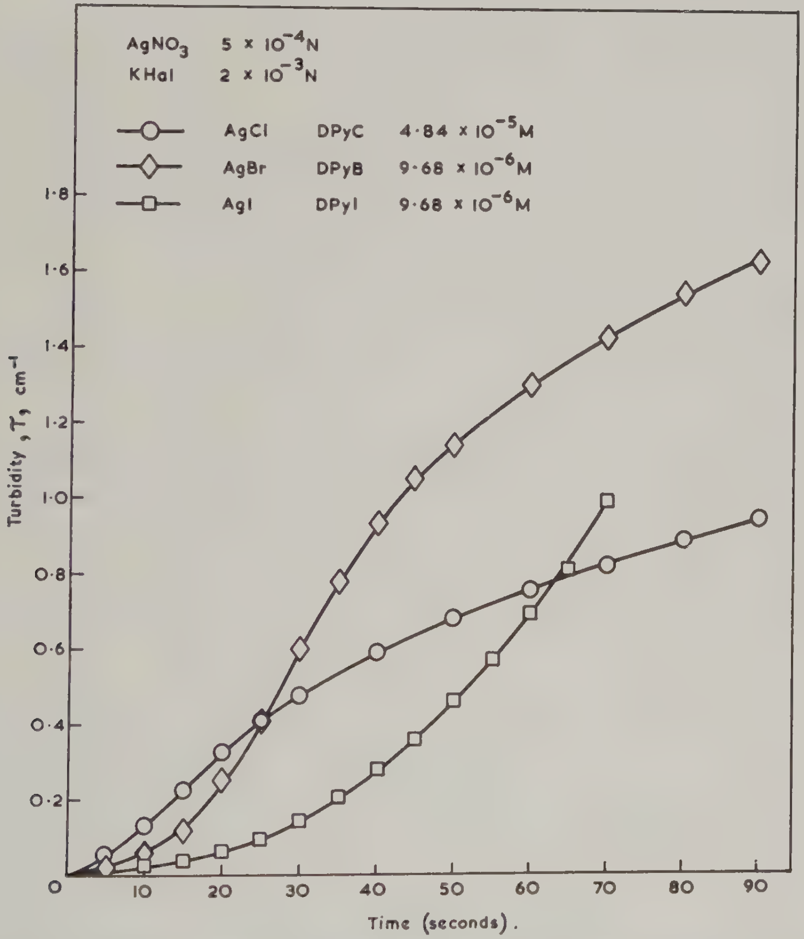

FIG. 7. Turbidity versus time (seconds) curves for silver chloride—dodecylpyridinium chloride (-○-), silver bromide—dodecylpyridinium bromide (-◇-), and silver iodide—dodecylpyridinium iodide (-□-). Sol concentration 5 × 10^{-4} *M*.

versus time curves for the three silver halides coagulated by the same detergent counter ion, choosing for comparison curves at comparable coagulation limits. As expected, the delay period for silver chloride is the shortest and for silver iodide the longest. In Fig. 4 the experimental points which were obtained from S-shaped turbidity-time curves are indicated by small arrows. These invariably occurred at the critical coagulation limit (boundary *A–B*). Only in the case of silver bromide did such curves occur throughout the whole region of coagulation maxima and minima, suggesting that at higher detergent concentrations the formation of primary particles is slower for silver bromide than for the other silver halides.

Comparison of mobility and turbidity curves (Fig. 6) shows that a maximum in turbidity corresponds with virtually uncharged particles, whereas a turbidity minimum corresponds to charged particles. Hence it would appear that turbidity maxima correspond to the point where adsorption of a monolayer of detergent occurs on the initially negatively charged sol particles leading to their neutralization. Further, since the hydrocarbon chain is orientated outwards the particle becomes oleophobic and coagulation takes place. Adsorption of a second layer of detergent molecules due to van der Waals' attraction between the hydrocarbon chains is then possible with the ionized groups of the second layer orientated towards the solution. Therefore, when the particles have a "twofold layer" they attain a high positive charge which causes repulsion between the particles and consequently stabilization of the sol. This is represented by a turbidity minimum.

On this basis, in the simplest case, only one coagulation maximum would be expected and a complete turbidity-concentration curve would consist of a region of negatively charged sol particles at low concentration of detergent, a region of uncharged particles having an adsorbed monolayer of detergent (coagulation, turbidity maximum), and a region of positively charged particles with a "twofold layer" (stabilization, low turbidity) at high detergent concentrations. Such simple systems were obtained in the case of silver chloride— DPyC and silver bromide—DQuB.

The appearance of periodic maxima and minima in most of the curves shown in Figs. 2–5 can be explained if a comparison is made of turbidity, electrophoretic, and electron micrograph data. The observed maxima and minima are a consequence of the competition between two rate processes, particle formation and adsorption. The electron micrographs of the silver iodide-DPyI system give clear evidence that the resultant particle size decreases with increasing detergent concentration. Therefore, the total solid phase area exposed is increasing; hence, greater concentrations of detergent are needed for monolayer or twofold layer formation. According to the ratio of the total particle area and detergent concentration a series of conditions will occur in which either a complete or incomplete monolayer, or "twofold" adsorption layer is possible. The decrease of particle size does not appear to be a continuous function of increase in detergent concentration. Therefore, when the concentration of detergent is high enough to neutralize the charge, coagulation occurs giving maximum turbidity. With a small increase of detergent the particle size remains fairly constant, and reversal of charge occurs leading to stabilization (turbidity minimum). However, with larger increases in detergent concentration the particle size becomes smaller, and the phenomenon is repeated. This occurs several times, leading to a number of turbidity maxima and minima.

When the critical micelle concentration is reached the conditions of the system are completely different and the detergents act as protective colloids, drastically reducing the rate of formation of silver halides. The solutions beyond the critical micelle concentration remained optically clear for long periods of time (see Figs. 2 and 3).

The "normal" behavior of the two systems silver chloride—DPyC and silver bromide—DQuB may be the result of two different factors. In the case of silver chloride—DPyC the rate of growth of particles is so high that the total area is always small; the known variation of charge of the silver halides (26, 27) would not seem to be the decisive influence. DQuB, on the other hand, has such a large head group that a much larger critical particle size is necessary for adsorption, and thus apparent inhibition of silver bromide coagulation occurs at lower concentrations than with the other detergents of smaller head group.

The investigation of this type of system represents an important transition region between coagulation by simple inorganic ions and coagulation by macromolecules, especially, since detergents represent well-defined pure chemical compounds. The structure of macromolecules is often unknown—a factor leading to results which are often difficult to explain.

ACKNOWLEDGMENT

We wish to thank the Governing Body of Trinity Hall for a Consolidated Zinc Corporation grant to one of us (E.M.).

REFERENCES

1. KRUYT, H. R., AND HORSTING, C. W., *Rec. trav. chim.* **57**, 737 (1938).
2. HERAK, J., AND TEŽAK, B., *Arkiv Kem.* **22**, 49 (1950).
3. FREUNDLICH, H., *Z. physik. Chem.* **44**, 135 (1903).
4. KRUYT, H. R., AND TROELSTRA, S. A., *Kolloid-Beih.* **54**, 262 (1943).
5. FREUNDLICH, H., "Colloid and Capillary Chemistry," p. 420. Methuen, London, 1926.
6. LOTTERMOSER, A., AND STEUDEL, R., *Kolloid-Z.* **82**, 319 (1938).
7. LOTTERMOSER, A., AND STEUDEL, R., *Kolloid-Z.* **83**, 37 (1938).
8. TAMAMUSHI, B., *Kolloid-Z.* **150**, 44 (1957).
9. TEŽAK, B., MATIJEVIĆ, E., AND SCHULZ, K. F., *J. Phys. & Colloid Chem.* **55**, 1557, 1567 (1951). MATIJEVIĆ, E. AND TEŽAK, B., *Kolloid-Z.* **125**, 1 (1952).

10. Matijević, E., Schulz, K. F., and Težak, B., *Croatica Chemica Acta* **28,** 81 (1956).
11. Kruyt, H. R., and Klompé, M. A. M., *Kolloid-Beih.* **54,** 484 (1943).
12. Ottewill, R. H., and Rastogi, M. C., to be published.
13. Ottewill, R. H., and Parreira, H. C., to be published.
14. Ottewill, R. H., and Sirs, J. A., *Bull. Photoelectric Spectrometry Group* **10,** 262 (1957).
15. Boyer, P. D., and Segal, H. L., "The Mechanism of Enzyme Action," p. 520. Johns Hopkins Press, Baltimore, 1954.
16. Mattson, S., *J. Phys. Chem.* **32,** 1532 (1928); *ibid.* **37,** 223 (1933).
17. Henry, D. C., *J. Chem. Soc.* **1938,** 997.
18. Ottewill, R. H., and Horne, R. W., *Kolloid-Z.* **149,** 122 (1956).
19. Troelstra, S. A., and Kruyt, H. R., *Kolloid-Beih.* **54,** 225 (1943).
20. Oster, G., *J. Colloid Sci.* **2,** 291 (1947).
21. Horne, R. W., Matijević, E., and Ottewill, R. H., *Kolloid-Z.*, to be published.
22. Volmer, M., "Kinetik der Phasenbildung." Steinkopff, Dresden and Leipzig, 1939.
23. La Mer, V. K., *Ind. Eng. Chem.* **44,** 1270 (1952).
24. Schulz, K. F., and Težak, B., *Arkiv Kem.* **26,** 187 (1954).
25. Težak, B., *Arkiv Kem.* **19,** 19 (1947).
26. Verwey, E. J. W., and Kruyt, H. R., *Z. physik. Chem.* **A167,** 137 (1933).
27. Basiński, A., *Rec. trav. chim.* **59,** 331 (1940).

JOURNAL OF COLLOID SCIENCE **13**, 257–265 (1958)

ON THE VISCOELASTIC PROPERTIES OF CRYSTALLINE POLYMERS

I. POLYTETRAFLUOROETHYLENE

Kazuo Nagamatsu, Tatsuya Yoshitomi, and Tatsuro Takemoto

Department of Applied Science, Faculty of Engineering, Kyushu University, Fukuoka, Japan

Received December 2, 1957

I. Introduction

Great progress has been made in the field of viscoelastic properties of high polymeric materials. Most of the recent investigations, however, are limited to the properties of so-called amorphous polymers. Few studies have been conducted on crystalline polymers (1).

As is well known, the viscoelastic properties of materials can be expressed by the aid of a generalized Maxwell model with an appropriate relaxation time spectrum (2). For the amorphous polymers, it is also known that the method called Ferry's reduction (3) gives a powerful means of constructing such relaxation time spectra for a wide range of time scale from the rheological data of limited time range at different temperatures.

In 1955, Tobolsky and his co-workers measured the stress relaxation of some crystalline polymers, namely, polytrifluorochloroethylene (4) and polyethylene (5) and reported that Ferry's reduction method was inapplicable to these crystalline polymers. The determination of the relaxation time spectra of crystalline polymers, therefore, presents an attractive problem in the rheology of high polymeric substances.

Recently two of the authors (6) have succeeded in finding some possibility of applying Ferry's reduction method to the crystalline polymers, and have determined the relaxation time spectrum of Nylon 6 over a wide range of time scale. They have shown that in order to apply this method to the crystalline polymers, the whole course of the measurement must be carried out under the smallest values of strain and the specimen carefully conditioned before each measurement. After this success, a similar method was applied to the measurement of the viscoelasticity of polytetrafluoroethylene. As will be seen in this paper, this polymer was selected because of its well-known transition phenomena at room temperature, chemical stability, and especially its non-water-absorbing property. These characteristic features allow the experiment to be carried out easily, and a good example of the relation between the rheological behavior and the transition phenomena is obtained.

II. Experimental Methods

The stress relaxation properties of polytetrafluoroethylene were measured with ribbon-like specimens cut from commercial Teflon film, under a very small tensile strain. The apparatus is shown schematically in Fig. 1. Here, *A* is a strain gauge of the unbonded type with sensitivity of 0.035 mv./g. at 6 v. input voltage; *B* is the driving screw to pull up the sliding support of the strain gauge *A*; *C* is a 6 v. (36 AH) battery supplying the potential to the strain gauge; and *D* is a dial gauge for determining the vertical translation of the strain gauge, or the applied net strain on the specimen. A piece of sample ribbon *H* (6.12 mm. wide, 130.0 mm. long, and 0.060 mm. thick) is fixed between two clamps *F* and *G*. The upper clamp *F* is connected to the link pin *E* of the strain gauge by a thin piano string, and the lower clamp *G* is mounted on the fixed bed. The stress originated by straining the specimen is detected by the strain gauge and converted into an electrical potential.

The whole specimen is dipped into the thermostat *J*. The temperature fluctuation of this bath was less than 0.1° C. at an arbitrary temperature, and near the transition temperature the fluctuation was reduced to 0.01°C. The specimen was kept in this bath under no stress about 1 day to ensure thermal equilibrium before each measurement. After this pretreatment, the screw *B* was rotated rapidly and the clamp *F* was pulled up with the strain gauge *A*. The strain thus applied to the specimen *H* was measured by the dial gauge *D*. The stress was recorded automatically by the millivoltmeter *I* ranging from several seconds to several hours.

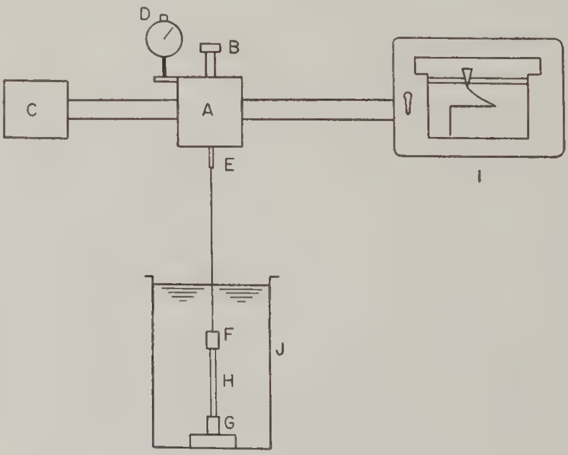

Fig. 1. Schematic diagram of the apparatus.

The measurement was carried out over the temperature range between 15° and 70°C. The strain was always kept below 0.7%, corresponding to 0.27 kg./mm.^{2} in stress, or 0.9 mm. in absolute length. Throughout these series of measurements, the maximum stress was 100 g. and the minimum was 34 g. This meant that the shift of the strain gauge link pin was less than 0.012 mm., which is negligibly small compared to the absolute elongation of the specimen.

The stress relaxation measurements were carried out as follows. At first the relaxation at the highest temperature was measured. After this measurement, the temperature of the bath was adjusted to the second highest temperature, and the specimen was kept in this bath about 1 day for preconditioning at this new temperature. This process was repeated until the lowest temperature was reached. To ascertain the reproducibility and linearity of the measurement, such series were repeated with the same specimen under several different strains. The results were quite satisfactory under these ranges of temperature, strain, and treatments. Such reproducibility and linearity show that there is no change in the structure of the specimen such as a change of crystallinity by heat treatment.

III. Results

The stress relaxation curves measured at different temperatures are shown in Figs. 2 and 3. The curves are divided into two groups for the reason that will be mentioned later. By the application of Ferry's reduction method, two master curves shown in Fig. 4 are obtained with good overlapping. One of them corresponds to the curves shown in Fig. 2 (measure-

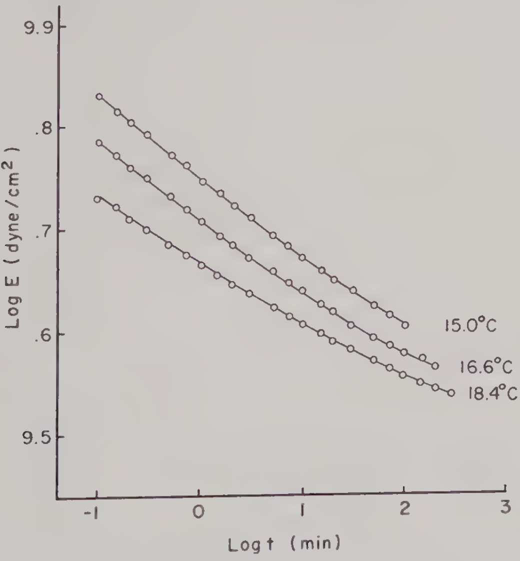

FIG. 2. Stress relaxation curves of polytetrafluoroethylene below 18.4°C.

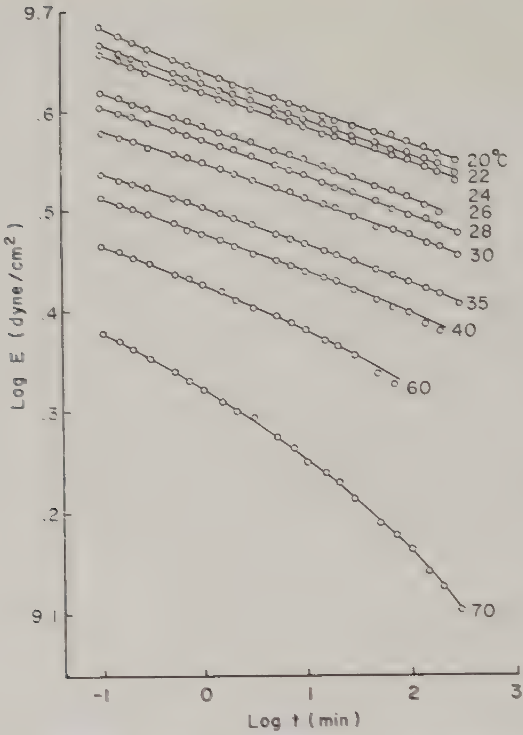

FIG. 3. Stress relaxation curves of polytetrafluoroethylene above 20.0°C.

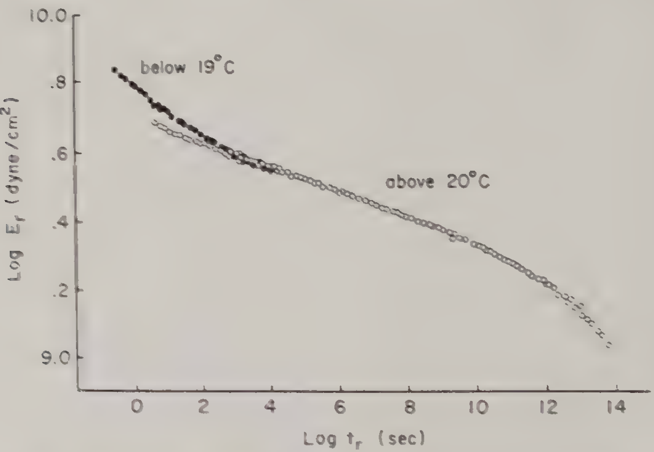

FIG. 4. Stress relaxation master curves of polytetrafluoroethylene reduced to 20°C.

ments below 18.4°C.) and the other to the curves shown in Fig. 3 (measurements over 20.0°C.).

Although these two master curves cross in one region, they can never be made to superimpose by any simple translation along the time axis. Thus it should be considered that there is a quite distinct point of temperature at which this polymer makes a remarkable change in its properties. This point lies between 18.4° and 20.0°C., probably 19°C. Accordingly, it must be concluded that polytetrafluoroethylene has a distinguishable

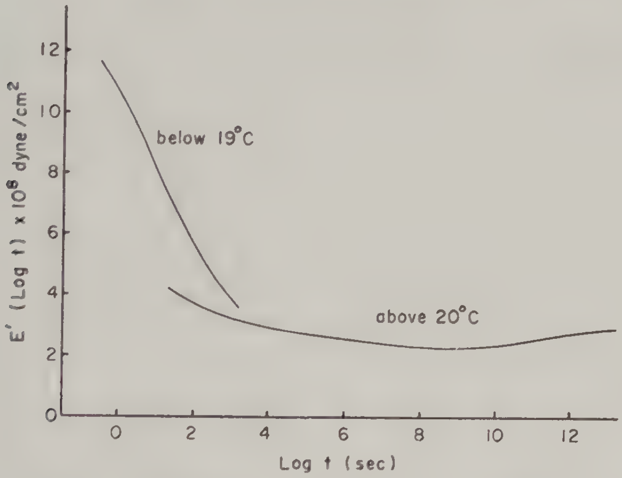

FIG. 5. Relaxation tiem spectra of polytetrafluoroethylene.

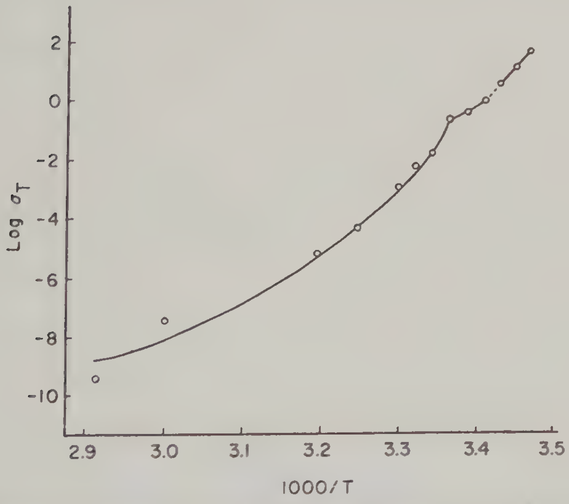

FIG. 6. Relation between Ferry's reduction factor a_T and temperature.

transition point at about 19°C., and the states above and below this temperature are quite different. The relaxation time spectra corresponding to these two states can be easily calculated by the first-order approximation method (7). The spectra thus obtained are shown in Fig. 5. Here the relaxation time spectrum corresponding to the state below 19°C. is made so as to coincide with the state at the standard temperature, i.e., 20°C., by shifting it properly along the time axis by extrapolating Ferry's reduction constant a_T to this standard temperature.

In Fig. 6, the reduction factors a_T are plotted against $1/T$. Differentiating this curve, the relation between the so-called apparent activation energy and the temperature can be obtained. As is clearly seen in the result of this

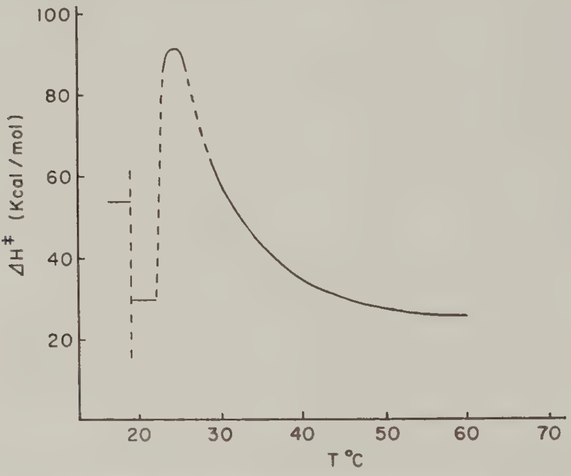

FIG. 7. Relation between the apparent activation energy $\Delta H^{\ddagger}$ vs. temperature.

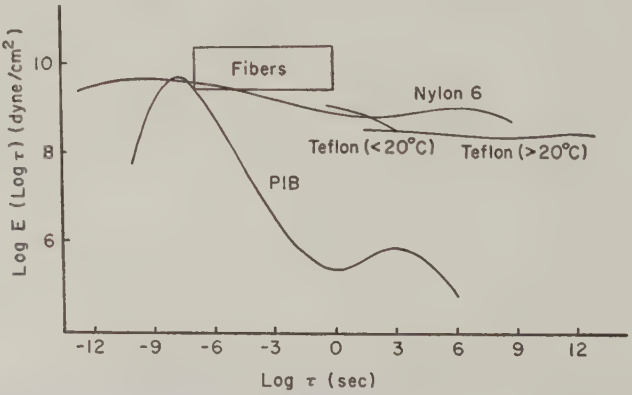

FIG. 8. Relaxation time spectra of polytetrafluoroethylene, with those of several other high polymers.

calculation shown in Fig. 7, it has a sharp maximum at about 25°C. From this figure, it must be concluded that this polymer has another irregular point in its viscoelasticity at 25°C.

For the comparison with other several high polymeric substances, Fig. 8 is drawn with the usual scales of axis. It contains the relaxation time spectrum of polytetrafluoroethylene along with the famous result of polyisobutylene (8) distributed by the National Bureau of Standards, the relaxation time spectrum of Nylon 6 (6) determined by two of the authors, and that of several fibers measured by Fujino and his co-workers (9).

IV. Discussion

As has been mentioned above, the experimental results clearly show that this polymer has two fairly distinct irregular points in its viscoelastic properties, namely, at 19° and 25°C. The irregularity at 25°C. appears in the form of a sharp maximum in the apparent activation energy vs. temperature diagram. This type of irregularity is often seen as the so-called second-order transition temperature of high polymeric materials (10). The existence of such a transition at about 30°C. has already been established for this polymer by several different methods (11). About the exact nature of this transition phenomenon, however, there is no decisive experimental evidence as yet. The authors are convinced through their experiments that the irregularity found at 25°C. can be considered as a sort of so-called second-order transition. The discrepancy of 5°C. between our 25°C. and the 30°C. of others may be attributed to the difference of cooling rate used in our experiments.

On the other hand, the irregularity at 19°C. has a character quite different from that at 25°C. The relaxation time spectrum of this material splits into two definitely different parts above and below this temperature. From the rheological point of view, it is quite unusual for the same material to have two different relaxation time spectra at different temperatures. It suggests that the material is in quite a different state above and below this temperature. Bunn (12) has revealed in his X-ray research that the polymer chains in the crystalline region begin to rotate at about 20°C. This rotational transition has been clearly seen by the sudden change in the X-ray diffraction pattern, and it has been concluded that this is a first-order transition. The abrupt change in relaxation time spectrum in our experiment will be easily understood from this feature of the X-ray diagram. It must be considered that the start of rotation of polymer chains in the crystalline regions affects the viscoelastic properties of this polymer, and changes the relaxation time spectrum. The difference in the natures of irregularities at 19° and 25°C. found in our study is thought to be a good support for the suggestion of Bunn, who considers that the transition at 20°C. is different in character from that at the higher temperature.

It must be also noted that the relaxation time spectra shown in Fig. 8 have very high and flat values all over the measured range of time scale. It suggests that polytetrafluoroethylene still has characteristic features of crystalline polymers (9) above its transition at 25°C.

In addition to these conclusions, it must be also mentioned that these experimental results give strong support to the possibility of application of Ferry's reduction method to the rheological data of crystalline polymers under appropriate experimental conditions.

Referring to the possible range of such application of Ferry's method, the authors wish to note here, in the case of polytetrafluoroethylene, slight disagreements which begin to take place in the overlapping of relaxation curves at different temperatures below 15°C. Such limit of the applicability of the reduction method suggests an interesting study in the rheology of high polymers. A detailed discussion of this problem will be left for another occasion.

V. Summary

As is shown in the previous paper (6), it is possible to apply Ferry's reduction method to the crystalline polymers, if the strain is sufficiently small and the specimen is carefully conditioned. This method is applied to results for the tensile stress relaxation of polytetrafluoroethylene. The analysis shows that this polymer has two transition points: one at 19°C. and the other at 25°C. These two transitions have distinctly different natures. The one at 25°C. is thought to have the nature of a so-called second-order transition whereas the other at 19°C. is quite different in character and is thought to be originated by the rotational change of polymer chains in crystallites. This explanation clarifies the nature of the transition phenomena of polytetrafluoroethylene, which had been left in doubt by other methods of investigation. The relaxation time spectra of this polymer show characteristic features of crystalline polymers.

Acknowledgment

The authors wish to express their thanks to all the members of the rheologists' group in this university, especially to Mr. Tetsuo Takemura, for their valuable suggestions and discussions throughout the course of this work.

References

1. Ferry, J. D., *in* H. A. Stuart, "Die Physik der Hochpolymeren," Vol. 4, p. 425. Springer, Berlin, 1956. Nagamatsu, K., Takemura, T., and Yoshitomi, T., *Chem. High Polymers* (*Japan*) **6**, 527 (1957).
2. Alfrey, T., "Mechanical Behavior of High Polymers." Interscience Publishers, New York, 1947. Eirich, F. R., "Rheology, Theory and Applications." Academic Press, New York, 1956.
3. Ferry, J. D., *J. Am. Chem. Soc.* **72**, 3746 (1950).
4. Tobolsky, A. V., and McLoughlin, J. R., *J. Phys. Chem.* **59**, 989 (1955).

5. Catsiff, E., Tobolsky, A. V., and Offenbach, J., *J. Colloid Sci.* **11,** 48 (1956).
6. Yoshitomi, T., Nagamatsu, K., and Kosiyama, K., *J. Polymer Sci.* **27,** 335 (1958).
7. Andrews, R. D., *Ind. Eng. Chem.* **44,** 707 (1952).
8. Marvin, R. S., *Proc. 2nd Intern. Congr. on Rheology*, p. 156 (1954).
9. Fujino, K., Kawai, H., and Horino, T., *Textile Research J.* **25,** 852 (1956).
10. Catsiff, E., and Tobolsky, A. V., *J. Appl. Phys.* **25,** 1092 (1954). Bueche, F., *J. Appl. Phys.* **26,** 738 (1955).
11. Quinn, F. A., Roberts, P. E., and Work, R. N., *J. Appl. Phys.* **22,** 1085 (1951). Schmieder, K., and Wolf, K., *Kolloid-Z.* **134,** 149 (1953). Smith, J. A. S., *Discussions Faraday Soc.*, No. **19,** p. 207 (1955).
12. Bunn, C. W., and Howells, E. R., *Nature* **174,** 549 (1955).

JOURNAL OF COLLOID SCIENCE **13**, 266–272 (1958)

THE SHAPE OF SOAP MICELLES AND OTHER POLYIONS AS OBTAINED FROM ANISOTROPY OF ELECTRICAL CONDUCTIVITY

K. G. Götz and K. Heckmann

Max-Planck-Institut für Physikalische Chemie, Göttingen, Germany

Received January 27, 1958

INTRODUCTION

The Anisotropy of Electrical Conductivity in Flowing Solutions

The translational mobility of an anisometric particle in solution depends on its orientation relative to the direction of motion. Thus, if the particle is electrically charged, as, for example, a polyion, its contribution to electrical conductivity will depend on its orientation. A field of orienting forces applied to a solution of such particles will therefore induce an overall anisotropy of conductivity in the solution. This effect (hereafter designated anisotropy) was demonstrated a few years ago (1–3) and has recently received theoretical treatment (4).

In the experiments described here the particles were aligned by mechanical shear in a Couette apparatus.

The shape of the polyions can be obtained directly from measurements of the electrical anisotropy in chosen directions. From the dependence of the anisotropy on the gradient of the orienting forces the rotation diffusion constant of the particles may be found, and hence if their shape is known the dimensions can be calculated. Allowance must be made, however, for possible particle interaction. Joly (5) has shown that the behavior of interacting particles of a given size approximates to that of freely moving but proportionately larger particles. Thus, whereas determination of the shape is largely independent of particle interaction, only the "apparent" size (larger than the real size) is obtainable at high concentrations.

If a sufficiently steep gradient of forces (Fig. 1) is applied to a system of rod- or disc-shaped particles, the shapes of which approximate to prolate or oblate ellipsoids of revolution, respectively, they rotate irregularly such that their most probable orientation is that in which the longest axes are parallel to the line of forces (y), and the shortest axes parallel to the force gradient (x). Now the translational mobility of the particles is greatest in the direction of their longest axes. Hence, assuming they are electrically charged, in both cases the total electrical conductivity of the system in-

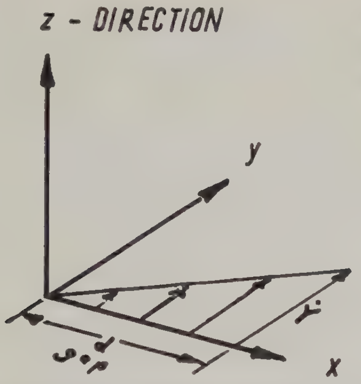

FIG. 1. Vector diagram in gap of Couette apparatus. x: force gradient. y: line of forces. z: perpendicular to x and y. d: gap width.

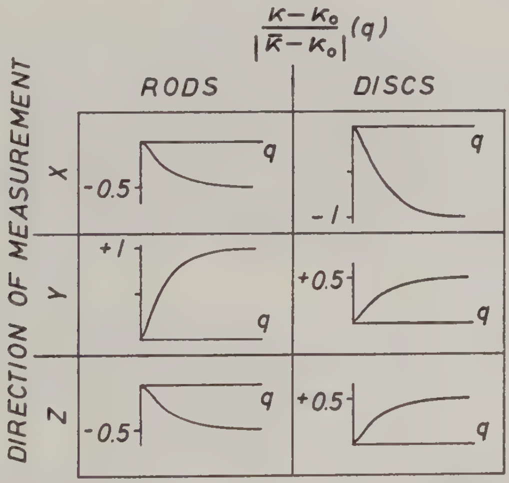

FIG. 2. Relative anisotropy of conductivity in x-, y-, and z-directions (Fig. 1) as a function of the velocity gradient q, showing the essential features of the curves predicted by Schwarz (4).

creases in the y-direction and decreases in the x-direction. In the z-direction, however, an increase in conductivity appears for discs and a decrease for rods, since oriented discs have a long axis in this direction and rods, a short axis (Fig. 2). In the case of full orientation the conductivity change in the direction parallel to the axis of symmetry is always twice that in a perpendicular direction, and of opposite sign. This is clear since mobilities in all directions perpendicular to the axis of symmetry must be equal, and the sum of the changes in conductivity in three mutually perpendicular directions must be zero.

The change of conductivity in a given direction is $k - k_0$, where k_0 is the average conductivity, measured for random distribution of particles. Figure 2 shows qualitatively the changes of conductivity, $k - k_0$, with velocity gradient q. Here $k - k_0$ is expressed as a fraction of the absolute value of the maximum conductivity change, $\bar{k} - k_0$, where $\bar{k}$ is measured in the direction of the fully oriented axes of symmetry. The scale of q depends on the rotation diffusion constant and so on the size of the particles. It is seen that the shape of stable particles can be recognized from the arithmetical sign of a single measurement in the z-direction. In the case of unstable particles, $k_0(q)$ in general does not remain constant. The expression $k_0(q \rightarrow \infty) - k_0(0)$ is a measure of the shear damage. The value of $k_0(q)$ can be calculated from the ratio of any two of the x-, y-, and z-direction anisotropies which have opposite signs. Once $k_0(q)$ is known, the shape and apparent size even of unstable particles can be deduced from the anisotropy curves.

Experimental Technique

The measurements were carried out in a Couette apparatus (Fig. 3) which has been described in detail by Heckmann (6). The gap between two concentric cylinders is filled with the solution under investigation; the inner cylinder (stator) is fixed and the outer cylinder (rotor) can be rotated by a continuously variable drive. The frequency of rotation ν is measured stroboscopically. The velocity gradient in the gap between rotor and stator is calculated from ν, the width of the gap d (0.05 cm.),

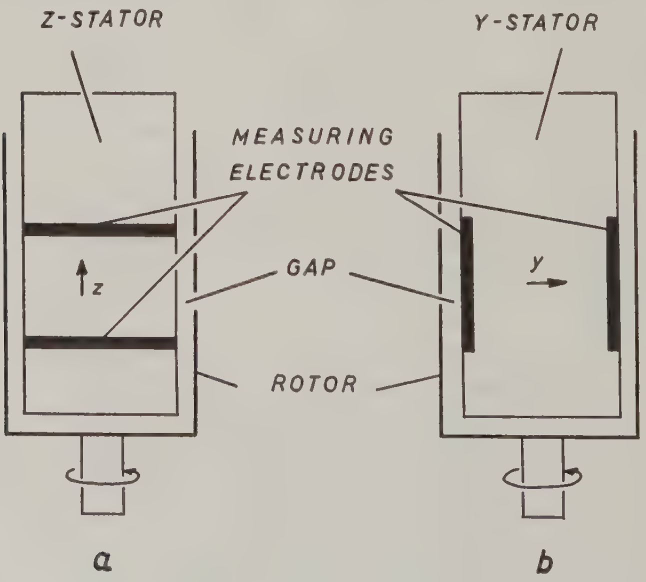

Fig. 3. Couette apparatus (outline).

and the inner radius r of the rotor:

$$q = \frac{2\pi r v}{d}.$$

The temperature of both cylinders is controlled by a thermostat. In the surface of the stator are the measuring electrodes and electrical thermometers. The temperature measurement in the gap is necessary for the calculation of the anisotropy isotherms, since with increasing velocity gradient the solution is unavoidably warmed by internal friction.

The conductivity in the z- and y-directions is measured by means of an impedance bridge at 1000 c.p.s. The experimental errors are of the order of 0.1% for the conductivity and ±0.02°C. for the temperature. In order to complete the present investigations, a y-stator was constructed, similar to the z-stator previously described (6) (Fig. 3).

RESULTS

Experimental Test of the Theory

To verify the theoretical results shown in Fig. 2, the anisotropies of rod-shaped and disc-shaped particles (polyphosphate and graphitic acid, respectively) were investigated in the z- and y-directions.

1. Polyphosphate (Rods). For the production of polyphosphate a method of Malmgren and Lamm's (7) was used, whereby KH_2PO_4 is dehydrated and then annealed at 660°C. for 10 hours. The diluted polyphosphate solution then contains unbranched stretched chains of PO_3^- groups up to 20,000 A long. Using such a solution, Schindewolf (8) has already made qualitative measurements of the anisotropy in a capillary tube (Strömungsrohr).

Figure 4*a* shows graphically the quantitative measurements in the Couette apparatus of the anisotropy in the z- and y-directions, using a 2.5×10^{-3} N polyphosphate solution at 24°C. By fitting the calculated curves (solid line) to the experimental points, a chain length of 6600 A was found from measurements in both directions. The saturation values of the experimental curves were -20% and $+38\%$, respectively. This is in fairly good agreement with the ratio of -1 to $+2$ predicted by the theory for rods.

2. Graphitic Acid (Discs). For the production of a graphitic acid sol, powdered graphite was treated with a strong oxidizing agent according to Ruess's method (9). The graphitic acid should appear in the form of two-dimensional macromolecules in solution, and Thiele (10) has in fact observed a positive double refraction of flow in graphitic acid sols, indicating anisometric particles.

The results of quantitative measurements on the electrical anisotropy of a weakly alkaline graphitic acid solution at 24°C. are shown graphically in Fig. 4*b*. In both directions (z and y) the positive anisotropy curve required for discs is obtained. As the discs are not quite circular and have their

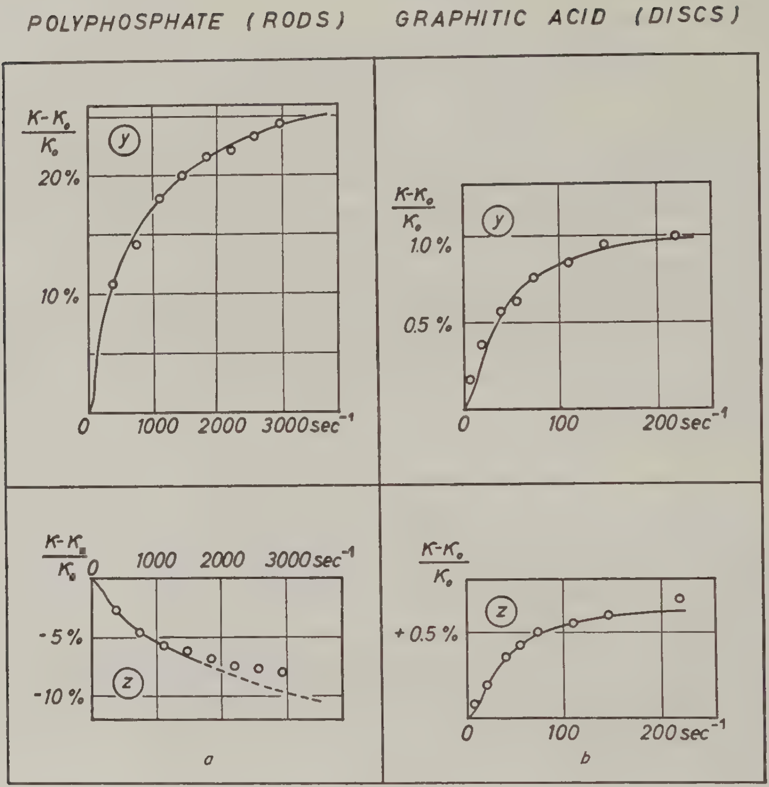

FIG. 4. Anisotropy of conductivity in z- and y-directions as a function of the velocity gradient q. Experimental (circles): (a) Polyphosphate (2.5×10^{-3} N; 24°C.). (b) Graphitic acid (11.7% by wt.; 24°C.). Theoretical (solid lines): (a) rods of approx. length 6600 A. (b) discs of approx. diam. 10,000 A.

longest axes aligned in the direction of flow, the effect in this direction (y) is somewhat larger than that in the z-direction. Fitting the calculated curves (solid line) to the experimental points, an apparent average diameter of about 10^4 A was found from measurements in each direction. (The average grain size of the graphite powder used in the production of graphitic acid was about 3×10^4 A.)

Determination of the Shape of Soap Micelles

The structure of soap micelles, especially in concentrated solutions, is still controversial. Hartley assumes the existence of small spherical micelles over the whole concentration range; on the other hand Hess, Stauff, Harkins and McBain each interpreted their X-ray interference measurements on Na-oleate or other soaps as indicating the presence of a laminated micellar structure at high concentrations (11, 12). Later, however, Corrin

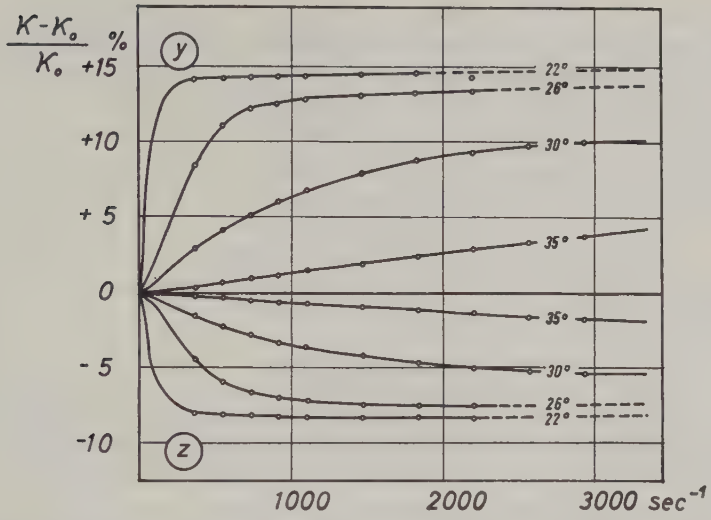

FIG. 5. Anisotropy of conductivity in z- and y-directions of cetyl trimethylammonium bromide (CTAB) as a function of the velocity gradient q. Comparison with Fig. 2 shows that the CTAB micelles are rods.

(13) suggested that X-ray interference methods may be unsuitable for determining micelle shapes, as X-ray diffraction patterns could be produced even by small spherical Hartley micelles if their forces of interaction are sufficient to induce ordered arrays. Using the light-scattering method, Debye and Anacker (14) have found rod-shaped micelles in very dilute cetyl trimethylammonium bromide (CTAB) solutions to which large amounts of electrolyte had been added.

In the present paper investigations are described using CTAB which had been purified by several recrystallizations. The negative anisotropy effect of CTAB, measured in the z-direction, has already been reported (6). Figure 5 shows the anisotropy curves of a CTAB solution (19 % by weight), measured in the z- and y-directions. Comparison with Fig. 2 shows that the curves are characteristic of the anisotropy behavior of rods. The saturation anisotropies are in the approximate ratio of -1 to $+2$, indicating that $k_0(q)$ is practically constant; the applied shear was evidently not sufficient to damage the CTAB micelles. The same results were obtained at concentrations between 12 % and 22 % by weight. Measurements on Na-oleate at concentrations varying from 10 % to 28 % by weight also indicated the presence of rod-shaped micelles, in contrast to some of the reports mentioned above (11, 12). However Corrin's view (13) could easily be interpreted so as to explain this discrepancy.

The "apparent" length of CTAB micelles increases with decreasing temperature and increasing concentration. In the temperature range 22° to 35°C. "apparent" lengths between 3600 A (35°C.) and 47000 A (22°C.)

were found from the anisotropy curves (Fig. 5). It is interesting that even at high concentrations these micelles appear to be stretched, in contrast to the straight-chain polyions (8). If it is assumed that the diameter of a rod micelle is about twice the length of a soap ion (about 50 A) (14), so that its cross section is about 400 times that of a polyphosphate chain, the difference in their behavior is understandable.

Two reports of further investigations are being prepared (15, 16).

Acknowledgment

We are gratefully indebted to our late Professor K. F. Bonhoeffer for his interest and encouragement in these experiments.

Summary

The translational mobility of anisometric dissolved polyions depends on their orientation relative to the direction of motion. If such particles are oriented by means of the flow gradient in the gap of a Couette apparatus, for example, the electrical conductivity of the solution becomes anisotropic. Measurements in a suitable direction (perpendicular to the plane of flow) enable rod-shaped and disc-shaped particles to be distinguished from one another, merely by the arithmetical sign of the change in conductivity. The "apparent size" of particles can be calculated from the shape of the anisotropic curves plotted against the orienting forces. This is in general larger than the real size, but approaches it as the particle interaction vanishes. Determinations of shape and size are possible even when the particles undergo flow damage. The theory of conductivity anisotropy is tested on a disc-shaped model (graphitic acid) and a rod-shaped model (polyphosphate), and confirmed. Measurements on concentrated cetyl trimethylammonium bromide and sodium oleate sols indicate the presence of rod-shaped micelles.

References

1. Heckmann, K., *Naturwissenschaften* **40,** 478 (1953).
2. Jacobson, B., *Rev. Sci. Instr.* **24,** 949 (1953).
3. Schindewolf, U., *Naturwissenschaften* **40,** 435 (1953).
4. Schwarz, G., *Z. Physik* **145,** 563 (1956).
5. Joly, M., *Kolloid-Z.* **126,** 77 (1952).
6. Heckmann, K. *Z. physik. Chem.* [N.F.] **9,** 318 (1956).
7. Malmgren, H., and Lamm, O., *Z. anorg. Chem.* **252,** 256 (1944).
8. Schindewolf, U., *Z. Elektrochem.* **58,** 697 (1954).
9. Ruess, G., *Kolloid-Z.* **110,** 17 (1945).
10. Thiele, H., *Kolloid-Z.* **111,** 15 (1948).
11. McBain, J. W., "Colloid Science." Heath, Boston, 1950.
12. Kruyt, H. R., "Colloid Science." Elsevier, New York, 1949.
13. Corrin, M. L., *J. Chem. Phys.* **16,** 844 (1948).
14. Debye, P., and Anacker, E. W., *J. Phys. & Colloid Chem.* **55,** 644 (1951).
15. Götz, K. G., and Heckmann, K. *Z. physik. Chem.* [NF], in preparation.
16. Heckmann, K., and Götz, K. G. *Z. Elektrochem.* **62** (1958), in press.

JOURNAL OF COLLOID SCIENCE **13**, 273–274 (1958)

WILHELMY'S PLATE AND YOUNG'S EQUATION

A. J. G. Allan*

Polychemicals Department, E. I. du Pont de Nemours and Company,
Inc., Du Pont Experimental Station, Wilmington, Deleware

Received November 11, 1957

In his recent criticisms of the Young equation (1), Bikerman (2, 3) cites the Wilhelmy plate method for surface tension (4) as evidence for his argument. He refers to a diagram similar to Fig. 1 with γ_{13} representing the surface tension of the solid, γ_{23} the interfacial tension along the solid-liquid boundary, and γ_{12} the surface tension of the liquid making an angle θ with the solid. He states "As Wilhelmy's method gives correct results, . . . it may be concluded that the vertical component of γ_{12} is not compensated by $\gamma_{13} - \gamma_{23}$ but exerts a pull on the solid. Thus, Young's equation is not in accord with observations."

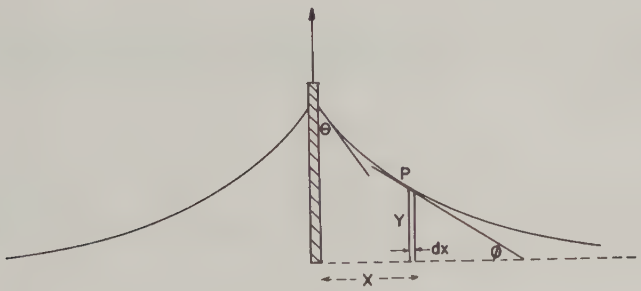

FIG. 1

First, it should be emphasized that the Wilhelmy plate method gives correct results only when the contact angle is zero or when there is "no contact angle" (5).

Secondly, it can be shown that the net pull on the vertical plate is not caused by the liquid surface tension vector per se but by the weight of the liquid lifted in the meniscus by the spreading of the liquid up the plate. The shape of a liquid surface in contact with a plane solid surface has been frequently discussed (6, 7), and in the case of the ring method the weight of liquid lifted by the ring has been calculated (8) and an accurate relation for the surface tension also derived practically (9). The following calculation for the weight lifted by the Wilhelmy plate is simple but does not seem to have been stated explicitly.

---

* Present address: E. I. du Pont de Nemours Co., Inc., Bush House, Aldwych, London W.C. 2, England.

If we assume that end effects can be neglected, the hydrostatic pressure at a point $P(x, y)$ on the meniscus (Fig. 1) is given by

$$g\rho y = \frac{\gamma}{R}, \qquad [1]$$

where g = gravitational constant,
ρ = density difference across the fluid interface,
y = height of the liquid surface above the plane surface of the liquid at the point P, and
R = radius of curvature at the point P.

Now

$$\frac{1}{R} = \frac{d\phi}{dy} \sin \phi \qquad [2]$$

where ϕ is the angle to the horizontal made by the tangent to the meniscus at the point P. Hence the volume of liquid v per unit perimeter of plate length $2l$ is given by

$$v = \int_0^\infty y\, dx = \int_{\phi=90-\theta}^{\phi=0} \frac{\gamma}{\rho g} \frac{\sin \phi}{\tan \phi} \cdot d\phi, \qquad [3]$$

where θ is the contact angle of the liquid with the plate. Integrating [3] we have

$$v\rho g = \gamma \cos \theta \qquad [4]$$

and the total weight lifted by the plate, $v\rho g.\ 2l$, is thus $2\gamma l \cos \theta$ and is responsible for the net pull.

References

1. Young, T., *Phil. Trans. Roy Soc.*, p. 65 (1805).
2. Bikerman, J. J., paper presented at meeting of the American Chemical Society, Atlantic City, September, 1956.
3. Bikerman, J. J., "Proc. Second International Congress on Surface Activity." Butterworths, London, 1957.
4. Wilhelmy, J., *Ann. Physik* **119**, 177 (1863).
5. Gans, D. M., *J. Phys. Chem.* **49**, 165 (1945).
6. Poynting, J. H., Thomson, J. J., and Todd, G. W., "Properties of Matter," 14th ed., p. 180. Griffin & Co., 1947, London.
7. Thomas, W. H., *Nature* **179**, 776 (1957).
8. Freud, B. B., and Freud, H. Z., *J. Am. Chem. Soc.*, **52**, 1772 (1930).
9. Harkins, W. D., and Jordan, H. F., *J. Am. Chem. Soc.* **52**, 1751 (1930).

JOURNAL OF COLLOID SCIENCE **13**, 275–285 (1958)

SURFACE VISCOSITIES OF MIXED UNIMOLECULAR FILMS[1]

G. E. Boyd[2] and F. Vaslow[2]

Department of Chemistry, University of Chicago, Chicago, Illinois

Received January 10, 1958

Abstract

Variations of the surface viscosities with surface pressure of binary mixed monolayers of stearic acid with octadecanol and with arachidic acid were measured. A torsional surface viscometer was employed together with a horizontal-type film balance and a surface trough which was maintained at 25.00°C. The observed fluidities indicated that homogeneous surface solutions were formed throughout the entire composition ranges of both mixtures. The long-chain fatty acid mixtures appeared to give nearly perfect monolayer solutions, whereas complex intermolecular interactions occurred in the acid + alcohol solutions.

Introduction

Two-dimensional solutions, as typified by mixed, insoluble monolayers spread on water, appear to have been little investigated. From the viewpoint of a general theory of surface solutions and for practical applications of surface chemistry, however, the nature and degree of molecular interaction in such mixtures is of interest. By analogy with mixtures of ordinary liquids, the properties of condensed liquid monolayer mixtures have seemed especially relevant. Therefore, additional work using mixtures of stearic (C_{18}) and arachidic (C_{20}) acids, and of stearic acid with octadecanol spread on dilute acid solutions, was considered desirable.

Measurements of the areas per molecule, σ, and of the surface potentials, ΔV, of *equimolar* mixed films of the above compounds have shown (1, 2) that these properties can be described within experimental error by simple equations of the type:

$$\sigma = x_1\sigma_1 + x_2\sigma_2 , \qquad [1]$$

$$\Delta V = 4\pi n_1\mu_1 + 4\pi n_2\mu_2 , \qquad [2]$$

where x_1 and x_2 are the mole fractions, n_1 and n_2 are the numbers of molecules per square centimeter and μ_1 and μ_2 are the apparent surface dipole moments of the pure components, respectively. An heterogeneous film consisting of regions of pure species 1 and pure species 2, however, would also conform to Eqs. [1] and [2], so that the occurrence of homogeneous mixed films with liquid condensed monolayers of *n*-long chain acids and alcohols has not been proved.

---

[1] Presented before the Division of Colloid Chemistry, 131st National Meeting, American Chemical Society, Miami, Florida, April 7–12, 1957.

[2] Present address: Oak Ridge National Laboratory, Oak Ridge, Tennessee.

In a film where the components are molecularly dispersed it is probable that the resultant molecular area, surface potential, or surface viscosity (η^s) will not be proportionately related to the areas, potentials, and viscosities of the components because of intermolecular interaction. However, if the components are immiscible in their monolayers the fluidity ($\phi^s = 1/\eta^s$) of the heterogeneous film will be given by:

$$\phi^s = x_1\phi_1{}^s + x_2\phi_2{}^s\ , \tag{3}$$

where $\phi_1{}^s$ and $\phi_2{}^s$ are the surface fluidities of the respective pure components. An additional test for the absence or presence of a surface solution is therefore afforded by Eq. [3]. Moreover, in contrast to molecular areas and surface potentials, surface viscosity measurements will give a much more sensitive indication of interaction in binary liquid condensed monolayer systems. Thus, at 25°C., the viscosities of pure arachidic acid and of pure octadecanol films are approximately ten times larger than that of a stearic acid monolayer. Accordingly, in this further search for intermolecular interaction in mixtures of these compounds, film viscosities were determined at constant temperature as a function of composition and surface pressure, π.

EXPERIMENTAL

The stearic and arachidic acids and the octadecanol used were taken from the collection donated to this Laboratory by Professor E. E. Reid (3). They were purified additionally by sublimation in a high vacuum at temperatures slightly above their respective melting points, and then accurately weighed out and dissolved in purified ligroin to give solutions of concentrations between 0.5 and 1.0 mg./ml. Aliquots taken from these solutions were mixed and the desired mixed monolayers were spread on the surface of an aqueous 0.001 *N* hydrochloric acid solution. The water used in the preparation of the acid was doubly distilled from alkaline permanganate and condensed in block tin. The acid was of reagent grade.

Surface pressure and viscosity measurements were conducted using a stainless steel surface trough (4) which could be maintained at 25.00 ± 0.02°C. Surface pressures were estimated to 0.05 dyne cm.$^{-1}$ with an horizontal, or Langmuir-Adam type, surface balance. Surface viscosities were determined using a torsional surface viscometer previously employed in this Laboratory (5–7). A measure of the viscosity is given with this method by the logarithmic decrement of the torsional oscillations of a suspended brass cylinder (or sharp ring) the lower, paraffined surface of which just rests on the film. Viscosities were computed from the equation:

$$\eta^s = \Delta\lambda_{10}(2.3\ I/2\pi T)\ (1/a^2 - 1/b^2), \qquad [4]$$

where $\Delta\lambda_{10}$ is the change in the logarithmic decrement caused by the film, I, the moment of inertia of the cylinder (136.1 g. cm.^{2}), T, the period of oscillation (10.85 seconds), a, the radius of the cylinder (1.273 cm.), and b, the distance between the cylinder and the edge of the trough (12.88 cm.). As required by the theory of this method, T did not vary in going from the clean water to the film-covered surface. The observed logarithmic decrements for the monolayers, λ_f, were independent of the amplitudes of the torsional oscillations, indicating that the surface viscosity was always Newtonian (i.e., viscosity coefficient independent of shear rate).

Several important sources of error must be guarded against when using the oscillating disk method: (*a*) the film must adhere to the moving disk, as any slippage would cause a low apparent surface viscosity; (*b*) the lower face of the disk must be accurately circular and its oscillations must be strictly centered within the plane of the face; otherwise, the film-covered surface will be swept clean periodically and an impeding torque caused by surface tension will be present ("Maragoni effect"). There was no indication of (*a*) at any time during the measurements reported below. Care was exercised to insure that complication (*b*) was absent.

The oscillating disk method is relatively insensitive and is limited to measurements with monolayers possessing viscosities of approximately 1×10^{-3} surface poise and greater. The precision of measurements at this lower value is poor because of the fact that $\Delta\lambda_{10}$, which is defined by

$$\Delta\lambda_{10} = \lambda_{\text{film}} - \lambda_{\text{water}}, \qquad [5]$$

is then determined as the difference between nearly equal quantities. A typical logarithmic decrement observed with pure water was $\lambda_{\text{water}} = 0.00560 \pm 0.00002$. This decrement is relatively large because appreciable momentum is imparted to the bulk underlying water by the end of the disk (8). Thus, when a sharp-edged, 1-inch diameter ring, placed so that its edge just touched the surface, was used, a decrement of 0.00242 ± 0.00003 was found.

Despite its simplicity and convenience the torsional surface viscometer is not capable of giving absolute viscosity values. The values given, in fact, appear to be too large by approximately a factor of ten when compared with the film viscosities obtained with surface canal viscometers. The difficulty with the torsional viscometer as an absolute method appears to reside in the manner of estimating $\Delta\lambda_{10}$. According to Eq. [5] it is assumed that the damping effects caused by the viscosity of the bulk aqueous phase and by the film are additive. However, this can be true only if the monolayer

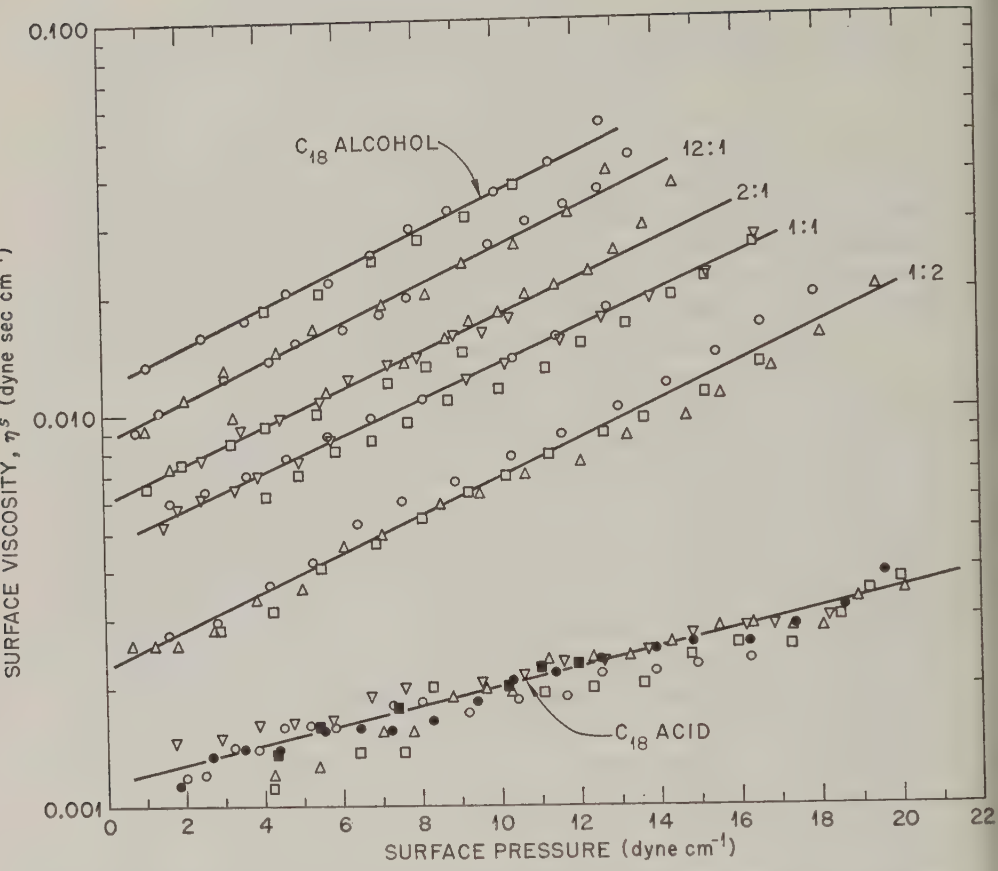

FIG. 1. Variations of the surface viscosities at 25°C. of mixed stearic acid + octadecanol films on 0.001 *N* HCl solutions with ratio of alcohol to acid and with surface pressure (note logarithmic scale on ordinate).

would slide freely on the substrate without adhering to it (9). Such a phenomenon has not been observed. To the contrary, there appears to be good experimental evidence (10–12) that no slippage occurs between the film and its aqueous substrate. The oscillating disk viscometer has been used in these studies in the absence of an adequate hydrodynamic theory because changes in the viscosity only are needed to detect molecular interactions. This method was considered to be adequate for this purpose, as it will yield self-consistent and precise relative surface viscosity values.

The experimental procedure was as follows: The paraffined surface trough (with attached surface balance) was filled with 1 liter of 0.001 *N* hydrochloric acid solution and allowed to stand for a time, usually 1 hour, sufficient for temperature equilibrium at 25°C. as indicated by thermocouple readings. The surface was then cleaned on both sides of the surface balance by repeated sweepings with paraffined "barriers." Next, the paraffined brass disk suspended by a fine phosphor bronze torsion wire was lowered precisely by means of a vertical micrometer screw until its lower face just touched the surface. The logarithmic decrement for the clean aqueous surface was determined as the average of five or more consecutive measurements in each of which ten complete torsional oscillations were taken. The desired film was spread at essentially zero surface pressure, and after 15 minutes for complete spreading it was compressed to about 0.5 dyne $cm.^{-1}$. A measurement of the decrement at this pressure was followed by further compression to a higher value and a further damping measurement. Approximately 3 minutes elapsed between consecutive surface viscosity determinations. The total time for an experiment varied from 40 to 100 minutes. At least two, and sometimes as many as five, separate films were measured for a given composition. Some of these measurements are shown in Fig. 1, wherein differing symbols are used for separate experiments.

EXPERIMENTAL RESULTS AND DISCUSSION

A portion of the measurements taken on the stearic acid + octadecanol mixtures are exhibited in Fig. 1. Similar variations of the surface viscosity with film pressure were observed with the stearic + arachidic acid mixtures examined and with other acid + alcohol mixtures omitted from Fig. 1 for clarity. For both binary mixtures, as well as for the pure compounds, log η^s varied linearly with π. The viscosities of the mixtures lay between those for the pure components, and appeared to increase proportionately to the mole fraction of the more viscous compound. With the acid + alcohol mixtures the surface pressure range over which Newtonian viscosities were observed decreased as the fraction of alcohol increased, because the liquid condensed, L_2, film was transformed in a "plastic" LS film (13) at progressively lower surface pressures. The dependence of these $L_2 \rightleftharpoons$ LS transition pressures (π_k) on film composition is shown in Fig. 4.

The observed variations of the monolayer fluidity, ϕ^s, with composition will be discussed in terms of Eq. [3], and, where homogeneous mixed films are indicated, in terms of the absolute rate theory for viscous flow as applied to surface films. In Eyring's formulation (14) of this theory the presence of "holes" in a liquid (or monolayer) is necessary for flow, and therefore the ability of a solvent to provide "holes" is a determining factor. Accordingly, it is to be expected that the average thermodynamic properties of the entire mixed film will be involved when any individual molecule flows. The equation for the shear rate, $\dot{s}$, in the film is:

$$\dot{s} = \lambda_n 2k_n' \sinh \alpha_n f_n \qquad [6]$$

where f_n is the shear stress, k_n' the rate constant for the flow of a given unit, n, $\alpha_n = (\lambda\lambda_2)_n/2kT$ and λ_1, and λ_2, and λ are the molecular parameters in the theory (13). As pointed out recently by Ree and Eyring (15), the flow rate of a system is a function of (I) the relaxation times of the flow units which contribute in the flow process, $\beta_n = 1/\lambda_n 2k_n'$, (II) the distribution of such relaxation times, and (III) the deformation of the system with stress. With the monomolecular films considered here it will be assumed that only one group of flow units occurs and that the third factor is not important (16). Further, assuming: (*a*) $\alpha f \ll 1$; (*b*) $\lambda_1 = \lambda$; and (*c*) setting $\lambda\lambda_2$ equal to the cross-sectional area of the units which flow, σ, Eq. [6] may be reduced to:

$$\phi = (\sigma/h)e^{-\Delta F^\ddagger/kT}, \qquad [7]$$

which is the equation of Moore and Eyring (17). Assumption (*a*), of course, requires that Newtonian flow holds. The quantity, σ, has been found to be approximately equal to the cross-sectional area per molecule in the film. Utilizing several assumptions about the free energy of activation, $\Delta F^\ddagger$, for flow in monolayers, Eq. [7] leads to the prediction that the logarithm of the surface viscosity should increase linearly with surface pressure, in agreement with experimental observations (6 and Fig. 1).

In an homogeneous binary mixed film the free energy of activation will be given by:

$$\Delta F^\ddagger = x_1\Delta \bar{F}_1^\ddagger + x_2\Delta \bar{F}_2^\ddagger, \qquad [8]$$

where $\Delta \bar{F}_1^\ddagger$ and $\Delta \bar{F}_2^\ddagger$ are the partial molar activation free energies for the flow of species 1 and 2. If these partial molar quantities take their molar values, and, if $\sigma_1 \approx \sigma_2$, then on substitution of Eq. [8] into Eq. [7] and simplifying:

$$\log \phi = x_1 \log \phi_1 + x_2 \log \phi_2 . \qquad [9]$$

In view of the assumptions, it is to be expected that Eq. [9] will describe the fluidity of perfect binary monolayer solutions.

If the assumption of the approximate equality of the molecular areas is retained, but if

$$\Delta \bar{F}_1^\ddagger = \Delta F_1^\ddagger + \delta x_1 x_2 \qquad [10a]$$

$$\Delta \bar{F}_2^\ddagger = \Delta F_2^\ddagger + \delta x_1 x_2 \qquad [10b]$$

the equation for the fluidity becomes:

$$\log \phi = x_1 \log \phi_1 + x_2 \log \phi_2 + \delta x_1 x_2/RT. \qquad [11]$$

The empirical parameter, δ, will be a measure of the molecular interaction to a first approximation, and it might reasonably be related to some simple function of $\Delta F_1^\ddagger$ and $\Delta F_2^\ddagger$.

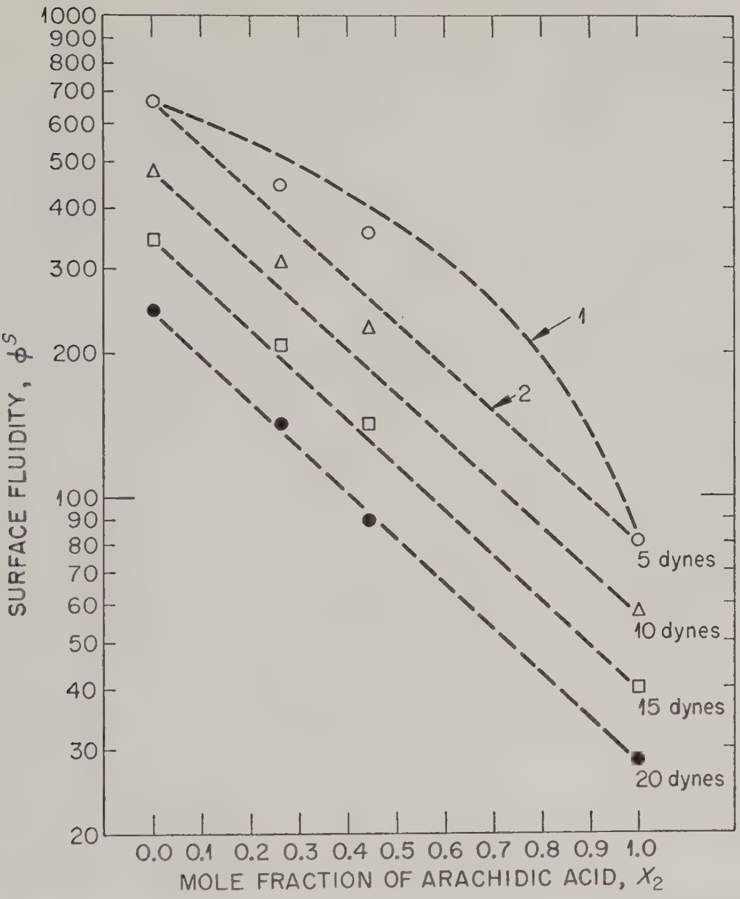

FIG. 2. Variations of the logarithm of the surface fluidities of mixed stearic + arachidic acid films with composition and surface pressure. Curve 1 from Eq. [3]; Curve 2 from Eq. [9].

The surface viscosity data obtained in this study were employed in the construction of the surface fluidity-composition, (ϕ, x), diagrams shown in Figs. 2 and 3, where the data are compared with the expectations according to Eq. [3], Curve 1; Eq. [9], Curve 2; and Eq. [11], Curve 3.

The variations of the surface fluidities of the mixed stearic + arachidic acid monolayers (Fig. 2) indicate fairly conclusively that truly homogeneous solutions are formed, and, because Eq. [9] is obeyed reasonably well, that these solutions are nearly perfect with little or no intermolecular interactions. Some departure from logarithmic additivity appears to occur at a surface pressure of 5 dyne cm.^{-1}. However, there is no agreement, even in this case, with Curve 1 for a heterogeneous film. The general compliance of the surface fluidities of these mixed long-chain, fatty acid monolayers

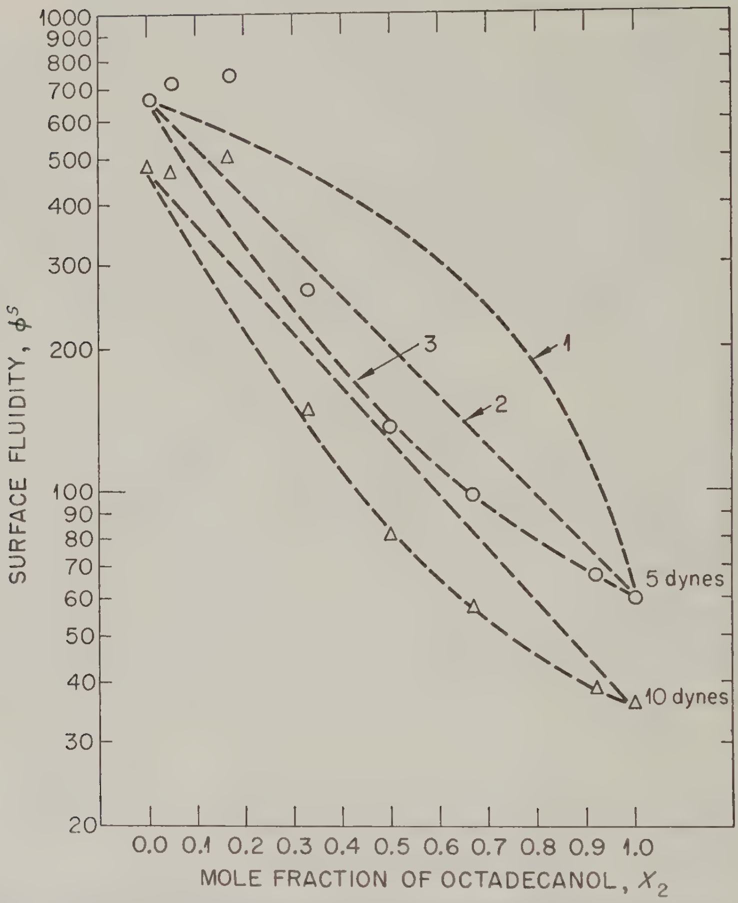

FIG. 3. Variations of the logarithm of the surface fluidities of mixed stearic acid + octadecanol films with composition and surface pressure. Curve 1 from Eq. [3]; Curve 2 from Eq. [9]; Curve 3 from Eq. [11] with $\delta = -400$ cal. mole^{-1}.

with Eq. [9] is not surprising. The areas per molecule of the components differ by only 3% (4) and probably the free energy of activation for viscous flow in the mixed film is given to a good approximation by the "weighted average" of the *molar* free energies.

The composition variations in this mixed film may be regarded as equivalent to modifying the molecules in an initially pure stearic acid film by lengthening some of its hydrocarbon chains by two carbon atoms keeping the polar group constant. The results in Fig. 2 suggest that the ends of the longer chains do not protrude above the top of the film, so that their terminal ethyl groups do not fully interact during the flow process, but, rather, that the molecular disposition in the mixed monolayer is such as to permit complete chain interactions. Such behavior seems to be consistent with the view that the long hydrocarbon chains in the monolayer possess a degree of flexibility sufficient to lower the surface tension at the top of the film from what it would be for rigid, protruding chain-ends. Clearly, more data are desirable if this interpretation is to be established.

The composition variations in the mixed stearic acid + octadecanol monolayers may be regarded as equivalent to changing some of the carboxyl to carbinol groups keeping the chain length constant. If the chain interactions remain unchanged, the surface fluidity variation might be ascribed to polar group interactions. As may be seen from Fig. 3, homogeneous monolayers were formed and a complex behavior was found. The fluidity increased somewhat *above* that for pure stearic acid, until the mole fraction of alcohol reached a value of 0.17; then a rapid decrease took place. For small additions of octadecanol, the actual mixed film appeared to be even more fluid than an hypothetical heterogeneous monolayer (Curve 1), suggesting that small amounts of alcohol either "break the structure" of the stearic acid film or introduce defects which permit easier viscous flow.

A possible cause of "structure-breaking" may reside in the unequal sizes of the polar groups in these two compounds, if it is assumed with N. K. Adam (18) that the molecular cross-sectional areas in their respective liquid condensed films on dilute acid solutions are determined by the "close-packed heads rearranged by compression." Accurate measurements (4) of the limiting area per molecule at zero film pressure for stearic acid and for octadecanol L_2 films have given values of 24.4_1 and 21.8_2 sq. A., respectively. The substitution of octadecanol with its smaller polar group into the two-dimensional array of close-packed carboxyl groups of the stearic acid monolayer may therefore act to give more freedom of movement to the hydrocarbon chains and hence increased fluidity. This picture is also consistent with the view that the greater fluidity of long-chain acid over alcohol monolayers is to be attributed to the fact that the greater size of the carboxyl group preserves to a greater extent the liquid-like nature of the hydrocarbon superstructure.

Ultimately, as the substitution of alcohol for acid progresses, the close-packed head-group structure in the acid film will be broken down more or less completely, and the fluidity will decrease rapidly as a consequence of a tighter packing of the hydrocarbon chains. The composition at which the greatest fluidity change occurs may be that where there are a sufficient number of carbinol groups in the film to require that they become neighbors in an hexagonal, close-packed array (i.e., $> 1{:}6$ or $x_2 > 0.14$).

Above a mole fraction of *ca.* 0.30, negative deviations from logarithmic additivity (Curve 2) were observed. The data for the change of fluidity with the composition for the "alcohol-rich" mixtures may be described by Eq. [11] with $\delta = -400$ cal. mole^{-1}. It is of interest to compare this value with a

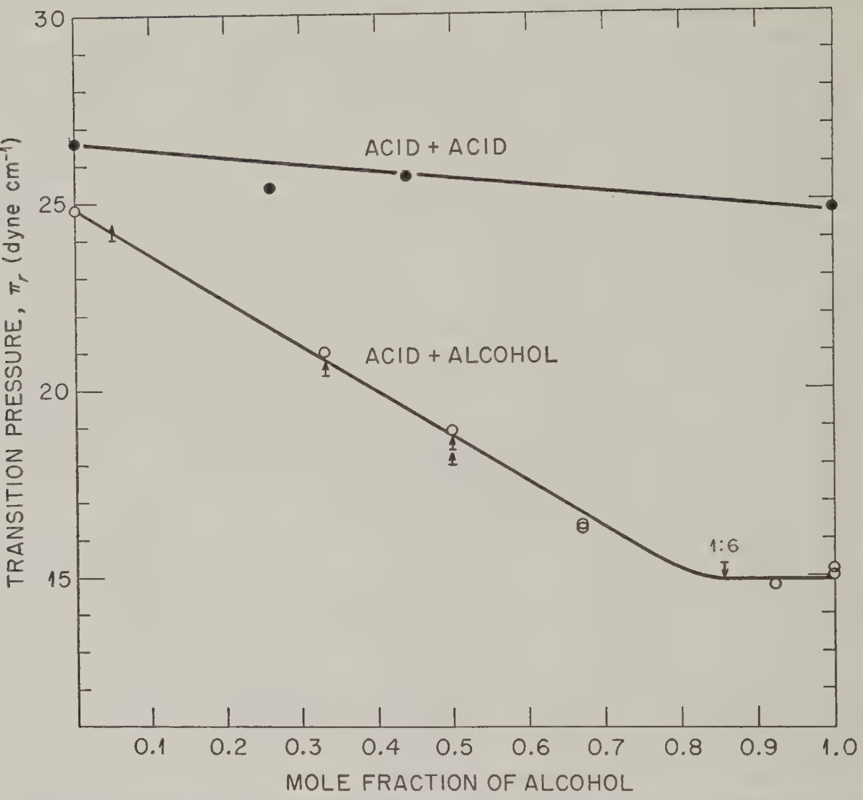

FIG. 4. Variations of the transition pressures, π_k, for stearic + arachidic acid and for stearic acid + octadecanol mixed films with composition.

value of -300 cal. mole^{-1} obtained recently (19) for the excess free energy of mixing in films containing sixteen carbon-atom chains.

It is to be expected, in accordance with the interpretation expressed above, that the addition of octadecanol to a stearic acid monolayer will act to lower the surface pressure, π_k, for the transition of the Newtonian, liquid condensed film, L_2, to the non-Newtonian, "plastic," LS, monolayer where the hydrocarbon chains are closely packed and vertically oriented (20, 21). Thus, the presence of smaller alcohol head-groups allows the mixed film to be compressed to an area of *ca.* 20 sq. A. per molecule at a lower pressure. From the results plotted in Fig. 4, it would appear, however, that the addition of small amounts of stearic acid to an octadecanol monolayer does not increase π_k. In this case it may be supposed that the strong, van der Waals' forces between the long chains in the LS film state are sufficient to permit small numbers of larger carboxyl head-groups to be accommodated. When the number of these latter exceeds 1:6 so that carboxyl groups must become neighbors (i.e., $x_2 < 0.86$), the structure of the hydrocarbon superstructure is broken and π_k increases.

REFERENCES

1. Harkins, W. D., and Florence, R. T., *J. Chem. Phys.* **6,** 847 (1938).
2. Marsden, J., and Schulman, J. H., *Trans. Faraday Soc.* **34,** 748 (1938).
3. Meyer, J. D., and Reid, E. E., *J. Am. Chem. Soc.* **55,** 1574 (1933).
4. Nutting, G. C., and Harkins, W. D., *J. Am. Chem. Soc.* **61,** 1180 (1939).
5. Fourt, L., and Harkins, W. D., *J. Phys. Chem.* **42,** 897 (1938).
6. Boyd, G. E., and Harkins, W. D., *J. Am. Chem. Soc.* **61,** 1188 (1939).
7. Copeland, L. E., Harkins, W. D., and Boyd, G. E., *J. Chem. Phys.* **10,** 357 (1942).
8. Langmuir, I., and Schaefer, V. J., *J. Am. Chem. Soc.* **59,** 2400 (1937).
9. Ewers, W. E., and Sack, R. A., *Australian J. Chem.* **7,** 40 (1954).
10. Merigoux, R., *Compt. rend.* **202,** 2049 (1936).
11. Schulman, J. H., and Teorrel, T., *Trans. Faraday Soc.* **34,** 1337 (1938).
12. Crisp, D. J., *Trans. Faraday Soc.* **42,** 619 (1946).
13. This nomenclature follows that given by Harkins, W. D., "Physical Chemistry of Surface Films," p. 106. Reinhold, New York, 1952.
14. Eyring, H., *J. Chem. Phys.* **4,** 283 (1936).
15. Ree, T., and Eyring, H., *J. Appl. Phys.* **26,** 793 (1955).
16. However, below 20° films of octadecanol appear to change their structure with compression (see refs. 7 and Trapeznikov, A., *Compt. rend. acad. sci.* URSS **30,** 321 (1941).
17. Moore, W. J., and Eyring, H., *J. Chem. Phys.* **6,** 391 (1938).
18. Adam, N. K., "The Physics and Chemistry of Surfaces," 3rd ed., p.54. Oxford University Press, London, 1941.
19. Goodrich, F. C., "2nd International Conference on Surface Activity," ed. by J. H. Schulman, Vol. 1, Paper M39. Butterworth's, London, 1957.
20. Alexander, A. E., *Proc. Roy. Soc.* (*London*) **A179,** 486 (1942).
21. Stenhagen, E., "Determination of Organic Structures by Physical Methods," edited by E. A. Braude and F. C. Nachod, Chapter 8. Academic Press, New York, 1955.

JOURNAL OF COLLOID SCIENCE **13,** 286–290 (1958)

LETTERS TO THE EDITOR

SOLUBILITY OF LONG-CHAIN AMINES IN WATER

In connection with the proposed use of several amine salts in adsorption experiments, values for the solubilities of the free amines in water were required. Since there were no values recorded in the literature for the compounds under consideration, solubility determinations were carried out by means of a technique involving potentiometric titration with the hydrogen electrode.

A platinum black hydrogen electrode was employed in conjunction with a calomel electrode to which was attached a liquid junction tube containing saturated potassium chloride solution. The cylinder hydrogen used was purified by passage over copper gauze at 700°C. and through a solution containing potassium hydroxide and pyrogallic acid, to remove oxygen and carbon dioxide, respectively. Water used in the experiments was double distilled and free of carbon dioxide. Caustic soda solutions were kept in polythene containers fitted with soda-lime tubes to prevent attack by carbon dioxide. The amine salts used were decylammonium acetate, dodecylammonium chloride, and tetradecylammonium acetate, all of which were supplied by Armour and Company in a state of high purity.

The accuracy of the measurement of pH by the electrode system used was checked frequently by means of standard buffer solutions at pH 7 and pH 10.

A high degree of accuracy, within 0.01 pH unit, was obtainable. Aqueous solutions of the amine salts were made up under purified nitrogen in the glass titration vessel which was then fitted with the rubber stopper holding the electrode system, the hydrogen inlet and outlet, and the buret containing sodium hydroxide solution. The solution in the buret was protected from the air by a soda-lime tube and air was also excluded from the titration vessel.

The reaction between amine salt (RNH_3X) and sodium hydroxide may be written:

$$RNH_3^+ + X^- + Na^+ + OH^- \rightleftharpoons RNH_2 + H_2O + Na^+ + X^-$$

The basic dissociation constant of the amine, K_b, is given by the relation

$$K_b = \frac{[RNH_3^+][OH^-]}{[RNH_2]}$$

TABLE I

Solubilities of Long-Chain Amines in Water

Amine	Solubility (*moles/liter*)	No. of tests	Initial salt concentration (*moles/liter*)	Temperature (°*C.*)	pH range
Decylamine	$(5.2 \pm 0.3) \times 10^{-4}$	2	4.01×10^{-3}	24	7–11
			4.32×10^{-3}	23	
Dodecylamine	$(2.0 \pm 0.2) \times 10^{-5}$	4	$3.96\text{–}9.97 \times 10^{-4}$	20–23	7–10.5
Tetradecylamine	$(1.2 \pm 0.1) \times 10^{-6}$	2	8.33×10^{-4}	23	7–9.5
			9.80×10^{-4}	21	

from which the amine concentration may be determined if the other quantities are known. The hydroxyl ion concentration is found from the pH measured by the hydrogen electrode.

The amine ion concentration is found from the amount of sodium hydroxide added to the solution, a correction being made for the quantity of alkali required to bring the test solution to the hydroxyl ion concentration found.

The values of K_b used were taken from the work of Ralston (1), being 4.4, 4.3, and 4.2×10^{-4} for the C_{10}, C_{12}, and C_{14} amines.

During all experiments the solutions became milky in appearance when the solubilities of the amines used had been exceeded. Froth formed above the solutions when the amine salt was almost totally converted to the amine (solubility not exceeded) or when the solubility of the amine had been exceeded. The measured values of solubility are shown in Table I.

The value for the solubility of dodecylamine is in agreement with estimates made previously, on the basis of light-scattering and adsorption density measurements, by de Bruyn (2).

The work was performed while the author was Armour Fellow in the Department of Mineral Engineering, Massachusetts Institute of Technology.

The thanks of the author are due to Professor A. M. Gaudin, Richards Professor of Mineral Engineering, and Professor J. Th. G. Overbeek, Visiting Professor, M.I.T., for advice and encouragement.

REFERENCES

1. Ralston, A. W., "Fatty Acids and their Derivatives." Wiley, New York, 1948.
2. De Bruyn, P. L., "Flotation of Quartz by Cationic Collectors," *Mining Eng.* **7,** 291–296 (1955).

Hornby, Oakley Road,
Cheltenham, Glos.,
England

D. J. Brown

Received March 24, 1958

A SIMPLE DERIVATION OF AN ELECTROVISCOUS EQUATION

A simple derivation of an equation for the electroviscous effect in suspension flow is possible following the approach used by Bull (1) for flow through capillaries. A similar simplified derivation was reported by Elton to describe the electroviscous retardation, of flow in capillaries (2), and of sedimenting particles (3).

Consider a suspension containing N particles per cubic centimeter of suspension, each particle having a radius a and a surface charge of Q. There is relative movement during flow between the liquid and the particles, and the force per particle necessary to cause it is F_2. However, this relative motion gives rise to a potential (analogous to a streaming or sedimentation potential) which causes a "back force" on the particles. Hence if the force originally imposed on a particle causing this movement is F and if the "back force" is $(-F_1)$ then the force actually causing the movement is

$$F_2 = F + (-F_1); \qquad \text{i.e.,} \quad F = F_1 + F_2 .$$

If the relative velocity of the particles and the fluid is v then the apparent viscosity of the film of water surrounding a particle is

$$\eta_a = F/6\pi a v, \tag{1}$$

whereas the actual viscosity is

$$\eta = F_2/6\pi a v. \tag{2}$$

The potential E across unit length of flow caused by the relative motion is

$$E = \frac{NQv}{K},$$

and since

$$v = \frac{F_2}{6\pi\eta a}$$

it follows that

$$E = \frac{F_2 NQ}{6\pi\eta K a}; \qquad \text{i.e.,} \quad F_2 = \frac{6\pi\eta K a E}{NQ}$$

(K is the conductivity of the electrolyte solution).

The "back force" caused by E is given by,

$$F_1 = QE.$$

Therefore

$$F = F_1 + F_2 = \frac{6\pi\eta K a E}{NQ} + QE.$$

Now since from [1] and [2]

$$\eta_a = \frac{F}{F_2}\,\eta$$

it follows that:

$$\eta_a = \eta\left(\frac{6\pi\eta KaE}{NQ} + QE\right)\frac{NQ}{6\pi\eta KaE};$$

thus

$$\eta_a = \eta\left(1 + \frac{NQ^2}{6\pi\eta Ka}\right).$$

Now the volume concentration

$$\varphi = \tfrac{4}{3}\,\pi a^3 N, \qquad \text{i.e.,}\quad N = \frac{3\varphi}{4\pi a^3}$$

and $Q^2 = (D\zeta a)^2$, where ζ is the zeta-potential and D is the dielectric constant.

And so,

$$\eta_a = \eta\left(1 + \frac{\varphi}{2a^2\eta K}\left(\frac{D\zeta}{2\pi}\right)^2\right).$$

In the Einstein equation for suspension flow,

$$\frac{\eta_s}{\eta_0} = 1 + 2.5\varphi,$$

η_0 should be replaced by η_a in order to allow for the electroviscous effect; then

$$\frac{\eta_s}{\eta} = 1 + 2.5\varphi\left[1 + \frac{\varphi}{2a^2\eta K}\left(\frac{D\zeta}{2\pi}\right)^2\right].$$

It is interesting to observe that this equation has the form

$$\frac{\eta_s}{\eta} = 1 + k_1\varphi + k_2\varphi^2,$$

TABLE I

Comparison of Calculated and Observed k_2

Equilibrium solution	k_2 (measured)	k_2 (calculated)
1	80	270
2	100	97
3	30	27
4	10	4.5
6	8	1

as observed by Harmsen, van Schooten, and Overbeek (4) in their work on the AgI sol. Harmsen *et al.* list experimental values for k_2 which are reproduced in Table I together with values calculated from $k_2 = k_1(f/2)$, where the f values (at $\zeta = 200$ mv.) are taken from Harmsen *et al.* (5).

More generally, in electrolyte solutions, since $Q^2 = (D\zeta a)^2 (1 + \kappa a)^2$, where κ is the reciprocal of the Debye characteristic length,

$$\frac{\eta_s}{\eta} = 1 + 2.5\varphi \left[1 + \frac{\varphi}{2a^2 \eta K} \left(\frac{D\zeta}{2\pi} \right)^2 (1 + \kappa a)^2 \right].$$

REFERENCES

1. BULL, H. B., *Kolloid-Z.* **60,** 130 (1932).
2. ELTON, G. A. H., *Proc. Roy. Soc.* (*London*) **A194,** 259 (1948).
3. ELTON, G. A. H., *Proc. Roy. Soc.* (*London*) **A197,** 568 (1949).
4. HARMSEN, G. J., VAN SCHOOTEN, J., AND OVERBEEK, J. TH. G., *J. Colloid Sci.* **8,** 72 (1953).
5. HARMSEN, G. J., VAN SCHOOTEN, J., AND OVERBEEK, J. TH. G., *J. Colloid Sci.* **10,** 120 (1955).

University of Illinois

NORMAN STREET

Received May 1, 1958

BOOK REVIEW

Excited States in Chemistry and Biology. C. Reid. Academic Press Inc., New York. 215 pp. Price $7.50.

This book attempts to combine within 215 pages an introduction to the quantum theory of chemical bonds, molecular spectra, mechanisms of excitation and energy exchanges, with brief chapters dealing with certain areas of chemistry and biochemistry from which examples of qualitative applications of the foregoing theories are drawn. An appendix of 26 pages deals with the Hermitian character of the Hamiltonian operator, group theory, time-dependent perturbation theory, long-range intermolecular energy transfer, and transition probabilities.

The first part is necessarily cursory and highly selective, and frequently unprecise without being consistently elementary. It will nevertheless serve as a stimulus to the previously unoriented reader to add to his theoretical equipment in understanding the phenomena of chemical combination and catalysis. References are given which will serve such a reader as a guide. The second part, which deals with luminescent reactions, vision, and selected chemical effects of radiation, including intracellular processes, is even more selective, and must be considered purely illustrative. For the most part, only qualitative or conceptual use is made of the theoretical apparatus developed in the first half of the book. The ideas presented are usually suggestive, rather than conclusive. Many examples, such as protection against radiation by added substances, are taken from the recent literature.

As may be gathered, the treatment of each field is too selective to serve as either an introduction or summary of its present status. Although the references are numerous, they sometimes give an impression of capriciousness, since in some cases they are neither representative nor exhaustive, nor consistent as documentation of the text. The index is particularly inadequate, even for referring back to material already read. Careless proofreading (such as reference to a figure (34), by incorrect number (35)) sometimes leads to confusion.

Within the limitations noted, this monograph can be recommended as a condensed introduction to quantum interpretations of chemical phenomena and as a convenient recapitulation of recent work widely scattered in the current literature. Its value as an introduction would have been greater if the presentation had not been characterized by an effect of breathlessness; thus there is a profusion of casually introduced undefined terms and concepts, which makes the text needlessly hard going, and sometimes downright unintelligible to the previously uninitiated for whom it was supposedly intended.

Jacinto Steinhardt, Cambridge, Massachusetts

Biophysical Chemistry

By JOHN T. EDSALL, *Harvard University, Cambridge, Massachusetts*
and JEFFRIES WYMAN, *UNESCO, Cairo, Egypt*

Volume 1

Thermodynamics, Electrostatics, and the Biological Significance of the Properties of Matter

February 1958, 699 pp., illus., $14.00

Biophysical Chemistry is based on a course taught by the authors dealing with the physical chemistry of biochemical systems. Emphasis has been placed on broad general principles and fundamental concepts in order to provide the reader with the basic understanding of the quite difficult problems of current interest in the field of biophysical chemistry.

Volume 1 presents a lucid discussion and a detailed analysis of the biological significance of the properties of matter. The second volume will be devoted to the physical chemistry of biological macromolecules, and their study by such methods as osmotic pressure, light scattering, diffusion, sedimentation, viscosity and electrophoresis.

These volumes will be indispensable to graduate students and advanced undergraduates familiar with the fundamentals of differential and integral calculus. This work will be of basic interest to investigators in organic and physical chemistry, biology, and biochemistry.

CONTENTS OF VOLUME 1:

Biochemistry and Geochemistry. Water and Its Biological Significance. Problems of Protein Structure. Thermodynamics. Electrostatics: Its Application to Polar Molecules and Ionic Solutions. Dielectric Constants and Their Significance. Conductivity of Electrolytes. Acid-Base Equilibria. Polybasic Acids, Bases, and Ampholytes, Including Proteins. Carbon Dioxide and Carbonic Acid. Some General Aspects of Molecular Interactions. AUTHOR INDEX—SUBJECT INDEX.

Volume 2, in preparation

Physical Chemistry of Macromolecules and of Blood

Descriptive leaflet available upon request

ACADEMIC PRESS INC., *Publishers*
111 FIFTH AVENUE, NEW YORK 3, NEW YORK

JOURNAL OF COLLOID SCIENCE **13**, 293–307 (1958)

PARTICLE MOTIONS IN SHEARED SUSPENSIONS

VII. INTERNAL CIRCULATION IN FLUID DROPLETS (THEORETICAL)[1]

W. Bartok[2] and S. G. Mason

Physical Chemistry Division, Pulp and Paper Research Institute of Canada, and Department of Chemistry, McGill University, Montreal, Canada

Received April 5, 1958

List of Symbols

b = radius of sphere.
c = volume fraction of particles in suspension.
G = velocity gradient (rate of shear).
h = displacement between center of drop and streamline measured along Y-axis at large distances from sphere.
k_1 = streamline constant inside drop in plane hyperbolic flow.
k_2 = streamline constant inside drop in laminar shear flow.
p = viscosity ratio = η'/η_0.
r = radius vector measured from origin of coordinate system.
t = time.
T = period of rotation at the surface of fluid sphere.
T_c = mean period of circulation inside fluid sphere.
u, v, w = velocity components along X, Y, Z-axis of shear field.
u', v', w' = velocity components along X', Y', Z'-axis of hyperbolic flow.
α_0 = intrinsic viscosity.
α = angle between rotating systems of coordinate axis.
η', η_0, η = viscosity of disperse phase, continuous phase, and of suspension, respectively.
ϕ = polar coordinate angle measured from Y-(or Y'-) axis.

INTRODUCTION

Einstein's theoretical treatment (1) of the viscosity of a suspension of rigid spherical particles in a liquid was extended by Taylor (2) to the case of small immiscible fluid spheres. The particles create a disturbance of the fluid motion which thereby causes an increase in viscosity. The viscous drag exerted by the surrounding medium is predicted to cause circulation currents inside the drops provided that transmission of tangential stresses across the interface is not inhibited by the formation of a rigid film around the particles.

---

[1] Contribution from Physical Chemistry Division, Pulp and Paper Research Institute of Canada, and Department of Chemistry, McGill University, Montreal, Canada. This research was conducted with financial assistance from the Defense Research Board of Canada (DRB Grant 9510–05).

[2] Holder of a Studentship from the National Research Council of Canada, 1956–57.

The circulation inside a fluid sphere moving in a field of gravitational sedimentation has been studied by a number of workers (3–12). The purpose of the present paper is to derive the equations of fluid motion outside and inside a fluid sphere suspended in the fields of plane-hyperbolic and of laminar shear flow.

1. Plane-Hyperbolic Flow

The field of plane-hyperbolic flow was chosen by Taylor (2) to derive the velocity components of fluid motion, both outside and inside the drop. The undisturbed field of motion is defined by

$$u' = \frac{G}{2}x'; \qquad v' = -\frac{G}{2}y'; \qquad w' = 0. \tag{1}$$

The constant G was chosen by Taylor in such manner that if the coordinate axes X', Y' are rotated with a constant angular velocity $G/2$ and if the coordinate axes X, Y of the uniform laminar shear flow defined by Eq. [12] lie instantaneously at 45° to the axes X', Y', then the two fields of flow become identical. This transformation, which will be performed later, is illustrated in Fig. 1.

Taylor (2) assumed the following boundary conditions to render the hydrodynamical analysis of the contribution of fluid particles to the viscosity of the suspension tractable:

1). The diameter of the suspended drops and the velocity of distortion of the fluid are so small that the interfacial tension keeps the drops nearly spherical.

2). There is no slip at the drop-medium interface.

3). The tangential stress parallel to the surface is continuous at the surface of the drop, so that any film existing between the two fluids merely transmits tangential stress from one fluid to the other.

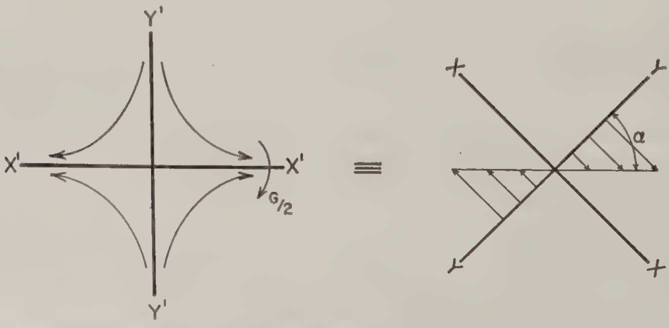

FIG. 1. Transformation of hyperbolic flow (left) to shear flow (right) by rotation of the coordinate axes.

a). *Velocity Components.* By satisfying the above boundary conditions, Taylor obtained the following components of velocity in the fluid outside a drop the center of which was placed at the origin of the coordinate system X', Y', Z' of Fig. 1.

$$\begin{aligned}
u' &= \frac{A_{-3}}{2} b^3 x' \frac{x'^2 - x'^2}{r^5} + B_{-3} b^5 \left[\frac{-5x'(x'^2 - y'^2)}{r^7} + \frac{2x'}{r^5} \right] + \frac{G}{2} x'; \\
v' &= \frac{A_{-3}}{2} b^3 y' \frac{x'^2 - y'^2}{r^5} + B_{-3} b^5 \left[\frac{-5y'(x'^2 - y'^2)}{r^7} - \frac{2y'}{r^5} \right] - \frac{G}{2} y'; \quad [2] \\
w' &= \frac{A_{-3}}{2} b^3 z' \frac{x'^2 - y'^2}{r^5} + B_{-3} b^5 \left[\frac{-5z'(x'^2 - y'^2)}{r^7} \right].
\end{aligned}$$

Similarly, the velocity components inside the drop are:

$$\left.\begin{aligned}
u' &= \frac{A_2}{b^2} \left[\frac{5}{21} x'r^2 - \frac{2}{21} x'(x'^2 - y'^2) \right]^* + 2B_2 x'; \\
v' &= \frac{A_2}{b^2} \left[-\frac{5}{21} y'r^2 - \frac{2}{21} y'(x'^2 - y'^2) \right] - 2B_2 y'; \\
w' &= \frac{A_2}{b^2} \left[-\frac{2}{21} z'(x'^2 - y'^2) \right];
\end{aligned}\right\} \quad [3]$$

where b is the radius of the drop, and r is the radius vector of a fluid element measured from the origin. Thus r is given by

$$r^2 = x'^2 + y'^2 + z'^2. \quad [4]$$

The constants A_{-3}, B_{-3}, A_2, and B_2 were determined by the boundary conditions to be

$$\left.\begin{aligned}
A_{-3} &= \frac{5G}{2} \frac{p + 2/5}{p + 1}; \qquad & B_{-3} &= -\frac{G}{4} \frac{p}{p + 1}; \\
A_2 &= \frac{21G}{4(p + 1)}; & B_2 &= -\frac{3G}{8(p + 1)};
\end{aligned}\right\} \quad [5]$$

where p is the ratio η'/η_0 of the viscosity of the drop to the viscosity of the fluid surrounding it.

The intrinsic viscosity α_0 of a suspension of fluid spheres of volume fraction c was calculated by Taylor from Eqs. [2], [3], and [5] to be:

$$\begin{aligned}
\alpha_0 &= \lim_{c \to 0} \frac{\frac{\eta}{\eta_0} - 1}{c}; \qquad [6] \\
&= \frac{5/2\,p + 1}{p + 1}.
\end{aligned}$$

---

* In the original article by Taylor (2), the first term in this bracket is shown negative. This appears to be a misprint, since the boundary conditions are satisfied only if the sign is reversed.

For a suspension of solid spheres, for which $p = \infty$, Eq. [6] yields the familiar Einstein coefficient $\alpha_0 = 5/2$; while for $p = 0$, $\alpha_0 = 1$.

b). Circulation inside a Fluid Sphere ($r < b$). To simplify the mathematical analysis, the treatment in all the derivations which are to follow will be restricted to the horizontal equatorial plane of a spherical drop. The equation of the streamlines inside a drop in the plane defined by $z' = 0$, $x'^2 + y'^2 = r^2$ is given by

$$\frac{dx'}{u'} = \frac{dy'}{v}. \qquad [7]$$

Combining Eqs. [3], [5], and [7] yields:

$$y'\left[-\frac{7x'^2}{b^2} - \frac{3y'^2}{b^2} + 3\right]dx' = x'\left[\frac{3x'^2}{b^2} + \frac{7y'^2}{b^2} - 3\right]dy'. \qquad [8]$$

The equation of the streamlines in terms of polar coordinates defined by

$$x' = r\sin\phi';\ y' = r\cos\phi' \qquad [9]$$

reduces to

$$\frac{\dfrac{10r^2}{b^2} - 6}{r\left(1 - \dfrac{r^2}{b^2}\right)}\,dr = 3\,\frac{\cos^2\phi' - \sin^2\phi'}{\sin\phi'\cos\phi'}\,d\phi'. \qquad [10]$$

Integrating Eq. [10], we obtain

$$\frac{r^3}{b^3}\left(1 - \frac{r^2}{b^2}\right) = \frac{k_1}{(\sin 2\phi')^{3/2}}. \qquad [11]$$

It follows from Eq. [11] that the center of the drop is a stagnation point. Furthermore, since $r/b = 0$ is a trivial solution of Eq. [11], two values of (r/b) will correspond to any value of ϕ', i.e., the circulation path of a fluid element is a closed curve in each quadrant. The streamlines are symmetrical about the line $\phi = \pi/4$, since r/b is a function of $\sin 2\phi'$. Close to the center of the drop the streamlines are rectangular hyperbolas since Eq. [11] reduces to

$$\frac{r}{b} = \frac{k_1^{1/3}}{\sqrt{\sin 2\phi'}}$$

for $r/b \ll 1$.

The implicit relationship of Eq. [11] can be solved graphically by plotting the left-hand side as a function of (r/b); for a fixed value of k_1, the right hand side of Eq. [11] is calculated at various values of ϕ' and the corresponding (r/b) is determined from the plot. It should be noted that the left-hand side is a maximum at $(r/b) = \sqrt{3/5}$. It follows that on this radius each streamline is radial and stagnation points exist at four positions, corresponding to $\phi' = \pm \pi/4$ and $\pm 3\pi/4$.

The circulation inside a fluid sphere in plane hyperbolic flow is shown in Fig. 2, where the graphical method described above has been used to calculate the streamlines.

2. Transformation of Plane Hyperbolic Flow to Laminar Shear

Undisturbed laminar shear flow is defined by the velocity components

$$u = Gy; v = w = 0. \tag{12}$$

Referred to Fig. 1, the coordinates of the two flow systems are related by

$$\begin{aligned} x &= x' \sin \alpha + y' \cos \alpha; \\ y &= y' \cos \alpha - y' \sin \alpha, \end{aligned} \tag{13}$$

where α is the angle between the rotating axes X', Y', and the axes X, Y at any instant. The components of the laminar shear motion are obtained by differentiating Eq. [13] with respect to time. Thus

$$\begin{aligned} u &= u' \sin \alpha + v' \cos \alpha + (x' \cos \alpha - y' \sin \alpha) \frac{d\alpha}{dt}; \\ v &= u' \cos \alpha - v' \sin \alpha - (x' \sin \alpha + y' \cos \alpha) \frac{d\alpha}{dt}. \end{aligned} \tag{14}$$

In the present case $d\alpha/dt = G/2$ and the instantaneous value of $\alpha = \pi/4$.

Substituting into Eq. [14], the transformation equations for the velocity

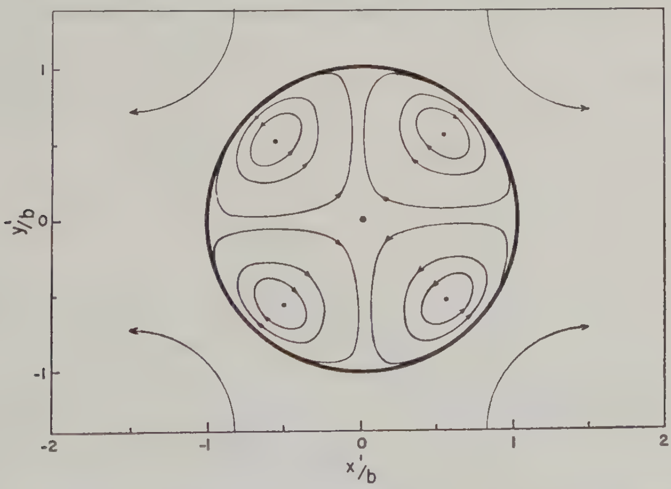

FIG. 2. Circulation inside a fluid sphere of unit radius in plane hyperbolic flow. The streamlines are calculated from Eq. [11].

components between the two fields of motion are

$$\left.\begin{aligned} u &= \frac{1}{\sqrt{2}}\left[u' + v' + \frac{G}{2}(x' - y')\right]; \\ v &= \frac{1}{\sqrt{2}}\left[u' - v' - \frac{G}{2}(x' + y')\right]. \end{aligned}\right. \qquad [15]$$

It follows from Eq. [13] that

$$\left.\begin{aligned} x &= \frac{1}{\sqrt{2}}(x' + y'); \\ y &= \frac{1}{\sqrt{2}}(x' - y'); \\ z &= z'. \end{aligned}\right\} \qquad [16]$$

Combining Eqs. [1], [15], and [16], u, v, and w are given by

$$u = Gy, v = w = 0$$

in accord with Eq. [12].

3. Laminar Shear Flow

a). Velocity Components. Using the above transformations, we can derive from Taylor's equations the components of fluid velocity outside and inside a drop in a laminar shear field.

The velocity components *outside* the drop ($r \geq b$) are given by transforming Eq. [2] with the aid of Eqs. [15] and [16] to yield

$$\left.\begin{aligned} u &= \frac{Gy}{p+1}\left[\frac{5b^3}{2}\left(p\frac{b^2}{r^2} - p - \frac{2}{5}\right)\frac{x^2}{r^5} - \frac{pb^5}{2r^5} + p + 1\right]; \\ v &= \frac{Gx}{p+1}\left[\frac{5b^3}{2}\left(p\frac{b^2}{r^2} - p - \frac{2}{5}\right)\frac{y^2}{r^5} - \frac{pb^5}{2r^5}\right]; \\ w &= \frac{Gz}{p+1}\left[\frac{5b^3}{2}\left(p\frac{b^2}{r^2} - p - \frac{2}{5}\right)\frac{xy}{r^5}\right]. \end{aligned}\right\} \qquad [17]$$

As before, r is the radius vector measured from the origin of the coordinate system, placed at the center of the drop. At large distances from the drop, Eq. [17] reduces to a field of undisturbed shear corresponding to Eq. [12]. For $p = \infty$ the velocity components given by Eq. [17] are identical with those calculated by Burgers (13) outside a rigid sphere.

The velocity components of the fluid *inside* the drop can be calculated in a similar manner, using Eqs. [3], [5], [15], and [16]. Thus, u, v, and w inside the drop are

$$\left.\begin{aligned} u &= \frac{Gy}{4(p+1)}\left[\frac{5r^2}{b^2} - \frac{4x^2}{b^2} + 2p - 1\right]; \\ v &= \frac{Gx}{4(p+1)}\left[\frac{5r^2}{b^2} - \frac{4y^2}{b^2} - 2p - 5\right]; \\ w &= -\frac{Gz}{(p+1)} \cdot \frac{xy}{b^2}. \end{aligned}\right\} \qquad [18]$$

b). *Streamlines outside a Fluid Sphere in a Shear Field* $(r > b)$. Consider the plane passing through the equator of the drop, i.e., points lying in the plane defined by

$$z = 0;$$
$$r^2 = x^2 + y^2.$$

The equation of the streamlines is obtained by following the procedure used to derive Eq. [10]. This yields the following differential equation for the streamlines in plane polar coordinates:

$$\begin{aligned} r\left[\frac{5b^3}{2(p+1)r^3}\left(p\frac{b^2}{r^2} - p - \frac{2}{5}\right) - \frac{pb^5}{(p+1)r^5} + 1\right] \sin\phi \cos\phi \, d\phi \\ = \left[\frac{pb^5}{2(p+1)r^5}(\sin^2\phi - \cos^2\phi) + \cos^2\phi\right] dr. \end{aligned} \qquad [19]$$

Equation [19] can be solved analytically for any value of p by neglecting the terms which contain $(b/r)^5$. Inspection of Eq. [19] shows that the error introduced by using the above approximation is maximum for $p = \infty$, and becomes smaller for decreasing values of p. For the limiting case of $p = 0$ the analytical solution becomes exact.

Using this approximation the differential equation of the streamlines reduces to

$$\frac{\sin\phi\cos\phi}{\cos^2\phi}\, d\phi = \frac{r^2\, dr}{r^3 - \left(\dfrac{5p+2}{2p+2}\right) b^3}. \qquad [20]$$

Integration of the above equation yields

$$\frac{r}{b} = \left(\frac{K^3}{\cos^3\phi} + \frac{5/2p + 1}{p+1}\right)^{1/3}, \qquad [21]$$

where K is a constant of integration. As $\phi \rightarrow \pi/2$, i.e. at large distances from the sphere, Eq. [21] reduces to

$$\frac{r}{b} = \frac{K}{\cos\phi}.$$

In this region, the streamlines become parallel with the X-axis. Hence

$$y = r \cos \phi = h,$$

where h is the displacement of any given streamline from the X-axis of the coordinate system, measured in the direction of the velocity gradient. Therefore, the constant which determines the location of the streamline is

$$K = h/b,$$

and Eq. [21] can be written in the form

$$\frac{r}{b} = \left(\frac{h^3}{b^3 \cos^3 \phi} + \frac{\frac{5}{2}p + 1}{p + 1}\right)^{1/3}. \qquad [22]$$

Equation [22] indicates that the distortion of the streamlines caused by the presence of a fluid sphere is least when $p = 0$, since $(\frac{5}{2}\,p + 1)/(p + 1)$ is then minimum. This is in agreement with Eq. [6], which predicts that the contribution to the viscosity of the medium is least when $p = 0$. It is interesting to note that the second term in the brackets of Eq. [22] is identical with α_0 given by Eq. [6]. The streamlines around a rigid sphere calculated from Eq. [22] for $p = \infty$ are shown in Fig. 3. The streamlines calculated for $p = 0$, and shown in Fig. 4, are seen to be less distorted than the streamlines around a rigid sphere.

c). Angular Velocity and Mean Period of Rotation at the Surface of a Fluid Sphere. The condition of continuity of velocity requires that the components of fluid velocity outside and inside a drop suspended in another fluid should

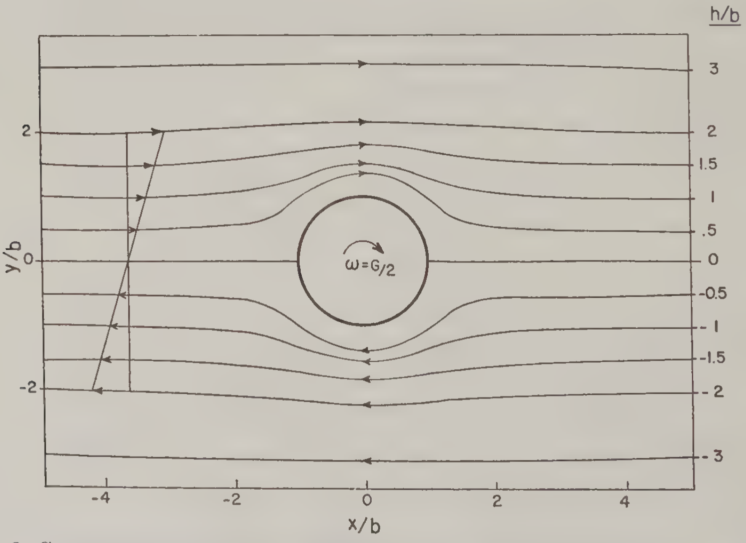

FIG. 3. Streamlines around a rigid sphere in a shear field. The lines are calculated from Eq. [22] for $p = \infty$.

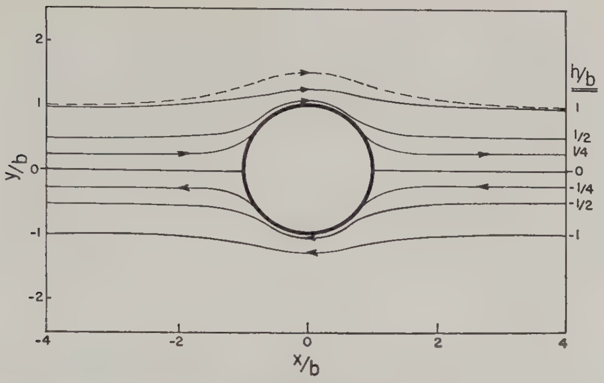

FIG. 4. Streamlines around a fluid sphere for $p = 0$. The lines are calculated from Eq. [22]. A streamline around a rigid sphere for $h/b = 1$ is shown as a broken line.

become identical at the interface. This condition is satisfied by Eqs. [17] and [18], since at $r = b$ both equations become

$$\left.\begin{aligned} u &= \frac{Gy}{p+1}\left(-\frac{x^2}{b^2} + \frac{p}{2} + 1\right); \\ v &= \frac{Gx}{p+1}\left(-\frac{y^2}{b^2} - \frac{p}{2}\right); \\ w &= \frac{Gz}{p+1}\left(-\frac{xy}{b^2}\right). \end{aligned}\right\} \qquad [23]$$

It follows from the above equations that for $p = \infty$, i.e. a solid sphere, the components of velocity are

$$\left.\begin{aligned} u &= \frac{Gy}{2}; \\ v &= -\frac{Gx}{2}; \\ w &= 0; \end{aligned}\right\} \qquad [24]$$

which corresponds to a rigid rotation of the surface with an angular velocity $G/2$, as predicted theoretically (1) and verified experimentally (14, 15).

The surface of a fluid sphere in a shear field also describes rotations. The angular velocity at the equatorial perimeter of the drop ($r = b$, $z = 0$) can be determined from

$$\frac{d\phi}{dt} = \frac{u}{y} = -\frac{v}{x}. \qquad [25]$$

Substituting u (or v) from Eq. [23], the angular velocity at $r = b$, $z = 0$

is given by

$$\frac{d\phi}{dt} = \frac{G}{(p+1)}\left[-\frac{x^2}{b^2} + \frac{p}{2} + 1\right]. \tag{26}$$

Transformation of Eq. [26] into polar coordinates yields

$$\frac{d\phi}{dt} = \frac{G}{2(p+1)}\left[p + 2 - 2\sin^2\phi\right]. \tag{27}$$

It is seen that Eq. [27] yields

$$\frac{d\phi}{dt} = \frac{G}{2} \tag{28}$$

for $p = \infty$. For the limiting case of $p = 0$, an inviscid drop, Eq. [27] gives

$$\frac{d\phi}{dt} = \frac{G}{2}\cos^2\phi.$$

For any value of $p > 0$, however, $d\phi/dt$ is always positive and never becomes zero, i.e., the fluid at the surface of the drop circulates with a variable angular velocity but always in the same direction.

The period of circulation at the surface can be calculated using Eq. [27]. Considering the angle ϕ to vary from 0 to $\pi/2$ for convenience, integration of Eq. [27] yields

$$\int_0^{\pi/2} \frac{d\phi}{1 - \dfrac{2}{p+2}\sin^2\phi} = \int_0^{T/4} \frac{G(p+2)\,dt}{2(p+1)},$$

where T is the mean period of rotation at $r = b$, $z = 0$. Integration of both sides of this expression yields the following relationship:

$$\frac{TG}{4\pi} = \frac{p+1}{\sqrt{p(p+2)}}. \tag{29}$$

Values of $TG/4\pi$ calculated from Eq. [29] for various values of the viscosity ratio are given in Table I. In agreement with Eq. [28], $TG/4\pi = 1$ for a solid sphere ($p = \infty$). The period of rotation becomes infinite in the hypothetical case when $p = 0$, since the angular velocity at the surface is zero at the points corresponding to $\phi = \pi/2$ and $\phi = 3\pi/2$. Table I indicates, however, that $TG/4\pi$ rapidly approaches unity as p increases from zero.

d). *Internal Circulation.* The pattern of internal motion can be determined by deriving an expression for the streamlines *inside* the drop. In the equatorial plane the velocity components are

$$\left.\begin{aligned} u &= \frac{Gy}{p+1}\left[\frac{1}{4}\frac{x^2}{b^2} + \frac{5}{4}\frac{y^2}{b^2} - \frac{3}{4}\right] + \frac{Gy}{2}; \\ v &= \frac{Gx}{p+1}\left[\frac{5}{4}\frac{x^2}{b^2} + \frac{1}{4}\frac{y^2}{b^2} - \frac{3}{4}\right] - \frac{Gx}{2}; \\ w &= 0. \end{aligned}\right\} \tag{30}$$

TABLE I

Period of Rotation at the Surface of a Fluid Sphere

$(z = 0, r = b)$

p	$\frac{TG}{4\pi}$
0.001	22.4
0.01	7.14
0.1	2.40
0.5	1.34
1.0	1.15
2.0	1.06
5.0	1.01
10.0	1.005
100.0	1.000

The equation of the streamlines becomes (cf. Eq. [7])

$$\frac{ydy}{xdx} = \frac{5x^2 + y^2 - b^2(2p + 5)}{x^2 + 5y^2 - b^2(1 - 2p)}. \qquad [31]$$

Replacing y^2 by Q and x^2 by R, we obtain

$$\frac{dQ}{dR} = \frac{5R + Q - b^2(2p + 5)}{R + 5Q - b^2(1 - 2p)}. \qquad [32]$$

Introducing the following change of variables

$$\left.\begin{aligned} R &= \lambda + \frac{b^2}{2}(p + 2); \\ Q &= \mu - \frac{b^2 p}{2}; \end{aligned}\right\} \qquad [33]$$

the differential equation becomes homogeneous:

$$\frac{d\mu}{d\lambda} = \frac{5\lambda + \mu}{\lambda + 5\mu}. \qquad [34]$$

Integration of Eq. [34] yields, after replacement of the variable,

$$\left[\frac{x^2}{b^2} - \frac{y^2}{b^2} - (p + 1)\right]^3 \left[\frac{x^2}{b^2} + \frac{y^2}{b^2} - 1\right]^2 = -k_2. \qquad [35]$$

Transforming to plane polar coordinates, Eq. [35] becomes

$$\left[\frac{r^2}{b^2}\cos 2\phi + (p + 1)\right]^3 \left[\frac{r^2}{b^2} - 1\right]^2 = k_2. \qquad [36]$$

The streamlines for any p can be calculated from Eq. [36] graphically, by plotting the left-hand side of the expression at various fixed values of ϕ versus r/b. The intersections of any constant ordinate with such a family of curves gives the streamlines inside the drop. It should be noted that in plane hyperbolic flow the streamlines inside the drop are independent of p, whereas in shear flow the pattern of internal circulation varies with p, owing to the rotation of the hydrodynamic field.

For $p > \frac{1}{2}$ the streamlines are oval in shape, and their ellipticity decreases with displacement from the origin. A set of streamlines calculated from Eq. [36] for $p = 1$ inside a fluid sphere of unit radius is shown in Fig. 5.

For $p > \frac{1}{2}$, the oval paths of circulation become narrower as the streamlines pass close to the center of the drop.

It follows from Eq. [36] that the left-hand side may have a maximum if $p > \frac{1}{2}$. Taking the first partial derivative with respect to r at constant ϕ, and equating to zero, the maximum will occur when

$$\frac{r^2}{b^2} = \frac{3}{5} - \frac{2(p+1)}{5 \cos \phi}. \qquad [37]$$

Equation [37] has real solutions only if $p < \frac{1}{2}$. When $\phi = 0$, Eq. [37] reduces to

$$\frac{r^2}{b^2} = \frac{3}{5} - \frac{2(p+1)}{5}, \qquad [38]$$

and the two roots of Eq. [38] determine two stagnation points in the fluid. The circulation pattern for $p = \frac{1}{4}$ is illustrated in Fig. 6, where the stagnation points occur at $r/b = \sqrt{0.1}$, corresponding to $\phi = 0$ and $\phi = \pi$. Two distinct "pockets" of circulation exist around these stagnation points close to the center of the drop, which are enveloped by the two loops of

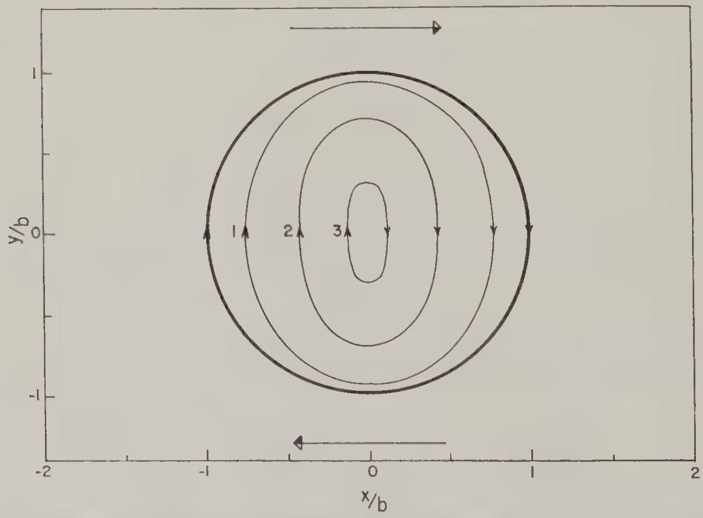

FIG. 5. Circulation inside a fluid sphere in a shear field for $p = 1$. The streamlines are calculated from Eq. [36] for $k_2 = 0.5$ (curve 1), $k_2 = 4.0$ (curve 2), and $k_3 = 7.5$ (curve 3).

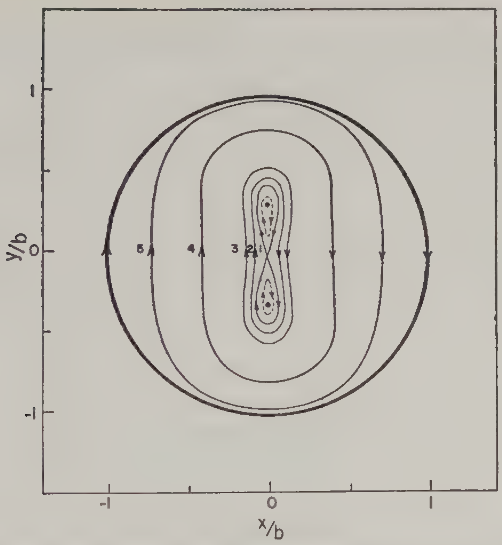

FIG. 6. Circulation inside a fluid sphere in a shear field for $p = \frac{1}{4}$. The streamlines are calculated from Eq. [36] for $k_2 = 1.952$ (curve 1), $k_2 = 1.90$ (curve 2), $k_2 = 1.80$ (curve 3), $k_2 = 0.90$ (curve 4), and $k_2 = 0.10$ (curve 5).

the streamlines passing through the center of the drop. Outside this region the streamlines are oval in shape.

e). *Mean Period of Circulation for* $p > \frac{1}{2}$. The mean period of circulation T_c inside a fluid sphere along a streamline can be calculated in the following manner. Transforming Eq. [31] into polar coordinates the equation of the streamlines is

$$\frac{dr}{d\phi} = \frac{6r\,(r^2/b^2 - 1)\sin\phi\cos\phi}{\frac{5r^2}{b^2}(\cos^2\phi - \sin^2\phi) + 6\sin^2\phi + (2p-1)}. \qquad [39]$$

The velocity component along the X-axis is given by

$$u = \frac{dx}{dt} = \left(r\cos\phi + \sin\phi \cdot \frac{dr}{d\phi}\right)\frac{d\phi}{dt}. \qquad [40]$$

The mean period of circulation can be calculated by substituting $dr/d\phi$ from Eq. [39] and u expressed in polar coordinates from Eq. [40]:

$$u = \frac{Gr\cos\phi}{4(p+1)}\left(\frac{5r^2}{b^2} - \frac{4r^2\sin^2\phi}{b^2} + 2p - 1\right)$$

and integrating the result.

To facilitate the mathematics, T_c will be calculated for $p > \frac{1}{2}$ and for positions close to the center of the drop, so that terms which contain $(r/b)^2$

TABLE II

Period of Circulation Close to the Center of a Fluid Sphere

$p > \frac{1}{2}$

$(z = 0,\ r^2 = x^2 + y^2)$

p	$\frac{T_cG}{4\pi}$	$\frac{T_c}{T}$
1.0	1.51	1.31
1.5	1.25	1.15
2.0	1.15	1.08
5.0	1.03	1.02
10.0	1.01	1.005
100.0	1.000	1.000

can be neglected. Thus

$$\frac{dr}{d\phi} = -\frac{6r \sin \phi \cos \phi}{6 \sin^2 \phi + (2p - 1)} \qquad [41]$$

and

$$u = \frac{Gr \cos \phi(2p - 1)}{4(p + 1)} \qquad [42]$$

for $r \ll b$, $p > \frac{1}{2}$ in the plane $z = 0$. Substituting for $dr/d\phi$ and u from Eq. [41] and [42], respectively, Eq. [40] yields for the first quadrant

$$\int_0^{T_c/4} \frac{G}{4} \frac{dt}{(p + 1)} = \int_0^{\pi/2} \frac{d\phi}{6 \sin^2 \phi + (2p - 1)}. \qquad [43]$$

Integration of the above expression results in the relation

$$\frac{T_cG}{4\pi} = \frac{2(p + 1)}{\sqrt{(2p + 5)(2p - 1)}} \qquad [44]$$

for $p > \frac{1}{2}$ near the center of a drop.

It follows from Eq. [44] that as $p \rightarrow \infty$, $T_cG/4\pi = 1$, which corresponds to the exact equation for rigid spheres. In Table II values of $T_cG/4\pi$ for various values of p ($> \frac{1}{2}$) are shown and are compared with the corresponding values of $TG/4\pi$ at the surface of the drop calculated from Eq. [29]. For a given value of p, the mean period of circulation is greater inside the drop than at its surface since

$$\frac{T}{T_c} = \frac{1}{2}\sqrt{\frac{4p^2 + 8p - 5}{p^2 + 2p}}$$

and $(4p^2 + 8p - 5)/(p^2 + 2p) < 4$ for any finite value of $p > \frac{1}{2}$.

Acknowledgment

The authors are indebted to Dr. W. C. G. Fraser, Computation Centre, University of Toronto for assistance in the solution of Eq. [31].

SUMMARY

Equations are derived for the streamlines inside and outside a viscous fluid sphere suspended at the origin of an infinite body of an immiscible viscous liquid which is undergoing plane-hyperbolic deformation using a set of equations for velocity components derived by G. I. Taylor. By means of a simple transformation, the same set of equations has been used to determine the streamlines inside and outside a liquid drop undergoing laminar shear flow. Equations are also derived for the time of internal circulation for streamlines close to the surface and near the center, respectively.

REFERENCES

1. EINSTEIN, A., *Ann. Physik* **19,** 289 (1906); *ibid.* **34,** 591 (1911).
2. TAYLOR, G. I., *Proc. Roy. Soc. (London)* **A138,** 41 (1932).
3. HADAMARD, J., *Compt. rend.* **152,** 1735 (1911).
4. RYBYCZYNSKI, W., *Bull. acad. sci. Cracovie* **1,** 40 (1911).
5. BOUSSINESQ, J., *Ann. Chem. Phys.* **29,** 364 (1913).
6. BOND, W. N., *Phil. Mag.* [Ser. 7] **4,** 889 (1927).
7. BOND, W. N., AND NEWTON, D. A., *Phil. Mag.* [Ser. 7] **5,** 794 (1928).
8. GARNER, F. H., *Trans. Inst. Chem. Engrs. (London)* **28,** 88 (1950).
9. GARNER, F. H., AND HAMMERTON, D., *Chem. Eng. Sci.* **3,** 1 (1954).
10. GARNER, F. H., AND SKELLAND, A. H. P., *Chem. Eng. Sci.* **4,** 149 (1955).
11. HABERMAN, W. L., AND MORTON, R. K., Report 802, Navy Department, The David W. Taylor Model Basin, Washington, 1953.
12. SAVIC, P., Report No. MT-22, National Research Council of Canada, Ottawa, 1953.
13. BURGERS, J. M., Second Report on Viscosity and Plasticity, p. 129, Academy of Sciences, Amsterdam, 1938.
14. TREVELYAN, B. J., AND MASON, S. G., *J. Colloid Sci.* **6,** 354 (1951).
15. MANLEY, R. ST. J., AND MASON, S. G., *J. Colloid Sci.* **7,** 354 (1952).

JOURNAL OF COLLOID SCIENCE **13**, 308–328 (1958)

SOLUTION PROPERTIES OF BRANCHED DEXTRANS

Kirsti A. Granath

Institute of Physical Chemistry, University of Uppsala, and Research Laboratory, Pharmacia Ltd., Uppsala, Sweden

Received May 27, 1957; revised December 23, 1957

The class of polysaccharides called dextrans consists of a great variety of α-polyglucosans produced by *Leuconostoc mesenteroides* and closely related bacteria under suitable environmental conditions. Jeanes *et al.* (1) have made an extensive study of the chemical structure of dextrans from many bacterial strains and have established the structural dependence of the dextran upon the causative bacterial strain.

The present paper deals with a study of the solution properties of dextrans having various degrees of branching, and was carried out in order to obtain a more complete picture of the hydrodynamic behavior of branched polymer molecules. Measurements have been made on the viscosity, light-scattering, sedimentation, and other solution properties, and results have been compared with those of Wales *et al.* (2, 3), Senti *et al.* (4), and Ogston and Woods (5).

Experimental

The materials used were two structurally different dextrans. One, designated B512-Ph, was a partially hydrolyzed native dextran produced in Sweden from *Leuconostoc mesenteroides* NRRL-B512; the other, designated A179, was clinical type dextran produced in Germany. It has been established (6) that dextran from the NRRL-B512 strain has 5% branch points; the A179 dextran appears to be more highly branched.

The clinical dextran was fractionated without any further treatment; the partially hydrolyzed native B512-Ph dextran was purified by several reprecipitations prior to fractionation. Both materials were separated into fractions by the method of fractional precipitation in several stages with ethanol as precipitant.

For the characterization of the fractions and for the comparison of the solution properties of the two different dextrans determinations were made of degree of branching, viscosity number, and average molecular weight on a number and weight basis. On several of the fractions sedimentation and diffusion coefficients were also measured.

Degree of Branching

In order to study branching properties of the dextrans, formic acid produced on periodate oxidation was measured. This method, of course, does not differentiate the nonreducing end groups from the 1,6-linked glucose units (1), so in reality the so-called 1,6-linked units here include both of these types of units. Furthermore, the method obviously gives the maximum degree of branching, since some of the non-1,6-linked units may be in the main chain and not necessarily at a branch point.

A slight modification of the periodate oxidation method of Jeanes and Wilham (7) was used. After drying the samples at 100°C. in a vacuum, they were dissolved in water and the amount of dextran in solution was checked by the anthrone method (8). The formic acid produced was titrated with 0.1 N NaOH using an Agla-micrometer buret. Titrations were made in a carbon dioxide free nitrogen atmosphere with phenolphthalein as indicator and the solutions were stirred magnetically.

For fractions of high molecular weight the ratio of the observed amount of formic acid produced on periodate oxidation to the theoretical amount for a dextran consisting of entirely 1,6-linked units, where 1 mole formic acid is produced per anhydrous glucose unit, gives the proportion of 1,6-linked glucose (plus terminal nonreducing) units in the molecules. However, if the amount of 6-linked terminal reducing end groups is not negligible in the sample ($M_n < 200\ 000$), a correction has to be made for the amount of formic acid produced by these end groups (9).

By carefully controlling the technique and making duplicate determinations, the average error in the experimental values of per cent 1,6-linkages could be reduced to ±0.3%.

The fractions selected for use in this study did not vary in content of 1,6-linkages more than ±1%; no effect of this variation upon the solution properties could be observed. The average amount of 1,6-linkages was 94.2% and 69.7% in dextran B512-Ph and A179, respectively.

Viscosity Numbers

The viscosities of the aqueous solutions of the dextran fractions were measured in an Ostwald viscometer at 20 ± 0.01°C. The solutions were filtered through a sintered glass filter and dilutions were carried out in the viscometer. The shear dependence was found to be negligible in the range of molecular weights investigated. The kinetic energy correction was small and could be neglected. In Tables II and III the results are collected.

Simha (10, 11) has pointed out that the value of k' in Huggins' equation

$$\eta_{sp/c} = |\eta| + k'|\eta|^2 c$$

depends upon the shape of the molecules. It should be increased by branching and cross-linking but should be independent of molecular weight as long as the coiling does not change. Experimental findings confirm the theoretical predictions of the influence of branching on k' (12–14). However, for dextran, Senti *et al.* (4) obtained a definite increase in k' with molecular weights $>4 \times 10^5$. However, the viscosity exponent a decreased simultaneously, indicating that the molecules become more compact coils.

For the dextrans investigated here, no dependence of k' on molecular weight was obtained. It appears that a very large amount of measurements would be required to decide if k' varies with the degree of branching for dextrans. In Table I are tabulated average values of k', as calculated from measurements on 20 to 100 fractions of each type of dextran listed. Some dependence of k' on branching (as measured by the value of the exponent a in the viscosity-molecular weight relation) can be noticed. Sample B65 is a condensation product of glucose, and it is quite possible that the high degree of cross-linking might be partly responsible for the high value of k' in this case.

Average Molecular Weights

The number average molecular weights, M_n, were determined by the Somogyi phosphate method (15). In this alkaline copper phosphate reagent is reduced by the terminal aldehyde groups of the polysaccharide. Isomaltose and isomaltotriose are expected to have the same equimolecular reducing power as dextran and were here used as standards in the computation of M_n. Determinations were made at least in duplicate and the reproducibility was within ±3%.

The weight-average molecular weights, M_w, were determined by light scattering. Some of the measurements were carried out in a Brice-Speiser light-scattering photometer (16), but in most cases a photometer built at this Institute was used (17, 18). The turbidity for Debye's polystyrene standard was in both photometers $\tau = 3.50 \times 10^{-3}$ cm.$^{-1}$ at 436 mμ, and measurements on the same fraction gave identical results in both photometers.

The solutions were clarified by filtering through sintered Jena G5 filters and Zsigmondy membrane "fein" filters. The water used for solutions was freshly distilled in a double distilling quartz column. A stock solution was prepared, filtered, and measured. Then its concentration was determined

TABLE I

Viscosity Coefficient k' as a Function of a

Sample	k'	a
B512-NRRL (4) $M < 250{,}000$	0.50 ± 0.01	0.50
B512-Ph	0.53 ± 0.02	0.43
A179	0.57 ± 0.02	0.37
B65	0.85 ± 0.03	0.31

from the optical rotation. The values of $(\alpha)_D^{20}$ were +199° and +206.7° for B512-Ph and A179, respectively. At least three solutions were prepared by successive dilutions of the stock solution; they were filtered directly into the cell and their turbidity was measured at 436 mμ. The value used for the refractive index increment at this wavelength was 0.151 ml./g. (19). From the $(Hc/\tau, c)$-plot the molecular weight, M_w, and second virial coefficient, A_2, were obtained. The results are compiled in Tables II and III and some representative measurements are shown in Fig. 1.

Sedimentation and Diffusion Measurements

The sedimentation measurements were made in a Svedberg oil turbine ultracentrifuge at 260.000 *g*. The buffer was 0.05 *N* Na_2HPO_4 + 0.05 *N*

TABLE II

Molecular Weights, Viscosity, Sedimentation, and Diffusion Data for Fractions of B512-Ph Dextran

No.	$\|\eta\|$	$M_w\times10^{-3}$	$M_n\times10^{-3}$	M_v	$s_0\times10^{13}$	$D_A\times10^7$	$M_{s,D}\times10^{-3}$	f/f_0
1	0.666	723	263	537	—	—	—	—
2	0.624	526	305	446	9.82	1.40	437	3.22
3	0.464	265	199	251	6.75	2.11	200	2.77
4	0.462	257	235	246	6.35	2.20	181	2.75
5	0.419	193	136	176	5.62	2.22	159	2.84
6	0.397				5.17	2.52	129	2.69
7	0.385				5.45	2.57	133	2.60
8	0.368				4.71	2.62	113	2.70
9	0.338				5.0	2.84	110	2.51
10	0.324	116,4	74	101	4.27	2.89	92.5	2.61
11	0.274				3.95	3.65	67.8	2.30
12	0.248	38			—	—	—	—
13	0.242				3.52	4.24	52	2.16
14	0.206	37.9	26.3	33.5	2.93	4.92	37.3	2.08
15	0.191				2.76	4.91	35.2	2.12
16	0.165				2.44	5.58	27.4	2.03
17	0.160	21.6	17	20	—	—	—	—
18	0.140				1.96	6.20	19.8	2.03
19	0.105				1.57	8.80	11.2	1.74

TABLE III

Molecular Weights, Viscosity, Sedimentation, and Diffusion Data for Fractions of A179 Dextran

No.	$\|\eta\|$	$M_w\times10^{-3}$	$M_n\times10^{-3}$	$M_v\times10^{-3}$	$s_0\times10^{13}$	$D_A\times10^7$	$M_{s,D}\times10^{-3}$	f/f_0
A_1	0.293	213	118.6	178	4.73	2.30	125	2.98
A_2	0.260	137	96	123	4.05	2.95	84	2.66
A_3	0.214	87.8	67.4	79.5	3.47	(3.52)[a]	60.2	2.48
A_4	0.194	65.4	53.7	61	3.21	3.95	49.6	2.36
A_5	0.165	39.8	29	35.5	2.55	(5.40)	28.8	2.07

[a] Interpolated values.

NaH_2PO_4. Sedimentation coefficients, s, were determined at four concentrations. Diffusion measurements were made at three concentrations in a diffusion cell according to Claesson (20). Within the limit of the experimental error the value of the diffusion coefficient was found to be independent of concentration. The values of sedimentation and diffusion coefficients were reduced to the standard conditions of water at 20°C. Figure 2 shows some plots of reciprocal sedimentation coefficients vs. concentration. The partial specific volume in the buffer used had the values 0.611 ± 0.002 and 0.603 ± 0.003 for dextran B512-Ph and for A179, respectively. Molecular weights, $M_{s,D}$, were calculated with the aid of Svedberg's formula

$$s_0 = \frac{M(1 - \bar{V}\rho)}{Nf}, \quad \text{or} \quad M = \frac{RTs_0}{D_A(1 - \bar{V}\rho)},$$

using the mean value of the diffusion constants, calculated by the area method D_A. Values of s_0, D_A, and $M_{s,D}$ are given in Tables II and III.

HETEROGENEITY

From the M_n- and M_w-values in Tables II and III it is evident that the fractions are not homogeneous. As all theories of polymer solutions are valid only for sharp fractions it is necessary to correct the data for the effects of polymolecularity. For this purpose a knowledge of a frequency function of the molecular weights is required. Following other workers (2–4) it is convenient to assume the Lansing-Kraemer distribution in the fractions. Figure 3 shows a comparison between the theoretical L-K dis-

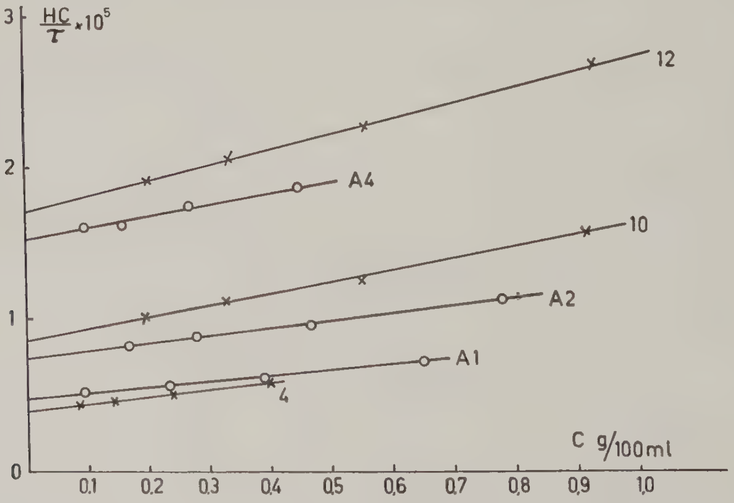

FIG. 1. Plots of $\frac{H_c}{\tau}$ vs. c for some fractions of B512-Ph and A179 dextran.

tribution for a clinical batch of B512-Ph dextran of known M_w and M_n, and the distributions of the same sample as determined experimentally by turbidimetry and extraction fractionation. The agreement is good, thus supporting the assumption of the *L-K* distribution.

RESULTS

The experimental results are collected in Tables II and III, and in Figs. 4 and 5 logarithmic plots are given of $|\eta|$ vs. molecular weight and log s_0

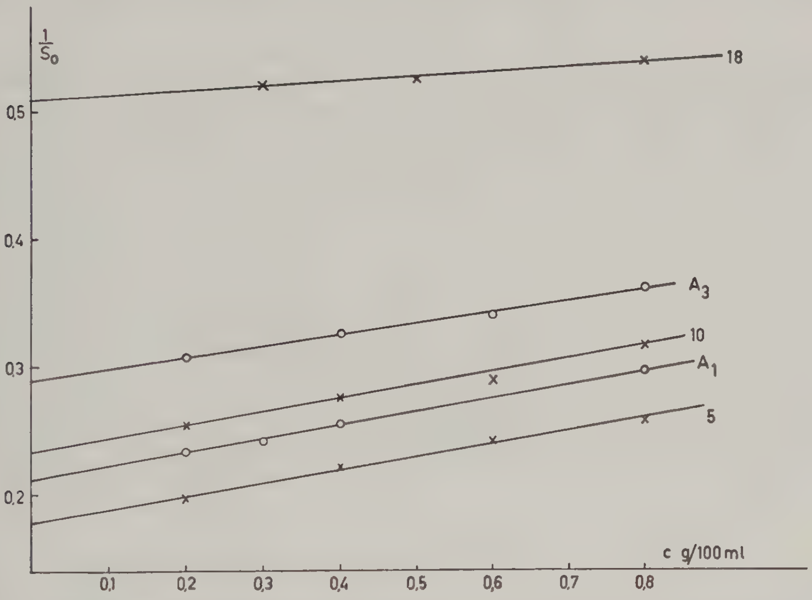

FIG. 2. Reciprocal sedimentation coefficients as a function of concentration for some fractions of B512-Ph and A179 dextran.

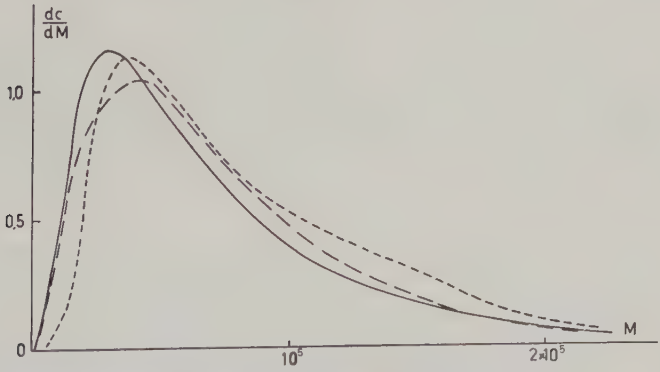

FIG. 3. Molecular weight frequency curves of a dextran sample. ——— Lansing-Kraemer distribution, calculated from M_w and M_n; – – – Turbidimetrically determined distribution; ---------- Distribution obtained by extraction fractionation.

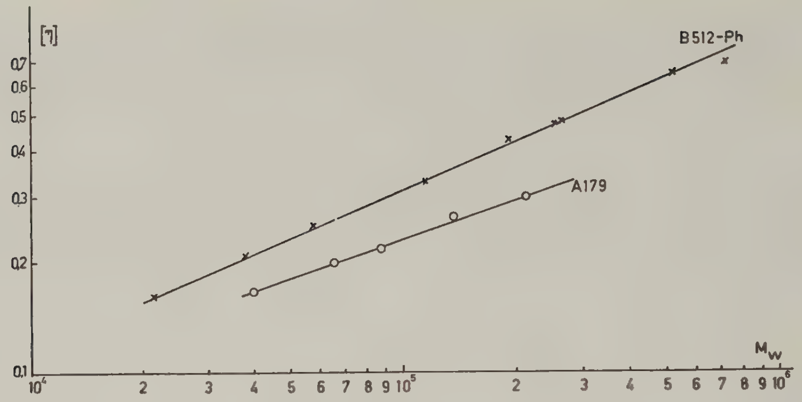

FIG. 4. Log-log plot of viscosity number vs. M_w for fractions of B512-Ph and A179 dextran.

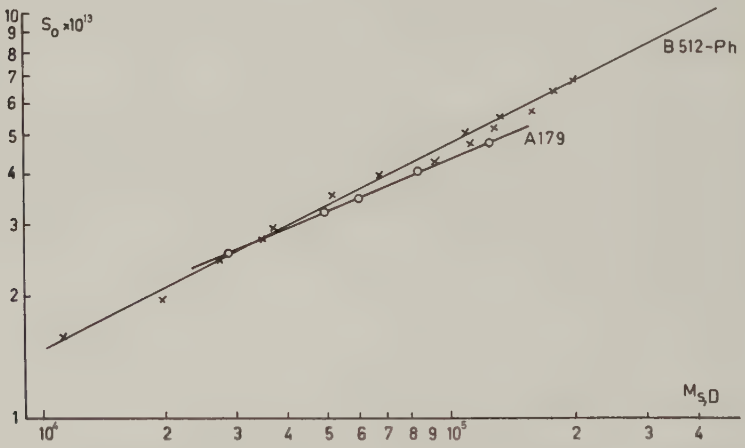

FIG. 5. Double logarithmic plot of sedimentation coefficient against $M_{s,D}$ for fractions of B512-Ph and A179 dextran.

vs. log $M_{s,D}$, respectively. With respect to the relation between the viscosity number and molecular weight the heterogeneity of the fractions makes it most correct to use the viscosity-average molecular weight, defined by

$$M_v = M_0 e^{\frac{1}{4}\beta^2(a+2)},$$

where M_0 and β are parameters of the *L-K* distribution function and a is the exponent in the viscosity-molecular weight relation. The straight lines in these figures are represented by the equations below

B512-Ph	*A179*
$\mid \eta \mid = 2.43 \times 10^{-3} M_w^{0.42}$	$\mid \eta \mid = 4.4 \times 10^{-3} M_w^{0.34}$
$\mid \eta \mid = 2.23 \times 10^{-3} M_v^{0.43}$	$\mid \eta \mid = 3.5 \times 10^{-3} M_v^{0.37}$

$$|\eta| = 0.74 \times 10^{-3} M_{s,D}^{0.53} \qquad |\eta| = 2.7 \times 10^{-3} M_{s,D}^{0.40}$$

$$s_0 = 1.45 \times 10^{-15} M_{s,D}^{0.50} \qquad s_0 = 3.43 \times 10^{-15} M_{s,D}^{0.42}$$

$$f \sim \frac{M}{s_0} = \sim M^{0.50} \qquad f = \sim M^{0.58}$$

Obviously the molecular weight exponents in these equations are quite remarkably influenced by the degree of branching. A similar influence has been found for branched polystyrenes (21).

DISCUSSION

Wales *et al.* (2, 3) and Senti *et al.* (4) have discussed the evidence for and against a nonrandom distribution of branches in dextran molecules. Furthermore it appears from their results that the Flory-Fox (22–25) viscosity theory for linear molecules is not applicable to branched dextrans. The experimental data obtained in the present and in above-mentioned investigations will now be treated in the light of a more general theory. For this purpose the Stockmayer modification (26, 27) of the Flory-Fox viscosity theory will be used. The ratio, Φ'/P', the radius of gyration, $\sqrt{\overline{R^2}}$, and the effective hydrodynamic radius, R_h, have been calculated for the dextrans here investigated, and compared with results of Senti *et al.* The effect of branching on the thermodynamic properties of dextran, as reflected in the unusual behavior of the second virial coefficient, is considered. Finally the effective bond length, b, is calculated, and the shape of dextran molecules is discussed.

Solution Properties and Branching

The Flory relationship for the viscosity number of flexible linear polymers is

$$|\eta|_{lin} = \Phi(\sqrt{\overline{L^2}})_0^3 \alpha^3 M^{-1} = \Phi'(\sqrt{\overline{R^2}})^3 M^{-1}, \tag{1}$$

where $(\sqrt{\overline{L^2}})_0$ is the unperturbed mean end-to-end distance, $\sqrt{\overline{R^2}}$ is the radius of gyration, and Φ is a universal constant.

In order to relate branched and unbranched polymers of the same chemical structure, Zimm and Stockmayer (28) introduced a parameter, g, defined by

$$g = \frac{(\sqrt{\overline{R^2}})_{0br}^2}{(\sqrt{\overline{R^2}})_{0lin}^2}. \tag{2}$$

With the use of this relation, Eq. [1] could then be generalized to be valid for any random flight chain polymer as follows (2):

$$|\eta| = \Phi'(\sqrt{\overline{R^2}})^3 M^{-1} = K M^{1/2} g^{3/2} \alpha^3. \tag{3}$$

Stockmayer (27) modified Eq. [1] to the more general form

$$|\eta| = \Phi(\sqrt{\overline{L^2}})_0^3 \alpha_r^2 \alpha_h M^{-1} = \Phi'(\sqrt{\overline{R^2}})^2 R_h M^{-1}, \qquad [4]$$

where R_h is the hydrodynamic radius and α_r and α_h are expansion factors corresponding to $\sqrt{\overline{R^2}}$ and R_h in nonideal solvents. According to Stockmayer, α_h is slightly smaller than α_r. Hence for linear polymers with increasing excluded volume effect, R_h should increase less rapidly than $\sqrt{\overline{R^2}}$. This has been experimentally confirmed by Krigbaum and Carpenter (29).

The effect of branching on the hydrodynamic radius, R_h, is by Stockmayer described by the ratio

$$h = \frac{(R_h)_{0br}}{(R_h)_{0lin}}, \qquad [5]$$

Using a cruciform molecule as a model Stockmayer (26) has shown that $h > \sqrt{g}$, i.e., the hydrodynamic radius is less sensitive to branching than the radius of gyration (Eqs. [2] and [5]).

For cruciform molecules of high molecular weight

$$h = \sqrt{f}/(2 - f + \sqrt{2}(f - 1)); \qquad [6]$$

$$g = (3f - 2)/f^2, \qquad [7]$$

where f is the number of branches. The relation between g, h, and gh is shown in Fig. 6.

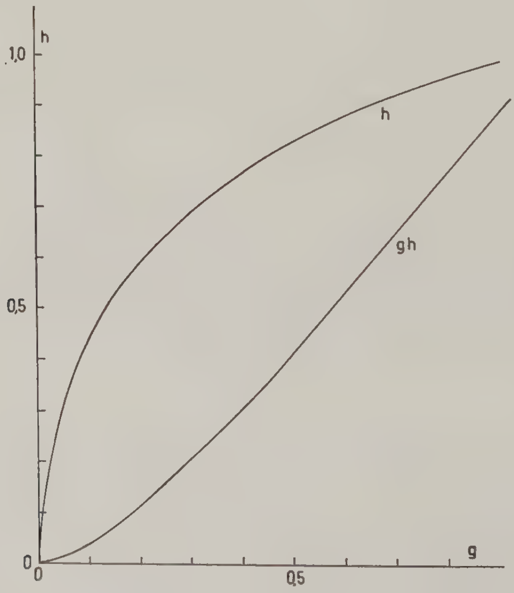

Fig. 6. Plot of h vs. g [cf. Eqs. (3) and (8)].

Assuming the above relationships (Eqs. [6] and [7]) to be generally applicable for branched molecules, then, if $\Phi_{lin} = \Phi_{br}$ and also α is independent of branching, it follows from Eqs. [2], [4], and [5]

$$gh = \frac{|\,\eta\,|_{br}}{|\,\eta\,|_{lin}}. \qquad [8]$$

In the range of gh values occurring in the investigations referred to here, log g, and then also log h, is a linear function of log M. The function log g vs. log M_v is illustrated by Fig. 7.

Introducing Eq. [8] in good solvents Eq. [4] becomes

$$|\,\eta\,| = KM^{1/2}gh\alpha^3, \qquad [9]$$

or, expressing the different parameters as functions of molecular weight,

$$|\,\eta\,| \sim M_v^{0.5+3a_\alpha+a_g+a_h}, \qquad [10]$$

$$(\sqrt{\overline{R^2}})^2 \sim M_v^{1+2a_\alpha+a_g}; \qquad [11]$$

$$R_h \sim M_v^{0.5+a_\alpha+a_h}. \qquad [12]$$

It should perhaps be pointed out that these relations assume Flory constants Φ and P to be constant. If this is not true then the terms a_Φ and a_p must also be included in the exponent in Eqs. [10] and [12].

From measurements of viscosity and molecular weight in a Θ-solvent, Wales *et al.* (2, 3) determined K and g in Eq. [3], according to the relation

$$|\,\eta\,|^{2/3}M^{-1/3} = gK^{2/3} \qquad [13]$$

for two dextrans of very different degree of branching, B512 and B742. On the basis of experimental data for B512 dextran in water the expansion

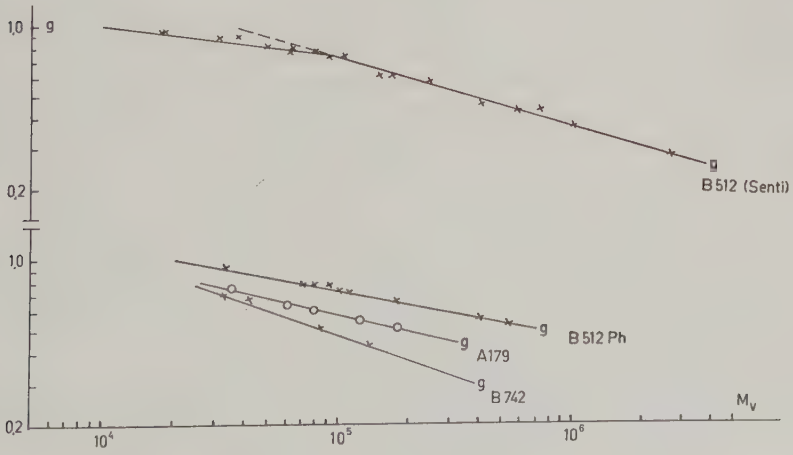

FIG. 7. Plot of log g vs. log M_v for some dextrans.

factor α was related to molecular weight as

$$\alpha^3 = 0.2\, M^{0.175}. \qquad [14]$$

Assuming α to be insensitive to branching, the viscosity number of hypothetical linear dextran in water was calculated to be

$$|\,\eta\,|_{lin} = 1.99 \times 10^{-4} M^{0.675}. \qquad [15]$$

Senti *et al.* (4) determined the molecular weight-viscosity relation for a dextran B512-NRRL, similar to one of the materials used by Wales, using 24 fractions which covered the range $1.7 \times 10^4 < M_w < 9.5 \times 10^6$. The relation was linear only for $M_w < 10^5$ and was in agreement with the results of Wales for the same M_w-range. The *z*-average radius of gyration, R_z, was calculated from light scattering for fractions covering the range $4 \times 10^5 < M_w < 2.7 \times 10^6$. By means of this radius, corrected for the polydispersity of the fractions, they obtained the value of 55.2×10^{21} for the proportionality constant Φ'. For linear polymers the accepted value for Φ' is 30.8×10^{21}. As Senti *et al.* point out, this difference should indicate that different relations exist for linear and branched molecules between the root-mean-square radius from light-scattering measurements and the hydrodynamic radius effective in viscosity. At the same time the value of the quotient $(\Phi')^{1/3}/P'$ was found to be $2.0 \times 10^6 \pm 0.1 \times 10^6$ as compared to 2.5×10^6 usually found for linear polymers. Finally Senti *et al.* suggest that the *g*-values given by Wales should be corrected by multiplying them with the factor $(30.8/55.2)^{2/3}$; they then proceed to discuss the structure of dextran on the basis of these corrected values.

Other workers have also encountered anomalies in viscosity parameters when working with branched molecules. For example, Arond and Frank (30) in a study of native dextran found Φ' to decrease with increasing molecular weight and interpreted this result as being due to variations in the heterogeneity and degree of branching of the fractions. Thurmond and Zimm (31) have reported similar effects for branched polystyrenes.

The Stockmayer treatment, as referred to above, apparently obviates some of these discrepancies. The results obtained by analyzing the experimental data from the present investigation as well as those of Wales *et al.* (2, 3) and Senti *et al.* (4) are collected in Table IV.

In order to apply Eqs. [10], [11], and [12] to dextran it is necessary to know the viscosity number as a function of molecular weight for hypothetical linear dextran. For this purpose we use the relation given by Wales (Eq. [15]). Our aim is now to arrive at values of $\sqrt{\overline{R^2}}$ and R_h for the dextrans investigated. This was done as follows.

With $|\,\eta\,|_{br}$ known from the experimental data and $|\,\eta\,|_{lin}$ from Eq. [15], *gh* is calculated from Eq. [8]. The corresponding values of *g* and *h* are then readily obtained from Fig. 6 and are expressed in Table IV as func-

TABLE IV

Molecular Parameters According to Eqs. [10], [11], and [12] Calculated for Different Dextrans

Sample	$[\eta]$	g_h	g	$\sqrt{\overline{R^2}} \times 10^8$	$R_h \times 10^8$	% 1, 6 linkages
Linear dextran (2)	$1.99 \times 10^{-4} M^{0.675}$	1.0	1.0	$0.19 M^{0.56}$	$0.19 M^{0.56}$	
B512-NRRL (4), $M < 10^5$	$9.78 \times 10^{-4} M_v^{0.50}$	$4.90 \; M_v^{-0.17}$	$3.9 M_v^{-0.14}$	$0.37 M_v^{0.48}$	$0.24 M_v^{0.53}$	95.2
B512-NRRL (4), $M > 10^5$	$1.3 \times 10^{-2} M_v^{0.28}$	$65.4 \; M_v^{-0.39}$	$22.9 M_v^{-0.30}$	$0.83 M_v^{0.41}$	$0.54 M_v^{0.47}$	95.2
B512-Ph, $M < 5 \times 10^5$	$2.23 \times 10^{-3} M_v^{0.43}$	$11.2 \; M_v^{-0.24}$	$6.8 M_v^{-0.19}$	$0.50 M_v^{0.46}$	$0.31 M_v^{0.51}$	94.2
A179, $M < 2 \times 10^5$	$3.5 \times 10^{-3} M_v^{0.37}$	$17.6 \; M_v^{-0.31}$	$9.1 M_v^{-0.24}$	$0.57 M_v^{0.44}$	$0.42 M_v^{0.49}$	69.7
B742 (3), $M < 2 \times 10^5$	$2.3 \times 10^{-2} M_v^{0.18}$	$116.0 \; M_v^{-0.50}$	$34.7 M_v^{-0.36}$	$1.12 M_v^{0.38}$	$0.64 M_v^{0.42}$	~57

tions of M. For linear dextran $g = h = 1$, and because the difference between α_h and α_r is neglected, then $(\sqrt{\overline{R^2}})_{lin} = (R_h)_{lin}$. On the assumption that the value for the Flory constant in good solvents ($\Phi \doteq 2.1 \times 10^{21}$) (29) is valid for linear dextran in water, then numerical values of $(\sqrt{\overline{R^2}})_{lin} = (R_h)_{lin}$ can be calculated from Eq. [4]. Thence using Eqs. [3] and [5] values of $\sqrt{\overline{R^2}}$ and R_h may be obtained for branched dextran.

For B512-NRRL dextran in the M_w-range $10^5 - 2.7 \times 10^6$ the relation $|\eta| = 1.3 \times 10^{-2} M_w^{0.28}$ represented the experimental data fairly well, and from it the corresponding $\sqrt{\overline{R^2}}$ and R_h values shown in Table IV were calculated. At $M > 10^5$ this dextran behaves as if it is rather highly branched. Possibly it reaches a coil density similar to that of a dextran with lower molecular weight but higher degree of branching.

In Fig. 8 log $|\eta|$ is plotted against log M_v for the dextrans mentioned in Table IV. In the molecular weight range investigated this relation is linear for B512-Ph, A179, and B742. All these lines in Fig. 8, if extended, cross the line for linear dextran between $1.0 \times 10^4 < M < 2.0 \times 10^4$; it is obvious that such an occurrence is unrealistic. It seems most probable that the lines should curve downwards at lower molecular weights, not least because it has been found that branching in dextrans diminishes rapidly when M approaches 10^4 (32).

It is of interest to compare the radii of gyration calculated from the Stockmayer treatment with those obtained directly from light-scattering measurements. For this purpose the data of Senti *et al.* (*cf.* Fig. 8) were used. (For the dextrans investigated here the molecular weights were too low to obtain accurate R_z-values.)

In Fig. 9 a comparison is made between these calculated $\sqrt{\overline{R^2}}$ values

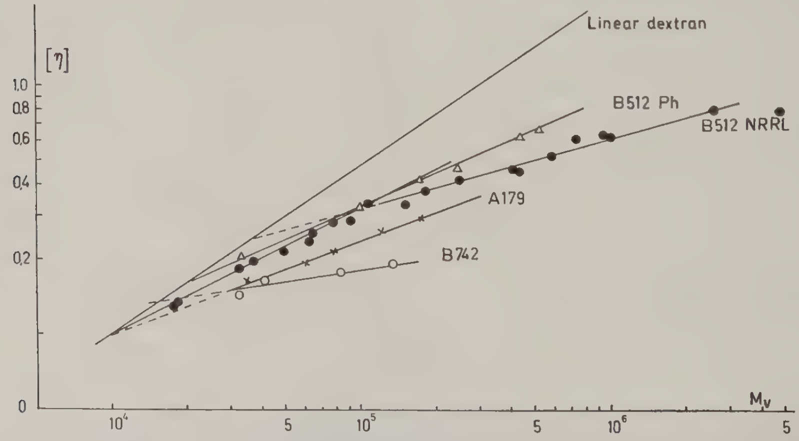

FIG. 8. Log-log plots of $|\eta|$ vs. M_v for some branched dextrans and for a hypothetical linear dextran.

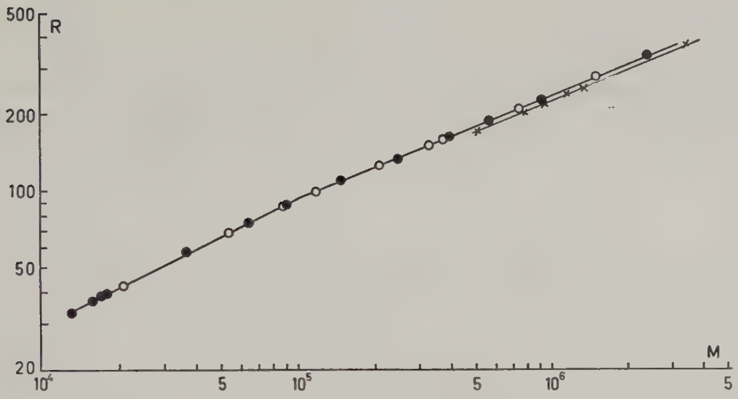

FIG. 9. Log-log plot of radius of gyration as a function of M. ● = $\overline{R^2}$ vs. M_v; ○ = $\overline{R^2}$ vs. M_0; × = R_z vs. M_z.

and the corresponding R_z-values obtained by Senti *et al.* from light scattering. The question arises as to what kind of average is represented by these calculated $\sqrt{\overline{R^2}}$ values. Applying a polydispersity correction on the basis of the *L-K* distribution function one obtains

$$\overline{R_0}^2 = \overline{R^2}(e^{-1/4\beta^2 a(a+2)}) \left(\frac{M_0}{M_v}\right)^{\gamma}, \qquad [16]$$

where a is the exponent in the relation $|\eta| = KM_v^a$ and γ is defined by $M_v^{\gamma} \sim M_v/R_h$. The relation $\sqrt{\overline{R_0}^2}$ vs. M_0 is also plotted in Fig. 9. Strictly speaking only corresponding averages may be compared, and therefore in Fig. 9 R_z has been plotted against M_z, which was obtained from the values of M_n and M_w given by Senti *et al.*, assuming a *L-K* distribution. The calculated and observed radii of gyration differ systematically by about 4%, which, however, is within the limits of the experimental error. The agreement is therefore satisfactory and strongly supports the validity of applying the Stockmayer equations to dextran molecules.

Evaluation of Φ'/P'

Mandelkern *et al.* (33) have shown that the frictional coefficient may be represented by the relationship

$$f/\eta_0 = P' \sqrt{\overline{R^2}}, \qquad [17]$$

where P' is a universal constant analogous to Φ' of the viscosity theory and η_0 is the viscosity of the solvent. By combining Eq. [17] with Eq. [1] and the Svedberg sedimentation equation the following relation between the sedimentation coefficient and viscosity number is obtained:

$$\frac{s_0 |\eta|^{1/3}}{M^{2/3}} = \frac{(\Phi')^{1/3}}{P'} \frac{1 - \bar{V}\rho}{N\eta_0}. \qquad [18]$$

As pointed out above, the accepted value for $(\Phi')^{1/3}/P'$ is 2.5×10^6 (33, 34) for linear polymers. It is to be noted, however, that Eqs. [1] and [17] are valid only for linear polymers, and therefore Eq. [18] should not be expected to be a priori applicable to branched polymers. According to Stockmayer, in the case of branching Eq. [17] becomes

$$f/\eta_0 = P'R_h, \qquad [19]$$

where R_h has the previously mentioned significance. Combining this with Eq. [4] and the Svedberg equation it follows that

$$\frac{s_0 \mid \eta \mid}{(\sqrt{\overline{R^2}})^2} = \frac{\Phi'}{P'} \frac{1 - V\rho}{N\eta_0}. \qquad [20]$$

In Table V are given the values of $(\Phi')^{1/3}/P'$ and Φ'/P', calculated from the data in Tables II, III, and IV using Eqs. [18] and [20], respectively. The effects of polydispersity have been taken into consideration by modifying the left-hand side of Eq. [18] to $\frac{s_0 \mid \eta \mid^{1/3} M_v{}^{1/3}}{M_{s,D}}$ and of Eq. [20] to

$$\frac{s_0 \mid \eta \mid M_v}{M_{s,D}(\sqrt{\overline{R^2}})^2}.$$

For B512-NRRL s_0 values were correlated to M_v instead of $M_{s,D}$, which could not be calculated through lack of diffusion data. This correlation is of course not quite correct, and might be partly responsible for the observed decrease of $(\Phi')^{1/3}/P'$ with M.

It is seen (Table V) that the ratio Φ'/P' is constant within the limits of the experimental error for the dextrans investigated. The numerical value of this ratio is in good agreement with the corresponding value for linear polymers, thus supporting that Φ' of linear polymers can be used for branched dextrans if a correction term h is introduced into the viscosity equation as suggested by Stockmayer.

Second Virial Coefficient and Branching

The second virial coefficient, A_2, was determined in order to study the influence of branching on the thermodynamic properties.

Earlier experiments confirm the theories of Zimm (35), Stockmayer (26),

TABLE V

Values of $\frac{(\Phi')^{1/3}}{P'}$ *and* $\frac{\Phi'}{P'}$ *for Some Dextrans*

Sample	$\frac{(\Phi')^{1/3}}{P'} \times 10^{-6}$	$\frac{\Phi'}{P'} \times 10^{-21}$
B512-NRRL	2.1 to 1.6	2.2 ± 0.1
B512-Ph	2.3 ± 0.1	2.2 ± 0.1
A179	2.3 ± 0.1	2.3 ± 0.1

and Flory-Krigbaum (36) that A_2 decreases with branching. Figure 10 shows that the above predictions are verified also for dextrans.

By combining Zimm's single contact theory with Flory's viscosity theory Krigbaum (37) has shown that for linear macromolecules the following relationships are valid:

$$A_2M_w/|\eta| \approx 160 \qquad [21]$$

and

$$A_2M_w^2/(\sqrt{\overline{R_w^2}})^3 \approx 4.4 \times 10^{24}. \qquad [22]$$

For polyvinylacetate in good solvents the constancy of Eqs. [21] and [22] has been verified by Shultz (38). Similar conclusions can be drawn from the published data for gelatin (39) and polyvinylpyrrolidone (40) in water.

In Fig. 11 $A_2M_w/|\eta|$ is plotted against M_w for some dextrans. For A179 and B512-Ph the quotient is constant and has the approximative values of 110 and 130, respectively. On the other hand, for B512-NRRL, where the molecular weight range is sufficiently wide for excluded volume effects to come into play, the value of the quotient increases from approximatively 130 to 200. Since the branching increases in the order B512-NRRL < B512-Ph < A179 (*cf.* Table IV), it is clear that the value of the quotient in Eq. [21] decreases with increasing branching. The most probable reason for this is the decreased solvent-solute interaction with increasing branching.

The Effective Bond Length

For linear molecules with random flight chains the end-to-end distance in the unperturbed condition is

$$\overline{L_0^2} = 6\overline{R_0^2} = N_0b^2, \qquad [23]$$

where N_0 is the number of links and b is the effective bond length.

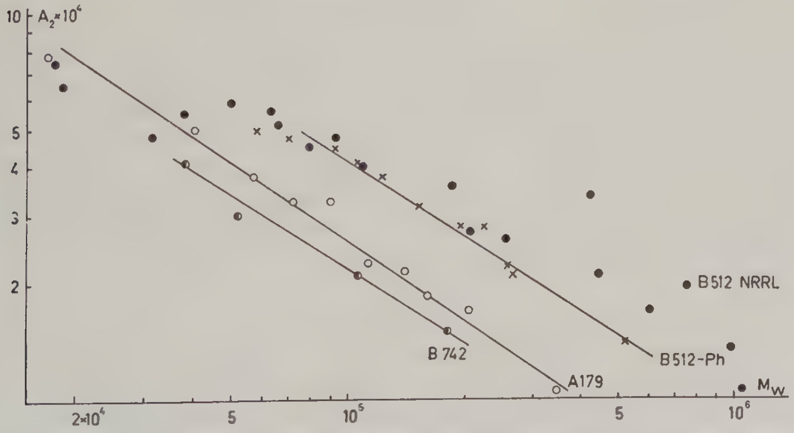

FIG. 10. Double logarithmic plot of second virial coefficient A_2 for some dextrans of different degree of branching.

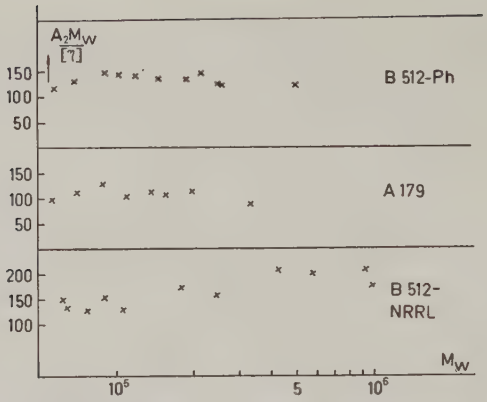

FIG. 11. $A_2M_w/[\eta]$ plotted against M_w for dextrans B512-NRRL, B512-Ph and A179.

In good solvents Eq. [23] should include a correction for excluded volume effects. This has been done in the general expression, given by Sadron (41),

$$\overline{L^2} = \overline{R^2}\,(2 + \epsilon)\,(3 + \epsilon), \qquad [24]$$

where ϵ is an increasing function of the second virial coefficient. Various explicit expressions have been worked out for the function ϵ (*cf.*, for example, references 42–44).

For branched molecules the following relationship is given by Stockmayer and Fixman (26):

$$\overline{L_0^2} = N_0b^2g; \qquad [25]$$

then, if N is assumed to be the same for linear and branched molecules,

$$b_{br} = \sqrt{g}\,b_{lin}. \qquad [26]$$

Since g is a function of M, b_{br} must also vary with M.

Values of b, calculated for different dextrans, are given in Table VI. They were calculated from Eq. [25] using the data for $(\sqrt{\overline{R^2}})_0$ and g given in Table IV.

The low values obtained strongly suggest that dextran molecules are highly flexible. This is also in agreement with conclusions drawn from the streaming birefringence behavior of dextran (45).

Molecular Shape

Asymmetry and hydration contribute to the frictional resistance of a sedimenting molecule, and both parameters must be taken into consideration in evaluating the shape of the molecule from its hydrodynamic properties.

TABLE VI

Sample	b(A) $M = 10^5$	b(A) $M = 2\times10^5$
Linear dextran	10	10
B512-NRRL	8.8	7.7
B512-Ph	8.7	8.2
A179	7.6	7.0
B742	7.4	6.6
Cruciform model	6.25	
Glucose ring	5.15	

Using a spherical model, Wales and Holde (46) have shown that

$$k_s = \frac{\Lambda N(\Phi^{1/3}P^{-1})^{-3}}{16{,}200\pi^2}\,|\,\eta\,|, \qquad [27]$$

where k_s may be defined by the well-known sedimentation equation

$$1/s = 1/s_0(1 + k_s c) \quad \text{or} \quad k_s = \frac{d(1/s)}{dc}\,s_0, \qquad [28]$$

and Λ is a numerical constant given by

$$s = \frac{s_0}{1 + \Lambda n v}$$

(n is the number of molecules in unit volume and v is the volume of a molecule). If the quotient $(\Phi)^{1/3}/P$ is constant, it follows that $k_s/|\,\eta\,|$ must be constant, independent of the molecular weight, as has indeed been found for many vinyl polymers. However, for polymethylmethacrylate a slight increase of both $k_s/|\,\eta\,|$ and $(\Phi)^{1/3}/P$ with molecular weight has been reported (47).

In Fig. 12 k_s is plotted against M for several dextrans. The value of k_s is found to be approximately proportional to $M^{0.6}$ in all cases. If a is the molecular weight exponent in the viscosity relation, then it follows that $k_s/|\,\eta\,|$ is proportional to $M^{0.6-a}$, and hence the increase of $k_s/|\,\eta\,|$ with molecular weight should depend on the degree of branching in the same way as a. Indications of such a tendency have indeed been found, but the limits of experimental error in the available data are such that no definite statement can be made at present.

By means of the assumptions of Wales and Holde, it may readily be shown that the quotient $k_s/|\,\eta\,|$ for branched molecules is given by

$$k_s = \frac{4/3\,\pi N \Lambda R_h^{\,2}}{100\Phi'(\sqrt{\overline{R^2}})^2}\,|\,\eta\,|. \qquad [29]$$

From this formula it is obvious that, as indicated above, $k_s/|\,\eta\,|$ must increase with M, since R_h increases faster with M, than $\sqrt{\overline{R^2}}$.

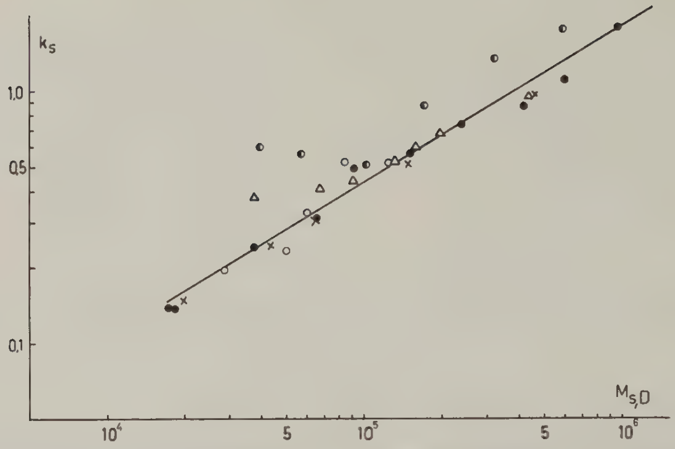

FIG. 12. Log-log plot of k_s against $M_{s,D}$ for some dextrans. △ = B512-Ph; ● = B512-NRRL (4); ○ = A179; ◐ = values of Scholz (49); × = values of Ogston (5).

Ogston and Woods (5) have studied a rather highly branched dextran of Birmingham strain and found it to be strongly hydrated but not very asymmetric.

Using a solid spheroid as a model they arrive at the relation (48) which, introducing Eq. [28], becomes

$$\frac{\zeta}{k}\,\frac{k_s}{|\eta|} = \frac{\chi^2(J)}{\xi(J)\psi(J)}. \qquad [30]$$

Equation [30] shows that a knowledge of $k_s/|\eta|$ may provide information about the molecular axial ratio. If $k_s/|\eta|$ increases with M, as suggested above, then $\chi^2(J)/\xi(J)\psi(J)$ also increases with M. There must then be a corresponding decrease in the axial ratio, a/b, as may indeed be observed from the data tabulated by Ogston (48). To express the matter pictorially, the molecules become more symmetrical with increase in the molecular weight.

Axial ratios calculated with the help of Eq. [30] include hydration contributions through the function $\xi\,(J)$. If such effects are not taken into consideration the axial ratio for dextran is found to increase rather rapidly with M, for example, for B512-Ph

$$a/b = 0.4\, M_{s,D}^{0.40} \quad \text{and for A179} \quad a/b = 0.1\, M_{s,D}^{0.56}.$$

This seems to be in contradiction to the high flexibility of dextran molecules.

ACKNOWLEDGMENTS

I wish to acknowledge my indebtedness to the director of the Institute of Physical Chemistry, Professor Stig Claesson, and to the director of the Research Laboratory of Pharmacia Ltd., Dr. Björn Ingelman, for their interest and for the many facilities they have placed at my disposal.

SUMMARY

In this discussion an attempt has been made to correlate the hydrodynamic properties of some dextrans as a function of their degree of branching. The effects of possible variations in the distribution of the branches along the chain and in the distribution of their lengths have not been considered here. As Senti *et al.* have pointed out the parameters g and h are not sufficient to provide such information.

REFERENCES

1. JEANES, A., *et al.*, *J. Am. Chem. Soc.* **76,** 5041 (1954).
2. WALES, M., MARSHALL, P. A., AND WEISSBERG, S. G., *J. Polymer Sci.* **10,** 229 (1953).
3. WALES, M., *et al.*, *Ann. N.Y. Acad. Sci.* **57,** 353 (1953).
4. SENTI, F. R., *et al.*, *J. Polymer Sci.* **17,** 527 (1955).
5. OGSTON, A. G., AND WOODS, E. F., *Trans. Faraday Soc.* **50,** 635 (1954).
6. VAN CLEVE, J. W., SCHAEFER, W. C., AND RIST, C. E., *J. Am. Chem. Soc.* **78,** 4435 (1956).
7. JEANES, A., AND WILHAM, C. A., *J. Am. Chem. Soc.* **72,** 2655 (1950).
8. SCOTT, T. A., JR., AND MELVIN, E. H., *Anal. Chem.* **25,** 1656 (1953).
9. DIMLER, R. J., *et al.*, *J. Am. Chem. Soc.* **77,** 6568 (1955).
10. SIMHA, R., *J. Research Natl. Bur. Standards* **42,** 409 (1949).
11. SIMHA, R., *J. Colloid Sci.* **5,** 386 (1950).
12. WALKER, O. J., AND WINKLER, C. A., *Can. J. Research* **B28,** 298 (1950).
13. CRAGG, L. H., AND FERN, G. R., *J. Polymer Sci.* **10,** 185 (1953).
14. CRAGG, L. H., AND BIGELOW, C. C., *J. Polymer Sci.* **16,** 177 (1955).
15. ISBELL, H. S., *et al.*, *J. Research Natl. Bur. Standards* **50,** 81 (1953).
16. BRICE, B. A., HALWER, M., AND SPEISER, R., *J. Opt. Soc. Amer.* **40,** 768 (1950)
17. BENGTSSON, A., unpublished.
18. MANLEY, R. ST. J., *Arkiv Kemi* **9,** 519 (1956).
19. NATL. BUR. STANDARDS, (U.S.), Rept. 1952, p. 72.
20. CLAESSON, S., *Nature* **158,** 834 (1946).
21. THURMOND, C. D., AND ZIMM, B. H., *J. Polymer Sci.* **8,** 477 (1952).
22. FLORY, P. J., *J. Chem. Phys.* **17,** 303 (1949).
23. FOX, T. G., AND FLORY, P. J., *J. Phys. & Colloid Chem.* **53,** 197 (1949).
24. FLORY, P. J., AND FOX JR., T. G., *J. Polymer Sci.* **5,** 745 (1950).
25. FLORY, P. J., "Principles of Polymer Chemistry," Cornell Univ. Press, Ithaca 1953.
26. STOCKMAYER, W. H., AND FIXMAN, M., *Ann. N.Y. Acad. Sci.* **57,** 334 (1953).
27. STOCKMAYER, W. H., unpublished.
28. ZIMM, B. H., AND STOCKMAYER, W. H., *J. Chem. Phys.* **17,** 1301 (1949).
29. KRIGBAUM, W. R., AND CARPENTER, D. K., *J. Phys. Chem.* **59,** 1166 (1955).
30. AROND, L. H., AND FRANK, H. P., *J. Phys. Chem.* **58,** 953 (1954).
31. THURMOND, C. D., AND ZIMM, B. H., *J. Polymer Sci.* **8,** 477 (1952).
32. GRANATH, K. A., unpublished.
33. MANDELKERN, L., *et al.*, *J. Chem. Phys.* **20,** 1392 (1952).
34. NEWMAN, S., *et al.*, *J. Polymer Sci.* **14,** 451 (1954).
35. ZIMM, B. H., *J. Chem. Phys.* **14,** 164 (1946).
36. FLORY, P. J., AND KRIGBAUM, W. J., *J. Chem. Phys.* **18,** 1086 (1950).

37. Krigbaum, W. R., *J. Polymer Sci.* **18,** 315 (1955).
38. Shultz, A. R., *J. Am. Chem. Soc.* **76,** 3422 (1954).
39. Gouinlock, E. W., Flory, P. J., and Scheraga, H. A., *J. Polymer Sci.* **16,** 386 (1955).
40. Levy, G., and Frank, H. P., *J. Polymer Sci.* **17,** 247 (1955).
41. Sadron, Ch., *Nature* **177,** 205 (1956).
42. Debye, P., and Bueche, A. M., *J. Chem. Phys.* **16,** 573 (1948).
43. Peterlin, A., *J. Colloid Sci.* **10,** 586 (1955).
44. Peterlin, A., *J. Polymer Sci.* **5,** 473 (1950).
45. Yang, Jen Tsi, and Foster, J. F., *J. Polymer Sci.* **18,** 1 (1955).
46. Wales, M., and van Holde, K. E., *J. Polymer Sci.* **14,** 81 (1954).
47. Eriksson, A.F.V., *Acta Chem. Scand.* **10,** 378 (1956).
48. Ogston, A. G., *Trans. Faraday Soc.* **49,** 1481 (1953).
49. Scholz, J. J. *Dissertation Abstr.* **15,** 724 (1955).

JOURNAL OF COLLOID SCIENCE **13**, 329-336 (1958)

VARIATION OF GAMMA RADIATION RATES FOR DIFFERENT ELEMENTS FOLLOWING AN UNDERWATER NUCLEAR DETONATION[1]

W. J. Heiman[2]

Applied Research Branch, Chemical Technology Division, United States Naval Radiological Defense Laboratory, San Francisco 24, California

Received October 24, 1957

ABSTRACT[3]

Calculations are made of the gamma radiation rates for the 13 chemical elements whose radioisotopes contribute the major portion of gamma radiation from a deep underwater nuclear detonation. These calculations are carried out for 14 different times after the burst ranging from 40 min. to 3 years. The gamma emitters include activities induced in sea water and possible bomb components as well as fission products.

INTRODUCTION

This paper examines the question of which chemical elements are chiefly responsible for the gamma radiations from nuclear detonations. As part of a systematic study, these effects are estimated for an underwater detonation. This information assists greatly in the investigation of decontamination of surfaces by providing a guide as to which elements must be removed. By describing the gamma radiation in terms of ionization rate, a quantity is obtained which is proportional to roentgens per hour. In addition, the data can be used in devising a radioactive simulant for gamma-emitting nuclides from an underwater detonation. The information essential to the preparation of such a radioactive simulant is very difficult to obtain experimentally, particularly at short times after the burst. Therefore this paper attempts a description of the gamma radiations by combining the available empirical data with some theoretical considerations.

---

[1] It is recognized by the authors of this and the succeeding two papers that the treatment is oversimplified. A complete picture of fallout radioactivity and its removal from contaminated surfaces requires a better knowledge of:

1). The decay rates, gamma energies, and relative yields of the fission products and induced activities associated with fast neutron fission in various weapon types.

2). Mechanisms of association of the activities with inactive weapon component material and environmental material drawn into the cloud.

3). Fractionation of the activities during cloud formation and transport.

4). Decontamination behavior of characteristic systems.

Work is in progress on these aspects of the problem. The present papers illustrate the nature of the problem and some of the preliminary approaches to its solution.

[2] Now at Westinghouse Electric Corp., Pittsburgh, Pennsylvania.

[3] The opinions or assertions contained herein are the private ones of the writer and are not to be construed as official or as reflecting the views of the Navy Department or of the Naval Service at large.

Calculations are made for the chemical elements contributing to the gamma radiation rate at 14 different times after the burst. These calculations are not applicable to thermonuclear weapons without important modifications.

Information on the fission product beta-activities resulting from 10,000 slow fissions of U^{235} has been given by Hunter and Ballou (1). Their calculations involved beta emission rates, whereas this paper is concerned with gamma emission rates. The present work gives induced activities as well as fission product activities for 10,000 fissions of U^{235}. The resulting radiation rate for each important element is expressed as a percentage. Of course there are external radiological hazards caused by alpha and beta radiation (2), but these pose different problems and are not treated here. The internal hazard from such sources should also be considered separately, although there are indications that it would be minor, at least in the case of an early acute exposure of short duration (3).

To obtain the rate of gamma radiation, the number of beta transformations per minute is multiplied by its corresponding total gamma-ray energy per beta disintegration. This product, million electron volts per minute, is approximately proportional to roentgens per hour as measured in air.

Total gamma-ray energy was obtained by considering the total energy of the quanta associated with one beta disintegration of the nuclide. Gamma rays of different energies emitted by the same nuclide were weighed according to their abundance. Energies were taken from the latest tabulations (4, 5).

Calculation of the total gamma-ray energy per beta disintegration is illustrated below for Rh^{106} (see Fig. 1). This is a typical calculation, although somewhat more complicated than that for the usual radionuclide.

Series of gammas in cascade such as the 0.87, 1.04, and 0.51 m.e.v. photons may be considered as a single gamma with an energy of 2.42 m.e.v., since this calculation is based upon the total ionization produced.

6% × 2.42 m.e.v. = 0.145 m.e.v.
3% × 1.55 m.e.v. = 0.047 m.e.v.
12% × 1.14 m.e.v. = 0.137 m.e.v.
11% × 0.51 m.e.v. = 0.056 m.e.v.
68% × 0 m.e.v. = 00 m.e.v.

Total gamma energy per
beta disintegration = 0.385 m.e.v.

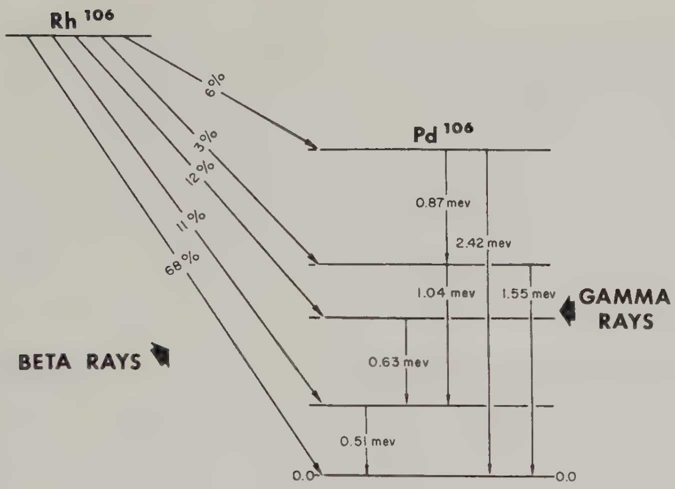

FIG. 1. Disintegration of Rh^{106}

It is recognized that this calculation will lead to a high value of the average energy wherever internal conversion of the emitted photon is important (low gamma energies at any step in the cascade).

ESTIMATION OF UNKNOWN GAMMA-RAY ENERGIES

There are a number of gamma-ray energies which are unknown, especially for the radionuclides with short half-lives. Furthermore, there is no decay scheme for many nuclides; the only information listed is the word "gamma." In such cases the gamma energies were estimated by use of the Bohr-Wheeler equations (6). These equations are based upon the liquid drop model of the nucleus and permit an estimation of the energy associated with a beta transition from a fission product. The beta-ray energies have been measured for a number of the fission products with unknown gamma energies; thus it is possible to subtract these measured values from the total calculated energy and obtain values for the gamma-ray energy. A few of the calculated gamma-ray values were rather high, e.g., 4.5 m.e.v. for La^{144}; therefore, it appeared desirable to obtain more reasonable values. In a survey of all known gamma-ray energies for fission products it was found that the highest observed energy was 2.8 m.e.v.; hence this was taken arbitrarily as the maximum value probable for any nuclide of unknown gamma energy.

Some of the estimated gamma energies possibly may be high, especially in the case of short-lived activities, since they are known to have very energetic betas. The energy of these beta rays has not been measured because of the experimental difficulties encountered in working with short-lived activities.

The applicability of the semiempirical Bohr-Wheeler equation to the particular radionuclides of interest was examined by using the equation to calculate the beta-transition energies for a number of known nuclides. Nuclides were chosen which had the same atomic number and the same "odd-even" mass number-atomic number relationship. Thus the only parameters changed in the equation were two which varied only slowly with mass number. Hence, it was assumed that, if the calculated and observed energies of the known nuclides were in reasonable agreement, then the same would apply to the unknown energies. In almost every case it was evident that the calculated value allowed a satisfactory estimate of the actual energy.

It was possible to estimate the gamma-ray energies for several nuclides by referring to the original papers which describe these particular activities. The gamma rays were reported, but the absorption curves had not been evaluated. Hence, by analyzing the curves for half-thickness, the gamma energies could be estimated. Values determined in this way were considered more reliable than those obtained by the Bohr-Wheeler estimates.

The gamma-ray energies estimated by the preceding methods are probably correct within a factor of two. Errors, if present, are more than likely on the high side. Because the unknown gamma energies are all short-lived, none of the estimates will affect the evaluation of gamma radiation after approximately 12 hr.

Rate of Gamma Radiation from Radionuclides Produced in an Underwater Nuclear Detonation

There are three sources of radionuclides in an underwater nuclear detonation: (*1*) fission products, (*2*) activity induced in sea water, and (*3*) activity induced in the bomb materials. It is assumed that the explosion occurs in deep water; therefore activity induced in the sea bottom need not be considered.

Activity from Fission Products

The number of beta disintegrations per minute for each radioactive fission product at various times after detonation were taken from the Hunter-Ballou curves (1). These values were multiplied by the corresponding total gamma-ray energies per beta disintegration to produce the rate of gamma radiation at the time in question. Radionuclides with no gamma rays or with a very small activity were neglected, as were the noble gases. All others were summed and their relative contribution to the rate of gamma radiation was calculated for each of the following times: 40 min.; 1, 3.5, and 12 hr.; 1, 2, 4, 7, 14, 28, 105, and 210 days; and 1 and 3 years.

The major portion of the radiation hazard was contributed by a few predominating radionuclides. This is especially true at long times after the burst. Preliminary calculations of the relative contribution of radiations to the decontamination characteristics of the contaminant were made on the basis of the different chemical groups. However, after observing that in a number of cases the entire contribution of a group was caused by one nuclide, it was decided to express the gamma radiation as represented by the individual elements. Another weakness of indicating radiation by chemical groups is the lack of information on whether all the elements in a group have the same decontamination characteristics (e.g., does lanthanum decontaminate in the same manner as yttrium?). For the decontamination studies 11 fission product elements were used to cover the range from 40 min. to 3 years. This number may be somewhat reduced after investigating the decontamination characteristics of these nuclides, since some of the elements may decontaminate in a similar manner. The rare gases xenon and krypton make an appreciable contribution to the radiation at early times but are not considered important, since they do not contaminate surfaces. However, the daughter activities of xenon and krypton are solids and do contaminate surfaces; radiation from those substances is included in the calculations.

The 11 fission product elements are listed in Table I with their percentage contributions at 14 different times. It is evident that, if these elements are used individually for decontamination experiments, their rates of gamma radiation are additive and represent a major contribution to the total radiation field.

TABLE I

Contribution of Important Gamma-Emitting Elements to Total Gamma Radiation Rate Maximum Neptunium Contribution Assumed to be 50 %

Element	Percentage Contribution to Gamma Radiation Rate at Various Times after Burst													
	40 min.	1 hr.	3.5 hr.	12 hr.	1 day	2 days	4 days	7 days	14 days	28 days	105 days	210 days	1 yr.	3 yr.
Sr	4.56	3.21	9.08	10.17	6.55	2.54	0.18	0	0	0	0	0	0	0
Y	22.37	18.88	11.53	21.12	12.87	3.59	0.25	0	0	0	0	0	0	0
Zr	0.23	0.37	2.03	6.59	8.33	7.03	2.99	2.17	4.86	11.97	32.80	29.20	24.10	0.18
Nb	0.12	0.21	1.65	6.28	7.63	6.29	1.97	0.49	1.37	5.54	44.70	58.60	55.90	0.39
Ru	0.09	0.17	0.99	1.22	0.51	0.01	0.57	1.19	2.60	5.14	10.11	5.00	1.76	0
Te	9.78	11.59	9.39	1.26	1.33	1.89	2.16	1.96	1.22	0.42	0.38	0.13	0.51	0
I	6.30	10.39	24.97	16.86	14.88	11.52	10.10	10.04	8.36	3.54	0	0	0	0
Cs	13.29	15.07	4.57	0	0	0	0	0.04	0.09	0.13	0.37	1.02	4.35	67.80
La	11.60	9.47	7.28	0.59	1.24	4.33	12.08	26.44	50.30	59.44	7.14	0.01	0	0
Ce	3.82	5.25	11.22	4.81	5.38	5.85	4.76	2.63	1.53	2.28	3.02	2.21	5.04	12.70
Pr	5.50	6.31	0.75	0	0	0	0	0.01	0.03	0.07	0.41	0.92	2.50	6.10
Np	0.23	0.45	3.03	12.37	23.06	40.41	50.00	40.54	11.92	0.39	0	0	0	0
Na	0.24	0.37	1.96	5.47	7.11	4.76	0.90	0	0	0	0	0	0	0
Others[a]	21.87	18.26	11.55	13.26	11.11	11.78	14.04	14.49	17.72	11.08	1.07	2.91	5.84	12.83

[a] Per cent of total gamma radiation not represented by the elements listed in this table.

INDUCED ACTIVITY IN SEA WATER

The relative activities induced in sea water may be calculated from the equation:

$$N = In\sigma, \qquad [1]$$

where N is the relative number of activated atoms at zero time, I is the number of neutrons available from the bomb for inducing activities, n is the number of atoms per cubic centimeter of the target, and σ is the cross section of the target nuclide for radiative capture of slow neutrons.

This same method was used by Mandeville for calculating activities induced in the Schuylkill River (7).

After the relative numbers of the product atoms are known, they may be normalized to the total number of reactions occurring. This number may be taken as the total number of available neutrons, since it is reasonable to assume that essentially all of them will be taken up by the sea water.

The following evaluations were made for the quantities in Eq. [1]. For simplicity it was assumed that 2 neutrons were produced per fission. Therefore 1 neutron per fission or 10,000 neutrons from 10,000 fissions are available for inducing activities. In addition it is hypothesized that almost all these neutrons escape from the center of the weapon to the surrounding sea water; thus the value for I is taken as 10,000 neutrons; this is clearly an upper limit, with sea water capture treated independently of tamper capture.

The number of target atoms per cubic centimeter, n, was obtained from the concentrations of the various elements present in sea water (8). The minimum concentration considered was that of aluminum, which was present to the extent of 2×10^{-5} mole per liter of sea water. Each stable nuclide was corrected for its percentage abundance. The slow neutron capture cross sections, σ, were taken from tabulated values.

The resulting *gamma-emitting* activities are N^{16}, F^{20}, Na^{24}, Mg^{26}, Al^{28}, S^{37}, Cl^{38}, Ca^{47}, Sc^{47}, Ca^{49}, K^{42}, Br^{80m}, Br^{80}, Br^{82}, Sr^{85}, and Sr^{87}. It should be noted that 99% of the product atoms are either nonradioactive (deuterium) or of very long half-life (chlorine—36; 3×10^5 years, no γ).

After obtaining the relative numbers of product atoms and normalizing them to the total number of reactions the activity at time zero may be calculated for each radionuclide. The only appreciable gamma activity induced in sea water is that of Na^{24}, which may contribute 7% (or more, if the Np contribution is reduced) at one day after the burst. (See Table I.)

RADIOACTIVITY INDUCED IN BOMB COMPONENTS

There will be a number of activities induced in the casing and other parts of the bomb itself. These will vary with the size, type, and design of the weapon. One of the most important contributors to this activity would be the tamper, which may be composed of a high-density, high atomic weight element (9, 10), such as natural uranium, thorium, lead, or tungsten.

Calculations based on:

1. Isotopic constitution of the natural elements,

2. Cross sections for radiative neutron capture, and

3. Gamma energies and half-lives of the resulting induced and daughter gamma activities, indicate that uranium, tungsten, and thorium may contribute significantly at various times after the burst. Tungsten and thorium may be somewhat less important than uranium.

If the tamper is composed of natural uranium, a most important induced gamma radiation would come from Np^{239}. This results from radiative neutron capture in U^{238} to form U^{239}, which decays with a 23.5 min. half-life to Np^{239}. The resulting 2.3 day gamma activity of Np^{239} may make a large contribution to the total gamma radiation at times up to two weeks after the burst, and its parent U^{239} would provide a small fraction of the gamma radiation rate at times up to 2 hours. Since uranium is probably the most significant tamper element from the point of view of induced activities, the Np^{239} contribution should be considered in our tables of the important gamma-emitting elements.

This is shown in Table I, where it is assumed that 50% of the gamma radiation rate at 4 days is due to neptunium. This percentage is chosen arbitrarily to indicate clearly the period when neptunium may be a significant contributor. The table may be recomputed for other assumed Np contributions as follows:

Let a_0 = fraction of Np contribution in Table I at time t.
z = ratio of new Np contribution to a_0.
f_0 = percentage contribution of element A in Table I at time t.

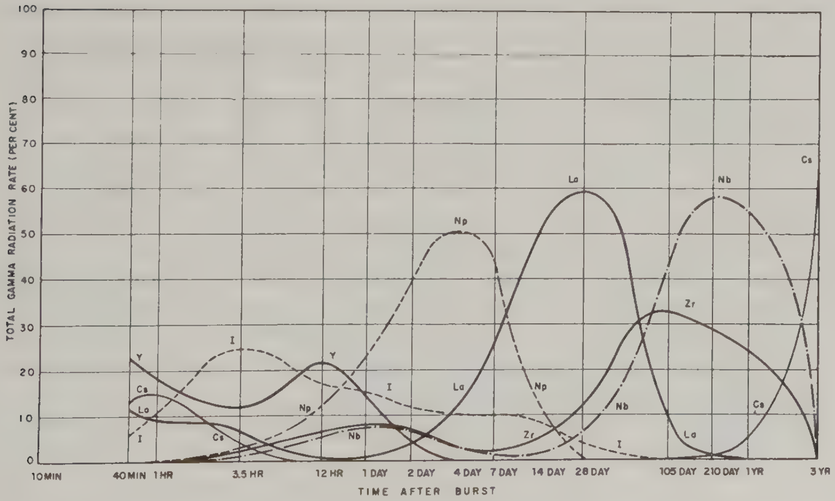

FIG. 2. Percentage contribution of elements to gamma radiation rate as a function of time after burst. (Maximum neptunium contribution assumed to be 50%.)

f = percentage contribution of element A at time t, for new Np contribution.

Then

$$f = f_0 \left[\frac{1 - za_0}{1 - a_0} \right]. \qquad [2]$$

As an example, assume a 25% Np contribution ($z = 0.5$) at 4 days. Calculate the La contribution at 4 days and at 1 day.

At 4d:

$$f = f_0 \left[\frac{1 - (0.5)(0.5)}{1 - 0.5} \right] = 1.5\, f_0 \text{ (any element).}$$

$$f_{La} = (1.5)(12.08\%) = 18.11\%.$$

At 1d:

$$f = f_0 \left[\frac{1 - (0.5)(0.2306)}{1 - 0.2306} \right] = 1.15\, f_0 \text{ (any element).}$$

$$f_{La} = (1.15)(1.24\%) = 1.43\%.$$

The information in Table I is plotted in Fig. 2 for the seven most important elements, showing gamma radiation rate as a function of time after burst.

REFERENCES

1. HUNTER, H. F., AND BALLOU, N. E., Fission Product Decay Rates, *Nucleonics* **9**, (No. 5), C-2 to C-7 (Nov. 1951) (C), February, 1947.
2. THE EFFECTS OF ATOMIC WEAPONS, U. S. Government Printing Office, Washington, D. C., September, 1950.
3. COHN, S. H., RINEHART, R. W., ROBERTSON, J. S., GONG, J. K., MILNE, W. L., CHAPMAN, W. H., AND BOND, V. P., "Internal Radioactive Contamination of Human Beings Accidentally Exposed to Radioactive Fallout Material," USNRDLTR-86, May 9, 1956.
4. "NUCLEAR DATA," *Natl. Bur. Standards* (*U.S.*) *Circ.* **499**.
5. HOLLANDER, J. M., PERLMAN, I., AND SEABORG, G. T., "Table of Isotopes" (December, 1952) UCRL-1928-revised. (cf. *Revs. Mod. Phys.* **25**, 469–651 (1953).)
6. BOHR, N., AND WHEELER, J. A., *Phys. Rev.* **56**, 426 (1939).
7. MANDEVILLE, C. E., *J. Franklin Inst.* **252**, 297–308 (Oct. 1951).
8. SVERDRUP, H. U., JOHNSON, M. W., AND FLEMING, R. H., "The Oceans, Their Physics, Chemistry and General Biology", Table 36. Prentice-Hall, New York, 1942.
9. SMYTH, HENRY DEWOLF, "Atomic Energy for Military Purposes," p. 210. Princeton University Press, Princeton, 1948.
10. GLASSTONE, S., "Sourcebook on Atomic Energy," p. 395. Van Nostrand, New York, 1950.

JOURNAL OF COLLOID SCIENCE **13**, 337–347 (1958)

DECONTAMINATION REACTIONS OF SYNTHESIZED FALLOUT DEBRIS FOR NUCLEAR DETONATIONS

I. NUCLEAR DETONATION IN SEA WATER

Carl F. Miller, Richard Cole, and Warren J. Heiman

Radiological Capabilities Branch, Chemical Technology Division, United States Naval Radiological Defense Laboratory, San Francisco 24, California

Received October 24, 1957

ABSTRACT

The expected general composition of fallout from a nuclear detonation in a homogeneous liquid medium (sea water) is discussed. Simplified contaminants each containing a single fission product (FP) element and sea water applied to a painted surface were decontaminated by water washing. Decontamination as a function of initial level or surface density of most of the FP elements used was found to follow the modified Freundlich relationship

$$R = aI^n \qquad [7]$$

in which I is the initial level, R is the level remaining after decontamination, and a and n are constants for each element.

INTRODUCTION

Three principal components of fallout from a nuclear detonation near the surface in deep sea water are sea water residue, radioactive elements, and material from the bomb structure. In this investigation the decontamination (removal of contaminant) reactions of a simulated contaminant consisting of various combinations of the first two components are described. By neglecting the third component, a contaminant can be defined the surface interactions of which are simple. A complete investigation of decontamination would include the determination of the effect of this component on the simple interactions; however, such treatment is beyond the scope of this report. The radioactive elements used in the present experiments consist mainly of the major gamma-emitting fission product (FP) elements.

If one knows the composition of sea water and that of the FP mixture at a given time after detonation, the first step in the formulation of a synthetic contaminant is the determination of the ratio between the two components in the fallout mixture. Although no ratio has been reported, it is possible to estimate its maximum and minimum limits from published data (1) for a 20-kt. weapon as follows:

1. 20 kt. = 3 × 10^{24} fissions.

2. Energy released = 2×10^{13} cal.

3. Bikini Baker shot at a depth of less than 200 ft. of water raised about 2×10^6 tons of material.

The 3×10^{24} fissions create 10 moles of FP, and 2×10^6 tons of sea water are equivalent to 1.8×10^9 liters; hence if all the water were used to dilute the FP elements, the total FP concentration would be 5.6×10^{-9} mole/liter. However, it is unlikely that all the water thrown up would actually mix with the FP elements. Therefore the concentration obtained by the above calculations is a minimum value. On the other hand, if it is assumed that about 1/2 of the energy released is available to vaporize sea water, whose heat of vaporization is about 10^4 cal./mole, then 10^9 moles of sea water (1.8×10^7 liters) would be vaporized. Now if the FP and this water are thoroughly mixed in the fireball along with the sea water salts which would be present (about 10^7 moles as NaCl) in the vapor state, the mole ratio of FP to H_2O equivalents would be $1/10^8$ and the FP concentration would be 5.6×10^{-7} mole/liter. Thus the expected concentration of fission products in the liquid carried upward in the cloud should be between 5.6×10^{-9} and 5.6×10^{-7} mole/liter.[1]

Furthermore, if the assumptions about vaporization and complete mixing are valid, then the resulting oxidized FP atom surrounded by 10^8 molecules of water is, precisely, a hydrated ion. Since it is reasonable to expect that the FP elements would be present in their most stable oxidation state and physical state in the sea water environment, the above process would result essentially in the same final aqueous solution as that obtained when soluble salts of the FP elements are dissolved in sea water at the appropriate concentration.

The radiation field from such a contaminant spread over a given area can also be estimated. The Hunter-Ballou (2) calculations on the decay of FP from 10,000 fissions together with estimates for induced activities (3) show that this mixture of radioactivity would be decaying at the rate of about 100 dis/min at $H + 1$ hr. (H is the hour of detonation). Hence, at this time, the total activity of the 20-kt. bomb would be about 1.4×10^{10} curies, and the minimum specific activity of the fallout material would be about 7.6×10^{-3} curie/ml. at $H + 1$ hr. It has also been reported (1) that 1 megacurie (of photons) per square mile produces an ionization rate in air of 4 r/hr. 3 ft. above the surface. For a beta-to-gamma ratio of one, this would mean that 8.2×10^{-3} ml./sq. in. of the solution at the minimum FP concentration spread over a large flat area would produce 1 r/hr. at 1 hr. after burst; at the maximum concentration, 8.2×10^{-5} ml./sq. in. would produce the same field. In a real detonation a single ratio of FP to sea water could be produced somewhere between the two extremes; or, if the assumptions about complete mixing are in error, the concentration could vary from about the lower limit to a value even higher than the calculated maximum.

---

[1] The expected physical state of the fallout material is considered in detail below.

The contaminant, once thrown up, could fall back to earth as fine crystalloid particles, a fine mist, or a rather heavy rain, depending on the weather conditions and the height to which the material is thrown. From higher altitudes, it would take longer for the material to fall, which would give the water a better opportunity to evaporate. From lower altitudes, the general dispersion would not be as great because of higher atmospheric pressures and higher relative humidity over water, and there would be little time available for evaporation. In the present investigation, involving a 20-kt. weapon, weather conditions were assumed such that the contaminant would return to earth as a rain very shortly after detonation. For such conditions, the contamination of test surfaces was simulated by applying the contaminant in liquid form to a surface.

The Hunter-Ballou (2) curve and Heiman's (3) calculations together with the decay schemes of the FP radionuclides were used to determine the percentages of those elements which contribute significantly to the gamma radiation up to $H + 3$ yr. These are: Cs, Sr, Y, La, Ce, Pr, Zr, Nb, Te, Ru, and I. These elements used one at a time comprised the FP radioactive component for a set of simplified two-component contaminants. This report describes the behavior of their decontamination from a painted surface.

THEORETICAL CONSIDERATIONS

Consider a spherical cloud in which the radioactive elements and sea water are homogeneously mixed. If this cloud were to settle back to sea without drifting away from the point of detonation, the accumulated amount of material per unit area if collected at the surface of the water would be proportional to $(a^2 - r^2)^{1/2}$, where a is the radius of the cloud and r is the radial distance of the point from ground zero. This simple picture of the phenomenon permits the generalization that a surface in the region could receive an amount of fallout ranging from zero to some maximum amount depending upon its location relative to the point of detonation. This generalization is acceptable even if the FP elements and sea water are not homogeneously mixed. This concept of a varying surface density of radioactive atoms along with its corresponding gamma radiation flux is termed the "level of contamination." In carrying out the experiments and in treating the data it was convenient to vary the ratio of FP to sea water by varying the concentration of the FP elements in sea water. This procedure kept the ionic strength of all the solutions essentially constant. In the case of complete mixing, in which the ratio of FP to sea water would be constant, the surface density of both FP and sea water would vary with the level of contamination. However, the above procedure was used, since previous experiments had indicated that the decontamination results were not very sensitive to the ratio at the FP concentrations used.

Let the area of contamination of a test surface with a given volume of contaminant be considered the unit area covered; then the initial level of contamination, I, will be proportional to the concentration of the FP element. When a volume, V_0, of the solution is deposited on a nonporous surface the ionic and/or colloidal species present in the solution will immediately begin to adsorb upon the surface. Under equilibrium conditions, the amount ultimately adsorbed depends upon the charge of the ion (colloid), its size, its concentration, and the nature of the surface. However, in the case of the present contaminant-paint surface system, the water is allowed to evaporate so that the salt concentration increases as the water evaporates, and if sufficient salt is present visible salt crystals precipitate out when both the surface and the liquid become saturated. At this time further adsorption by the surface ceases and the remaining unadsorbed material deposits as crystals over the surface.

For this process, let

I_1 = amount of radioactive element(s) adsorbed by the unit area of surface at any time after contamination.

I_2 = amount of radioactive element(s) in liquid phase (up to the time of crystallization).

For equilibrium adsorption at the time of surface saturation let

$$I_1 = a_1 I_2^n, \tag{1}$$

in which a_1 and n are constants. Equation [1] is an adaptation of the Freundlich adsorption isotherm.

When the liquid comes in contact with the surface, the initial adsorption rate is quite rapid. However, as soon as the liquid layers just above the surface become depleted of ions, the rate slows to that controlled by the rate of diffusion of the ion (or colloid). In the evaporating drop, the concentration increases around the periphery of the drop and in most cases the resulting concentration gradient produces a forced diffusion. It is during this period that saturation and final drying occur. If the rate of evaporation is too rapid many of the ions are not able to reach the surface; these are finally trapped in the crystal layer about the surface. In such a case the ion concentrations are increasing very rapidly at the vapor-liquid interface, and, with the interface moving almost as rapidly as the diffusing ions, saturation and crystallization at this interface predominate over adsorption at the paint surface-liquid interface.

Since forced diffusion is likely to be in progress at the time of interest, let us assume that it occurs over the whole evaporation period, and for overall concentration in the drop, let

$$dC/dt = 0, \tag{2}$$

in which $C = I_2/V$ is the concentration of the radioactive element in the liquid where V is the volume of the drop at time t. This states that material is being adsorbed by the surface at the same rate at which evaporation is increasing the average concentration in the drop. At constant temperature, the rate of evaporation will be constant up to the time of saturation; the volume is then given by

$$V = V_0(1 - gt), \quad 0 < t < t_d, \tag{3}$$

in which V_0 is the initial liquid volume, t_d is the drying time, and $g = 1/t_d$. Combining Eqs. [2] and [3] and substituting I_2 for CV gives

$$-\,dI_2/I_2 = \frac{gdt}{1 - gt}. \tag{4}$$

Integrating under the condition that $I_2 = I$ at $t = 0$ gives

$$I_2 = I(1 - gt). \tag{5}$$

At the time of saturation, t_s less than t_d, the quantity $(1 - gt_s)$ is a positive constant, say k_2. It may be noted that with almost any adsorption process different from that described by Eq. [2] but subject to the above limits of integration, evaluation at $t_s < t_d$ would give the result that I_2 is proportional to I at t_s. Then, since the total salt in the sea water deposit (*ca.* 0.5 molar) is constant for all values of I for all FP, it follows that t_s is constant for each FP and independent of I. Hence Eq. [1] can be written as

$$I_1 = a_1 k_2^n I^n. \tag{6}$$

If the element is chemisorbed by the surface so that little or no desorption occurs during decontamination or if the desorption rate is very slow, then only that fraction of the radioactive element which is in the crystal layer will be removed by a simple water wash.

The amount remaining after decontamination, R, will be equal to that adsorbed by the surface, I_1, and is given by

$$R = aI^n \tag{7}$$

in which $a = a_1 k_2^n$. Then the fraction remaining, or the decontamination ratio ($F = R/I$), is

$$F = aI^{n-1}. \tag{8}$$

EXPERIMENTAL DETAILS

The sea water component was prepared from a formula given by Sverdrup *et al.* (4). Concentrations for inactive carriers for the 11 FP elements were calculated from the fission (5) yield curve by decaying the appropriate chains to $H + 24$ hr. and calculating the relative numbers of atoms (active plus inactive) of each of the 11 FP. The minimum estimated concentration of all the FP combined, 5.6×10^{-9} mole/liter, was designated as the $1C$-level of total activity and was used to calculate the carrier concentrations given in Table I; the 11 FP elements listed comprise about 72% of all the FP atoms at $H + 24$ hr. The radionuclides used as tracers for the 11 FP elements were Cs^{134}, Sr^{89}, Y^{91}, La^{140}, Ce^{144}, Pr^{144}, Zr^{95}, Nb^{95}, Te^{127}, I^{131}, and Ru^{106}.

In addition to the FP elements listed in Table I, experiments were made on salt water solutions containing Na^{22} and Np^{239} to represent possible induced activities (3). All the tracers were obtained from the Isotopes Division of Oak Ridge National Laboratory with the exception of the Np activity, which was produced on the 60-in. cyclotron at the Crocker Laboratory of the University of California at Berkeley.

Although the complete chemical treatment given each radionuclide and carrier is not given here, the general procedure was to select or prepare a soluble salt of the element (carrier and tracer) which was compatible with its most stable thermodynamic state at a pH of 7 and which would permit complete exchange between tracer and carrier (except Np, for which no carrier was available). A separate contaminant was prepared for each of the 11 FP elements with the FP carrier at a concentration corresponding to the 1000 C-level or greater. Then that solution was diluted with sea water to obtain lower C-levels as desired. The Na of the sea water carried the Na^{22}; the true Np concentration was estimated from the counting geometry. All contaminants were adjusted to a pH of 7 before use.

The test surfaces used were aged Navy Gray paint surfaces (Haze Gray 5H) prepared on aluminum plates, 1¼ in. square by ⅛ in. thick. The test surfaces were contaminated in triplicate by pipetting 300 μl. of

TABLE I

Concentration of Fission Product Elements at 1C-Level[a]

Element	Percentage of total fission products at 1 day	Concentration *(moles/liter)* $\times 10^{10}$
Cs	9.2	5.2
Sr	8.2	4.6
Y	2.9	1.6
La	3.5	2.0
Ce	10.2	5.7
Pr	3.9	2.2
Zr	17.0	9.6
Nb	1.0	0.56
Te	5.2	2.9
I	3.2	1.8
Ru	7.6	4.3

[a] Concentration equivalent for $1C$-level of gamma radiation.

contaminant solution on them and allowing the deposit to evaporate and dry in an oven at 30°C. for about 18 hr. The surfaces were then counted, decontaminated, again counted, and then radioautographed.

The samples were all decontaminated by immersing them in 250 ml. of gently stirred water for 5 min. and then rinsing them in clean water before drying and counting.

The samples were counted with the USNRDL Model 1A proportional counter. All counts were corrected for background, standard, decay, coincidence loss, and self-absorption. The decay, coincidence loss, and self-absorption corrections were experimentally determined. Each radionuclide was counted on the basis of the individual characteristics of its nuclear radiations which, for Ce^{144}–Pr^{144} and Zr^{95}–Nb^{95}, required differential counting techniques.

RESULTS

The data for the decontamination as a function of *C*-levels are given in Table II. The data for Np are given in Table III. Except for Sr and Nb

TABLE II

Decontamination as a Function of Initial Level

Element	*I*(*C*-Level)	*F*(%)
Na	—	0.007 ± 0.0001
Cs	3.50	2 ± 1
	32.6	0.75 ± 0.22
	349	0.32 ± 0.06
	3,110	0.16 ± 0.06
	38,500	0.066 ± 0.002
Sr	0.28	7.1 ± 1.6
	2.63	8.5 ± 2.3
	24.6	7.5 ± 1.2
	232	7.5 ± 0.7
	2,610	7.0 ± 0.4
Y	48.3	92.5 ± 2.9
	348	90.0 ± 1.6
	2540	85.6 ± 1.6
	31,250	69.2 ± 2.0
La	138	85.8 ± 4.6
	1,540	80.0 ± 2.8
	17,500	76.8 ± 0.7
Pr	251	64.3 ± 3.2
	2,430	61.6 ± 3.6
	22,730	51.2 ± 0.9
Ce	0.77	90.3 ± 1.8
	2.23	84.5 ± 1.6
	9.80	81.0 ± 4.2
	77.6	78.9 ± 2.4
	877	71.5 ± 1.5
Zr	5.00	96. ± 18
	25.0	88. ± 7
	244	68.6 ± 2.3
	2,190	49.4 ± 3.5
	20,560	38.9 ± 6.1
Nb	312	66.4 ± 5.8
	3,530	69.9 ± 2.0
	41,070	73.0 ± 4.2
Te	412	26 ± 10
	4,140	19.8 ± 2.7
I	15.5	7.1 ± 0.7
	138	3.26 ± 0.13
	1,220	1.73 ± 0.02
	11,100	0.94 ± 0.03
Ru	38.2	79 ± 11
	376	77.2 ± 3.3
	2,330	69.3 ± 7.2

the fraction remaining for all the elements decreased as the initial level increased. For Nb, the data showed a slight increase. The Na and Sr data are independent of level because their concentrations were maintained constant by the sea water. A least-squares fit of Eq. [7] to the data was used to obtain the constants summarized in Table IV. These constants were used to calculate the lines drawn through the data points plotted in Fig. 1. The initial levels for Np are given in fractions of the total FP C-level so that for a given Np-to-FP atom ratio (at 1 day after detonation), the data could be easily converted to C-levels; as given, the constants would apply directly if the ratio were 1. At a C-level of 1, the constant a is a direct measure of the degree of adsorption or retentivity of the element by the surface in the presence of the sea water; the elements in increasing order of extent of adsorption at that level were: Cs $<$ Sr $<$ I, (Np) $<$ Te, Nb $<$ La, Ce, Pr, Ru $<$ Y, Zr. Over the whole range of concentrations, the order would be: charge 1 ions $<$ charge 2 ions $<$ charge 3 ions $\cong$ colloidal elements.

The average area covered by 300 μl. of solution as measured from the radioautographs was 0.251 sq. in., giving an average surface density of

TABLE III

Decontamination of Np as a Function of Initial Level

I (*counts/min.*)	I (*moles/liter*)	Fraction of a FP C-Level	F(%)
85	2.3×10^{-14}	4.1×10^{-5}	28 ± 6
508	1.4×10^{-13}	2.5×10^{-4}	20.5 ± 3.2
5,353	1.4×10^{-12}	2.5×10^{-3}	17.5 ± 1.4
51,330	1.4×10^{-11}	2.5×10^{-2}	14.8 ± 0.7
500,700	1.3×10^{-10}	0.23	12.4 ± 0.4

TABLE IV

Constants for Decontamination Equations for Dried Single-Carrier Contaminants on Navy Gray Paint Based on the C-Level Concentration Parameter[a]

Elements	a	n	Time of contact (*hr.*)
Cs	0.029 ± 0.003	0.637 ± 0.012	18.5
Sr	0.075 ± 0.004	1.00	18.6
Y	1.155 ± 0.224	0.955 ± 0.024	17.8
La	0.857 ± 0.041	0.992 ± 0.009	18.0
Ce	0.880 ± 0.012	0.970 ± 0.004	17.8
Pr	0.870 ± 0.122	0.949 ± 0.019	19.6
Zr	1.218 ± 0.063	0.886 ± 0.008	20.6
Nb	0.593 ± 0.006	1.020 ± 0.001	19.0
Te	0.528	0.882	18.5
I	0.156 ± 0.012	0.694 ± 0.013	17.8
Ru	0.898 ± 0.074	0.969 ± 0.014	19.2
Np	0.106 ± 0.007[b]	0.912 ± 0.010	21.0

[a] For equation, $R = aI^n$.

[b] For I = fraction of the FP C-level.

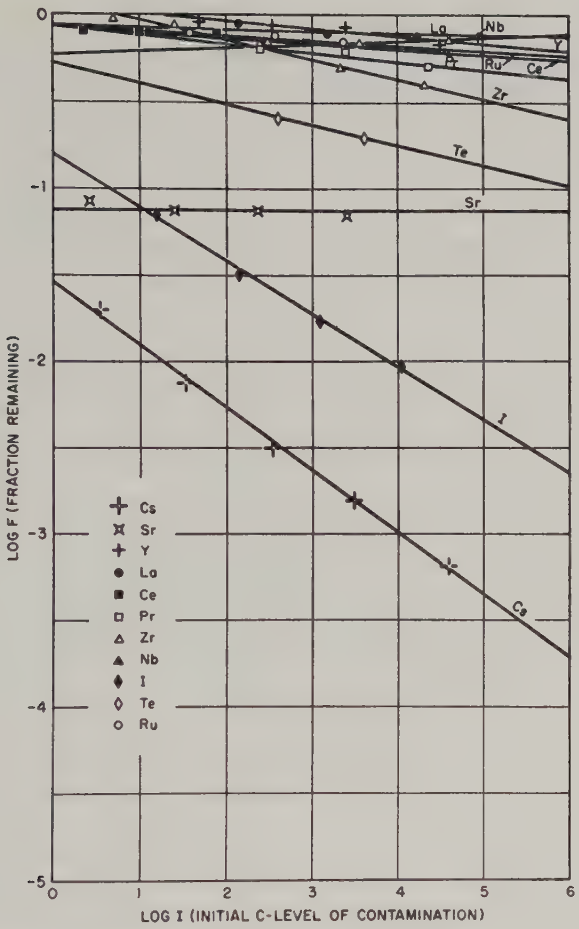

FIG. 1. Decontamination of 11 FP elements as a function of initial level.

1.20 ml./sq. in. Since it has been estimated that a surface density of 8.2×10^{-3} ml./sq. in. of a 1 *C*-level solution containing all the FP would produce 1 r/hr. at 1 hr., the 1 *C*-level at the surface density used in these experiments should be equivalent to 150 r/hr. at 1 hr. Since the method of contamination maximized the surface density of contamination for a horizontal surface without having run-off, the 150 r/hr. at 1 hr. is the maximum radiation level (assuming the same surface density of radioactivity over a large area) that could be associated with the 1 *C*-level contaminant solution containing all the FP.

From the data in Tables I and IV the fraction of all the FP atoms remaining after decontamination can be calculated by making the assumption that the remaining 28% of the FP would decontaminate to about the same extent as the 72% represented by the 11 elements for which the data were obtained. Using a maximum F of 1.00 for Y and Zr where required, the calculations give 65.1 %, 60.1 %, 51.9 %, 45.2 %, and 39.8 % remaining at the 1, 10, 100, 1000, and 10,000 C-levels. At the four higher levels a least-squares fit of the results to Eq. [7] gives $a = 0.686 \pm 0.007$ and $n = 0.940 \pm 0.001$. These values were used to determine the dotted line in Fig. 1. All the data are in terms of the fraction of FP atoms remaining. A better estimate of the reduction in gamma radiation field could be made by weighting each element according to its contribution to the total gamma flux being emitted by the combined FP radionuclides at the time (after fission) of interest.

Summary and Conclusions

The contamination and decontamination reactions of some elements representative of the most important gamma-emitting radionuclides produced by an atomic detonation near the surface in deep sea water have been investigated. The contaminant mixture was a simplified one containing only the major sea water elements and a single radioactive element (plus inactive carrier) at a time. With the use of published data and a number of assumptions, calculations were made establishing a concentration range of 6×10^{-9} to 6×10^{-7} mole/liter for the total FP elements. These limiting concentrations have been arbitrarily designated the 1 C-level and the 100 C-level, respectively. If the geometric mean of the range is taken as the most probable concentration, then the 10 C-level or 6×10^{-8} mole/liter solution would be the most likely FP-to-sea-water ratio to result from a nuclear detonation near the surface in deep sea water (according to complete mixing assumptions). Further, this ratio should be independent of yield, at least for weapons detonated at geometrically scaled depths according to commonly accepted scaling laws (6). Instead of varying the surface density of the 10 C-level solution on the surface to obtain a range of equivalent gamma radiation levels, the authors chose to use equal volumes of solutions of constant ionic strength and varied the FP-to-sea-water ratio to give a range of FP surface densities. This procedure was acceptable, since changes in the ratio at constant FP concentration had little effect on the interaction being measured.

All the elements the actual concentration of which varied with the C-level designation were found to decontaminate according to

$$F = aI^{n-1}, \qquad [8]$$

in which F is the fraction remaining and I the initial level and a and n are constants for each element. In terms of radiation levels, the surface density of material used in these experiments was estimated to be equivalent to 150 r/hr. at 1 hr. at 1 C-level; hence the term C-level, as used, has a dual meaning.

Although the contaminants used in the experiment were extremely simple compared to one which would contain all the components of atomic detonation debris, this experiment is a good example of the kind of data required for the understanding and analysis of the radiological recovery problem. Since chemical systems which have to be dealt with in decontamination originate with a nuclear detonation as the source of atomic debris, the chemical systems used in the decontamination experiments must reflect, to some degree, a consideration of the whole process: contaminate formation, contaminant distribution or dispersion, surface interaction (contamination), and recovery by a method of decontamination. These, in essence, are the physical processes which are associated with a possible radiological situation and to which data of the kind presented can be applied.

References

1. "The Effects of Atomic Weapons," Superintendent of Documents, United States Government Printing Office, Washington, D. C., September, 1950 (revised).
2. Hunter, H. F., and Ballou, N. E., *Nucleonics* **9**, (No. 5), C-2 (Nov. 1951).
3. Heiman, W. J., *J. Colloid Sci.* **13**, 329 (1958).
4. Sverdrup, H. V., Johnson, M. W., and Fleming, R. H., "The Oceans, Their Physics, Chemistry, and General Biology." Prentice Hall, New York, 1946.
5. Siegel, J. M., *J. Am. Chem. Soc.* **68**, 2411 (1946).
6. Cole, R. H., "Underwater Explosions." Princeton University Press, Princeton, New Jersey, 1948.

JOURNAL OF COLLOID SCIENCE **13**, 348–357 (1958)

DECONTAMINATION REACTIONS OF SYNTHESIZED FALLOUT DEBRIS FOR NUCLEAR DETONATIONS

II. LAND-SURFACE NUCLEAR DETONATION

Carl F. Miller, Richard Cole, W. B. Lane, and J. L. Mackin

Radiological Capabilities Branch, Chemical Technology Division,
United States Naval Radiological Defense Laboratory,
San Francisco 24, California

Received October 24, 1957

ABSTRACT

The decontamination of San Francisco harbor bottom soil, Nevada test site soil, and a commercial clay from a paint surface has been investigated. Decontamination was achieved with stirred water and sprayed water. The surface density of soil remaining after decontamination was found to depend on the initial condition according to the equation,

$$R_m = R_M(1 - e^{-ay})$$

in which R_M is a constant related to the mean particle size remaining, a is a constant related to the mean particle size and density of the deposited soil, and y is the surface density of the initial deposit. Estimates are made for the gamma radiation intensity over the contaminated and decontaminated surfaces for the case in which the surface area is large and the soil is fallout from a surface land atomic detonation.

INTRODUCTION

When a nuclear device—or any explosive material—is detonated on or beneath the surface of dry land, soil particles are thrown up or drawn into a "chimney" of hot rising gases and raised aloft. In the case of a nuclear device, two important processes occur: (*1*) vaporized radioactive fission product elements condense onto the soil particles, and (*2*) many of the soil particles rise thousands of feet into the air before they begin falling back, permitting the winds to scatter the particles over areas much greater than the cross section of the original mushroom cloud. Thus when the particles reach the earth they may be far from their origin and are contaminated with radioactivity. The particular concern over these particles is associated with the radioactivity they carry. In this report, preliminary experiments are presented to illustrate how such particles decontaminate (wash off) from a smooth, impervious surface. These experiments do not consider the radioactive disposal problem; they were designed primarily to give information on the extent to which the particles stick to such a surface.

THEORETICAL CONSIDERATIONS

Suppose a number of test surfaces were placed in some pattern under a cloud of particles. If one were to observe at high magnification a small area of one of the surfaces as the cloud passes overhead, one would see particles land one after another—or perhaps many at a time if the area is not too small. One would notice that the larger particles arrive first, and that some late arrivals land on other particles. An observer at a second test surface would probably not see his initial particle at the same time as the observer at the first test surface; nor would the size of the initial particles or the mean size of all the particles be necessarily the same at the two sites.

The gross amount of particles received by the various test surfaces depends among other things upon the amount of soil thrown into the air, the winds at all altitudes, and the site of the test surface. The particles could arrive either over a short period of time or over many hours; in either case, the time period or rate of deposition will not affect the following discussion. The main point is that, if enough test surfaces were placed over a large area, the gross deposit would be observed to vary from zero to some maximum surface density of soil particles. When the particle-size groups are distributed about a mean value, it is convenient to represent the deposit by the mass per unit area. Let y be the mass of material per unit area on the surface at any time and f be the fraction of the unit area covered by the group of particles of total mass y. The increase in the fraction of area covered by particles as the fallout progresses will be proportional to the amount of clean area available, or

$$df/dy = a(1 - f), \tag{1}$$

in which a is a constant dependent on the mean particle size and on density. Integrating under the limits stated above gives

$$f = 1 - e^{-ay}. \tag{2}$$

Knowledge of the precise time dependence of y and/or f is not required since this is reflected in the total mass received at the various locations which were exposed to fallout for various periods.

If, upon decontamination, all the particles not touching the surface are removed and, of those contacting the surface, all greater than a mean size are removed, then the remaining mass per unit area is

$$R_m = \rho V_m f, \tag{3}$$

in which ρ is the density of the soil and V_m is the volume of remaining mass per unit area for complete coverage of the surface ($f = 1$). If the particles are assumed to cover an area equal to their maximum horizontal cross section, then V_m for cubic particles is simply their mean vertical diameter; for spherical particles in close-packing it is ⅔ of the mean diameter (within 10%).

The fraction of the original mass remaining (decontamination ratio) is given by

$$F_m = \frac{R_m}{y} = \frac{R_M(1 - e^{-ay})}{y}, \qquad [4]$$

in which $R_M = \rho V_m$.

The radiation intensity equivalent of Eq. [4] for a given detonation can be estimated. For a 20-kt. weapon detonated near the surface of sea water, it has been estimated (1) that the maximum concentration of fission product would be about 5.6×10^{-7} mole/liter and that a surface density of 8.3×10^{-5} ml./sq. in. of that material would produce 1 r/hr. at 1 hr. after fission. If it is assumed that the same weapon detonated on land would throw out about the same volume of soil and that this soil would scavenge or condense-out all of the radioactivity, then it is possible to calculate a specific activity for the soil. Thus for a soil density of 2.5 g./cu. cm., the surface density of material required to produce a radiation flux of 1 r/hr. at 1 hr. would be 0.21 mg./sq. in.[1] The fraction, 0.21 mg./sq. in./r/hr. at 1 hr., is defined as the mass contour ratio and is given in general by

$$y/I_r(1) = M_r(1) \qquad [5]$$

in which $I_r(1)$ is the $H + 1$ hr. radiation intensity prior to decontamination and $M_r(1)$ is the 1-hr. mass contour ratio. The decontamination ratio, F_r, in terms of r/hr. at 1 hr. will be

$$F = \frac{R_R(1 - e^{-mI_r(1)})}{I_r(1)} \qquad [6]$$

in which $R_R = \rho V_m / M_r(1)$ and $m = aM_r(1)$.

Equation [6] implies the assumption that the radioactivity is "fixed" onto the particles and will not leach from them during the decontamination procedure. Equations [4] and [6] predict that F will vary inversely with the initial level for initial contamination levels equal to or greater than that required to cover the surface completely ($f = 1$). As $I_r(1)$ approaches zero, F_r approaches the value $mR_R = aR_M$.

EXPERIMENTAL DETAILS

The soils used in this investigation were an average grade clay obtained from the Harris Clay Co., two core samples from the San Francisco harbor bottom, and dirt from the Nevada Test Site. The latter was passed through a 50-mesh sieve to remove rocks and organic material.

---

[1] If the geometric mean of the estimated maximum and minimum FP concentrations (1) is used and if it is assumed that equal weights of soil and water are thrown up and mixed with the FP, then the surface density of material required to produce 1 r/hr. would be 0.83 mg./sq. in.

The test surfaces used were Navy gray paint (Haze Gray, 5H) on aluminum plates (1¼ by 1¼ by ⅛ in.). They were aged for 6 weeks and then exposed in an Atlas weatherometer for 90 hr.

The experiments were carried out by two methods. In the first method, water slurries of the harbor bottom and clay soils were prepared at 0.2%, 0.5%, 1.0%, 2.0%, and 5.0% by weight of soil. The test surfaces in triplicate were contaminated with slurries by pipetting 1 ml. from a vigorously stirred slurry onto a previously weighed plate. The contaminated plate was dried at 30°C. overnight, after which it was weighed, decontaminated, and again weighed. This set of samples will be identified by the term "slurried" soils.

In the second method the Nevada Test Site dirt and clay soils were tagged with about 1 mc. of Ce^{144} by making a slurry of 100 g. of each soil in 500 ml. of water containing the tracer. The slurries were slowly evaporated down to dryness, oven-dried overnight, and fired at 900°C. for 1 hr. Small portions of the fired material were washed with water. A count assay of the wash water showed that less than 1% of the Ce^{144} was removed from the soil. A definite area (1 sq. in.) of each test surface was bounded by a template and contaminated with the tagged soils. The template was an aluminum plate (3 by 3 by ¼ in.) with a 1-in. square hole machined at its center. An additional ⅛ in. around the hole was machined out on the underside deep enough to seat the test sample. The contaminated plates thus had a ⅛-in. clean border around their outer edges. Weighed test surfaces were placed under the template one at a time and contaminated by dropping the soil in small amounts through a Tyler 35 sieve from 2 in. above the plate. Attempts were made to contaminate the surfaces with about 0.2, 2, 20, 200, and 2000 mg. of soil. After contamination, the plates were reweighed and counted on a gamma scintillation counter. The specific count rate thus obtained was used to convert all the counting data to mass data.

Half of the samples contaminated with the tagged soils were placed in a high humidity chamber for 12 hr. and then oven-dried at 30°C. for 1 hr. This set of samples will be termed "prewet" soils.

All weighings were made on a Sartorius semi-micro balance.

A spray chamber and a stirring apparatus were used to decontaminate the test surfaces. In the spray (or hosing) method the samples were exposed in a chamber to a spray of water applied through a fine nozzle at 50 p.s.i.g. for 30 sec. In the stirring method the samples were immersed in 250 ml. of water and gently stirred for 5 min., after which they were rinsed in a vertical position in clean water to drain all the loosened particles from the plate.

In the case of the tagged soils, the amount of soil remaining after decontamination was determined from the observed count and the specific

TABLE I

Decontamination by Stirred Water

San Francisco harbor soil (slurried)			Clay (slurried)		
I_m (*mg./in.*^{2})	F_m(obs.) (%)	F_m(calc.) (%)	I_m (*mg./in.*^{2})	F_m(obs.) (%)	F_m(calc.) (%)
11.7	13 ± 4	12.9	12.9	25 ± 10	25.4
23.7	8.8 ± 1.7	8.8	24.7	12 ± 10	21.0
49.6	5.4 ± 1.0	4.8	47.8	15 ± 5	15.0
96.0	2.2 ± 0.5	2.5	96.1	9.8 ± 1.0	8.6
226	1.1 ± 0.2	1.1	235	3.1 ± 0.5	3.6

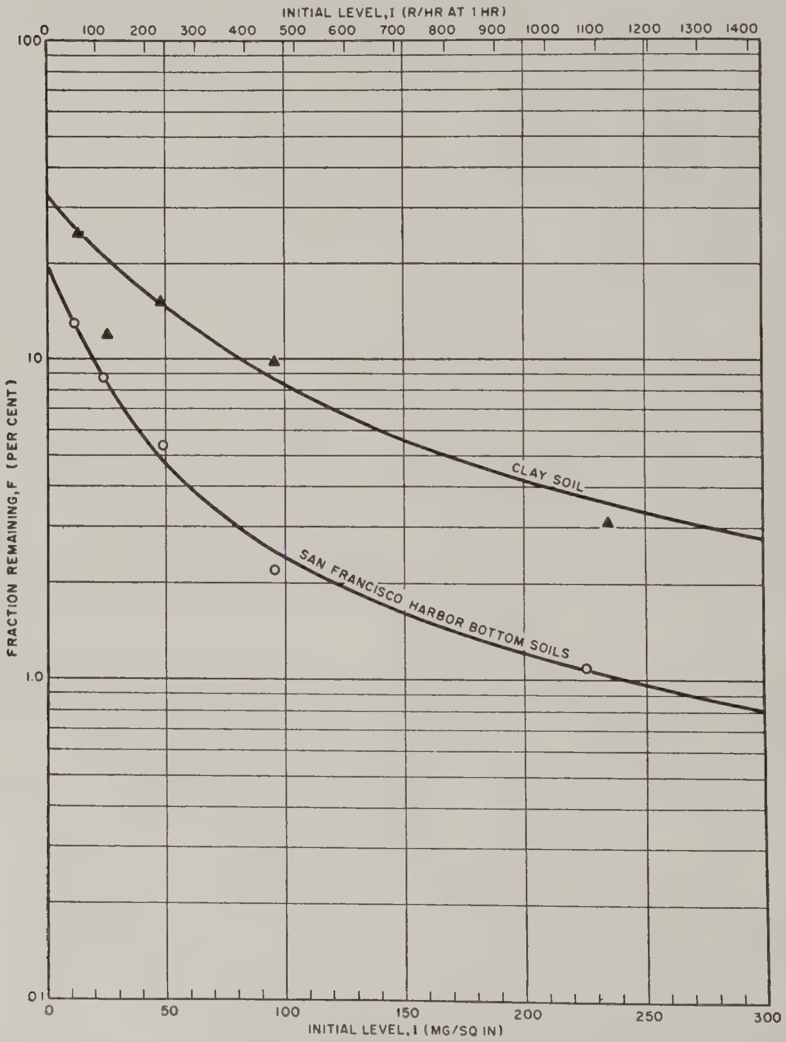

FIG. 1. Stirred water decontamination of untagged soils.

count rate of the soil. The untagged harbor bottom and clay soils were decontaminated by the stirred method only and the amount of soil remaining was determined by weighing.

RESULTS

The data for the San Francisco harbor bottom soil and the clay soil are given in Table I and are plotted in Fig. 1. The values of $I_m (I_m = y)$ and F_m for the harbor soils are averages of six samples (three for each core sample); data for the clay are averages of three samples. The data for the tagged soils are given in Tables II and III and are plotted in Figs. 2 and 3. The smoothed curves were calculated from the equation constants summarized in Table IV. Although initial deposits up to about 1500 mg./sq. in. were used, the figures are plotted only to 300 mg./sq. in. (about 1400 r/hr. at 1 hr.). The usual method of obtaining the constants was to average the remaining amounts at levels greater than about 100 mg./sq. in., where, in most cases, f is almost 1; that value (R_M) was used to calculate the constant

TABLE II

Decontamination by Stirred Water Using Tagged Soils

Nevada soil			Nevada soil (prewet)			Clay			Clay (prewet)		
I(*mg./in.*²)	*F*(%)	*F*(calc.) (%)	*I*(*mg./in.*²)	*F*(%)	*F*(calc.) (%)	*I*(*mg./in.*²)	*F*(%)	*F*(calc.) (%)	*I*(*mg./in.*)	*F*(%)	*F*(calc.) (%)
0.497	11.1	7.44	0.724	13.5	12.4	0.172	11.6	3.98	0.354	66.6	6.3
5.26	7.62	6.75	0.988	14.3	12.3	0.730	3.15	3.94	0.414	67.4	6.2
6.47	6.71	6.60	4.46	9.89	10.8	0.912	5.92	3.88	6.20	9.35	5.62
13.9	4.16	5.74	6.88	9.66	9.83	1.03	4.66	3.84	6.83	10.6	5.54
16.1	4.88	5.52	18.8	3.41	6.59	21.5	1.55	2.75	27.0	2.79	3.93
119	1.80	1.56	106	1.67	1.49	41.5	1.14	2.06	28.2	2.84	3.86
121	1.06	1.54	1260	0.122	0.125	150	0.497	0.710	82.4	1.35	1.94
1430	0.119	0.131	1500	0.130	0.111	1120	0.158	0.096	900	0.246	0.184

TABLE III

Decontamination by Sprayed Water Using Tagged Soils

Nevada soil			Nevada soil (prewet)			Clay			Clay (prewet)		
I(*mg./in.*²)	*F*(%)	*F* (calc.) (%)	*I*(*mg./in.*²)	*F*(%)	*F* (calc.) (%)	*I*(*mg./in.*²)	*F*(%)	*F* (calc.) (%)	*I*(*mg./in.*²)	*F*(%)	*F* (calc.) (%)
0.242	1.0	0.32	0.682	3.52	2.43	0.828	0.63	0.15	0.448	25.9	2.72
6.25	0.288	0.28	1.24	2.90	2.38	1.86	0.86	0.14	0.516	12.0	2.72
19.8	0.0909	0.22	4.79	1.84	2.08	26.8	0.056	0.093	3.08	3.54	2.61
21.6	0.102	0.21	5.03	1.67	2.05	32.2	0.053	0.086	3.72	3.55	2.59
88.9	0.0405	0.086	21.1	0.725	1.20	164	0.017	0.024	11.6	1.67	2.23
122	0.0205	0.064	88.5	0.380	0.349	206	0.016	0.019	15.7	1.07	2.03
1420	0.0116	0.056	127	0.250	0.243	1230	0.0037	0.0032	—	—	—
1480	0.0118	0.053	1240	0.0212	0.025	1300	0.0035	0.0030	—	—	—

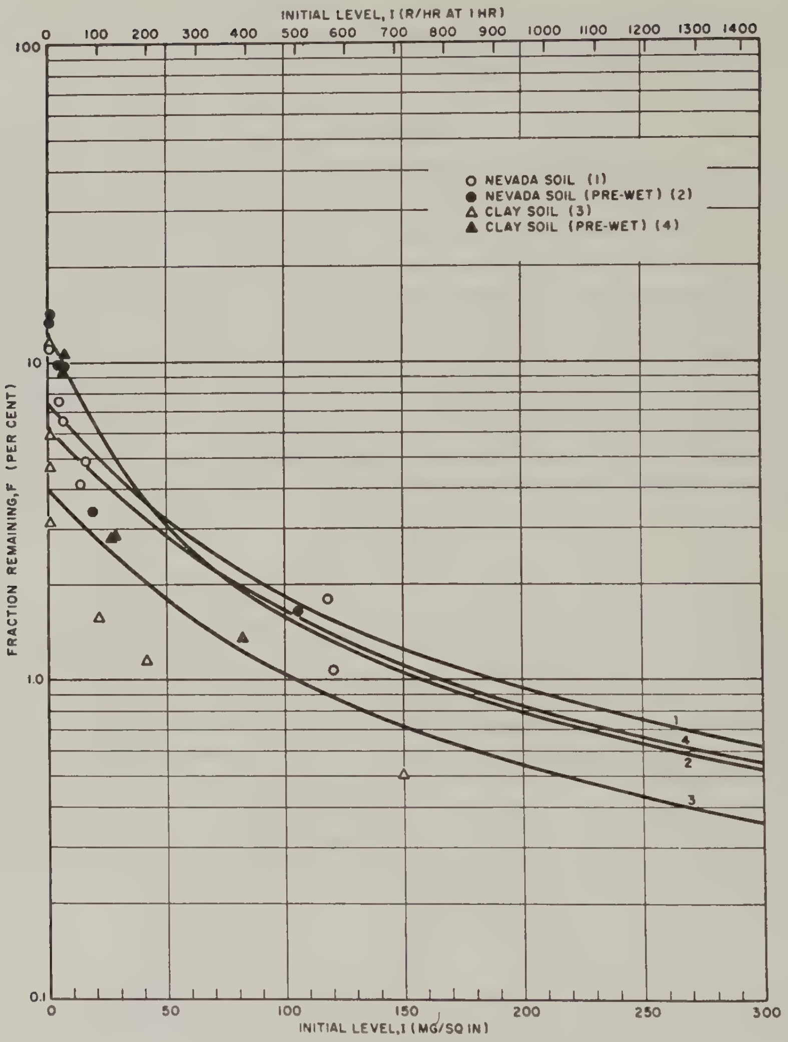

FIG. 2. Stirred water decontamination of tagged soils.

a from each of the remaining data points. Since a should be independent of the method of decontamination, the value given in Table IV is an average of the a's for both methods. The constant R_M for the spray method on the prewet clay was obtained by first using the above procedure to calculate a for the stirrer method on the prewet clay; then using the a thus obtained, the value of R_M was calculated from the data for the spray decontamination. The mean particle size, V_m, and the maximum radiation

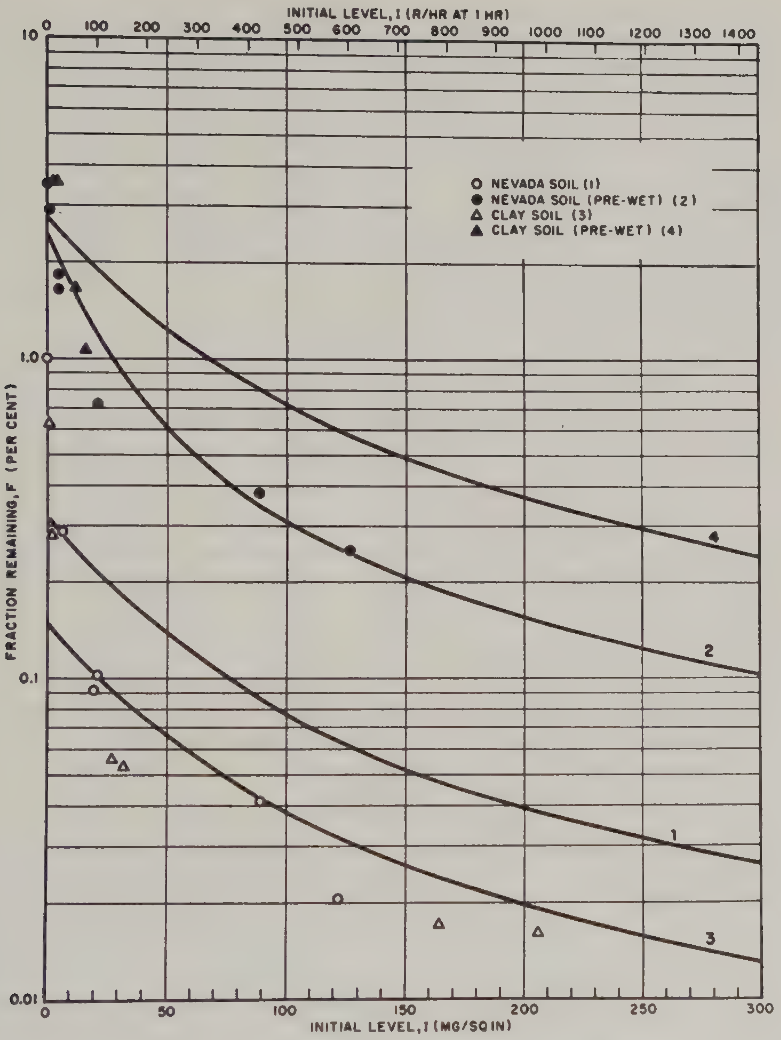

FIG. 3. Sprayed water decontamination of tagged soils.

level remaining after decontamination are summarized in Table V. The scatter in F values at low values of $I_r(1)$ of the tagged soils is to be expected for this kind of experiment, since it involves the detection of a mass of the order of 0.001 mg./sq. in. Even with as much tracer as was used, the gamma count of the decontaminated surface was often as small as 2% to 5% of background which, even with extended counting periods, involved considerable statistical fluctuation.

TABLE IV

Summary of Derived Constants for Eq. [6]

	Stirrer method			Spray method		
	R_M (mg./in.²)	a (in.²/mg.)	aR_M (%)	R_M (mg./in.²)	a (in.²/mg.)	aR_M (%)
Nevada soil	1.87	0.040	7.5	0.079	0.040	0.32
Nevada soil (prewet)	1.58	0.081	12.8	0.309	0.081	2.5
Clay	1.07	0.037	4.0	0.039	0.037	0.15
Clay (prewet)	1.66	0.038	6.3	0.73	0.038	2.8
SF harbor bottom soil (slurried)	2.43	0.083	20.2	—	—	—
Clay (slurried)	8.35	0.039	32.7	—	—	—

TABLE V

Mean Particle Size and Maximum Radiation Level Remaining on Surface

	Stirrer method		Spray method	
	V_m* (μ)	R_R (r/hr. at 1 hr.)	V_m* (μ)	R_R (r/hr. at 1 hr.)
Nevada soil	1.2	8.8	0.05	0.4
Nevada soil (prewet)	1.0	7.5	0.19	1.5
Clay	0.7	5.1	0.02	0.2
Clay (prewet)	1.0	7.9	0.45	3.5
SF harbor bottom soil (slurried)	1.5	12	—	—
Clay (slurried)	5.2	40	—	—

* $\rho = 2.5$ for all soils.

SUMMARY

The decontamination of a group of soil particles from three soil sources has been carried out over a range of initial simulated dose-rate intensities associated with a mass surface density of particles ranging from 0.2 to 1500 mg./sq. in. (estimated to be from 1 to 7500 r/hr. at 1 hr.). The amount remaining after decontamination increased with initial level until a maximum was reached, after which it remained constant; for the stirring method the maximum varied from about 1 to 8 mg./sq. in. (5 to 40 r/hr. at 1 hr.); for the spray method the maximum varied from 0.04 to 0.7 mg./sq. in. (0.2 to 4 r/hr. at 1 hr.). These numbers are a measure of the quantity of small particles of the particle groups which are strongly held in the residual force field of the test surfaces rather than a measure of the decontamination effectiveness which might be achieved in a large-scale decontamination operation. The mean particle sizes as estimated by the constant, V_m, are too large to attribute their retention to van der Waals' adsorption. The sizes are in the near-colloidal range; the particles are undoubtedly charged, and hence are probably chemisorbed by the surface. In the stirring method, the interfacial tension between the small particles and the water is not sufficient to overcome the attractive force field exerted by the surface on the particle. In the spray method, the water molecules strike the particles with a higher energy, removing more particles and also decreasing the mean size of the remaining particles.

For the Nevada soil, the spray method was about 24 times as effective as the stirrer method; for prewetted Nevada soil it was about 5 times as effective. The prewetting appeared to increase the area covered per gram of soil for the coarser soils as reflected in the value of a; no trend was apparent for the finer clay. The effect of the prewetting on the spray method appeared in the larger value of R_M. The effect of the prewetting as used might be compared to an exposure of the deposits to an overnight dew while the slurry deposition might be compared to an exposure to rain, each with a subsequent later drying out before decontamination.

Although the procedure employed to apply the radioactive tracer proved satisfactory, the experimental technique used to apply the soils as a simulated radioactive contaminant to the surface did not correspond well with the way they would arrive in a real fallout, where the particles would "statistically" accumulate on the surface with the larger particles arriving first. Even though a great deal of care was used to get an "even" distribution of particles over the surface, it was virtually impossible to obtain a satisfactory even deposit over the whole area with deposits less than 100 mg. from the height at which the soil was dropped. Of the two methods of application, the slurry method, where the water tended to suspend the finer particles for some length of time, probably came closer to the real situation. Wide variations in the distribution of the particles over the surface for the ligher deposits are reflected in the dispersion of the F's at low initial deposits and hence in the value of a in Eq. [6]. Although the precision of the data is not of the degree required to substantiate the theoretical equations rigorously, the empirical fit in itself is useful for extrapolation and interpolation which would not otherwise be possible.

These preliminary experiments on the decontamination of simulated debris from a nuclear detonation on land are presented as an example of the methods employed to aid in the understanding and description of the chemistry and physics of the fallout material. Data of this kind are applicable, in a practical way, to the formulation of basic concepts of radiological recovery following an atomic attack.

REFERENCE

1. MILLER, C. F., COLE, R., AND HEIMAN, W. J., *J. Colloid Sci.* **13,** 337 (1958).

JOURNAL OF COLLOID SCIENCE **13**, 358–371 (1958)

BASIC FACTORS IN THE FORMATION AND STABILITY OF NONSOAP LUBRICATING GREASES

I. A STUDY OF THE FACTORS RESPONSIBLE FOR GEL FORMATION

G. J. Young and J. J. Chessick

The Surface Chemistry Laboratory Lehigh University, Bethlehem, Pennsylvania

Received March 10, 1958

Abstract

The oil-thickener interface was recognized as the seat of important properties in nonsoap greases. In order to index the nature and extent of this interface, in a variety of systems, first the surface characteristics of several thickening agents and the physical properties of several oils were measured. These properties of the oils and solids were correlated with the behavior of grease systems formulated from them. Modification of the interfacial region by water and its effect on grease building by inducing flocculation was then investigated.

For hydrophobic thickeners, grease building efficiency depends directly on surface area for those above 200 m.^{2}/g., and falls off sharply for thickness of lower surface area. The amounts of thickeners required to give greases of a specified consistency vary as the square of their surface areas. For hydrophilic thickeners, the amounts of water adsorbed at the oil-thickener interface can be much larger than for hydrophobic thickeners and, indeed, control the consistency. Temperature, relative humidity, and amount of working of the grease affect the amount of water at the interface. The polarity of the oil has little effect on the grease building by hydrophobic thickeners, but greatly affects those built with hydrophilic thickeners. In the latter case, water enhances thickening in nonpolar vehicles but somewhat surprisingly thins those made with polar, water-miscible oils.

Introduction

Nonsoap greases, in contrast to soap greases, are thickened with finely divided inorganic or oil-insoluble organic solids instead of metal soaps. The advantages of the nonsoap greases arise primarily from the greater thermal stability of the thickening agents and the resulting gel structures. For example, consistency changes found with soap greases due to phase changes or to temperature-solubility relations of the soap and oil are not found with the nonsoap greases which have no true dropping point.

The mechanism of gel formation by various types of finely divided solids in organic liquids is not entirely understood. Hence, the selection of proper thickening agents and prediction of the stability and behavior of the resulting grease systems generally have been decided by trial-and-error procedures. Scientific understanding of such factors as thermal, pressure, and working stability, and of bleeding and syneresis during storage has not yet been developed. The effect of additives added for specific purposes such as increasing dispersion, corrosion inhibition, reduction of the effect of pressure and temperature on reducing lubrication properties, and possibly undesirable interrelated effects, are at best only artfully known. The present paper is the initial report of an investigation of the basic factors involved in gel formation in nonsoap lubricating greases and the relation of certain of these variables to the stability of the gel systems. Specifically, the influence of surface area of the solids on thickening ability and of small amounts of water were examined.

MATERIALS AND METHODS

A variety of oils and thickener powders were chosen to cover as wide a practical range of materials which would develop greaselike systems.

Oils

The oils employed in this investigation are listed in Table I where densities, viscosities, surface tensions, and dielectric constants are listed. Plexol 201 (Rohm and Haas Co.), Ucon Adipate 465 and Ucon Lubricant DLB-62-E (Carbide and Carbon Chemical Co.) are diester type synthetic oils; the latter contains additives to reduce the pressure and temperature coefficient of viscosity. Paraffin Oil (Matheson, Coleman, and Bell) is a mixture of aliphatic hydrocarbons. Sunvis 11 (Sun Oil Co.) is a petroleum oil obtained from the solvent refining of mixed base crudes and is predominantly paraffinic. Circo X Light (Sun Oil Co.) is derived from Gulf Coastal crude petroleum oil and is predominantly naphthenic. Disiloxane MLO 8200 (Oronite Chemical Co.) is a disiloxane designed for use as a high-temperature hydraulic fluid. Silicone DC 550 (Dow Corning Co.) is a methyl phenyl silicone oil.

TABLE I

Physical Properties of Oils at 25°C.

	Density (*g./ml.*)	Viscosity (*centipoises*)	Surface tension (*ergs/cm.^{2}*)	Dielectric constant
Plexol 201	0.912	17.6	31.3	3.85
Ucon Adipate 465	0.946	6.1	30.7	5.31
Paraffin Oil	0.873	87.5	31.0	—
Ucon Lubricant DLB-62-E	0.950	16.5	28.9	12.4
Sunvis 11	0.855	31.0	30.1	—
Circo X Light	0.910	38.6	31.6	—
Disiloxane MLO 8200	0.923	40.0	26.1	2.64
Silicone DC 550	1.062	129	27.1	—

Thickeners

The thickening agents employed in this investigation are listed in Table II with their measured surface properties.

Aerosil (Godfrey L. Cabot Co.), Santocel ARD and Santocel 54 (Monsanto Chemical Co.) are nonporous silicas. Their surface areas, particle sizes, and particle shapes are similar; however, they differ in the nature of their surfaces. The heats of immersion and water vapor adsorption indicate that the Aerosil surface is much less hydrophilic than those of the Santocels. The Carbolacs, Supercarbovar, and Monarch 71 (Godfrey L. Cabot Co.) are carbon blacks of varying surface area and porosity and with differing amounts of volatile matter on their surfaces (1). Graphon (Godfrey L. Cabot Co.) is a graphitized carbon black with a homopolar, homogeneous surface (2) possessing lower heats of immersion and water vapor adsorption than other carbon blacks. HiSil (Columbia Southern Chemical Corporation)

TABLE II

Surface Characteristics of Thickening Agents[a]

Thickening agent	Surface area (*$m.^2/g.$*)	Average particle size (*microns*)	Particle shape	Heat of immersion in water (*$ergs./cm.^2$*)	Heat of immersion in Plexol 201 (*$ergs/cm.^2$*)	Water adsorption (*$mg./m.^2$ at R.H. 30%*)
Aerosil (Cabosil)	147–187	0.015 to 0.020	Irregular grains	180	170	0.07
Santocel ARD	170	0.015	I.G.	340	270	0.13
Permagel	180–200	0.045	Needles	380–500	180	0.57
Carbolac "1"	820–1000	0.011	I.G.	80–90	115	0.07
Carbolac "2"	660–700	0.014	I.G.	90	130	0.12
Carbolac "46"	525–600	0.014	I.G.	110	—	—
Supercarbovar	350–430	0.014	I.G.	85	120	0.07
Monarch "71"	250–420	0.018	I.G.	65	110	0.07
G. S. Hydrophobic Silica	270	*ca.* 0.012	I.G.	26	85	0.01
Estersil	290–300	0.010	I.G.	*ca.* 10	66	0.01
Copper phthalocyanine	74	0.050	Platelike prisms	34	112	0.03
Bentone "34"	6–11	—	Flat platelets	440	250	1.90
Ebco "1"	13–15	—	Platelets	300	—	0.14
Graphon	75–95	—	I.G.	32	110	0.00
HiSil	129	—	I.G.	460	—	—
TiO_2 (MP997)	105	—	I.G.	(550)	—	—

[a] A smaller heat of wetting in water compared to the organic liquid, Plexol 201, indicates surface hydrophobicity. For the hydrophilic solids, the magnitude of the heat of wetting is a measure of the degree of surface polarity.

and the TiO_2 (MP997) (National Lead Co.) are highly polar solids as measured by heats of immersion in water or organic liquids.

G. S. Hydrophobic Silica and Estersil (E. I. du Pont de Nemours) (3) are silicas that have been given hydrophobic organic surface coatings.

Bentone 34 (National Lead Co.) and Ebco 1 (Edgar Bros. Co.) are clays that have been given hydrophobic organic surface coatings. In both cases, only a portion of the surface is effectively hydrophobic. Bentone 34 is prepared from a montmorillonite (bentonite) clay; Ebco 1 is prepared from a kaolinite.

Copper phthalocyanine (E. I. du Pont de Nemours) is a thermally stable, oil-insoluble organic and is hydrophobic; this grade was produced specifically for use as a grease thickener.

The surface characteristics of the thickeners are listed in Table II. Surface areas were measured by nitrogen adsorption. Particle shapes and sizes were estimated from electron micrographs. Heats of immersional wetting were measured in a calorimeter previously described (4).

Preparation

The production of complete and reproducible dispersions, particularly in the absence of dispersing agents, is a considerable problem. To accomplish this, all preparations were finally milled on a "floating roll" three-roll mill (5). With this mill, major milling variables such as clearance, force on the rolls, and roll temperature could be adjusted to give the best dispersion possible. For each system, maximum dispersion was developed as measured on a fineness of grind gage, the NPIRI Grindometer (6). Agglomerate particle sizes larger than about 0.5 μ were not tolerated. Even those thickeners generally believed to require dispersing agents or special thermal treatment could be properly dispersed by careful control of the milling variables. The dispersions were further checked by light microscopy and in some cases by electron microscopy.

For some of the work, it was desirable to store the oil and thickener at different relative humidities prior to formulation. Exposure to atmospheric conditions occurred only during the rapid final roll milling step.

Testing

Flow curves of these highly filled grease systems cannot be established with precision rotational viscometers. Presumably slippage occurs as the shear rate is increased. For this reason, consistency was established in each case by measuring penetration with a standard ASTM penetrometer using the prescribed procedure (7). The lower the penetration value, the higher is the grease consistency.

For stability measurements, the greases were worked in an ASTM motor-driven grease worker (7) for 100,000 double strokes. A comparison of penetration values before and after working was used as a measure of stability.

Results and Discussion

Two-component grease systems were formulated at a variety of thickener concentrations from many of the possible combinations. Analysis of the properties readily led to the conclusion that hydrophobic and hydrophilic thickeners produced two distinct families.

Grease Building Efficiency of Hydrophobic Thickeners

In general, the decrease in penetration of a grease with increasing amount of thickening agent is not a linear function. At low concentrations of thickener, the penetration of the grease is strongly dependent on small changes in the thickener concentration and also on other factors influencing consistency. At high loadings of thickener, the penetration of the grease is relatively insensitive to changes in thickener concentration or other factors. This behavior is illustrated in Fig. 1, where the worked penetrations of several greases are plotted as a function of the weight percentage thickener. These greases were formulated with hydrophobic thickeners in Disiloxane MLO 8200. Similar, although limited results, were found for these solids dispersed in the other vehicles described in Table I.

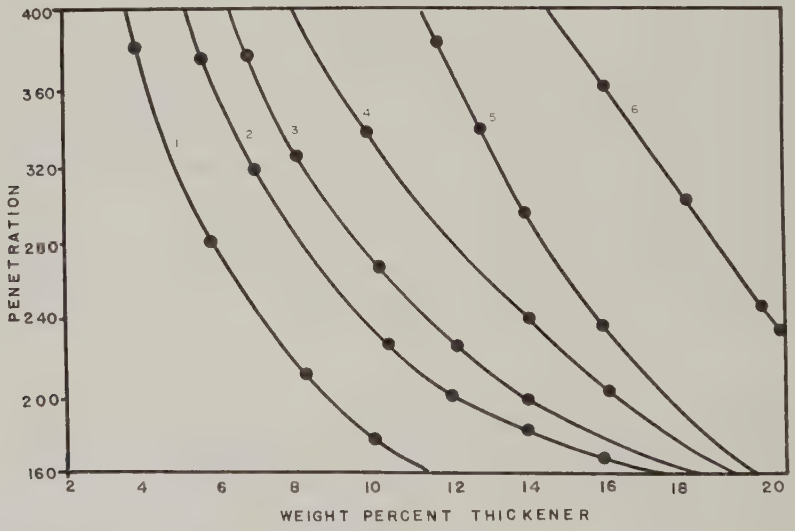

FIG. 1. Variations in penetration of nonsoap greases with thickener concentration. Hydrophobic thickeners in MLO 8200. Curve *1*: Carbolac 1; Curve *2*: Carbolac 2; Curve *3*: Carbolac 46; Curve *4*: Supercarbovar; Curve *5*: Monarch 71; Curve *6*: Estersil.

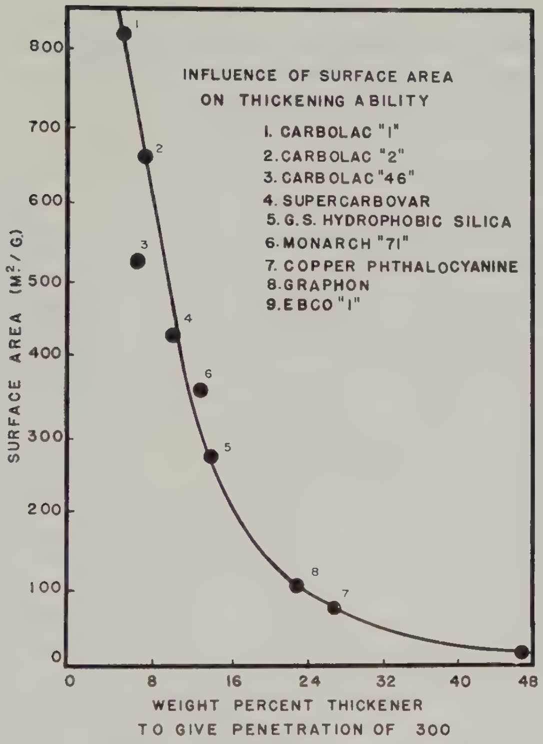

FIG. 2. Influence of surface area on the thickening ability of hydrophobic solids.

The manner in which the penetration of a grease changes with thickener concentration is an important consideration when comparing the effect of other factors which influence the grease consistency. For example, an additive may drastically alter the penetration of a grease at low thickener concentrations but have only a slight effect at high loadings.

At sufficiently high thickener concentrations the penetration curves generally tend to level off to a nearly constant penetration value. The thickener concentration where this occurs and the resulting penetration is specific for each grease system. This plateau usually begins beyond the useful range of thickener concentration and probably represents a sufficiently dense structural packing arrangement of thickener particles so that more thickener does not appreciably increase gel strength.

The influence of surface area on thickening ability is illustrated in Fig. 2, where surface areas of the thickeners are plotted against the weight per cent thickener required to give a penetration of 300 in Disiloxane. Since porosity is a minor factor for the different thickeners plotted here, the surface area was taken as a first approximation of the effective extent of the oil-thickener interfacial region. The thickeners represented in Fig. 2 are all assumed to have the same surface hydrophobicity, have similar particle shapes, have similar heats of immersion, and thus differ mainly in surface area. These results are typical for these thickeners in other oils and at different penetrations.

The amounts of thickener required to yield a grease of the specified penetration increases almost linearly with decreasing surface area until the surface area falls below ca. 200 m.^{2}/g. Below this surface area, the required amounts increase rapidly with decreasing surface area, and the resulting greases begin to assume properties more like those of heavily loaded suspensions than gels. This change in the nature of the grease at high loadings becomes more pronounced as the surface area of the thickener falls to very low values. For example, several greases were formulated from low surface area (below 20 m.^{2}/g.) pigments and clays. A product of suitable penetration usually can be obtained at high loadings, but the resulting dispersions tend to flow, have considerable length, bleed oil at high rates, and exhibit other behavior suggestive of a heavily loaded suspension rather than of a properly built grease.

The question arises as to whether as a first approximation thickening ability can be related to the potential number of contacts the particles can make in developing a flocculated gel structure. Thus, the thickening ability would be dependent on the number of particles per gram, *N*, and their average diameter, *d*. The per cent thickener required to yield a gel of a given

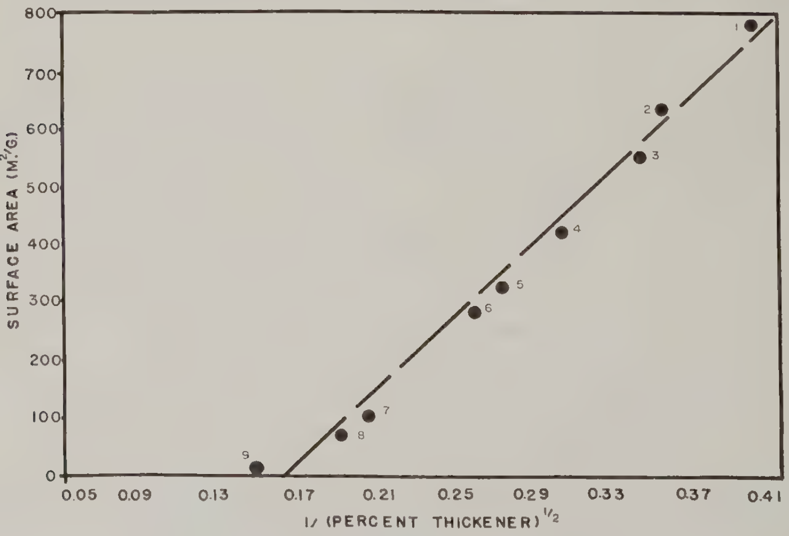

FIG. 3. The dependence of the thickening ability of a solid on its surface area.

consistency is inversely related to its thickening ability, hence to $1/Nd$. This relation can be put in terms of the surface area, A, and the density, ρ, of the thickener:

$$\begin{array}{l}\text{Per cent thickener} \\ \text{(for a perscribed penetration)}\end{array} \quad \alpha \quad \frac{1}{A^2\rho}. \qquad [1]$$

For hydrophobic thickeners, this relation is followed closely as exemplified in Fig. 3 for the systems from Fig. 2. The densities of these materials are sufficiently close so that this factor has negligible influence. Such plots can be developed for various consistency levels so that predictions as to thickening ability can readily be made.

Hydrophobic vs. Hydrophilic Thickeners and the Influence of Trace Water

Whereas the thickening ability of hydrophobic thickeners has been related to their surface areas, no such simple relation applies to hydrophilic thickeners. Table III gives an indication of the average weight per cent of both hydrophobic and hydrophilic solids required to prepare greases. Lesser amounts of the hydrophilic thickeners are required. For example, only about 12 wt. % of the polar solid Aerosil is necessary to form a grease of penetration 176, whereas 15 wt. % of the nonpolar solid Estersil is required to form a grease of penetration 231, even though the area of Estersil is nearly twice that of Aerosil. On the basis of such accumulated evidence, hydrophilic solids were judged to be more effective thickeners than hydrophobic solids.

The first studies were conducted with "as is" thickeners and with oils, usually nonpolar, which were not specially dried and contained small amounts of dissolved water. Whether the greater thickening ability of the polar solids resulted from the more energetic solid-oil interaction, from a greater attraction between the solid particles, or from the influence of these small amounts of water acting as a flocculating agent had not been es-

TABLE III

Thickening Ability of Solids in Paraffin Oil

Solid	Area (*m.*^{2}*/g.*)	Heat of immersion in water (*ergs/cm.*^{2})	Wt. % solid	Penetration
		Polar Solids		
Aerosil	140–180	154–180	12	176
HiSil	130	460	17	158
Rutile	80	550	25	183
		Nonpolar Solids		
Estersil	290–300	10	15	231
Carbolac 2	660–700	90	10	224
Copper phthalocyanine	74	34	33	232

tablished. Careful studies were then conducted with the polar solid Santocel 54 in Plexol 201 under increasingly anhydrous conditions.

Dispersions of 14 wt. % Santocel 54 in Plexol 201, when no special precautions are taken, yield a micropenetrometer reading of about 160. Preparations based on the dried solid (100° for several days) give a considerably lower consistency and penetration values 25% higher. If the oil is also dried, no significant increase is found. The so-called dry preparations were made in a dry box containing P_2O_5 except for the final rapid milling step. At most only trace amounts of water (likely less than a monomolecular layer at the solid-liquid interface) could be taken up.

The influence of water on the flocculation of polar solids in nonpolar liquids was first studied by Kruyt and van Selms (8). These workers showed that comparatively thick films of water led to coalescence between particles based on the reasonable mechanism of the concomitant decrease in interfacial tension. Here, on the other hand, *trace* amounts of water, certainly fractions of a monolayer, were shown to be effective. For a remarkable decrease in structure and consistency is achieved if small weighed portions of P_2O_5 or anhydrous $MgSO_4$ are added by spatula to the "dry" greases. Thus, the 14% Santocel 54 in Plexol 201 grease becomes so fluid that it can be poured; the greaselike characteristics gradually return on aging in air. The amount of P_2O_5 required to fluidize well-dried greases is far less than that required to react with the amount of water required to form a monomolecular surface film on the dispersed solids. On the other hand, greases based on hydrophobic thickeners are unaffected by desiccants.

This evidence for flocculation induced by trace amounts of water has far-reaching significance. Mobility of the water molecules at the interface to junction points between particles, there to form the bridges, seems to be required. Bridge formation would lead to immobilization of the adsorbed molecules. When surface diffusion coefficients on packed powders are sought as a function of coverage (9), such behavior might be responsible for the present conclusion that nominal film thicknesses below the monolayer values tend to be immobile.

The Role of Increasing Amounts of Water on Consistency

Since trace amounts of water markedly increase the thickening ability of hydrophilic solids in nonpolar oils, it is pertinent to inquire about the behavior of these grease systems as the water content is progressively increased. A simple method for introducing a controlled amount of water into the grease is to adsorb a definite amount of water vapor onto the surface of the thickener before incorporation. Evidence indicates that practically all the water introduced in this manner remains at the thickener-oil interface where its influence on the system is manifested. First, the viscosity of the system is not altered much by mere admixture with the oil.

Second, the influence on the curves of penetration versus amount of water preadsorbed parallels the water adsorption isotherm on the thickener.

Two contrasting types of thickeners were selected for a study of the effects of increasing amounts of water: Aerosil, a hydrophilic solid, and G. S. Hydrophobic Silica, a hydrophobic solid. Both thickeners dispersed readily in Plexol 201. Prior to formulation, quantities of the thickening agents were preconditioned in desiccators at increasing relative humidities. Greases formulated at 0% relative humidity were made from oils and thickeners that had been dried and mixed in a sealed dry box with P_2O_5 as a desiccant. By drying the thickeners in a vacuum over P_2O_5 for 72 hours all the physically adsorbed water was removed. It must be remembered that at least trace amounts of water (as determined by treatment with P_2O_5) are present in the finished grease owing to brief exposure to moist air during dispersion on the mill despite this stringent drying.

The variation in penetration of these two grease systems with the relative humidity at which the thickening agent was preconditioned prior to formulation into the grease is shown in Fig. 4. The difference in behavior between the two greases is striking. The grease formulated from the hydro-

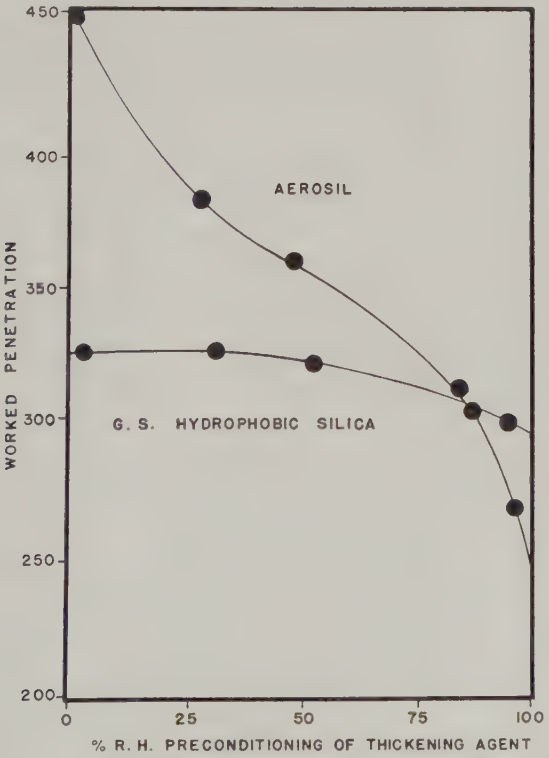

FIG. 4. The influence of water on the consistencies of greases containing hydrophobic or hydrophilic thickeners.

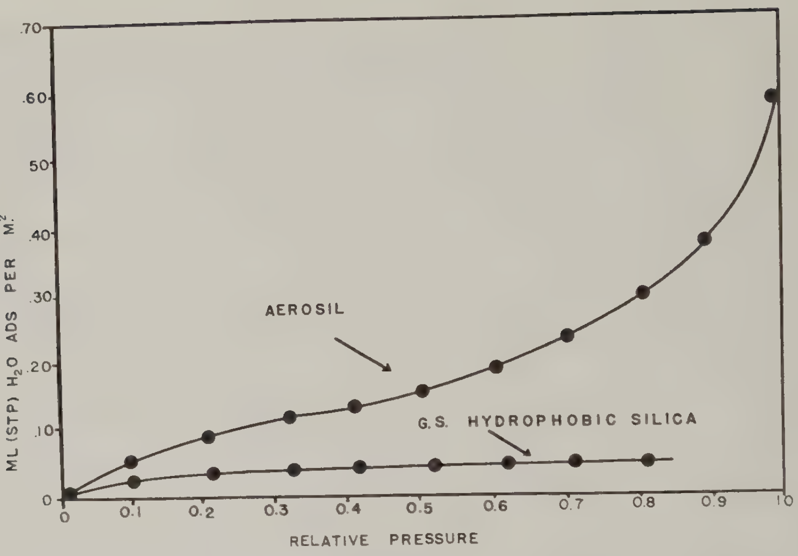

FIG. 5. The adsorption of water vapor on grease thickeners at 25°C.

philic Aerosil shows large and continuous changes in penetration with changes in the preconditioning relative humidity. In contrast, the G. S. Hydrophobic Silica grease has nearly the same consistency over the entire range of relative humidity.

An explanation for this behavior is suggested by the water vapor adsorption isotherms for the two thickeners. These isotherms are given in Fig. 5, where the amount of water vapor adsorbed is plotted against the relative humidity. It is seen that Aerosil adsorbs much larger amounts of water vapor than does the G. S. Hydrophobic Silica. Indeed, the change in consistency in the two greases is almost directly related to the amount of water vapor the thickeners adsorb. It seems reasonable to hypothesize that the adsorption of water vapor on the surface of the thickener leads to stronger particle-to-particle interaction and thus yields a grease of greater consistency. Water displaces the oil from the surface of a hydrophilic thickener. Hydrophobic thickeners adsorb water sparingly, however, especially in the presence of oil, and hence are not subject to large changes in the strength of particle-to-particle interaction.

Excess water was milled directly into grease systems formulated under various relative humidities. The resulting penetrations of the grease systems are always approximately those of the systems formulated under saturation conditions. This finding substantiates the conclusion that the influence of the water resides at the thickener interface and, once the thickener has adsorbed the amount of water normally taken up by the surface, further additions of water have little effect on consistency.

It is interesting to note that another immiscible liquid besides water has been found to cause a sharp increase in consistency of a grease thickened with the polar solid, Aerosil. Ethylene glycol, for example, thickens Aerosil-Plexol 201 greases in much the same manner as does water. Evidently, here also flocculation is increased as the concentration of ethylene glycol is increased owing to coalescence of particles and the reduction of interfacial tension between adsorbed ethylene glycol and the vehicle. Undoubtedly, other immiscible liquids with high interfacial tensions measured against the vehicle, and which are preferentially adsorbed by the solid, could cause flocculation by this same mechanism. Low molecular weight amines, alcohols, acids, aldehydes, etc., might be expected to thicken greases formulated with polar solids in nonpolar vehicles in direct contrast to the more usual thinning effect of the larger straight-chain heptyl compounds discussed in the following paper.

Work Stability of Greases

The influence of traces of water in nonsoap grease systems formulated from hydrophilic thickeners is not limited to the effect on the initial consistency. If the amount of adsorbed water at the thickener-oil interface is altered after formulation, the penetration of the grease would be expected to change. It is found that heating, evacuation, and mechanical working all can alter the concentration of water in the grease system. Table IV shows the change in penetration after working 100,000 double strokes in a grease worker for grease systems preconditioned at various relative humidities. The results for the Aerosil greases suggest that the grease tends to equilibrate with the water vapor in the atmosphere. Thus, the grease formulated at 0% R. H. becomes thicker presumably by picking up water vapor from the atmosphere, the grease formulated at 50% R. H. retains its original penetration, and the grease formulated at 87% R. H. becomes thinner because of loss of water from the interfacial region. These three greases ended with essentially the same consistency after mechanical working.

On the other hand, the presence or absence of water in the grease system

TABLE IV

Influence of Preconditioning Relative Humidity on Work Stability

Grease system	Preconditioning relative humidity	Initial worked penetration	Penetration after 100,000 double strokes
Plexol 201, 10% Aerosil	0%	ca. 400	332
Plexol 201, 10% Aerosil	50%	353	350
Plexol 201, 10% Aerosil	87%	293	349
Plexol 201, 15% G. S. Hydrophobic Silica	0%	311	267
Plexol 201, 15% G. S. Hydrophobic Silica	52%	310	283

has little effect on the mechanical stability of greases made with hydrophobic thickeners.

Thickening of Polar Vehicles by High Area Solids

If water is important for the flocculation of polar solids, its influence would be greatest in nonpolar vehicles (like common grease vehicles) and least in polar vehicles (like ethylene glycol). That is, a given quantity of water is more available for adsorption at the interface in a nonpolar vehicle which dissolves only small quantities. Secondly, in nonpolar vehicles the water is preferentially adsorbed by the solid producing an extensive interface between the immiscible adsorbed water and the vehicle. This interface is absent in pure water or even in water containing polar vehicles like ethylene glycol; consequently, in such cases flocculation by coalescence of film-covered particles is impossible. Experimentally, it was found that 10 to 15 wt. % Aerosil or HiSil (amounts sufficient to form a grease with nonpolar vehicles) do not gel ethylene glycol. In fact, amounts as high as 50 wt. % and higher are still ineffective. In contrast, normal amounts of the carbon blacks and Estersil form greases as effectively with ethylene glycol as with the usual grease vehicles.

Additional work, however, demonstrated the surprising fact that the inability to form gels even with high concentrations of polar solids in ethylene glycol is due to the presence in the dispersion of water itself. The directly opposite effect, of course, was found in nonpolar vehicles. Addition of P_2O_5 to a 45 wt. % Aerosil-glycol dispersion by spatulation causes considerable heat evolution indicating the presence of water. But P_2O_5 or $MgSO_4$ added in this manner causes the fluid dispersion to thicken. In addition, a grease dispersion was prepared from 30 wt. % Aerosil in ethylene glycol after both the solid and vehicle were rigorously dried before milling. Evidently water does preferentially adsorb onto the surface of Aerosil, but since ethylene glycol and water are miscible in all proportions, no sharp interface exists between the adsorbed film and vehicle. Flocculation by water bridges or by coalescence of water covered particles as in the case of the water-polar solid-nonpolar vehicle systems is thus impossible. Furthermore, since flocculation in glycol occurs by particle-to-particle contact if water is absent, it is logical to conclude that the decrease in free energy on the adsorption of water is greater than that which occurs by particle-to-particle interaction in the absence of water.

ACKNOWLEDGMENT

This work was performed under Air Force Contract AF 33(616)-2440 under the monitorship of the Materials Laboratory, Wright Air Development Center, Wright-Patterson Air Force Base, 1, Ohio.

REFERENCES

1. "Cabot Carbon Blacks Under the Electron Microscope," 2nd ed., Godfrey L. Cabot, Boston, Massachusetts, 1950.
2. YOUNG, G. J., CHESSICK, J. J., HEALEY, F. H., AND ZETTLEMOYER, A. C., *J. Phys. Chem.* **58,** 313 (1954).
3. ILER, R. K., U.S. Patent 2,657,149, October 27, 1953.
4. ZETTLEMOYER, A. C., YOUNG, G. J., CHESSICK, J. J., AND HEALEY, F. H., *J. Phys. Chem.* **57,** 649 (1953).
5. GAMBLE, E., WALKER, W. C., AND ZETTLEMOYER, A. C., *Am. Ink Maker* **31,** 72 (1953).
6. WALKER, W. C., AND ZETTLEMOYER, A. C., *Am. Ink Maker* **27,** 9 (1949); WALKER, W. C., AND ZETTLEMOYER, A. C., *Am. Ink Maker* **28,** 7 (1950).
7. ASTM Standards, Part 5, 1952, p. 119 ff.
8. KRUYT, H. R., AND VAN SELMS, F. G., *Rec. trav. chim.* **62,** 407 (1943).
9. CARMAN, P. C., AND RAAL, F. A., *Trans. Faraday Soc.* **50,** 842 (1954); CARMAN, P. C., *S. African Ind. Chemist*, June, 1955.

JOURNAL OF COLLOID SCIENCE **13**, 372–382 (1958)

BASIC FACTORS IN THE FORMATION AND STABILITY OF NONSOAP LUBRICATING GREASES

II. THE MECHANISM OF GEL FORMATION

J. J. Chessick, A. C. Zettlemoyer, and G. J. Young

The Surface Chemistry Laboratory, Lehigh University, Bethlehem, Pennsylvania

Received March 10, 1958

Abstract

High-area hydrophobic and hydrophilic solids flocculate in *pure* or *dry* liquids to form grease gels by particle-to-particle contact. In these systems, particle diameter and concentration of thickener are more important in gel formation and resulting consistency than the degree of polarity of the solid surface or of the liquid. When water is present, on the other hand, the formation of structure depends greatly on whether the dispersed solid is hydrophilic or hydrophobic. Trace water markedly influences the flocculation of hydrophilic solids dispersed in polar or nonpolar vehicles; however, trace water has little effect on the flocculation process of hydrophobic thickeners. In nonpolar vehicles, water enhances the flocculating ability of polar solids; in polar vehicles, the opposite effect is found.

Heptyl alcohol and amine (and their benzene analogs) drastically thin greases built with polar solids. Heptyl aldehyde, chloride, and acid generally have small influence. As the polarity of the solid is increased, the thinning ability of the additives increases. Distinctly different are carbon black built greases which are not influenced by these additives. Greases built with Estersil, which possess a predominantly but not entirely hydrophobic surface, are affected somewhat differently from the greases made from predominantly polar solids. In the presence of additives and water, the degree of surface polarity determines whether one component (water or additive) will be displaced by increasing concentrations of the second component.

Introduction

The mechanism of gel formation in organic liquids is not entirely understood. Hence, selection of a proper thickening agent and predictions of the formation, stability, and behavior of a grease gel have been arrived at by empirical methods. The first paper in this series (1) described the experimental results of a study of the variables important in the formation of grease structure. Here, these experimental findings are used to give a unified picture of the mechanism of flocculation of hydrophobic and hydrophilic thickener solids in a variety of pure liquids and in liquids containing water, organic additives, or both these components.

The forces of repulsion tending to prevent flocculation appear to be of two kinds. The one is due to interaction of adsorbed aliphatic chains; this force which sterically prevents flocculation needs a more quantitative definition (2). Nevertheless this force no doubt becomes a factor in the thinning effect in greases produced by aliphatic additives. The other is the double layer repulsion which seems to operate even in liquids with dielectric constants lower than a magnitude of five to ten (3); however, repulsion due to double layers need not be taken into account to explain grease behavior.

The forces of attraction are the usual London or Lifschitz van der Waals' forces (4) coupled with those brought on by any reduction in interfacial free energy. This reduction through the coalescence of interfacial immiscible liquids, particularly due to omnipresent water, is most important, as shown in the first paper in this series (1). Even trace water can apparently operate by moving to points of juncture there to form bridges. This factor appears often to be the dominant one in grease building by polar solids.

Experimental

Greases were prepared from representative samples of the thickeners and oils already described (1). The preparation and measurement of the properties of the greases were also the same. In addition, the influence of straight-chain, heptyl additives on the consistency of prepared greases was investigated. The additives included the alcohol, acid, aldehyde, amine, and chloride. Limited studies of the influence on grease consistency of the benzene analogs of these additives were also made. These additives were all research grade and were redistilled before use.

The additives were milled directly into the grease and penetration readings were taken at definite weight per cents of additive as previously described (1).

Results and Discussion

A Comparison of the Properties of Grease Gels Formed from Hydrophilic and Hydrophobic Thickeners

There is good evidence to suggest that of the solids used in this investigation the hydrophilic solids under certain circumstances flocculate to form a grease gel differently than do hydrophobic thickeners. This evidence resulted from a study of the behavior of dispersions of these solids in pure liquids or in liquids containing water, organic additives, or both. The properties of various grease systems after different treatments are listed in Table I. They were formulated under as anhydrous conditions as possible but contained trace amounts of water (1). Whereas hydrophilic and hydrophobic thickeners were included, only relatively nonpolar grease vehicles were used.

In studying the data of Table I it should be noted first that the hydrophilic solids have much smaller areas than the hydrophobic thickeners,

TABLE I

Properties of Greases on the Addition of Water, P_2O_5, or Organic Additives

Solids	Wt. %[a] solids	Nonpolar vehicles[b]		
		Effect on the Consistency of a Grease on the Addition of		
		Trace or larger quantities of H_2O	Heptyl additives	P_2O_5
Carbolac 2 600–700 m.^{2}/g.	8	No effect	No effect	No effect
G. S. Hydrophobic Silica 300 m.^{2}/g.	15	Little or no effect	Thins	No effect
HiSil, Aerosil	8–12	Large effect (thickens)	Thins or no effect	Large effect (fluidizes)

[a] To give grease of penetration 300.

[b] Plexol 201, Paraffin Oil, MLO 8200, Ucon Adipate.

yet nearly the same amount of both produces greases of about the same consistency. Secondly, the addition of small amounts of P_2O_5 causes consistency changes only in those greases containing the hydrophilic solids: these greases are thereby fluidized. Formation of grease structure by these concentrations of polar solids is impossible in the absence of water. Relatively large quantities of water also have a large influence on the consistencies of these greases, but only a negligible influence on the greases containing the blacks or the hydrophobic silica. However, the consistency of a G. S. Hydrophobic Silica grease is strongly changed by certain of the organic heptyl additives but in a different manner than are the greases containing polar solids. The heptyl additives do not alter the consistency of carbon black greases. The influence of additives will be discussed further below.

Eight to fifteen weight per cent of the hydrophobic solids is sufficient to form grease gels in either dried or undried vehicles irrespective of the polarity of the vehicle. Eight to twelve weight per cent of the polar solids is also effective in thickening the nonpolar vehicles but only in the presence of at least trace amounts of water. However, 30 to 40 wt. % of these hydrophilic solids is required to gel *dry* ethylene glycol. Wet ethylene glycol can not be thickened by the hydrophilic solids at any loading. Obviously, there are basic differences (and similarities) in the properties of greases thickened by hydrophilic and hydrophobic solids. Thickeners, representative of these groups, are discussed in detail below.

The Influence of Water on the Properties of Grease Gels Formed from Hydrophilic Solids Dispersed in Nonpolar Vehicles

Because of the large amount of available experimental data, the surface properties and dispersion characteristics of the silica, Aerosil (Cabosil), will be singled out for discussion. The heat of immersion of different lots of Aerosil in water range from 155 to 180 ergs/cm.^{2} These values suggest that the surface of Aerosil is weakly polar if all surface sites are of the same adsorption energy. Differences between water and nitrogen adsorption measurements, however, have shown that only about 25% of the total Aerosil surface is polar. It is generally accepted that the hydrophilic portions of silicas of this type are composed of silanol groups which adsorb water, whereas the hydrophobic portion is made up of siloxane groups. The suggestion has only recently been made that the hydrophobicity of the siloxane portion of silica surfaces results from its lack of ionic character (5). It is obvious that these two types of surfaces can behave differently depending on conditions. For example, the nonpolar portions of the surface are important when it is dispersed in polar vehicles containing nonpolar additives. The polar portion of the surface is most important in nonpolar vehicles containing polar components, particularly water.

Ten weight per cent Aerosil will form a grease structure in nonpolar vehicles if at least trace amounts of water are present (1). The formation of a structure by trace amounts of water requires bridges made up of small quantities of water—perhaps even a few molecules per bridge between the solid particles. Certainly in the stringently dried systems only a fraction of a monolayer of water could have been present at the interface. Solids dried by heating and vehicles dried by treatment with anhydrous $MgSO_4$ did not form a gel structure when premixed in a dry box containing P_2O_5. A grease was formed during milling under atmospheric conditions. The amount of P_2O_5 added to the grease to cause fluidization was less than that required to react one-fourth of a monolayer on the surface of the solid particles. This mechanism requires mobility of adsorbed molecules to points of junction between particles which flocculate to very close distances, probably not more than about 2 to 4 A. units apart. The concept of attractive forces operating through distances of 100 A. or more (4) is not required here.

Other polar solids such as HiSil and rutile behave similarly to Aerosil in nonpolar vehicles containing trace amounts of water. Although the polarity of the surfaces of these solids as revealed by heat of wetting and adsorption measurements (1) increases in the order:

$$\text{Aerosil} < \text{HiSil} < \text{rutile},$$

the influence of trace water in promoting gel structure in dispersions of these materials is nearly the same. These results reveal the important fact that surface hydrophilicity alone rather than the degree of polarity of the surface is sufficient to cause flocculation. Further, a surface need not be completely hydrophilic for trace water to be important as in the case of Aerosil. A certain minimum amount of surface hydrophilicity appears necessary, however, since it is well accepted that hydrophobic surfaces usually possess a minor fraction of hydrophilic area (6, 7) yet do not behave as polar solids.

Aerosil has a density of 2.2 g./c.c., so that a 12 wt. % dispersion is about

6.0 volume %. In the absence of water no grease gel can be formed at this solids concentration in nonpolar vehicles even though there are enough solid particles present to form a loose network structure of coordination number three (8). Evidently, at this packing level, the bonds between adjacent silica particles are not strong enough to impart structural properties to the dispersion. Water, however, makes a grease gel possible even with this loose structural arrangement because of the strong bonds between flocculated particles. Studies in dry polar ethylene glycol revealed that 30 to 40 wt. % solid Aerosil (coordination number between four and five) is necessary to form a grease, although even at these weight concentrations the particle-to-particle bonding is not strong as revealed by high penetration values.

Systems in Which the Influence of Small Amounts of Water is Negligible

It is interesting to compare the gelling ability of both hydrophobic and hydrophilic thickeners in pure liquids or in liquids, polar and nonpolar, where the influence of trace impurities present is negligible. Approximately 15 wt. % of Estersil will thicken ethylene glycol; the total interface per 100 g. sample amounts to 4500 m.^{2}, assuming complete dispersion and reliability of the nitrogen area as a measure of the solid-vehicle interface. About 35 wt. % Aerosil is required to form a grease of similar consistency in this vehicle; the calculated total solid-vehicle interface also amounts to about 4900 m.^{2} This finding is significant when one considers that in nonpolar vehicles containing trace amounts of water about 15 wt. % Estersil is also required to form a grease. In nonpolar vehicles, 10 to 12 wt. % Aerosil produces a similar grease—a marked decrease in total interface of solid considering that the Aerosil area is about one third that of the Estersil. There is no doubt that the influence of water in certain systems far overshadows the role of the total interface.

The Hydrophobic Thickener Solids

Estersil is a silica gel the surface hydroxyls of which have been converted to —OR groups by treatment with primary or secondary alcohols. Although the material is quite hydrophobic, the surface is not completely covered by these silica ester groups. Water vapor and nitrogen adsorption measurements reveal that this material has hydrophilic surface sites which occupy about 3.5% of the surface. Flocculation may result, therefore, from an interlocking of the hydrocarbon groups of adjacent particles fitting in at uncovered areas, or by hydrogen bonding between unreacted hydroxyl groups on the surfaces of adjacent particles. Additives of the straight-chain, heptyl type apparently decrease flocculation by adsorbing preferentially onto the unesterified sites. Comparison of Figs. 1 and 2 shows that the thinning effect of these additives on Estersil greases is not the same as for the silica, HiSil, Aerosil, and Santocel greases.

It is important to point out, too, that the consistency changes of Estersil thickened greases at *high* water concentrations are not insignificant as was the case with unpellitized G. S. Hydrophobic silica gel. As the ratio of the unesterified portions to the organic portions of the surface increases so does the influence of water. All hydrophobic materials studied thus far contain some hydrophilic sites on their surfaces. When the hydrophilic sites increase to a given number for a given solid, the material behaves as a hydrophilic solid even though the surface hydrophobicity as measured by adsorption and calorimetric techniques is in excess of the polar portions. Compare the hydrophilic behavior of Aerosil (75% surface hydrophobicity) with the hydrophobic behavior of Estersil (96.5% surface hydrophobicity): trace amounts of water cause Aerosil dispersions to flocculate, but not Estersil dispersions.

Carbon blacks are different in behavior from the other thickeners studied in that neither P_2O_5, heptyl additives, nor amounts of water up to 3 to 4 wt. % significantly alter the consistency of greases made from them. McBain (9) has pointed out that blacks adsorb organics most strongly from water or polar vehicles like glycol, much less from hydrocarbons. Hence, it is quite likely that in the carbon black greases studied here, the blacks are preferentially wet by the nonpolar, hydrocarbon vehicles. Surprisingly, the heptyl derivatives also have small effect on the consistency of a carbon black-ethylene glycol grease in concentrations up to 6 wt. %.

If flocculation results in a decrease in interfacial free energy, then the thickening ability of the blacks should be greatest in polar vehicles where flocculation would cause the greatest decrease in interfacial free energy. That this is so is indicated by the following results: The penetration of 10 wt. % black, XC-72, in glycol was 301; 12 wt. % black was required in the less polar Plexol 201 to give the equivalent penetration of 299. This effect, however, is minor compared to the flocculating ability of water or other immiscible additives in polar solid-nonpolar vehicle grease systems.

Influence of Simple Additives on Grease Systems

Preliminary work has been carried out on the influence of simple, monofunctional additives on the formation and stability of nonsoap greases. Initially, two contrasting types of gel systems were studied. These were formulated from paraffin oil with Aerosil, a polar-behaving solid, and Estersil, a nonpolar solid. The grease thickeners and oils were dried. The dissolved water, picked up during dispersion as previously pointed out, is important in giving structure to greases containing the polar thickeners. The organic additives were all seven-carbon, straight-chain compounds with a single functional group. The functional groups were selected to cover a wide range of dipole moments and represented functional groups encountered in more complex grease additives.

Small amounts of heptyl alcohol and heptyl amine fluidize Aerosil-

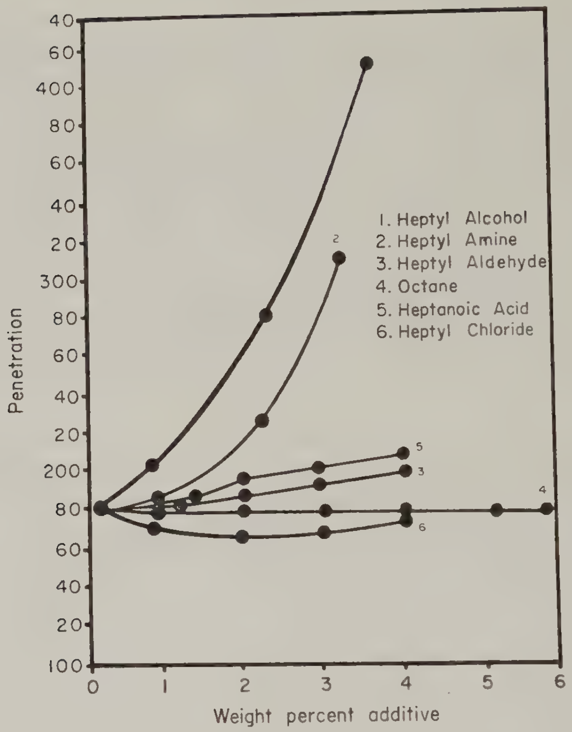

FIG. 1. The influence of heptyl additives on the consistency of an Aerosil-paraffin oil system.

paraffin oil greases, and the other additives produce no effect or a much smaller one. The results of this study are summarized in Fig. 1, where penetration is plotted as a function of the per cent additive.

The marked thinning actions of the amine and alcohol no doubt result from a preferential adsorption of these compounds by Aerosil. The adsorbed organic film prevents the flocculation of particles by the trace water present in the system. Indeed, the drying agents, $MgSO_4$ and P_2O_5, have similar effects on this system. On the other hand, limited adsorption in the additive concentration range studied can account for the small effects of the chloride, aldehyde, and acid. The possibility also exists that specificity occurred during adsorption from solution and that the amine and alcohol are exclusively and possibly chemisorbed onto the silica surface. To establish these conjectures, numerous heats of wetting determinations were made for the immersion of Aerosil and several other polar solids in the pure additive liquids and in solutions of these additives in paraffin oil. All measured heat values were much too low to be attributed to any but physical interactions. The reasons for additive influence are now being studied and will be reported later; one of the most important factors is the heat of solution of additive in the vehicle.

The following hydrophilic solids: Aerosil, HiSil, rutile, were also studied in one or more of the following oils: paraffin oil, Plexol 201, MLO-8200, and Ucon Adipate 465. The results are similar to those found for the Aerosil-paraffin oil system. However, an important finding is that greases containing more polar thickeners, such as rutile and HiSil, suffer larger consistency changes on the addition of the additives. Indeed, all the additives with the exception of the chloride thin rutile-built greases to varying degrees and do so at low concentration of additive, and this is attributed to the high surface polarity of this solid. It will be shown later that the water is displaced most readily from the more polar solids by these simple additives. The heptyl additives are not unique in their behavior since similar results are found with their benzene analogs, but to a lesser degree.

The heptyl additives were also found to influence the system Estersil-paraffin oil. The nonpolar Estersil surface (3.5% hydrophilic) was not

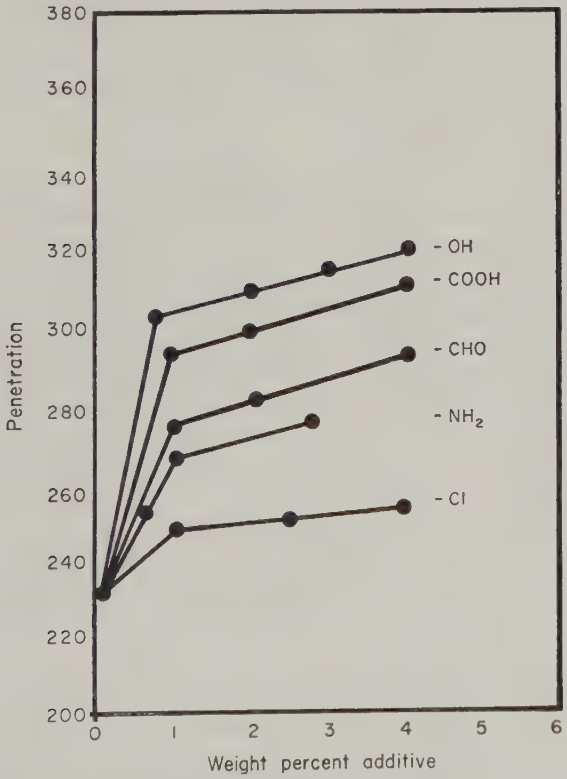

FIG. 2. The influence of heptyl additives on the consistency of Estersil-paraffin oil system.

expected to have a large and specific adsorptive capacity for these additives. In addition, marked differences in additive action were found. The influence of these same additives on the Estersil-paraffin oil system is markedly different from the Aerosil-paraffin oil system as shown in Fig. 2. The changes in consistency of the Estersil greases are linear after a minimum amount of each additive is present, and the slopes of the curves can be explained by considering that the larger changes in consistencies at low concentrations are due to adsorption of the additive on the surface making the Estersil even more hydrophobic. After this initial large change, smaller linear changes occur owing to dilution of the grease by the liquid additives. This explanation requires that the surface have a different adsorptive capacity for each additive.

Experimentally, the carbon blacks were found to behave more like ideal hydrophobic solids when dispersed in grease vehicles. Greases prepared from Carbolac 2 in Sunvis 11 and Mogul in Plexol 201 do not undergo significant changes in consistencies with any of the heptyl additives or with water. Heat of wetting measurements, water adsorption studies, and measurements of volatile matter content of these solids all indicate the presence of polar, hydrophilic surface sites. Unlike Estersil, however, these sites are apparently unavailable to adsorb the heptyl additives; they are no doubt much less polar.

Mixed Water-Additive Effects

The study of complex systems of solid, vehicle, water, and additives is important because these results become more pertinent to the behavior of greases and other practical dispersions like paint and inks. Measurements were made of the mixed influence of water and additives in Aerosil, HiSil, and rutile greases formulated in the usual nonpolar grease vehicles. It is important to note that the solids were all hydrophilic and are listed in order of increasing surface polarity. The addition of 2 to 3 wt. % water by milling into well-dried samples of these greases causes an expected sharp increase in consistency, as measured by the penetrometer. Addition to these water-solid-vehicle greases of additives effective as thinners in the presence of trace water, particularly the amine or alcohol, cause marked fluidization in all cases. Evidently, the mechanism of displacement of water from the surface with consequent rupture of the water bridges or bonds necessary for flocculation and gel formation applies.

On the other hand, if samples of these greases are first fluidized by 2 to 4 wt. % additives and then if water is added, much different results are experienced. With the grease containing the weakly polar Aerosil, sufficiently high concentrations of water displace any of the heptyl additives and cause considerable thickening. Also, sufficiently high concentrations of additive displace water from the Aerosil surface and cause fluidization.

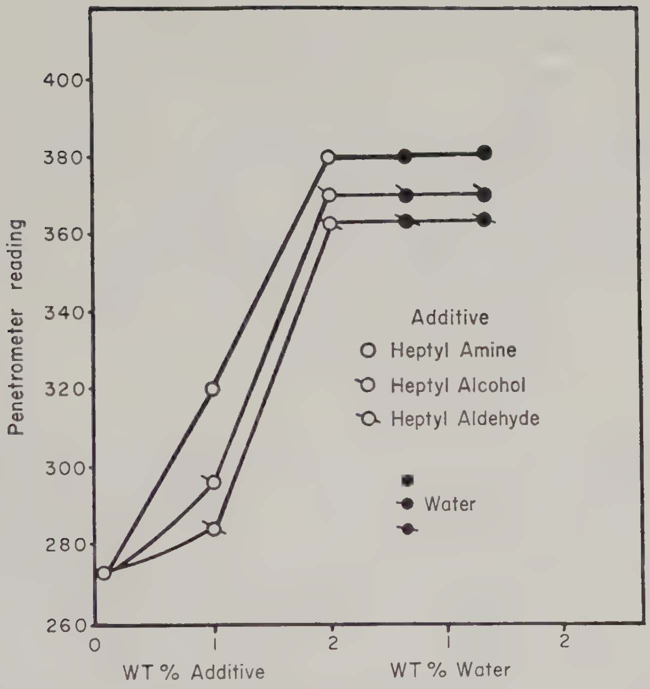

FIG. 3. Penetration vs. Weight per cent heptyl additive in a system of 37 wt. % rutile in paraffin oil.

As the polarity of the solid increases, however, water will not displace additive molecules from the surface with ease. In fact, the consistency of rutile-paraffin oil-additive grease is not changed by increased amounts of water up to 4 wt. %, as is illustrated in Fig. 3. Studies at higher water concentrations were not conducted. It is quite evident that the degree of polarity of the dispersed solid is most important in determining the resulting structure in these complex dispersions.

ACKNOWLEDGMENT

This work was performed under Air Force Contract AF 33(616)-2440 under the monitorship of the Materials Laboratory, Wright Air Development Center, Wright-Patterson Air Force Base 1, Ohio.

REFERENCES

1. "Basic Factors in the Formation and Stability of Nonsoap Greases. I. A Study of the Factors Responsible for Gel Formation." *J. Colloid Sci.* **13,** 358 (1958).
2. "Flocculation and Coagulation," Sheffield, England, 1954, *Discussions Faraday Soc.* **18** (1955).
3. KOELMANS, H., *Philips Research Repts.* **10,** 161 (1955).

4. Lifschitz, E. M., *Doklady Akad. Nauk S.S.S.R.* **97,** 643 (1954); Kitchener, J. A., and Prosser, A. P., *Proc. Roy. Soc.* (*London*) **A242,** 403 (1957).
5. Young, G. J., *J. Colloid Sci.*, **13,** 67 (1958).
6. Young, G. J., Chessick, J. J., Healey, F. H., and Zettlemoyer, A. C., *J. Phys. Chem.* **58,** 313 (1954).
7. Chessick, J. J., Healey, F. H., and Zettlemoyer, A. C., *J. Phys. Chem.* **60,** 1345 (1956).
8. Manegold, E., "Kapillarsysteme, Band 1," p. 242. Chemie und Technik Verlagsgesellschaft m. b. H., Strassenbau, 1955.
9. McBain, J. W., "Colloid Science," p. 46. Heath, Boston, 1950.

JOURNAL OF COLLOID SCIENCE 13, 383-396 (1958)

THE EFFECT OF ADDITIVES UPON THE PROCESS OF CRYSTALLIZATION

I. CRYSTALLIZATION OF CALCIUM SULFATE

E. R. McCartney and A. E. Alexander*

New South Wales University of Technology

Received January 8, 1958

Numerous observations have been reported concerning the influence of trace impurities upon crystal habit, and more recently workers in varied fields have noted their effects in preventing, or reducing the rate of, crystallization from supersaturated solutions. Many such examples are observed in industrial practice; thus calcium sulfate and phosphate crystallize in the form of scale in boilers and in process equipment such as evaporators and crystallizers in the sugar industry. Certain impurities have a major effect on such crystal growth. For example, Deitz (1) describes the action of certain organic nonsugars occurring in raw sugar in preventing the precipitation of calcium sulfate. He found that the solubility of calcium sulfate appeared to be five times higher in a solution made up from raw sugar than in one with the same concentration of pure sucrose. He believed that there was a correlation between the increased apparent solubility of the calcium sulfate and the presence of organic anions, particularly those from aconitic, malic, citric, fumaric, glycolic, and succinic acids.

Lowy (2) noted that citric acid prevented the precipitation of calcium sulfite from sugar liquors after the addition of sodium hydrosulfite for bleaching. He found that the organic acids, citric, aconitic, malonic, maleic, tartaric, itaconic, and succinic could all prevent precipitation of calcium sulfite. Their activity decreased in the order given above.

Evidence from conductimetric measurements indicates that calcium citrate forms a complex ion (3), thus increasing the effective solubility of calcium citrate, but the authors point out that even a heavily supersaturated solution needs a long time to come to equilibrium.

In a recent patent, Johnson (4) claims that polymeric compounds "having two carboxylic groups adjacent to one another and spaced along the polymeric chain" are useful for preventing the precipitation of calcium carbonate in steam boilers.

The setting of gypsum plaster can be regarded at least partly as a case of crystallization, and a number of the substances reported as hindering the crystallization of calcium sulfate also occur in the group of materials used as retarders for the setting of plaster, e.g., citric, malic, and succinic acids. Other commonly used retarders are borax, gelatin, and the degraded keratin material known as "scutch."

---

* Present address: Department of Physical Chemistry, The University of Sydney.

The present paper reports part of a study of the crystallization of calcium sulfate. The kinetics of the crystallization of pure calcium sulfate from solution have been examined, and the results will be published elsewhere (5). The object of the work described here was to characterize the substances most active in inhibiting the crystallization of calcium sulfate and to elucidate the mechanism of their action.

EXPERIMENTAL

Obtaining the appropriate degree of supersaturation in solution presents peculiar difficulties in the present case, since calcium sulfate exhibits a very small temperature coefficient of solubility which becomes negative above 35°C. The method adopted made use of the fact that calcium sulfate hemihydrate is more soluble on a molecular basis than calcium sulfate dihydrate. A slight excess of hemihydrate was stirred with water for 1 minute and filtered quickly under suction. The filtrate was then a supersaturated solution of dihydrate. The hemihydrate used was May and Baker's "calcium sulfate exsiccated," A.R. grade.

The supersaturated solution was placed in a thermostatted water bath controlled to ±0.01°C. and the change in concentration was followed by means of a Philip's A.C. bridge, type GM4249/01, and dip-type conductivity cell. All readings were made at a frequency of 1000 cycles per second. Readings of resistances on the 1000-ohm scale of the bridge were found to be repeatable to ±0.5 ohm.

The crystallizing vessel was cylindrical, of about 400 ml. capacity, and had two necks. To minimize evaporation the stirrer was fitted through a stirrer gland mating with a standard B14 cone joint while the conductivity cell was a neat fit through the second neck. The vessels were cleaned with dichromate sulfuric acid cleaning mixture, then $2N$ hydrochloric acid, and thoroughly rinsed with distilled water. They were then dried in an air-oven. No special precautions were taken to exclude stray nuclei. (This point is referred to again in the discussion section.) The inhibitor under study was added to the calcium sulfate solution immediately after filtration.

Of the materials reported as retarders of the setting of gypsum plaster the colloidal substances gelatin and degraded keratin are by far the most effective, but owing to their complex composition, their active constituents have never been characterized. In the present study, in addition to these complex materials, a range of pure chemicals was also tested for activity to indicate what molecular groupings, molecular weights, and states of dissociation are most effective.

Changes in crystal habit and rate of growth were recorded, but owing to the difficulty of attaching a quantitative value to the former the relative activities were assessed mainly from the reduction in rate of crystallization.

The principal groups of substances tried were:

1. The homologous series of fatty alcohols methyl to amyl.

2. The dyestuffs indocarbocyanine, chlorazol fast red, chlorazol yellow, aniline orange, chlorazol sky blue, and quinoline yellow.

3. The carbolan dyestuffs blue BS, violet 2RS, green GRS, crimson BS, and yellow RS.

4. The wetting agents "Teepol" (anionic) and cetyl trimethyl ammonium bromide (cationic).

5. Ammonium oxalate; ammonium acetate, borax.

6. The amino acids glycine, aspartic acid, alanine, cystine, arginine, and glutamic acid.

7. Potassium and sodium hydroxides.

8. Sulfuric, hydrochloric, and chloracetic acids.

9. Glycerol, sucrose, starch.

10. Citric, oxalic, malonic, succinic, and tartaric acids.

11. A copolymer of glycine and alanine; a Nylon intermediate.

12. Gelatin and degraded keratin, some samples of which had been filtered through a collodion membrane of pore diameter 10 mμ. These are designated "through collodion."

14. Polyacrylic and polymethacrylic acids of molecular weights of approximately 40,000.

15. Methyl cellulose and carboxymethyl cellulose.

16. Alginic acid.

17. Polyethylene oxides (Carbowaxes) of molecular weights 1000 and 6000.

18. Methoxy-polyethylene glycol, of molecular weight 1250.

Attention was directed towards finding additives active at low concentrations. Using both unstirred solutions and solutions stirred at standardized rates, the substances were added in concentrations of 10^{-5} mole % for the low molecular weight substances, and, except where otherwise indicated, 0.0026 gm. per 200 ml. of solution (i.e., 13 p.p.m.) for the high molecular weight substances and polymers.

The initial concentration of calcium sulfate in solution was 40 millimoles of $CaSO_4$ per liter at 30°C., at which temperature a saturated solution contains 15.36 millimoles.

RESULTS

The great majority of substances tested exerted no effect on either rate or habit. Those which reduced the rate could be grouped as follows:

a. Low molecular weight materials (borax, citric, succinic, and tartaric acids).

b. Proteinaceous materials (gelatine, degraded keratin).

c. Long-chain polymers with carboxy side chains (alginic acid, carboxy methyl cellulose, polyacrylic acid, polymethacrylic acid).

The second-order dependence of rate on supersaturation, found for pure solutions (5), still held in the presence of the retarding substances, as shown by the plots of reciprocal of supersaturation against time for retarded runs in Fig. 1. The effect of an additive can therefore be stated as the ratio of the rate of crystallization in the presence of additive to the rate of crystallization of the pure solution at the same initial concentration and temperature. The results are set out in Tables I–IV.

Consideration of the tabulated data shows that the additives which interact with the crystals of calcium sulfate are those with polar groups on a chain structure, particularly the two groups previously mentioned, proteinaceous and polycarboxylic materials. The retarding power increased markedly with molecular weight. Thus in the protein group, the simple amino acids had no effect, the alanine-glycine copolymer had only a slight effect, and gelatine and degraded keratin had a marked effect.

The trend was clearer and generally more definite in the case of the polycarboxylic materials. The retarding power increased through malonic, succinic, and citric acids. Upon adding polyacrylic acid and carboxymethyl cellulose at the usual concentrations, crystallization was completely inhibited over the usual period of a run (about 5 hours), although a very slight deposit of modified stumpy crystals appeared overnight. Even when the concentration of polyacrylic acid was reduced to 1.3 p.p.m., it still

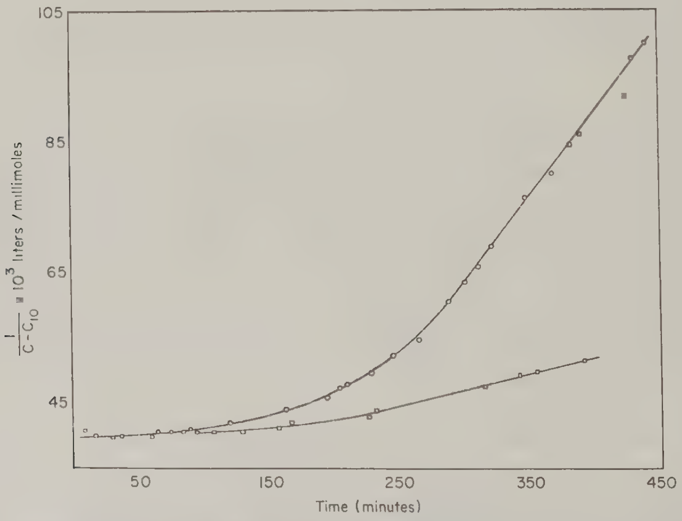

FIG. 1. Reciprocal of supersaturation as a function of time for calcium sulfate solutions crystallizing at 30°C. ○ in presence of alginic acid; □ in presence of gelatin which had been filtered through a collodion membrane. Solutions unseeded.

TABLE I

The Retarding Power of Additives

Amino Acids

I Run no.	II Additive	III Specific rate[a]	IV Initial concn.[b]	V Specific rate in pure soln.	VI Ratio $\frac{III}{V}$
69	Glycine	0.99	41.8	1.16	0.85
181	Glycine	1.28	40.6	1.08	1.18
72	1-Cystine	1.018	41.2	1.12	0.91
185	1-Cystine	1.035	39.6	1.00	1.04
73	Glutamic acid	1.01	41.0	1.1	0.92
187	Glutamic acid	1.06	39.1	0.98	1.08
74	Aspartic acid	1.37	41.7	1.15	1.19

[a] All rates are in liter per (gram mole) (minute).

[b] All concentrations are in millimoles per liter of solution.

TABLE II

The Retarding Power of Additives

Low Molecular Weight Materials Other Than Amino Acids

I Run no.	II Additive	III Specific rate	IV Initial concn.	V Specific rate in pure soln.	VI Ratio $\frac{III}{V}$
91	Borax	0.8	40.6	1.08	0.74
93	Citric acid	0.44	40.6	1.08	0.41
119	Glycerol	0.99	39.8	1.01	0.98
121	Malonic acid	1.07	41.3	1.11	1.05
122	Succinic acid	0.71	39.8	1.01	0.71
123	Tartaric acid	0.84	40.2	1.04	0.81
126	Succinic acid (pH 10.6)	0.84	40.6	1.08	0.78
129	Succinic acid (pH 7.2)	0.69	38.3	0.92	0.75

TABLE III

The Retarding Power of Additives

Acids and Alkalis

I Run no.	II Additive	III Specific rate	IV Initial concn.	V Specific rate in pure soln.	VI Ratio $\frac{III}{V}$
109	Potassium hydroxide	0.42	40.6	1.08	0.39
143	Hydrochloric acid (pH 3.60)	0.47	44.0	1.30	0.36
178	Sodium hydroxide (pH 11)	0.49	40.6	1.08	0.46
179	Hydrochloric acid (pH 3.5)	0.56	39.1	0.98	0.57
186	Sulfuric acid (pH 3.2)	0.48	40.6	1.08	0.44
195	Chloracetic acid (pH 2.3)	1.24	41.8	1.18	1.05

TABLE IV

Retarding Power of Additives

High Molecular Weight Materials

I Run no.	II Additive	III Specific rate	IV Initial concn.	V Specific rate in pure soln.	VI Ratio $\frac{\text{III}}{\text{V}}$
78	Keratin	0.64	41.7	1.15	0.56
81	Keratin (through collodion)	0.35	41.7	1.15	0.31
83	Gelatin	0.04	41.0	1.10	0.04
128	Keratin (pH 4) (HCl)	0.56	40.6	1.08	0.03
84	Gelatin (through collodion)	0.032	40.6	1.08	0.03
86	Gelatin (through collodion)	0.048	40.6	1.08	0.04
90	Starch	1.143	41.2	1.12	1.02
92	Nylon intermediate	0.85	41.0	1.10	0.77
95	Copolymer (glycine-alanine)	0.70	38.7	0.94	0.75
192	Copolymer	1.2	41.1	1.11	1.08
130	Copolymer (pH 10.8)	0.82	41.3	1.12	0.74
180	Polyvinyl alcohol (M.W. 1500)	1.15	39.8	1.02	1.13
188	Polyvinyl alcohol (M.W. 15,000)	1.44	41.1	1.11	1.3
149	Carbowax (M.W. 1000)	0.717	38.1	0.9	0.80
150	Carbowax (M.W. 4000)	0.94	40.2	1.05	0.90
98	Polyacrylic acid	0	40.2	—	0
99	Polymethacrylic acid	0.36	40.2	1.05	0.34
100	Methyl cellulose	0.66	40.2	1.05	0.63
101	Carboxymethyl cellulose	0	40.6	—	0
102	Polyacrylic acid and alkali	0	—	—	0
103	Polyacrylic acid and acid (HCl)	0.15	40.6	1.08	0.14
104	Carboxymethyl cellulose and acid (HCl)	0	—	—	0
106	Carboxymethyl cellulose and alkali (NaOH)	0	—	—	0
107	Polyacrylic acid (0.00026 g. per 200 ml.)	0	—	—	0
108	Polyacrylic acid (0.000026 g. per 200 ml.)	0.9	0.0429	1.23	0.73

I Run no.	II Additive	III Specific rate	IV Initial concn.	V Specific rate in pure soln.	IV Ratio $\frac{\text{III}}{\text{V}}$
124	Polyacrylic acid (0.0001 g. per 200 ml.)	0	—	—	0
189	Polyacrylic acid (0.00005 g. per 200 ml.)	0.47	42.2	1.18	0.40
120	Sucrose	1.12	0.0414	1.13	0.99
162	Alginic acid	0.69	0.0429	1.23	0.56
163	Alginic acid (pH 8.0)	0.26	0.0406	1.08	0.24
182	Methoxy polyethylene glycol	0.89	0.0383	1.0	0.89

prevented crystallization up to 5 hours, but again a small deposit appeared overnight. At a further reduced concentration of 0.13 p.p.m., polyacrylic acid showed a retarding activity similar to that of borax at 20 p.p.m.

The result of adding polyacrylic acid to a crystallizing solution after nucleation had taken place, compared with the result of adding a similar concentration of keratin, illustrated the much greater activity of the former. Polyacrylic acid, at 10 p.p.m., produced a very marked change, whereas the others produced only a very gradual and slight change. Polymethacrylic acid showed much less activity than polyacrylic acid at the same concentration. Fig. 2 shows some of the results.

The hydrogen ion concentration of the solution influenced the retarding power of the active additives. Those substances which produced a retarding effect at their natural pH, produced a greater effect in alkaline solution. The result of addition of acids was investigated most fully in the case of polyacrylic acid. When hydrochloric acid was added to solutions containing polyacrylic acid at a concentration of 13 p.p.m., crystallization occurred at a rate greater than in the presence of polyacrylic acid alone. When hydrochloric or sulfuric acids were added to solutions containing polyacrylic acid at 0.25 p.p.m., the rate of crystallization was less than in the presence of polyacrylic acid alone. However, when the hydrochloric or sulfuric acids were replaced by chloracetic acid, it reduced the retarding power of the additive in all cases examined. These results are discussed later.

In order to eliminate the possibility of the difference in activity between polyacrylic and polymethacrylic acids being due to a large difference in molecular weight, the degree of polymerization of the two samples was determined by viscosity measurements following the procedure recommended by Katchalsky and Eisenberg (6). This gave a value of approximately 500 for the degree of polymerization in each case, corresponding to molecular weights of approximately 43,000 for the polymethacrylic and 36,000 for the polyacrylic acid.

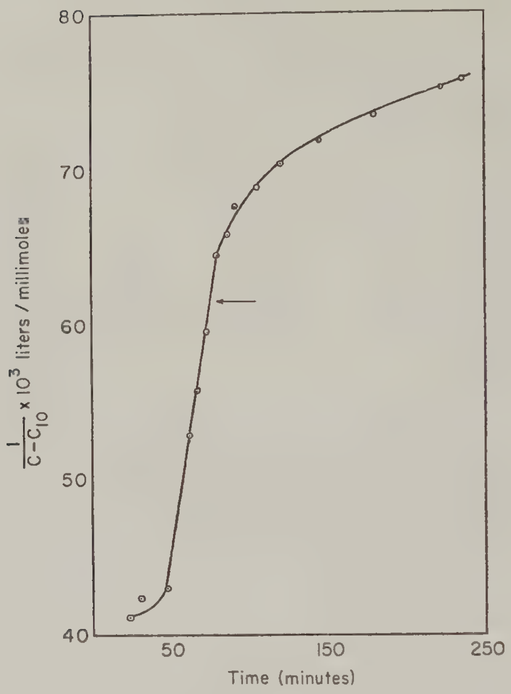

Fig. 2 (*a*).

Fig. 2 (*a*). Result of adding polyacrylic acid (13 p.p.m.) to a crystallizing solution of calcium sulfate after nucleation is complete. Temp. 30°C.

Discussion

a. The Effect of Additives on the Kinetics of Crystal Growth

With all the substances found to retard crystallization of calcium salts the effective entity would seem to be an anion. This appears to apply to the carbonate, phosphate, sulfite, and sulfate (and even to sucrose), but the present discussion will be confined to calcium sulfate.

The marked efficiency of substances containing carboxyl groups regularly spaced along a chain structure, together with the inactivity of the alanine-glycine copolymer, makes it highly probable that the proteinaceous materials owe their activity to their carboxyl side chains (e.g., aspartic and glutamic acids). The amino acid composition varies with the source, but the following figures have been given as typical (7):

	Grams of amino acid per 100 g. of protein	
	Hair (keratin)	Gelatin
Aspartic acid	8.0	6.7
Glutamic acid	17.9	11.2

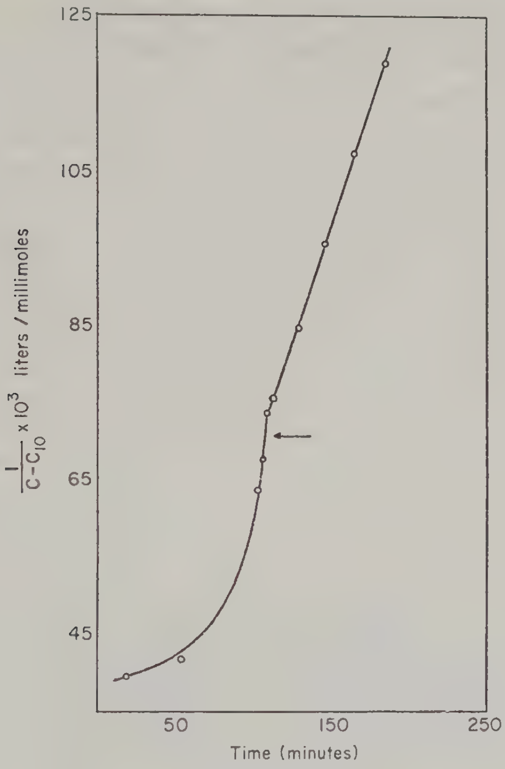

FIG. 2 (*b*).

Result of adding gelatin (13 p.p.m.) to a crystallizing solution of calcium sulfate after nucleation is complete. Temp. 30°C.

The effect of pH on retarding power may be correlated with the degree of ionization of polyacrylic acid and carboxymethyl cellulose, using the data of Kagawa and Katsuura (8) and of Kern (9). Between pH 3 and pH 11, the degree of ionization increases from approximately 10% to approximately 90%. Addition of alkali increased the retarding action of polyacrylic acid and carboxymethyl cellulose parallel with the increased ionization. The effect of acid on the retarding power of polyacrylic acid depended on the concentration of the polyacrylic acid and the type of acid used. It has been shown that, even in the absence of other additives, sulfuric and hydrochloric acid both exert a retarding action on the crystallization. In the case of hydrochloric acid this would be due to an increase in the solubility of the calcium salts.

Although sulfuric acid increases the solubility of calcium sulfate, the effect would be negligible in the concentrations used, so that it must be attributed to a change in the activity of the calcium sulfate brought about by the divalent negative ion. No retardation was produced by the presence of chloracetic acid alone; the addition of chloracetic acid to polyacrylic acid caused a reduction in retarding power corresponding to the decreased ionization of the latter.

In summation, when a strong acid is added to a solution of one of the polycarboxylic materials, the latter's ionization is suppressed and its retarding power largely destroyed. In the case of hydrochloric and sulfuric acids, the rate of crystallization is still retarded by the specific action of these acids. If the concentration of the polyacrylic acid is such that its retarding power is less than that of the acids at the particular concentration, then the addition of the acids causes an increased retardation. In Fig. 3, the percentage reduction in rate of crystallization is plotted on the same diagram as the degree of dissociation.

In connection with viscosity measurements of solutions of polyelectrolytes, Katchalsky and Eisenberg (6) have pointed out another result of varying pH. In low concentrations of alkali, the ionization of the carboxyl group is nearly complete and the like negative charges on these groups repel one another, making the molecule much more rigid. In higher concentrations of alkali, the high ionic strength neutralizes the effect of electrostatic repulsions and the molecule again becomes randomly coiled. This change in the rigidity of the molecule may be a contributing factor in changing its adsorption on the calcium sulfate lattice.

The inductive effect of the methyl group in polymethacrylic acid has only a slight effect on its ionization, which is given by a curve similar to that for polyacrylic acid. The molecular weights of the samples of poly-

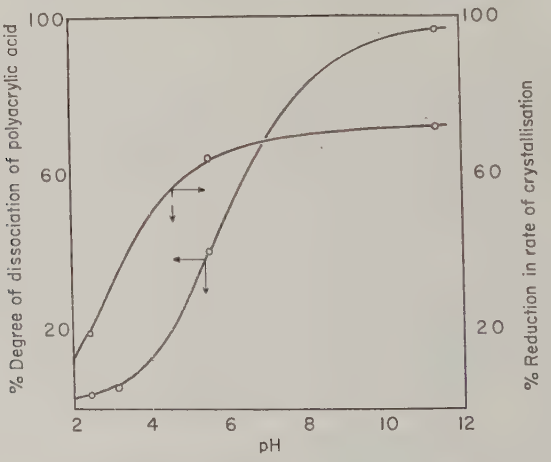

FIG. 3. Relationship between retarding power and degree of ionization of polyacrylic acid. Concentration of polyacrylic acid: 0.25 p.p.m. in solutions of calcium sulfate at 30°C.

acrylic acid and polymethacrylic acid have been shown to be similar, so that the relatively small retarding power of the polymethacrylic acid must be attributed to steric hindrance by the methyl group interfering with the adsorption of the molecule on the crystal structure.

These changes in rate of crystallization could be brought about through one or both of two mechanisms:

1. Interaction of the additive with calcium ions in solution altering the activity of these ions.

2. Adsorption of the additive on the crystal surface either generally or on particular crystal faces or points such as dislocations.

Many of the substances which are effective as retarders do form weak complexes with calcium ions, but this does not appear to be a sufficient condition to produce a marked change in the crystallization process. Ethylene diamine tetraacetic acid, which forms one of the most stable complexes with calcium ions, has no effect on the crystal habit of calcium sulfate and affects the rate of crystallization only to the extent that it removes a stoichiometric proportion of calcium. In complex mixtures such as sugar syrups, it is probable that both complexing and adsorptive effects

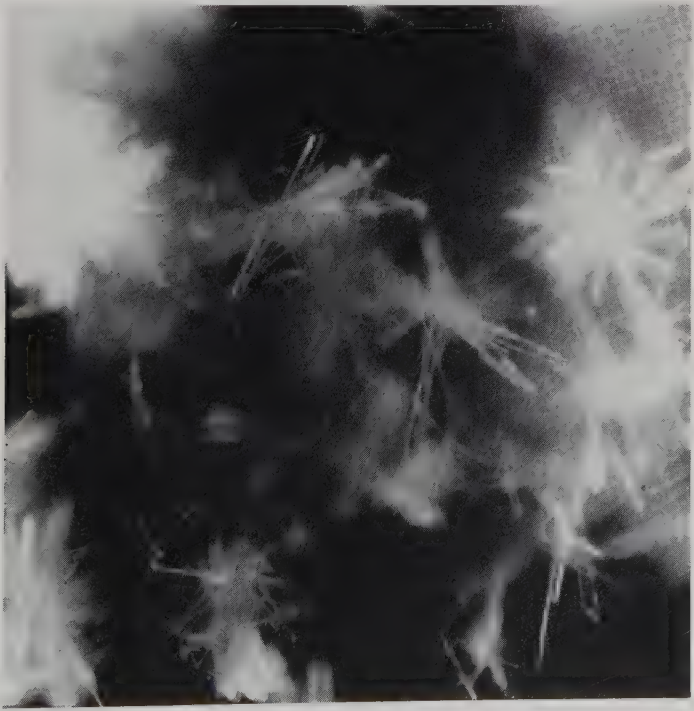

FIG. 4. Clumps of needle-shaped crystals of calcium sulfate dihydrate from pure solution (×156).

are operative. Polyacrylic acid and carboxymethyl cellulose prevent crystallization in concentrations so small that the formation of a complex with calcium ions would not significantly reduce the supersaturation.

If the action of the substances, which stabilize supersaturated solutions of calcium sulfate, is to be adsorbed on the crystal embryos and prevent their growth, the question arises why the nuclei do not go on forming until all the stabilizing material has been used up, since the formation of nuclei involves a negligible change in the concentration of the solution. There are two possible reasons for this. Nucleation may take place only on a limited number of "stray nuclei," or it may be that the stabilizing substances stop development of the nuclei below the critical size and they redisperse, freeing the stabilizing material to interact with other embryos. The latter is more in accord with the suggestion that homogeneous nucleation takes place and is consistent with the observation that the active additives do not significantly reduce the rate of solution of calcium sulfate dihydrate.

b. *The Effect of Additives on Crystal Habit*

This work has established a relationship between the action of additives in slowing the rate of nucleation and crystal growth and the modification of crystal habit. The greatest modification of crystal habit was produced by the protein materials, gelatin and keratin retarder, in alkaline solution.

The characteristic crystals which formed in pure solution were a mixture of three-dimensional balls of needles radiating from a center and a propor-

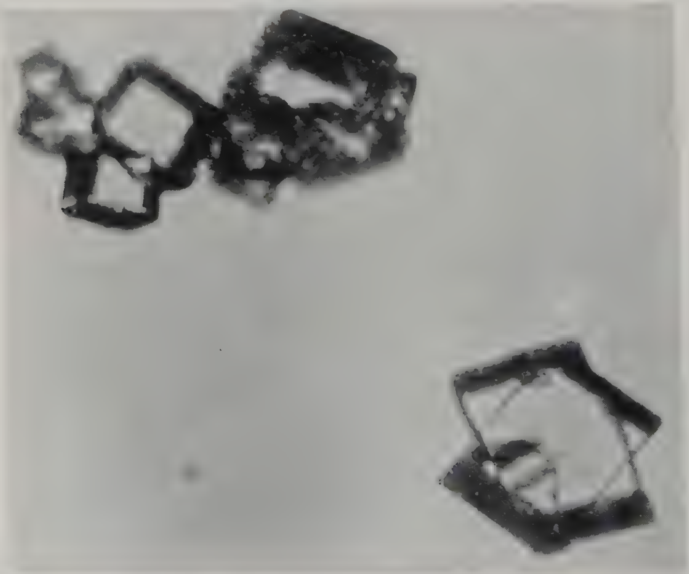

Fig. 5. Crystals of modified habit from calcium sulfate solutions containing gelatin at a natural pH of 5.8 (×194).

tion of twinned crystals. Typical examples are shown in Fig. 4. The presence of gelatin or keratin retarder in alkaline solution (pH 10.5) produced much more stumpy crystals, i.e., elongation parallel to the C-axis was restricted (Fig. 5). Adjustment of the pH to about 3 caused the habit modification to disappear completely (Fig. 6).

The habit modification is not due to the alkali, since this alone has the opposite effect. Crystals from solutions adjusted to pH 10 with potassium hydroxide were extremely elongated and formed an oriented fibrous mass, which, even to the naked eye, had a noticeable luster.

The few small crystals which formed from solutions containing polyacrylic acid and carboxymethyl cellulose were modified clumps.

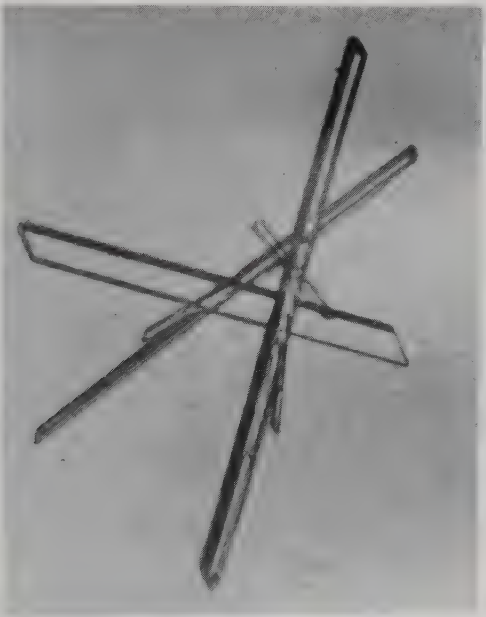

FIG. 6. Needle crystals of calcium sulfate from a solution containing gelatin and hydrochloric acid (pH 3.1).

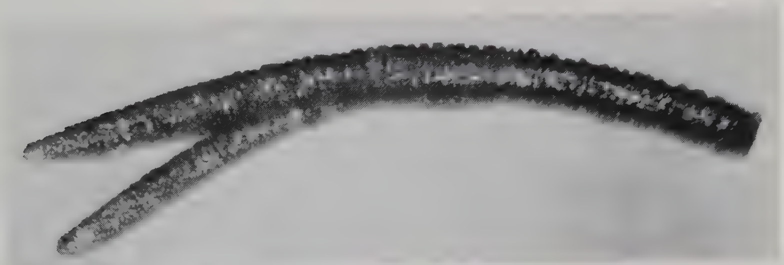

FIG. 7. Curved crystal of calcium sulfate dihydrate from solution containing polyacrylic acid at 70°C.

Interesting results were obtained upon heating a solution of calcium sulfate which contained sufficient polyacrylic acid to prevent crystallization at 30°C. At about 70°C a deposit of crystals appeared and grew extremely rapidly to such a size that the general shape could be distinguished with the naked eye. A typical needle is shown in Fig. 7. It is seen to be curved and highly imperfect in accordance with the extreme haste of its growth. It appears that, upon heating, the polyacrylic acid cannot completely prevent nucleation and, once a few nuclei form, the excess solute is very rapidly deposited on them.

The growth of calcium sulfate dihydrate crystals from pure solution consists mainly in the growth normal to themselves of the (111) faces. It is postulated that, in alkaline solution, the anionic polymers are strongly adsorbed on the (111) faces of the crystals, attaching themselves to the calcium ions in the edges of the growing steps, thereby slowing or, at high concentrations, stopping the growth of these faces. (The (111) face consists of calcium and sulfate ions together with water molecules.)

CONCLUSIONS

1. The rates of nucleation and crystal growth of calcium sulfate dihydrate are most strongly reduced by colloidal materials having regularly spaced, ionized carboxyl groups on a chain structure. The materials appear to act by being adsorbed on the crystal surface, the strength of the adsorption increasing with increasing molecular weight of the additive and decreasing size of the crystal or embryonic crystal.

2. The crystal habit of calcium sulfate dihydrate is modified by adsorption of anionic polymers which occurs most strongly on the (111) faces of the crystals.

REFERENCES

1. DEITZ, V. R., Investigations of the Bone Char Research Project, Inc., Natl. Bureau of Standards Rept. 5269.
2. LOWY, K., "The Role of Aconitic Acid in Sugar Refining," paper presented to the Bone Char Conference, 1957.
3. CARRUTHERS, A., OLDFIELD, J. F. T., SHORE, N., AND WOOTTON, A. E., "Studies Relating to the Solubility of Calcium Compounds in Juice," Ninth Annual Technical Conference of the British Sugar Corporation, Ltd.
4. JOHNSON, C. E., U. S. Patent 2,723,956.
5. McCARTNEY, E. R., to be published.
6. KATCHALSKY, A., AND EISENBERG, H., *J. Polymer Sci.* **6,** 145 (1951).
7. NEURATH, H., AND BAILEY, K., "The Proteins." Academic Press, New York, 1953.
8. KAGAWA, I., AND KATSUURA, K., *J. Polymer Sci.* **7,** 89 (1951).
9. KERN, W., *Biochem. Z.* **301,** 338 (1939).

JOURNAL OF COLLOID SCIENCE **13**, 397–406 (1958)

ON PHYSICAL ADSORPTION

X. ADSORBED MONOLAYERS OF ARGON AND NITROGEN ON BORON NITRIDE AND ON A GRADED SERIES OF PARTIALLY GRAPHITIZED CARBON BLACKS

Sydney Ross and W. W. Pultz[1]

Department of Chemistry, Rensselaer Polytechnic Institute, Troy, New York

Received March 13, 1958

ABSTRACT

Low-pressure adsorption isotherms of argon and nitrogen at 77.8° and 90.1°K. were measured on members of a graded series of a carbon black, which had been partially graphitized in an inert atmosphere at temperatures of 1000, 1500, 2000, and 2700°C. An increasing homogeneity of the surface accompanies graphitization and is reflected in a number of adsorption phenomena, all of which gradually become more pronounced with increasing degree of surface homogeneity: (*a*) the two-dimensional van der Waals' equation provides a description of the isotherm over a greater range of surface concentrations; (*b*) the two-dimensional critical temperature of the adsorbate increases regularly toward the theoretical value expected of an ideally uniform substrate; (*c*) the mobilities of the adsorbed monolayers correspond over an increasingly greater range of surface concentration to that of a two-dimensional gas on a uniform substrate.

A sample of boron nitride was also used as adsorbent for monolayers of argon and nitrogen at 77.8 and 90.1°K. A comparison of the results for boron nitride with those for the carbon black series shows that the boron nitride surface would correspond to a carbon black of the present series graphitized at 1800°C.

INTRODUCTION

In an earlier paper of this series, Ross and Winkler (1) reported monolayer adsorption isotherms, at 77.8° and 90.1°K., for argon and nitrogen on a highly graphitized sample of carbon black; they offered an interpretation of their observations in terms of the known properties of the adsorbates and the nature of the adsorbent surface. Since the ultimate objective of the present researches is the characterization of surface energies of solids, we have now observed adsorption phenomena on samples of carbon black, all taken from the same original specimen, but subjected to different degrees of graphitization so as to form a graded series. The members of the series exhibit an increase of surface homogeneity with higher temperature of heat treatment. We also include for comparison monolayer adsorption isotherms on a boron nitride adsorbent. Boron nitride has a crystalline lattice similar to that of graphite and the structure of its principal cleavage plane is identical with that of the corresponding plane in graphite. Our conclusions show that the behavior of the adsorbates is the same on the boron nitride as on the relatively highly graphitized members of our series of carbon blacks.

---

[1] Based on a thesis presented by W. W. Pultz, in partial fulfillment of the requirements for the degree of Doctor of Philosophy, to the Department of Chemistry, Rensselaer Polytechnic Institute, June, 1958. The experimental observations are reported in full in the original thesis, copies of which may be obtained from University Microfilms, Ann Arbor, Michigan.

Materials, Apparatus, and Methods

A series of samples of a carbon black, P-33 (also known as Sterling F.T.), of surface area approximately 12m.^{2}/g., were supplied by the courtesy of Dr. W. R. Smith, of Godfrey L. Cabot, Incorporated. These carbon black samples had been heat-treated for 2-hour periods in an induction furnace at temperatures ranging from 1000° to 2700°C. Virtually all the air was driven off in the initial heating stages and excluded for the duration of the heating period. More complete details of the preparation, X-ray crystallite dimensions, and other physical properties of the resulting partially graphitized carbon black are given by Schaeffer, Smith, and Polley (2). The present samples are from the same lots for which Polley, Schaeffer, and Smith (3) determined the adsorption of argon, nitrogen, and oxygen at 78°K. These authors found a gradual development of stepwise isotherms for the progressively more graphitized carbon black. In accordance with modern theories this result was interpreted as evidence for a transition from heterogeneous to homogeneous surfaces as graphitization increased. Almost no data were reported, however, in the range below monolayer coverage, which is the province of the present paper.

The adsorption of argon and nitrogen on P-33 (2700°) has been reported previously by S. Ross and W. Winkler (1); the present work includes a redetermination of the nitrogen adsorption at 77.8°K.; the two sets of data are in good accord.

The sample of boron nitride (Batch 210484) was manufactured by the Norton Co. It was selected from a number of boron nitride samples because it gave adsorption isotherms that closely resembled those of the highly graphitized carbon black; the other boron nitride samples gave isotherms resembling less graphitized carbon black. The surface area of the boron nitride sample is approximately 18m.^{2}/g.

Spectroscopically pure grades of argon, nitrogen, and helium were obtained from the Matheson Company.

The measurements were determined on two different volumetric apparatuses, one for the range 2–50 μ, and the other for the range 0.05–14 mm. Each apparatus and details of the method used have been described previously (1). The initial desorption of each sample was carried out *in vacuo* at 150°C. for 12 hours.

EXPERIMENTAL RESULTS

The adsorption isotherms were determined in as much detail as those reported by Ross and Winkler (1). The isotherms were determined chiefly by adsorption, with enough points by desorption to show that the data are true equilibrium values. The range of adsorption measurement for which the two apparatuses overlap (i.e., at the high-pressure end of the low-pressure apparatus and the low-pressure end of the high-pressure apparatus) shows excellent agreement, save for results on the original non-graphitized P-33. The deviation here probably arises from differences in the initial desorption carried out in the two apparatuses, where, in spite of using the same temperatures and times of desorption, differences in the sample-tube size, the amount of sample, surface area exposed, and density of packing could all contribute to variations in the loss of a volatile surface-impurity. The visible presence of such an impurity in the untreated carbon black samples was actually detected in one experiment.

The data were plotted on large-scale graph paper as $\ln p$ versus V, and smooth curves were drawn to connect the points. The resulting curves can be represented by a fifth-order power series, for which the coefficients have been determined conveniently by means of Gerber's "Equameter".[2] The additional error introduced by the use of the interpolation equations is negligible (max. error in $\ln p = \pm 0.02$).

The interpolation equation has the form:

$$\ln p = a + bV + cV^2 + dV^3 + eV^4 + fV^5,$$

in which p is in millimeters of mercury, and V is in milliliters of adsorbate at S.T.P. per gram of adsorbent. The values of the coefficients are given in Table I. The large range of pressures covered by the measurements would require two sets of interpolation equations for an adequate description of all the data obtained. The equations of Table I represent the higher pressure values, amounting to about 95% of the measurements taken; the data for the pressure range 2–50 μ are available in the original thesis.

Interpolation equations of the type used here are useful not only for a concise reporting of the data, but also because they allow mathematical operations, such as obtaining derivatives, second derivatives, or integrals, to be performed analytically. There is less loss of precision by analytic operations on a good interpolation equation than by graphical operations with the original data.

---

[2] The Gerber Scientific Instrument Co., 162 State St., Hartford 3, Connecticut.

TABLE I

Interpolation Equations of Argon and Nitrogen Adsorption Isotherms on a Series of Carbon Blacks and Boron Nitride

Sample	Temp. (°K.)	Range of V	a	bV	cV^2	dV^3	eV^4	fV^5	V_m
I. Argon Adsorption Isotherms									
P-33 (original)	77.8	0.10–2.30	−6.2275	+18.2550	−24.5824	+18.3453	−6.6924	+0.9400	4.10
	90.1	0.10–1.00	−3.9860	+27.9346	−73.7780	+113.5939	−88.3445	+27.0390	3.94
P-33 (1000°)	77.8	0.15–2.80	−4.4404	+4.1542	−1.9619	+0.4109	+0.0517	−0.0150	3.50
	90.1	0.15–2.00	−3.0017	+9.6784	−12.1775	+8.9473	−3.2726	+0.4802	3.36
P-33 (1500°)	77.8	0.20–2.72	−3.8015	+4.7335	−4.8754	+2.9898	−0.9534	+0.1296	3.50
	90.1	0.25–2.30	−1.8647	+5.8945	−6.5024	+4.2586	−1.4256	+0.2009	3.36
P-33 (2700°)	77.8	0.30–3.10	−3.0890	+2.9782	−3.0096	+1.8564	−0.6332	+0.0955	3.60
	90.1	0.20–2.70	−1.1441	+3.8082	−3.9348	+2.4268	−0.7820	+0.1095	3.46
BN	77.8	0.10–3.20	−3.0380	+7.0181	−7.8766	+4.4674	−1.2191	+0.1278	5.06
	90.1	0.10–3.20	−1.0281	+7.4837	−8.5407	+4.9289	−1.3584	+0.1439	4.26
II. Nitrogen Adsorption Isotherms									
P-33 (original)	77.8	0.10–1.90	−5.6058	+13.3820	−14.1633	+9.5872	−3.3540	+0.4675	3.70
	90.1	0.10–0.85	−4.3486	+32.8470	−103.2697	+194.7234	−184.8532	+68.3791	3.52
P-33 (1000°)	77.8	0.35–2.40	−6.0680	+9.3500	−8.8528	+5.0976	−1.4101	+0.1615	3.00
	90.1	0.15–1.65	−3.7791	+11.9926	−17.1031	+15.4685	−7.1549	+1.3360	2.85
P-33 (1500°)	77.8	0.10–2.50	−4.9385	+9.3744	−13.7289	+11.1204	−4.3505	+0.6701	2.95
	90.1	0.10–1.80	−3.1176	+12.4510	−22.0098	+21.8757	−10.6525	+2.0323	2.80
P-33 (2700°)	77.8	0.15–2.55	−3.8807	+4.7692	−5.2709	+3.6186	−1.3286	+0.2176	2.86
	90.1	0.15–2.25	−2.2555	+7.2830	−9.5413	+7.1388	−2.6378	+0.3993	2.72
BN	77.8	0.15–3.50	−3.1217	+6.5474	−6.6114	+3.4957	−0.8921	+0.0892	4.23
	90.1	0.10–3.10	−0.9965	+6.7294	−7.3266	+4.3460	−1.2491	+0.1388	3.70

DISCUSSION OF RESULTS

1. *Estimation of Monolayer Capacity, V_m*

The determination of the monolayer capacity, V_m, for the present series of carbon blacks is based on the isotherm "b" point, as the B.E.T. plots are not linear. Polley, Schaeffer, and Smith (3) report surface areas, based on the nitrogen adsorption isotherms at 78°K. The same authors in a private communication have kindly given us the values of V_m for the argon isotherms at 78°K., also based on the isotherm "b" point. We have estimated the V_m values at 90°K. by using the ratio of the cross-sectional areas of the adsorbate molecules (4) at 90° and 78°K., namely, for nitrogen 16.2/15.4 and for argon 15.2/14.6. Table I contains the value of V_m used for each isotherm in the calculation of θ, the fraction of the surface covered by the adsorbate monolayer, where $\theta = V/V_m$.

2. *Application of Two-Dimensional van der Waals' Equation*

It was shown by Ross and Winkler (1) that the two-dimensional van der Waals' equation was applicable to argon and nitrogen adsorbed on P-33 (2700°), and this application yielded an estimate of the two-dimensional critical temperatures of the adsorbates. In the same way as previously described this equation is found to be valid for the adsorption of argon and nitrogen on the following samples: P-33 (2000°), which is not otherwise reported here because of its close similarity to the 2700° sample; P-33 (1500°); P-33 (1000°); and boron nitride. The range of application of the van der Waals' equation as a description of the data (see Figs. 6 and 7 of reference 1) increases progressively as the carbon black samples are more graphitized. For the isotherms that are described adequately by a two-dimensional van der Waals' equation, the range of surface concentration that is so described is approximately from 5% to 40% of the monolayer. Each of these descriptions yields an estimate of the two-dimensional critical temperature of the adsorbate, T_{c_2}, which are reported in Fig. 1. Figure 1 includes for comparison a theoretically calculated T_{c_2} for argon and nitrogen, which is taken as 50% of the normal three-dimensional critical temperature (5). It is interesting to observe that as graphitization produces a more homogeneous surface, the value derived for T_{c_2} more closely approaches the theoretical value, which is, of course, based on the assumptions of a mobile film and a perfectly homogeneous substrate.

The two-dimensional critical temperatures estimated from the van der Waals' equation can be compared with the observed phase transitions of argon on graphite reported by Jura and Criddle (6). The two-dimensional critical temperature calculated from their data by de Boer and Kruyer (7) is 66.3°K., which is a little higher than even the most highly graphitized carbon of the present series.

The boron nitride adsorbent causes the T_{c_2} of argon and of nitrogen to

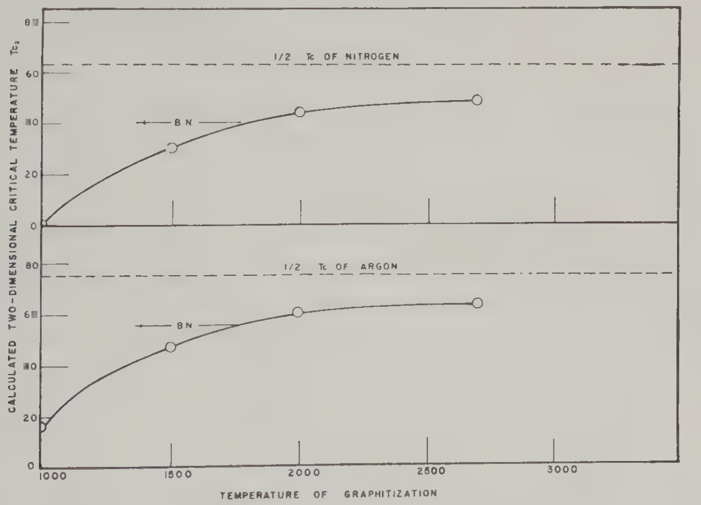

FIG. 1. The variation of estimated two-dimensional critical temperatures of adsorbed argon and nitrogen as a function of the graphitization temperature of carbon black adsorbents. The interpolated point represents T_{c_2} on a boron nitride adsorbent. Each value is an average of the estimated T_{c_2} from the 77.8° and 90.1°K. isotherms.

fall in a range that would correspond to a carbon black of the present series graphitized at 1800°C.; presumably the surface heterogeneity of the boron nitride is of the same nature as that occurring on carbon black surfaces.

3. Entropy and Mobility of Adsorbed Monolayers

J. H. de Boer and S. Kruyer (7) in a recent series of papers have described a procedure for calculating the differential entropy of adsorption from experimental data. The difference in free energy between the standard state of the three-dimensional gas at temperature T_1 and the adsorbed molecules is given by

$$\Delta F_1 = -RT_1 \ln p^\circ/p_1,$$

where p° is the standard pressure (760 mm. Hg). Similarly ΔF_2 for the same degree of surface coverage at temperature T_2 is given by

$$\Delta F_2 = -RT_2 \ln p^\circ/p_2.$$

As

$$\Delta F_1 = \Delta H - T_1 \Delta S$$

and

$$\Delta F_2 = \Delta H - T_2 \Delta S,$$

where ΔH is the differential heat of adsorption and ΔS the differential entropy of adsorption, both ΔH and ΔS can be calculated. De Boer and Kruyer introduce two entropically ideal adsorption states: for the model of a mobile adsorbed monolayer the original translational entropy of an ideal gas (${}_gS_{tr}$) is transformed to the translational entropy of an ideal two-dimensional gas, (${}_aS_{tr}$), the internal vibrations and rotation remaining unchanged; in the model of "entropically ideal site adsorption" the original translational entropy of the ideal gas is completely lost. From the experimentally derived figures for ΔS at different degrees of coverage we calculate, on the basis of each model, alternative values of ΔS°, representing the difference in the differential entropy between the three-dimensional gas in its standard state and the standard state of the adsorbed monolayer, whether mobile or immobile. For the two models the equations developed by de Boer and Kruyer are, respectively:

$$-\Delta S_m{}^\circ = -\Delta S - R \ln \frac{\sigma^\circ}{\sigma}; \qquad [1]$$

$$-\Delta S_i{}^\circ = -\Delta S - R \ln \frac{\theta}{1 - \theta}, \qquad [2]$$

where θ is the degree of surface coverage given by the ratio V/V_m, σ is the area per molecule, and σ° is the area per molecule at the standard state of the mobile adsorbed monolayer. The forms of the last terms in Eqs. [1] and [2] are determined by the standard states of the adsorbed mobile and immobile monolayers, respectively, as chosen by de Boer and Kruyer. An improvement of Eq. [1] can be made in the term for configurational entropy of the adsorbed molecules, which is given by de Boer and Kruyer as $R \ln \sigma$, whereas the actual area available to every adsorbed molecule is diminished by the area covered by molecules already adsorbed (8). Therefore for σ we substitute $(\Sigma - N_a b)/N_a$, where Σ is the specific surface area per gram of adsorbent, N_a is the number of adsorbed molecules, and b is the average limiting molecular area of the adsorbate, taken, for convenient reference, as given by Yates (4). With this correction and with the introduction of the standard state as selected and defined by de Boer and Kruyer, Eq. [1] becomes:

$$-\Delta S_m{}^\circ = -\Delta S - R \ln \frac{4.08T}{b}\left(\frac{\theta}{1-\theta}\right). \qquad [1a]$$

For comparison with the values of ΔS° obtained from the experimental data by means of Eqs. [1*a*] and [2], corresponding values of ΔS° for entropically ideal models of mobile and immobile monolayers are derived from the following equations:

$$-\Delta S_m{}^\circ = {}_gS^\circ_{tr} - {}_aS^\circ_{tr}; \qquad [3]$$

$$-\Delta S_i{}^\circ = {}_gS^\circ_{tr}. \qquad [4]$$

The term ${}_gS^\circ_{tr}$ in Eqs. [3] and [4] is given by the Sackur-Tetrode equation for the standard molar entropy of an ideal gas:

$${}_gS^\circ_{tr} = R \ln (M^{3/2}T^{5/2}) - 2.30.$$

The term ${}_aS^\circ_{tr}$ in Eq. [3] is derived by de Boer and Kruyer, based on a two-dimensional ideal gas, and a two-dimensional pressure of 0.338 dyne/cm. as the standard state of the adsorbed monolayer:

$${}_aS^\circ_{tr} = \tfrac{2}{3}\,{}_gS^\circ_{tr} + 1.52 \log T - 3.04. \qquad [5]$$

By this treatment experimental data can be tested to find if the model of a mobile or an immobile adsorbed monolayer gives the closer correspondence. The experimental data are used in Eqs. [1*a*] and [2], which are based, respectively, on each model, to give values that are to be compared with the theoretical results obtained from Eqs. [3] and [4], again based, respectively, on each model.

The data of the present communication (Table I) are treated in the manner just described and the results are collected in Tables II and III. These tables use the same symbols and are arranged in the same way as those published by de Boer and Kruyer (7). The temperature is 84°K., the arithmetic mean of the two temperatures at which the isotherms were determined.

TABLE II

Entropies of Adsorption of Nitrogen on Boron Nitride and on Carbon Blacks at 84°K.

2700 P-33

θ	$-\Delta H$ (cal./mole)	$-\Delta S_i^\circ$	$-\Delta S_m^\circ$
0.1	2310	15.5	9.4
0.2	2410	15.9	9.8
0.3	2470	16.3	10.2
0.4	2560	17.6	11.0
0.5	2610	17.4	11.3
0.6	2680	18.1	12.0

Boron Nitride

θ	$-\Delta H$ (cal./mole)	$-\Delta S_i^\circ$	$-\Delta S_m^\circ$
0.1	2290	18.1	12.0
0.2	2330	18.2	12.1
0.3	2390	18.6	12.5
0.4	2390	18.4	12.3
0.5	2380	17.8	11.8
0.6	2350	17.2	11.1

1500 P-33

θ	$-\Delta H$ (cal./mole)	$-\Delta S_i^\circ$	$-\Delta S_m^\circ$
0.1	2420	16.2	10.2
0.2	2490	17.0	10.9
0.3	2550	17.5	11.4
0.4	2650	18.2	12.5
0.5	2650	18.7	12.6
0.6	2820	20.8	14.7

1000 P-33

θ	$-\Delta H$ (cal./mole)	$-\Delta S_i^\circ$	$-\Delta S_m^\circ$
0.1	2710	19.3	13.2
0.2	2720	19.2	13.2
0.3	2710	19.5	13.4
0.4	2700	19.7	13.6
0.5	2680	19.9	13.8
0.6	2630	20.0	13.9

${}_gS^\circ_{tr} = 29.60$ e.u.

${}_gS^\circ_{tr} - {}_aS^\circ_{tr} = 10.00$ e.u.

Examination of Tables II and III shows that for all the substrates the model of mobile adsorption describes the situation better than the model of site adsorption. This conclusion is founded on the closer agreement between the results based on Eqs. [1*a*] and [3], compared to results based on Eqs. [2] and [4].

An entropy loss, calculated from Eq. [1*a*], greater than the entropy loss given by Eq. [3], is interpreted by de Boer and Kruyer (7) as caused by some restriction of the free translational movement of the adsorbed molecule on the surface. This interpretation is almost inevitably true at higher surface concentrations. The increase of the entropy loss ($-\Delta S_m^\circ$) with coverage is caused at first by the change of the surface monolayer from ideal to nonideal; which is reflected also by the entropy loss being close to ideal entropy loss only at low values of surface coverage, where the entropy loss could still be legitimately compared with an idealized entropy loss derived from an ideal, two-dimensional equation of state. The first restrictions of the free translational motion of the adsorbed molecules are, therefore, brought about by the increasingly nonideal character of the adsorbed monolayer. At still higher surface concentrations a quasi-ordered packing of the adsorbed molecules brings about additional restrictions on the mobility, though far from enough to warrant comparison with an ideally immobilized monolayer.

The adsorption of argon on P-33 (2700°) at very low surface concentration corresponds well to the concept of the idealized mobile film: on

TABLE III

Entropies of Adsorption of Argon on Boron Nitride and on Carbon Blacks at 84°K.

2700 P-33

θ	$-\Delta H$ (cal./mole)	$-\Delta S_i°$	$-\Delta S_m°$
0.1	2330	17.4	11.2
0.2	2500	17.9	11.7
0.3	2600	18.4	12.2
0.4	2670	18.7	12.5
0.5	2800	20.0	13.8
0.6	2840	18.8	13.8

Boron Nitride

θ	$-\Delta H$ (cal./mole)	$-\Delta S_i°$	$-\Delta S_m°$
0.1	2220	17.8	11.6
0.2	2280	17.9	11.7
0.3	2330	17.9	11.7
0.4	2390	18.0	11.8
0.5	2490	18.7	12.5
0.6	2510	19.1	12.9

1500 P-33

θ	$-\Delta H$ (cal./mole)	$-\Delta S_i°$	$-\Delta S_m°$
0.1	2370	16.6	10.4
0.2	2480	17.5	11.3
0.3	2570	18.2	12.0
0.4	2670	19.0	12.9
0.5	2790	20.0	14.0
0.6	2870	21.2	15.0

1000 P-33

θ	$-\Delta H$ (cal./mole)	$-\Delta S_i°$	$-\Delta S_m°$
0.1	2710	19.7	13.5
0.2	2780	20.6	14.4
0.3	2750	20.3	14.3
0.4	2680	19.6	13.6
0.5	2710	20.3	14.1
0.6	2730	20.8	14.6

${}_gS^\circ_{tr} = 30.68$ e.u.
${}_gS^\circ_{tr} - {}_aS^\circ_{tr} = 10.35$ e.u.

extrapolating low coverage values of $-\Delta S_m°$, which are approximately linear up to about $\theta = 0.40$, to zero coverage, we obtain $-\Delta S_m° = 10.70$ e.u., which compares favorably with the idealized value of 10.35 e.u. Adsorbed nitrogen, however, at low surface concentration loses less entropy on the same substrate than that lost on the basis of the model of an ideal mobile film; which means that on transferring the atoms from the gas to the surface, there is not a complete loss of the entropy of translational motion perpendicular to the surface: a vertical vibration remains of such a frequency $\upsilon < 10^{14}$ sec.$^{-1}$ that it still contributes towards entropy. Kemball (9) has named this adsorbed condition "the super-mobile state"; it has been found (7) for argon adsorbed on charcoal at temperatures above 200°K., and for mercury on charcoal at 66.6°K.

An increase in $-\Delta S_m°$ above the entropically ideal value is readily interpreted for a monatomic molecule as a restriction in the translational movement; for a diatomic molecule the same interpretation is not necessarily valid; appropriate comparisons, however, between argon and nitrogen, of entropy changes at the same heat of adsorption, show that for the present substrates the increase in $-\Delta S_m°$ for nitrogen can also be interpreted as a restriction in the translational movement, while free rotation in both directions is unhindered. The argument used here follows one developed by de Boer and Kruyer based on data of Brunauer and Emmett (10) in which they likewise demonstrate that "there is a certain restriction of the free translation of the nitrogen molecule over the surface.

The rotation of the molecules, however, is not hindered. There is therefore, no mutual orientation."

ACKNOWLEDGMENT

The authors gratefully acknowledge a research grant, NSF-G3015, from the National Science Foundation, for the support of these researches.

REFERENCES

1. ROSS, S., AND WINKLER, W., *J. Colloid Sci.* **10,** 319 (1955).
2. SCHAEFFER, W. D., SMITH, W. R., AND POLLEY, M. H., *Ind. Eng. Chem.* **45,** 1721 (1953).
3. POLLEY, M. H., SCHAEFFER, W. D., AND SMITH, W. R., *J. Phys. Chem.* **57,** 469 (1953).
4. YATES, D. J. C., *Proc. Roy. Soc.* (*London*) **224A,** 526 (1954).
5. DE BOER, J. H., "The Dynamical Character of Adsorption," p. 147. Clarendon Press, Oxford, 1953.
6. JURA, G., AND CRIDDLE, D., *J. Phys. & Colloid Chem.* **55,** 163 (1951).
7. DE BOER, J. H. AND KRUYER, S., *Koninkl. Ned. Akad. Wetenschap. Proc.* **55B,** 451 (1952); *ibid.* **56B,** 67, 236, 415 (1953); *ibid.* **57B,** 92 (1954); *ibid.* **58B,** 61 (1955).
8. TOMPKINS, F. C., *Trans. Faraday Soc.* **46,** 569, 580 (1950).
9. KEMBALL, S., "Advances in Catalysis," Vol. 2, p. 233. Academic Press, New York, 1950.
10. BRUNAUER, S., AND EMMETT, P. H., *J. Am. Chem. Soc.* **59,** 2682 (1937).

JOURNAL OF COLLOID SCIENCE **13**, 407–409 (1958)

LETTER TO THE EDITOR

THE GLASS SCRATCH EFFECT

We offer here additional information on the phenomenon recently described (1). The equipment is of the utmost simplicity. We use tubes of a standard type[1] and 3-mm. soft glass stirring rods. The immediate effect of the scratch is best viewed if the tubes are half immersed in a beaker filled with water, against a dark background, with light coming almost horizontally from a source facing the observer. After settling, the sediments are examined with the help of a small concave mirror. We have studied more closely the three following features.

1. The smear reaction. This is given by all polar compounds of comparatively low molecular weight containing an active hydrogen (e.g., water, lower alcohols, and amines), and is extremely characteristic. The white deposit of glass dust can be streaked on the wall and requires vigorous and prolonged stirring to detach it. Its macroscopic stickiness is in marked contrast to its microscopic appearance, which reveals freely mobile particles, presumably negatively charged (2), which seem to repel each other and show intense translatory and rotatory Brownian motion. We have concluded, from a close observation of the phenomenon, that it is hydrodynamic and a manifestation of the Bernoulli, or Magnus, effects: The particles roll as they fall along the wall in a region where, because of molecular orientation at the surfaces (3), the viscosity of the medium is increased, and thus experience a "lift" toward the wall, which keeps them from dispersing through the medium. This view is supported by the following observation: If these particles in water, or, for example, erythrocytes in 0.14 M NaCl, are allowed to slide down a hanging immersed glass plate, they are deflected under the plate as they reach its lower edge, before resuming their downward motion. Since this interpretation would not apply to particles unable to rotate freely, the intensity of the smear in the glass scratch effect may be taken as a measure of the freedom of the dust from aggregation.

2. Seizure and abrasion. The abrasive power of organic fluids on glass, under the conditions of the test, in general decreased with cyclic structures and with increasing molecular weight (1). A quantitative estimation of the effect has not yet been successful (cf. Engelhardt's results with quartz (4)). A different technique, described below, suggests that seizure of glass sur-

---

[1] Five-milliliter round-bottom test tubes, boro-silicate glass N51-A, Kimble Glass Company, Philadelphia.

TABLE I

Relation between Chemical Constitution and Angle of Seizure

Compound	Angle of seizure Degrees from vertical	Abrasion	Smear
Water	45	+	+
Methanol, ethanol, *n*-propanol	30	+	+
Iso-propanol	25	+	+
n-butanol, sec.-butanol	20	+	+
Tert.-butanol	10	+	+
n-decanol	<10	−	−
Allyl alcohol	35	+	+
Ethanolamine	40	+	+
n-propylamine	40	+	+
n-butylamine	35	+	+
Diethylamine	30	+	+
Triethanolamine	10	±	−
Acetic acid	35	+	±
Acetone	20	+	−
Acetylacetone	30	−	−
Diacetyl	15	−	−
Ethylether	15	+	−
CCl_4, $CHCl_3$, CS_2, hexane	10–15	+	−
Benzene	10	+	−
Benzyl chloride	10	−	−
Benzyl alcohol	30	−	−
Nitrobenzene	10	+	−
Aniline	15	±	+
Pyridine	30	+	Not visible
Dry glass (freshly cleaned)	5–10		

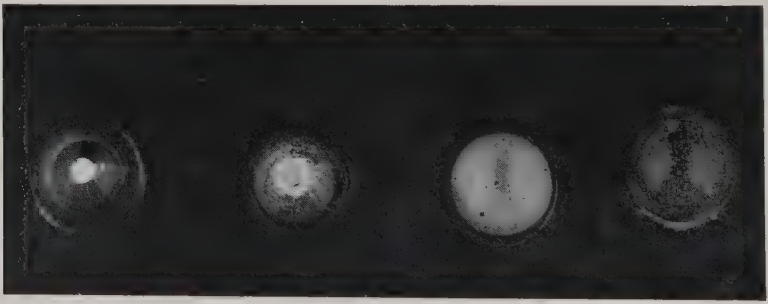

FIG. 1. CCl_4-ethanol system. Sedimentation pattern of glass dust produced by CCl_4 mole fractions of 0, 0.53, 0.96, and 1.0.

faces under slight pressure, and abrasion, are different phenomena: A microscope slide is placed on the bench and a protractor set up vertically behind it. A glass rod, drawn to a thread about 20 cm. long and 0.2 mm. thick, is held above the slide, its tip pointing downwards and touching lightly the middle of the slide, on which a few drops of fluid have been placed. Starting with the rod in a vertical position, the slide is gently poked with the tip, while the hand is slowly displaced along an arc, so as to increase the angle between the rod and the vertical. At first, the rod seizes and jumps off the slide, until an angle is reached beyond which the rod no longer seizes, but glides smoothly over the surface. This angle is given in Table I for a few substances, together with results from the test performed in a tube.

The angle is largest with substances possessing an active hydrogen in a polar group, the same that give a strong smear effect. It seems to be unrelated to abrasive power. Contrast the small angle and fairly good abrasion of nonpolar solvents or nitrobenzene with acetylacetone or benzyl alcohol, which offer the opposite picture.

3. The sediments. Nonaggregated sediments, little white pellets at the tip of the tubes, look much alike; aggregated sediments vary considerably in appearance and bear an obvious relation to the nature of the fluid in which they are produced, as if the latter mediated the abrasion and left its imprint, so to speak, on the particles as they are torn from the wall. Sediments from mixtures offer a bewildering variety, which it has not yet been possible to correlate clearly with the other physical properties of the solutions. For example, the methylal-CS_2 system (cf. reference 5), described schematically:

Mole per cent CS_2:	
0–7	Pellet surrounded by fine deposit
7–52	Coarse aggregate
52–95	Pellet surrounded by coarse deposit
95–98	Coarse aggregate
98–100	Scant aggregate

Ethanol in mixtures yielded a pellet when its mole fraction exceeded approximately 0.5 with nonpolar solvents; 0.2 with ethyl ether; 0.1 with acetone. With water, it produced, strangely enough, a middle zone of aggregation between ethanol mole fractions of 0.3 and 0.9.

Figure 1 offers an illustration of the ethanol-CCl_4 system. The second tube shows the transition point. The third illustrates the general observation that a small amount of a polar fluid added to a nonpolar fluid is enough to increase considerably the abundance and fineness of the sediment.

REFERENCES

1. Bourdillon, J., *Nature* **180,** 1475 (1957).
2. Quist, J. D., and Washburn, E. R., *J. Am. Chem. Soc.* **62,** 3169 (1940).
3. Henniker, J. C., *Revs. Mod. Phys.* **21,** 322 (1949).
4. von Engelhardt, W., *Nachr. Akad. Wiss. Göttingen, Math.-physik. Kl.*, No. 2, 34 pp. (1942), *C. A.* **38,** 4485 (1944); *Naturwiss.* **33,** 195 (1946).
5. Moelwyn-Hughes, E. A., "Physical Chemistry," p. 738. Pergamon Press, London and New York, 1957.

Division of Laboratories and Research,
New York State Department of Health,
Albany, New York.
Jaques Bourdillon

Received March 24, 1958; revised May 19, 1958.

PHYSICAL CHEMISTRY: A Series of Monographs

Edited by Eric Hutchinson and P. Van Rysselberghe

Department of Chemistry, Stanford University, Stanford, California

Volume 6

ESTIMATION OF Thermodynamic Properties of Organic Compounds

By **GEORGE J. JANZ**, *Rensselaer Polytechnic Institute, Troy, New York*

June 1958, 211 pp., illus., $6.00

This new book stresses the use of thermodynamics as a guide to studies in the field of chemical reactions. The thermodynamic approach, based on a prediction of free energy changes and equilibria, is all too frequently limited because complete data are lacking. This volume provides not only an up-to-date survey of the estimation methods developed for computing thermodynamic properties but also a comprehensive compilation of tables of increments required for the application of each method in practice.

CONTENTS:

Part I. METHODS OF ESTIMATION (pp. 1–133)
The Free Energy Change in a Chemical Reaction. Thermodynamic Properties of Simple Polyatomic Systems by Statistical Thermodynamic Methods. Thermodynamic Properties of Long Chain Hydrocarbons. The Method of Structural Similarity. The Methods of Group Contributions. The Method of Group Equations. Heat of Formation and Heat Capacity. Applications of the Thermodynamic Method.

Part II. NUMERICAL DATA (pp. 135–200) 48 Tables

AUTHOR INDEX—SUBJECT INDEX (pp. 201–211).

Volume 5

Synthetic Polypeptides

PREPARATION, STRUCTURE, AND PROPERTIES

By C. H. Bamford, A. Elliott, and W. E. Hanby

1956, 445 pp., illus., $10.00

REVIEW: ". . . We owe a great deal to the authors for this most excellent, comprehensive and timely book, which has the property of making itself indispensable from the moment one sets eyes on it."

—*British Journal of Applied Physics*

Volume 1, 1952, 558 pp., illus., $12.00

Diffusion in Solids, Liquids, Gases

By W. Jost

Volume 2, 1954, 244 pp., illus., $7.00

Structure of Molecules and Internal Rotation

By S. Mizushima

Volume 3, 1955, 329 pp., illus., $8.50

Degradation of Vinyl Polymers

By H. H. G. Jellinek

Volume 4, 1955, 259 pp., illus., $7.00

Solubilization and Related Phenomena

By Mary E. L. McBain and E. Hutchinson

ACADEMIC PRESS INC., Publishers
111 Fifth Avenue, New York 3, New York

JOURNAL OF COLLOID SCIENCE **13**, 411–417 (1958)

CONDUCTANCE OF DIALKYL SODIUM SULFOSUCCINATE SURFACE-ACTIVE AGENTS

M. L. Miller and J. K. Dixon

American Cyanamid Company, Research Division, Stamford, Connecticut

Received June 4, 1958

Abstract

The conductance of solutions of very carefully purified di-*n*-octyl, di-*n*-hexyl, di-*n*-amyl, di-*n*-butyl, and di(2-ethylhexyl) sodium sulfosuccinate was measured at 29.92°C. Plots of equivalent conductance against the square root of the concentration showed that only di-*n*-hexyl and di(2-ethylhexyl) had the sharp break in equivalent conductance that was considered characteristic of surface-active agents. The equivalent conductance of di-*n*-octyl sodium sulfosuccinate had a flat maximum at concentrations just above the critical micelle concentration. Plots of the equivalent conductance of di-*n*-amyl and di-*n*-butyl sodium sulfosuccinate were smooth curves.

Critical micelle concentrations were estimated from plots of specific conductance against concentration and, where possible, from plots of equivalent conductance against the square root of concentration. Except for di(2-ethylhexyl), values of the critical micelle concentrations obtained from conductance agreed nicely with critical micelle concentrations from surface tension. The reason for the difference between the values for the critical micelle concentration of di(2-ethylhexyl) sodium sulfosuccinate when measured by conductance and by surface tension has been considered.

Introduction

Williams, Woodberry, and Dixon (1) studied the surface tension of solutions of seven exceptionally pure dialkyl sodium sulfosuccinates and estimated critical micelle concentrations (CMC) from surface tension data. The conductance of five of these highly purified surface-active agents (di-*n*-octyl, di-*n*-hexyl, di-*n*-amyl, di-*n*-butyl, and di(2-ethylhexyl)) has now been measured on the same preparations that were used for surface tension studies and CMC's have been estimated from conductance data. With the exception of di(2-ethylhexyl) sodium sulfosuccinate, these compounds constitute a series of surface-active agents which have straight alkyl groups containing from four to eight carbon atoms and which have CMC's from 0.20 to 0.00068 mole per liter.

The conductance was measured at 29.92°C. over a range of concentrations, for each compound, which included the CMC determined by surface tension.

EXPERIMENTAL

Materials

The preparation and purification of the dialkyl sodium sulfosuccinates is described in reference (1). Ion-exchanged water with a conductance of 0.85×10^{-6} mho. cm.$^{-1}$ was collected from relatively fresh resin beds. Dilutions were never extended to a concentration where the water correction became greater than 10% of the total conductance.

Apparatus

The conductance bridge was a shielded fixed ratio-arm bridge similar to that described by Shedlovsky (2). It could be balanced to a precision of better than four significant figures. Measurements were made in an oil bath at 29.92 ± 0.01°C. The temperature was read on a thermometer calibrated at the National Bureau of Standards.

To cover the wide concentration range, four cells were used. Three were of Washburn type and one was a flask-type dilution cell similar to the cell used by Shedlovsky (3). Calibration at 29.92°C. was based on Bremner's data for very dilute KCl solutions (4).

Solutions

The purified salts, which were very hygroscopic, were freeze-dried and sealed in vials. Subsequent handling was in a dry box.

All solutions and dilutions were by weight. Except at high concentrations and when working with the flask-type dilution cell, each concentration was made up separately. In work with the flask-type dilution cell the conductance of the water was measured in the cell and a stock solution of salt was injected through a Parafilm closure into the cell by a weighed syringe. After a series of such additions a final dilution with water restored the concentration to its initial value and also restored the conductance to its initial value. This procedure served as a check against contamination by carbon dioxide.

The densities of di-*n*-butyl and di-*n*-amyl sodium sulfosuccinate solutions, which were needed to convert concentrations from a weight to a volume basis, were measured in water at 29.87°C. These densities, d(in g./ml. at 29.87°C.), were represented by the following equations.

Di-*n*-butyl to 12%:

$$d = 0.99570 + 0.10338\ C - 0.0307\ C^{3/2},\ \sigma = 0.00024.$$

Di-*n*-amyl to 7%:

$$d = 0.99570 + 0.09113\ C - 0.02120\ C^{3/2},\ \sigma = 0.0001.$$

Here σ is the average difference between calculated and observed densities, and C is the concentration in moles per liter. The densities of solutions of di-n-octyl, di-n-hexyl, and di(2-ethylhexyl) sodium sulfosuccinate were computed by the equation:

$$d = 0.9957 + 0.0830\ C,$$

where $C < 0.1$

All measurements were made at 1000 cycles. Supplementary measurements by Dr. W. C. Schneider showed that the conductance of a 4% solution of di-n-amyl sodium sulfosuccinate was independent of frequency from 500 to 500,000 cycles.

Results

The conductance measurements are summarized in Tables I and II. Figures 1 and 2 plot the equivalent conductance, Λ, against the square root of the concentration, $C^{1/2}$. These plots show that only di-n-hexyl and di-(2-ethylhexyl) have a sharp break in the plot of Λ vs. $C^{1/2}$ which can be used to estimate CMC's. The plot of Λ vs. $C^{1/2}$ for di-n-octyl sodium sulfosuccinate has a flat maximum just above the CMC. Similar maxima in the conductance of surface-active agents *which have CMC's at very low concentrations* have been observed by other workers. The reason for these maxima has been considered by McDowell and Kraus (5), who also reviewed the literature.

Plots of Λ vs. $C^{1/2}$ for di-n-amyl and di-n-butyl sodium sulfosuccinates *which have CMC's at relatively high concentrations* are smooth curves from which it is impossible to estimate CMC's. The conductance of diisobutyl sodium sulfosuccinate, a compound with a short, branched alkyl group,

TABLE I

Conductance of Dialkyl Sodium Sulfosuccinates at 29.92°C.

n-Butyl		*n*-Amyl		*n*-Hexyl	
C (moles/liter)	Specific conductance (*mho. cm.*$^{-1}$)	C (*moles/liter*)	Specific conductance (*mho. cm.*$^{-1}$)	C, (*moles/liter*)	Specific conductance (*mho. cm.*$^{-1}$)
0.3762	0.01913	0.2577	0.01463	0.04793	0.2831×10^{-2}
0.3144	0.01677	0.2008	0.01183	0.04029	0.2462
0.2525	0.01378	0.1231	0.007706	0.02951	0.1939
0.2088	0.01183	0.09261	0.006014	0.01874	0.1355
0.1733	0.01008	0.05567	0.003864	0.01291	0.09884
0.1299	0.007870	0.04164	0.002979	0.006180	0.04957
0.06769	0.004410	0.02819	0.002073	0.002929	0.02425
0.02786	0.001931	0.02049	0.001537	0.001284	0.01092
				0.0007610	0.006610

TABLE II

Conductance of Dialkyl Sodium Sulfosuccinates at 29.92°C.

(2-Ethylhexyl)		*n*-Octyl	
$C \times 10^2$ (*moles/liter*)	Specific conductance $\times 10^5$ (*mho. cm.*$^{-1}$)	$C \times 10^2$ (*moles/liter*)	Specific conductance $\times 10^5$ (*mho. cm.*$^{-1}$)
0.009214	0.7340	0.009811	0.6922
0.01813	1.422	0.01978	1.4355
0.02496	1.918	0.03525	2.5424
0.06964	5.331	0.03883	2.8247
0.08410	6.494	0.06472	4.7148
0.1555	11.821	0.08117	6.0056
0.1773	13.390	0.08883	6.5036
0.2779	21.255	0.09106	6.8149
0.3590	27.259	0.1338	10.355
0.5518	41.168	0.1424	10.855
0.7144	51.989	0.2128	15.856
1.1122	76.80	0.2774	20.040
1.4525	96.26		
2.2400	137.23		

was measured by Haffner, Piccione, and Rosenblum (6). The plot of Λ vs. $C^{1/2}$ for this sulfosuccinate was also a smooth curve.

The CMC's of di-*n*-hexyl and di(2-ethylhexyl) sodium sulfosuccinate have been estimated by passing straight lines ("least squared") through the values of Λ above and below the break in the curve and solving for the concentration at which the two lines intersected.

Because of the maximum in Λ the CMC of di-*n*-octyl sodium sulfosuccinate had to be obtained graphically from a large plot.

CMC's can also be estimated from plots of the specific conductance, κ, vs. C. There is evidence of a slight break in the plots of κ vs. C for di-*n*-butyl and di-*n*-amyl sodium sulfosuccinates, whereas there is no evidence of a break in the plots of Λ vs. $C^{1/2}$. The fact that plots of κ often show a break when plots of Λ do not was pointed out by Wright *et al.* (7). CMC's have been estimated from specific conductance for di-*n*-butyl, di-*n*-amyl, di-*n*-hexyl, and di(2-ethylhexyl)sodium sulfosuccinates. This was done by passing straight lines through the value of κ at high and at low concentrations.[1]

---

[1] Because of the very gradual change in slope of plots of κ vs. C for di-*n*-butyl and di-*n*-amyl sodium sulfosuccinate, it was sometimes difficult to tell whether a given point, at an intermediate concentration, should be included among the points at high concentrations or among the points at low concentrations. This question was decided by carrying out the computation twice, first with the point in question included among the points at high concentrations and second with the same point included among the points at low concentrations. The set of lines which best fitted the experimental data was considered to be based on the best allocation of the point in question. In general, the allocation of these intermediate points made little difference in the value of CMC.

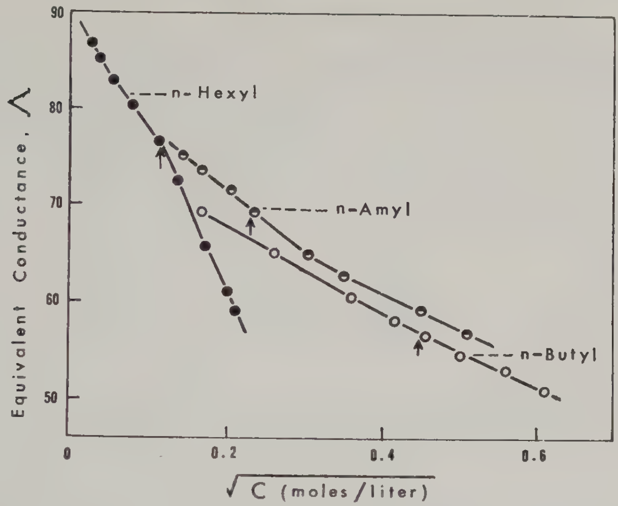

FIG. 1. Equivalent conductance of di-*n*-alkyl sodium sulfosuccinates. Arrows designate critical micelle concentrations measured by surface tension.

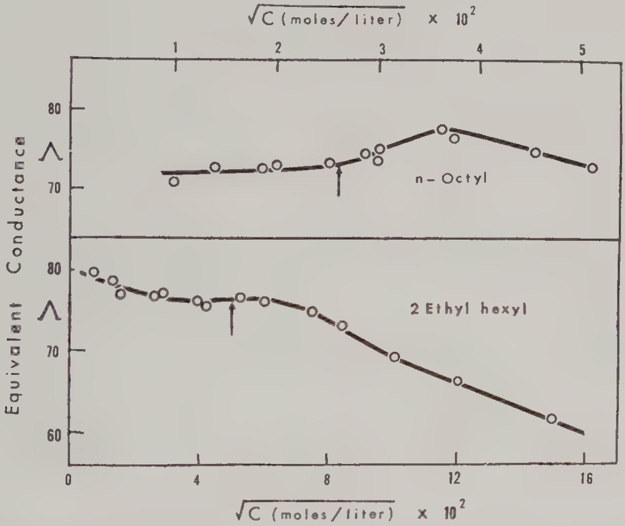

FIG. 2. Equivalent conductance of di-*n*-octyl and di(2-ethylhexyl) sodium sulfosuccinates. Arrows designate critical micelle concentrations measured by surface tension.

The CMC's of the five sodium alkyl sulfosuccinates studied here are listed in columns 3 and 4 of Table III. Column 2 gives, for comparison, the CMC's that were obtained from surface tension measurements by Williams *et al.* (1). Notice that, for the di-*n*-cotyl, di-*n*-hexyl, and di-*n*-butyl sodium sulfosuccinates there is excellent agreement between CMC's measured by conductance and by surface tension. In view of the indefi-

TABLE III

Critical Micelle Concentrations of Dialkyl Sodium Sulfosuccinates

Compound	Critical micelle concentration (*moles/liter*) from			
	Surface tension at 25°C.	Specific conductance at 29.92°C.	Equivalent conductance at 29.92°C.	Conductance, ref. (6), at 25°C.
n-Butyl	0.20	0.21	—	—
n-Amyl	0.053	0.073	—	—
n-Hexyl	0.0124	0.0128	0.0119	—
n-Octyl	0.00068	—	0.00064	<0.0009
2-Ethylhexyl	0.0025	0.0061	0.0056	0.0055

niteness of the micellar break with short-chain compounds, the agreement between the CMC's from the two techniques for di-*n*-amyl sodium sulfosuccinate (0.073 mole/l. from conductance and 0.053 mole/l. from surface tension) is as good as can be expected. The CMC for di(2-ethylhexyl) sodium sulfosuccinate (0.0056 to 0.0061 mole/l.) which we have obtained by conductance measurements at 29.92°C. agrees nicely with the CMC (0.0055 mole/l.) which Haffner and co-workers (6) found from their conductance measurements at 25°C. On the other hand, this value is very different from the CMC (0.0025 mole/l.) found by Williams *et al.* (1) from surface tension measurements at 25°C. This difference is far outside the limits of error of either technique. The following considerations make it seem likely that the CMC determined by surface tension is the correct one.

It is possible that those factors (fully discussed by McDowell and Kraus (5)) which caused the maximum in the plot of Λ vs. $C^{1/2}$ for di-*n*-octyl sodium sulfosuccinate also increased the conductance of di(2-ethylhexyl) sodium sulfosuccinate *immediately above* the CMC. If this happened, the break in the conductance curve would occur at a concentration somewhat higher than the CMC. The shape of the plot of Λ vs. $C^{1/2}$ (Fig. 2) for di(2-ethylhexyl) sodium sulfosuccinate in the immediate neighborhood of the break is consistent with this interpretation.

CONCLUSIONS

The break in the plot of the equivalent conductance of sodium alkyl sulfosuccinates at the critical micelle concentration decreases in sharpness as the length of the alkyl chain decreases and as the critical micelle concentration moves to higher and higher concentrations. This is true for sulfosuccinates with both straight and branched alkyl groups. A similar but less pronounced decrease in the sharpness of the break in the surface tension at the critical micelle concentration has been reported previously for sulfosuccinates with short alkyl groups (1). The decreased sharpness in the micellar break in plots of the equivalent conductance of *short-chain* sodium alkyl sulfosuccinates, as contrasted to *long-chain* sodium alkyl sulfosuccinates, results from the fact that with short-chain compounds the formation of micelles takes place over a relatively wide range of concentrations rather than at a single critical concentration (1).

Except for special cases critical micelle concentrations from conductance data are in good agreement with critical micelle concentrations from surface tension measurements.

References

1. Williams, E. F., Woodberry, N. T., and Dixon, J. K., *J. Colloid Sci.* **12,** 452 (1957).
2. Shedlovsky, T., *J. Am. Chem. Soc.* **52,** 1793 (1930).
3. MacInnes, D. A., "The Principles of Electrochemistry" Reinhold, 1939, New York, p. 43.
4. Bremner, R. W., *J. Am. Chem. Soc.* **66,** 444 (1944).
5. McDowell, M. J., and Kraus, C. A., *J. Am. Chem. Soc.* **73,** 2173 (1951).
6. Haffner, F. D., Piccione, G. A., and Rosenblum, C., *J. Phys. Chem.* **46,** 662 (1942).
7. Wright, K. W., Abbott, A. D., Sivertz, V., and Tartar, H. V., *J. Am. Chem. Soc.* **61,** 549 (1939).

JOURNAL OF COLLOID SCIENCE **13,** 418–428 (1958)

CORRELATION BETWEEN DILATOMETRIC AND VISCOELASTIC DATA ON A SERIES OF POLY-*n*-ALKYL METHACRYLATES[1]

Hiroshi Fujita and Akira Kishimoto

Physical Chemistry Laboratory, Department of Fisheries, University of Kyoto, Maizuru, Japan

Received March 6, 1958

INTRODUCTION

In a previous paper (1), we have shown that the lowering of the glass transition temperature of an amorphous polymer due to the addition of a low molecular weight diluent can be correlated quantitatively with the concentration dependence of its viscoelastic behavior through the variation of the average local free volume around the polymer chain as functions of temperature and diluent concentration. The average local free volume in the polymer may also vary with the size of a side group attached to the backbone polymer chain. Therefore, if we compare polymers prepared from a series of homologous monomers, such as poly-*n*-alkyl methacrylates, we may find the local free volume to increase systematically as a function of the increased number of carbon atoms contained in their side chains. This situation may resemble that which we obtain when an increasing amount of a diluent is added to a given polymer. Macroscopically, the increase in side chain size manifests itself as an increase in specific volume of the polymer. Thus, it is anticipated that there will be a close correlation between the local free volume and the specific volume for consecutive members of a series of polymers with homologous side groups. In the present paper, we show that dilatometric and viscoelastic data of such a polymer series can be correlated in a simple form on appropriate assumptions for this relation as well as for the viscous motion of a monomeric unit in the polymer matrix. Rogers and Mandelkern (2) have recently presented a treatment of the glass transition temperature for a homopolymer series (here by homopolymer series is meant a series of polymers prepared from homologous monomers) on assumptions similar to those given below. However, our treatment differs from theirs in that we consider glass transition to occur at a state of iso-volume fraction of local free space.

---

[1] Abbreviations: PMMA = polymethyl methacrylate; PEMA = polyethyl methacrylate; PPMA = poly-*n*-propyl methacrylate; PBMA = poly-*n*-butyl methacrylate; PHMA = poly-*n*-hexyl methacrylate; POMA = poly-*n*-octyl methacrylate.

THEORY

Let us consider a homopolymer series in which the backbone polymer structure of each member is the same and its side chain varies systematically according to a homologous series. Let us call its member with the shortest side chain the reference polymer and give it a number 1. The successive polymers in the series are then given numbers 2, 3, $\cdots$, n in the order of their side chain lengths. We denote by $f(n, T)$ the average volume fraction of local free spaces in polymer n at temperature T and by $v(n, T)$ its specific volume at the same temperature. Since increase of the side chain length may change both f and v, there must be a definite relation between the two quantities for a given series of homopolymers. We assume that this relation can be represented in the form:

$$f(n, T) - f(1, T) = F[v(n, T) - v(1, T)], \qquad [1]$$

where F denotes a certain function of its argument and obviously $F(0) = 0$. The form of F should be characteristic of a given series at a given temperature but may vary with T. In their treatment of a similar problem, Rogers and Mandelkern (2) have assumed a linear relation between v and the free volume itself. It is not clear to us which of the free volume itself and its volume fraction is more closely responsible for the actual behavior of polymeric systems. In connection with this, we should like to note that the WLF equation (3), which has proved so useful to describe the temperature dependence of viscoelastic behavior of a wide variety of polymers in bulk and in concentrated solution, is essentially based on the variation of the average free volume fraction with temperature.

We next assume, in agreement with the derivation of Williams, Landel, and Ferry (WLF) (3), that the fractional free volume of polymer n increases linearly with temperature according to the relation:

$$f(n, T) = f(n, T_g{}^n) + \alpha_n(T - T_g{}^n), \qquad [2]$$

where $T_g{}^n$ is the glass transition temperature of polymer n and α_n is the difference between its thermal expansion coefficients above and below $T_g{}^n$. To this approximation, α_n should be independent of T but may vary from member to member in the series. This latter fact is indicated by subscript n.

By combining Eqs. [1] and [2], putting $T = T_g{}^1$, and assuming that glass formation occurs at a state of *iso-free volume fraction* for all polymers, we obtain

$$T_g{}^n = T_g{}^1 - (1/\alpha_n)F[v(n, T_g{}^1) - v(1, T_g{}^1)]. \qquad [3]$$

This equation may be compared to Eq. [6] in Rogers and Mandelkern's paper (2). Their equation differs from ours in that it assumes a linear function for F and in that it does not specify T contained in $v(n, T)$. This latter condition is due to the fact that they have neglected the variation of $\Delta\alpha_n$ with n, where $\Delta\alpha_n$ is the difference between the linear volume-temperature coefficients of member n above and below T_g^n.

According to the recent theory of Rouse (4), Bueche (5), or Nakada (6), that part of the relaxation spectrum of a linear polymer which is controlled by fairly long-range (but not long-range enough to introduce complications from entanglements and loose ends) cooperative motions of the backbone polymer chain is linear on a log-log plot with a slope of $-\frac{1}{2}$, and its position on the logarithmic time axis is wholly determined by a molecular parameter $a^2\zeta/T$, where a^2 is the mean square length of a monomer unit, ζ is the monomeric friction coefficient, and T is the absolute temperature of the system. It follows then that the predicted relaxation spectrum should be independent of molecular weight for a given polymer species and that changes in either external or internal conditions which affect the value of $a^2\zeta/T$ should simply shift the logarithmic time scale of the spectrum, without altering its shape. Many recent experiments have demonstrated that such behavior, in fact, can be observed for many amorphous or primarily amorphous polymer systems in the transition region from glasslike to rubberlike consistency, although the observed shapes of the spectra are not exactly in conformity with the predicted one.

Introduction of a side chain into a given backbone polymer structure may cause the magnitude of $a^2\zeta$ to change, so that a shift of the relaxation spectrum along the logarithmic time axis may appear. Actually, this shift may be accompanied with a change in shape of the spectrum. However, if comparison of the original and the shifted spectra is made in the part near the bottom end of the transition region, only the shift effect may actually be observed, because in this part the cooperative motions of the polymer chains are sufficiently long-range to conform to the conditions assumed in the theory. The same may hold between relaxation spectra of any pair of members in a given homopolymer series, provided they are compared in the region noted above. It should still be the case even though the molecular weights of the members compared are different, since, as the theory predicts and also as many recent experiments support (7–10), the relaxation spectrum in this region is not affected by the molecular weight of the sample, provided it is sufficiently high.

From these considerations, it is expected that the variation of the monomeric friction coefficient ζ with increasing size of the side group in a homopolymer series can be assessed from the relative positions on the logarithmic time axis of the relaxation spectra of its members in the part near the bottom end of the transition region. It should be mentioned that, to a first approximation, the factor a may be regarded as the same throughout the series. For this comparison to be made, of course, all relaxation spectra concerned have to be reduced to the same temperature, since not only is ζ extremely temperature-dependent but also a^2 changes slightly with temperature. For this temperature reduction, the WLF equation (3) may be used most effectively, provided all necessary informations for its application are available.

Let us plot temperature-reduced relaxation spectra for members of a given homopolymer series on a log-log graph with relaxation time distribution intensity H (dynes/cm.^{2}) as the ordinate and relaxation time τ (sec.) as the abscissa. Then, let us examine whether the plotted curves are parallel with each other in the part of the transition region in question. When this is actually the case, we measure the horizontal distance between the spectrum of the reference polymer 1 and that of another polymer n at a value of H, say $\log H = 6.5$, and denote it by $\log a(n, T)$. Here T is the temperature taken as the reference for the temperature reduction of the spectra. Then it follows from the theory of Rouse, Bueche, or Nakada that

$$\log a(n, T) = \log \zeta(n, T) - \log \zeta(1, T), \qquad [4]$$

where $\zeta(n, T)$ denotes the monomeric friction coefficient of member n at temperature T.

The force required to translate a monomeric unit through the polymer matrix may depend primarily upon both the chain flexibility and the looseness of the "local liquid structure." The latter factor may be closely related to the pattern and strength of the intermolecular field of forces. For a series of homopolymers at constant temperature both the chain flexibilities and the patterns of the intermolecular force field of the respective members are not significantly different owing to the similarity in the chemical nature of their repeating units, but the strength of their force field (cohesive energy density) decreases with increasing size of the side group (2). The less cohesive energy density allows a chain segment to jump and rotate more freely, provided the other controlling factors are the same. Thus it is expected that for the members of a homopolymer series at constant temperature the friction coefficient changes systematically with the average free volume that each repeating unit occupies. The following is an attempt to put this relation into a quantitative form.

We assume that an equation similar in form to the Doolittle viscosity equation (11) as modified by Williams, Landel, and Ferry (3) holds between ζ and f, i.e.,

$$\ln \zeta(n, T) = A(n) + B(n)/f(n, T). \qquad [5]$$

Here $A(n)$ and $B(n)$ are constants characteristic of the monomeric unit of polymer n. Probably $B(n)$ is of the same nature as the parameter B appearing in the derivation of the WLF equation and, following Williams, Landel, and Ferry, may simply be set equal to unity for all members of the series. On the other hand, $A(n)$ should depend on the molecular volume of the monomeric unit as does the parameter A in the modified Doolittle equation on the weight-average molecular weight of the sample, often in accordance with the familiar 3.4 power law (12). By analogy with the macroscopic case, the dependence of $A(n)$ on the molecular weight of a monomer unit will be of the form:

$$A(n) = K + \epsilon \log m(n); \tag{6}$$

where K and ϵ are constant for a given series and $m(n)$ is the molecular weight of a monomer unit of its member n. Assuming that the viscous motion of a monomer through the polymer matrix follows Stokes' law, the factor ϵ should be of the order less than unity. If this is the case, the variation of $A(n)$ with increasing size of the side group may be quite limited, at least for the first few members of a homopolymer series where the range of $m(n)$ is usually within a factor of 5 or so. Furthermore, f is generally so small (of the order of 10^{-2}) that even its slight variation produces a pronounced change in the term B/f in Eq. [5]. Thus it may be considered that, to a first approximation, the variation of ζ with n originates wholly from the change in fractional free volume with increasing size of the side chain. With these considerations in mind, substitution of Eq. [5] into Eq. [4] gives

$$\log a(n, T) = (1/2.303)[1/f(n, T) - 1/f(1, T)]. \tag{7}$$

Substitution for $f(n, T)$ from Eq. [1] and arrangement leads to

$$-\frac{2.303[f(1, T)]^2 \log a(n, T)}{1 + 2.303[f(1, T)] \log a(n, T)} = F[v(n, T) - v(1, T)]. \tag{8}$$

For $T = T_g^1$ the right-hand side of this equation can be combined with Eq. [3] to eliminate the unknown function F, giving

$$-\frac{2.303[f(1, T_g^1)]^2 \log a(n, T_g^1)}{1 + 2.303[f(1, T_g^1)] \log a(n, T_g^1)} = \alpha_n(T_g^1 - T_g^n). \tag{9}$$

This is rewritten in the form:

$$-\frac{1}{\log a(n, T_g^1)} = 2.303f(1, T_g^1) + \frac{2.303[f(1, T_g^1)]^2}{\alpha_n(T_g^1 - T_g^n)}. \tag{10}$$

The values of $\log a(n, T_g^1)$ may be obtained from experimental relaxation spectra for successive members of a given homopolymer series, first by reducing them to a temperature corresponding to the glass transition temperature T_g^1 of the reference polymer and then by applying the procedure described in the foregoing lines. Both α_n and $T_g^1 - T_g^n$ may be evaluated from a set of separate dilatometric data for the same homopolymer series. Equation [10] indicates that when these viscoelastic and dilatometric data are plotted on a graph with $-1/\log a(n, T_g^1)$ as the ordinate and $1/[\alpha_n(T_g^1 - T_g^n)]$ as the abscissa, a straight line is obtained with a slope equal to 2.303 $[f(1, T_g^1)]^2$ and an intercept on the ordinate axis equal to 2.303 $[f(1, T_g^1)]$. The values of $f(1, T_g^1)$ calculated from both the slope and the intercept must agree with each other. Thus, for Eq. [10] to be valid not only the linearity of the plot but also the correlation of its slope and intercept must be satisfied. It is also important to observe that Eq. [10] holds independent of the functional form of F which correlates fractional free volume and specific volume at a given temperature.

APPLICATION

Recently, Ferry and his associates (13–15) have published extensive data on dynamic properties of several poly-n-alkyl methacrylates, i.e., polyethyl methacrylate (PEMA), poly-n-butyl methacrylate (PBMA), and poly-n-hexyl methacrylate (PHMA). The relaxation spectra they gave cover the complete range of the transition from glasslike to rubberlike consistency for all the polymers studied and have been reduced to a temperature of 100°C. Fortunately, this is the temperature corresponding to the glass transition of polymethyl methacrylate (PMMA), the first member of this homopolymer series, as shown below. Therefore, their relaxation spectrum data are immediately utilized for the evaluation of the quantity $\log a(n, T_g^1)$, provided the corresponding data are available for PMMA. Such data are obtained from the work of McLoughlin and Tobolsky (9) which gives the relaxation spectrum at 40°C. for a sample of PMMA and the shift factors necessary for temperature reduction. In Fig. 1 are plotted on a log-log graph the relaxation spectra of these four polyalkyl methacrylates at 100°C.; for convenience only the data in the transition region are indicated. It is seen from the figure that the four spectra are surprisingly similar in shape over a wide range of the transition region, in good agreement with the prediction mentioned above. Of course, some specific differences are noted among the curves shown, but these do not violate significantly the discussion which follows. Values of $\log a(n, T_g^1)$ have been determined from this graph at a value of $\log H = 6.5$ (see the horizontal dashed line indicated in the figure), and are listed in the second column of Table I.

The corresponding dilatometric data are obtained from the work of Rogers and Mandelkern (2), who determined very accurately specific volume-temperature curves for the first few members of the poly-n-alkyl methacrylate series. The values of T_g^n, $v(n, T_g^n)$, and $\Delta\alpha_n$ taken from Table II of their paper are listed in the second, third, and fourth columns

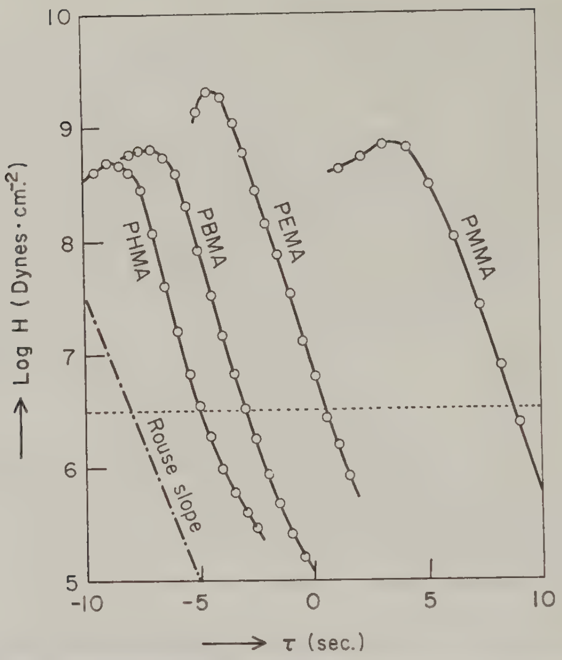

FIG. 1. Relaxation spectra in shear of poly-*n*-alkyl methacrylates reduced to 100°C. (glass transition temperature of PMMA). Reference (1) on PMMA concerns data in tension, which are converted to those in shear assuming Poisson's ratio to be 0.5 and plotted in this graph.

TABLE I

Shift Factors and Glass Transition Temperature Lowerings of Poly-n-Alkyl Methacrylates Relative to Polymethyl Methacrylate

Polymer	$-\log a(n, T_g{}^1)$	$T_g{}^1 - T_g{}^n$ (°C.)
PMMA	0	0
PEMA	8.0	35
PBMA	11.6	80
PHMA	13.6	105

in Table II of this paper. Here $\Delta\alpha_n$ is the difference between the linear temperature coefficients of specific volume above and below $T_g{}^n$. Rogers and Mandelkern record a value of 105°C. for $T_g{}^1$, the glass transition temperature of PMMA. However, inspection of their specific volume vs. temperature curve for this polymer shows that the knick of the curve occurred at $T = 100$°C., so that $T_g{}^1$ must be identified as 100°C., as indicated in Table II. The fifth and sixth columns of Table II record the values of α_n and $v(n, T_g{}^1)$, respectively. Here α_n has been calculated from the measured values of $v(n, T_g{}^n)$ and $\Delta\alpha_n$ using the definition

$$\alpha_n = \Delta\alpha_n / v(n, T_g{}^n),$$

TABLE II

Some Dilatometric Characteristics of Poly-n-Alkyl Methacrylates (2)

Polymer	T_g^n (°C.)	$v(n, T_g^n)$ (cm.³g.⁻¹	$\Delta\alpha_n \times 10^4$ (cm.³g.⁻¹ deg.⁻¹)	$\alpha_n \times 10^4$ (deg.⁻¹)	$v(n, T_g^1)$ (cm.³g.⁻¹)[a]
PMMA	100	0.868	2.45	2.82	0.868
PEMA	65	0.900	2.65	2.94	0.917
PPMA	35	0.931_5	2.65	2.85	0.967
PBMA	20	0.947_5	2.30	2.43	0.991
PHMA	−5	0.972	2.00–2.80 (2.40)	2.52[b]	1.040
POMA	−20	1.002	1.90–2.80 (2.35)	2.35[b]	1.076

[a] Determined graphically from Fig. 1 of reference (2).

[b] Calculated using mean values of $\Delta\alpha_n$ indicated in the parentheses.

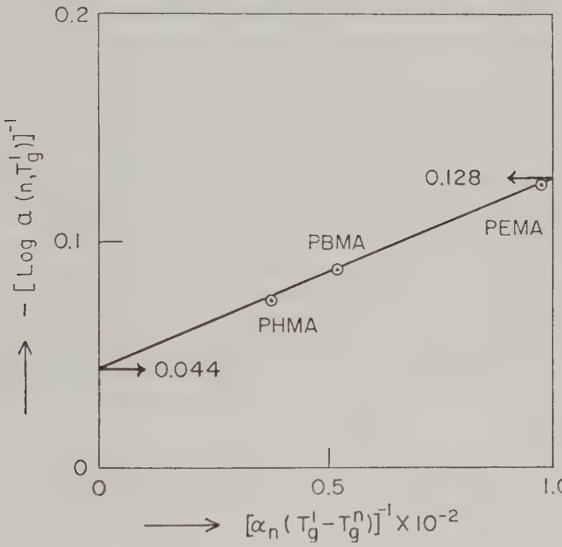

FIG. 2. Test of Eq. [10] on poly-*n*-alkyl methacrylates.

and $v(n, T_g^1)$ has been read off Fig. 1 of Rogers and Mandelkern. For reference, the values of $T_g^1 - T_g^n$ for PMMA, PEMA, PBMA, and PHMA are given in the third column of Table I.

The numerical values given in Table I and II are combined and plotted in the form as suggested by Eq. [10]. Figure 2 shows the results obtained. It is seen that the plotted points follow satisfactorily a linear relation, in conformity to the prediction. The slope and the intercept of the straight line drawn are 8.4×10^{-4} and 4.4×10^{-2}, respectively, which both, in turn, lead to an entirely identical value of $f(1, T_g^1)$, 0.019_1, in perfect agreement with another requirement of Eq. [10]. These results, especially the amazing agreement of the two calculated values of $f(1, T_g^1)$, might be more or less fortuitous, considering the fact that the data used to test

Eq. [10] have been taken from three independent sources. Nevertheless, it would not be too drastic to suppose that there must be a definite correlation between the dilatometric and viscoelastic properties of successive members of a homopolymer series. It is of great interest to check the validity of Eq. [10] on other series of homopolymers, but at present no such series for which a complete set of data to test Eq. [10] is available is yet found in the literature, so far as we are aware. It is hoped that further tests of the present theory will soon be possible.

From Eq. [3] it is expected that plots of $\alpha_n(T_g^1 - T_g^n)$ against

$$v(n, T_g^1) - v(1, T_g^1)$$

should fall on a single curve characteristic of a given homopolymer series at temperature T_g^1. That this is the case can be seen in Fig. 3, which has been prepared by substituting the data listed in Tables I and II. Evidently, this curve gives graphically the functional form of F at a temperature of T_g^1 and shows a definite curvature. It is readily confirmed that this curvature is primarily associated with the variation of α_n with increasing size of the alkyl side chain. In fact, if α_n is replaced by an average value throughout the members herein concerned, an approximately linear relation is obtained between $T_g^1 - T_g^n$ and $v(n, T_g^n) - v(1, T_g^1)$ over the range, in agreement with Rogers and Mandelkern (2). It will be a challenging problem to work out the derivation of the functional form of F in terms of molecular models.

The value obtained above for $f(1, T_g^1)$ is consistent with, but much smaller than, 0.025, which is now generally accepted as the average frac-

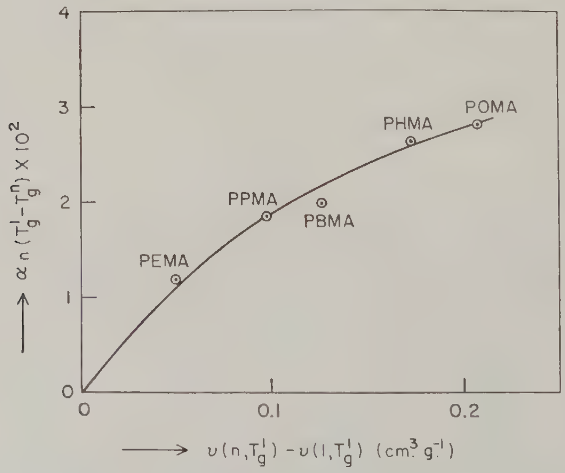

FIG. 3. Functional form of F for polyalkyl methacrylates at T_g^1 (glass transition temperature of PMMA).

tional free volume for many polymers (amorphous or primarily amorphous) at their glass transition temperatures. However, it should be noted that this value depends on the choice of $B(n)$ in Eq. [5], which, in the present discussion, has simply been set equal to unity, in agreement with Williams, Landel, and Ferry (3). It is apparently doubtful whether the simplification $B(n) = 1$ is valid for the equation of microscopic viscosity given by Eq. [5]. In connection with our low $f(1, T_g^1)$ value, it is of interest that Ferry and Landel (16) have deduced a value of 0.02 for this quantity from application of the WLF equation to dynamic mechanical data of a sample of poly-n-butyl methacrylate. In the present discussion, we are satisfied only with a check of the internal consistency of Eq. [10], leaving the disagreement of our $f(1, T_g^1)$ value from the "universal" one for future research. It is quite apparent that the theory presented above is yet so premature that no guarantee is given for the absolute value of $f(1, T_g^1)$ obtained.

Note added in Proof

After the completion of this work, a paper dealing with a similar subject has appeared [Dannhauser, W., Child, Jr., W. C., and Ferry, J. D., *J. Colloid Sci.* **13,** 103 (1958)]. The authors wish to thank Professor Ferry for calling their attention to it.

Acknowledgment

This work is part of a cooperative research program on the physical properties of high polymeric systems, supported financially by the Ministry of Education of the Government of Japan. We are indebted to Professor S. Oka of Gakusyuin University, Tokyo, who allowed us to participate in this research program.

Summary

On the basis of the assumptions (*1*) that for a series of polymers in which the backbone polymer structure of each member is the same and its side chain varies systematically according to a homologous series, the fractional free volume of its member n relative to that of member 1 (polymer with the shortest side chain in the series) is given by a function of the difference between their specific volumes; (*2*) that the fractional free volume of a given member increases linearly with temperature; and (*3*) that glass transition occurs at a state of iso-fractional free volume, a relation is derived which gives the glass transition temperature of any member of the series relative to that of its first member as a function of the change in specific volume between the two members at a temperature corresponding to the glass transition of the first member. It is shown that for such a series of polymers relaxation spectra of the respective members reduced to the same temperature are compared in the part near the bottom end of the transition region to obtain information about the relative magnitudes of the friction coefficients of their monomer units. A relation is assumed

for the monomeric friction coefficient as a function of the average fractional free volume, by analogy with the Doolittle equation as modified by Williams, Landel, and Ferry for the description of the temperature dependence of the steady-flow viscosity of polymers. Combination of these relations leads finally to the prediction that there should be a definite relation between dilatometric and viscoelastic data for polymers with the same backbone chain structure but with the side groups varying in accordance with a homologous series. Data on poly-n-alkyl methacrylates are taken from recent publications of Rogers and Mandelkern, Ferry and associates, and McLoughlin and Tobolsky and used to test the predicted relation, with a quite satisfactory result. A value of 0.019 is obtained for the average fractional free volume of each member of this series at its glass transition temperature. This value is consistent with but much smaller than that (0.025) generally accepted as the "universal" value for this quantity.

REFERENCES

1. FUJITA, H., AND KISHIMOTO, A., *J. Polymer Sci.*, in press.
2. ROGERS, S. S., AND MANDELKERN, L., *J. Phys. Chem.* **61**, 985 (1957).
3. WILLIAMS, M. L., LANDEL, R. F., AND FERRY, J. D., *J. Am. Chem. Soc.* **77**, 3701 (1955).
4. ROUSE, P. E., JR., *J. Chem. Phys.* **21**, 1272 (1953).
5. BUECHE, F., *J. Chem. Phys.* **22**, 603 (1954).
6. NAKADA, O., *J. Phys. Soc. Japan* **10**, 804 (1955); *ibid.* **11**, 1218 (1957)
7. BROWN, G. M., AND TOBOLSKY, A. V., *J. Polymer Sci.* **7**, 221 (1951).
8. ANDREWS, R. D., AND TOBOLSKY, A. V., *J. Polymer Sci.* **7**, 221 (1951).
9. MCLOUGHLIN, J. R., AND TOBOLSKY, A. V., *J. Colloid Sci.* **7**, 355 (1952).
10. NINOMIYA, K., AND FUJITA, H., *J. Colloid Sci.* **12**, 204 (1957).
11. DOOLITTLE, A. K., *J. Appl. Phys.* **22**, 1471 (1951); *ibid.* **23**, 236 (1952).
12. FOX, T. G, AND LOSHAEK, S., *J. Appl. Phys.* **26**, 1080 (1955).
13. FERRY, J. D., CHILD, W. C., ZAND, R., STERN, D. M., WILLIAMS, M. L., AND LANDEL, R. F., *J. Colloid Sci.* **12**, 53 (1957).
14. CHILD, W. C., JR., AND FERRY, J. D., *J. Colloid Sci.* **12**, 327 (1957).
15. CHILD, W. C., JR., AND FERRY, J. D., *J. Colloid Sci.* **12**, 389 (1957).
16. FERRY, J. D., AND LANDEL, R. F., *Kolloid-Z.* **148**, 1 (1956).

JOURNAL OF COLLOID SCIENCE **13**, 429–440 (1958)

A MODIFIED METHOD FOR MEASURING SURFACE VISCOSITY

R. Bulas and C. A. Kumins

The Research Laboratories, Interchemical Corporation, New York, New York

Received March 10, 1958

Abstract

The oscillating disk method for measuring the surface viscosity has been used without recourse to a reference liquid.

It has been found that for a pure liquid the logarithmic decrement obtained with the disk positioned in the liquid is twice as large as that obtained with the disk oscillating at the surface of the liquid, providing the distance from the disk to the surface of the liquid and to the bottom of the container is greater than a critical distance h_c.

A method of determining the critical distance is described and an equation describing the relationship between h_c and the bulk viscosity of the solution is presented.

The results obtained in the determination of surface viscosity using this method are shown and are compared with those obtained with the conventional technique using an external standard.

Introduction

The measurements of the surface viscosity of either an insoluble monolayer on water or of a detergent solution are based on the following methods: (*1*) the flow of the film through a narrow channel (1–3); (*2*) the damping of the oscillation (3–6); or (*3*) the retardation of a rotating disk or ring (3, 4, 7–10). Methods (*2*) and (*3*) require two separate measurements, i.e., the damping or the torque must be determined first on the surface of a pure liquid and second, either on the surface of the same liquid covered by the film or on the surface of a solution of detergent in the liquid. The surface viscosity is then calculated from the difference in the respective values by means of an appropriate equation. This procedure is used in order to account for the viscous drag arising from the underlying liquid, usually water. However, it is impossible to use such a technique with complex systems for which a reference liquid is not obtainable. Just such a complex situation occurs in pigmented media, and the methods described above cannot be used to investigate the possibility of surface structure in such systems. It was therefore desirable to develop a means for measuring surface viscosity without recourse to a reference liquid.

This paper describes a method based on measuring the damping of an oscillating disk within the bulk of the material and also at the air-liquid interface. It is shown that where no surface viscosity exists the damping at the air-liquid interface is one half of that obtained within the bulk. Conversely the existence of surface viscosity is indicated when the damping at the air-liquid interface is greater than one half of that obtained within the bulk. These conditions hold only when the distance from the disk to the surface of the liquid and to the bottom of the container is greater than a critical distance, h_c.

THEORY OF MEASUREMENTS

The torsional oscillations of a disk suspended from a thin wire and immersed in a liquid are described by the differential equation [1].

$$I\ddot{\theta} + K\dot{\theta} + F\theta = 0, \qquad [1]$$

where θ is the angular displacement of the disk, I is the effective moment of inertia, F is the restoring force per unit angular displacement, and K is the opposing couple per unit angular velocity arising from the frictional resistance of the liquid. The damping of the oscillation results from the work performed against the viscous resistance of the liquid. It is usually described by the logarithmic decrement λ, defined as the natural logarithm of the ratio of the successive amplitudes.

The decrement λ is related to the surface viscosity η_s by the equation (5)

$$\eta_s = \frac{2.303\Delta\lambda I}{2\pi T}\left(\frac{1}{r_1^2} - \frac{1}{r_2^2}\right). \qquad [2]$$

In this equation I is the effective moment of inertia of the disk, T is the period of oscillation, r_1 and r_2 are the radii of the disk and the container, respectively, and $\Delta\lambda$ is the difference between the logarithmic decrement obtained with the disk oscillating at the surface of the pure liquid and that covered by the film. In other words, the correction is applied for the damping caused by the viscous resistance of the underlying liquid.

From theoretical consideration of the motion of the liquid around an oscillating disk it was believed that such a correction could be made by measuring the logarithmic decrement with the disk submerged in the solution the surface viscosity of which is to be determined, without measuring the pure liquid.

According to Lamb (11) and subsequently Rouse and Sittel (12), the transverse velocity v of the liquid at a distance y from a plane executing steady oscillations in an infinite volume of liquid is given by equation

$$v = v_0 e^{-\gamma y} e^{i\omega t}, \qquad [3]$$

where V_0 is the maximum velocity of the particles of liquid, i is $\sqrt{-1}$, ω

is the angular frequency, t is time, and γ is the propagation constant equal to $(i\omega\rho/\eta)^{1/2}$. Here ρ and η are the density and viscosity of the liquid, respectively. Since the motion of the liquid is attenuated very rapidly as the distance from the source of excitation increases, Eq. [3] can be applied to a finite volume of liquid as well, providing the distance from the oscillating plane to the boundaries of the liquid is larger than the distance to which any significant vibrations of the liquid penetrate. Under such conditions the shearing wave generated in the liquid is not affected by the boundary surfaces of the liquid, and the motion of the layers of liquid on both sides of the oscillating plane is symmetrically distributed. In the case of an oscillating disk the velocity transferred to the particles of liquid facing both planes of the disk may be represented by two identical solids of revolution with a common base formed by the plane of the disk. The sides of these solids are curved to fit the exponential form of Eq. [3], and their altitudes represent the distance from the source of excitation.

Similarly, the energy dissipated, owing to the internal resistance of the liquid, can be assumed to be equal on both sides of the disk.

If the disk oscillated at the surface of a pure liquid, only half the energy need be dissipated and the damping of the oscillation (resulting from the work performed against the frictional resistance of the liquid) should be half as large as that case in which the disk oscillates in the bulk of such a liquid.

If the surface layer of the liquid is physically different from the rest of the liquid, as may be the case with a detergent solution, then the damping at the surface should be greater than one half of that obtained in the bulk of the liquid. This difference then should represent the contribution of the surface layer alone.

Thus, by determining the logarithmic decrement in the bulk of a solution either containing surfactant or covered by a film, with the disk positioned at a predetermined distance from the boundary surfaces of the liquid, and by subtracting one half of its value from that obtained at the surface, it should be possible to arrive at a value for $\Delta\lambda$ from which the surface viscosity can be calculated according to Eq. [2].

In the preceding analysis it has been assumed that the viscous drag due to the edge of the disk and that due to the supporting shaft are negligible. Further it has been assumed that the viscous drag due to the air acting on the upper surface of the disk positioned at the surface of the liquid is of no significance and therefore can be neglected.

Description of the Viscometer

The torsion pendulum used in this work is essentially the same as that described by Wilson and Ries (4). The measuring element consisted of a brass disk, 5.08 cm. in diameter and 0.1 cm. thick, connected to a support which could be loaded with lead disks of predetermined moment of inertia.

The range and sensitivity of the pendulum were altered by using different wires and applying different loads. The effective moments of inertia used varied from 5654 g.-cm.^{2} to 15266 g.-cm.^{2}, depending upon the surface and the bulk viscosity of the liquid. The torsion wires used in various determinations were of the MacMichael type; steel piano wires were also used. In the early stages of our work the oscillations were induced by turning the head assembly, to which the upper end of the torsion wire was attached; in the later stages an electromagnetic device was used. It consisted of two electromagnets placed 180° apart on a ring which could be rotated around the support. A soft iron bar was placed across the support which held the lead disks. The strength of the magnetic field between the poles of the electromagnets could be varied by means of a rheostat and therefore the amplitude of the initial oscillation could be controlled. The schematic diagram of the viscometer is shown in Fig. 1.

The liquid to be measured was contained in a large Petri dish, 14.8 cm. in diameter, which rested upon a small jack that could be raised and lowered to any desired height. The large diameter of the dish was chosen in order to reduce the effect of the walls of the container.

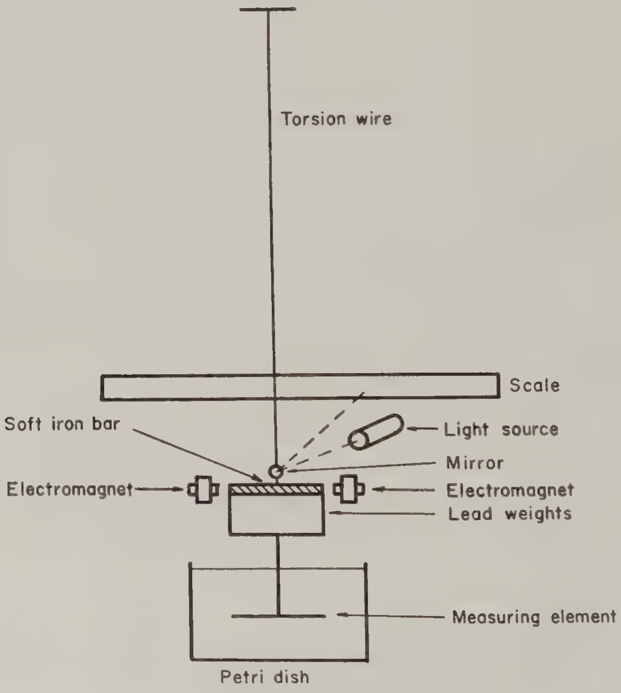

FIG. 1. Oscillating disk viscometer.

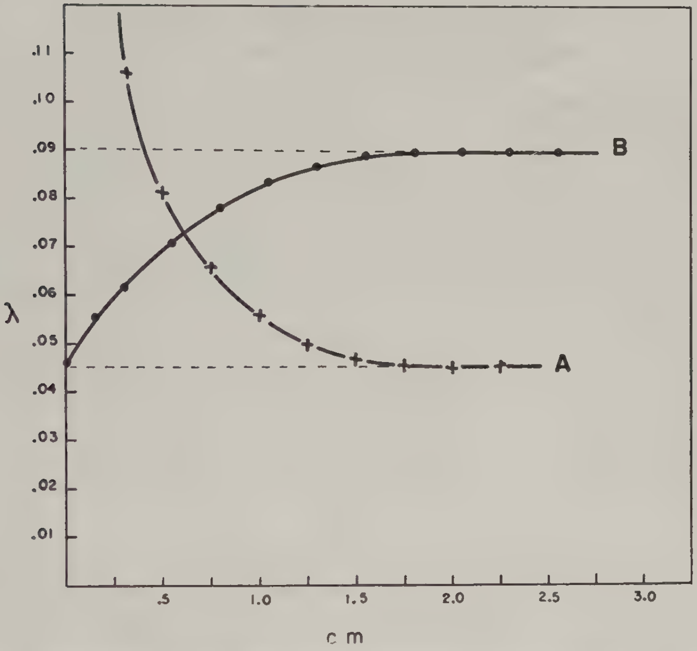

FIG. 2. Dependence of the logarithmic decrement on the position of the disk in the liquid.

Curve A

(Disk kept at the surface of the liquid; distance from the bottom of the container varied.)

λ	*h* in cm.	λ	*h* in cm.
0.45918	0.10	0.04741	1.50
0.13972	0.25	0.04554	1.75
0.08133	0.50	0.04561	2.00
0.06694	0.75	0.04429	2.25
0.05602	1.00	0.04523	2.50
0.05075	1.25		

Curve B

(Disk kept at a distance 1.75 mm. from the bottom of the container: depth of submergence of the disk varied.)

λ	*h* in cm.	λ	*h* in cm.
0.04606	0.00	0.08638	1.30
0.05575	0.15	0.08889	1.50
0.06179	0.30	0.09000	1.80
0.07083	0.55	0.08995	2.05
0.07831	0.80	0.09008	2.30
0.08337	1.05	0.08989	2.55

EXPERIMENTAL PROCEDURE AND DATA

Determination of the Critical Distance h_c

The distance to which any significant vibrations penetrate into the liquid has been determined by measuring the logarithmic decrement λ as a function of the distance h between the disk and the bottom of the container and the air-liquid interface, respectively.

Curve *A* in Fig. 2 shows the relationship between λ and h with the disk oscillating on the surface of a pure liquid. When h is small the value of λ is extremely high. It decreases in approximately exponential manner as h

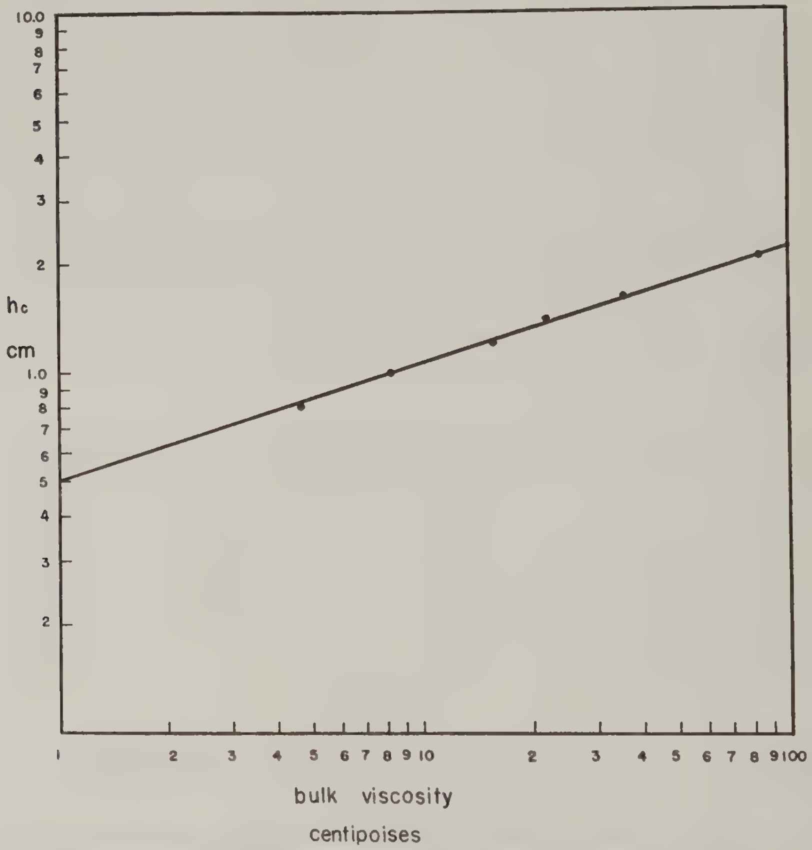

FIG. 3. Dependence of the critical distance h_c on the bulk viscosity of the solution.

Bulk viscosity	h_c in cm.
4.7 centipoises	0.8
8.3 centipoises	1.0
16.0 centipoises	1.2
24.0 centipoises	1.4
36.0 centipoises	1.62
84.0 centipoises	2.08

increases and, for all practical purposes, may be considered constant when h_c is equal to 1.75 cm., in this particular case. If the disk is kept at the distance h_c from the bottom and the depth of submergence of the disk is changed by adding more liquid, then curve B is obtained. In this case λ increases gradually until the distance from the air-liquid interface reaches the h_c value and then remains constant. In this paper h_c is referred to as the critical distance. The value of λ obtained with the disk on the surface of the liquid is, within the limits of experimental error, equal to one half that obtained with the disk immersed in the liquid.

The critical distance h_c has been determined, in the manner described above, for solutions of glycerol and water ranging in viscosity from 8 to 112 centipoises. The plot of log h_c vs. log of the bulk viscosity is shown in Fig. 3. This relationship may be represented by the equation

$$h_c = K\eta_b^a, \tag{4}$$

where η_b is the bulk viscosity of the liquid and K and a are constants. The

TABLE I

Comparison of the Logarithmic Decrements Obtained at the Surface of Pure Liquids with the Half Values of the Logarithmic Decrements Obtained in the Solutions Containing SLS, at a Predetermined Distance h_c from the Boundary Interfaces

Solution no.	Bulk viscosity (*centipoises*)	(λs pure)	($\frac{1}{2}\ \lambda_c h$SLS)	% difference
1	8.3	0.03256	0.03487	+7.1
2	16.0	0.02697	0.02383	−11.6
3	24.0	0.03410	0.03233	−5.2
4	36.0	0.02998	0.02787	−7.0
5	56.7	0.03406	0.03447	+1.2
6	84.0	0.04844	0.04326	−10.7
7	112.0	0.06615	0.05591	−15.4

TABLE II

Comparison of the Differences in Logarithmic Decrements ($\Delta\lambda$'s) *Obtained According to the Conventional Technique with Those Obtained According to the Critical Distance Technique*

(The difference between ($\lambda_{s\ \mathrm{pure}}$) and ($\lambda_{s\ \mathrm{SLS}}$) represents the former and the difference between ($\frac{1}{2}\ \lambda_{h_c\mathrm{SLS}}$) and ($\lambda_{s\ \mathrm{SLS}}$) the latter technique.)

Solution No.	(λs SLS)	(λ_s SLS) − (λ_s pure)	(λ_s SLS) − ($\frac{1}{2}\lambda_{h_c}$SLS)	% difference
1	0.33146	0.29890	0.29659	−0.8
2	0.22677	0.19980	0.20294	+1.6
3	0.35196	0.31786	0.31963	+0.6
4	0.12977	0.09979	0.10190	+2.1
5	0.06503	0.03097	0.03056	−1.3
6	0.12231	0.07387	0.07905	+7.0
7	0.23512	0.16897	0.17921	+6.1

disk used in this work was 5.08 cm. in diameter and the period of oscillation was 17.3 seconds; K and a were found to be equal to 0.5 and 0.32, respectively.

Comparison of the Methods for Measuring Surface Viscosity

The reliability of this method was tested on the series of liquids used previously for measuring the critical distance. By dividing each liquid in two fractions two series were obtained and to one series 0.5% of technical grade sodium lauryl sulfate (SLS) was added. Subsequently the logarithmic decrements were determined on the series containing SLS with the disk positioned in the liquid at a predetermined distance (h_c) from the boundary interfaces.

The half values of the logarithmic decrements obtained in this way, indicated by ($\frac{1}{2}\lambda_{h_c\text{SLS}}$), were then compared with the logarithmic decrements measured on the surface of the corresponding pure liquids. The latter values are indicated by ($\lambda_{s\text{pure}}$). These results are shown in Table I.

Subsequently the logarithmic decrements were measured on the surfaces of solutions containing SLS. They are indicated by ($\lambda_{s\text{SLS}}$). These measurements were carried out on the solutions which had been aged in the viscometer for approximately 18 hours in order to develop high surface viscosity.

TABLE III

Comparison of Surface Viscosities Obtained According to the Conventional Technique with Those Obtained According to the Critical Distance Technique

Solution No.	Surface viscosity in surface poises		% difference
	Conventional technique	Critical distance technique	
1	1.497	1.485	−0.8
2	2.027	2.059	+1.6
3	3.199	3.217	+0.6
4	1.681	1.716	+2.1
5	0.635	0.626	−1.4
6	1.515	1.621	+7.0
7	3.469	3.679	+6.1

TABLE IV

Effect of the Time on the Surface Viscosity of Solution No. 1

Age of the surface	Apparent surface viscosity in surface poises
Freshly formed	0.018
25 minutes old	0.243
1 hour old	0.683
4 hours old	1.233

The differences in logarithmic decrements or $\Delta\lambda$'s were obtained by subtracting ($\lambda_{s\text{pure}}$) from ($\lambda_{s\text{SLS}}$), and ($\frac{1}{2}\lambda_{h_c\text{SLS}}$) from ($\lambda_{s\text{SLS}}$); the differences between ($\lambda_{s\text{SLS}}$) and ($\lambda_{s\text{pure}}$) representing the conventional method, and those between ($\lambda_{s\text{SLS}}$) and ($\frac{1}{2}\lambda_{h_c\text{SLS}}$) representing the critical distance technique. It should be noted that the same values of ($\lambda_{s\text{SLS}}$) were used in both cases. Therefore the possibility of errors due to the aging of the surface films was eliminated. The results are compared in Table II. The values of $\Delta\lambda$ were then used to calculate the surface viscosities by means of Eq. [2]. The results are listed in Table III.

Measurements of the Surface Viscosity as a Function of Time

During the measurement of the surface viscosity of solutions containing SLS it was observed that the "consistency" of the surface layer was greatly influenced by the age of the surface. The subsequent measurements of the surface viscosity as a function of the age of the surface yielded the results which are shown in Table IV.

A qualitative observation was also made regarding the effect of the bulk viscosity on the speed of formation of the surface layer. It was noted that in general it took much longer for a solution having higher bulk viscosity to develop an appreciable surface structure than for one the viscosity of which was lower.

The surface viscosities of all solutions containing 0.5% *SLS* were non-Newtonian. This was indicated by the fact that the differences between the log of amplitudes of successive swings were not constant.

For that reason, the results listed in Table IV represent the apparent surface viscosities in the same sense as applied to the three-dimensional systems.

The non-Newtonian character of the surface viscosity can best be shown by the flow curve in which the shearing stress is plotted against the rate of shear. Such flow curves are shown in Fig. 4. They are obtained in the following way: The surface viscosity η_s is calculated for several angular displacements according to Eq. [2].

The shearing stress F at each displacement corresponding to the surface viscosity at that point is calculated from the relationship

$$\tau = I\alpha = Fr2\pi r,$$

where τ is the torque, I is the moment of inertia, α is the angular acceleration, and r is the radius of the disk. Now α equals $\Delta\omega/t$ or $(\theta_1 - \theta_2)/t^2$, where ω is the angular velocity, θ_1 and θ_2 are the angular displacements, and t is time.

In calculating α it is assumed that the angular velocity is constant during each swing and for that reason, the angular displacements of successive swings are considered. Since the angular displacement of a preceding swing

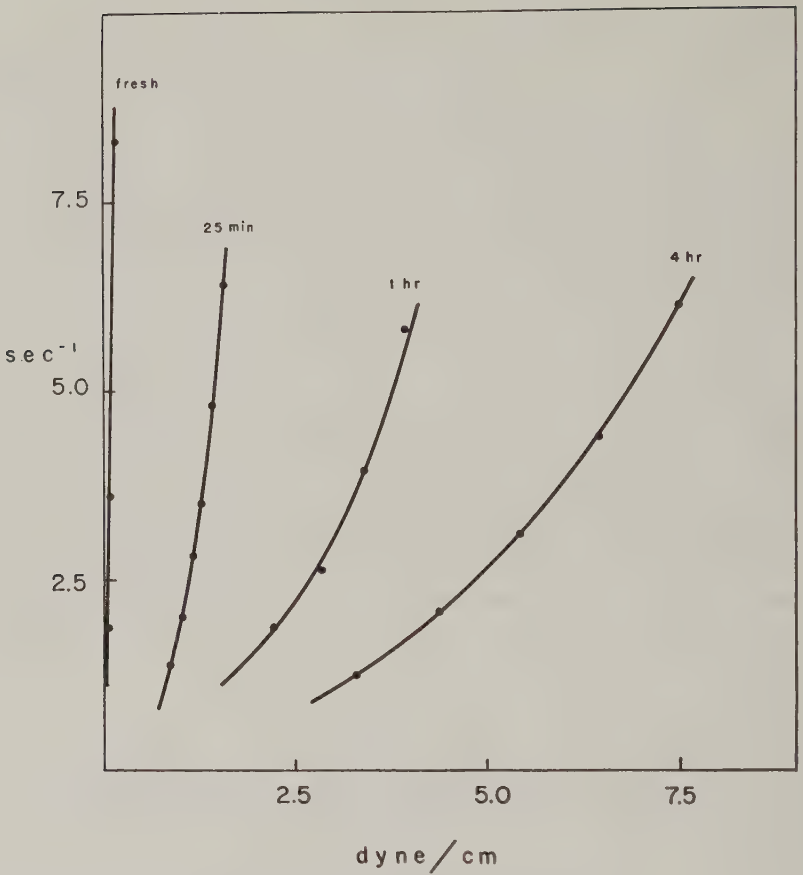

FIG. 4. Effect of the time on the surface viscosity of solution No. 1.

is greater than that of a successive swing, α represents a deceleration rather than an acceleration.

The deceleration due to the surface film alone is given by the difference of successive swings obtained with the disk oscillating at the surface of the solution minus one half of that obtained with the disk oscillating in the liquid at the critical distance from the boundary interfaces for the same angular displacement. Following the determination of α and subsequently of F, the rate of shear is calculated from Newton's equation $F = \eta \frac{dv}{dr}$ using the previously determined values of surface viscosity according to Eq. [2].

DISCUSSION OF THE RESULTS

The overall agreement between the logarithmic decrements (λ_{spure}) and ($\frac{1}{2}\lambda_{h,\text{cSLS}}$) is considered to be reasonably good, especially since the measurements were made at room temperature. The maximum difference between these values amounts to 15%, the average difference being 8%. It is felt that this difference is due largely to the error involved in determining the logarithmic decrement at the air-liquid interface. These measurements are subject to error because of difficulty in reproducing the position of the disk at the surface of the liquid. According to Cridle (13) the accuracy of such measurements can be improved greatly by using a conically shaped knife-edged disk. The effect of the shaft of the disk on the measurements of the logarithmic decrement with the disk immersed in the liquid seems to be negligible. Otherwise, one would expect that the results obtained for $(\frac{1}{2}\lambda_{h_c \mathrm{SLS}})$ would always be larger than those obtained for $(\lambda_{s \mathrm{pure}})$.

The errors due to the positioning of the disk or due to the drag exerted by the shaft of the disk become less important if the surface viscosity is appreciable. This is apparent when the values of $\Delta\lambda$, from which the surface viscosities are calculated, are compared. The maximum difference in this case amounts to 7% and the average difference is 2.8%. As previously mentioned, both $\Delta\lambda$'s were calculated using the same value of $(\lambda_{s\ \mathrm{SLS}})$. This was done in order to avoid the possibility of an error due to the aging of the film.

Our observations on the time effect of the surface viscosity of SLS solutions, Table IV, are in agreement with the results obtained by the other of investigators who have studied the properties of monolayers (3, 13, 14). According to Joly (3), the time effects are associated with the non-Newtonian behavior of the surface viscosity and are the result of the structural changes in the monolayer. It is interesting to note, however, that the fresh solution containing SLS indicates practically Newtonian behavior. The plastic character of the surface viscosity becomes apparent only after the surface has been aged for some time. The transition from Newtonian behavior toward plastic type of flow is shown by the flow curves in Fig. 4, which represent graphically the results summarized in Table IV. In contrast to the tabulated results, which indicate only the overall changes in apparent surface viscosity with time, the flow curves show the transition from one flow type to another and the changes in plastic viscosity and yield value of the surface layer at different stages of aging.

If one assumes that the formation of the viscous interfacial layer depends upon the rate of diffusion of the molecules of the surfactant to the surface, then one should expect the fastest build-up in the surface viscosity in solutions having low bulk viscosity. These solutions permit faster diffusion to the surface and subsequent formation of structure there. Our qualitative observations in regard to the effect of the bulk viscosity of the solution on the rate of build-up of the surface viscosity seemed to support such a theory. We intend to investigate the relationship between the bulk viscosity and the rate in the build-up of the surface viscosity in a quantitative manner in our future studies.

REFERENCES

1. MYERS, R. J., AND HARKINS, W. D., *J. Chem. Phys.* **5,** 501–603 (1937).
2. EWERS, H. E., AND SACK, R. A., *Australian J. Chem.* **7,** 40–54 (1954).
3. JOLY, M., *Kolloid-Z.* **126,** 1 (1952).
4. WILSON, R. E., AND RIES, E. D., *Colloid Symposium Monograph,* pp. 145–173 1923).
5. FOURT, L., AND HARKINS, W. D., *J. Phys. Chem.* **42,** 897–910 (1938).
6. BLAKEY, B. C., AND LAWRENCE, A. S. C., *Discussions Faraday Soc.* **18,** 268–276 (1954).
7. VAN WAZER, J. R., *J. Colloid Sci.* **2,** 223–236 (1947).
8. BROWN, A. G., THUMAN, W. C., AND MCBAIN, J. W., *J. Colloid Sci.* **8,** 508–519 (1953).
9. ELLIS, S. C., LAHHAM, A. F., AND PANKHURST, V. G. A., *J. Sci. Instr.* **32,** 70–73 (1955).
10. DE BERNHARD, L., "The Proceedings of the Second International Congress of Surface Activity," Vol. 1. To be published.
11. LAMB, H., "Hydrodynamics," pp. 619. Dover Publications, New York, 1945.
12. ROUSE, P. E., JR., AND SITTEL, K., *J. Appl. Phys.* **24,** 690–696 (1953).
13. CRIDLE, D. W., AND MEADER, A. L., JR., *J. Appl. Phys.* **26,** 838–842 (1938).
14. JOLY, M., *J. Chim. Phys.* **44,** 213–220 (1947).

JOURNAL OF COLLOID SCIENCE **13**, 441–458 (1958)

COALESCENCE OF LIQUID DROPS AT OIL-WATER INTERFACES

Lawrence E. Nielsen, Robert Wall,[1] and George Adams[2]

Monsanto Chemical Company, Plastics Division, Springfield, Massachusetts

Received March 20, 1958

Abstract

Measurements were made of the length of time single drops can exist at an oil-water interface before coalescence takes place with a bulk phase of the same composition as the drop. The effect of stabilizing agents soluble in either the oil or water phases was investigated. Factors investigated included: (*1*) temperature; (*2*) size of drops and curvature of O-W interfaces; (*3*) O/W vs.W/O drops; (*4*) kind of oil; (*5*) mutual solubility of oil and water phases; (*6*) type of stabilizing agent, its concentration, pH, interfacial viscosity, and rigidity.

The stability of drops decreases as the temperature is raised; the temperature dependence depends upon both the type of oil and the stabilizing agent. Oil drops are generally more stable than water drops when the stabilizing agent is water-soluble; the opposite is true for oil-soluble stabilizers. Oil-water phases which are mutually saturated with each other form more stable drops than unsaturated systems. The lifetime of drops depends roughly upon the cube root of the concentration of stabilizing agent in general. Stabilizers which produce a large viscosity or rigidity at the O-W interface also give stable drops; however, some good stabilizers show no interfacial viscosity or rigidity. Polyelectrolytes such as polymethacrylic acid and carboxymethyl cellulose stabilize drops better as acids than as salts; this behavior correlates with the interfacial viscosity behavior but not with the bulk solution viscosity.

Simple mechanical models of drop coalescence can explain only some of the observed results. Many of the data may be understood in terms of the generalizations: (*1*) any factor which disturbs the O-W interface on a molecular scale decreases the stability of drops; (*2*) many stabilizers are most effective when they are on the verge of precipitation.

I. Introduction

The coalescence of liquid drops at an interface has been studied for many years; however, the complexity of the phenomena and the difficulty in getting reproducible results have prevented a complete understanding of why liquid drops may have an appreciable lifetime before coalescing. Some of the most recent work on the stability of liquid drops at oil-water interfaces has been done by Cockbain and McRoberts (1) and by Gillespie and Rideal (2).

---

[1] Now at Chemistry Department, Pennsylvania State University, University Park, Pennsylvania.

[2] Now at Research Laboratory, Sprague Electric Company, North Adams, Massachusetts.

When the oil and water phases are pure liquids, the drops have a lifetime of about a second before they coalesce with a bulk phase. However, when certain substances, called stabilizing agents, are dissolved in the oil or water phases, the drops may have lifetimes of minutes or even hours. It is the purpose of this paper to discuss some of the physical factors affecting drop stability and to test various theories or hypotheses on the stability of emulsions. One such theory assumes an adsorbed film of high viscosity or rigidity around the drops and at all oil-water interfaces. In order to test this theory, interfacial viscosity and rigidity measurements were compared with drop stability measurements.

II. Apparatus and Experimental Techniques

The apparatus used to measure the lifetime of liquid drops before they coalesce at an oil-water interface was essentially the same as that used by Cockbain and McRoberts (1). The drop stability apparatus consists of a thermostated glass vessel similar to a short distillation condenser about 4½ inches long and 2 inches in diameter in which a layer of oil floats on top of a layer of water. The oil-water interface was concave on the oil side when the vessel had a clean untreated surface, but the interface could be made concave on the water side by using a glass vessel which had been given a silicone treatment.

Drops were formed on the tips of hypodermic needles which had been ground to give a flat end. The volume of the drops was measured by a calibrated micrometer screw which moved the plunger of a syringe to which the hypodermic needle was attached. When oil drops were being studied, the hypodermic needle entered the water phase through the stopper in the bottom of the glass vessel. When water drops were being studied, the apparatus was partially inverted and the needle tip was immersed in the oil phase through the top of the glass vessel. The time a drop rested at the oil-water interface before coalescing with the bulk phase was measured by an ordinary electric timer or stop watch. In order to determine the distribution of lifetimes of the drops, 30 to 100 drops were studied for each run.

The size of the drops was changed by using hypodermic needles with exterior diameters of 0.0254, 0.0445, and 0.0910 cm.

The distribution of lifetimes was plotted either as log N vs. t or N vs. log t, where N is the percentage of drops having a lifetime longer than time t. From such plots the half-life $t_{1/2}$, the maximum lifetime, and the minimum lifetime were obtained.

Great care must be used to get reproducible results. The interfaces must be kept scrupulously clean, and any dirt or scum must be removed by means of a hypodermic needle inserted at the interface. The curvature of the interface must also be controlled. Air dissolved in the water was found to increase the lifetimes of drops, so the distilled water was always boiled shortly before using. Aqueous solutions were made up with freshly boiled, distilled water and stored in sealed bottles until used; solutions in general were not used later than 2 days after being made. Solutions were also filtered through fine-pore glass filters to remove any insoluble particles. The apparatus was thermostated with a temperature variation of less than 0.2°C. However, except in a few cases the liquid in the syringe was at 24°C., the temperature of the air-conditioned room. The drops were formed slowly, so by the time they left the needle and came to rest at the interface, they were at about the same temperature as the liquids in the thermostated chamber. Experiments were carried out which indicated that room vibrations and mild agitation had only a slight effect on the rate of coalescence of drops. Likewise the distance between the hypodermic needle tip and the oil-water interface was found to be unimportant.

With great care, duplicate runs would generally give lifetimes which agreed to within about 10%. However, occasionally variations as great as 50% or even 100% were found. Half-lives were generally more reproducible than minimum lifetimes or the slope of the distribution curves.

Surface and interfacial viscosity and elasticity were measured by a torsion pendulum apparatus similar to that used by Criddle and Meader (3) or by Wilson and Ries (4). A stainless-steel double cone 2 inches in diameter with an edge making an angle of 30° was immersed in the interface. The cone oscillated through an angle of about 1 or 2 degrees. Part of the restoring force on the cone came from a torsion wire 2 feet long and 0.007 inch in diameter, and the remainder of the restoring force came from the magnetic lines of force of a differential transformer acting on the transformer core. The Schaevitz[3] linear variable differential transformer not only acted as a spring on the torsion pendulum, but also was used as transducer for recording the oscillations of the pendulum on a Sanborn[4] recorder. The surface viscosity η_s and real part of the surface rigidity G'_s were calculated from the following equations (5), which may be derived in a manner analogous to the equations for dynamic mechanical properties (6).

$$\eta_s = \frac{2I}{K}\left(\frac{\delta_s}{P_s} - \frac{\delta_L}{P_L}\right); \qquad [1]$$

$$G'_s = \frac{4\pi^2 I}{K}\left(\frac{1}{P_s^2} - \frac{1}{P_L^2}\right) - \frac{I}{K}\left(\frac{\delta_s^2}{P_s^2} - \frac{\delta_L^2}{P_L^2}\right), \qquad [2]$$

where I is the moment of inertia of the oscillating system,

$$\frac{1}{K} = \frac{1}{4\pi}\left(\frac{1}{R_1^2} - \frac{1}{R_2^2}\right),$$

[3] Schaevitz Engineering Company, Crescent Boulevard at Drexel Avenue, Camden, New Jersey.

[4] Sanborn Company, Waltham 54, Massachusetts.

where R_1 is the radius of the cone, R_2 is the radius of the dish in which the cone is immersed (100 mm.), P_s and P_L are the period of oscillation of the cone in a solution and in the pure liquid, respectively, and δ_s and δ_L are the logarithmic decrement of the oscillating system in the surface of a solution and in the surface of the pure liquid, respectively. These equations are for the cone oscillating at a liquid-air interface, but analogous equations hold for oil-water interfaces. If a dissolved substance appreciably changes the bulk viscosity of the liquid being used, a correction must be made to the δ_L term.

Some of the substances used in this study were: Mallinckrodt analytical-grade benzene and toluene; Phillips Petroleum research grade *p*-xylene; pharmaceutical grade Nujol; Fisher's highest purity grade *n*-butyl chloride, methyl *n*-butyrate, and 3-pentanone (made by Eastman); Dupont's highest viscosity, 88% hydrolyzed polyvinyl alcohol; Hercules Cellulose gum-type 70 high carboxymethyl cellulose; Eastman's practical-grade gelatin and saponin; Monsanto's commercial-grade styrene monomer, polystyrene (methanol-soluble material removed), solium salt of sulfonated polystyrene, vinyl acetate-maleic anhydride copolymer, and sodium salt of polyacrylic acid. The polymethacrylic acid was a specially purified material of high molecular weight made by Q. Trementozzi.

III. Experimental Results

A. Curvature of Interface and Size of Drops

The lifetime of a drop may be varied by changing the curvature of the oil-water interface. If the drop is on the concave side of the interface so that the interface tends to curve around the drop, the lifetimes before coalescence occurs are considerably longer than when the drop is on the convex side of the interface.

It appears that the stability of a drop can either decrease or increase as the size of the drop changes, depending upon the oil-water system and the type of stabilizing agent. Typical data are shown in Table I. In one case the lifetimes increased with the size of the drops; in the other case, the lifetimes decreased.

The buoyancy effect can be shown to have an effect upon the rate of coalescence of drops even though it is usually overwhelmed by other factors. The size of drops and the difference in density between the oil and water phases determine the force which a drop exerts on an interface. The greater the force pushing a drop against an interface, the shorter the lifetime of the drop. This effect can be illustrated very accurately (keeping the total volume of drops constant in all cases) by not allowing the drops to get large enough to escape from the tip of the hypodermic needle and then adjusting the force between the drop and the O-W interface by changing the height of the interface above the needle tip. The position of the interface can be adjusted by moving a glass rod up or down in the aqueous phase. If the interface is high so the drop barely touches the interface, the force between the drop and the O-W interface is small and the lifetimes are large. If the interface is low, the drop is pushed into the interface with a large force and the lifetimes of the drops are short. By alternately measuring lifetimes with the interface high and then low, accurate relative distribution curves can be obtained. Figure 1 shows the results of measurements using a 0.20% solution of polyvinyl alcohol as the aqueous phase and

TABLE I

Effect of Drop Size on Stability

Stabilizing agent	Conc. (%)	Drops[1]	Curvature of interface[2]	Drop radius (*cm.*)	Half-life (*sec.*)	Min. life-time	Max. life-time
Polyvinyl[3] alcohol	0.25	O/W	a	0.191	54.6	9.0	379
Polyvinyl alcohol	0.25	O/W	a	0.0683	230	8.1	>900
Na sulf.[4] polystyrene	0.23	O/W	a	0.287	44.8	11.2	>150
Na sulf. polystyrene	0.23	O/W	a	0.0807	20.3	2.8	73
Na sulf. polystyrene	0.23	W/O	b	0.307	16.3	6.4	63.6
Na sulf. polystyrene	0.23	W/O	b	0.208	12.8	2.4	29.7

[1] O/W = oil in water drops. W/O = water in oil drops.

[2] a = O/W interface bowed up. b = O/W interface bowed down.

[3] Styrene = oil phase.

[4] *p*-Xylene = oil phase. T = 24°C.

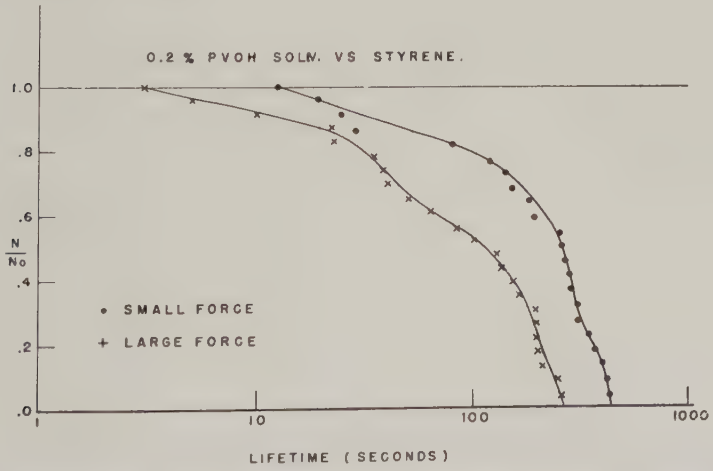

FIG. 1. Distribution of lifetimes of drops at an interface with: (*1*) a small force pushing the drops into the O-W interface (top curve); (*2*) a large force pushing the drops into the interface (bottom curve).

styrene as the oil phase. The results are as expected, but, unfortunately, it is difficult to measure quantitatively the total force or the force per unit area acting between a drop and an interface by such experiments.

The results in Table II show that in general the buoyancy effect is overpowered by other factors in determining lifetimes. The aqueous phase in these experiments was a 0.10% solution of polyvinyl alcohol. There is no correlation with density; many other similar examples were found during the course of the investigation.

B. Temperature and Temperature Gradients

In nearly all cases, increasing the temperature decreases the lifetimes of drops at an O-W interface. Figure 2 shows how the distribution of lifetimes changes with temperature for drops of benzene in an aqueous solution of polyvinyl alcohol (0.28%). Not all stabilizing agents give the same temperature dependence with a given oil. For instance, Fig. 3 shows the distribution of lifetimes using sodium sulfonated polystyrene as the stabilizing agent at a concentration of 0.23%. The changes in lifetimes with temperature are greater for polyvinyl alcohol than for sodium sulfonated polystyrene solutions.

TABLE II

Buoyancy vs. Lifetimes of Drops

Oil	Density of oil-density of water	Average lifetimes of drops
Nujol	0.121	2000 sec. approx.
Trioctyl phosphate	0.071	2 sec. approx.
Dioctyl phthalate	0.011	2000 sec. approx.

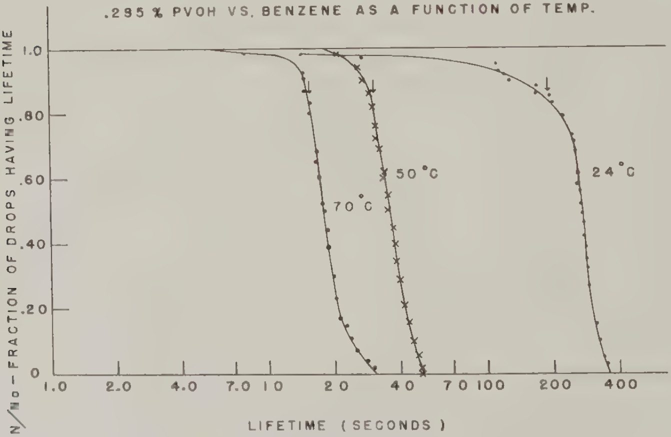

FIG. 2. Distribution curves of the lifetimes of benzene drops at an interface made up of benzene and a 0.28% solution of polyvinyl alcohol. Arrows indicate drainage times t_D.

A small part of the data on effect of temperature on lifetimes of drops is given in Table III. In all these experiments the O-W interface was bowed up for oil drops and sagged down for water drops. By this technique the interface always tended to curve around the drop and to maximize their lifetimes.

Cockbain and McRoberts (1) and Gillespie and Rideal (2) report that temperature gradients and convection currents in the apparatus decrease the lifetimes of drops. Experiments to check this effect were made at elevated temperatures. As the drop stability tests were normally carried out, the liquid in the syringe was 24°C. while the rest of the system might be at some other temperature. This may give rise to temperature gradients between the drops and the O-W interface. In a series of special experiments the temperature gradients were eliminated not only by thermostating the glass condenser-like vessel with circulating hot water, but also by putting the whole apparatus including the syringe in an air oven at the same temperature as the circulating water. The apparatus was operated by means of long gloves built into the side of the air oven, so the door of the oven did

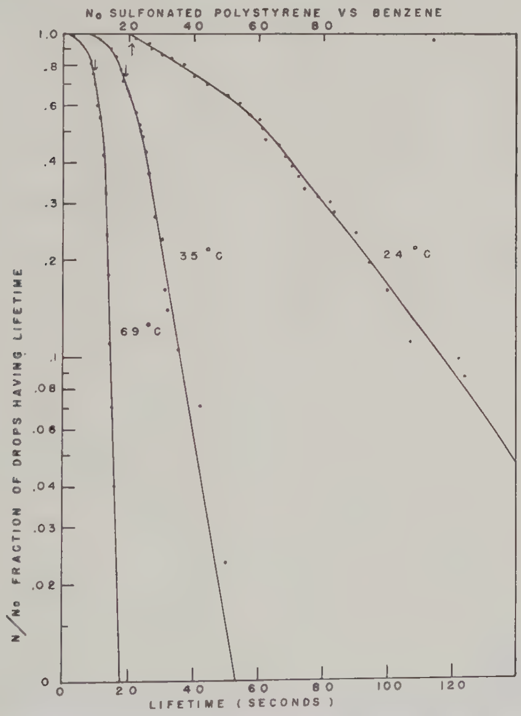

FIG. 3. Distribution curves of the lifetimes of benzene drops at a benzene-0.23% solution of sodium sulfonated polystyrene in water interface. Arrows indicate drainage times t_D.

TABLE III

Effect of Temperature on Drop Stability

Stabilizing agent	Temp. (°C.)	Oil phase	Drops	Half-life (*sec.*)	Minimum lifetime	Maximum lifetime
0.20% sodium sulfonated polystyrene	24	Styrene	O/W	13.8	2.8	57.7
	60	Styrene	O/W	13.5	1.9	30.3
	80	Styrene	O/W	12.1	2.9	26.7
0.28% polyvinyl alcohol	24	Toluene	O/W	285	25.9	400
	70	Toluene	O/W	25.6	17.2	32.9
	24	*p*-Xylene	O/W	435	66	>1000
	50	*p*-Xylene	O/W	46	6.1	79
	70	*p*-Xylene	O/W	26.5	17.0	35
0.23% sodium sulfonated polystyrene	24	Toluene	O/W	61.3	21.0	>200
	66	Toluene	O/W	10.8	2.6	18.2
	83	Toluene	O/W	7.6	3.2	11.0
	24	*p*-Xylene	O/W	30.7	12.0	97.7
	70	*p*-Xylene	O/W	11.2	3.6	20.1
	11	Benzene	W/O	11.4	1.5	31.3
	24	Benzene	W/O	10.3	2.1	21.9
	29	Benzene	W/O	6.1	1.7	11.2
	12	Toluene	W/O	20.1	2.9	33.2
	24	Toluene	W/O	12.2	1.5	30.0
	30	Toluene	W/O	7.5	1.4	22.9
	11	*p*-Xylene	W/O	19.1	2.0	86.4
	24	*p*-Xylene	W/O	12.6	1.7	84.1
Vinyl acetate-maleic anhydride copolymer, 0.23%	38	Benzene	O/W	74.4	24.8	150
	48	Benzene	O/W	61.1	34.6	110
	59	Benzene	O/W	35.8	8.9	53
	52	Toluene	O/W	49.5	9.4	95
	66	Toluene	O/W	26.3	10.9	47
	57	*p*-Xylene	O/W	43.2	10.2	127
	76	*p*-Xylene	O/W	16.9	5.0	31

not have to be opened at any time. The drops were formed more rapidly than the usual rate, which required nearly 1 minute. However, numerous other tests were made to show that generally the lifetimes were nearly independent of time of formation over the range from a few seconds to several minutes.

For the system polyvinyl alcohol solution with benzene drops, temperature gradients had no effect on the lifetimes, even though the interface was at 70°C. and the benzene in the syringe was at 24°C. However, when a vinyl acetate-maleic anhydride copolymer was used as the stabilizing agent and *p*-xylene was the oil phase, it was found that temperature gradients apparently cut the half-life of drops from 88 seconds to 43 seconds and the maximum lifetimes from 181 to 127 seconds. In this case the interface was kept at 57°C.

On the basis of these experiments, it was concluded that the elevated temperature measurements could be in error in some cases. However, the temperature gradients were normally very small as the drops were formed slowly on the needle tip over the course of about a minute, so the errors should not be great from this cause.

C. Effect of Concentration of Stabilizing Agent

Figure 4 shows that increasing the concentration of stabilizing agent increases the stability of drops. The half-life of styrene drops at 24°C. is plotted against concentration of polyvinyl alcohol or sodium sulfonated polystyrene in the aqueous phase. These and other data indicate in general that the lifetimes $t_{1/2}$ depend upon the concentration C according to the relation

$$t_{1/2} = KC^n, \qquad [3]$$

where K and n are constants. The constant n is in the range of 0.3 to 0.45. If the minimum and maximum lifetimes are examined, it is found that changes in concentration have a much greater effect upon the maximum lifetimes than upon the minimum lifetimes; i.e., the distribution of lifetimes broadens as the concentration increases.

D. Oil vs. Water Drops

For any given O-W interface oil drops coalesce with the bulk oil phase at a rate which is different from the rate at which water or aqueous drops

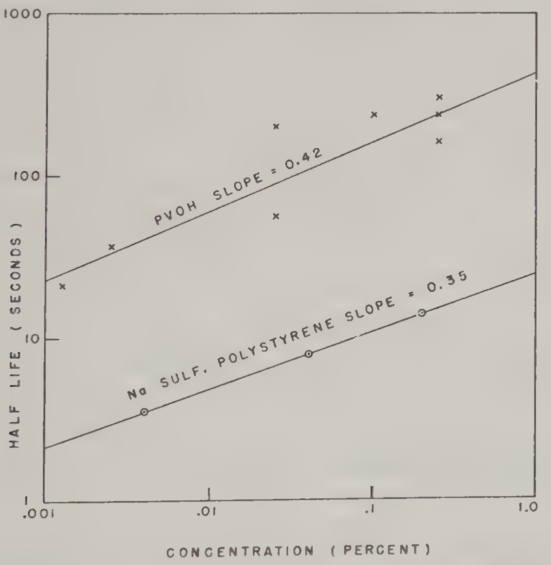

FIG. 4. Half-life of styrene drops as a function of concentration of stabilizing agent. *Top curve:* Polyvinyl alcohol solutions as the aqueous phase. *Bottom curve:* Solutions of sodium sulfonated polystyrene as the aqueous phase.

coalesce with the bulk aqueous phase. Typical data at 24°C. are given in Table IV.

In general these results indicate that oil drops are stabilized by water-soluble stabilizing agents, and water drops are stabilized by oil-soluble stabilizing agents. It is interesting to note that the lifetime of both O/W and W/O drops can be long. As polystyrene is added to styrene in the sodium polyacrylate system, both O/W and W/O drops increase in lifetime; there is no decrease in lifetime of O/W drops as the inversion point to W/O stable drops is approached.

E. Mutual Solubility of Oil and Water Phases

The solubility of oil in water or water in oil may have a large effect on the rate of coalescence of drops. This can be shown by comparing unsaturated oil and water phases with phases which are mutually saturated with each other. Table V illustrates this point.

The solubility of 3-pentanone in water is 4.7 g./100 ml.; the solubility of water in 3-pentanone is also roughly 5%. The solubility of styrene in water is only 0.027%. The mutually saturated phases always give longer lifetimes than the unsaturated phases. This effect is noticeable even when the solubility is very slight.

TABLE IV

Stability of Oil and Water Drops

Stabilizing agent	Oil phase	Drops	Half-life (*sec.*)	Minimum lifetime	Maximum lifetime
None	Styrene	O/W	3.2	1.6	9.8
	Styrene	W/O	2.3	1.0	5.9
0.25% polyvinyl alcohol	Styrene	O/W	175	6	940
	Styrene	W/O	10	1	77
0.10% vinyl acetate-maleic anhydride copolymer	Butyl chloride	O/W	16.5	1.6	64
	Butyl chloride	W/O	2.7	0.8	8.4
	Methyl butyrate	O/W	124	8.9	260
	Methyl butyrate	W/O	4.8	1.3	7.0
0.25% lauryl peroxide in oil phase	Butyl chloride	O/W	0.4	0.1	4.3
	Butyl chloride	W/O	6.4	0.8	14.0
0.20% polyacrylic acid (Na salt)	Benzene	O/W	62	9.2	150
	Benzene	W/O	1.7	0.6	5
0.20% polyacrylic acid (Na salt) in water and 12.5% polystyrene in oil phase	Benzene	O/W	111	40	225
	Benzene	W/O	87	30	293
10% polystyrene in oil phase	Styrene	O/W	6.3	3.1	23.2
	Styrene	W/O	59.2	20.8	109.5

TABLE V

Rate of Coalescence with Saturated and Unsaturated Phases

Stabilizing agent	Oil phase	Drops	Condition of phases	Half life (*sec.*)	Minimum lifetime	Maximum lifetime
0.20% Na sulfonated polystyrene	3-Pentanone	O/W	Unsaturated	3.9	0.4	6.8
	3-Pentanone	O/W	Saturated	9.2	0.8	33
0.10% polyvinyl alcohol	3-Pentanone	O/W	Unsaturated	7.6	5.4	9.2
	3-Pentanone	O/W	Saturated	99.5	17.0	170
	3-Pentanone	W/O	Unsaturated	4.3	2.2	5.1
	3-Pentanone	W/O	Saturated	9.2	2.1	10.3
None	Styrene	W/O	Unsaturated	2.3	1.0	5.9
	Styrene	W/O	Saturated	5.4	2.2	11.1

F. Effect of pH and Salts on Stability of Drops

The properties of some stabilizing agents such as proteins and polyelectrolytes are very dependent upon the pH or concentration of salts in solution. This is illustrated in Table VI using styrene as the oil phase.

The polyelectrolytes (polymethacrylic acid and carboxymethyl cellulose) give much more stable drops in the acid form at low pH than in the form of their sodium salts at high pH. The temperature dependence of the lifetimes of the acid form of polymethacrylic acid is abnormally large between 24°C. and 60°C. However, at higher temperatures the drops become more stable again. This unusual behavior seems to be related to the fact that polymethacrylic acid precipitates out of acid solutions at high temperatures. The acid form of carboxymethyl cellulose also has a very large temperature dependence of drop stability when the drops are styrene, but the temperature dependence is small when the drops are aqueous solution.

Gelatin is a polyampholyte with an isoelectric point at about pH 4.75. The half-life and maximum lifetime go through a maximum near the isoelectric point, where the gelatin itself is least stable and tends to precipitate easily.

Saponin forms stable drops at room temperature even at concentrations as low as 0.01 %, but the stability decreases rapidly at higher temperatures. Salts increase the stabilizing effect of saponin; calcium chloride is especially effective in this respect. The coalescence phenomenon is different with saponin than with most other stabilizing agents. With most stabilizing agents a drop coalesces nearly instantaneously like the puncturing of a balloon. However, saponin forms a tough film at the O-W interface (especially in the presence of $CaCl_2$), and the drops disappear more gradually like a leaky balloon.

TABLE VI

Effect of pH and Salts on Coalescence of Drops

Stabilizing agent	pH	Temp.	Drops	Half-life	Minimum lifetime	Maximum lifetime
0.10% polymethacrylic acid	2.25	24	O/W	217	32.1	427
	4.05	24	O/W	89.4	1.5	800
	10.75	24	O/W	29.5	3.5	60
	2.25	60	O/W	20.4	8.8	30
	4.60	60	O/W	6.2	0.7	14
	10.75	60	O/W	8.4	1.3	13
	2.25	80	O/W	108	16.1	923
0.10% carboxymethyl cellulose	2.85	24	O/W	660	25.4	>1600
	6.4	24	O/W	27.7	6.1	99
	2.85	24	W/O	24.4	3.2	45
	6.4	24	W/O	2.0	0.5	6
0.25% gelatin	2.15	24	O/W	20.5	3.1	37
	4.50	24	O/W	29.0	11.7	81
	4.75	24	O/W	22.7	4.9	250
	6.15	24	O/W	17.8	3.1	61
	9.05	24	O/W	12.2	3.1	92
0.01% saponin	5.3	24	O/W	23.0	6.0	250
	5.3	80	O/W	3.0	1.2	13
0.01% saponin + 0.1*M* KCNS	5.3	24	O/W	172	115	279
	5.2	80	O/W	1.9	0.9	6.1
0.01% saponin + 0.1*M* K_2SO_4	5.0	24	O/W	153	99	253
0.01% saponin + 0.1*M* $CaCl_2$	5.0	24	O/W	295	22	1495
0.01% saponin	5.3	24	W/O	47	5.4	159
0.01% saponin + 0.1*M* KCNS	5.5	24	W/O	63	1.2	151
0.01% saponin + 0.1*M* $CaCl_2$	5.0	24	W/O	165	5.0	1199

G. Correlation of Interfacial Viscosity and Rigidity with Drop Stability

On the basis of a mechanical model of drop stability one expects that a rigid film or a very viscous layer at an oil-water interface should decrease the rate of drop coalescence. Such a concept has some merit. In nearly all cases where a large interfacial rigidity or interfacial viscosity was found, the drops were very stable. However, there were a number of cases where stable drops could be made but no interfacial viscosity or rigidity could be measured. Table VII gives the surface viscosity η_s, surface rigidity G'_s, interfacial viscosity η_i, and interfacial rigidity G'_i for a number of stabilizing agents at 24°C. Surface values refer to the air-aqueous solution interface; interfacial values refer to the styrene-water solution interface.

A comparison of the drop stability measurements in Table VI with the mechanical properties of interfaces given in Table VII reveals a number of interesting results. Saponin not only shows tremendous viscosity at interfaces but also is very rigid. The interfacial viscosity correlates with the drop stability measurements for the saponin and saponin-salt solutions. For this substance the surface rigidity and the interfacial rigidity also correlate with drop stability.

Gelatin solutions do not show a measurable rigidity, but they do show surface and interfacial viscosity which go through a maximum near the isoelectric point. Figure 5 shows that the viscosities correlate fairly well with the lifetimes of drops as the pH of the gelatin solutions is varied.

Polymethacrylic acid and its sodium salt show interesting viscosity behavior. In solution the ionized salt has a much greater specific viscosity than the uncharged acid; this is the usual behavior of polyelectrolyte sub-

TABLE VII

Surface and Interfacial Viscosities and Rigidities

Stabilizing agent	Conc. (%)	pH	η_s	η_i	G'_s	G'_i
Saponin	0.01	5.5	17.0	1.07	18.9	0.03
Saponin + 0.1M KCNS	0.01	5.4	18.2	9.30	44.5	1.88
Saponin + 0.1M $CaCl_2$	0.01	4.8	13.7	14.2	56.0	16.0
Gelatin	0.25	2.10	0~	0~	0	0
	0.25	4.75	0.14	0.19	0	0
	0.25	6.0	0.21	0.05	0	0
	0.25	8.7	0.012	0.027	0	0
Polymethacrylic acid	0.25	4.15	0.013	—	0.031	—
	0.25	1.6	0.164	1.19	0.076	0.69
Carboxymethyl cellulose	0.10	6.50	0	0	0	0
	0.10	4.3	0.035	—	0	—
	0.10	2.95	0.40	—	0	—
	0.10	2.25	—	0.122	—	0.004
Polyvinyl alcohol	0.25	5.8	0+	0.016	0	0
Sodium sulfonated polystyrene	0.22	6.1	0	0	0	0

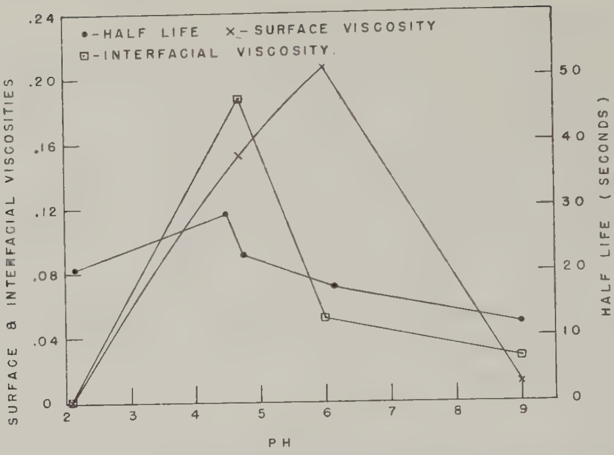

Fig. 5. Correlation of the stability of styrene drops with surface and interfacial viscosities of gelatin solutions at different values of pH. ○ half-life; X surface viscosity; ⊡ interfacial viscosity.

stances. The solution viscosity increases greatly as the pH increases. However, the surface viscosity decreases as the pH increases. The lifetimes of styrene drops correlate with the surface viscosity but not with the solution viscosity. Carboxymethyl cellulose behaves very much like polymethacrylic acid; again the drop stability changes in the same manner as the surface or interfacial viscosity.

IV. Discussion

A number of mechanisms have been proposed to explain the stability of emulsions or suspensions of drops and why oil and water drops in general coalesce at different rates at the same O-W interface.

The factors which determine the relative stability of oil and water drops are somewhat better understood than the factors which determine the absolute values of their lifetimes. A rule taken from emulsion technology which in general (but not always) allows one to predict the relative stability of oil and water drops is: If the stabilizing agent is soluble in the water phase, then oil drops will be more stable than water drops; if the stabilizing agent is oil-soluble, water drops will be more stable than oil drops. In most cases where this rule broke down it was observed that a precipitate formed at the O-W interface. If the stabilizing agent is soluble in water and insoluble in the oil, then it will collect on the outside of oil drops and tend to prevent their coalescence. However, if the drops are water instead of oil, the stabilizing agent is inside the drops and there is very little film to prevent coalescence when two drops come in contact as the molecules of stabilizing agents are free to move back into the water phase. This results in unstable W/O drops.

The simplest mechanical theories of drainage and coalescence do not take into account the properties of the stabilizing agent but assume that the most important factor is the bulk viscosity of the continuous liquid phase. It is assumed that as the liquid drains out of the space between two interfaces, coalescence takes place when the interfaces get very close together. The action of a stabilizing agent in these mechanical models is to increase the viscosity of the continuous phase and thereby decrease the rate at which two interfaces can approach each other. As with other investigators, the results of this work show such a concept to be inadequate. The correlation of lifetimes with viscosity is very poor when a stabilizing agent is used.

In order to overcome some of the shortcomings of the viscosity theory, one can replace the bulk viscosity by the interfacial viscosity or rigidity. This is an improvement. When the interfacial viscosity or rigidity are large, the experimental values of the lifetimes tend to be great. However, some materials are good stabilizing agents even though they show no viscosity at an oil-water interface.

Although the simple mechanical models of drop coalescence are inadequate in many respects, they do offer an explanation of many of the observed phenomena such as: (*1*) the lifetimes of drops depend upon the curvature of the O-W interfaces. Lifetimes are longest where the O-W interface curves around the drop, and they are shortest where the interfaces are curved so as to easily allow the liquid of the continuous phase to flow away from the interfaces as when two drops approach each other. (*2*) The greater the force pushing two interfaces together, the shorter the lifetimes of drops when all other factors are held constant.

Most of the emphasis has been placed upon the half-life of drops. However, in order to characterize a distribution curve one must know something about the width of the distribution or the difference between the minimum and maximum lifetimes. Cockbain and McRoberts (1) expressed their distribution curves in the form

$$\ln N = \ln N_0 - k(t - t_D), \qquad [4]$$

where N is the number of drops having a lifetime greater than time t, N_0 is the total number of drops, k is a constant called the rate constant, and t_D is the drainage time. Large values of k indicate a sharp distribution of lifetimes. Most of the results of this investigation did not give good straight line when $\log N/N_0$ was plotted against t, but the deviation from a straight line was slight for N/N_0 between the limits of 0.025 and 0.50. (See Fig. 3, for instance.)

It is generally possible also to estimate approximate values of k from

$$k = \frac{3.0}{t_{\text{max.}} - t_{1/2}}. \qquad [5]$$

This equation arises from the manner used to obtain k from the log N/N_0 vs. t plots which were generally fairly linear between the limits of 0.5 and and 0.025 for N/N_0.

A statistical analysis of tens of thousands of drops and many dozens of systems gave the following relationship between the value of k and the lifetimes $t_{1/2}$ and $t_{\text{min.}}$:

$$\log_{10} k = 0.279 - 1.013 \log_{10} (t_{1/2} - t_{\text{min.}}), \qquad [6]$$

where $t_{1/2}$ is the half-life and $t_{\text{min.}}$ is the minimum lifetime of a drop. The correlation coefficient relating k to the lifetimes has a value of 0.877 and a level of significance of over 99%. One might expect the slope of the log-log plot to be -1.00; the experimental value is -1.013. A general conclusion based on this equation is that the distribution of lifetimes broadens as the half-life increases.

Stabilizing agents change the longer lifetimes more than they do the minimum lifetimes. This indicates that stabilizing agents have somewhat less effect on the drainage of liquid between interfaces than they have upon the nature of the interface itself. This work shows the following results. (*1*) With no suspending agent, k is large, i.e., the distribution is sharp. (*2*) The value of k increases with temperature. (*3*) As the concentration of stabilizing agent increases, k decreases. (*4*) The value of k is greater for W/O drops than for O/W drops when a water-soluble stabilizing agent is used.

Gillespie and Rideal (2) suggest plotting ln N/N_0 vs. $(t - t_{\text{min.}})^{3/2}$. Straight lines were obtained for only a few of the systems studied and then only over the part of the distribution curves represented by the short lifetimes.

The energy of activation ΔH^* of the coalescence process may be calculated from the temperature dependence of k by

$$\frac{d \ln k}{dT} = \frac{\Delta H^*}{RT^2}. \qquad [7]$$

Values of ΔH^* vary from 2000 to 32,000 cal./mole. Typical values are 13,800 cal./mole for the system polyvinyl alcohol solution-benzene and 5900 cal./mole for the system sodium sulfonated polystyrene solution-styrene.

In many cases it was noticed that volatile oils had shorter lifetimes than nonvolatile oils with the same stabilizing agent. However, an analysis of the results shows that although there is a tendency for lifetimes to decrease as the vapor pressure increases, the correlation is poor and a constant vapor pressure does not correspond to a constant lifetime. In addition to the generalizations already discussed, several other fairly reliable generalizations have resulted from this work. The first of these is: Factors which disturb the oil-water interface on a molecular scale decrease the lifetimes of drops. Thus, oils with high vapor pressure tend to have short lifetimes. Also, if the oil and water phases are not saturated with respect to each other, the lifetimes are decreased because of the interdiffusion of molecules across the interface. Increasing the temperature increases the Brownian motion and decreases the lifetimes. Temperature gradients may decrease drop stability by changing the concentration of stabilizing agent over the surface of the drops.

A second generalization is: A stabilizing agent gives the most stable drops when it is near the point of precipitation from solution. This is illustrated by the results with polymethacrylic acid and its salts—the less soluble acid form gives the most stable drops. Another example is gelatin at its isoelectric point, where its stabilizing action is greatest. Also, the work of Biehn and Ernsberger (7) with polyvinyl alcohols of various polyvinyl acetate contents shows that it is best as a stabilizing agent when the polyvinyl alcohol has an acetate content great enough to cut down its solubility in water.

Cockbain and McRoberts (1) separate the distribution curve into two parts—coalescence that occurs during drainage and coalescence that occurs after drainage has ceased. This separation into two parts may not be completely justified. Since k and $t_{1/2}$ are so closely related, the same factors must be affecting both of them. In nearly all cases if $t_{1/2}$ is large, the distribution of lifetimes is broad. If two independent factors were involved, one might expect to find cases where even though $t_{1/2}$ were large, the distribution of lifetimes would be sharp.

The results of this work in general agree with the concept advanced by earlier workers that some part of the drop must "wet" the bulk liquid before coalescence can occur. However, until an experimental method of measuring this wetting is perfected, one can only speculate on the validity of this idea. If the concept of wetting is correct, the results on mutually saturated liquids versus unsaturated liquids are difficult to explain unless in the saturated systems the stabilizing agent is less soluble and tends to precipitate out at the interface. This, however, still leaves unexplained the results where no stabilizing agent was used in the styrene-water system in Table V.

ACKNOWLEDGMENTS

The authors are indebted to Dr. F. D. Stockton for a discussion of some of the results and to C. O. Baumann for a statistical analysis of the data.

REFERENCES

1. COCKBAIN, E. G., AND MCROBERTS, T. S., *J. Colloid Sci.* **8,** 440 (1953).
2. GILLESPIE, T., AND RIDEAL, E. K., *Trans. Faraday Soc.* **52,** 173 (1956).
3. CRIDDLE, D. W., AND MEADER, A. L., JR., *J. Appl. Phys.* **26,** 838 (1955).
4. WILSON, R. E., AND RIES, E. D., Colloid Symposium Monograph **1,** 145 (1923).
5. HARKINS, W. D., *in* "Physical Methods of Organic Chemistry" (A. Weissberger, ed.), Vol. 1, Part 1, Chap. 10. Interscience, New York, 1949.
6. NIELSEN, L. E., *Rev. Sci. Instr.* **22,** 690 (1951).
7. BIEHN, G., AND ERNSBERGER, M., *Ind. Eng. Chem.* **40,** 1449 (1948).

JOURNAL OF COLLOID SCIENCE **13**, 459–471 (1958)

DIELECTRIC DISPERSION IN METHACRYLATE POLYMERS AND ITS CORRELATION WITH MECHANICAL PROPERTIES

John D. Ferry and Stephen Strella[1]

Department of Chemistry, University of Wisconsin, Madison, Wisconsin, and Samuel Feltman Ammunition Laboratories, Picatinny Arsenal, Dover, New Jersey

Received April 17, 1958

INTRODUCTION

Recent measurements (1–3) of the dielectric properties of a series of four methacrylate polymers—the ethyl, *n*-butyl, *n*-hexyl, and *n*-octyl esters—have provided data over a wide range of temperatures and frequencies. Two of the same polymers, with some other methacrylates, have also been studied by de Brouckère and Offergeld (4, 5) with similar results. In the present communication, the data of references 1–3 are examined with respect to the applicability of reduced variables, the calculation of relaxation spectra, and comparison of the shapes of the latter as well as their temperature dependence with those of other dielectric spectra. Finally, the results are compared with measurements of mechanical properties on the same materials (6–9), and the general question of correlation of dielectric and mechanical properties is discussed.

APPLICATION OF REDUCED VARIABLES

General Considerations

In certain cases, it has been possible to separate the temperature and frequency dependence of the real (ϵ') and imaginary (ϵ'') components of the dielectric constant in polymer systems by the method of reduced variables, based on the assumption that although there is a distribution of relaxation mechanisms all relaxation times depend identically on temperature (10–12). This procedure has been questioned (13–15), even though it is inherent in several molecular theories for dispersion in polymers (15–17). Actually, examination of individual cases appears to reveal three classes of polymer systems, summarized in Table I; they can be most readily distinguished by the temperature dependence of the product $\epsilon''_m T/\rho$, where ϵ''_m is the maximum in ϵ'' as a function of frequency, T is the absolute temperature, and ρ is the density.

In Class A, both $\epsilon''_m T/\rho$ and $(\epsilon_0 - \epsilon_\infty)T/\rho$ are independent of T, where

---

[1] Present address: Monsanto Chemical Company, Everett, Massachusetts.

TABLE I

Classes of Behavior of Polymer Systems with Respect to Temperature Reduction of Dielectric Properties

Class	Characteristics	Examples
A	$\epsilon''_m T/\rho$ independent of T; reduced variables superpose at different temperatures	Polyvinyl chloride gels in dimethyl thianthrene ($\leq$ 40% polymer) (10) Polyvinyl acetal (11, 18)
B	$\epsilon''_m T/\rho$ decreases with increasing T; normalized variables superpose at different temperatures	Polyvinyl acetate (11, 19) Polyvinyl chloroacetate (11, 19) Polymethyl acrylate (11, 20)
C	$\epsilon''_m T/\rho$ increases with T; neither reduced nor normalized variables superpose	Polyvinyl chloride plasticized with diphenyl and tetrahydronaphthalene ($>$ 60% polymer) (21) Styrene-acrylonitrile polymers (22)

ϵ_0 and ϵ_∞ are the low- and high-frequency limiting values of ϵ'. Plots of the reduced variables as originally defined, $\epsilon'' T\rho_0/T_0\rho$ and $(\epsilon' - \epsilon_\infty)T\rho_0/T_0\rho$, against the logarithm of the frequency are identical in shape at different temperatures and superpose to give composite curves within a close approximation when shifted along the logarithmic frequency axis by a distance log b_T which depends on temperature alone. Of course, b_T must be the same for both real and imaginary components; a more recently imposed criterion for a satisfactory treatment is that its temperature dependence must follow the form of the WLF equation (23), though not necessarily with the approximate "universal" coefficients originally proposed for the latter (24). The function $b_T(T)$ then fully represents the temperature dependence of the dielectric properties; while the composite curves for $\epsilon' - \epsilon_\infty$ and ϵ'', reduced to a reference temperature by the shifts, represent the frequency dependence.

In Class B, both $\epsilon''_m T/\rho$ and $(\epsilon_0 - \epsilon_\infty)T/\rho$ decrease with increasing T. Thus, the contributions to polarization fall off abnormally with increasing temperature. But the effect appears throughout the dispersion region so that after normalization of the real and imaginary components—dividing through by $\epsilon_0 - \epsilon_\infty$—superposition is achieved as before; the shapes of the normalized dispersion curves are still independent of temperature.

In Class C, $\epsilon''_m T/\rho$ *increases* with increasing T, and the sharpness of the inflection in ϵ' increases; with or without normalization, the shapes of the dispersion curves change, and application of reduced variables except within a very limited temperature range is impossible. We shall return later to interpretation of these differences.

Application to Methacrylate Polymers

Now, examining the data (1–3) on the ethyl, n-butyl, n-hexyl, and n-octyl methacrylate polymers, we find that the features of both Classes B and C are evident. Although $(\epsilon_0 - \epsilon_\infty)T/\rho$ is nearly independent of temperature for the ethyl and *n*-butyl polymers, it decreases with increasing temperature for the other two, reflecting the drop in polarization contributions characteristic of Class B. By contrast, $\epsilon''_m T/\rho$ increases with temperature for all the polymers, so a change in shape characteristic of Class C is superimposed on the behavior.

For consistency, the data on all four polymers have been normalized to give the components $(\epsilon' - \epsilon_\infty)/(\epsilon_0 - \epsilon_\infty)$ and $\epsilon''/(\epsilon_0 - \epsilon_\infty)$, after calculating ϵ_0 and ϵ_∞ from the formulas given in Table II, where t is Centigrade temperature. The formulas for ϵ_0 were obtained from the measurements of ϵ' at the highest temperatures and lowest frequencies. Those for ϵ_∞ are based on equating ϵ_∞ to the square of the refractive index, n. For the ethyl and *n*-butyl polymer, n was taken from the measurements of Wiley and Brauer (25); the room temperature values for the *n*-octyl and the *n*-hexyl, respectively, were measured directly on an Abbé refractometer and obtained by an interpolation from a plot of specific refraction against number of carbon atoms in the side chain; and the temperature dependences for the *n*-octyl and *n*-hexyl were obtained from the thermal expansion coefficients, assuming the specific refraction to be independent of temperature.

To obtain a survey of the dispersion of the normalized components and its dependence on temperature, the complex plane plot of Cole and Cole (26) was employed. The results are shown in Fig. 1. Several conclusions are at once apparent from these curves. First, the breadth of dispersion increases with decreasing temperature, as already emphasized (1–5); if the method of reduced variables were applicable, a single arc locus would have been obtained for each polymer. Second, the left intersections of the loci with the real axis are not at the origin, but at values ranging from 0.13 to 0.23, showing that ϵ_∞ for the dispersion is actually somewhat higher than n^2. Strictly, this distorts the normalization, but the effect is slight. A similar, though smaller, difference was noted by de Brouckère and Offergeld (5). Third, the shape of the locus does not conform to the symmetrical arc of Cole and Cole (26) nor the unsymmetrical one of Davidson and Cole (27). The latter is sketched in for three of the polymers, based on a value of 0.400 for the parameter β determined from the initial slope at the left in each case; this function deviates markedly at the high-temperature–low-frequency end at the right.

Even though, for a given polymer, a separate locus is given at each tem-

TABLE II

Values of ϵ_0 and ϵ_∞ for Normalization

Polymer	ϵ_0	ϵ_∞
Ethyl	$4.819-0.0108(t-100)$	$2.150-0.00102(t-100)$
n-Butyl	$3.983-0.0071(t-100)$	$2.196-0.00080(t-25)$
n-Hexyl	$3.500-0.0086(t-100)$	$2.188-0.00113(t-25)$
n-Octyl	$3.839-0.00706(t-25)$	$2.178-0.00098(t-25)$

perature, the arcs tend to coincide at high temperatures, indicating that the shape of the dispersion approaches constancy there. This behavior has some theoretical precedent; the model of Hoffman (28, 29) for dipole molecules with alternative orientational sites in a crystal leads to an asymmetrical dispersion which broadens with decreasing temperature but approaches a Debye dispersion at high temperatures. Such an assortment of sites, associated with the steric hindrance caused by the methyl group in methacrylate polymers, could when superimposed on the more usual polymeric relaxation spectrum produce the effect shown in Fig. 1. It is clear from the reasoning of de Brouckère and Offergeld, and by analogy with the earlier results on polymethyl methacrylate by Deutsch, Hoff

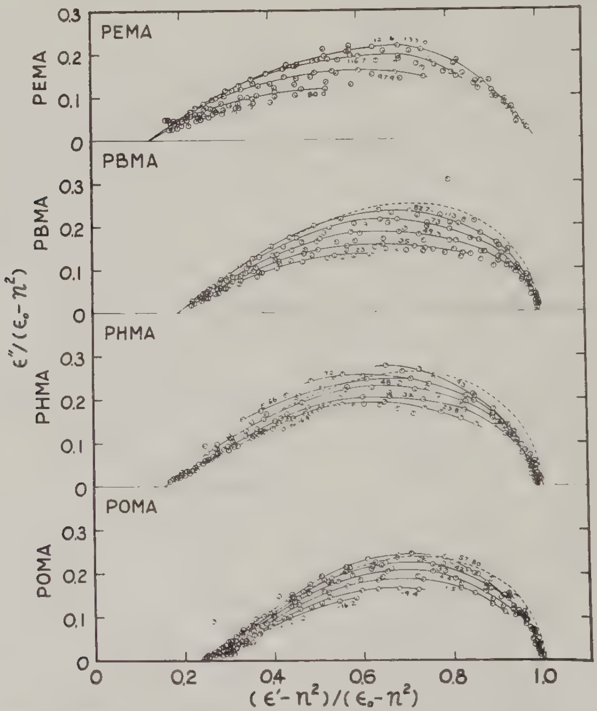

FIG. 1. Complex plane plots of normalized components of the dielectric constant. PEMA, polyethyl methacrylate: pip up, 55.1°; successive 45° rotations clockwise, 62.4°, 67.4°, 73.8°, 80.0°, 85.6°, 93.2°, 97.9°, 107.5°, 112.0°, 116.7°, 121.6°, 125.7°, and 133.0°. PBMA, poly-*n*-butyl methacrylate: pip down, 23.2°; successive 45° rotations clockwise, 30.1°, 35.5°, 41.1°, 54.6°, 64.7°, 73.4°, 82.7°, 92.6°, 103.2°, and 113.8°. PHMA, poly-*n*-hexyl methacrylate: pip left, 0.4°; successive 45° rotations clockwise, 9.0°, 16.9°, 23.8°, 32.6°, 40.0°, 48.0°, 56.3°, 66.8°, 72.3°, 81.2°, 92.3°, and 106.0°. POMA, poly-*n*-octyl methacrylate: pip right, −36.8°; successive 45° rotations clockwise, −23.9°, −16.2°, −9.4°, 1.5°, 6.1°, 14.4°, 21.5°, 27.4°, 35.3°, 42.9°, 49.7°, 57.6°, 66.8°, 74.3°, and 80.7°. Some of the temperatures are identified numerically. Dashed lines are Davidson-Cole arcs with $\beta = 0.400$.

and Reddish (30), that the dispersion in Fig. 1 involves primarily motion of the ester side chains (a so-called β mechanism); and Heijboer (31) has shown that the mechanical manifestations of this mechanism are closely associated with the steric hindrance of the methyl group.

We have therefore attempted to apply reduced variables only to the data at higher temperatures where the shape of the complex locus is nearly constant: for the ethyl polymer, from 107.5° to 133.0°; for the *n*-butyl, from 73.4° to 113.8°; for the *n*-hexyl, from 48.0° to 106.0°; and for the *n*-octyl, from 42.9° to 80.7°. Logarithmic plots of $(\epsilon' - n^2)/(\epsilon_0 - n^2)$ and $\epsilon''/(\epsilon_0 - n^2)$ against frequency were prepared, and the differences $\Delta \log b_T$ were measured with dividers; in most cases the shifts for both real and imaginary components agreed well, and the logarithm of the total shift from a given reference temperature was a linear function of $1/T$. In other words, the apparent activation energy ΔH_a for the relaxation processes is constant over the rather limited temperature ranges concerned, and the Arrhenius equation serves instead of the more complicated WLF equation. The values of ΔH_a are given in Table III; the comparison with the other values which appear will be discussed subsequently.

Using these values of ΔH_a, $\log b_T$ was calculated for each temperature based on the choice of 100°C. as a reference. With these calculated (rather than the original empirical) shift factors, logarithmic plots of the normalized components against ωb_T were prepared and are shown in Fig. 2. The superposition is reasonably satisfactory except at the low frequencies for polyoctyl methacrylate where the second, low frequency rise in ϵ'' is entering. (The values in this region are omitted in subsequent calculations for all the polymers, since the origin of the loss is uncertain.)

RELAXATION DISTRIBUTION FUNCTIONS

From the reduced plots in Fig. 2, the normalized distribution of electrical relaxation times, Ψ_n, was calculated by the second approximation formulas of Williams and Ferry (32, 11). The values are listed in Table IV and plotted in Fig. 3. The agreement between the calculations from the real and the imaginary components is in most cases excellent.

The values of $\log \tau_m$ where Ψ_n reaches a maximum and of Ψ_n at the maximum are summarized in Table V. In comparing these four polymers, it must be remembered that their molecular weights and degrees of poly-

TABLE III

Apparent Activation Energies for Relaxation (kcal.)

Polymer	Dielectric	Mechanical (β)	Mechanical (α) at 100 C.
Ethyl	31	31	69
n-Butyl	24	24	37
n-Hexyl	21	13	27
n-Octyl	18	—	21

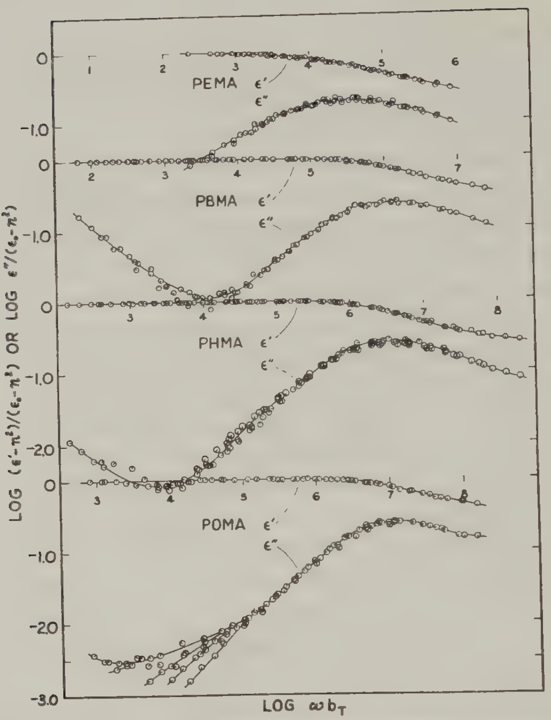

Fig. 2. Normalized components of the dielectric constant plotted logarithmically against the reduced frequency, reduction to 100°C. having been made by the apparent activation energies in Table III. Polymers and temperatures identified as in Fig. 1; temperature ranges as specified in the text.

merization are all different. Nevertheless, there is good evidence that in the range covered here the dielectric dispersion is essentially independent of molecular weight; unpublished data on another fraction of polyethyl methacrylate (33), as well as those of de Brouckère and Offergeld on four samples of poly-*n*-butyl methacrylate (5), support this conclusion. Thus, the differences in log τ_m in Table V can be correlated directly with side chain length. As the latter is increased, the progressive drop in log τ_m reflects enhanced dipole mobility at constant temperature. By contrast, it is striking that the maximum value of Ψ_n varies very little with side chain length. In fact, the entire shapes of the distribution functions (except for the ethyl polymer at long times) are quite similar, as shown in Fig. 4, where log Ψ_n is plotted against log τ/τ_m for the four polymers. The distributions are asymmetrical, being steeper on the long time side.

Comparison of Side Chain and Backbone Dispersions

The evidence that the dispersion treated here involves side chain motions appears to be convincing. The ΔH_a values in Table III agree well

TABLE IV

Normalized Relaxation Distribution Function Reduced to 100°C.

	$\log \Psi_n$			$\log \Psi_n$	
$\log \tau$	From ϵ'	From ϵ''	$\log \tau$	From ϵ'	From ϵ''
Polyethyl methacrylate			Poly-*n*-hexyl methacrylate		
−6.0	−1.19	−1.35	−8.0	−1.43	−1.26
−5.5	−1.07	−1.10	−7.5	−1.17	−1.02
−5.0	−0.92	−0.93	−7.0	−0.88	−0.87
−4.5	−0.88	−0.89	−6.5	−0.72	−0.79
−4.0	−1.02	−0.99	−6.0	−0.96	−0.95
−3.5	−1.20	−1.23	−5.5	−1.52	−1.60
−3.0	−1.57	−1.58	−5.0	−2.20	−2.00
−2.5	−2.05	−1.94	−4.5	−2.58	—
			−4.0	—	−3.00
Poly-*n*-butyl methacrylate			Poly-*n*-octyl methacrylate		
−7.5	−1.22	−1.43	−8.0	−1.01	−1.01
−7.0	−1.07	−1.07	−7.5	−0.90	−0.89
−6.5	−0.83	−0.87	−7.0	−0.76	−0.86
−6.0	−0.78	−0.88	−6.5	−1.06	−1.11
−5.5	−1.07	−0.98	−6.0	−1.77	−1.85
−5.0	−1.61	−1.57	−5.5	−2.34	−2.28
−4.5	−2.36	−2.18	−5.0	—	−3.00
−4.0	—	−2.51			

with the corresponding values deduced for the β mechanism from dynamic mechanical measurements (6–8), also given in the table; they are definitely smaller than the values for the α mechanism, which are also given in the table for comparison at 100°C., though of course they change rapidly with temperature in accordance with the WLF equation. (A similar conclusion was also stressed by de Brouckère and Offergeld for polymethyl methacrylate (5); they did not, however, obtain the same ΔH_a values for the ethyl and *n*-butyl polymers as ours, since they calculated ΔH_a from the position of the maximum in ϵ'' at lower temperatures where the distribution is changing in shape.)

The polymeric dispersions which we have examined earlier (10, 11) and fall into Classes A and B of Table I are sharply differentiated from the methacrylate dispersions by the fact that the temperature dependence of their relaxation times follows the WLF equation; moreover, wherever the mechanical data are available, this temperature dependence is *identical* with that of the mechanical relaxation times obtained from measurements which obviously reflect the α mechanism or backbone motions. These electrical dispersions have therefore been attributed to cooperative motions of backbone segments. Apparently for such motions the application of reduced variables is much more successful and the broadening of the distribution with decreasing temperature is not apparent.

Despite these contrasts between the α and β dielectric dispersion types, the breadth of the relaxation distribution is surprisingly similar for the

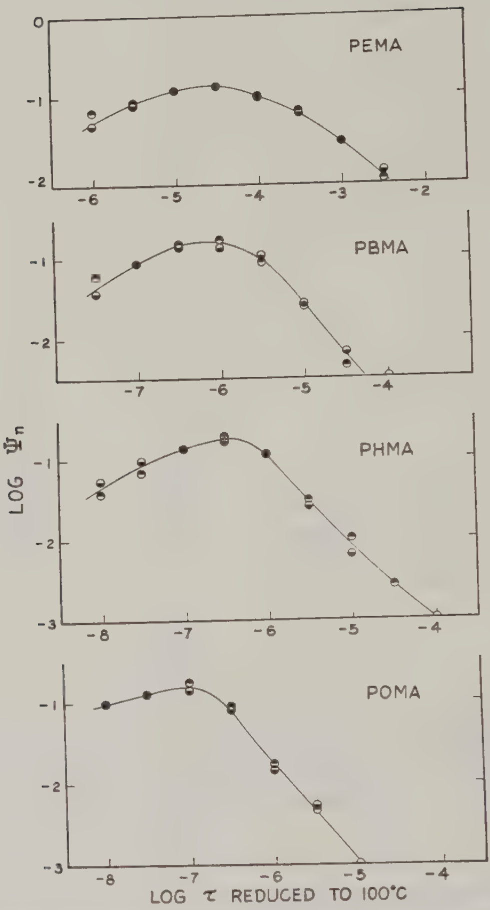

Fig. 3. Normalized electrical relaxation spectra plotted logarithmically, reduced to 100°C. Polymers identified as in Fig. 1. Points top black, from real component; bottom black, from imaginary component.

two classes. The maximum of 0.16 ± 0.02 in Ψ_n for the methacrylate β dispersions may be compared with values of 0.08, 0.17, 0.20, and 0.18 for what are presumably α dispersions in polymethyl acrylate, polyvinyl acetate, polyvinyl chloroacetate, and polyvinyl acetal; and 0.13 and 0.085 for 10% and 40% compositions of polyvinyl chloride in dimethyl thianthrene (10, 11). The theories of Kirkwood and Fuoss (16) and Hammerle and Kirkwood (17), which treat dipoles rigidly attached to the polymer chain and hence a dispersion involving backbone motions, predict values of 0.25 and 0.30, respectively, for the maximum in Ψ_n. Thus both the observed α and β dispersions are only moderately broader than the theory. The two theoretical curves for Ψ_n are also drawn in Fig. 4.

TABLE V

Parameters Characterizing Relaxation Distributions

	Ethyl	*n*-Butyl	*n*-Hexyl	*n*-Octy
Log τ_m at 100°C. (sec.)	−4.60	−6.15	−6.45	−7.05
Ψ_n at maximum	0.14	0.16	0.18	0.15
Log ζ_0 at 100°C. (dynes-sec./cm.)	−0.21	−3.51	−5.21	−5.78

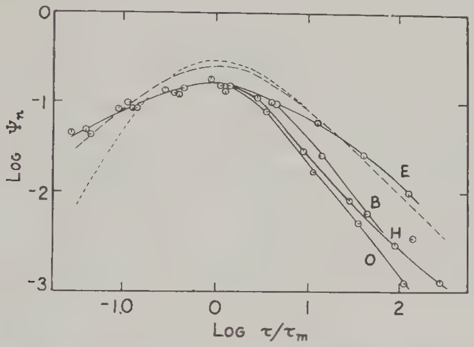

FIG. 4. Normalized electrical relaxation spectra plotted logarithmically against τ/τ_m, where τ_m is the relaxation time at the maximum of the spectrum. E, B, H, and O identify the ethyl, *n*-butyl, *n*-hexyl, and *n*-octyl polymers. Curves with long dashes, theory of Kirkwood and Fuoss; with short dashes, Hammerle and Kirkwood.

COMPARISON OF ELECTRICAL AND MECHANICAL DISPERSIONS

In comparing (30, 34) dispersion of the complex dielectric constant $(\epsilon' - i\epsilon'')$ with that of the complex mechanical compliance $(J' - iJ'')$ it must be remembered that in passing through its dispersion ϵ' may change by a factor of 2, or possibly 10, while J' in an α dispersion can change by a factor of 10^4. It follows that the maximum in ϵ''/ϵ' is close to that in ϵ'', on the frequency scale, but the maximum in J''/J' may lie several logarithmic decades to the right of that in J''. The functions ϵ'' and J'' most nearly reflect the distribution functions Ψ and L which determine the electrical and mechanical properties, respectively. In our present analysis, we have separated out the time dependence in the form of Ψ and L and the temperature dependence in the form of the factors b_T and a_T, respectively.

Temperature Dependence

It has already been mentioned that for the electrical dispersions in Classes A and B of Table I the temperature dependence is identical with that of the mechanical α dispersion. On the other hand, the temperature dependences for the electrical dispersions in the methacrylate polymers, identified with β mechanisms, are close to those for the respective mechanical β mechanisms. (It should be remarked, however, that the ΔH_a

values for the mechanical dispersion are obtained from data at somewhat lower temperatures where the electrical dispersion has started changing in shape; this makes the comparison somewhat uncertain.) The α mechanisms follow the WLF equation; the β, the Arrhenius equation. Thus the correlations between the respective temperature dependences seem to be clear.

Time Dependence

In previous comparisons for α mechanisms, it has been pointed out that the Ψ_n spectrum lies several logarithmic decades to the left of the L spectrum (10, 35), presumably because the short-time contributions are weighted more heavily in Ψ than in L; contributions to polarization are practically independent of molecular length, but contributions to L are directly to proportional to it. A similar comparison of Ψ_n and L for the β dispersions of the methacrylate polymers is made in Fig. 5. Again the electrical spectra lie at shorter times than the mechanical. The heights of the mechanical spectra are arbitrary, since normalization constants are not yet available; their shapes are not known with sufficient confidence to make detailed comparisons, but the ethyl appears to be somewhat broader than the n-butyl and n-hexyl just as in the electrical group. For polymethyl methacrylate, the β mechanical dispersion appears to be much broader than for even the ethyl (36, 8); and the same is apparently true for the β electrical dispersion, since from the data of de Brouckère and Offergeld on polymethyl methacrylate Ψ_n at its maximum can be estimated to be about 0.06, as compared with 0.14 ± 0.02 for the higher members of the series in Table V.

Nature of Molecular Motions

The identity of temperature dependence for electrical and mechanical α dispersions suggests that the resistance to dipole orientation involves primarily translatory friction of chain segments, even though some of the

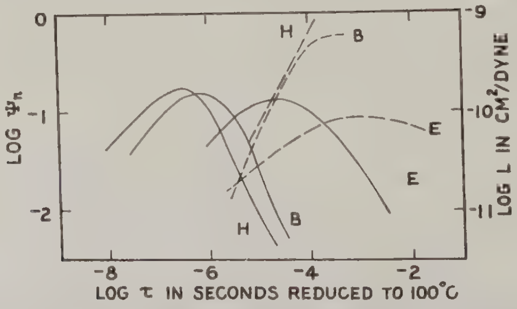

FIG. 5. Normalized electrical relaxation spectra (solid curves) and (unnormalized) mechanical retardation spectra (dashed curves) reduced to 100°C. Polymers identified as in Fig. 4.

polymers in Classes A and B of Table I have dipoles on side groups. For the β dispersions, a different sort of resistance is evidently involved, in which steric hindrance and potential barriers may play a role—as evidenced by the sharpening of the dispersion with increasing temperature. From molecular models it appears that the carbonyl dipole in a methacrylate polymer can orient in certain directions without much displacement of the backbone, but in other directions cooperation of the backbone is necessary. It is not clear just how the side group motions produce response to mechanical stress in the mechanical β mechanism. Cooperation of neighboring backbones has been postulated, especially when the side groups are short (7). The resistance to motion diminishes with increasing side chain length at constant temperature, but not nearly as rapidly as the translational friction of the backbone diminishes, as shown by the comparison in Table V of $\log \tau_m$ and $\log \zeta_0$ which characterize the two processes. Here ζ_0 is the translational friction coefficient per monomer unit, derived from the mechanical dispersion (24).

MAGNITUDE OF THE ELECTRICAL POLARIZATION

It has been pointed out (2, 3) that the contribution of orientation to the dielectric constant divided by the number of dipoles per unit volume, as measured for example by $(\epsilon_0 - \epsilon_\infty)M_0/\rho$, is higher for polyethyl methacrylate than fo the other polymers in the series. We suggest that this difference may be related to Fuoss's remarks (37) on the abnormally high dielectric constants of polymers in general compared with polar liquids. In a polymer, there is less cancellation of the fields of neighboring dipoles because of the restrictions of attachment to the molecular chain. If the restrictions are less in the butyl and higher homologs than in the ethyl polymer—as the activation energies in Table III suggest—then the cancellation will be somewhat greater in the higher members of the series.

Such an effect may also be responsible for the abnormal temperature dependence of $\epsilon_0 - \epsilon_\infty$ of the polymers listed in Class B of Table I. It is worth noting that the polymers of Class A, which do not show this dependence, have their dipoles rigidly attached to the chain backbone. The polymers in Class B have their dipoles on side groups but lack the hindering methyl group which characterizes the methacrylates.

ACKNOWLEDGMENTS

This work was supported by the Ordnance Corps, Department of the Army. We are much indebted to Mrs. Garrett Droppers and Mrs. William C. Frazier for many of the derived calculations.

SUMMARY

The dielectric measurements of Strella on ethyl, n-butyl, n-hexyl, and n-octyl methacrylate polymers at Picatinny Arsenal have been further examined. The frequency and temperature dependence of ϵ' and ϵ'' reveal

combined characteristics of two different classes of polymer systems previously recognized: a decrease in $(\epsilon_0 - \epsilon_\infty)T/\rho$ with increasing temperature; and an increase in $\epsilon''_m T/\rho$ with temperature, representing a sharpening of the relaxation spectrum and attributed to overcoming steric barriers associated with the backbone methyl groups. Despite the latter effect, at high temperatures the shape of the dispersion approaches constancy and the real and imaginary components of the dielectric constant can be superposed at different temperatures in accordance with the method of reduced variables after normalization by $\epsilon_0 - \epsilon_\infty$. The temperature shift factors follow the Arrhenius equation with apparent activation energies close to those obtained for the β mechanism in the dispersion of mechanical compliance. From the resulting composite curves, the normalized relaxation spectra Ψ_n can be calculated with good agreement between the values from real and imaginary components. The shapes of Ψ_n are very similar for the three highest homologs; that for the ethyl polymer is somewhat broader. At its maximum, Ψ_n is 0.16 ± 0.02 for the four methacrylate polymers, not far from values found for dielectric α dispersions in other polymer systems, and only moderately lower than the 0.25 and 0.30 predicted by the theories of Kirkwood-Fuoss and Hammerle-Kirkwood. Nevertheless, the temperature dependence of the polymethacrylate dispersions and their relation to the data of Hoff and of de Brouckère clearly identify them as of the β type. At 100°C., the Ψ_n maximum shifts to shorter times with increasing side chain length, but not as rapidly as the monomeric friction coefficient characterizing the mechanical α dispersion changes. The mechanical β retardation spectra lie at longer times than the electrical β relaxation spectra, but their relative positions and shapes are qualitatively similar in comparing the ethyl, butyl, and hexyl homologs.

REFERENCES

1. Strella, S., and Zand, R., *J. Polymer Sci.* **25,** 97 (1957).
2. Strella, S., and Zand, R., *J. Polymer Sci.* **25,** 105 (1957).
3. Strella, S., and Chinai, S. N., *J. Polymer Sci.*, in press.
4. Offergeld, G., *Nature* **178,** 1460 (1956).
5. De Brouckère, L., and Offergeld, G., *Bull. soc. chim. Belg.* **67,** 96 (1958).
6. Ferry, J. D., Child, W. C., Jr., Zand, R., Stern, D. M., Williams, M. L., and Landel, R. F., *J. Colloid Sci.* **12,** 53 (1957).
7. Child, W. C., Jr., and Ferry, J. D., *J. Colloid Sci.* **12,** 327 (1957).
8. Child, W. C., Jr., and Ferry, J. D., *J. Colloid Sci.* **12,** 389 (1957).
9. Dannhauser, W., Child, W. C., Jr., and Ferry, J. D., *J. Colloid Sci.* **13,** 103 (1958).
10. Ferry, J. D., and Fitzgerald, E. R., *J. Colloid Sci.* **8,** 224 (1953).
11. Ferry, J. D., Williams, M. L., and Fitzgerald, E. R., *J. Phys. Chem.* **59,** 403 (1955).
12. Williams, M. L., *J. Phys. Chem.* **59,** 95 (1955).
13. Broens, O., and Müller, F. H., *Kolloid-Z.* **141,** 20 (1955).

14. Cole, R. H., *J. Chem. Phys.* **23,** 493 (1955).
15. Van Beek, L. K. H., Thesis, Leyden, 1955.
16. Kirkwood, J. G., and Fuoss, R. M., *J. Chem. Phys.* **9,** 329 (1941).
17. Hammerle, W. G., and Kirkwood, J. G., *J. Chem. Phys.* **23,** 1743 (1955).
18. Funt, B. L., and Sutherland, T. H., *Can. J. Chem.* **30,** 940 (1952).
19. Mead, D. J., and Fuoss, R. M., *J. Am. Chem. Soc.* **63,** 2832 (1941).
20. Mead, D. J., and Fuoss, R. M., *J. Am. Chem. Soc.* **64,** 2389 (1942).
21. Fuoss, R. M., *J. Am. Chem. Soc.* **63,** 378, 2410 (1941).
22. Ehrlich, P., and de Lollis, N. J., *J. Research Natl. Bur. Standards* **51,** 145 (1953).
23. Williams, M. L., Landel, R. F., and Ferry, J. D., *J. Am. Chem. Soc.* **77,** 3701 (1955).
24. Ferry, J. D., and Landel, R. F., *Kolloid-Z.* **148,** 1 (1956).
25. Wiley, R. H., and Brauer, G. M., *J. Polymer Sci.* **3,** 647 (1948).
26. Cole, K. S., and Cole, R. H., *J. Chem. Phys.* **9,** 341 (1941).
27. Davidson, D. W., and Cole, R. H., *J. Chem. Phys.* **19,** 1484 (1951).
28. Hoffman, J. D., and Axilrod, B. M., *J. Research Natl. Bur. Standards* **54,** 357 (1955).
29. Hoffman, J. D., *J. Chem. Phys.* **23,** 1331 (1955).
30. Deutsch, H., Hoff, E. A. W., and Reddish, W., *J. Polymer Sci.* **13,** 565 (1954).
31. Heijboer, I., *Kolloid-Z.* **148,** 36 (1956).
32. Williams, M. L., and Ferry, J. D., *J. Polymer Sci.* **11,** 169 (1953).
33. Strella, S., and Zand, R., unpublished measurements.
34. Thurn, H., and Wolf, K., *Kolloid-Z.* **148,** 16 (1956).
35. Williams, M. L., and Ferry, J. D., *J. Colloid Sci.* **9,** 479 (1954).
36. Sato, K., Nakane, H., Hideshima, T., and Iwayanagi, S., *J. Phys. Soc. Japan* **9,** 413 (1954).
37. Fuoss, R. M., *in* "The Chemistry of Large Molecules," edited by R. E. Burk and O. Grummitt. Interscience, New York, 1943.

JOURNAL OF COLLOID SCIENCE **13**, 472–482 (1958)

AEROSOL SIZE AND RELATIVE HUMIDITY[1]

Clyde Orr, Jr., F. Kenneth Hurd, and William J. Corbett

Georgia Institute of Technology, Atlanta, Georgia

Received April 18, 1958

ABSTRACT

A theoretical and experimental investigation was made of the gain and loss of water with humidity change for particles of NaCl, $(NH_4)_2SO_4$, $CaCl_2 \cdot 6H_2O$, AgI, PbI_2, and KCl having radii between 0.01 and 0.1 micron. Predictions were made using a combination of adsorption theory, the Kelvin equation, Ostwald's theory, and other thermodynamic considerations. Where actual data were nonexistent, empirical relations were employed to arrive at reasonable approximations.

The indicated behavior of hygroscopic particles exposed to increasing humidity is to adsorb moisture amounting to a few molecular layers at low relative humidities; to dissolve as humidity increases, becoming saturated droplets and at the same time undergoing an abrupt size increase; and thereafter, as humidity increases still further, to grow larger and more dilute. The indicated behavior for decreasing humidity is for the droplet size to decrease as humidity decreases and, at a humidity considerably lower than that at which the particle initially dissolved, to recrystallize, undergoing an abrupt size decrease. For nonhygroscopic compounds, no abrupt solution or recrystallization irregularities are predicted. The predictions are in satisfactory agreement with experimental findings.

INTRODUCTION

The behavior of aerosol particles and droplets under varying humidities is of practical concern in studies of air pollution, visibility, microwave energy propagation, aircraft icing, fog formation, artificial weather modification, and cloud physics in general. For certain conditions the characteristics to be expected have been established by previous investigators. La Mer and associates (1, 2) showed that liquid droplets follow the Kelvin equation at least to sizes as small as 0.03 μ radius. Insoluble solid particles pick up small amounts of moisture by physical adsorption in accordance with one of several equations (3). Soluble aerosol particles, as shown by Junge (4) for the case of very small atmospheric ions, are solids at low

---

[1] The work reported herein was conducted at the Georgia Institute of Technology, Engineering Experiment Station, through sponsorship of the Geophysics Research Directorate, Air Force Cambridge Research Center, Air Research and Development Command, under Contract No. AF 19(604)-1086. Reproduction of this article in whole or in part is permitted for any purpose of the United States Government.

humidities and dissolved droplets at high humidities, undergoing a transition at some intermediate condition.

The purpose of this article is to describe the behavior of solid (at low humidities) hygroscopic aerosol particles over a wide range of humidities and to show that results in reasonable agreement with experimental ones may be estimated, although extension of data into regions of supersaturation are required.

THEORETICAL

A. Solid Particles at Low Relative Humidities

All solids in contact with the atmosphere attract a part of the atmosphere's gases to their surface because of unsatisfied molecular forces in their surface layers. The most condensable gases are adsorbed in the greatest quantities, so, even at low relative humidities, some water vapor is present on aerosol particles. For adsorption occurring on a free surface, i.e., one not exhibiting capillary cracks or pores, physical adsorption is expressed by the relation (5)

$$\frac{v}{v_m} = \frac{C\left(\frac{P}{P_0}\right)}{\left(1 - \frac{P}{P_0}\right)\left[1 + (C - 1)\frac{P}{P_0}\right]}, \qquad [1]$$

where v = volume of gas adsorbed at pressure P, v_m = volume of adsorbed gas to give a unimolecular film over the entire adsorbing surface, P = adsorbing gas pressure, P_0 = vapor pressure of adsorbing gas at experimental temperature, and $C = e^{(E_1 - E_L)/RT}$; where E_1 = heat of adsorption of gas in first layer, E_L = heat of liquefaction of gas, R = gas constant, and T = absolute temperature, °K.

The quantity $E_1 - E_L$ is considered to be the energy released by the adsorbing gas or vapor above that normally released by condensation. Ordinarily it is calculated from adsorption measurements. Lacking experimental data for water vapor adsorbed on the materials of interest, values for the quantity were obtained by assuming that, if the solid dissolves in the condensed vapor, the adsorbed vapor satisfies the surface forces of the solid, or that $E_1 - E_L$ is approximately equal to the surface energy of the solid. Surface energies have been measured and also calculated from theoretical considerations for some of the more common materials.

Granted the validity of the assumption regarding the quantity $E_1 - E_L$, the ratio v/v_m of Eq. [1] may be calculated for any relative humidity and temperature when surface energy data are available. For example, sodium chloride, having a surface energy (6) of 276 ergs/cm.^{2}, exposed to water vapor, each molecule of which, according to Livingston (7), occupies

10.8 A^2, would at 25° C. and 30% relative humidity be covered with a film of water averaging 1.42 molecules thick. Therefore a single NaCl particle with a diameter of 0.05 μ when dry is predicted to increase in size by approximately 0.001 μ or about 2% owing to adsorbed water. The contribution of physically adsorbed water is thus not great as far as size is involved.

Figure 1 presents curves (segment *A*) calculated in this fashion for the materials studied. Surface energy data were taken from the literature or estimated from Fig. 2, which shows surface energies as a function of cold water solubility.

B. Transition from Solid Particles to Droplets

If a particle is soluble in water, its adsorption of water vapor will cause it to gain a water envelope which may then dissolve the particle at some relative humidity less than 100%. To predict the humidity at which a solid surrounded by its liquid film will shift into a completely dissolved droplet requires that assumptions be made regarding the state of the liquid film. Very probably a concentration gradient actually exists across it during the transition, the inner layer being nearly a concentrated solution while the outer layer is more nearly pure water. For present purposes, it will be

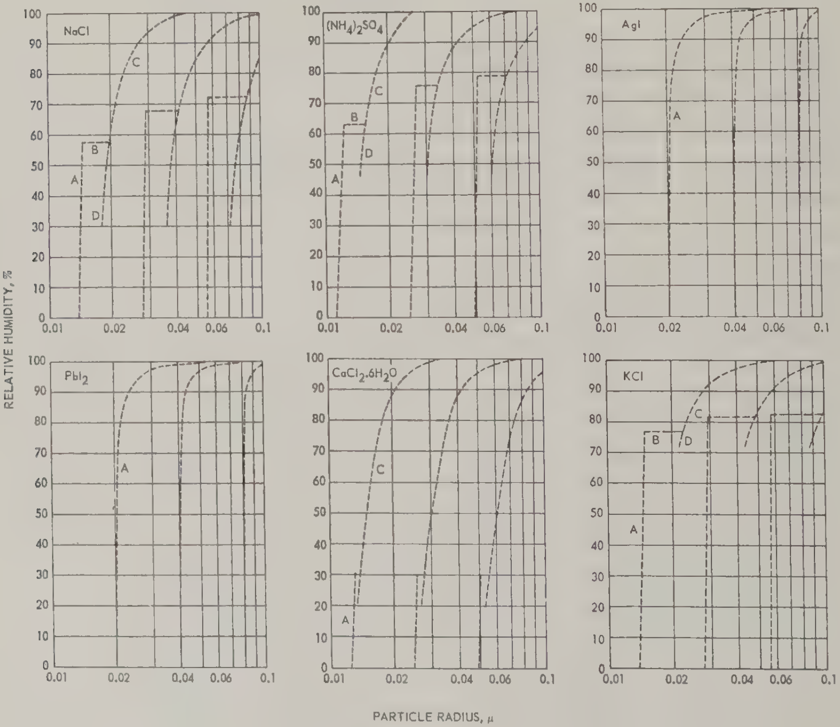

FIG. 1. Calculated aerosol size as a function of relative humidity.

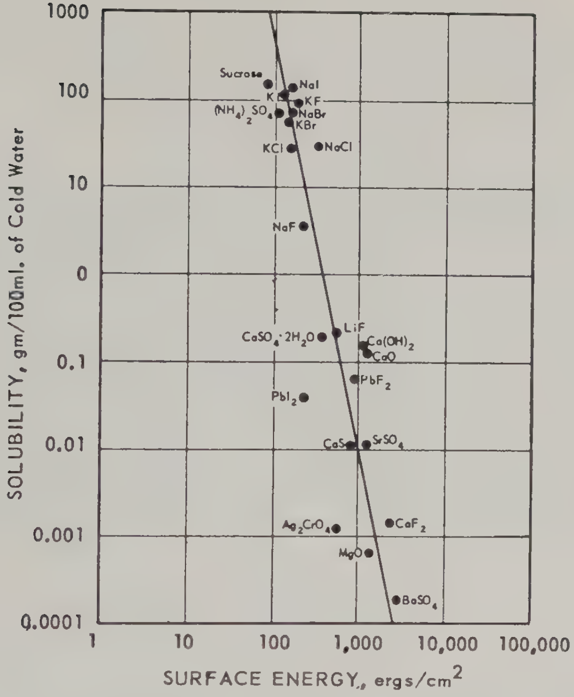

FIG. 2. Surface energy as a function of cold water solubility.

assumed that there is no concentration gradient across the liquid phase. The undissolved particle with its film of liquid surrounded by air containing water vapor will be considered as a three-phase system in equilibrium. The undissolved particle will be considered as in equilibrium with a saturated solution, the concentration of which is discussed below. The liquid film surrounding the particle will be considered to be in equilibrium with the atmosphere.

The film of liquid surrounding a particle will exhibit a vapor pressure like any other liquid, and this pressure will determine whether more vapor condenses from the atmosphere or whether some of the film evaporates. The vapor pressure will, however, be altered by two independent effects. The dissolved component will reduce the vapor pressure as shown by Raoult's law and the film's very great curvature will increase its vapor pressure. This increase in vapor pressure is given by the Kelvin equation.

The concentrations of solutions in equilibrium with small particles are dependent on particle size and surface energy, as well as temperature and the other usual considerations. The smaller the size, the greater is the concentration of the solution with which the particle is in equilibrium. The relationship between particle size, surface energy, and equilibrium concentration can be obtained for ionic solutions from considerations of the first law of thermodynamics and the Gibbs free energy. This fundamental expression is

$$\ln\left(\frac{a_2}{a_1}\right) = \frac{2\sigma M}{\rho RT}\left(\frac{1}{r_2} - \frac{1}{r_1}\right), \qquad [2]$$

where a_1 = activity of solute in a solution produced with particles of radius r_1 (r_1 is usually chosen sufficiently large for the term $1/r_1$ to be negligible), a_2 = activity of solute in a solution produced with particles of radius r_2, σ = surface free energy of solute, M = molecular weight of solute, ρ = density of solute, R = gas constant, 8.32×10^7 dynes cm./gram-mole °K, and T = absolute temperature, °K. This relation is quite general and holds regardless of the extent of dissociation of the solute into ions. When the necessary data are available, the activity of the solute in a film of liquid adhering to a particle can be calculated. From this solute activity the vapor pressure of the solution can be determined as outlined in a following section.

In the absence of activity data, an approximate equation of Dundon and Mack (8)

$$i \ln\left(\frac{S_2}{S_1}\right) = \frac{2\sigma M}{\rho RT}\left(\frac{1}{r_2} - \frac{1}{r_1}\right), \qquad [3]$$

where S_2 = solubility of a small particle of radius r_2, S_1 = solubility of a large particle (usually taken as one of infinite size) of radius r_1, and i = van't Hoff factor, can be used to approximate the concentration of a solution that would exist in equilibrium with a small solute particle. Because of insufficient data it was necessary to use Eq. [3] instead of Eq. [2] in the case of $(NH_4)_2SO_4$, for example.

Curvature of surface is related to vapor pressure by the Kelvin equation

$$\ln\left(\frac{p}{p_0}\right) = \frac{2M_s\gamma}{RT\rho_s r}, \qquad [4]$$

where p = vapor pressure of a solution droplet of radius r (= partial pressure of water vapor in air = water vapor pressure × per cent relative humidity), P_0 = vapor pressure of a solution of infinite extent, M_s = molecular weight of solvent, γ = surface tension of solution, R = gas constant, 8.32×10^7 dynes cm./gram-mole °K, T = absolute temperature, ρ_s = solution density, and r = droplet radius.

These relations predict, as may easily be seen, that a soluble particle will shift rather suddenly into a liquid droplet. As relative humidity increases, the particle which already was enveloped in a film of absorbed water, picks up a little more water from the surroundings. The extra solvent dilutes the liquid of the film so that it is no longer saturated with respect to the solid inside. As a result, more material is dissolved from the surface of the particle, thereby reducing its size. But as particle size decreases, the concentration of solution with which the particle can be in equilibrium increases. Increased solution concentration reduces vapor pressure, and causes more moisture to be condensed from the atmosphere; moisture condensing causes the particle to grow in size, reducing surface curvature and reducing vapor pressure still further. At a certain relative humidity the situation clearly is unstable, and equilibrium is re-established only after the complete dissolution of the particle.

The relative humidity just below that at which a particle dissolves may be calculated, assuming, of course, that the conditions postulated and the relations expressing them mathematically, as given above, are reasonably correct. For example, a cubical particle of NaCl 0.04 μ on an edge has a surface area equal to, and for purposes of this calculation equivalent to, a spherical particle having a radius of 0.0277 μ. Using a surface energy of 276 ergs/cm.^{2}, a solute density of 2.163 g./cm.^{3}, an activity of 0.986 for a saturated solution of bulk material at 25° C., solution of Eq. [2] gives the change in activity due to particle size, yielding a value of 1.22 for a_2. From a plot of solute activity versus solution vapor pressure, the vapor pressure of this solution, assuming it to be of infinite extent, is 15.70 mm. Hg.

With the vapor pressure established, other quantities were then evaluated for substitution into the Kelvin equation (Eq. [4]) to arrive at the corresponding relative humidity. This equation requires information on concentration, surface tension, and solution density among other things. Such data are not easily obtainable for supersaturated solutions. They usually must be obtained by extrapolation and estimation; the details of these methods are also discussed in a following section. Once obtained, these values, when substituted into Eq. [4], yielded a vapor pressure of 16.25 mm. Hg for the droplet. Compared with a water vapor pressure at 25° C. of 23.75 mm. Hg, this represents a relative humidity of 68.5%. Thus it is predicted that a cubical particle of NaCl 0.04 μ on an edge will dissolve in the film condensed about it when the relative humidity reaches 68.5%.

The solubility, the surface curvature, and all the other factors determining the condition of solubility change with particle size. As a result the shift from particle to droplet occurs at lower and lower relative humidities as particle size decreases. As size increases the change-point becomes asymptotic to a line drawn, in the case of NaCl, at about 75% relative humidity, indicating that large particles would all go into solution at this point. This value compares favorably with the 75.5% given by Twomey (9) for NaCl particles observable in the microscope.

Segments *B* of Fig. 1 present the calculated transition points. Predicted curves are not given for $CaCl_2 \cdot 6H_2O$, AgI, and PbI_2 because the necessary data could not be found. However, rough estimates show that the $CaCl_2 \cdot 6H_2O$ transition would fall below about 15%, whereas the AgI and PbI_2

transition would lie well above the highest relative humidity employed experimentally, about 95%.

C. Droplets and Increasing Relative Humidity

Once a particle is dissolved, the droplet's further growth with increasing relative humidity is described by the Kelvin equation using the properties of the solution and paying particular attention to the vapor pressure lowering due to dissolved components. Segments *C* of Fig. 1 were calculated in this manner. The necessary data in the cases of AgI and PbI_2 could not be found, and, if they were available, would undoubtedly have applied only to extremely high relative humidities.

D. Droplets and Decreasing Relative Humidity

As relative humidity decreases, droplet size decreases. The Kelvin equation is equally applicable to decreasing relative humidity and size conditions as it is to increasing ones. For concentrations greater than the normal limits of solubility, this equation was employed to obtain segments *D* in Fig. 1 using extrapolated vapor pressure, surface tension, and density data.

A droplet subjected to decreasing relative humidity conditions is predicted to follow first down segment *C*, then down segment *D* for an undetermined distance, and finally shift suddenly back to *A*. Below the humidity condition established by the intersection of lines *B*, *C*, and *D*, i.e., line *D*, conditions must be regarded as metastable because the droplet solution is supersaturated. At present there are no good methods for predicting the point at which a supersaturated solution will crystallize. When crystallization does occur, it will occur spontaneously and the particle size will shift over to line *A*. This explains the often-noted lingering of smogs (2) below the humidities at which they first appeared.

E. Methods of Arriving at Supersaturated Solution Data

Vapor pressures of aqueous NaCl solutions at 25° C., the concentrations of which were greater than the normal limit of solubility (26.4% by weight), were predicted by extrapolation of the activity coefficients of NaCl in unsaturated solutions. The values of these coefficients up to concentrations of 6.0 molal were taken from Robinson and Stokes (10). They were plotted versus concentration and the resulting curve was extrapolated to 15.0 molal using as a guide for the extrapolation similar curves for LiCl and $CaCl_2$. The activity coefficient curves for these latter materials are similar to that of NaCl below 6.0 molal, and, owing to the high solubility of these compounds, data are available for them over a greater range. The validity of this extrapolation for NaCl is supported by the fact that experimental data are available for some materials, in particular $CaCl_2$, in the supersaturated region, and for such materials, the curves extend smoothly from the unsaturated to the supersaturated region.

From the activity coefficients of NaCl in solution obtained by the extrapolation, NaCl activities were calculated using the relationship

$$a_s^{1/2} = \gamma_s m, \qquad [5]$$

where a_s = the activity of NaCl in solution, γ_s = the activity coefficient of NaCl in solution, and M = the molality of the solution.

The solvent, or water, activity was calculated from the activities of NaCl by the relationship

$$\ln\left(\frac{a'_w}{a_w}\right) = -\int_{a_s}^{a'_s} \frac{x_s}{x_w}\, d \ln a_s, \qquad [6]$$

where a'_w = the activity of the solvent at the mole fraction x'_w of the solvent, a_w = the activity of the solvent at the mole fraction x_w of the solvent, a'_s = the activity of NaCl at the mole fraction x'_s of NaCl, and a_s = the activity of NaCl at the mole fraction x_s of NaCl.

Since the solvent activity, a_w, is defined as the ratio of the partial pressure of the solvent p_1 at concentration, x_w, to the vapor pressure of the pure solvent, $p_1{}^0$, the relationship

$$a_w = \frac{p_1}{p_1^0} \qquad [7]$$

can be written. Hence,

$$\ln\left(\frac{a'_w}{a_w}\right) = \ln\left(\frac{p'_1}{p_1}\right). \qquad [8]$$

Equation [6], requiring graphical integration for evaluation, was written in the form

$$\ln\left(\frac{p'_1}{p_1}\right) = -\int_{a_s}^{a'_s} \frac{x_s}{a_s\,(1 - x_s)}\, da_s, \qquad [9]$$

where p'_1 = the partial pressure of the solvent at the concentration where the NaCl activity = a'_s, and P_1 = the partial pressure of the solvent at the concentration where the NaCl activity is a_s. By means of Eq. [9] and the data of Robinson and Stokes (10) for the activity of aqueous solutions of NaCl, curves of vapor pressure versus solute activity and vapor pressure versus solution concentration were predicted for solutions up to 50% by weight of NaCl. The curve of vapor pressure versus solution concentration checked very closely with data from the *International Critical Tables* for the unsaturated region (11), lending confidence in the accuracy of the supersaturated portion of the curves.

The vapor pressures of $(NH_4)_2SO_4$ solutions were predicted from the equation of Edgar and Swann (12),

$$\ln\left(\frac{p_1}{p_2}\right) = i(x_2 - x_1) - \frac{Q}{R}\left(\frac{1}{T_1} - \frac{1}{T_2}\right), \tag{10}$$

where p_1 = the vapor pressure of the solution of mole fraction x_1 at temperature T_1, p_2 = the vapor pressure of the solution of mole fraction x_2 at temperature T_2, Q = the heat of vaporization of H_2O, R = gas constant, 1.987 cal./gram-mole °C., and i = the van't Hoff factor, using the data of these same investigators for saturated solutions. The vapor pressures of aqueous $(NH_4)_2SO_4$ solutions, at 25° C., were predicted in this manner from zero to 75% concentration by weight. The van't Hoff factor, calculated as shown below, was assumed to be constant for these calculations. The vapor pressure curve calculated in this manner checked very well in the unsaturated region with data from the International Critical Tables (13), indicating that vapor pressures for the supersaturated region predicted in this manner are reasonably correct.

Vapor pressures of aqueous $CaCl_2$ solutions at 25°C. were obtained by means of Eq. [8], these activities having been determined well into the supersaturated region (14).

Activity and vapor pressure data for KCl solutions at 25° C. were obtained from Robinson *et al.* (15).

The van't Hoff factor for $(NH_4)_2SO_4$ was calculated from data on the vapor pressure lowering (16), boiling point elevation (17), and freezing point lowering (18). Because of the lack of data in the supersaturated region, the van't Hoff factor was evaluated from data at saturation. Other properties of solutions show no discontinuity in going from the saturated to the supersaturated region; therefore it was assumed that the van't Hoff factors behave in a similar manner. Also, these factors do not change value appreciably with concentration in the unsaturated region, thus indicating that use of the values obtained at saturation for slightly supersaturated solutions does not greatly affect the accuracy of the calculations.

Data for the surface tension (19, 20) and solution density (21, 22) for NaCl and $(NH_4)_2SO_4$ in the unsaturated region were obtained from the *International Critical Tables*. The data of Harkins and Gilbert (23) for surface tension and solution density of unsaturated $CaCl_2$ solutions were used. The surface tension data for unsaturated KCl solutions were obtained from the work of Jones and Ray (24). The solution densities of unsaturated KCl solutions were obtained from the *International Critical Tables* (25). Surface tension and solution density curves, for the compounds considered, were extended into the supersaturation region by simple extrapolation.

The normal limit of solubility for all compounds considered was obtained from the data of Seidell (26).

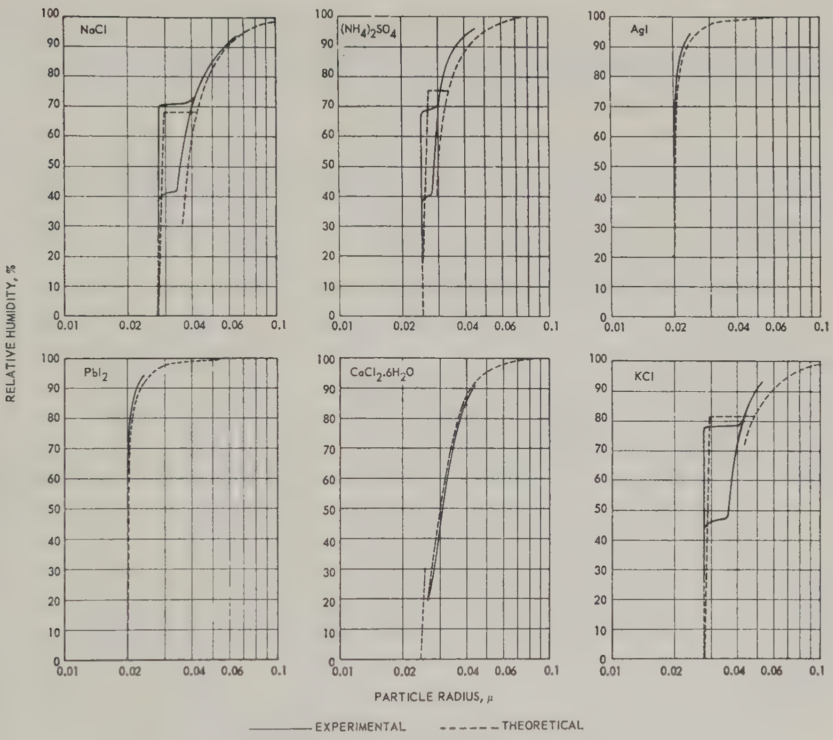

FIG. 3. Comparison of experimental and calculated results.

EXPERIMENTAL

Since the experimental apparatus and technique are described elsewhere (27, 28), they will not be dwelt on here. Both were patterned after the descriptions of Israel (29) and Junge (4). Briefly it may be stated that particle (and droplet) size and size change were determined from mobility measurements, i.e., the movement of the particles under imposed electric fields. Refinements in the method of interpretation of the mobility data allowed specific size information to be obtained in contrast to earlier work which yielded only average values for the entire size distribution. Crystal or low-humidity particle size was confirmed with electron photomicrographs.

The results in every case checked the predicted curves. Typical correspondence of calculated and experimental data is shown by curves in Fig. 3.

CONCLUSIONS

Making assumptions which were supported by experimental data from similar systems or comparable conditions, the behavior of aerosol particles was calculated under changing humidity conditions. With better data for the properties of surfaces and supersaturated solutions, more exact predictions could undoubtedly have been obtained. The methods employed are believed valid for particles of compositions other than those studied.

REFERENCES

1. La Mer, V. K., and Gruen, R., *Trans. Faraday Soc.* **48,** 410 (1952).
2. La Mer, V. K., and Cotson, S., *Science* **118,** 516 (1953).
3. Brunauer, S., "The Adsorption of Gases and Vapors." Princeton University Press, Princeton, New Jersey, 1945.
4. Junge, C., *Ber. deut. Wetterdienstes, U. S. Zone* **38,** 264 (1952).
5. Brunauer, S., Emmett, P. H., and Teller, E., *J. Am. Chem. Soc.* **60,** 309 (1938).
6. Van Zeggeren, F., and Benson, G. C., *Can. J. Chem.* **35,** 1150 (1957).
7. Livingston, H. K., *J. Colloid Sci.* **4,** 447 (1949).
8. Dundon, M. L., and Mack, E., Jr., *J. Am. Chem. Soc.* **45,** 2479 (1923).
9. Twomey, S., *J. Appl. Phys.* **24,** 1099 (1953).
10. Robinson, R. A., and Stokes, R. H., "Electrolyte Solutions." Academic Press, New York, 1955.
11. "International Critical Tables," Vol. 3, p. 297. McGraw-Hill, New York, 1933.
12. Edgar, Graham, and Swann, W. O., *J. Am. Chem. Soc.* **44,** 570 (1928).
13. "International Critical Tables," Vol. 3, p. 363. McGraw-Hill, New York, 1933.
14. Stokes, R. H., *Trans. Faraday Soc.* **41,** 637 (1945).
15. Robinson, R. A., and Stokes, R. H., "Electrolyte Solutions." Academic Press, New York, 1955.
16. Robinson, R. A., and Stokes, R. H., "Electrolyte Solutions," p. 363. Academic Press, New York, 1955.
17. Robinson, R. A., and Stokes, R. H., "Electrolyte Solutions," p. 325. Academic Press, New York, 1955.
18. Robinson, R. A., and Stokes, R. H., "Electrolyte Solutions," p. 255. Academic Press, New York, 1955.
19. "International Critical Tables," Vol. 4, p. 465. McGraw-Hill, New York, 1933.
20. "International Critical Tables," Vol. 4, p. 464. McGraw-Hill, New York, 1933.
21. "International Critical Tables," Vol. 3, p. 80. McGraw-Hill, New York, 1933.
22. "International Critical Tables," Vol. 3, p. 60. McGraw-Hill, New York, 1933.
23. Harkins, W. D., and Gilbert, E. C., *J. Am. Chem. Soc.* **48,** 604 (1926).
24. Jones, Grinnel, and Ray, W. A., *J. Am. Chem. Soc.* **59,** 187 (1937).
25. "International Critical Tables," Vol. 3, p. 87. McGraw-Hill, New York, 1933.
26. Seidell, A., "Solubilities of Inorganic and Metal Organic Compounds," Vol. 1, 3rd ed. Van Nostrand, New York, 1940.
27. Orr, Clyde, Jr., Hurd, F. Kenneth, Hendrix, Warren P., and Corbett, William J., "An Investigation into the Growth of Small Aerosol Particles with Humidity Change." Final Report, Project No. A-162, Engineering Experiment Station of the Georgia Institute of Technology, Atlanta, Georgia, December 31, 1956.
28. Orr, Clyde, Jr., Hurd, F. Kenneth, Hendrix, W. P., and Junge, Christian, "The Behavior of Condensation Nuclei under Changing Humidities." To be published by the *J. Meteorol.* **15,** No. 2 (1958).
29. Israel, H., *Gerlands Beitr. Geophys.* **31,** 173 (1931).

JOURNAL OF COLLOID SCIENCE **13**, 483–487 (1958)

THE SWELLING BEHAVIOR OF NATURAL RUBBER LATEX

P. W. Allen

The British Rubber Producers' Research Association, Herts, England

Received May 2, 1958

Abstract

The distribution of a swelling agent (methyl methacrylate) among the particles of natural rubber latex has been shown to be nonuniform. Large particles absorb more swelling agent than do small particles. The data are analyzed by means of the thermodynamic treatment of Morton, Kaizerman, and Altier.

Introduction

The distribution of a swelling agent among the particles of natural rubber latex is of interest in connection with several problems. A study by Morton, Kaizerman, and Altier (1) indicated that the equilibrium uptake of swelling agents by latex particles should increase with particle size, and experiments with polystyrene latex quantitatively confirmed their equation. From this it seemed likely that, in the case of a very heterodisperse latex such as natural rubber, the distribution of a swelling agent should be nonuniform, favoring the larger particles. This paper describes a test of this hypothesis, using as swelling agent a vinyl monomer methyl methacrylate. This choice was made because of interest in vinyl polymerization in rubber latex (2).

Experimental

The latex used was a 60 % commercial concentrate, diluted to the concentration stated with 1.5 % ammonia solution.

The monomer contents of latex particles of various sizes were obtained by making use of an oil-soluble dye Waxoline Blue (Imperial Chemical Industries Ltd.). If monomer containing 0.5 %–1 % of this dye is added to dilute (2 % solids) latex, some of the monomer dissolves in the serum and a small amount of the dye is precipitated. This precipitate can be removed by filtration. It is assumed that the amount of monomer in an individual particle is proportional to the amount of dye in it, which can be estimated colorimetrically. The swollen latex is fractionated by a centrifuging technique and the monomer content of each fraction is measured from the color.

The detailed procedure is as follows. The latex was diluted to give a solids content of 2% and a suitable amount of monomer (containing 1% of the dye) was added. The latex was rotated end-over-end for several hours and then filtered. About 40 ml. were placed in a centrifuge tube and centrifuged in a trunnion-type machine at 2000 r.p.m. (measured with a stroboscope). The centrifuge was stopped at intervals and 2 ml. of latex were removed from a fixed point in the centrifuge tube. The range of particle sizes corresponding to a given time of centrifuging was then calculated by Stokes' law; this is essentially the method of Nisonoff, Messer, and Howland (3). It is convenient that the density of methyl methacrylate is close to that of natural rubber so that, for a fixed particle radius, centrifuging behavior is not much affected by monomer content. The successive fractions are cumulative, each containing all particles less than a given size.

The 2 ml. samples were dried and weighed in tared dishes. A small quantity of benzene was added to each dish, which was then covered and left until the dye was uniformly distributed; the amount of added benzene was checked by reweighing. The color of the benzene solutions was measured in a colorimeter (Hilger-Spekker). Calibration measurements with the dyed monomer at various concentrations in benzene enabled the amount of monomer in each dish to be measured. Control experiments in which a known amount of dyed monomer was added to latex, which was not subsequently fractionated, showed that the method for monomer estimation was quantitatively satisfactory.

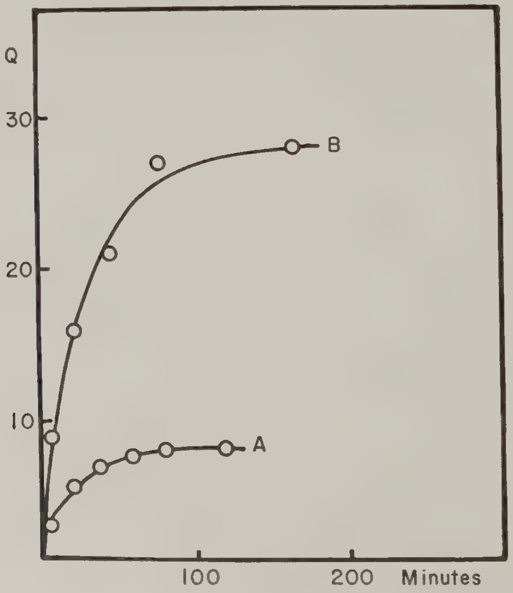

FIG. 1. Uptake of swelling agent as a function of time. Comparison between whole latex (curve *A*) and a large-particle fraction (curve *B*).

RESULTS

It was first necessary to establish that natural rubber latex behaved qualitatively in the same way as polystyrene latex towards swelling agents. Figure 1 shows the swelling ratio Q measured as a function of time for (a) a whole latex; (b) a large-particle fraction from the same latex, obtained by fractional creaming with ammonium alginate (4). The equilibrium uptake of methyl methacrylate by the large-particle fraction is substantially greater than that of the whole latex. The relative *rate* of swelling of the large-particle fraction is somewhat less, owing to the smaller surface area. The results of Fig. 1 were obtained by rotating latex/monomer mixtures end-over-end at room temperature for varying times, followed by separation of the undissolved monomer by centrifuging.

Of more interest is the distribution of monomer among the latex particles in a whole latex, measured by the procedure described in the last section. Figure 2 shows the results for three different ratios of added monomer to

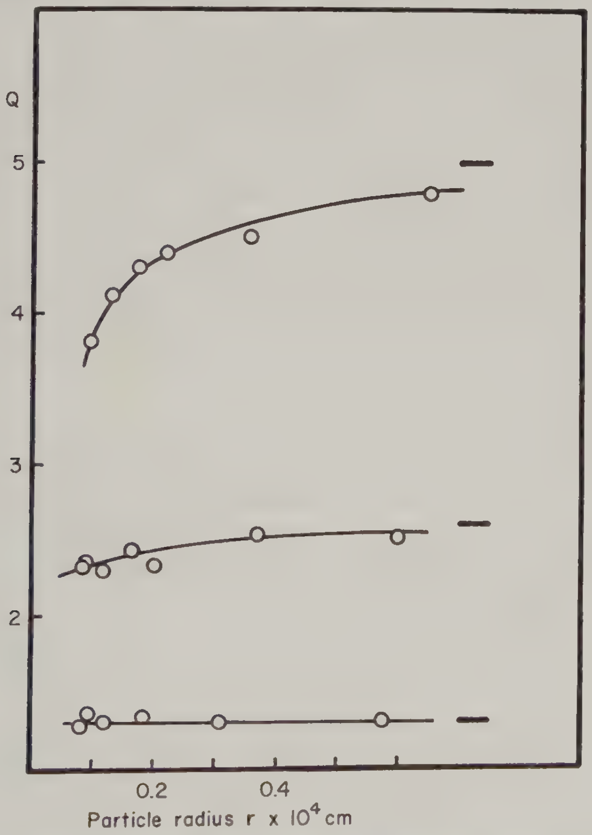

FIG. 2. Cumulative values of Q as a function of particle radius. The heavy lines represent the overall values of Q for each experiment.

latex, corresponding to swelling ratios of 1.3, 2.6, and 5.0. For larger amounts of monomer the swollen latices were insufficiently stable for examination.

The particle radius scale is only semiquantitative, since its assessment depends on exact measurements of the geometry of the centrifuge, e.g., distance from axis of rotation to sampling point, which are difficult to perform with the instrument used. The data represent 70% of the total latex; the smallest particles were not centrifuged under the conditions used. Two points should be borne in mind in examining Fig. 2: (*a*) the *Q*-scale is cumulative, since each sample removed from the centrifuge contains all particles of sizes less than that plotted; (*b*) the particle radii are, of necessity, those for the swollen particles.

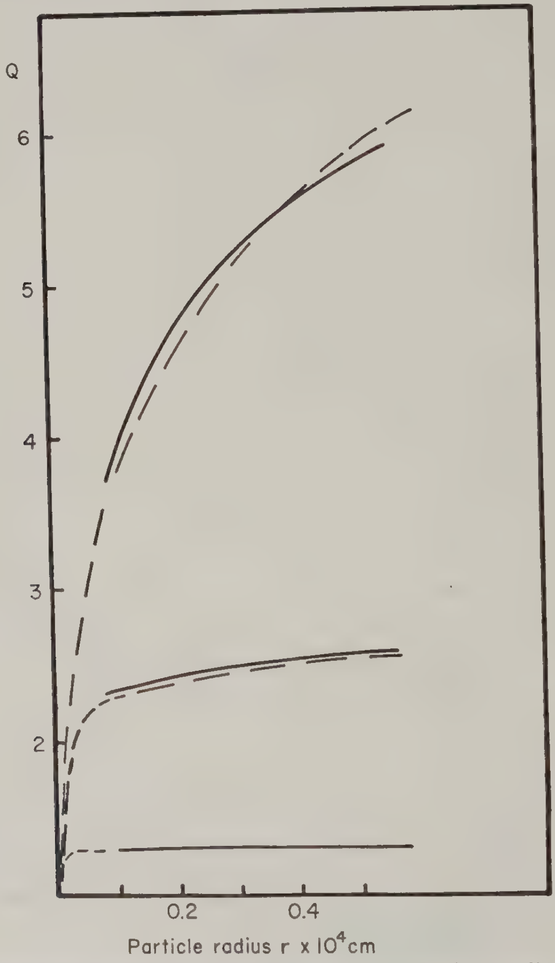

FIG. 3. Theoretical values of *Q* as a function of particle radius. The solid lines are computed from the experimental values of $Q_{cum.}$.

Discussion

The thermodynamics of swelling of small particles has been evaluated by Morton *et al.* (1). The equation they derive is analogous to that for the swelling of a polymer network (5), the force opposing swelling being, instead of a network, the interfacial free energy between latex particles and serum

$$\Delta G = RT\,[\ln (1 - v_2) + v_2 + \chi v_2^2] + 2V_1\gamma/r = 0, \qquad [1]$$

where $v_2 = 1/Q$, is the volume fraction of rubber in the swollen particle; χ is the Flory-Huggins interaction constant; V_1 is the molar volume of the swelling agent; γ is the interfacial energy; and r is the particle radius. Equation [1] predicts that the equilibrium swelling ratio will increase with particle size and will be very dependent on χ. Figure 1 shows qualitatively that the particles of natural rubber latex exhibit the expected behavior. Since the particle sizes in this case were not known, quantitative comparison is not possible.

The situation in the second experiment (Fig. 2) is that where the amount of swelling agent absorbed is less than the maximum uptake possible. Under these conditions which were imposed by stability considerations, the free energy of swelling should be equal for every particle size, being given by non-zero values of ΔG from Eq. [1]. In each experiment the value of ΔG at one particular experimental value of r (and v_2) was calculated from Eq. [1]. This value of ΔG was then used, in conjunction with Eq. [1], for the calculation of v_2 for other values of r. Figure 3 shows the resulting plot of Q against r for the three experiments of Fig. 2. The broken lines in Fig. 3 show the theoretical dependence. The experimental curves were obtained from the cumulative values of Q by using the relation

$$Q = Q_{\text{cum.}} + w\,\frac{dQ_{\text{cum.}}}{dw}, \qquad [2]$$

where w is the total concentration (rubber + monomer) of each fraction.

For the theoretical curves, χ was taken as 0.5 and γ as 10 dynes/cm. These were considered to be reasonable values, though a closer fit could probably be obtained by adjustment. The agreement between the theoretical and experimental curves of Fig. 3 provides additional evidence for the validity of the thermodynamic treatment of Morton and co-workers.

This work forms part of a program of research undertaken by the Board of The British Rubber Producers' Research Association.

References

1. Morton, M., Kaizerman, S., and Altier, M. W., *J. Colloid Sci.* **9**, 300 (1954).
2. Bloomfield, G. F., and Swift, P. McL., *J. Appl. Chem.* **5**, 609 (1955).
3. Nisonoff, A., Messer, W. E., and Howland, L. H., *Anal. Chem.* **26**, 856 (1954).
4. Schmidt, E., and Kelsey, R. H., *Ind. Eng. Chem.* **43**, 406 (1951).
5. Flory, P. J., "Principles of Polymer Chemistry," p. 576ff. Cornell University Press, Ithaca, New York, 1953.

JOURNAL OF COLLOID SCIENCE **13,** 488–499 (1958)

DIELECTRIC RELAXATION OF POLYOXYETHYLENE GLYCOL (POEG) IN TOLUENE

A. B. Ruigrok and J. J. Hermans[1]

Laboratorium voor Anorganische en Fysische Chemie, Universiteit, Leiden

Received May 12, 1958

Abstract

Dielectric losses have been determined for polyoxyethylene glycol in toluene in the frequency ranges 0.3–300 kc. and 5–18 Mc. In one series, in the low-frequency range, the solvent was dioxane. The corrections necessary for the effects of certain undesired impedances in the measuring circuit are discussed in some detail because the losses are quite small. A simple Debye loss curve with a single relaxation time independent of molecular weight was found in the neighborhood of 6 Mc. Some very weak indications for the existence of a second dispersion at much lower frequencies are described, but they cannot be considered as convincing. The results are discussed in the light of recently developed theories.

The present work is concerned with the dielectric losses of POEG in toluene (in one series also in dioxane). These losses were found to be so small that corrections for parasitic impedances had to be considered carefully. For this reason, although the measurements were carried out in a commercial apparatus, some technical details will have to be discussed.

Apparatus; Evaluation of the Measurements

Frequencies Ranging from 0.5 to 30 Mc.

The cell containing the liquid was constructed in the manner described by de Brouckère and van Nechel (1); as a thermostat we used a Haake thermostating jacket, connected to a "Kältespeicher," Model *K*. The generator was a "Leistungs Mesz-sender" SMLR (Rhode and Schwarz, Munich), the detector an Eddystone receiver, Model 680-C, combined with either a Philips oscilloscope GM-5656 or an earphone or loudspeaker. As a bridge we used the Twin-T Impedance Measuring Circuit 821-A, General Radio Company. To measure an unknown admittance $Y_x = G_x + iB_x$, the bridge is first brought into balance, then connected to the unknown admittance and again brought into balance by adjusting the condensors C_G and C_B (see Fig. 1*a*). The values of G_x and B_x follow from the relations

$$G_x = (R\omega^2 C'C''/C''')(C_{G2} - C_{G1}); \qquad B_x = \omega(C_{B1} - C_{B2}),$$

where $\omega = 2\pi f$ (f is the frequency), while the index 1 refers to the situation before and the index 2 to that after adjustment.

---

[1] Present address: Cellulose Research Institute, State University College of Forestry at Syracuse University, Syracuse 10, New York.

For frequencies exceeding 5 MHz it is necessary to correct for the effects of impedances in the measuring circuit. These can be accounted for by the substitution diagram of Fig. 1*b*; the values of $L_c R_c L''$ and L′ are given by General Radio (2). It became apparent from our results, however, that the value of 6.1×10^{-9} henry given for L_c was not quite correct; it was redetermined by us, following a method indicated by Sinclair (3). To this end we made measurements with a condensor, using various initial

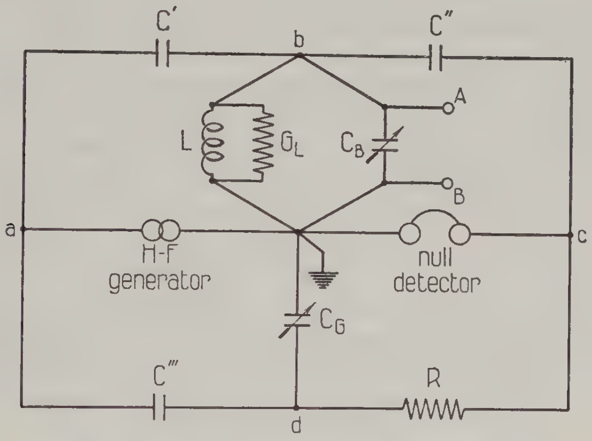

FIG. 1*a*. Principle of the Twin-T bridge.

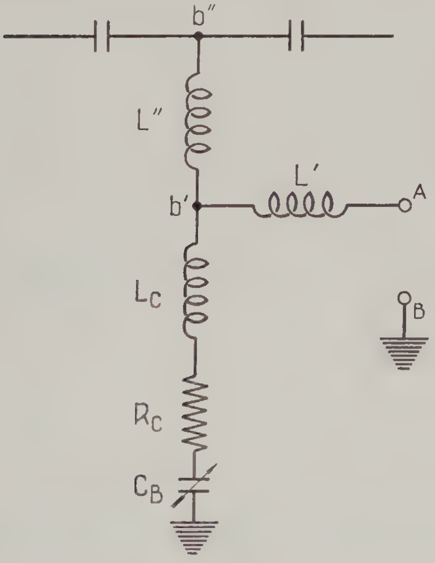

FIG. 1*b*. Substitution diagram for the susceptance condenser C_B.

values (C_1) of C_B. Both the initial and the adjusted value must be corrected for L_c, the effective capacitances being

$$C_1^* = C_1(1 - \omega^2 L_c C_1)^{-1}; \qquad C_2^* = C_2(1 - \omega^2 L_c C_2)^{-1}. \tag{1}$$

From these equations it follows that approximately:

$$C_1^* - C_2^* = C_x^* = (C_1 - C_2)[1 - \omega^2 L_c(C_1 + C_2)]^{-1}. \tag{2}$$

A plot of $C_1 - C_2$ versus $C_1 + C_2$ will, therefore, be a straight line with a slope $-\omega^2 L_c C_x^*$ and an intercept C_x^* with the ($C_1 - C_2$)-axis, so that L_c is found as $-(1/\omega^2)$ times the ratio between slope and intercept. It was found experimentally that L_c was a linear function of the frequency, being 5.3×10^{-9} henry at 30 Mc. and 4.2×10^{-9} henry at 1 Mc.

Using the values found for L_c, C_1^* and C_2^* were now calculated, and subtracted to give C_x^*, which is related to the real capacitance C_x as follows:

$$C_x^* = C_x(1 + \omega^2 L_x' C_x^*), \tag{3}$$

where L_x' is the sum of L' and L_x, the inductance of the cell. Plots of $1/C_x^*$ versus ω^2 are straight lines, from which L_x' can be derived. It was found that L_x' differed for different liquids in the cell, following a relation:

$$L_x' = 0.0545 + 0.700/C_x. \tag{4}$$

This can be explained by taking into account the capacitance C_a and inductance L_a of the connection between bridge and cell (see Fig. 2). Since the latter is present also in the absence of the cell, the effective capacitance is, in that case,

$$C_a^* = C_a(1 - \omega^2 L_a C_a)^{-1}.$$

After connecting the cell, the effective capacitance is

$$C_b^* = (C_a + C_x')[1 - \omega^2 L_a(C_a + C_x')]^{-1},$$

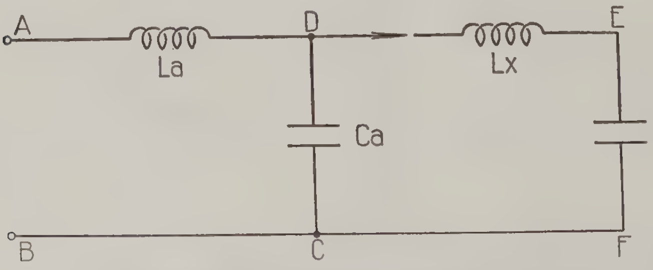

FIG. 2. Diagram of the connection between the cell and the Twin-T bridge (compare Fig. 1*a*).

where $C_x' = C_x(1 - \omega^2 L_x C_x)^{-1}$. From these equations it follows that, approximately,

$$1/C_x^* = 1/C_x - \omega^2(L_x + L_a + 2C_aL_a/C_x),$$

showing that a plot of $1/C_x^*$ against ω^2 gives, not L_x', but

$$L_x'' = L_x + L_a + 2C_aL_a/C_x,$$

in accordance with Eq. [4]. Using this equation, we calculated the L_x'' value specific for each substance. Substituting this for L_x' in Eq. [2] gives C_x. This is the total capacitance of the cell with the liquid, and may be written:

$$C_x = K\epsilon' + C_r, \tag{5}$$

where K and C_r are constants. Here C_r denotes the residual capacitance. We determined K and C_r by calibration with liquids for which the real part, ϵ', of the dielectric constant is known with accuracy (4): benzene, $\epsilon_{20}' = 2.2821$, $d\epsilon'/dT = -0.00199$; hexane,

$$\epsilon_{20}' = 1.888, \qquad d\epsilon'/dT = -0.0015.$$

This gave $K = 30.55 \pm 0.03$, $C_r = 5.45 \pm 0.02$, and determines ϵ' once C_x is known.

The imaginary part, ϵ'', of the dielectric constant is given by the ratio

$$\epsilon'' = G/\omega K, \tag{6}$$

where G is the conductance. The formula given by General Radio (2) to correct G for residual impedances is

$$G_x = [1 + \omega^2 L_x'(C_1^* - C_2^*)]^{-2}[G(1 - \omega^2 L'' C_1^*)^2 + R_c\omega^2(C_1^{*2} - C_2^{*2})]. \tag{7}$$

In view of the connection between bridge and cell, we replaced the factor $1 - \omega^2 L'' C_1^*$ in Eq. [7] by $1 - \omega^2 L''(C_a^* + C_1^*)$ and L_x' by L_x''. It was found, however, that the curves obtained for ϵ'' as a function of log f for all the solutions examined, including the pure solvent, showed an upward trend with increasing frequency f when f began to exceed 9 Mc. Now we must remember that the correction term $R_c\omega^2(C_1^{*2} - C_2^{*2})$ in Eq. [7] derives from a resistance in C_B. It is, therefore, indicated to assume a resistance R_x also in the circuit containing the cell, so that a proper balance can be achieved. Taking this into account we obtain, instead of Eq. [7]:

$$G_x = \frac{G[1 - \omega^2 L''(C_a^* + C_1^*)]^2 + R_c\omega^2(C_1^{*2} - C_2^{*2})}{[1 + \omega^2 L_x'(C_1^* - C_2^*)]^2} - R_x\omega^2 C_x^2. \tag{8}$$

To determine R_x we made use of the fact that ϵ'' of the pure solvent in the frequency range considered must be zero. This led to an R_x which increased with increasing frequency, suggesting a skin-effect. The values of R_x obtained were confirmed by accurate measurements with the empty cell: here again, the uncorrected ϵ'' was found to change with frequency, but on recalculating ϵ'' from Eq. [8], we found $\epsilon'' = 0$ in the entire frequency range examined.

Frequencies Ranging from 0.05 to 300 kc.

The generator was an R.C. oscillator 330-A, made by Peekel, Rotterdam, the detector an "Abstimmbarer Anzeigeverstärker UBM, BN-12121, made by Rhode and Schwartz, Munich, the bridge a Schering type "Capacitance Bridge," 716-C, of the General Radio Company (see Fig. 3 and reference 5). We used the substitution method.

Finally, the measuring cell was a DFL-1, made by the "Wissenschaftlich-Technische Werkstätten," Weilheim OBB, and the thermostat was the same as for the high-frequency range.

A variable capacitor 722-N of General Radio was used for C_p (see Fig. 3), in order to make it possible to choose a small value C_1 of the capacitor C_N. Here again $C_x = K\epsilon' + C_r$. The constants K and C_r were found by calibrating with toluene (6) and dioxane (4): $\epsilon_{25}(\text{tol}) = 2.3661$; $\epsilon_{25}(\text{diox}) = 2.314$; $d\epsilon/dT = -0.00338$. For the calculation of the dissipation factor, we refer to reference 5.

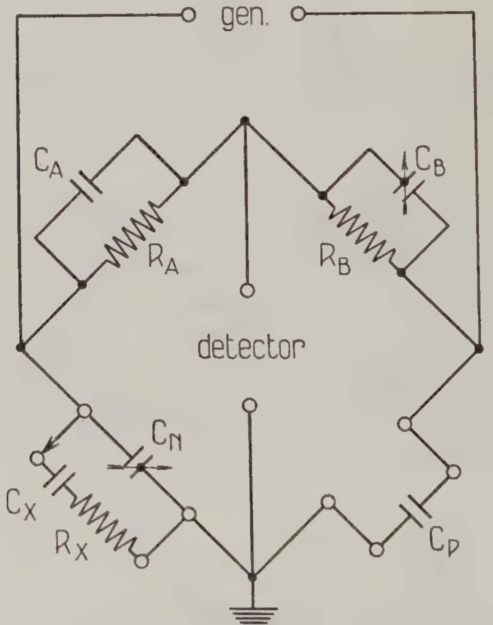

FIG. 3. Principle of the General Radio "Capacitance Bridge" 716-C.

Accuracy

According to General Radio, the maximum error in the capacitance when the Twin-T bridge is used amounts to 0.8 $\mu\mu F$. For comparative measurements, however, we are interested, rather, in the reproducibility, which proved to be better than 0.1 $\mu\mu F$.; in our measurements this corresponds to a relative error of 0.1%. The maximum error in the conductance is also given by General Radio; in our measurements this corresponds to 7%. In the majority of our experiments, however, the reproducibility was considerably better; in the remaining instances we averaged over a number of measurements.

With the type 716-C capacitance bridge (5) the maximum error is 0.2 $\mu\mu F$. In practice, however, we found 0.1%. The error in the dissipation factor is either $5 \times 10^{-5} \times C_1/C_x$ or 2%, whichever is the largest. This is why C_1 is kept as small as possible. In our case, C_1/C_x was usually about 3, so that the error in $\tan \delta$ is about 15×10^{-5} when $\tan \delta < 0.01$ but becomes 2% for higher values.

CHARACTERIZATION OF POLYMER AND SOLVENTS

POEG was fractionated by the method of Schulz and Nordt (7), which is based on the partition of the polymer between water and a chloroform-benzene mixture. The molecular weights were calculated from the results of viscosity measurements, using Rempp's equation (8):

$$[\eta] = A + KM^a, \qquad [9]$$

where a, K, and A are constants. The results are collected in Table I.

The solvent was Merck's toluene p.a., which was subjected to fractionated distillation, then dried over anhydrous $CaCl_2$ and finally over Na. It was freshly distilled for each series of measurements. The dioxane used in one series at low frequencies was Merck's dioxane puriss. We removed peroxides by boiling under reflux with anhydrous $SnCl_2$. This was followed by boiling with Na and fractionated distillation.

TABLE I

Data for the POEG Samples, Using Rempp's Values for a, A and K in Eq. [9]

Sample	$[\eta]$ (*ml./g.*)			$10^{-3}M$
	Benzene	Dioxane	Water	
I	9.8	9.75		2.5
II			50.1	25
III	21.4			8
IV (not fractionated)	36.4			17

RESULTS AND DISCUSSION

High-Frequency Measurements

The samples I and II were measured in the high-frequency range at -50, -40, and -30°C. Unfortunately, the losses were so low that polymer concentrations, as high as 20 g./100 g., had to be used. It should be mentioned, further, that at the low temperatures mentioned the solutions gelled, but it was found that the dielectric losses in the low-frequency range, where measurements could be made both below and above the temperature of gelling, did not show any essential difference in behavior between the gel and the solution.

The results for ϵ'' are shown in Fig. 4. It will be shown that the curves in this figure can be represented within experimental error by a Debye curve with a single relaxation time. To this end we give, by way of example, a plot of $\cosh^{-1}(\epsilon_m''/\epsilon'')$ versus $\log f$ in Fig. 5. Here ϵ_m'' is the value of ϵ'' at the maximum of the loss curve; according to the empirical relation of Fuoss and Kirkwood (9):

$$\epsilon'' = \epsilon_m''\mathrm{sech}(\alpha \ln f/f_m).$$

The slope α of the lines in Fig. 5 is 1 within experimental error, which means that the loss curve is a Debye curve. The same result was found for fraction II. An alternative check is found in Fig. 6. The straight line

$$\epsilon' = \epsilon_s - \omega\tau\epsilon'',$$

from which ϵ_s and τ may be derived, is a consequence of Debye's formula and is equivalent to a half-circular Cole-Cole plot of ϵ'' against ϵ'. From the fact that the slopes of the lines in Fig. 6 are equal, it is at once apparent that the relaxation time τ has the same value for the two samples, although the molecular weights differ by a factor of 10. This independence of molecular weight holds good also at the other temperatures. Table II summarizes the results: $\tau = (2\pi f_m)^{-1}$, ϵ_0 is the dielectric constant of toluene, ϵ_s and ϵ_∞ were calculated from the formulas for dielectric relaxation with a single relaxation time:

$$\epsilon_m' = \tfrac{1}{2}(\epsilon_s + \epsilon_\infty); \qquad \epsilon_m'' = \tfrac{1}{2}(\epsilon_s - \epsilon_\infty).$$

According to the theory of Hammerle and Kirkwood (10), τ is proportional to M^p, where $p = \tfrac{1}{2}$ for Gaussian chains but may lie between $\tfrac{1}{2}$ and 1 as a result of the excluded volume effect. Moreover, the theory predicts a loss curve that is broader than Debye's curve for a single relaxation time. Neither of these predictions is borne out by our experimental results at high frequencies. On the other hand, the application of the Rouse-Bueche model (11) by Zimm (12) and by Van Beek and Hermans (13) leads to a Debye curve with a τ-value which is independent of M.

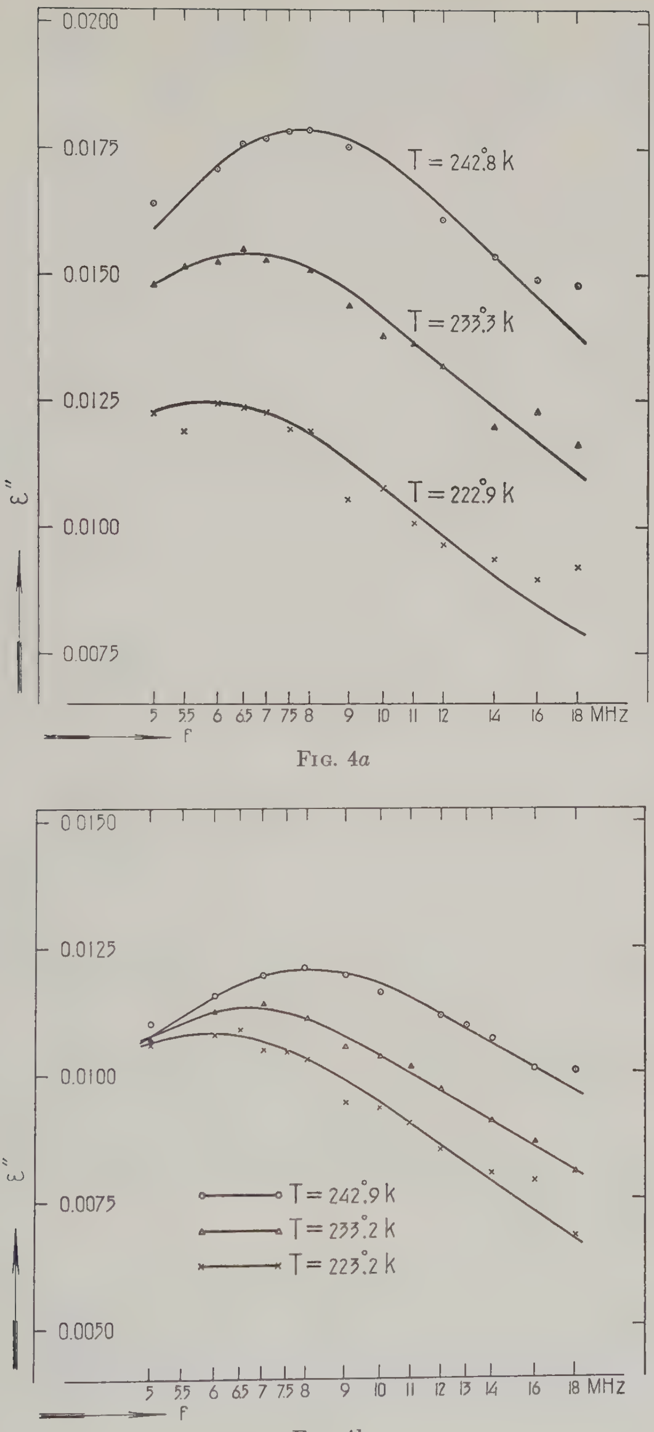

FIG. 4*a*

FIG. 4*b*

FIG. 4. Loss curve for POEG 20 g./100 g. in toluene at three temperatures; (*a*) sample I, (*b*) sample II.

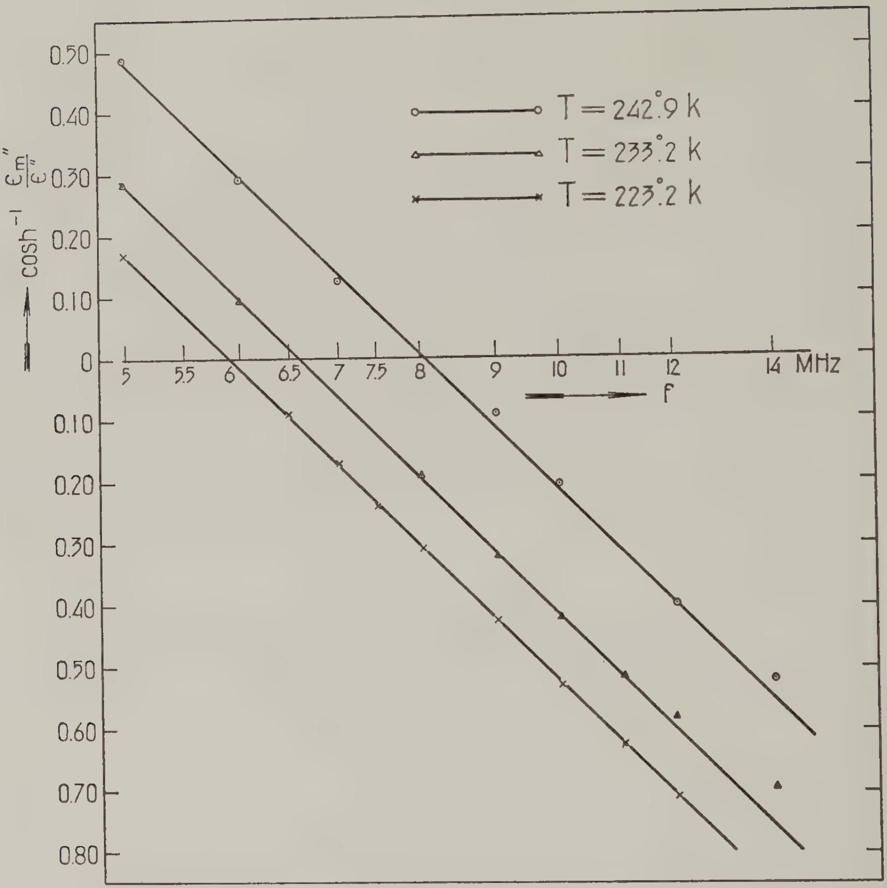

FIG. 5. Cosh^{-1} (ϵ_m''/ϵ'') versus log f according to the empirical Fuoss-Kirkwood relation; sample I.

The last-mentioned theory predicts, in addition, a second dispersion region at much lower frequencies. The maximum of this second loss curve corresponds to a τ-value which is proportional to M^2 when the molecules are free-drained and will be proportional to M^n (with $1 < n < 2$) when there is only partial free-draining. For this reason, we investigated the low-frequency range carefully.

Low-Frequency Measurements

These were carried out on (*a*) sample IV in toluene, concentration 20%, at 40, 24, and −51°C.; (*b*) sample III in toluene, concentration 20%, at 41, 22, and −51°C.; (*c*) sample III in toluene, concentration 2%, at 41, 22, and −51°C., and (*d*) sample III in 1,4-dioxane, concentration 2%, at

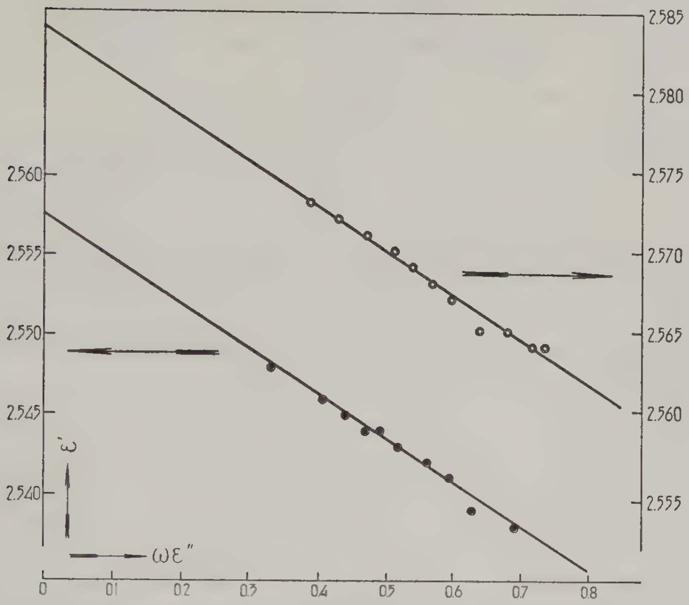

FIG. 6. A plot of ϵ' versus $\omega\epsilon''$ for POEG in toluene: ○ sample I at −50°C., ● sample II at −50°C.

TABLE II

Summary of the Results Obtained for Samples I and II; Conc. 20%

Sample	$10^{-3} M$	T(°K.)	$10^2 \epsilon''_m$	ϵ_m'	ϵ_s	ϵ_∞	ϵ_0	f_m (*Mc.*)	$10^8\tau$ (*sec.*)	α
I	2.5	223	1.24_5	2.571	2.584	2.559	2.589	5.9	2.70	1
		233	1.54	2.553	2.568	2.537	2.555	6.6	2.41	1
		243	1.79	2.530	2.548	2.512	2.525	8.1	1.97	1
II	25	223	1.08	2.546	2.557	2.535	2.588	5.8	2.74	1
		233	1.13	2.530	2.541	2.518	2.556	6.6	2.41	1
		243	1.20_5	2.514	2.526	2.502	2.524	8.0	1.99	1

23.5°C. The 20% solutions were liquid only at 40°; at the lower temperatures they gelled. The 2% solutions were all liquid except that in toluene at −51°C.

All our attempts to find the low-frequency dispersion were fruitless. It is true that the dissipation factor in all cases examined increased markedly with decreasing frequency from about 20 kHz downwards. The same effect was found by Conner (14) for solutions of methyl methacrylate in dioxane and in benzene and was attributed by him to traces of inorganic salt. There can be little doubt that the increase in tan δ in our experiments

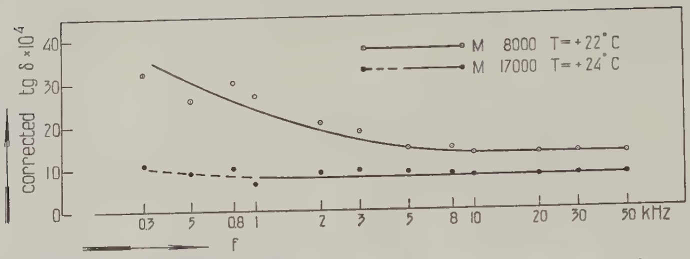

FIG. 7. Plot of tan δ, corrected for conductance, versus the frequency, for sample III (upper) and sample IV (lower curve). Concentration 20 g./100 g.

was likewise due to conductance. If we assume that the total conductance may be written

$$\sigma = \omega\epsilon'' + \sigma_0,$$

where σ_0 is frequency-independent, we may hope to eliminate the effect of σ_0 by plotting $\omega\epsilon''$ against ω. Extrapolating to $\omega = 0$, we get σ_0 and may then subtract σ_0/ω from the apparent ϵ'' values. An example of the result of this procedure is shown in Fig. 7, which shows a slight increase in the corrected value of tan δ at low frequencies. This could be interpreted as the tail of a dispersion curve, the more so since it was observed that ϵ' increases slightly in the same region. The fact that the curve for sample IV is so much flatter than for sample III would be in keeping with the fact that M is higher, so that f_m would be shifted to still lower frequencies. Moreover, this sample was not fractionated, which would make the loss curve still flatter.

Similar, very weak, indications for the existence of a second maximum were obtained in the other measurements, but the result cannot be considered as at all convincing. Van Beek and Hermans have expressed, as their opinion, that the maximum in the low-frequency range may never show up in practice, unless the molecular weight distribution is very sharp. In the present work an additional difficulty resided in the fact that the solutions had to be quite concentrated to obtain measurable losses. This need not have a pronounced effect on the high-frequency dispersion because this is due to the motion of chain segments, but in the low-frequency range, the dispersion must presumably be attributed to rotations of large parts of the entire particle (13).

As a final remark, we may point out that Koizumi and Hanai (15) found a small dielectric dispersion for low molecular weight POEG in the undiluted state between 0.5 and 50 kc. It is of further interest to note that Scherer, Levi, and Hawkins (16) found a dispersion between 1 and 40 kc. for cellulose acetate in dioxane, f_m being proportional to $M^{-3/2}$; in addition, there were indications for a second dispersion region beyond

100 kc., but this was not investigated further. For this reason, a more exhaustive study of cellulose acetate has been started.

REFERENCES

1. DE BROUCKÈRE, L., AND VAN NECHEL, R., *Bull. soc. chim. Belges* **61,** 261 (1952).
2. General Radio Co., operating instructions for type 821-A Twin-T Impedance Measuring Circuit.
3. SINCLAIR, D. B., *Proc. I.R.E.*, 310 (1940).
4. TREIBER, E., SCHURZ, J., AND KOREN, H., *Monatsh.* **82,** 32 (1952).
5. General Radio Co., operating instructions for type 716-C Capacitance Bridge.
6. TIMMERMANS, J., "Physico-Chemical Constants of Pure Organic Compounds." Elsevier, Amsterdam, 1950.
7. SCHULZ, G. V., AND NORDT, E., *J. prakt. Chem.* **155,** 115 (1940).
8. REMPP, P., *J. chim. phys.* **54,** 432 (1957).
9. FUOSS, R. M., AND KIRKWOOD, J. G., *J. Am. Chem. Soc.* **63,** 385 (1941).
10. HAMMERLE, W. G., AND KIRKWOOD, J. G., *J. Chem. Phys.* **23,** 1743 (1955).
11. ROUSE, P. E., *J. Chem. Phys.* **21,** 1272 (1953); BUECHE, F., *J. Chem. Phys.* **22,** 603 (1954).
12. ZIMM, B. H., *J. Chem. Phys.* **24,** 269 (1956).
13. VAN BEEK, L. K. H., AND HERMANS, J. J., *J. Polymer Sci.* **23,** 211 (1957).
14. CONNER, W. P., *J. Chem. Phys.* **9,** 591 (1941).
15. KOIZUMI, N., AND HANAI, T., *J. Chem. Phys.* **60,** 1496 (1956).
16. SCHERER, PH. C., LEVI, D. W., AND HAWKINS, M. C., *J. Polymer Sci.* **24,** 19 (1957).

JOURNAL OF COLLOID SCIENCE **13** 500–507 (1958)

ELASTIC MODULI IN MONOLAYERS

N. W. Tschoegl

Bread Research Institute of Australia, North Sydney, New South Wales

Received December 28, 1957

Abstract

The surface elastic moduli are the two-dimensional analogs of the elastic moduli in three dimensions. Experimental methods are reviewed briefly, and it is shown that Fourt's "elasticity index" for an oscillating vane or needle is dimensionally incorrect, whereas the formula proposed by Trapeznikov for an oscillating disk or ring is correct and can be derived exactly by regarding the film as an elastic annulus sheared in its own plane. A dimensionally correct formula is proposed for an oscillating needle as well as for an aperiodic needle type surface torsion pendulum.

The relationships between the four two-dimensional elastic constants of homogeneous isotropic films are derived and are shown to be different from the three-dimensional formulas. The maximal value of the surface Poisson's ratio is unity instead of one half.

Introduction

In a monolayer, being by definition one molecule in thickness, bonding between similar molecules can occur in two dimensions only. It is customary to regard such a system as a two-dimensional one and to define for it two-dimensional analogs of the relationships in three dimensions.

In this sense the rheology of monolayers may be referred to as two-dimensional or *surface rheology* in which, for instance, the elastic moduli have the dimensions of surface traction (force per unit length) instead of traction (force per unit area). Similarly, whereas bulk viscosity has the dimensions $ML^{1-}T^{-1}$, two-dimensional or *surface viscosity* has MT^{-1}, the c.g.s. unit being termed a "surface poise."

As the state of aggregation of the molecules in a monolayer is generally different from that in bulk, three-dimensional coefficients λ' calculated from surface rheological coefficients λ_s and the thickness d of the monolayer according to the formal relation

$$\lambda' = \frac{\lambda_s}{d} \tag{1}$$

are not identical with the "true" bulk coefficients λ. Thus Fourt and Harkins (1) found the "calculated" bulk viscosity of long-chain alcohols to be of the order of magnitude of the bulk viscosity of waxes and pitches.

The Two-Dimensional Elastic Moduli

Whereas surface (or interfacial) viscosity has received a good deal of attention, the other rheological properties of insoluble and adsorbed monolayers have been comparatively neglected.

The surface *compressional modulus* K_s can be obtained from the tangent of the surface pressure-area $(F - A)$ curve as the reciprocal of the *surface coefficient of compressibility* (2) c_s

$$K_s = \frac{1}{c_s} = A\left(\frac{dF}{dA}\right). \qquad [2]$$

Methods for the determination of the *surface shear modulus* G_s include the rotating disk method (3, 4), the resonance frequency method (5), the aperiodic torsion pendulum (6, 7), and the oscillating torsion pendulum method (8–10). No systematic study has yet been undertaken to compare these methods and the published data are too scanty to allow a comparison of the results.

The last-mentioned method was developed by Fourt (8), who derived the contribution of the film to the restoring torque of a surface torsion pendulum from the decrease in period as

$$C_f = 4\pi^2 I\left(\frac{1}{T^2} - \frac{1}{T_0^2}\right), \qquad [3]$$

where C_f is the increase in the effective torsional constant of the system due to the film, I is the moment of inertia of the pendulum, and T and T_0 are the periods measured with the film and the clean surface, respectively.

From Eq. [3] Fourt defined an "elasticity index"

$$E_s = \frac{4\pi^2 I}{l^3}\left(\frac{1}{T^2} - \frac{1}{T_0^2}\right) \qquad [4]$$

for an oscillating vane (or needle) instrument by introducing the third power of the length of the vane l as an empirical factor in order to render comparable the values obtained with vanes of different lengths.

Fourt's index does not have the dimensions of a surface shear modulus. Trapeznikov (9), working with an apparatus of circular symmetry, used the formula

$$E_s = \pi I\left(\frac{1}{T^2} - \frac{1}{T_0^2}\right)\left(\frac{1}{r_1^2} - \frac{1}{r_2^2}\right), \qquad [5]$$

where r_1 is the radius of the oscillating disk (or ring) and r_2 is the radius (or equivalent radius) of the film. Equation [5] was apparently obtained by multiplying C_f with the apparatus constant (6)

$$H = \frac{1}{4\pi}\left(\frac{1}{r_1^2} - \frac{1}{r_2^2}\right). \qquad [6]$$

Trapeznikov's formula is dimensionally correct and it can be shown that the elasticity index E_s determined from Eq. [5] is identical with the shear modulus G_s. The film contributing to the restoring torque of the surface torsion pendulum may be regarded as an elastic annulus sheared in its own plane. The torsional constant C_f of this annulus is subject to the relation

$$C_f\theta = L, \tag{7}$$

where θ is the angle of twist and L is the corresponding torque which must be constant throughout the annulus. It remains then to find an expression linear in θ and L, and containing G_s.

Now for small strains

$$G_s = \frac{s}{e}. \tag{8}$$

where s is the shearing stress and e is the shear strain. From known formula

$$s = \frac{L}{2\pi r^2}. \tag{9}$$

Further, as may be seen from Fig. 1,

$$e = \frac{du}{dr} = \frac{r\,d\theta}{dr}, \tag{10}$$

where du is the elemental tangential shift and $d\theta$ is the elemental angle. The desired relationship in its differential form therefore becomes

$$G_s = \frac{L}{2\pi r^3}\frac{dr}{d\theta}. \tag{11}$$

Integrating between the limits r_1 and r_2, and $\theta_1 = 0$, $\theta_2 = \theta$, and using Eqs. [7] and [3]

$$G_s = \pi I\left(\frac{1}{T^2} - \frac{1}{T_0^2}\right)\left(\frac{1}{r_1^2} - \frac{1}{r_2^2}\right). \tag{12}$$

Hence, from Eqs. [5] and [12], $E_s = G_s$.

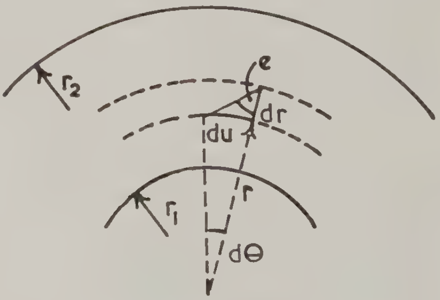

FIG. 1. Shear strain of an elastic annulus sheared in its own plane.

The oscillating needle offers certain experimental advantages over the disk or ring. Unfortunately no really satisfactory expression has as yet been proposed for the calculation of the coefficient of surface viscosity or the surface shear modulus determined with an oscillating needle or vane, since the problem is indeed very difficult to treat hydrodynamically. Fourt (8), however, derived a surface viscosity equation from the assumption that the resistance of the film may be localized as rupture at the ends of an oscillating vane and showed that the surface viscosities of long-chain fatty alcohols determined in this way with vanes of different lengths fell within the range of the results obtained with rings and disks of different diameters (1).

The "apparatus constant" in Fourt's equation is

$$H = \frac{2}{l^2} \qquad [13]$$

and combining Eqs. [13] and [3], one obtains the dimensionally correct relation

$$G_s = \frac{8\pi^2 I}{l^2}\left(\frac{1}{T^2} - \frac{1}{T_0^{\,2}}\right) \qquad [14]$$

for an oscillating vane or needle.

Applying the same type of reasoning to Langmuir and Schaefer's (6) equation for the surface shear modulus determined by a disk type aperiodic surface pendulum, one finds, for a vane or needle,

$$G_s = \frac{2C}{l^2}\left(\frac{\theta_H}{\theta_N} - 1\right), \qquad [15]$$

where C is the torsional constant of the pendulum and θ_H and θ_N are the angular displacements of the torsion head and the needle, respectively.

An endeavor to determine a *surface Young's modulus* Y_s was made by van Wazer (5) on adsorbed films of saponin but no attempt to measure the *surface Poisson's ratio*, μ_s has been published.

Since the four material constants are not independent of each other, Y_s and μ_s can be calculated from K_s and G_s. This necessitates a consideration of the appropriate relationships which will here be shown to differ from the well-known three-dimensional formulas.

The Relationships between the Two-Dimensional Elastic Constants

Van Wazer (5) comparing his surface shear modulus and surface Young's modulus states that elastic theory demands Young's modulus to be about three times as large as the shear modulus. This is true for incompressible bodies in three dimensions, but it will be shown that the surface Young's modulus of incompressible films must be four times as large as the surface shear modulus. Also, while the maximal value of Poisson's ratio is 0.5 in three dimensions, this value is 1.0 in two dimensions.

In order to derive the relationships between the four elastic constants in two dimensions we shall consider the case of simple push on a square area of unit length of the film. The resolution of the surface tractions is shown in Fig. 2.

The isotropic surface pressure of $-\frac{1}{2}F$ on the four sides of the square cause a uniform compression of $-\frac{1}{2}F/K_s$. The area of the square after compression is $1 - F/2K_s$ and the length of each side, taking the square root, expanding by the binomial theorem, and neglecting all powers of $F/2K_s$ higher than the first, is $1 - F/4K_s$. Hence, the isotropic surface pressure on each side of the square causes a contraction of $-F/4K_s$ in every direction.

The set of deviatoric (shearing) surface tractions will cause a contraction of $-\frac{1}{2}F/2G_s$ in the direction of the push and an elongation of $\frac{1}{2}F/2G_s$ at right angles to it [11]. Hence, the resultant total contraction in the direction of the push is

$$-\gamma = -\frac{F}{4K_s} - \frac{F}{4G_s} \qquad [16]$$

and the resultant total elongation at right angles to it is

$$\gamma' = -\frac{F}{4K_s} + \frac{F}{4G_s}. \qquad [17]$$

But according to Hooke's law, the contraction $-\gamma$ expressed in terms of the surface Young's modulus Y_s is

$$-\gamma = -\frac{F}{Y_s}. \qquad [18]$$

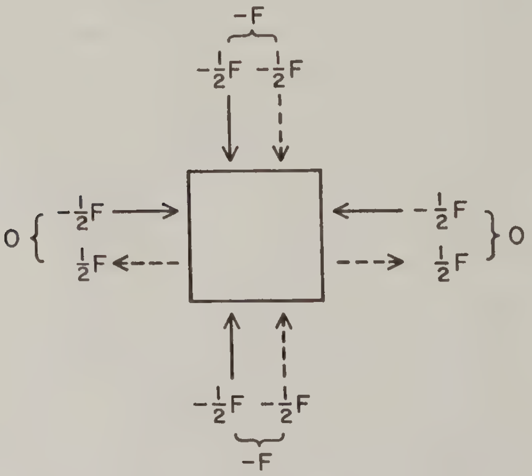

FIG. 2. Resolution of simple push into isotropic (——→) and deviatoric (- - -→) components.

and the elongation γ' in terms of Y_s and the surface Poisson's ratio μ_s is

$$\gamma' = \frac{\mu_s F}{Y_s}. \qquad [19]$$

We now obtain, from Eqs. [16] and [18],

$$Y_s = \frac{4K_s G_s}{K_s + G_s} \qquad [20]$$

and from Eqs. [17], [19], and [20]

$$\mu_s = \frac{K_s - G_s}{K_s + G_s}. \qquad [21]$$

From Eqs. [20] and [21] we further find

$$K_s = \frac{Y_s}{2(1 - \mu_s)}; \qquad [22]$$

$$G_s = \frac{Y_s}{2(1 + \mu_s)}. \qquad [23]$$

Equation [21] may be written as

$$K_s(1 - \mu_s) = G_s(1 + \mu_s), \qquad [24]$$

from which it is clear that Poisson's ratio in two dimensions cannot exceed unity. This can also be shown in a different way. Consider an infinitesimal extension ϵ of the length of a unit area of the film in one direction. If the film is incompressible, there is no change in area and we have

$$(1 + \epsilon)(1 - \mu'\epsilon) = 1, \qquad [25]$$

where μ' stands for $\mu_{s\,(\text{max.})}$.

From Eq. [25] we find

$$\epsilon - \mu'\epsilon - \mu'\epsilon^2 = 0, \qquad [26]$$

and, neglecting the second power of ϵ,

$$\mu' = \mu_{s(\text{max.})} = 1. \qquad [27]$$

That the maximal value of the surface Poisson's ratio must in fact be 1.0 instead of 0.5 is easily realized on considering that in two dimensions an extension in one direction is accompanied by a contraction in only one other direction whilst in three dimensions it is accompanied by contractions in the other two directions.

Inserting $\mu_s = 1$ into Eq. [23] we have, for an incompressible film,

$$Y_s = 4G_s \qquad [28]$$

as asserted above.

TABLE I

Relationships between the Four Elastic Material Constants

Material constant	Three dimensions	Two dimensions
Compressional modulus	$K = \frac{Y}{3(1 - 2\mu)}$	$K_s = \frac{Y_s}{2(1 - \mu_s)}$
Shear modulus	$G = \frac{Y}{2(1 + \mu)}$	$G_s = \frac{Y_s}{2(1 + \mu_s)}$
Young's modulus	$Y = \frac{9KG}{3K + G}$	$Y_s = \frac{4K_sG_s}{K_s + G_s}$
Poisson's ratio	$\mu = \frac{3K - 2G}{6K + 2G}$	$\mu_s = \frac{K_s - G_s}{K_s + G_s}$
Maximal value of Poisson's ratio	$\mu_{(\max.)} = 0.5$	$\mu_{s(\max.)} = 1.0$
Young's modulus (for $K = \infty$)	$Y = 3G$	$Y_s = 4G_s$

Van Wazer found his surface Young's modulus to be lower than the surface shear modulus and ascribed this to the fact that the Young's modulus was measured by a static method whilst a dynamic one (the resonance frequency method) was used to obtain the surface shear modulus. However, another explanation also seems possible. It can be seen from Eq. [23] that a Y_s smaller than G_s implies a negative value of Poisson's ratio, or, in other words, a lateral contraction instead of expansion on compression of the film. This is likely to have happened under van Wazer's experimental conditions where the film would not seem to have had complete freedom for lateral expansion.

The more important relationships for three and for two dimensions are tabulated for comparison (Table I). These formulas were derived assuming an isotropic material. It has been shown (12), however, that protein films at higher compression may be anisotropic. In this case there would be more than two fundamental elastic constants. The treatment, however, would again be the two-dimensional analog of three-dimensional elastic theory.

A mathematically more rigorous treatment of the general n-dimensional case of which the three- and two-dimensional ones are special cases only has been published elsewhere (13).

This work was carried out as part of a research project on the surface chemistry of wheat proteins.

References

1. Fourt, L., and Harkins, W. D., *J. Phys. Chem.* **42,** 897 (1938).
2. Alexander, A. E., and Johnson, P., "Colloid Science," p. 496. Clarendon Press, Oxford, 1950.

3. Mouquin, H., and Rideal, E. K., *Proc. Roy. Soc.* (*London*), **A114,** 690 (1927).
4. Cumper, C. W. N., and Alexander, A. E., *Australian J. Sci. Research, Ser. A*, **5,** 189 (1952).
5. van Wazer, J. R., *J. Colloid Sci.* **2,** 223 (1947).
6. Langmuir, I., and Schaefer, V. J., *J. Am. Chem. Soc.* **59,** 2400 (1937).
7. Tachibana, T., and Inokuchi, K., *J. Colloid Sci.* **8,** 341 (1953).
8. Fourt, L., *J. Phys. Chem.* **43,** 887 (1939).
9. Trapeznikov, A. A., *Doklady Akad. Nauk S.S.S.R.* **63,** 57 (1948).
10. Cumper, C. W. N., and Alexander, A. E., *Trans. Faraday Soc.* **46,** 235 (1950).
11. Searle, G. S. C., "Experimental Elasticity," 2nd ed., p. 10. Cambridge University Press, Cambridge, 1933.
12. Hughes, A. H., and Rideal, E. K., *Proc. Roy. Soc.* (*London*) **A137,** 62 (1932).
13. Tschoegl, N. W., *Australian J. Phys.* **11,** 154 (1958).

JOURNAL OF COLLOID SCIENCE **13**, 508–509 (1958)

LETTERS TO THE EDITOR

DISTRIBUTION OF PARTICLE SIZE IN COLLOIDAL SILICA BY ULTRACENTRIFUGATION

The particle size distribution in several Ludox preparations was studied by Alexander and Iler (1), using electron microscopy, light scattering, and nitrogen absorption. They came to the conclusion that the distribution is sharp, that the particles consist of rather dense silica, and that the particle radius is of the order of 10 mμ. These observations have been confirmed by us in centrifugation experiments, using a Spinco ultracentrifuge at a speed of about 12,500 r.p.m., i.e., an acceleration of about 10,000 times gravity.

It is easy to show that under these circumstances diffusion effects are negligible. The distribution curve for the sedimentation constant s may then be derived immediately from the refractive index gradient as a function of distance x from the center of rotation. The simplest relation is obtained when this distance may be considered as constant throughout the cell, which in most centrifuges is a good approximation. This constant will be denoted by X. Let the meniscus be at x_0 and let the original solution (at time $t = 0$) be homogeneous. We assume that $c_0(s)\, ds$ is the volume of the particles with sedimentation constant between s and $s + ds$ per milliliter liquid at $t = 0$. Here s is defined as the velocity when the acceleration is unity, i.e. $dx/dt = s\omega^2 X$. Particles with sedimentation constant s which at $t = 0$ are at x_1 will at time t be in $x = x_1 + s\omega^2 Xt$. Consequently, the volume concentration $f_s(x, t)\, ds$ of the particles with sedimentation constant between s and $s + ds$ at time t and distance x obeys the equation:

$$f_s(x, t) = f_s(x - s\omega^2 Xt, 0). \tag{1}$$

The total volume concentration $c(x, t)$ is obtained by integrating $f_s(x, t)$ over s. Making use of the fact that $f_s(x_1, 0) = c_0(s)$ when $x_1 > x_0$ and zero when $x_1 < x_0$, the result will be:

$$c(x, t) = \int_0^p ds\, c_0(s); \qquad p = (x - x_0)/\omega^2 Xt. \tag{2}$$

The refractive index gradient which is measured in the Spinco is proportional to $\partial c/\partial x$, and we find by differentiation of Eq. [2]:

$$\omega^2 Xt\partial c/\partial x = c_0(p), \tag{3}$$

which means that a plot of $t\partial c/\partial x$ versus $(x - x_0)/t$ is equivalent with a plot of $c_0(s)$ versus s, and must therefore be independent of time t. This was confirmed experimentally.

If the cell is sector-shaped, a similar reasoning leads to the following result, which replaces Eq. [3]:

$$(\partial c/\partial x)\omega^2 tx^3/x_0^2 = c_0(q); \qquad q = (1/\omega^2 t)\ln(x/x_0), \tag{4}$$

which is true irrespective of whether x is approximately the same throughout the cell or not.

From the distribution $c_0(s)$ we can derive the size distribution when the relation between s and size is known. When Stokes' law applies, a plot of $s^{\frac{1}{2}}c_0(s)$ against $s^{\frac{1}{2}}$ is equivalent with a plot of $g(R)$ versus R, where R is the particle radius and $g(R)\,dR$ the volume (or the weight) of the particles the radius of which lies between R and $R + dR$. The application to Ludox gave a curve the width of which was in good agreement with the results reported by Alexander and Iler.

REFERENCE

1. Alexander, G. B., and Iler, R. K., *J. Phys. Chem.* **57**, 932 (1953).

Cellulose Research Institute
State University College of Forestry,
Syracuse, New York
J. J. Hermans
A. M. Rÿke

Received August 18, 1958

A NOTE ON YOUNG'S EQUATION

A. J. G. Allen recently published (1) a mathematical proof of the equation

$$W = 2l\gamma \cos\theta, \tag{1}$$

in which W is the weight of the meniscus at a vertical wall, $2l$ the perimeter of the wall, γ the surface tension of the liquid, and θ the contact angle. An equivalent proof has also been given by J. F. Padday (2). It seems worth mentioning that Eq. [1] was first derived by Laplace in 1806 (3) and can be found in several textbooks, for example, reference 4.

Both Dr. Padday and Dr. Allen refer to Eq. [1] in connection with my criticism (5) of Young's equation. In reality, there is no connection. The fact that one of Laplace's formulas, as usual, is correct has no bearing on the correctness or otherwise of a relation proposed by Young.

REFERENCES

1. Allen A. J. G., *J. Colloid Sci.* **13**, 273 (1958).
2. Padday J. F., *Proc. 2nd Intern. Congr. Surface Activity* **3**, 187 (1958).
3. Laplace "Oeuvres complètes," Vol. 4, p. 432. Gauthier-Villars, Paris, 1880.
4. Neumann, Franz, "Vorlesungen ueber die Theorie der Capillarität," p. 97. Teubner, Leipzig, 1894.
5. Bikerman, J. J., *Proc. 2nd Intern. Cong. Surface Activity* **3**, 125 (1958).

J. J. Bikerman
Massachusetts Institute of Technology,
Cambridge, Massachusetts

Received August 20, 1958

JOURNAL OF COLLOID SCIENCE **13,** 510–511 (1958)

BOOK REVIEWS

Biophysical Chemistry, Volume I. Thermodynamics, Electrostatics, and the Biological Significance of the Properties of Matter. By John T. Edsall and Jeffries Wyman. Academic Press Inc., New York, 1958. 699 pp. Price $14.

The first volume of this unusually ambitious and well-executed text should be very useful in the teaching of biochemistry, quantitative biology, and general physiology at the graduate level, since no other work of anywhere nearly comparable scope has been hitherto available. It may well lead to the initiation in many institutions of much-needed introductory courses with the same general orientation. It should be none the less useful as a convenient, lucidly written reference book, since it includes more material on very recent results bearing on such active fields as, for example, protein stereo-chemistry, than are to be found in even very recently published monographic collections. The reviewer has been impressed by its usefulness in this respect and has made actual use of it in connection with his own work while preparing this review. The unusually complete and well-selected references for further reading on each subject treated contribute greatly to its usefulness.

The selection of topics treated is, in some respects, narrower than the title implies, since, for example, they are the subjects most amenable to essentially thermodynamical treatment; there is little emphasis on the kinetic and stationary-state processes that are so characteristic of living matter. Thus it appears that even after Volume II is published there will be no comprehensive discussion of redox systems, energy relations in biosynthesis, photo-biochemistry, nor the kinetics of metabolic cycles, growth, or differentiation. In other respects, however, the topics treated are even broader than the title implies. Thus the book begins with an excellent discussion of geochemistry, which includes considerable material on the evolution of the chemical elements; likewise, the third chapter contains a very full discussion of an essentially organic chemical subject (albeit investigated in part by physical methods)—the linear succession of amino acid residues in polypeptides and proteins. On the other hand, although many allusions are made to studies of protein denaturation, especially those that throw light on protein stereochemistry, there is no unified or comprehensive treatment of the great differences in properties between native proteins and their various "denatured" modifications.

Every reader will applaud the selection of particular topics in accordance with his own approach to biology and biochemistry, and possibly deplore the distribution of emphasis in respect to others. (The reviewer, for example, considers the chapter on electrostatics, though excellent and comprehensive in many respects, to overemphasize the contribution of the more complex aspects of this subject to biochemical understanding.) The prevailing impression, however, is one of great accomplishment, discrimination, and lucidity. The excellences that occur in every chapter, too numerous to mention (such as much-needed stress on protein lability, and the distinction between the state of a protein in the cell and a protein preparation), far outweigh the effect of a few omissions or oversimplifications (such as the treatment of protein homogeneity and the bearing of solubility data on this subject).

Jacinto Steinhardt, Cambridge, Massachusetts

Physico-Chemical Effects of Pressure. By S. D. Hamann. Academic Press Inc., New York, 1957. 246 pp. Price $8.50.

This book is in the form of a review of the effects of high pressures on physical and chemical phenomena. In general, it is concerned with changes brought about by pressures greater than 100 atmospheres, where the effects of pressure on molecular processes begin to become apparent. Readers attracted by the title or by a familiarity with the author's work may be led to expect a detailed account of the effect of pressure on chemical reactions. However, a wide range of physical and chemical topics is covered with little variation in emphasis. Chapters are devoted to experimental techniques, volumetric effects, phase changes, transport properties, dielectric and optical effects, electrolytic conduction, chemical equilibria, and chemical kinetics.

The most interesting sections of the book, to most readers, are likely to be the chapters on chemical equilibria and kinetics, since these subjects have not previously been discussed comprehensively from a mechanistic standpoint, and since they cover an area where the author's own contributions have been outstanding. Electrostriction is used as a unifying principle throughout the discussion of kinetic effects. Dr. Hamann's arguments in support of his position are indeed impressive, but some of his readers will undoubtedly wish to place other interpretations on some of his examples. Curiously, little use is made of this principle in the chapter on equilibria, the discussion here centering on compressibility effects.

This book provides an excellent survey of the present state of high-pressure research. The many references provide a convenient guide for those who may wish to delve further into selected areas.

Clayton Huggett, Philadelphia, Pennsylvania

Just published—Volume 1

Biophysical Chemistry

By JOHN T. EDSALL, *Harvard University, Cambridge, Massachusetts*
and JEFFRIES WYMAN, *UNESCO, Cairo, Egypt*

Volume 1

Thermodynamics, Electrostatics, and the Biological Significance of the Properties of Matter

February 1958, 699 pp., illus., $14.00

Biophysical Chemistry is based on a course taught by the authors dealing with the physical chemistry of biochemical systems. Emphasis has been placed on broad general principles and fundamental concepts in order to provide the reader with the basic understanding of the quite difficult problems of current interest in the field of biophysical chemistry.

Volume 1 presents a lucid discussion and a detailed analysis of the biological significance of the properties of matter. The second volume will be devoted to the physical chemistry of biological macromolecules, and their study by such methods as osmotic pressure, light scattering, diffusion, sedimentation, viscosity and electrophoresis.

These volumes will be indispensable to graduate students and advanced undergraduates familiar with the fundamentals of differential and integral calculus. This work will be of basic interest to investigators in organic and physical chemistry, biology, and biochemistry.

CONTENTS OF VOLUME 1:

Biochemistry and Geochemistry. Water and Its Biological Significance. Problems of Protein Structure. Thermodynamics. Electrostatics: Its Application to Polar Molecules, and Ionic Solutions. Dielectric Constants and Their Significance. Conductivity of Electrolytes. Acid-Base Equilibria. Polybasic Acids, Bases, and Ampholytes, Including Proteins. Carbon Dioxide and Carbonic Acid. Some General Aspects of Molecular Interactions. AUTHOR INDEX—SUBJECT INDEX.

Volume 2, in preparation

Physical Chemistry of Macromolecules and of Blood

Descriptive leaflet available upon request

ACADEMIC PRESS INC., *Publishers*
111 FIFTH AVENUE, NEW YORK 3, NEW YORK

PHYSICAL CHEMISTRY: A Series of Monographs

Edited by ERIC HUTCHINSON and P. VAN RYSSELBERGHE

Department of Chemistry, Stanford University, Stanford, California

Volume 6

ESTIMATION OF

Thermodynamic Properties of Organic Compounds

By **GEORGE J. JANZ**, *Rensselaer Polytechnic Institute, Troy, New York*

June 1958, 211 pp., illus., $6.00

This new book stresses the use of thermodynamics as a guide to studies in the field of chemical reactions. The thermodynamic approach, based on a prediction of free energy changes and equilibria, is all too frequently limited because complete data are lacking. This volume provides not only an up-to-date survey of the estimation methods developed for computing thermodynamic properties but also a comprehensive compilation of tables of increments required for the application of each method in practice.

CONTENTS:

Part I. METHODS OF ESTIMATION (pp. 1–133)

The Free Energy Change in a Chemical Reaction. Thermodynamic Properties of Simple Polyatomic Systems by Statistical Thermodynamic Methods. Thermodynamic Properties of Long Chain Hydrocarbons. The Method of Structural Similarity. The Methods of Group Contributions. The Method of Group Equations. Heat of Formation and Heat Capacity. Applications of the Thermodynamic Method.

Part II. NUMERICAL DATA (pp. 135–200) 48 Tables

AUTHOR INDEX—SUBJECT INDEX (pp. 201–211).

Volume 5

Synthetic Polypeptides

PREPARATION, STRUCTURE, AND PROPERTIES

By C. H. Bamford, A. Elliott, and W. E. Hanby

1956, 445 pp., illus., $10.00

REVIEW: ". . . We owe a great deal to the authors for this most excellent, comprehensive and timely book, which has the property of making itself indispensable from the moment one sets eyes on it."

—*British Journal of Applied Physics*

Volume 1, 1952, 558 pp., illus., $12.00

Diffusion in Solids, Liquids, Gases

By W. JOST

Volume 2, 1954, 244 pp., illus., $7.00

Structure of Molecules and Internal Rotation

By S. MIZUSHIMA

Volume 3, 1955, 329 pp., illus., $8.50

Degradation of Vinyl Polymers

By H. H. G. JELLINEK

Volume 4, 1955, 259 pp., illus., $7.00

Solubilization and Related Phenomena

By MARY E. L. MCBAIN and E. HUTCHINSON

ACADEMIC PRESS INC., Publishers

111 Fifth Avenue, New York 3, New York

JOURNAL OF COLLOID SCIENCE **13**, 513–521 (1958)

THE VELOCITY OF SOUND IN EMULSIONS

P. A. Allinson

Physics Department, King's College, University of Durham, Newcastle upon Tyne

Received March 19, 1958

Abstract

The velocity of sound in emulsions of benzene in water was measured, the viscosity of the continuous phase being varied by the addition of glycerine to the water, and the density of the disperse phase varied by the addition of carbon tetrachloride to the benzene.

The results so obtained were compared with two theories, one assuming the emulsions to be homogeneous mixtures of the two components of a mean density and compressibility, the second derived from considerations of the scattering of sound energy from the suspended particles. The experimental results lay close to the values derived from the first assumption.

Introduction

A simple expression for the velocity of sound in emulsions can be derived by assuming the emulsions to be homogeneous mixtures of their constituents, as, for example, Wood (1) has shown.

Then if V is the velocity of sound in the emulsion and V_0 the velocity of sound in the continuous phase

$$\frac{V^2}{V_0^2} = \left\{1 + \frac{c}{100}\left(\frac{m_2 - m_1}{m_1}\right)\right\}\left\{1 + \frac{c}{100}\left(\frac{\rho_2 - \rho_1}{\rho_1}\right)\right\}, \qquad [1]$$

where ρ_1 is the density and m_1 the compressibility of the continuous phase and ρ_2 and m_2 refer to the disperse phase, c being the volume concentration in per cent of the disperse phase. This will be referred to as the Homogeneous Assumption. Urick (2) has shown that the compressibility of finely divided substances can be determined by the use of Eq. [1].

An expression for the propagation constant of sound in media containing numerous small spherical particles was developed by Urick and Ament (3). The derivation depends on a consideration of the scattering produced by the dispersed particles, and in general the constant is complex. However, for the range of densities, viscosities, particle sizes, and frequencies obtaining in the present investigations, a simple expression for the velocity of sound is obtained which differs from [1] only in the final term

$$\frac{V^2}{V_0^2} = \left\{1 + \frac{c}{100}\left(\frac{m_2 - m_1}{m_1}\right)\right\}\left\{1 + \frac{c}{100}\left(\frac{\rho_2 - \rho_1}{2\rho_2 + \rho_1}\right)\right\}. \qquad [2]$$

This will be termed the First-Order Assumption. Considering these two expressions it becomes apparent that:

(*a*) Equation [1] gives a correct result for $c = 100\%$, whereas [2] does not.

(*b*) Equations [1] and [2] become identical for equidense continuous and disperse phases, i.e., $\rho_1 = \rho_2$.

(*c*) For a denser continuous phase $\rho_1 > \rho_2$, [1] yields a higher value for V than [2].

(*d*) Whereas for $\rho_2 < \rho_1$ [1] gives a lower value for V than [2].

PREPARATION OF EMULSIONS

The emulsions used in the present work were formed by violently mixing the two phases. A 1 inch diameter "Dispersator" manufactured by Premier Colloid Mills was employed. A Dispersator consists of a rotating hollow cylinder with a centrally spaced hole in its base. There are slots cut along the body of the cylinder, within which is a baffle dividing the inside into two parts.

When the device is rotated at high speed in a liquid, that portion inside the cylinder is carried around by the baffle and ejected through the slots by centrifugal force, new material being continuously drawn up through the hole in the base.

Thus to produce an emulsion the Dispersator was placed within the continuous phase, and the liquid to be dispersed was directed into its base. Emulsions so produced were stabilized by a small quantity of sodium oleate dissolved in the continuous phase.

The mass median diameter of the particles used was found to vary from 6.5 to 10 μ, the higher value corresponding to emulsions of 70% disperse phase concentration. At higher concentrations the phases tended to settle out rather quickly.

Other emulsions having much larger mass median diameters (up to 150 μ) were investigated, but no change of sound velocity with particle size was detected—a fact which supports the adequacy of the Homogeneous Assumption.

For viscosity measurements, a concentric cylinder viscometer was used, which was calibrated against sucrose solutions. The viscosity of the various liquids used to make emulsions, and also, of the emulsions themselves, was measured.

Continuous phase: glycerine in water (with 1% sodium oleate)

Per cent glycerine	0	10	20	30	40	50
Kinematic viscosity (Stokes)	0.012	0.015	0.021	0.030	0.043	0.065

Disperse phase: Benzene 0.007 Stokes; carbon tetrachloride 0.006 Stokes.

APPARATUS

Basically the apparatus used for the measurement of the velocity of sound consisted of an oscillator feeding a signal onto the transmitting crystal of the acoustic interferometer; a receiver, which amplified the signal taken from the receiving crystal and fed it into the cathode-ray oscilloscope that provided the final signal display.

The oscillator was of the Hartley Type, and was operated in the 2–10 Mc. range.

The acoustic interferometer, illustrated in the accompanying photograph (Fig. 1), consists of a carriage for a pair of matched X-cut quartz crystals, excited at resonance, the distance between which is variable. The crystal holders are immersed in the experimental fluid; one can be moved by an

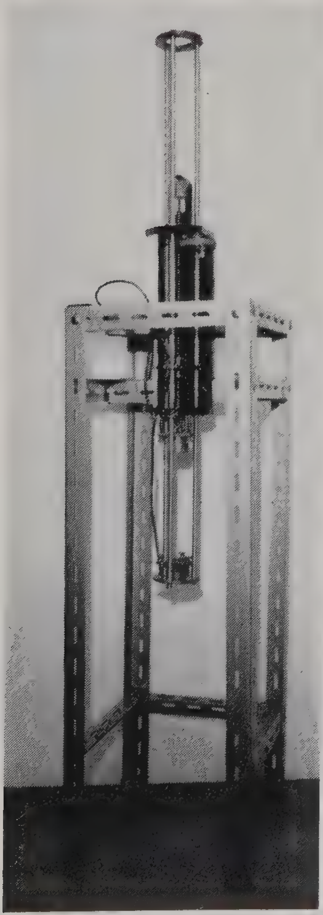

FIG. 1. Photograph of interferometer removed from liquid.

accurately cut screw thread and changes in path length found from a revolution counter and circular scale attached to the screw.

The receiver was a conventional superheterodyne amplifier consisting of one R. F. stage, a mixer stage, and two I. F. stages working at 500 kc./sec.; there was no detector.

Signal display. The received signal was displayed on a Cathode-Ray Oscilloscope. The amplifier of the oscilloscope also provided an increase in signal amplitude.

The frequency meter used in conjunction with the interferometer was of the crystal-controlled beat frequency type, and was used to set the oscillator

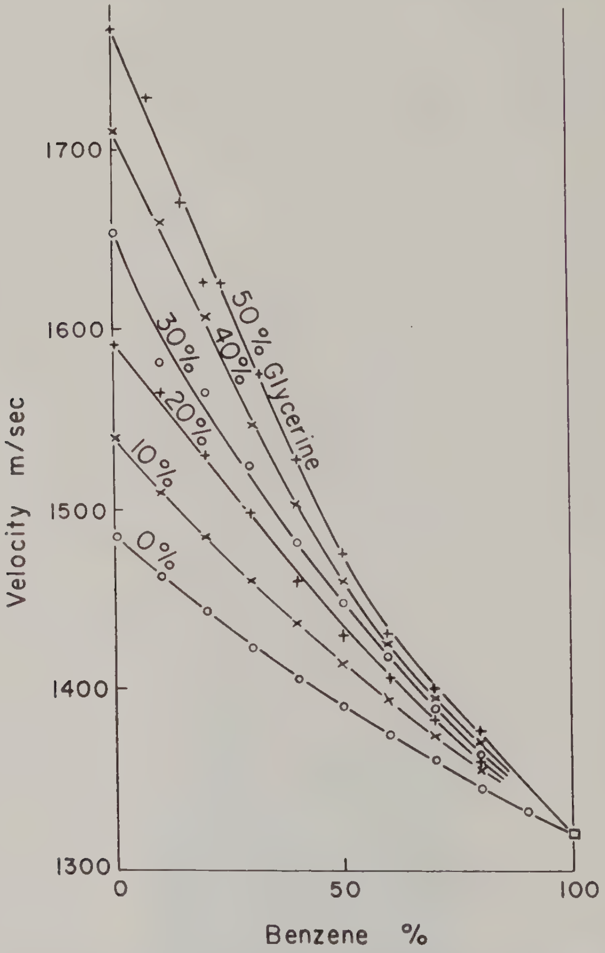

Fig. 2. Velocity of sound in emulsions of benzene in glycerine-water mixtures for different viscosities of continuous phase.

to the desired frequency, viz., the fundamental or an odd harmonic of the natural frequency of the crystal transducers.

Experimental Details

The measurement of the wavelength of the ultrasound in the emulsions depends on the setting up of a standing wave system in the fluid; this is achieved by feeding the transmitting quartz with oscillations of its natural frequency, or an odd harmonic of this frequency. In this way a standing wave system is set up, and successive half wavelengths are easily determined by moving the receiving crystal and observing the change of reaction on it as shown by the amplitude of the oscillogram, successive minima of which correspond to successive pressure nodes.

For highly attenuating emulsions it was found more convenient to feed some oscillation direct to the receiver, mixed with the signal from the receiving transducer. With the apparatus employed in this way the path length in the experimental liquid acts as a delay line. The transmitted and received signals are combined, the resultant signal weight passing through successive maxima as the path length is altered by one wavelength.

Results

The velocity of ultrasound in emulsions was measured at various frequences in the 2–10 Mc./sec. range.

TABLE I

Velocity of Sound (m/sec.) for Emulsions of Benzene in Glycerine-Water Mixtures

Continuous phase % glycerine in water	Expt.: E Calc.: H. Homo. I. 1st-Order	Disperse phase % benzene										
		0	10	20	30	40	50	60	70	80	90	100
0	E	1484	1464	1443	1423	1406	1391	1374	1362	1345	1332	1320
	H	1484	1459	1442	1424	1404	1386	1372	1362	1347	1331	1320
	I	1484	1442	1399	1371	1336	1301	1270	1242	1212	1186	1161
10	E	1540	1509	1488	1461	1437	1414	1394	1373	1363	—	1320
	H	1540	1509	1480	1452	1434	1405	1386	1368	1349	1334	1320
	I	1540	1486	1433	1374	1343	1298	1254	1225	1192	1152	1128
20	E	1592	1565	1530	1498	1460	1429	1407	1383	1365	—	1320
	H	1592	1545	1506	1459	1438	1415	1387	1363	1342	1333	1320
	I	1592	1527	1461	1397	1348	1300	1258	1217	1178	1144	1112
30	E	1654	1583	1566	1544	1482	1448	1418	1396	1363	—	1320
	H	1654	1597	1548	1505	1468	1434	1406	1380	1357	1337	1320
	I	1654	1565	1487	1417	1350	1294	1243	1197	1152	1110	1073
40	E	1711	1659	1607	1547	1502	1461	1425	1391	1371	—	1320
	H	1711	1640	1578	1528	1484	1446	1416	1385	1362	1340	1320
	I	1711	1605	1525	1429	1355	1272	1233	1182	1135	1088	1052
50	E	1766	1705	1626	1585	1527	1474	1431	1401	1377	—	1320
	H	1766	1678	1606	1549	1497	1457	1420	1387	1361	1339	1320
	I	1766	1649	1556	1467	1392	1327	1263	1210	1162	1122	1022

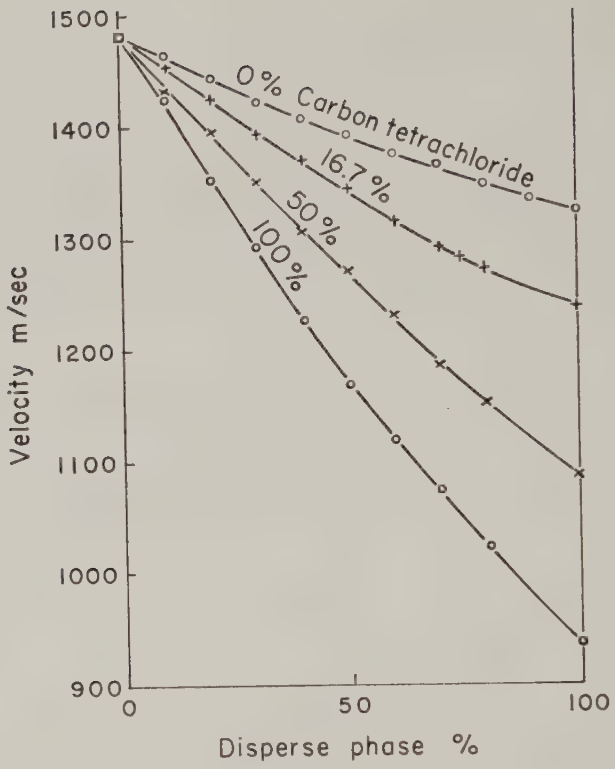

FIG. 3. Velocity of sound in emulsions for different relative densities.

TABLE II

Velocity of Sound (m./sec.) for Emulsions of Benzene-Carbon Tetrachloride Mixtures in Water

Continuous phase % carbon tetrachloride in benzene	Expt.:E Calc.: H. Homo. I. 1st-Order	Disperse phase %										
		0	10	20	30	40	50	60	70	80	90	100
0	E	1484	1464	1443	1423	1406	1391	1374	1362	1345	1332	1320
(p = 0.876)	H	1484	1459	1442	1424	1404	1386	1372	1362	1347	1331	1320
	I	1484	1442	1399	1371	1336	1301	1270	1242	1212	1186	1161
16.7	E	1484	1454	1425	1394	1368	1343	1314	1290	1271	—	1237
(p = 1.08)	H	1484	1452	1423	1398	1372	1344	1322	1297	1269	1258	1237
	I											
50	E	1484	1431	1396	1349	1305	1269	1230	1184	1151	—	1087
(p = 1.24)	H	1484	1433	1383	1338	1295	1255	1217	1183	1152	1117	1087
	I	1484	1437	1390	1330	1305	1267	1232	1196	1164	1132	1102
100	E	1484	1414	1353	1293	1226	1168	1118	1074	1023	—	937
(p = 1.64)	H	1484	1407	1330	1258	1205	1147	1102	1055	1012	974	937
	I	1484	1417	1352	1296	1242	1192	1148	1108	1068	1029	998

Figure 2 and Table I show the average values for the velocity of sound in emulsions of benzene, in glycerine-water mixtures, that is, emulsions having continuous phases of varying viscosity. The effect of varying the density of the disperse phase, by using mixtures of benzene and carbon tetrachloride, is shown in Fig. 3 and Table II.

DISCUSSION

It remains to compare the results obtained with the theoretical expressions: Eqs. [1] and [2]. Figures 4 and 5 and Tables I and II illustrate the

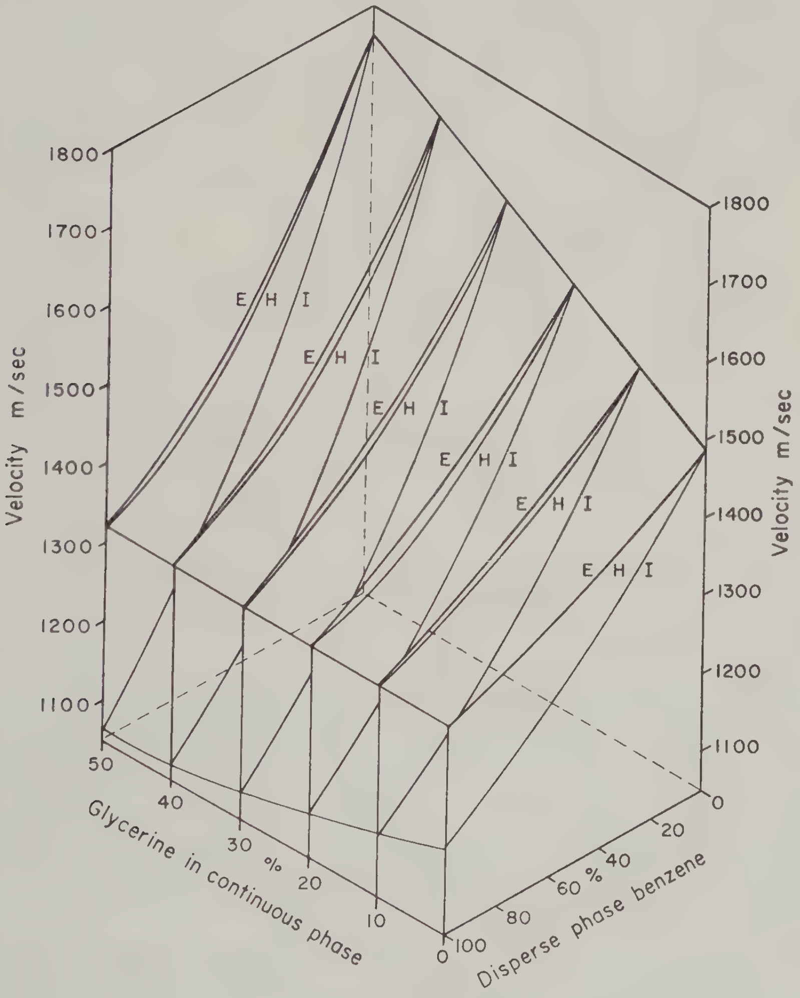

FIG. 4. Velocity of sound in emulsions, viscosity as variable: comparison of experimental results and theory.

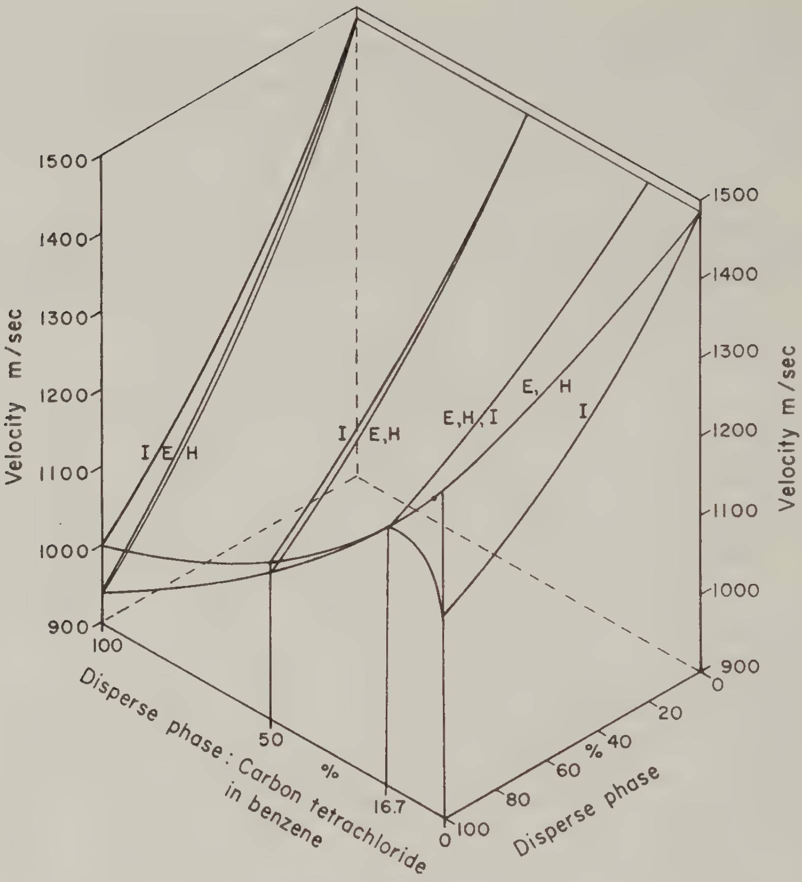

FIG. 5. Velocity of sound in emulsions, density as variable: comparison of experimental results and theory.

experimental results and the values obtained using the Homogeneous and First-Order Assumptions for the emulsions investigated.

It is evident that the Homogeneous Assumption accounts more closely for the experimental values and that where the disperse phase has a higher density, the First-Order values are consistently higher. The First-Order expression is, however, derived on the basis of single scattering, and so is applicable strictly only to emulsions of low concentration. The agreement between it and experimental results is striking for disperse phases of high density (e.g., for carbon tetrachloride in water).

The close agreement between the Homogeneous Assumption and the experimental results of the present work provides an adequate theory to employ in deriving the compressibility of emulsions from a knowledge of the velocity of sound in, and the density of, the constituent phases.

References

1. Wood, A. B., "A Text Book of Sound," 3rd ed., p. 361. Bell, London, 1955.
2. Urick, R. J., *J. Appl. Phys.* **18,** 983 (1947).
3. Urick, R. J., and Ament, W. S., *J. Acoust. Soc. Amer.* **21,** 115 (1949).

JOURNAL OF COLLOID SCIENCE **13**, 522–536 (1958)

COMPETITIVE ADSORPTION OF ALIPHATIC COMPOUNDS AND WATER ON SILICA SURFACES[1]

C. S. Brooks

Shell Development Co., Exploration and Production Research Div., Houston, Texas

Received April 17, 1958

Abstract

These experiments have established (*1*) the interfacial concentrations and orientation of three selected C_{18} straight-chain aliphatic compounds—a hydrocarbon (*n*-octadecane), a carboxylic acid (stearic acid), and a primary amine (*n*-octadecyl amine) —at the interface between the *n*-heptane solution of these solutes and silica with various thicknesses of water film present, and (*2*) the alterations in the water-adsorptive properties of silica surfaces due to adsorbed films of stearic acid and *n*-octadecyl amine.

Introduction

Information on the adsorption of organic materials on mineral surfaces and at oil-water interfaces is essential to our understanding of the processes for the accumulation and release of oil in source beds and for the retention and displacement of oil in reservoir formations.

A question on which we have a quite inadequate understanding is how organic materials accumulate on wet siliceous mineral surfaces in a marine environment.

Another question which may have some bearing on the processes of oil accumulation but which is more applicable to oil recovery processes is how the polar organics, especially those with acidic and basic functional groups, are adsorbed at oil-water and at oil-wet siliceous mineral surfaces. The adsorption of polar organics (whether they occur naturally in the oil or are introduced in flood water to facilitate recovery processes) at oil-water and at oil-silica interfaces has an important influence on recovery processes inasmuch as the oil-water interfacial tension and the wetting properties of the mineral surfaces affect the displacement of oil by water in porous sediments.

The actual oil, water, mineral systems which constitute oil source beds and reservoirs are quite complex. The oil phase may consist of a wide range of various types of polar and nonpolar aliphatic and aromatic organic compounds. The composition and salinity of the water phase may vary widely. A wide variety of heterogeneous mineral surfaces with different adsorptive properties are present in the actual systems. In addition, a number of complex variables such as pressure, temperature, and the relative amounts and compositions of the oil and water phases may vary in an undertermined manner with time, whether the process under consideration is that of accumulation or recovery.

---

[1] This paper was presented at the Symposium on Adsorption from Solution at the 131st meeting of the American Chemical Society in Miami, Florida, April 9, 1957. Publication No. 153, Shell Development Company, Exploration and Production Research Division, Houston, Texas.

The present experiments were designed primarily to establish the adsorptive behavior of a quite simple system, namely, the adsorption at 24°C. of normal C_{18} aliphatic compounds at *n*-heptane solution-silica interfaces, and secondarily to establish the change in the wetting properties of silica surfaces with preadsorbed organic films. A better understanding of the nature of the adsorption processes for this simple system should provide some clue to the behavior of the more complex systems encountered in oil source beds and reservoir formations.

In the adsorption experiments designed to demonstrate the effect of preadsorbed water films on the adsorptive capacity of silica surfaces for aliphatic compounds, straight-chain, high molecular weight compounds were adsorbed from their dilute solutions in *n*-heptane. Normal-octadecane was chosen as one adsorbate; the corresponding amine and acid, *n*-octadecyl amine and stearic acid, were chosen to demonstrate the role of polar functional groups on the adsorption process without alteration in the size and shape of the hydrocarbon chain. The adsorbent used was a high surface area nonporous silica (aerosil).

Water vapor isotherms at 30°C. on clean silica and on silica with preadsorbed films of stearic acid and *n*-octadecyl amine were also measured.

EXPERIMENTAL

Materials

The solutes selected for the preparation of the solutions for the adsorption experiments were *n*-octadecane (Eastman, m.p. 27°–28.5°C.), stearic acid (Matheson Coleman and Bell, m.p. 69°–70°C.), and *n*-octadecyl amine (Armour and Company, 98% primary amine, 93% octadecyl amine).

The solvent, *n*-heptane (Phillips Petroleum Company, 99 mole % purity), was dried and further refined to remove unsaturated hydrocarbons and any surface-active contaminants by percolation through activated silica gel.

The adsorbent was a nonporous silica (Dow-Corning Aerosil) with a specific surface area of 163 m.^{2} per gram (low-temperature nitrogen adsorption) and a particle diameter of the order of 0.015–0.020 μ (electron micrograph).

Adsorbent Preparation

The dry silica was prepared by evacuation for 6 hours at 110°C. at 10^{-5} mm. of mercury pressure. The silica adsorbent was placed in a special sample tube which could be connected directly to the high-vacuum pumping system. A three-way stopcock on the top of this special sample tube permitted switching from the high-vacuum manifold to a thistle tube holding the *n*-heptane solutions so that the solutions could be admitted to the dried, evacuated silica without exposure of the solid to the atmosphere. The three-way stopcock, thistle tube, and a tube for directing the solution into the adsorbent holder could be disassembled from the bottom part of the holder by means of a 34/45 standard taper ground joint to permit addition of the adsorbent. The adsorbent holder had a flat bottom to accommodate a glass-encased magnetic stirrer element. The holder had a capacity of about 120 ml. without the solution contacting the high-vacuum grease on the ground joint.

The silica adsorbent with the preadsorbed monolayer of water was prepared by equilibration for at least a week in a desiccator in which a relative humidity of about 58% was maintained over 40 weight % aqueous sulfuric acid.

The silica adsorbent with the multilayer water film was prepared by mixing the air-dry silica with water (about 270 weight %) to give a free-flowing powder, homogeneous in regard to water content and aggregate size.

The water content of the wet silicas was established by measuring the weight loss of portions evacuated at 110°C. in special adsorbent holders (1).

Procedure for Adsorption of Aliphatics on Silica

In the adsorption measurements on dry silica, about 1 g. of silica was placed in the special sample tube. The silica adsorbent was dried and 100 ml. of the *n*-heptane solution was admitted to the sample tube via the thistle tube.[2] The residual solution in the thistle tube was chased with 5 ml. of *n*-heptane solvent. The silica-solution mixture was agitated for an hour with a magnetic stirrer. This mixture was permitted to stand overnight, agitated again for 30 minutes, and the silica was permitted to settle out. The top of the sample tube was then removed and an 80- to 90-ml. portion of the clear supernatant equilibrium solution was pipetted out for analysis.

In the adsorption measurements on the "wet" silicas 100 ml. of the *n*-

---

[2] Even should the 100 ml. of *n*-heptane solution become saturated with water (0.0151 g. per 100 g. of *n*-heptane at 25°C.) during admission to the dried silica and all this water be adsorbed on the silica, the coverage of the surface could not exceed 15%. (See first isotherm, Table VII.)

TABLE I

Comparison of Chemical and Gravimetric Analyses for n-Octadecyl Amine in n-Heptane Solution

Analytical method	Solute concentration *equiv./l.* × 10^4	Standard deviation	95% confidence limits	$t = \frac{d\sqrt{n}}{S_d}$
Chemical	334			
Chemical	163			
Chemical	76			
Chemical	1.6	±1.8	±5.0	
Gravimetric	342			
Gravimetric	163			
Gravimetric	83			
Gravimetric	10.9	±3.5	±9.7	1.5

Per cent probability level (times critical *t* exceeded in 100 trials)	Critical values of *t* for four degrees of freedom
1	4.6
5	2.8

heptane solution was added to a 1–3 g. adsorbent sample in a glass-stoppered Erlenmeyer flask. The procedure was in all other respects the same as that described above in connection with the dry silica adsorbents.

The amount of solute adsorbed on the silica adsorbent[3] in each case was determined by establishing the total loss of solute from the solution based on the final equilibrium solution composition and on the initial solution concentration. All adsorption values reported are the average of duplicate determinations and are based on the weight of the silica dried by evacuation at 110°C.

Analytical Procedures for Aliphatic Solutes in n-Heptane Solution

The amine solutions were analyzed by a modified Kjeldahl procedure (2). The stearic acid solutions were analyzed by a potentiometric titration (3). The *n*-octadecane solutions were analyzed gravimetrically by evaporation of the *n*-heptane solvent at moderate temperatures (<200°C.) and de-

[3] $A/W = (C_1V_1 - C_2V_2)/W$, where A is the weight of adsorbate, W the weight of the silica dried by evacuation for 6 hours at 110°C., C_1 the initial volume concentration of the n-heptane solution, V_1 the initial volume of the n-heptane solution, C_2 the final volume concentration of the equilibrium n-heptane solution, and V_2 the final volume of the equilibrium n-heptane solution (V_1 plus any n-heptane solvent chaser added). When corrections were applied for the estimated partial molar volumes of the solute and solvent and maximum possible adsorption was assumed of the solvent, n-heptane, on the adsorbent (see R. S. Hansen, Y. Fu, and F. E. Bartell, *J. Phys. Chem.* **53**, 772 (1949)) it was estimated that the maximum correction on the apparent adsorption, $(C_1V_1 - C_2V_2)/W$, would be less than 1%. No such corrections were made on the adsorption values reported here.

termination of the weight of the residual solute. A comparison of the results obtained from the gravimetric procedure with the results obtained for the chemical procedures for the amine are given in Table I.

The standard deviations and the 95% confidence limits have been calculated from the differences between the duplicate determinations to indicate the precision obtained by the chemical and the gravimetric methods. The computed *t*-factors (4), 1.5 for the amine and 1.3 for the acid, obtained by a comparison of the averages of the analyses for the two methods are less than the critical values of 4.6 and 2.8 for 4 degrees of freedom at the 1% and the 5% probability levels, respectively. This demonstrates that the results obtained by the chemical and the gravimetric methods are in essential agreement.

Apparatus for Water Vapor Isotherms

The water vapor isotherms were measured with a helical spring sorption balance (5).

RESULTS

Adsorption of Aliphatics on Dry Silica

To determine how the presence of water films on silica surfaces affected the adsorptive capacity of the silica for the selected solutes (*n*-octadecane, *n*-octadecyl amine, and stearic acid) in solutions of *n*-heptane, it was necessary to determine first the amounts of these solutes adsorbed from *n*-heptane solutions on dry silica.

Results of these adsorption experiments, performed in the special sample

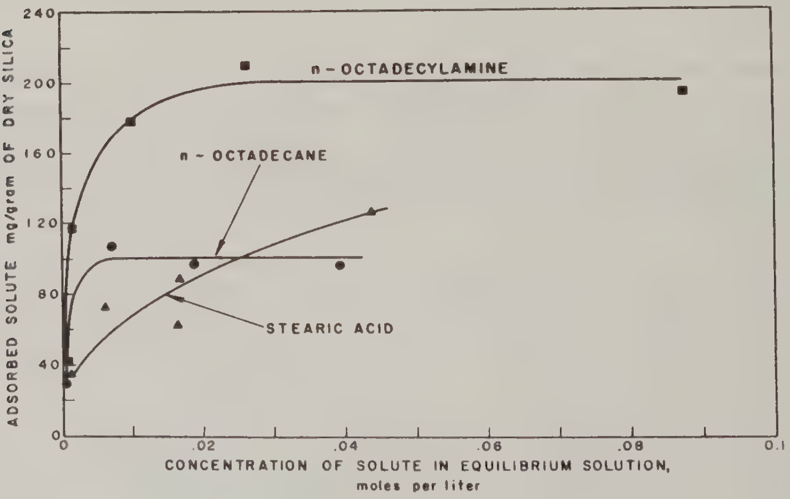

FIG. 1. Adsorption on dry silica surface.

tubes by the procedure described above, are shown in Fig. 1. The concentrations of the three solutes (*n*-octadecane, *n*-octadecyl amine, and stearic acid) in the equilibrium solutions ranged from 0.0002 to 0.09 mole per liter. The maximum concentrations of the amine and stearic acid used approach the solubility of these solutes in *n*-heptane at 24°C. *n*-Octadecane and stearic acid were adsorbed in amounts ranging from 29 mg. per gram of dry silica from the dilute solutions to 126 mg. per gram of dry silica from the most concentrated solutions. *n*-Octadecyl amine was adsorbed in appreciably greater amounts than the other two solutes, and for equilibrium solution concentrations in excess of 0.02 mole the amount of amine adsorbed was about twice the amount of *n*-octadecane or stearic acid adsorbed.

Adsorption of Aliphatics on Wet Silica

The presence of a water monolayer (4.6 weight % based on silica dried by evacuation at 110°C.) on the silica surfaces resulted in no appreciable change (>20%) in the adsorption of stearic acid or *n*-octadecyl amine (Fig. 2) compared with the adsorption of these solutes on dry silica (Fig. 1). The presence of the water monolayer completely inhibited the adsorption of *n*-octadecane at all solute concentrations used (Fig. 2).

The presence of a thick water film (equivalent to ~54 molecular layers) on the silica surfaces resulted in a quite appreciable reduction in the adsorption of the amine from all except the most concentrated solutions and there was a drastic reduction in the adsorption (<3 mg. per gram of dry silica) of stearic acid from the most concentrated solutions used (Fig. 3).

Determination of the change in water content (Karl Fischer) between

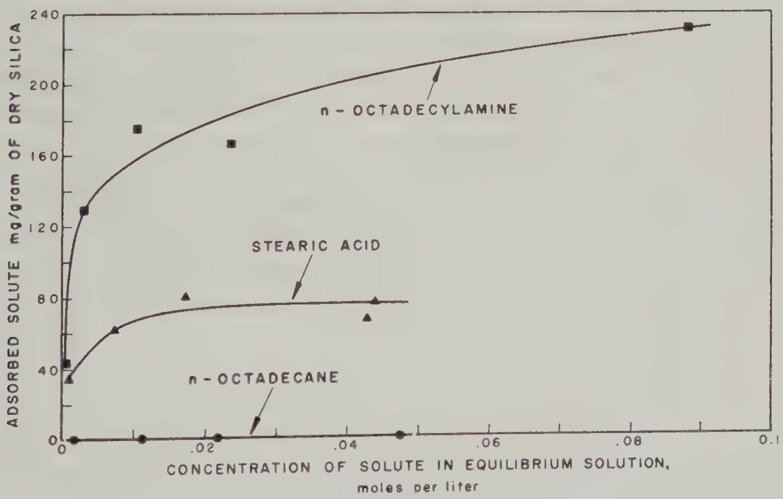

FIG. 2. Adsorption on silica with water monolayer.

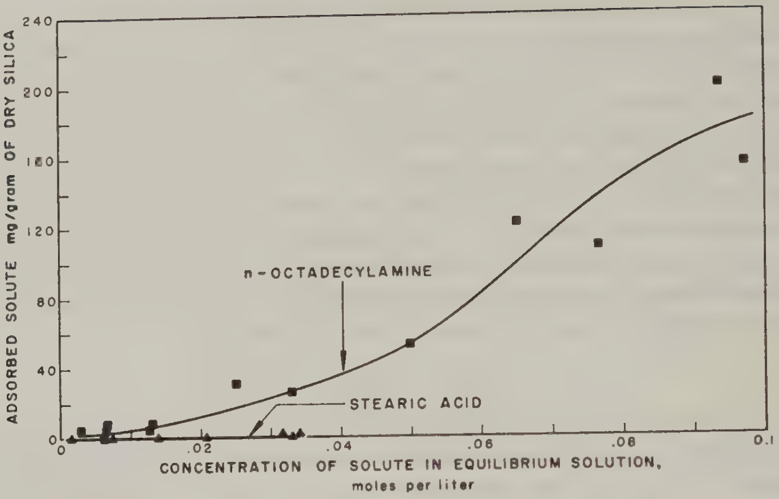

FIG. 3. Adsorption on silica with water multilayer (equivalent to ~54 molecular layers).

the initial solutions and the final equilibrium solutions of stearic acid and *n*-octadecyl amine which were equilibrated with the wet silicas (equivalent to ~54 molecular layer thick water film) established that the total water displaced from the wet silicas after agitation with the *n*-heptane solutions represented in no instance more than 1 weight % of the amount of water initially present on the silica surface.

To establish whether the rate of diffusion of the solute from the *n*-heptane solution to the *n*-heptane solution-water interface was a controlling factor in the amount of adsorption observed, one of the most concentrated stearic acid solutions (0.0328 M) was permitted to stand in contact with the wet silica with intermittent agitation for a week. This had no observable effect upon the amount of adsorption.

Similar tests were made with two concentrations (0.0989 and 0.0064 M) of *n*-octadecyl amine in *n*-heptane solution in contact with silica with a multilayer water film. Portions of the equilibrium solution were analyzed at intervals of overnight, 3 days, 10 days, and 30 days. Equilibrium adsorption was established overnight within the precision of the analytical methods used for determination of the solute.

Water Vapor Isotherms on Silica

Water vapor isotherms (desorption) at 30°C. were determined for the clean silica, silica with an adsorbed film of stearic acid, and silica with an adsorbed film of *n*-octadecyl amine (Fig. 4).

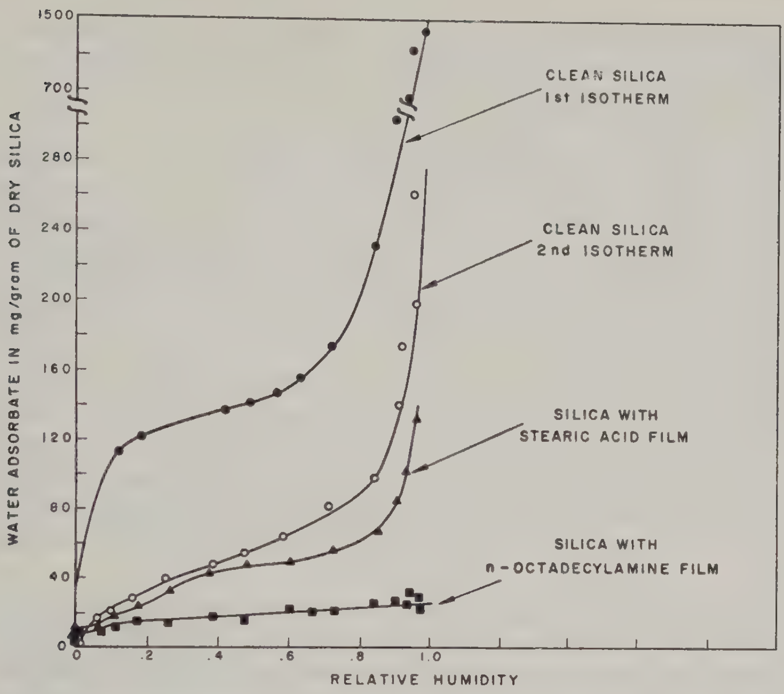

FIG. 4. Water isotherms at 30°C. on silica with preadsorbed organic films.

DISCUSSION

Concentration and Orientation of Aliphatic Adsorbates at n-Heptane Solution-Silica Interfaces

The difficulty of establishing with reasonable accuracy the liquid-solid interfacial area in order to express adsorption data in terms of interfacial concentration and to provide information on the nature of adsorbate orientation at a liquid-solid interface has, heretofore, discouraged such efforts. The aerosil adsorbent used in the present experiments offered the outstanding advantages of high specific surface area and essentially no internal pore structure, which justify use of the specific surface area of the dry adsorbent as a measure of the solution-silica interfacial area available to even comparatively large molecules.

The agreement between the specific surface area measured by nitrogen adsorption and the area calculated from the electron micrograph particle diameter and the helium displacement grain density provides reasonable assurance that the uncertainty in the specific surface area of the adsorbent does not exceed 10%. The uncertainty in the surface area combined with the uncertainty of correct determination of the amount of solute adsorbed should permit estimates to be made of interfacial concentrations and effective molecular coverage areas for these adsorbates at *n*-heptane-silica (dry and with a preadsorbed water monolayer) interfaces which are reliable to within 20%.

These adsorption experiments provide information on the concentration and orientation of the *n*-octadecane, *n*-octadecyl amine, and stearic acid molecules adsorbed at the interface between the *n*-heptane solutions of these solutes and the dry and wet silica surfaces. Some interfacial concentrations and the effective coverage areas per adsorbed solute molecule for the adsorption of these three solutes on dry and on wet silica surfaces are given in Table II.

In the cases of the adsorption of *n*-octadecane, stearic acid, and *n*-octadecyl amine on the dry silica surfaces and the adsorption of the acid and the amine on the silica surface with a preadsorbed water monolayer, it can be assumed, quite reasonably, that the interfacial area between the *n*-heptane solutions and the silica surface is essentially the same as the surface area of the silica as measured by the low-temperature adsorption of nitrogen.

In the case in which there is a water multilayer (equivalent to ~54 molecular layers thick) on the silica surfaces, the interfacial area between the *n*-heptane solution and the wet silica surface might very well be somewhat less than the surface area of the dry silica because of aggregation of the silica particles. Adsorption of the amine from the most concentrated solutions (0.09 M), however, yields essentially the same interfacial concentration (2.7×10^{14} molecules per square centimeter) that was obtained in the case of the dry silica and in the case of the silica with the water monolayer, assuming the nitrogen surface area of the dry silica to represent

TABLE II

Interfacial Concentration and Orientation of n-Octadecane, Stearic Acid, and n-Octadecyl Amine at n-Heptane Solution-Silica Interfaces (24°C)

			Adsorbed solute	
Surface condition of silica	Solute	Conc. of solute in equil. soln. (*moles/l.*)	Molecules/cm.^{2} soln.-silica Interface $\times 10^{-14}$	cm^2./molecule adsorbed solute $\times 10^{-16}$
Dry	OD	0.0397	1.4	71
Dry	SA	0.0439	1.6	61
Dry	ODA	0.0262	2.9	35
Water monolayer	SA	0.0438	0.99	101
Water monolayer	ODA	0.0230	2.3	44
Water multilayer	SA	0.0332	<0.07	—
(Equivalent to 47–60		0.0249	0.43	233
molecular layers)	ODA	0.0498	0.71	141
		0.0935	2.7	37

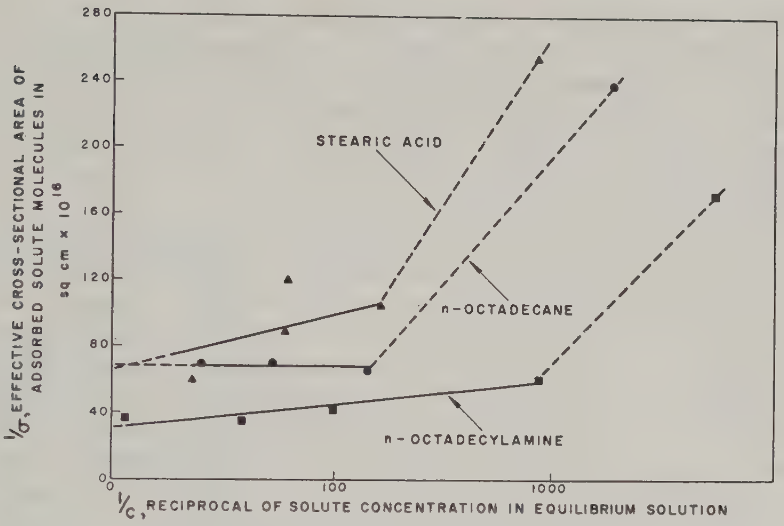

FIG. 5. Adsorption on dry silica surfaces.

the true interfacial area in each instance. Two possible explanations are (*1*) the amine has sufficient solubility in the water film that adsorption occurs at the water-silica as well as at the *n*-heptane-water interface, or (*2*) the high interfacial activity of the amine maintains a large *n*-heptane-water interfacial area comparable with the initial *n*-heptane-silica interface. Both factors may contribute, and it is not possible to decide which is the more correct.

It is interesting to note that if the effective particle size of this silica were increased from 175×10^{-8} cm. in diameter to about 500×10^{-8} cm. in diameter owing to the presence of an adsorbed water film equivalent to 54 molecular layers thick, the specific surface area would increase by a factor of 8.2, providing there was no reduction in the available area owing to the coalescence of adjacent wet spheres of silica. It is apparent, however, in the case of this silica with the multilayer water film that we have a very inexact knowledge of the interfacial area between the *n*-heptane solution and the water film on the silica, and that any estimates of interfacial concentrations and effective coverage areas for the adsorbate molecules must be regarded as rough approximations.

A plot of the effective cross-sectional area of the adsorbed solute molecules versus the reciprocal of the solute concentration in the equilibrium solutions is shown in Fig. 5 for the dry silica surface. Values can be extrapolated to infinite solute concentration to provide an estimate of the minimum effective cross-sectional areas of the adsorbed solute molecules under the conditions of closest packing and maximum orientation in the interface. The extrapolated values for the effective cross-sectional areas of the adsorbed *n*-octadecane and stearic acid on dry silica surfaces were 68 and 65×10^{-16} cm.^{2} per molecule, respectively. A value of 88×10^{-16} cm.^{2} per molecule was obtained for stearic acid on the silica with a water monolayer. The amine gave values of 30, 28, and 26×10^{-16} cm.^{2} per molecule, respectively, for the effective cross-sectional areas of the molecules adsorbed on the dry silica, on the silica with a water monolayer, and on the silica with a water multilayer.

These extrapolated values for the effective cross-sectional areas of all three solutes are appreciably greater than the value of 20.5×10^{-16} cm.^{2} observed in film balance experiments (6) for monolayer films of normal polar aliphatics at closest packing and maximum orientation where the molecules are perpendicular to the air-water interface. This makes highly questionable the determination of the surface areas of even nonporous solids by the adsorption from solution of normal aliphatics acids, such as stearic acid, when the effective coverage areas of the adsorbed molecules are assumed to approximate the values observed at air-water interfaces.

The appreciably greater affinity for adsorption on both the dry and wet silica surfaces that was observed for the *n*-octadecyl amine may be attributable to the weakly acid character of the surface hydroxyl groups on the silica so that the adsorption is in part physical and in part chemical in nature (7). The base-exchange capacity of this silica was quite small (0.028 meq. per gram) as determined by the conventional procedure of measuring the amount of ammonium ion adsorbed from acetate solution (8).

Much of the data in the literature in which a solute is adsorbed from solution on a solid adsorbent can be satisfactorily fitted to a Langmuir (9)-type equation, indicating that the adsorption is monomolecular in nature. There is good evidence (10–12), however, that solutes can be adsorbed from solution to form adsorbate films which are definitely multimolecular.

In the present experiments, the adsorption of aliphatic compounds from *n*-heptane solutions on silica surfaces appears to be essentially Langmuir in character.

The Langmuir equation can be expressed in the form

$$\frac{C}{\sigma} = \frac{1}{K\sigma_0} + \frac{C}{\sigma_0}. \qquad [1]$$

In the above equation σ is the amount adsorbed in molecules per sq. cm., σ_0 denotes a saturated monomolecular layer of adsorbate, and C is the solute concentration (in this instance, moles per liter); K is a constant dependent primarily upon the strength of the adsorptive forces.

A plot made of C/σ versus C was linear for all the solutes adsorbed on dry silica and on silica with a water monolayer, indicating that the Langmuir equation provides a reasonable fit for these data.

The concentrations, σ_0, of the *n*-octadecane, stearic acid, and *n*-octadecyl amine in the saturated condensed adsorbate films on the dry silica and

TABLE III

Saturated Monomolecular Layers for Adsorbate Films of n-Octadecane, Stearic Acid and n-Octadecylamine at n-Heptane-Silica Interfaces

(1)	(2)	(3)	(4)
		σ_0 in Molecules/cm.^{2}	
Solute	Adsorbent preparation	From slope of equation (1) plot $\times 10^{-14}$	From intercept of $1/\sigma$ vs. log $(1/c)$ plot (Fig. 5) $\times 10^{-14}$
n-Octadecane	Dried by evacuation at 110°C	1.43	1.47
Stearic acid	Dried by evacuation at 110°C.	1.56	1.54
n–Octadecyl amine	Dried by evacuation at 110°C.	2.73	3.33
Stearic acid	Preadsorbed water monolayer	0.98	1.14
n-Octadecyl amine	Preadsorbed water monolayer	2.96	3.57

on the silica with the preadsorbed water monolayer as obtained from extrapolation of a plot such as Fig. 5 to infinite solute concentration are given in column 4, Table III. These values are in reasonable agreement with the σ_0 values obtained from the Langmuir plot (column 3, Table III).

Water Vapor Isotherms on Silica (Clean and with Preadsorbed Organic Films)

Information on the alterations in the wetting and adsorptive properties of silica surfaces due to adsorbed films of stearic acid and *n*-octadecyl amine were provided by water isotherms at 30°C. (Table IV and Fig. 4). The BET nitrogen surface areas were measured before and after each of the water isotherms on each of the adsorbents, and the averages were used to estimate the areas available for water vapor sorption and the number of molecular layers of water adsorbate.

The first water isotherm measured on the clean silica yielded 2.1 molecular layers of water adsorbate at 0.1 relative humidity (the point on the water isotherm which corresponded to BET monolayer coverage) and 17 molecular layers of water adsorbate at 0.95 relative humidity. The second isotherm at 30°C. on this same clean silica yielded 0.92 molecular layer of water adsorbate at 0.27 relative humidity (the point on the water isotherm which corresponded to BET monolayer coverage), and 43 molecular layers of water adsorbate at 0.95 relative humidity. This silica was evacuated to constant weight at 50°C. in preparation for both isotherms. Only by heating at temperatures in excess of 110°C. could the water sorption capacity of the wetted silica be restored to that observed for the initial water isotherm. This provides good evidence that approximately one layer of water vapor was chemisorbed during the initial water isotherm when the silica was first exposed to a high relative humidity.

TABLE IV

Water Isotherms at 30°C. on Silica with Preadsorbed Organic Films

Adsorbent	Adsorbent preparation	Nitrogen surface area ($m^2/g.$)	BET water monolayer		Number of layers of water adsorbate based on nitrogen surface area	
			($mg./g.$)	($m^2/g.$)	At BET monolayer coverage	At 95% relative humidity
Clean silica (first Isotherm)	Evacuated to constant weight at 50°C.	169 *B*	100	351	2.1	17
Clean silica (second Isotherm)	Evacuated to constant weight at 50°C.	156 *A*	39	135	0.92	43
Silica with film of stearic acid (SA) (126 mg. SA/g. dry SiO_2)	Evacuated to constant weight at 50°C.	92 *B* 83 *A*	29	100	1.2	4.8
Silica with film of *n*-octadecyl amine (ODA) (210 g. ODA/g. dry SiO_2)	Evacuated to constant weight at 50°C.	83 *B* 88 *A*	13	47	0.53	1.0

B = before water isotherm.
A = after water isotherm.

This silica (Dow-Corning Aerosil) was manufactured by the vapor-phase hydrolysis of $SiCl_4$ with a combustible gas. The resultant silica surface would be expected to have a dehydrated or "siloxane" (7) character and the chemisorption of water vapor during the determination of the first isotherm may be attributed to the rehydration of the "siloxane" surface to a "silonal" (7) surface. Once the aerosil has been hydrated by exposure to high relative humidities or immersed in liquid water and a complete layer of chemisorbed water taken up subsequent water vapor isotherms will show a marked reduction in water sorption capacity compared with the initial isotherm so long as the adsorbent is never activated at temperatures high enough to reconvert the "silonal" back to a "siloxane" surface. This has been substantiated by recent experiments (13, 14).

The water isotherm on the silica with the preadsorbed film of stearic acid (126 mg. of stearic acid per gram of dry silica) yielded 1.2 molecular layers of water adsorbate at 0.23 relative humidity (the point on the water isotherm which corresponded to BET monolayer coverage) and 4.8 molecular layers of water adsorbate at 0.95 relative humidity.

The water isotherm on the silica with the preadsorbed film of *n*-octadecyl amine (210 mg. of *n*-octadecyl amine per gram of dry silica) yielded 0.53 molecular layer of water adsorbate at 0.1 relative humidity (the point which corresponded to BET monolayer coverage) and 1.02 molecular layers of water adsorbate at 0.95 relative humidity.

The assumptions involved here are (*1*) that essentially the same surface area is accessible for water vapor sorption at 30°C. as for low-temperature nitrogen adsorption, and (*2*) the effective coverage area of the water adsorbate molecule corresponds to hexagonal close packing of spheres with the normal liquid density at the given temperature.

It is quite evident from these water vapor isotherms that the presence of the preadsorbed films of stearic acid and *n*-octadecyl amine has reduced appreciably the distance, in terms of the number of molecular layers of water adsorbate, at which this normally strongly hydrophilic silica surface has any measurable effect. In the case of the amine, only partial coverage of the surface occurs with water adsorbate at low relative humidities, and complete coverage occurs only in the vicinity of 95% relative humidity.

If it is assumed that 20.5×10^{-16} cm.^{2} is the effective cross-sectional area of the adsorbed acid and amine molecules at closest packing and greatest orientation (6) on the silica and that the nitrogen surface area of the clean silica provides a reasonable estimate of the surface available for the adsorption of the acid and the amine from their solutions in *n*-heptane, it would appear that 34% of silica surface was covered by the stearic acid film and that 59% of the silica surface was covered by the *n*-octadecyl amine film. As is evident from the preceding discussion, these adsorption experiments indicate that the minimum coverage areas for these adsorbate molecules on silica surface are somewhat greater than the minimum coverage areas observed at air-water and oil-water interfaces.

The fact that the nitrogen surface areas of the silicas with the preadsorbed films of stearic acid and *n*-octadecyl amine were found to be 46% and 47% lower, respectively, than the nitrogen surface area of the clean silica has two possible explanations: (*1*) The average effective particle sizes of the silicas with the organic films were somewhat greater owing to agglomeration and to the presence of the organic film, or (*2*) there was only partial coverage of the available surface by the adsorbed nitrogen during the area determination. The first explanation appears to be the most plausible in view of the considerable evidence in the literature of the purely van der Waals, nonspecific character of nitrogen adsorption on a wide variety of high-energy and low-energy solid surfaces.

SUMMARY

1). These experiments have established (*a*) the interfacial concentrations and orientation of three selected C_{18} straight-chain aliphatic compounds—a hydrocarbon (*n*-octadecane), a carboxylic acid (stearic acid), and a primary amine (*n*-octadecyl amine)—at the interface between the *n*-heptane solution of these solutes and silica with various thicknesses of water film present; and (*b*) the alterations in the water-adsorptive proper-

ties of silica surfaces due to adsorbed films of stearic acid and *n*-octadecyl amine.

2). The adsorption data provide some understanding of the nature of the adsorption of high molecular weight polar and nonpolar aliphatic compounds on wet siliceous surfaces, which may be applicable to the processes of oil accumulation in marine sediments.

3). The experiments provide information which may be applicable also to oil production processes, in particular, the relative concentrations of high molecular weight aliphatics with acidic and with basic functional groups adsorbed at oil-wet silica interfaces.

Acknowledgments

The author wishes to express his appreciation to Mr. John E. Greaney for assistance in the experimental work, to Dr. H. van Olphen for advice and criticism in the preparation of this paper, and to the Shell Development Company for permission to publish.

References

1. Brooks, C. S., "Nitrogen adsorption experiments on several clay minerals," *Soil Sci.* **79,** 332 (1955).
2. Scott, W. W., "Standard Methods of Chemical Analysis," 5th ed., pp. 631–634. Van Nostrand, New York, 1939.
3. ASTM D664-54, "ASTM on Standards on Petroleum Products and Lubricants." 1955.
4. Youden, W. J. "Statistical Methods for Chemists," pp. 16, 28. Wiley, New York, 1951.
5. McBain, J. W., and Baker, A. M., "A new sorption balance," *J. Am. Chem. Soc.* **48,** 690 (1926).
6. Adams, N. K., "The Physics and Chemistry of Surfaces," 3rd ed. Oxford University Press, London, 1941.
7. Carman, P. C., "Constitution of colloidal silica," *Trans. Faraday Soc.* **36,** 964–973 (1940).
8. MacKenzie, R. C., "A micro method for determinations of cation-exchange capacity of clay," *J. Colloid Sci.* **6,** 219 (1951).
9. Langmuir, I., "The adsorption of gases on plane surfaces of glass, mica, and platinum," *J. Am. Chem. Soc.* **40,** 1361–1403 (1918).
10. Fu, Ying, Hansen, R. S., and Bartell, F. E., "Thermodynamics of adsorption from solutions. I. The molality and activity coefficient of adsorbed layers," *J. Phys. Chem.* **52,** 374–386 (1948).
11. Hansen, R. S., Fu, Ying, and Bartell, F. E., "Multimolecular adsorption from binary liquid solutions," *J. Phys. Chem.* **53,** 769–785 (1949).
12. Hansen, R. S., and Hansen, R. D., "The adsorption of hydrocarbons from methanol and ethanol solutions by non-porous carbons," *J. Phys. Chem.* **59,** 496–498 (1955).
13. DeBoer, J. H., Hermans, M. E. A., and Vleeskens, J. M., "The chemisorption and physical adsorption of water on silica I," *Koninkl. Ned. Akad. Wetenschap. Proc.* **60,** 145–153 (1957).
14. Young, G. J., "Interaction of water vapor with silica surfaces," *J. Colloid Sci.* **13,** 67–85 (1958).

JOURNAL OF COLLOID SCIENCE **13**, 537–552 (1958)

FIBER SWELLING AND DETERGENT ADSORPTION IN DETERGENT/TEXTILE FIBER SYSTEMS

H. C. Evans

"Shell" Research Limited, Thornton Research Centre, P.O. Box 1, Chester

Received October 14, 1957; revised received June 6, 1958.

SUMMARY

The adsorption of sodium alkyl sulfates and sodium oleate on various textile fibers passes through a maximum, and sometimes subsequently a minimum, as the concentration of surface-active material in the aqueous phase is increased. The transverse swelling of single fibers, constant in dilute solutions of surface-active compound, decreases at the concentration corresponding to maximum adsorption. The shape of the adsorption/concentration graph can be explained on the basis of adsorption of single ions on a changing surface, and this hypothesis can also explain the dialysis of surface-active compounds. The effects of alkali and inorganic electrolyte on the adsorption isotherms are also discussed.

INTRODUCTION

The adsorption of anionic surface-active compounds by textile fibers has received attention because of its importance in problems of detergency. Aickin (1) has determined the adsorption of sodium alkyl sulfates on wool; the adsorption of fatty acid soaps (2), sodium oleate (3), sodium dodecyl sulfate (4), and alkylarylsulfonates (5, 6) on cotton have also been measured. Weatherburn and Bayley (7) examined the adsorption of several pure anionic compounds on wool, cellulose acetate, nylon, viscose, and cotton, although usually only at a single concentration. Until 1949 only Aickin had reported fluctuations in the adsorption isotherm, but since then several investigators have found that the adsorption passes through a maximum as the liquid phase concentration is increased. This behavior seems to be general in the systems under discussion; it has not been reported more often because the isotherm has not been carried to sufficiently high concentrations.

The shape of the isotherm has been explained in one of two ways. Either, it is said, micelles and single ions are independently adsorbed, and the maximum is due to a decrease in the single ion concentration above a certain total concentration of solution; or hydrolysis of the detergent occurs and two species of molecule are adsorbed to varying extent. Whereas the latter explanation might be tenable for fatty acid soaps, it cannot be true for alkylarylsulfonates which are resistant to hydrolysis. Neither does the theory of micelle adsorption seem possible. Firstly, the anion-active molecules are usually thought to be adsorbed on the fiber surface through their lipophilic chains so that the polar heads are outwards, whereas ions comprising the micelles have only their polar heads exposed and the micelle as a whole is symmetrically hydrophilic and therefore not subject to adsorptive forces. Secondly there is in solution a dynamic equilibrium between micelles and single ions, so that when the latter are removed from solution by adsorption some micelles dissociate and the concentration of single ions is maintained. Further, neither theory can explain the existence of a minimum in the adsorption isotherm which sometimes occurs beyond the maximum adsorption.

The work now reported was carried out in 1948–1949. Although somewhat incomplete, the data, when considered in conjunction with other published results, lead to a hypothesis which appears to account, qualitatively at least, for the observed facts. For brevity the term "detergent" will be used to mean "anionic surface-active compound."

RESULTS

Adsorption Isotherms

The adsorption of sodium alkyl sulfates[1] on nylon, cellulose acetate, viscose, and cotton, and of sodium oleate on nylon, viscose, and cotton from buffered solutions of pH ranging from 8.5 to 12 have been studied at 30°C. The adsorption isotherms (Figs. 1–3) are similar to those of related systems: the adsorption of detergent passes first through a maximum, falls off somewhat, and may subsequently increase again. The shape of the isotherm will first be discussed, and then an attempt will be made to explain why the magnitude of the adsorption varies as the composition of the aqueous phase is altered.

a). *Adsorption near the Critical Micelle Concentration.* The critical micelle concentration (c.m.c.) of sodium oleate is 1.5×10^{-3} M (8); that of the sodium alkyl sulfates mixture is indeterminate but it will suffice to adopt the value 3.3×10^{-3} M for the C_{14} compound (9). Others (5, 6) have found discontinuities in the isotherm near the c.m.c., but in the figures smooth curves have been drawn for two reasons. First, sharp changes would not be expected with a mixture where micelles form over a considerable concentration range. Secondly, although for the sodium oleate isotherms some points appear well away from the curves the experimental method is not precise enough to be sure that a sharp break exists. Nevertheless it is probable that

---

[1] Commercial mixture with hydrocarbon chains of 10 to 18 carbon atoms.

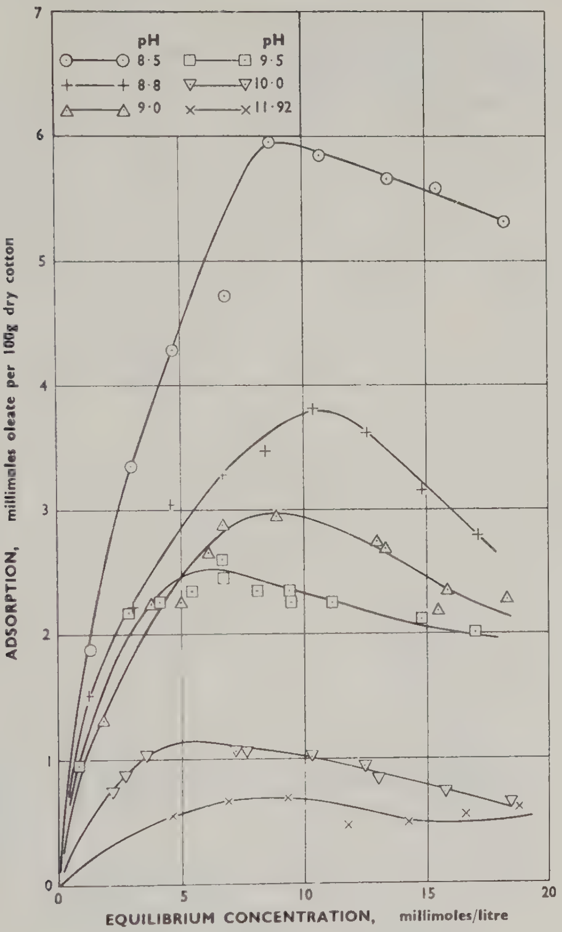

FIG. 1. Adsorption isotherm: cotton/sodium oleate.

adsorption increases when micelles form, although micelles themselves are not adsorbed. Hartley has pointed out (10) that although the tendency of surface-active molecules to form micelles in solution (indicated by c.m.c.) and their tendency to collect in the surface layers of the solution (indicated by foaming properties, surface tension, etc.) are manifestations of the same property of the molecule, these tendencies are competitive. In the adsorption system the ions at concentration just above the c.m.c. are likewise subject to conflicting tendencies; either they can form micelles or they can be adsorbed on the fiber surface; the free energy change of the two processes is approximately equal. A value of *ca.* 2 kcal./mole was obtained for the heat of adsorption of sodium alkyl sulfates on nylon at a concentration below the c.m.c. over the temperature range 30°–60°C.; for the adsorption

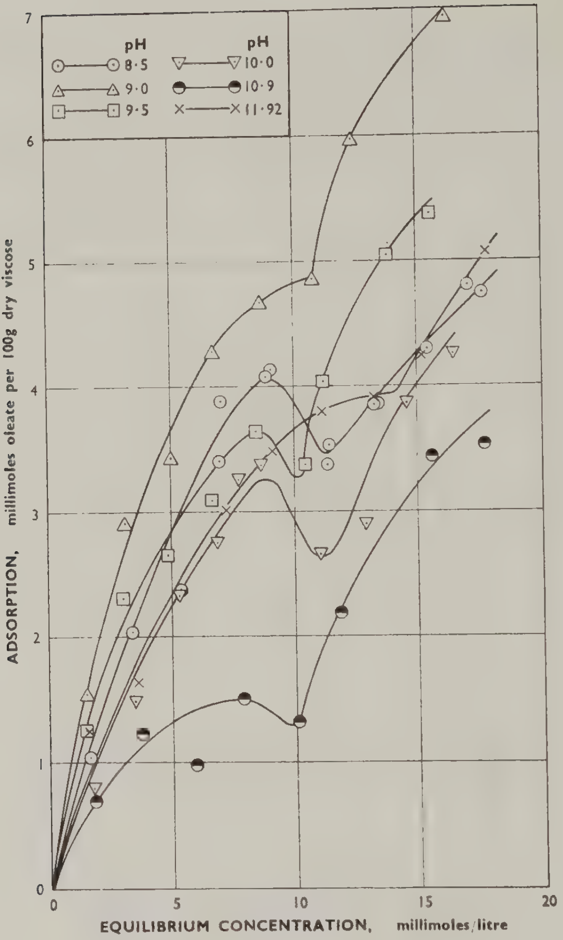

FIG. 2. Adsorption isotherm: viscose/sodium oleate.

of sodium alkyl sulfates and of sodium oleate on cotton over the range 20°–60°C. Wijga (11) calculated a value ≤1.3 kcal./mole, and Fava and Eyring (6) obtained a value *ca.* 1 kcal./mole for sodium dodecylbenzene sulfonate on cotton. These values are comparable with estimates of the energy of micellization (0.8 kcal./mole for sodium lauryl sulfate (12); 1 kcal./mole for potassium pentadecanoate (13)), and are much less than the heats of adsorption of various direct dyes on cotton (14) (11–22 kcal./mole).

b). *Adsorption above the c.m.c.* Larose (15) has observed that when wool is dyed with Orange II (sodium salt of β-naphthol azobenzene *p*-sulfonic acid) the amount of water vapor adsorbed is less after than before application of

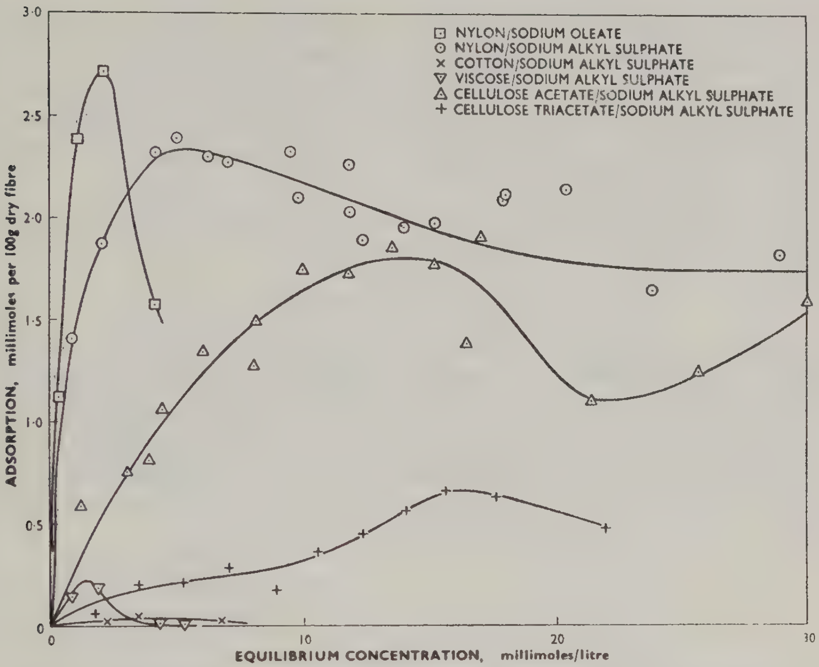

FIG. 3. Adsorption isotherms of sodium alkyl sulfates and sodium oleate.

the dye. Similarly Gillam (16) found that the regain of wool decreases after treatment with "sulfated detergent" at 1 g./l. active matter concentration. It seems therefore that the adsorption of surface-active compound may be associated with the amount of water held by the fiber; if at some stage the surface area of the fiber became reduced, the adsorption, which depends *inter alia* on the area of the fiber, would also be reduced. The following section describes experiments designed to test this idea.

Swelling of Fibers in Detergent Solutions

The diameters of single fibers before and after immersion in solution were measured at a linear magnification of about 500, swelling being expressed as a percentage increase in diameter. At least eight different fibers were measured at each detergent concentration, for replicate measurements show a very wide scatter. Thus the means of these replicates have the following 95% confidence limits:

Cotton	Viscose	Nylon	Cellulose Acetate
±5.8	±7.5	±1.4	±3.7

A feature of all the results is that the swelling, constant at low detergent concentration, decreases at concentrations between 5 and $10 \times 10^{-3}\ M$, then either becomes constant again or increases somewhat. Electrolytes have no such effect for with the system sodium sulfate/viscose the swelling is unchanged over the concentration range 0 to 100 × 10^{-3} M. It is evident that the adsorption maxima occur at about the same concentration as do changes in swelling, and consequently there is some relation between adsorption and fiber diameter.

The empirical Freundlich equation [1] relating adsorption (x) per unit weight of absorbent with equilibrium concentration (c)

$$\log x = \log k + n \log c \qquad [1]$$

of detergent solution is valid only when the surface area of the adsorbent remains unaltered, since the constant k includes a term which takes account of the surface area accessible for adsorption. For fibers this area will be greater than the geometric surface area, but we may suppose that changes in one will correspond with changes in the other. Deviations of the experimental adsorption y from the Freundlich adsorption x can be found by

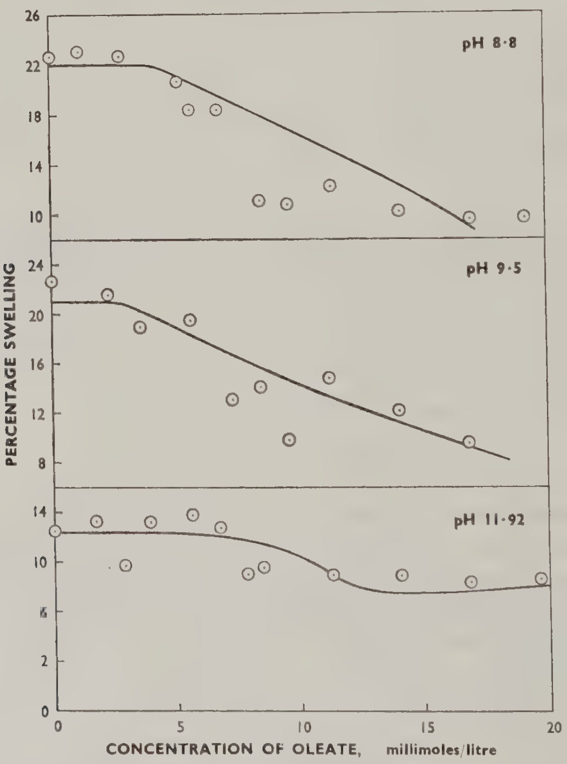

FIG. 4. Swelling of cotton in solutions of sodium oleate. (Circles represent experimental determinations. Lines represent expected swelling on basis of adsorption data.)

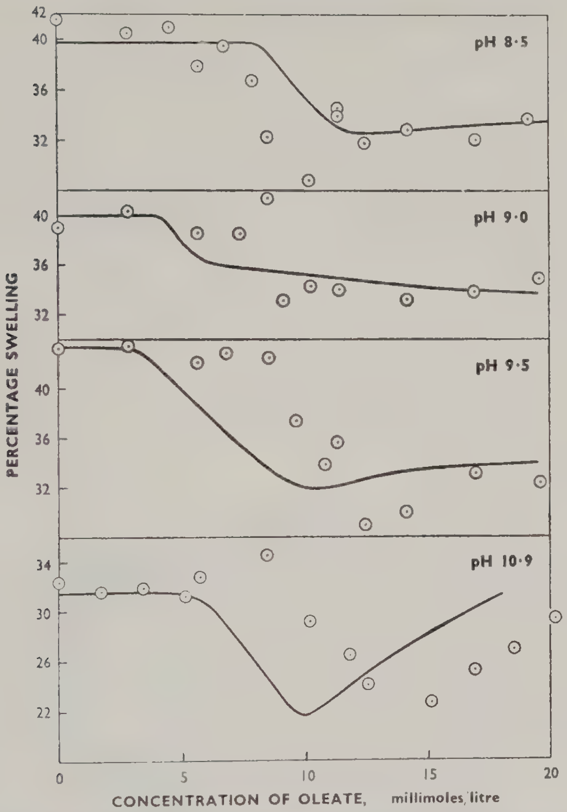

FIG. 5. Swelling of viscose in sodium oleate solutions. (Circles represent experimental determinations. Lines represent expected swelling on basis of adsorption data.)

plotting the adsorption isotherm on a logarithmic scale, drawing the line representing the Freundlich equation (which is valid at low concentrations) and plotting the values ($\log y - \log x$) at given concentrations. This done, it is at once apparent that ($\log y - \log x$) and swelling (I) can, to a first approximation, be related by an equation of the form

$$\log y - \log x = k_1(I - k_0). \qquad [2]$$

Figures 4–6 illustrate the relationships. The plots of ($\log y - \log x$) versus concentration are represented by the continuous lines, where the log adsorption scale has been adjusted so that the maximum decrease of ($\log y - \log x$) and of I are roughly in correspondence. The mean values of the swelling at stated concentrations are represented by points within circles. In view of the rather wide confidence limits given previously it will be seen

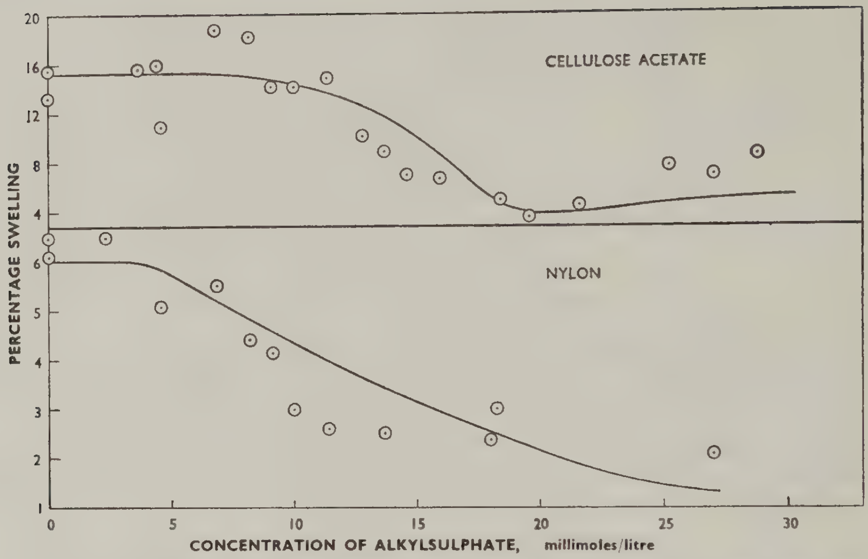

FIG. 6. Swelling of cellulose acetate and nylon in "Teepol." (Circles represent experimental determinations. Lines represent expected swelling on basis of adsorption data.)

that, in general, each line represents a reasonable fit to the experimental swelling data.

Since $y = x = 0$ when the fiber is in equilibrium with water (or buffer solution) alone, it follows that Eq. [2] can be written as

$$\log y - \log x = k_1(I - I_s) \qquad [2a]$$

where I_s is the fiber swelling at zero detergent concentration. Thus the actual adsorption y is associated with the actual swelling I, and the theoretical adsorption x with the initial swelling I_s; that is, if the swelling were unchanged at all concentrations of detergent the actual adsorption would increase throughout the concentration range.

The existence of a maximum and a minimum in the adsorption isotherm can now be explained. Combining Eqs. [1] and [2a], we have

$$\log y = n \log c + k_1 I + (\log k - k_1 I_s), \qquad [3]$$

where I is a function of concentration and decreases as Figs. 4–6 show, whilst the term within brackets remains constant throughout. The adsorption isotherm can then be represented as in Fig. 7, in which the upper dotted line represents the Freundlich isotherm with the constants n, k; and the lower line has the constants n, $k \times 10^{k_1(I_u - I_s)}$, where I_u is the swelling constant again at some higher concentration c_u. If the reduction in swelling occurs at a concentration where the Freundlich adsorption alters only slowly

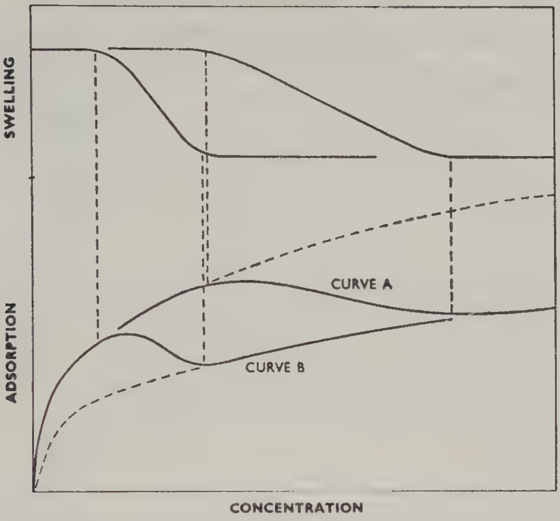

FIG. 7. Idealized adsorption isotherms and fiber swelling.

the experimental isotherm will contain a maximum and the adsorption will level off at some lower value (Curve A). If, on the other hand, the decrease in swelling occurs at a concentration when the Freundlich adsorption is still increasing rapidly the experimental adsorption will first decrease as the fiber swelling is lessened and then increase again when the fiber swelling becomes constant at its lower level (Curve B).

In the Freundlich isotherm the shape of the isotherm controls the value of n; if n is small the curvature is large and the isotherm quickly becomes flat at low equilibrium concentrations. Hence for a given detergent, if n is small one would expect a type A curve rather than a type B curve; if n is large a type B curve would be expected in preference to one of type A. This is in fact found; for cotton and viscose the average values of n are 0.64 and 0.78, respectively, while for cellulose acetate and nylon the values are 0.8 and 0.6, respectively. Viscose and cellulose acetate give type B curves (Figs. 2 and 3); nylon and cotton give type A curves (Figs. 1 and 3).

Effect of pH

Figures 1 and 2 show the effect of pH on the adsorption isotherm at an electrolyte concentration of 0.1 N. An isotherm of the unbuffered sodium oleate (natural pH 9) on cotton is almost the same as that of the pH 9.0 buffered solution, and at pH 10 changing the electrolyte concentration from 0.1 to 0.2 N merely displaces the maximum to a slightly lower equilibrium concentration. Hence the adsorption decrease in Figs. 1 and 2 cannot be an electrolyte effect. Addition of alkali to the system cotton/sodium alkyl

TABLE I

Effect of pH on Sodium n-Pentadecyl Sulfonate Adsorbed by Cotton (60°C.)
Initial concentration of detergent 2.70 × 10^{-3} *M*

pH	Adsorption (*millimoles/100 g.*)
7.2	0.75
8.5	0.36
9.2	0.34
10.0	0.28
10.4	0.29

TABLE II

Effect of Acid on Sodium Alkyl Sulfates Adsorption by Cotton (30°C.)
Initial detergent concentration 3.0 × 10^{-3} *M*

HCl concn.	Adsorption (*millimoles/100 g.*)
0.0 *N*	0.0
0.0138	0.16
0.0276	0.20
0.0552	0.17

sulfonate (11) gives a reduced adsorption (Table I). Again, the negligible adsorption of sodium alkyl sulfates on cotton (Fig. 3) is naturally not affected by alkali, but addition of acid increases the adsorption (17) (Table II). It is clear therefore that the variation of adsorption with change in pH cannot be due to hydrolysis of the detergent.

In a broad sense the decrease in adsorption with increase in alkalinity is due to competition of the hydroxyl ions and the detergent ions for the fiber surface. Adsorption of hydroxyl ions brings about an increase in the (negative) interfacial potential of the fiber surface (18) and the adsorption of detergent must therefore decrease. When the pH rises above 11.0, where the interfacial potential reaches a maximum, increased adsorption of detergent ions may again occur (viscose, Fig. 2). Water, hydroxyl ions, and detergent ions are all capable of adsorption on the fiber, and there is a considerable degree of interaction between the adsorbable species; in some cases a decreased adsorption of water (for fibers immersed in buffer solution only) accompanies a decreased adsorption of detergent.

Discussion

It has been possible to account for the observed phenomena only in a qualitative way. The main difficulty is the great imprecision of the swelling results. The ellipticity of the dry fiber (particularly cotton), which tends to become circular in the swollen state, introduces variations from fiber to fiber which can be overcome only by making many more measurements at the same concentration, but such a course would prolong the experiment unreasonably. Statistical examination of the data confirms that in each experiment the swelling decreases with increasing concentration. Although in any single experiment there is too much scatter to establish that the mathematical relation between swelling and concentration contains a cubic term (that is, the swelling has an increasing downward trend followed by a leveling off or increase), by taking the results as a whole a sharp downward trend of the type shown by the full lines in Figs. 4–6 is statistically significant. Despite this difficulty the deficiency in logarithmic adsorption follows the decrease in swelling reasonably well except in two experiments, viz., those with viscose at pH 9.5 and 10.9; here the swelling starts to decrease at a lower concentration than does the adsorption from the Freundlich isotherm.

Salt Effect

Small concentrations of inorganic electrolyte (up to 0.05 *N*) have little effect on the adsorption, but 0.3 *N* sodium sulfate increases the adsorption of sodium alkyl sulfates by cotton from zero to 0.5×10^{-3} mole/100 g. At higher salt concentrations, or for the same salt concentration in a solution of less soluble detergent, one would expect the adsorption to increase anal-

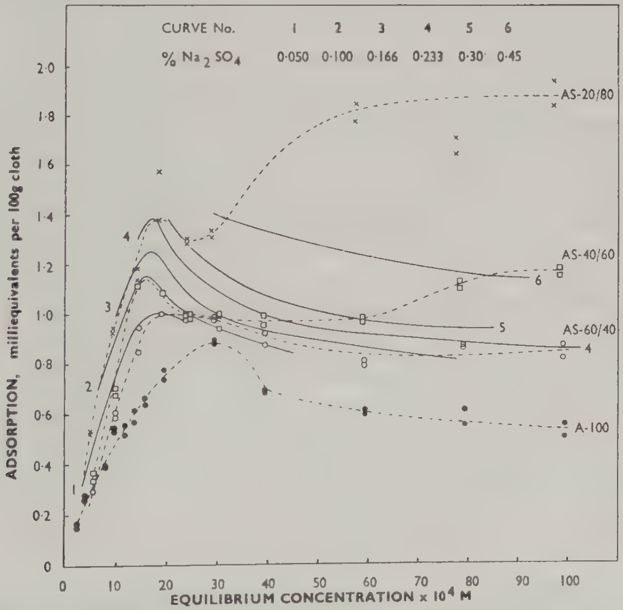

FIG. 8. Figure 1 of Meader and Fries' paper replotted. Sodium sulfate concentration constant.

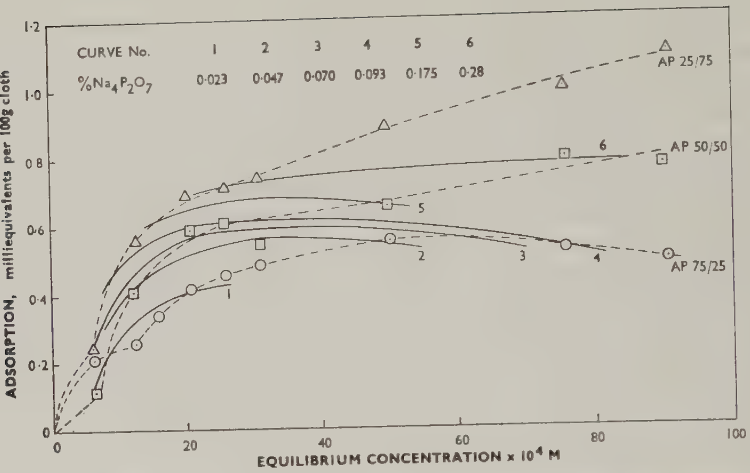

FIG. 9. Figure 3 of Meader and Fries' paper replotted. Sodium phosphate concentration constant.

ogously to a "salting out" effect of organic liquids, while the position of the maximum should be but little affected. At first sight the adsorption isotherms obtained by Meader and Fries (5) with added sodium sulfate and tetrasodium pyrophosphate (their Figs. 1 and 3) appear anomalous, but in their experiments the electrolyte and alkylarylsulfonate concentrations are varied simultaneously. Figure 8 shows the data of Meader and Fries plotted in terms of constant concentrations of sodium sulfate, although only three points are available for each curve. As the salt concentration is increased the adsorption of detergent increases, the maximum moves to a slightly lower equilibrium concentration, and the subsequent decrease in adsorption at higher detergent concentrations becomes less marked.

When tetrasodium pyrophosphate is added to the adsorption system the adsorption is greatly lowered at first; further additions cause an increase (Fig. 9). This initial reduction in adsorption is due to the pH of the pyrophosphate solution (*ca.* 10) and at the lowest salt concentration the adsorption isotherm resembles that of sodium oleate on cotton (Fig. 1). Higher concentrations of pyrophosphate cause an increase in adsorption and the maximum tends to disappear analogously with the effect of sodium sulfate. The same effect is seen when the results of Meader and Fries for adsorptions from solutions containing sodium pyrophosphate at 60°C. (their Fig. 4) are similarly replotted.

Mechanism of Swelling

The possibility exists that the decrease in adsorption as the fiber diameter is reduced may be due to the fact that the bulk solution, and not water, is absorbed by the fiber; as the fiber swelling is reduced the amount of detergent on the fiber is likewise reduced in proportion. However, calculation indicates that the amount of water withdrawn is, at most, *ca.* 10 ml. per 100 g. fiber. At the concentration where swelling decreases, the amount of detergent in this volume is much too small to account for the decrease in adsorption.

In the past attempts have been made to apply the Donnan theory of membrane equilibrium to the adsorption of dyes by fibers, but since neither the activity coefficient of the adsorbed species nor the effective volume of the fiber phase is known the transformation of adsorptions into activities involves arbitrary assumptions. This is also true of the present work, but consideration of the Donnan theory leads to a qualitative conception of the mechanism by which fiber swelling decreases above the c.m.c. of the detergent. The micelles then formed are not adsorbed and can be treated in the same way as the nondiffusible ions of the Donnan theory. If therefore constraint could be applied to the adsorption system so that water remained in the fiber, an osmotic pressure would be set up and the isotherm would not contain a maximum. Under experimental conditions, however, the osmotic pressure tendency has the effect of preventing some of the water from entering the fiber. Since the concentration of micelles increases continuously above the c.m.c., it might be objected that the fiber swelling should continue to lessen; it is probable, however, that a balance of forces exists between the osmotic effect and the energy of sorption of water by the fiber. As the concentration of water in the fiber is increased its heat of sorption is known to decrease rapidly.

The results of Mann and Morton (19) for the dyeing of cotton by anionic dyes confirm the hypothesis that swelling and adsorption are co-related. In dyeing it is generally considered that swelling of the amorphous regions of the fiber is a necessary preliminary to the adsorption of dyes: in the unswollen state the capillary spaces of the fiber are too small to admit the penetration of the dye molecules. This swelling is complete within a short time; Mann and Morton state that for viscose 10 seconds is sufficient. Although the molecular sizes of detergents are not as great as those of the majority of dyes, it is probable that the same condition holds; the fiber swelling is completed quickly and the much slower process of detergent adsorption follows. When the ability of water to swell the fiber becomes reduced the detergent ions are not able to penetrate the capillary spaces to the same degree, and adsorption is reduced.

The hypothesis also explains the results obtained by Klevens and Carr (20) on the equilibrium dialysis of detergent solutions through cellophane sheets. They found that at detergent concentrations below the c.m.c. equilibrium is established in a short time; above the c.m.c. the passage of detergent through the cellophane is much slower, and alkali or potassium chloride reduces the rate still further. They state that the controlling factor is the pore size of the membrane in relation to the micellar diameter, but cannot account for the extremely slow dialysis at concentrations above the c.m.c. We prefer to think of the process as one of adsorption followed by diffusion across the membrane. If the detergent solution is initially below the c.m.c., the cellophane is fully swollen on both sides and detergent ions can readily diffuse through. If, on the other hand, the initial concentration is well above the c.m.c. (in Klevens' experiments the factor is 10), the cellophane will not be swollen to its fullest extent and the detergent ions are not able to pass through so readily. The usual outcome will be that diffusion will occur until the concentrations on either side of the membrane are such that the adsorptions on either side are the same (i.e., the concentrations are on opposite sides of the maximum in the adsorption isotherm). The system will therefore be in equilibrium except for a concentration gradient for water across the membrane; water will thus pass through the membrane in a direction such that the bulk detergent concentrations tend to become equalized. Since the experiments were carried out under conditions which minimized the transfer of water, this process must be very slow. The effect of alkali on the dialysis process can be attributed to the reduced adsorption on the surface in the presence of hydroxyl ions, resulting in a slower diffusion process.

EXPERIMENTAL

Fibers

The cellulose acetate fibers were extracted once with petroleum spirit (40°–60° b.p.), four times with water at 55°C., and dried at 60°C. The acetate contents of the fibers were determined by Barnett's method (21): monoacetate and triacetate, 41% and 61% expressed as acetic acid. The viscose and nylon 66 fibers were extracted with ether, ethanol, and water in turn, and dried at 100°C. All these fibers were used as hanks of approximately 1 g. weight. The cotton, tarantulle fabric of weight *ca.* 100 g./m.^{2}, was desized with Nervanase (diastase), washed several times with boiling water, and dried. It was used in the form of approximately 5-cm. squares. The carboxyl content of the viscose and cotton was 5.0 and 0.2 meq./100 g., respectively (22). Before use all the materials were conditioned over saturated ammonium nitrate at 65% R.H.

Materials

Sodium oleate was prepared from purified oleic acid (neutralization value: 143; iodine number 89.9) and sodium hydroxide; the purity of the material was 99.3% as determined by titration against standardized cetyltrimethyl ammonium bromide. The sodium alkyl sulfates were obtained from a commercial detergent ("Teepol") which was desalted before use by adding isopropyl alcohol and separating off the aqueous layer. Buffer solutions for the pH range 8.5–10.0 were made with boric acid, potassium chloride, and sodium hydroxide; those for the range 10.0–12 were made with glycine, sodium chloride, and sodium hydroxide.

Adsorption Experiments

Adsorptions were carried out at 30 ± 0.05°C. For nylon 145 hours were allowed for the attainment of equilibrium; in fact further adsorption continued up to three weeks, but since the rate of adsorption is inversely proportional to the time elapsed, after 145 hours the rate is very low. For cotton, cellulose acetate, and viscose equilibrium was established after 4, 24, and 48 hours, respectively. The concentration of the equilibrium solution was measured by titrating an aliquot part against cetyl pyridinium bromide for sodium alkyl sulfates using methylene blue as indicator (23), or against cetyltrimethyl ammonium bromide for sodium oleate using Pontamine Fast Red as indicator. The fiber weight was corrected for the regain at 65% R.H.

Swelling Measurements

A single fiber was held on a microscope slide with spots of plasticine, a cover glass was placed over it, and its diameter was measured at a linear magnification of about 500 by positioning the image between the fixed and adjustable parallel hairs of a micrometer eyepiece. A single drop of solution was then run between the slide and cover glass from a capillary, and the diameter of the fiber was measured at the same position after a lapse of about 2 minutes. The ratio of fiber to solution is so small that the concentration of the solution is not appreciably changed by adsorption onto the fiber. Because of the very wide variation in results, replicate measurements were made on at least eight fibers at each detergent concentration.

ACKNOWLEDGMENTS

The author thanks Mr. S. R. Epton and Dr. P. A. Winsor for discussions, and the Directors of "Shell" Research Ltd. for permission to publish this work.

REFERENCES

1. Aickin, R. G., *J. Soc. Dyers Colourists* **60**, 60 (1944).
2. Acharya, B. G., and Wheeler, T. S., *Proc. Indian Acad. Sci.* **2A**, 637 (1935).
3. Gardiner, K. W., and Smith, L. B., *J. Am. Oil Chemists' Soc.* **26**, 194 (1949).
4. Vold, R. D., and Phanasalkar, A. K., *Rec. trav. chim.* **74**, 41 (1955).
5. Meader, A. L., and Fries, B. A., *Ind. Eng. Chem.* **44**, 1636 (1952).
6. Fava, A., and Eyring, H., *J. Phys. Chem.* **60**, 890 (1956).
7. Weatherburn, A. S., and Bayley, C. H., *Textile Research J.* **22**, 797 (1952).
8. Flockhart, B. D., and Graham, H., *J. Colloid Sci.* **8**, 105 (1953).
9. Evans, H. C., *J. Chem. Soc.* **1956**, 579.
10. Hartley, G. S., *Trans. Faraday Soc.* **37**, 130 (1941).
11. Wijga, P. W. O., private communication.

12. Flockhart, B. D., and Ubbelohde, A. R., *J. Colloid Sci.* **8,** 428 (1953).
13. Stainsby, G., and Alexander, A. E., *Trans. Faraday Soc.* **46,** 587 (1950).
14. Marshall, W. T., and Peters, R. H., *J. Soc. Dyers Colourists* **63,** 446 (1947).
15. Larose, P., *J. Soc. Dyers Colourists* **70,** 77 (1954).
16. Gillam, N. W., *Textile J. Australia* **21,** 535 (1946).
17. Epton, S. R., private communication.
18. Harrison, W., *J. Soc. Dyers Colourists* **27,** 279 (1911).
19. Mann, T. B., and Morton, T. H., *Discussions Faraday Soc.* **No. 16,** 75 (1954).
20. Klevens, H. B., and Carr, C. W., *J. Phys. Chem.* **60,** 1245 (1956).
21. Barnett, W. L., *J. Soc. Chem. Ind.* **40,** 9T (1921).
22. Neale, S. M., and Stringfellow, W. A., *Trans. Faraday Soc.* **33,** 881 (1937).
23. Epton, S. R., *Trans. Faraday Soc.* **44,** 226 (1948).

JOURNAL OF COLLOID SCIENCE **13**, 553–564 (1958)

I. MEASUREMENT OF DYNAMIC SURFACE TENSIONS OF AQUEOUS SOLUTIONS BY THE OSCILLATING JET METHOD

Raymond Defay and Jacques R. Hommelen

Université Libre de Bruxelles, Brussels, Belgium

Received May 27, 1958

Abstract

The rate of surface tension lowering of aqueous solutions of ten long-chain alcohols and two dicarboxylic acids has been measured by the oscillating jet method. The surface tensions have been calculated by the Bohr formula.

Seven orifices, standardized with water, have been used to determine the variation of surface tension with age for an aqueous solution of heptanol (0.4 g./l). The results obtained, which lie on a single curve, are compared with published values.

I. Introduction[1]—Principle and History of the Method

If a jet of the liquid to be examined is forced through a small elliptical orifice under constant pressure, stationary waves are produced on the stream; these waves oscillate about their equilibrium circular form, the restoring force being the surface tension. Determination of the outflow rate, the mean radius of the jet and the wavelengths is sufficient for the calculation of the surface tensions along the jet, for surface ages varying between 0.1 and 0.001 second. From the knowledge of the outflow rate, the surface age at any point on the stream can be calculated.

Bidone (2) in 1854 and Magnus (3) in 1855 were the first to observe the phenomenon. Rayleigh (4) in 1879 gave the first mathematical treatment to it; this allowed him to study the variation of surface tension with time for very short surface ages. He showed that the surface tensions of soap solutions were very near that of water for surface ages below 0.001 second. Pederson (5), Bohr (6), and Stocker (7) further improved the experimental technique.

Bohr, in 1908, derived a complete hydrodynamical treatment of the problem and obtained a practical equation with which he could measure the surface tension of pure water.

---

[1] This is the first of a series of three papers on the measurement of dynamic surface tensions and the discussion of the mechanism of adsorption of heavy alcohols and acids in dilute aqueous solutions. (Thesis subject (26).)

We have recently published a detailed bibliographical study of other methods of measuring dynamic surface tensions (1).

Bond and Puls (8) have used the method to check the results which had been obtained with their flowing sheet method on soap solutions.

Addison and his co-workers (9–15) have developed and utilized an empirical method, the results of which, obtained with solutions of heavy alcohols, differ from those obtained with the same solutions by Sutherland (16, 17), (28) using the Bohr equation.

Burcik and Newman (18–21), (25) have studied solutions of sodium salts of fatty acids using Addison's empirical procedure.

A process of elimination of the capillaries examined, leading to the selection of those which conform to the Bohr equation, must be carried out. Sutherland (17, p. 321) has shown that Addison's orifice is unsatisfactory for use with the Bohr equation.

This equation can be considerably simplified if values to within 0.2% only are required. Apart from its greater accuracy, this equation is also more convenient to use than the empirical treatment of Addison (17).

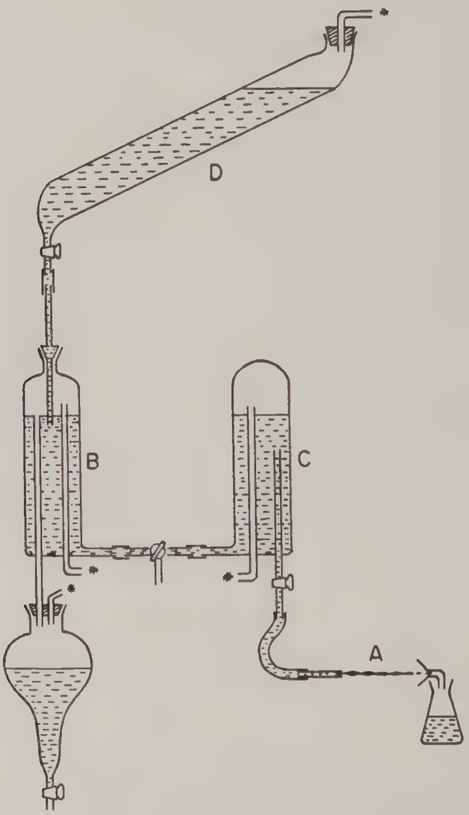

Fig. 1. Oscillating jet apparatus (*A*—oscillating jet).

Sutherland (16, 17, 22) was the first to apply the Bohr equation to the vibrating jet method to study some solutions of simple surface-active substances. He did not, however, succeed in obtaining results completely independent of the capillary orifice used.

A procedure to eliminate this difference for water has been evolved in the present work, and used to correct values obtained with aqueous solutions. In this way it is claimed that true surface tension values may be obtained at very short ages.

II. Description of the Apparatus

The apparatus can be seen on Fig. 1. It was kept at constant temperature (20° ± 0.5°C.). The outflow rate of solution through the elliptical capillary orifice (*A*) was maintained at a definite value by the constant-level device used. The vessel *C* was incorporated to damp out the pressure oscillations created by the overflow in *B*.

The tubes marked with an asterisk lead to an air vessel which was kept at a pressure greater than atmospheric by means of a compressed air system (not shown), which could be maintained thanks to another constant liquid level. The outflow rate from the orifice could thus be modified by varying the air pressure, without moving either the capillary tube or the constant-level vessels *B* and *C*. The whole apparatus was firmly fastened to a wall. In order to damp out the building vibrations, the orifice was attached to a heavy concrete mass lying on three small blocks of rubber which in turn rested on two consoles.

III. Measurement of the Dimensions of the Jets

1. Measurement of the Wavelengths

The method of measuring the wavelengths (λ) is essentially due to Stocker (7). The jet is illuminated with a parallel beam of light (Fig. 2). A pinhole in a tinfoil screen (*C*) forms a point source of light. The hole is illuminated by projecting on the screen the image of the filament of a cinelamp (*A*) using an Elmar Leica f.3.5–5 cm. lens. The point source *C*

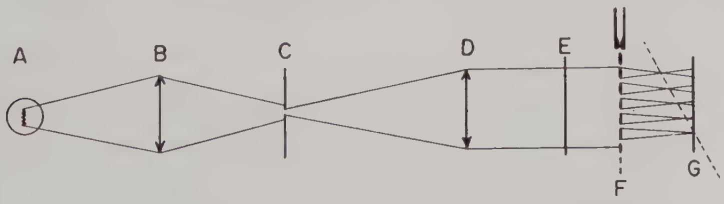

Fig. 2. Measurement of the wavelengths—optical system:
F—oscillating jet.
A—light source.
G—photographic plate.

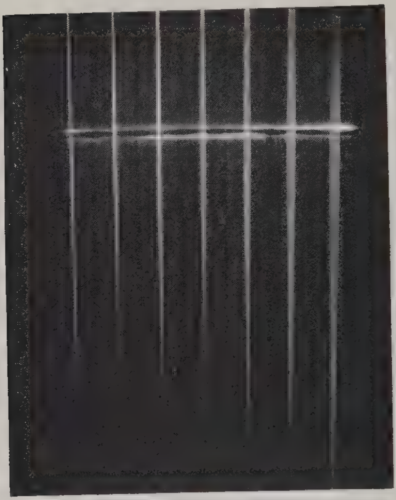

FIG. 3. Photographic figure for measurement of the wavelengths.

is placed at the focus of another lens D (f.4.5–21 cm.), and the resultant parallel beam of light is narrowed by a horizontal slit in the screen E to illuminate only the jet F.

Each wave of the jet acts as a cylindrical convergent lens, producing well-defined line images which can be observed on a focusing screen at G or recorded on a photographic plate (Fig. 3).

Owing to progressive amplitude variation of the waves, sharp images are obtained only if the plate is inclined at an angle α to the stream (7, 27) (dotted line Fig. 2). The distance between the line images on the photographic plate multiplied by $\cos \alpha$ gives the wavelength λ. If, however, the plate is parallel to the jet, the images, although unfocused and therefore of varying width, have sharp edges and hence their mid-points can be accurately determined. The error on $\cos \alpha$ is, in this latter case, reduced to a minimum. All wavelength values reported in the present work are obtained in this way, using a cathetometer, and are accurate to within 0.01 mm.

2. Measurement of the Jet Radius

Maximum and minimum radii of the stream were measured by observing it from above through a microscope with a moving reticular eyepiece. The moving reticle was calibrated with a spectrographic plate with very thin lines, the linear separations of which had been previously determined with a traveling microscope. In the eye-piece used, one hundred graduations on the reticle screw equaled a length on the plate of 0.01535 ± 0.0005 cm.

IV. MEASUREMENT OF OUTFLOW RATE

The outflow rate D was obtained by measuring, with a stop watch, the time necessary to collect 250 ml. of solution in a calibrated vessel. The volume was correct to within 0.1 ml. and the time to within 0.5 second.

V. CALCULATION OF THE SURFACE TENSIONS

Bohr has established the complete equation giving the surface tensions along the jet in terms of the wavelengths (λ), the outflow rate (D), and the maximum and minimum radii of the jet (r_x and r_i).

Sutherland (17) (28) has shown that, for dilute aqueous solutions the viscosity of which is not greater than 0.01 poise, correction factors in the Bohr equation can be neglected if surface tension values within 0.2% are acceptable.

The equation then becomes

$$\sigma = \frac{4\rho D^2 \left(1 + \frac{37}{24}\frac{b^2}{b^2}\right)}{6r\lambda^2 + {}^5\!/_3\pi^2 r^3}, \qquad [1]$$

where ρ = density of the solution;

$$\frac{a}{b} = \frac{r_x - r_i}{r_x + r_i};$$

$$r \approx \frac{r_x + r_i}{2}.$$

VI. PREPARATION OF ORIFICES

The elliptical capillaries were obtained by pressing circular Pyrex glass capillaries, previously softened in a Bunsen flame, between two parallel even surfaces of cold iron. Each capillary was sealed to a Pyrex glass tube of the same external diameter ($\approx$4 mm.) and then cut symmetrically about 2 mm. from the join.

The capillaries were tested in the apparatus using pure water and only those which produced no distortion on the photographs (7) and the wavelengths of which were constant after the fourth wave (within 0.01 mm.) were kept.

In order to discover the reason why Sutherland (16) could not obtain concordant results with two different orifices, about fifty different capillaries were made, and of these only seven of various radii and amplitudes were kept (Table I).

During the tests with pure water, various hydrostatic pressures were used in order to vary the outflow rates for a single orfice. It is important that the radius be measured on the jet itself and not on the orifice since the stream suffers a slight contraction after leaving the orifice.

VII. Standardizing of the Apparatus with Pure Liquids

Using Eq. [1], the results obtained with pure liquids are summarized in Table I. Each given value of λ is a mean value measured from the third to the tenth waves. The amplitude b/a decreases with increasing distance from the orifice, and an average value obtained from measurements on the sixth wave was used in each calculation. The values for the surface tension of water and carbon tetrachloride given in the International Critical Tables are 72.8 and 26.8 dynes/cm., respectively, at 20° C. From Table I it is seen that the calculated values for water, for the orifices and flow rates used, lie above the classical value by the following amounts $\Delta\sigma$ in dynes/cm.: -0.1; $+1.1$; $+0.6$; $+1.7$; $+2.0$; $+2.4$; $+1.2$; $+1.6$; $+0.2$.

These quantities $\Delta\sigma$ are outside the average variation from the mean, and there is therefore a systematic difference depending on the orifice and flow rate used. This indicates that the orifices do not conform perfectly with the Bohr equation.

In all determinations of the surface tension of solutions, the differences were allowed for by applying the particular correction appropriate to the orifice and flow rate used. This correction equals $\Delta\sigma/72.8$, multiplied by the uncorrected measured tension.

VIII. Comparison of Results with Published Data

Sutherland is the only author who has used the vibrating jet based on the Bohr equation to measure the dynamic surface tensions of aqueous alcoholic solutions. The results were found to depend on the particular orifice used (Fig. 4).

Addison derived an empirical equation for the calculation of surface tension from measured data, but apparently used only one orifice. It can be seen from Fig. 4 that his results with normal heptyl alcohol are completely different from those of Sutherland.

In an attempt to account for these differences, the series of capillaries mentioned earlier were used to examine normal heptyl alcohol of the same concentration as used by other workers (0.4 g./l.). The tension was calculated in each instance by means of Eq. [1]; applying the appropriate correction factor to each orifice and flow rate. The results, given in Table II and plotted in Fig. 4, show that the experimental values of surface tension lie on a single curve.

It is probable therefore that these results represent the true variation with time of the surface tension of the heptyl alcohol solution. The results obtained by Sutherland, although dependent on the orifice used, approximated closely to the values of the present authors (Fig. 4).

TABLE I

Standardization of the Oscillating Jet Method

20°C.	Radius of jet r (*cm.*)	Amplitude $\frac{b}{a}$	Outflow rate D (*cm.*^{3}/*sec.*)	Wavelength λ (*cm.*)	Surface tension σ (*dynes/cm.*)	
CCl_4 capillary I_2	0.0206	1/11	0.420	0.578	26.8	
	0.0206	1/11	0.420	0.580	26.7	
CCl_4 capillary II_2	0.0260	1/12	0.707	0.865	27.2	
H_2O capillary I_2	0.0205	1/11	0.523	0.341	73.0	72.7 ± 0.3[a] 0.2[b]
	0.0205	1/11	0.522	0.340	73.0	
	0.0208	1/11	0.534	0.346	72.5	
	0.0208	1/11	0.526	0.342	72.5	
H_2O capillary I_2	0.0210	1/23	0.400	0.249	73.7	73.9 ± 0.3[a] 0.3[b]
	0.0210	1/23	0.397	0.245	74.2	
	0.0210	1/23	0.398	0.246	74.1	
	0.0211	1/22	0.402	0.250	73.5	
H_2O capillary I_3	0.0204	1/8	0.532	0.349	73.5	73.4 ± 0.2[a] 0.2[b]
	0.0206	1/10	0.537	0.349	73.6	
	0.0206	1/9	0.538	0.350	73.5	
	0.0208	1/9	0.542	0.352	73.3	
	0.0208	1/9	0.542	0.352	73.3	
	0.0207	1/9	0.541	0.352	73.3	
H_2O capillary I_3	0.0210	1/16	0.403	0.249	74.8	74.5 ± 0.3[a]
	0.0209	1/16	0.407	0.252	74.3	
H_2O capillary II_2	0.0260	1/9	0.914	0.527	75.5	
H_2O capillary II_2	0.0261	1/13	0.683	0.387	74.6	74.8 ± 0.4[a] 0.3[b]
	0.0261	1/13	0.682	0.388	74.4	
	0.0261	1/11	0.695	0.393	74.8	
	0.0260	1/12	0.695	0.391	75.2	
	0.0261	1/11	0.690	0.391	75.1	
H_2O capillary II_6	0.0283	1/46	0.775	0.420	74.8	75.2 ± 0.5[a] 0.3[b]
	0.0282	1/46	0.772	0.417	75.2	
	0.0281	1/46	0.765	0.413	75.7	
H_2O capillary III_1	0.0332	1/11	1.115	0.568	74.0	74.0 ± 0.3[a] 0.2[b]
	0.0331	1/11	1.111	0.569	73.7	
	0.0330	1/10	1.118	0.571	74.2	
	0.0330	1/10	1.125	0.574	73.9	
	0.0331	1/10	1.129	0.576	74.2	
H_2O capillary III_2	0.0334	1/13	1.131	0.574	74.2	74.4 ± 0.2[a] 0.1[b]
	0.0335	1/14	1.130	0.572	74.3	
	0.0337	1/12	1.152	0.581	74.5	
H_2O capillary III_3	0.0302	1/8	0.924	0.498	73.0	

[a] Maximum variation.

[b] Average variation to the mean.

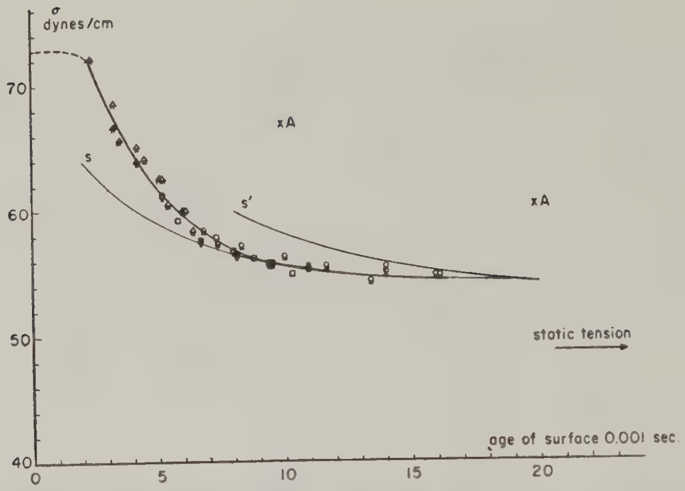

Fig. 4. Dynamic surface tensions of a normal heptyl alcohol solution 0.4 g./l.(20°C.).
S, *S′*—values obtained by Sutherland.
A —values obtained by Addison.

Data obtained for other alcohol and acid solutions are given below.

(In order to verify the absence of an evaporation effect, the jet was enclosed in a special box, with two optical glass walls parallel to the jet so as to allow the light beam to pass. The box contained a little solution under test. Under both conditions, identical results were obtained, and it is therefore unlikely that evaporation occurs to any significant extent.[2])

IX. Further Determinations of Dynamic Surface Tensions

In an attempt to assess the role played by diffusion in the adsorption mechanism,[3] the dynamic surface tensions of a number of other solutions have been determined.

Figure 5 shows the variations of surface tension with age for several aqueous solutions of alcohols, the concentrations used being such that the static or equilibrium surface tension was the same for each solution. The solutions of branched heptyl alcohols and those of hexyl alcohols reached their static tension within 0.01 second (curves *A*, *G*, *F*, *B*, *C*), whereas the normal heptyl alcohol and the branched octyl alcohols aged at a somewhat slower rate. The surface tensions of the normal octyl alcohol and the branched nonyl alcohol at these concentrations did not fall much below that of pure water within 0.015 second. It is seen that the three groups

---

[2] The selective evaporation of alcohols and acids of medium volatility from dilute aqueous solutions has been studied and discussed in this laboratory by one of us (23, 24), (26).

[3] See third paper of the present series.

TABLE II

Oscillating Jet Method—Normal Heptyl Alcohol Solution 0.4 Gram per Liter

Capillary	No.	r	$\frac{b}{a}$	D	λ	t	σ
I_2	3–4	0.0206	1/16	0.535	0.352	2.4	72.2
	4–5				0.366	3.3	66.7
	5–6				0.374	4.2	64.0
	6–7				0.378	5.1	62.5
	7–8				0.386	6.0	60.0
I_2	4–5	0.0207	1/27	0.396	0.257	3.3	68.7
	5–6				0.264	4.2	65.1
	6–7				0.269	5.1	62.7
	7–8				0.275	6.0	60.0
I_3	4–5	0.0210	1/27	0.404	0.266	3.5	65.7
	5–6				0.269	4.5	64.2
	6–7				0.277	5.4	60.6
	7–8				0.282	6.4	58.4
	8–9				0.284	7.3	57.6
II_2	5–6	0.0262	1/20	0.925	0.604	6.7	57.6
	6–7				0.610	8.1	56.5
	7–8				0.613	9.5	55.9
	8–9				0.615	10.9	55.5
II_2	4–5	0.0263	1/26	0.692	0.433	5.2	60.6
	5–6				0.447	6.6	56.9
	6–7				0.448	8.0	56.8
	7–8				0.451	9.4	55.8
II_6	4–5	0.0282	1/100	0.770	0.467	5.8	59.2
	5–6				0.473	7.3	57.8
	6–7				0.480	8.8	56.1
	7–8				0.484	10.3	54.8
III_1	7–8	0.0331	1/15	1.120	0.660	14	55.6
	8–9				0.665	16	54.9
III_3	4–5	0.0301	1/11	0.920	0.554	6.6	58.4
	5–6				0.560	8.3	57.2
	6–7				0.564	10.0	56.4
	7–8				0.567	11.7	55.8
	8–9				0.575	13.4	54.2

No.—wave number.
r—radius of jet (cm.).
b/a—mean amplitude.
D—outflow rate (cm.^{3}/sec.).
λ—wavelength (cm.).
t—age of surface (10^{-3} sec.).
σ—surface tension (dynes/cm.).

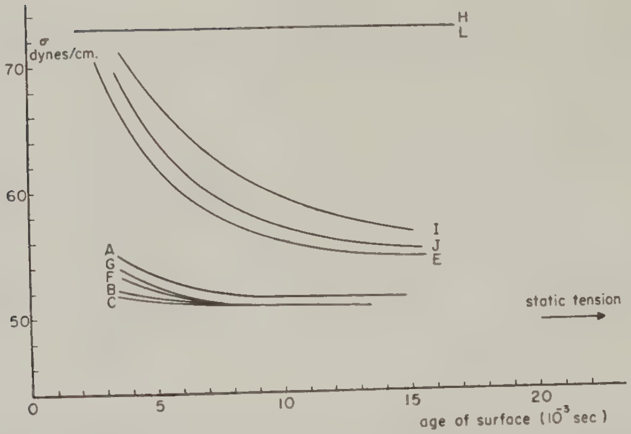

FIG. 5. Dynamic surface tensions of some alcohol solutions with same static surface tension (20° C.).

A —normal hexyl alcohol 1.29 g./l.
B —isohexyl alcohol 2.38 g./l.
C —1 methyl pentanol 2.47 g./l.
E —normal heptyl alcohol 0.4 g./l.
F —ethyl butyl carbinol 1.22 g./l.
G —dipropylcarbinol 1.26 g./l.
H —normal octyl alcohol 0.116 g./l.
I —methylhexylcarbinol 0.255 g./l.
J —2 ethyl hexanol 0.273 g./l.
L —3,5,5 trimethyl hexanol 0.114 g./l.

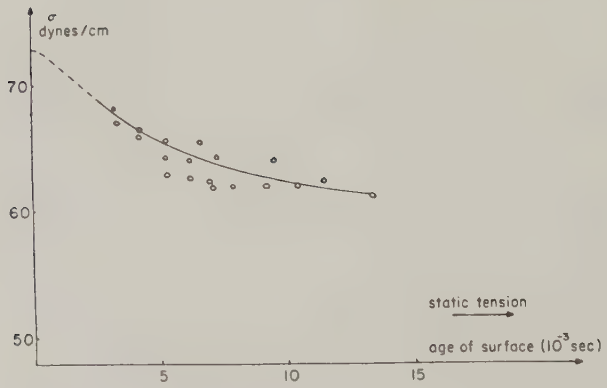

FIG. 6. Dynamic surface tensions of the azelaic acid solution 10^{-2} *M* (20°C.).

shown are mainly characterized by the concentration factor, suggesting that diffusion governs the adsorption mechanism.

Results for 0.01 *M* azelaic acid are given in Fig. 6 and show its behavior to be similar to that of the group *I J E* in Fig. 5 for surface ages up to

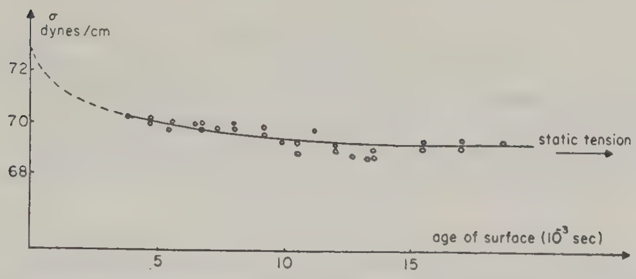

FIG. 7. Dynamic surface tensions of the adipic acid solution 0.1 *N* (20°C.).

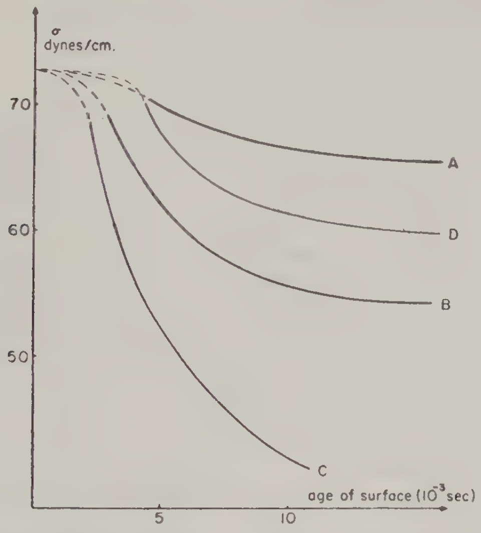

FIG. 8. Dynamic surface tensions of some alcohol solutions.

A—hexyl alcohol
B—heptyl alcohol } 3.44 10^{-3} mole/liter.
C—octyl alcohol
D—heptyl alcohol 2.43 10^{-3} mole/liter.

about 0.015 second. However, this solution does not attain its equilibrium tension until after 15 hours (29).

Adipic acid (0.05 *M*), on the other hand, attains its equilibrium tension within 0.01 second (Fig. 7).

Figure 8 shows the results for three different normal alcohols at the same concentration in moles/liter (*A*, *B*, *C*). The fourth curve refers to a different concentration of heptyl alcohol (*D*).

These curves have been determined, together with those obtained with the falling meniscus method,[4] for the calculation of the diffusion speed of the solute towards the surface.[5]

---

[4] See second paper of the present series.

[5] See third paper of the present series.

Acknowledgments

An important part of the equipment necessary for the present work was obtained through the generosity of the "Centre National de Chimie Physique Moléculaire" and the "Fonds National de la Recherche Scientifique."

We should like to express our gratitude to these two organizations.

References

1. Defay, R., and Hommelen, J., *J. Ind. Chim. Belg.* **XXIII** (no. 6) 597 (1958).
2. Bidone, "Experiences sur la Forme et la Direction des Veines et des Courants d'Eau lancés par diverses Ouvertures." 1854.
3. Magnus, P., *Pogg. Ann.* **95** (1855).
4. Rayleigh, Lord, *Proc. Roy. Soc.* (*London*) **29**, 71 (1879).
5. Pederson, P. O., *Phil. Trans.* **A207**, 341 (1906–1907).
6. Bohr, N., *Phil. Trans.* **A209**, 281 (1908–1909).
7. Stocker, H., *Z. physik. Chem.* **94**, 149 (1920).
8. Bond, W. N., and Puls, H. O., *Phil. Mag.* [7] **24**, 864 (1937).
9. Addison, C. C., *J. Chem. Soc.* **1943**, 535.
10. Addison, C. C., *J. Chem. Soc.* **1944**, 252.
11. Addison, C. C., *J. Chem. Soc.* **1944**, 477.
12. Addison, C. C., *Phil. Mag.* **36**, 73 (1945).
13. Addison, C. C., *J. Chem. Soc.* **1945**, 98.
14. Addison, C. C., *J. Chem. Soc.* **1945**, 354.
15. Addison, C. C., and Litherland, D., *Nature* **171**, 393 (1953).
16. Sutherland, K. L., *Revs. Pure and Appl. Chem.* (*Australia*) **1**, 35 (1951).
17. Sutherland, K. L., *Australian J. Chem.* [7] **4**, 319 (1954).
18. Burcik, E. J., *J. Colloid Sci.* **5**, 421 (1950).
19. Burcik, E. J., *J. Colloid Sci.* **6**, 522 (1951).
20. Burcik, E. J., *J. Colloid Sci.* **8**, 520 (1953).
21. Burcik, E. J., and Newman, R. C., "Technical report on a fundamental study of foams and emulsions." Pennsylvania State College, State College, Pennsylvania, 1953.
22. Rideal, E. K., and Sutherland, K. L., *Trans. Faraday Soc.* **48**, 1109 (1952).
23. Hommelen, J., *Bull. soc. chim. belges*, **66**, 476 (1957).
24. Hommelen, J., *J. Colloid Sci.*, in the press.
25. Burcik, E. J., and Newman, R. C., *J. Colloid Sci.* **9**, 498 (1954).
26. Hommelen, J., Doctor's thesis. Brussels, 1957.
27. Littaye, G., *Compt. rend.* **214**, 760 (1942).
28. Sutherland, K. L., Thesis. London, 1950.
29. Derycker, M., and Defay, R., *Bull. soc. chim. belges* **65**, 794 (1956).

JOURNAL OF COLLOID SCIENCE **13**, 565–568 (1958)

RADIOACTIVE TRACER STUDIES OF MONOLAYERS[1]
II. COMPARISON OF FLOATING AND BUILT-UP MONOLAYERS

Harry Sobotka, Margaret Demeny, and J. D. Chanley

Department of Chemistry, Mount Sinai Hospital, New York, New York

Received June 19, 1958

Abstract

The composition of built-up calcium stearate stearic acid layers has been studied with Ca^{45}. The results diverge from those obtained by conventional chemical analysis of the floating layers ("H-layers"), from which the built-up layers were formed. Similar discrepancies have been observed when building layers of fatty acids on a hypophase containing bivalent organic cations. In all these instances the cations seem to form an integral part of the H-film, but are eliminated, probably by exchange against protons, during the building-up operation.

Introduction

The radioactive labeling of monolayers provides an excellent analytical tool for the quantitative study of physical and chemical changes in these films (2). In order to understand the reactivity of molecular films, one should learn as much as possible about their composition. Langmuir and Schaefer (3) had studied stearic acid monolayers, skimmed off from a bath, containing Ba or Ca ions in 10^{-4} *M* solution; the pH values of the bath ranged from 4.5 to 10.5. The film was pushed with a glass skim-bar into a narrow strip, and the crumpled film was then collected by means of a scoop of thin platinum foil. The tray was thus skimmed about 10 times, yielding film of a total area of 3–4 m.^{2}. The material was blotted with filter paper, dried in a platinum boat, heated in the presence of a few drops of concentrated H_2SO_4, and was then weighed. The results are shown in Fig. 1, where the neutralized fraction of the stearic acid is plotted as ordinate against the pH as abscissa. A sigmoid curve was obtained, not unlike a dissociation curve, but of flatter slope.

Composition of Built-Up Films and pH

We have studied the relationship between pH of the hypophase and the percentual incorporation in the film of cations by radioactive tracer

---

[1] Presented before the Division of Colloid Chemistry, American Chemical Society, New York, September 1957. For the first paper of this series see reference 1.

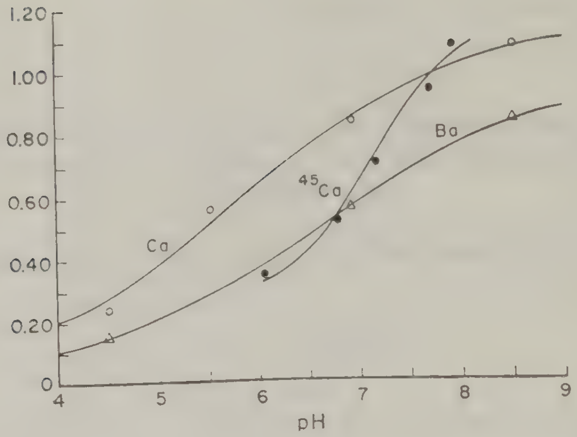

FIG. 1. Neutralization of stearic acid at varying pH.
●—experiments with Ca^{45}
○—experiments with Ca by Langmuir and Schaefer (3).
△—experiments with Ba by Langmuir and Schaefer (3).

techniques (4). This requires only small areas of monomolecular layers, which may be collected by Blodgett's building-up technique. In this procedure the filme emerge from the hypophase in completely dry condition; thus, errors caused by the salt content of adhering droplets are eliminated. It was most convenient to use for these studies Ca^{45} with a pure β-radiation of 0.25 m.e.v. and a half-life of ca. 180 days. The bath contained 1500 ml. of a 10^{-4} *M* $CaCl_2$ solution with 1.5 microcuries Ca^{45}. The pH was adjusted by means of $KHCO_3$ (0.2×10^{-4} to 8.0×10^{-4} *N*) to pH values between 6.2 and 7.9. Within these pH limits it was possible to build up films on chromium covered glass slides to a thickness of 100 layers and more.

The radiation was counted with a thin mica-window Geiger-Mueller Tube (1.4 mg. cm.^{2}). The area to be counted was limited by a circular blind of lucite to 3.6 cm.^{2}. If one assumes a density of 5.26×10^{18} molecules of stearic acid per square meter of film (weight 2.47 mg.), the amount of Ca equivalent to complete neutralization would be 174 μg. A film of 100 layers, such as was used in our experiments, of the area given above (3.6 cm.^{2}), corresponding to a total of 360 cm.^{2}, thus would contain 6.26 μg. of Ca if completely neutralized. In control experiments it was ascertained that this amount of Ca in the form of the chloride, when deposited by evaporation on a planchet of the same area (3.6 cm.^{2}), yielded a count of 124.8/min. (Table I).

The solid dots in Fig. 1 exemplify our results with this technique. A comparison with those of Langmuir and Schaefer (3) must take into account the fact that their layers were built up on a solid plate—a process which

TABLE I

Ca^{45} Content of Films as Function of pH

pH	Counts/min.	Stearic acid neutralized (%)
6.04	43.8	34.6
6.77	64.8	51.9
7.15	87.6	70.2
7.68	117.0	93.9
7.90	133.8	107.9
Control	124.8	100.0

appears to entail changes in the composition of the layers. We know that the deposition ratio under the conditions of the experiment is approximately 0.96, in other words, that the film is stretched out by about 4%. This minor factor does not explain why the slope of our curves is distinctly steeper than that of Langmuir and Schaefer.

Neither Langmuir's nor our own curves are as steep as an acid dissociation curve. The turning point at 50% neutralization is almost 2 pH units farther to the alkaline side in our case than the pK of stearic acid. If one expected that the dissociated fraction of the total stearic acid concentration gives rise to the formation of the Ca-soap, one must assume that the pH at the interface is considerably lower than the pH in the bulk phase. Such differences, up to several pH units, have been observed by Havinga (5), for example, in the comparison of lactonization in bulk and in the two-dimensional state and also in the color changes of indicators in monomolecular films; this effect is most pronounced towards alkaline reaction.

The divergence between our results and those of Langmuir and Schaefer indicates that an exchange between metal ions and protons takes place during the building-up process, so that part of the bivalent metal is left behind in the solution and exchanged against hydrogen ions—an effect that increases with the hydrogen ion concentration, i.e., towards lower pH values.

STEARIC ACID FILMS BUILT ON SOLUTIONS OF BIVALENT ORGANIC BASES

Additional light was thrown on these relationships by an unexpected observation. The building-up of double layers of stearic acid on a hypophase lacking bivalent metal ions is most unsatisfactory and irregular, although not altogether impossible. It occurred to us to use solutions of organic or other nonmetallic bivalent cations such as hydrazine, ethylene diamine, phenylene diamines, and benzidine as hypophase. Films of stearic acid, prepared on these solutions, behave in general like films prepared on barium solutions. However, owing to differences in surface tension, the solutions have a tendency to spread over the rim of the trough. Moreover, they emerge wet, like protein films, and must be dried by suction through a microcapillary before the next immersion; this slows up the building up of multiple layers. However, we succeeded in building films with all these bases and found to our surprise no significant difference in thickness between the various bivalent bases and metals, in spite of the substantial differences in molecular volume.

We developed a colorimetric method for the microanalysis of benzidine by diazotization, followed by coupling with N-α-naphthyl ethylene diamine, with a sensitivity of 1 μg./ml. We built, for example, 24 double layers of stearic acid from a benzidine hypophase on both sides (2 x 10 cm.^{2}) of a metal plate. The film (total area of 960 cm.^{2} in the monomolecular state) was dissolved in ethanol and tested for benzidine. To our surprise no benzidine could be detected, nor were any but traces of benzidine found when an H-layer of 20 x 40 cm. on a benzidine hypophase was skimmed and removed on a platinum spatula and subsequently tested. In either case, 30–40 μg. of benzidine had been expected according to our calculations for two-thirds neutralization. These results lead to the assumption that bivalent cations, either metallic or organic, are important for establishing those properties of an H-film which are prerequisite for its building up; however, the incorporation of the cations into the built up film does not necessarily follow but remains a question of relative solubility. In the case of barium or calcium soaps a considerable part of the metal ions remain in the layer on building up, whereas benzidine fully exchanges against protons during building up or skimming of the layer. This observation has enabled us to build up films of pure stearic acid and to compare their reactivity with that of the barium stearate/stearic acid films. As concerns the ellipsometric measurements, these films display exactly the same interference as the barium stearate films, indicating identical thickness under the assumption that there are no significant differences of refractive index.

Acknowledgment

The authors wish to acknowledge financial support form U. S. Public Health Service Grant No. RG-4736.

References

1. Sobotka, H., *J. Phys. Chem.* **62,** 527 (1958).
2. Beischer, D. E., *in* "Monomolecular Layers" (edited by H. Sobotka), p. 124. American Association for the Advancement of Science, Washington, 1954.
3. Langmuir, I., and Schaefer, V. J., *J. Am. Chem. Soc.* **58,** 284 (1936).
4. Sobotka, H., Demeny, M., and Chanley, J. D., Proc. 2nd Intern. Congr. Surface Activity, Vol. 1, p. 13. Butterworths, London, 1957.
5. Havinga, E., *in* "Monomolecular Layers" (edited by H. Sobotka), p. 192, especially pp. 194 and 199. American Association for the Advancement of Science. Washington, 1954.

JOURNAL OF COLLOID SCIENCE **13**, 569–575 (1958)

THE DISTRIBUTION OF ACETIC ACID BETWEEN SOLVENT AND SOAP MICELLES IN BENZENE SOLUTIONS

W. D. Bascom and C. R. Singleterry

U. S. Naval Research Laboratory, Washington 25, D. C.

Received July 22, 1958

ABSTRACT

The distribution of acetic acid between benzene and micelles of sodium dinonylnaphthalene sulfonate, magnesium dinonylnaphthalene sulfonate, and magnesium phenylstearate was examined by measurements of the vapor composition in equilibrium with such systems. In each case the initial increments are more firmly bound than later portions, the amount of strongly bound acid ranging from one to two molecules per cation present. The magnesium salts bind the acid more strongly than the sodium compound. The partition coefficient for acid at higher concentrations is one or two orders of magnitude smaller than that for the initial increments. Its magnitude depends on the nature of the anion in the micelle. Water was found to reduce the initial acid-binding capacity of the magnesium salts. The data indicate that the coordinating properties of the cation are a major factor in the initial firm binding of acetic acid by oil-soluble soap micelles, but that significant amounts of acid are more loosely held by forces which may be attributed to the organic anion present.

INTRODUCTION

A significant property of the micelle-forming oil-soluble soaps is their ability to solubilize, by inclusion in the micelle, substances which are otherwise difficultly soluble in the oil (1). Baker and co-workers (2) have noted that neutral sulfonate micelles appear to sequester acetic acid and thus reduce the corrosiveness and effective acidity of an acid-containing oil. Since acetic acid is usually miscible with oils in all proportions, the use of the term solubilization for this acid-sequestering process could be questioned if the original definition were strictly applied. However, the factors responsible for the uptake of polar molecules by the micelle are similar whatever the true molecular solubility of the solubilizate in the solvent phase. It appears justifiable to extend the term micellar solubilization to cover all cases in which the partition coefficient of a solute between the solvent and the micelles is such as to produce a higher mole fraction of the solute in the micellar microphase than in the solvent.

Solubilization in aqueous soap systems is considered to result mainly because the hydrocarbon centers of such micelles represent islands of low polarity environment into which hydrocarbon molecules (or molecules having a substantial hydrocarbon portion) may pass from water with a decrease in the free energy of the system. Solubilization of hydrocarbons is therefore controlled by the factors which influence simple molecular solubility. McBain and Hutchinson (1) have pointed out that many cases of solubilization can be described quantitatively as a partition of the solute between two immiscible phases. When the solubilizate carries a peripheral polar group it may orient appropriately in the surface of the micelle instead of passing into the interior, but even in this case the behavior may be approximately characterized by a simple distribution constant.

Solubilization in nonaqueous soap systems, as McBain and Hutchinson note from a consideration of the literature on dye solubilization, is highly specific to the micelle former and the solubilizate involved. This results from the strong and specific activity of the polar heads that are responsible for micelle formation in such systems. Solubilization in such micelles may be expected not only to be selective, but to exhibit stoichiometric peculiarities not encountered in aqueous soap solutions. Mathews and Hirschhorn (3) have reported the high apparent density of the first water solubilized by Aerosol OT in benzene as compared with the later increments, and the author and co-workers (4, 5) have noted indications that the first water solubilized by phenylstearate or dinonylnaphthalene sulfonate salts is more strongly bonded than succeeding portions.

The present paper reports a study of the partition of acetic acid between benzene and the micelles of three oil-soluble salts which might be expected to show distinctly different tendencies to interaction with the solubilizate. The distribution of acetic acid between solvent and micellar phase has been inferred from the measured acid content of gas in equilibrium with the solutions.

EXPERIMENTAL PROCEDURE

Materials

Water-pumped cylinder nitrogen was purified by successive passage through ascarite, drierite, anhydrous barium oxide, and finally through a dry ice-acetone trap.

Benzene (ACS reagent grade) was percolated through silica gel and dried over sodium. Glacial acetic acid, ACS reagent, was used without further purification.

Hydrochloric acid and potassium hydroxide solutions were prepared with the usual analytical precautions against CO_2, and standardized against potassium acid phthalate.

The sodium dinonylnaphthalene sulfonate (NaDNNS) was prepared according to Kaufman and Singleterry (5). The magnesium dinonylnaphthalene sulfonate, Mg(DNNS)$_2$, and the magnesium phenylstearate were prepared by precipitation from the corresponding sodium salts with $MgCl_2 \cdot 6H_2O$ (6). The preparations were lyophilized and stored in sealed ampoules under nitrogen.

Procedure

Vapor-liquid equilibrium data were obtained by passing purified nitrogen through the solution under study in two consecutive equilibrating vessels maintained at constant temperature. The effluent gas was passed through a cold trap and the condensate weighed and titrated for acid content.

The first equilibrator was a modified Corson bottle (7). The final equilibrating vessel was an unenclosed solution-filled coil through which gas was bubbled. The exposed coil equilibrator provides prolonged contact between each bubble and the solution, improves thermal equilibrium with the bath, and ensures orderly circulation of the fluid under study.

The cold trap was a small glass cylinder fitted with three standard taper necks and a well at the bottom about 15 mm. in diameter and 15–20 mm. in depth. A 7-mm. glass tube extended through the center neck to the top of the well. During operation the lower two thirds of the trap was immersed in powdered dry ice. The direction of gas flow through the trap was the reverse of normal practice to avoid sudden cooling of the entering vapors to form a fog; the vapors condensed gradually as the gas progressed down the wide cross section of the trap towards the cold zone.

The water bath was maintained at 24.8°C. and the room temperature between 25° and 26°C. to prevent vapor condensation in the lines.

The volume of carrier gas was metered by periodic readings of a capillary differential manometer. The flow rate was held constant by regulation of the cylinder pressure and the use of a ballast tank and bleeder tube.

The operational procedure consisted of collecting condensate in a weighed trap for a period of at least 1 hour with a gas flow rate of about 2 l. per hour. The trap inlet and outlet were then closed, and the condensate was thawed and allowed to drain into the well. Condensate that would not drain was distilled from the warm walls by refreezing the well only in dry ice. Finally, the trap was brought to room temperature and weighed.

Preliminary studies gave a calculated vapor pressure of 95.4 mm. Hg at 24.8°C. for percolated benzene as compared to 94.9 mm. Hg at 25.0°C. reported by Hovorka and Dreisbach (8). This indicates that saturation of the carrier gas stream with the vapor of the liquid in the equilibrator was essentially complete.

The acid contents of both the solution in the equilibrator and the condensate in the trap were determined by titration. An excess of standard KOH solution was added directly to the hydrocarbon to remove all acid to the aqueous phase. This system was then made faintly acid with standard

HCl and back-titrated with KOH. This sequence was found to give the sharpest end point. The electrometric end point for this titration was closely approached by an indicator composed of one part 0.1% phenol red sodium salt and one part 0.1% bromthymol blue sodium salt in water (9). This indicator exhibited a distinct blue-green at the equivalence point.

The microtitration of the condensate was conducted directly in the trap under an atmosphere of nitrogen. Standard HCl and KOH were introduced into the well from micropipettes (10) inserted through the trap side arm. The well contents were stirred magnetically by a teflon-coated iron slug.

RESULTS AND DISCUSSION

The results of the measurements are presented graphically in Fig. 1, which shows the acid content of the vapor phase as a function of acid concentration in the liquid. Data are shown for acetic acid alone and for acetic acid in the presence of sodium dinonylnaphthalene sulfonate, magnesium dinonylnaphthalene sulfonate, and magnesium phenylstearate. All the soaps were present at a concentration of 0.0182 mole per liter. The plot for the binary acetic acid-benzene system exhibits the curvature to be expected from the dimerization equilibrium for the acid in benzene. For the interpretation of the results with the soap solutions it is assumed that the concentration of acid in the solvent phase is equal to that in an acid-benzene solution having the same vapor composition.

The curves for the data in soap solutions, although markedly different from each other, all indicate that the first acid taken up is more strongly bound than later increments. The effect is much greater for the magnesium

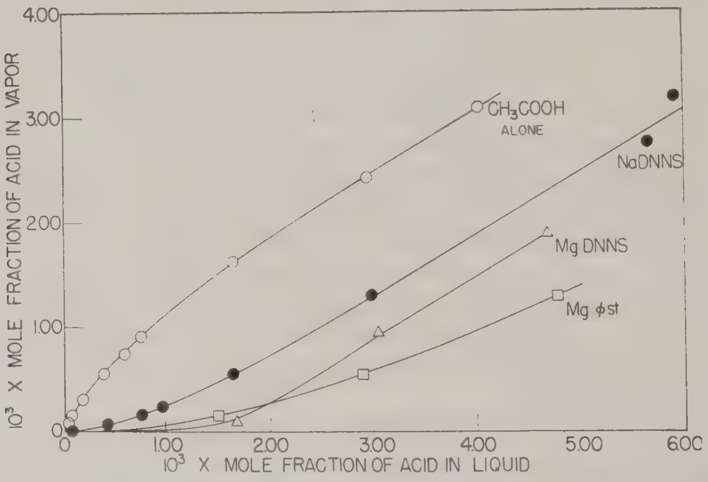

FIG. 1. Solubilization of acetic acid in benzene solutions of oil-soluble soaps. Soap concentration, 0.0182 mole per liter.

salts than for the sodium dinonylnaphthalene sulfonate. This difference suggests that the coordinating power of the cation is the controlling factor at low acid concentrations. Honig and Singleterry (4) found that coordinating ability strongly influenced the association of the phenylstearates to form polymeric soaps of high intrinsic viscosity. Kaufman and Singleterry (5) demonstrated positive correlation between the apparent densities of the hydrocarbon tails of the phenylstearate and dinonylnaphthalene sulfonate salts and the coordinating power of the cation. If the binding of the initial acid entering the micelles is a result of specific coordination bonding to metal ions, and if this bonding is an order of magnitude stronger than that of later increments entering the micelle after the coordination sites have been occupied, it might be expected that the equilibrium during saturation of these sites would be analogous to that of the Langmuir equation for the adsorption of a gas on a surface having a fixed number of adsorption sites. In this case a plot of $1/\theta$ vs. $1/p$ should be linear if θ is the fraction of coordination sites occupied and p is the mole fraction of acid in the vapor phase above the solution. Figure 2 presents such a plot of the data for the NaDNNS system, assuming that coordination effects are responsible for binding exactly 1 mole of acid per mole of soap. Such an assumption appears plausible from visual inspection of the curve. For

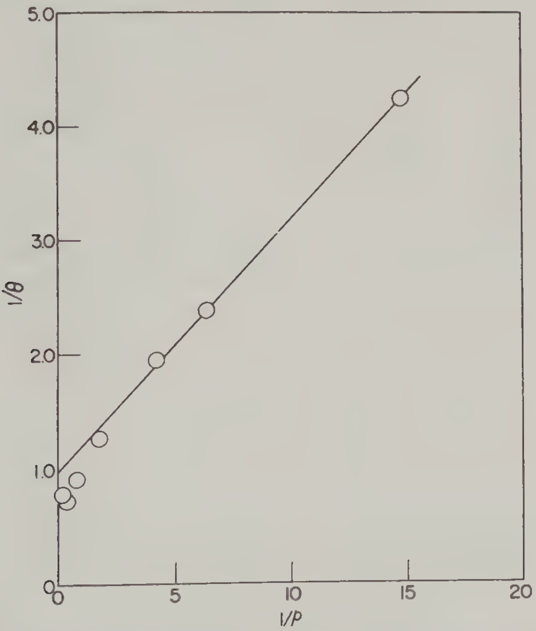

FIG. 2. Test of Langmuir adsorption isotherm for low acid concentrations assuming 1–1 binding of acid by soap molecules. Here θ = moles of acid solubilized per mole of soap; $p = 10^3 \times$ mole fraction of acid in vapor.

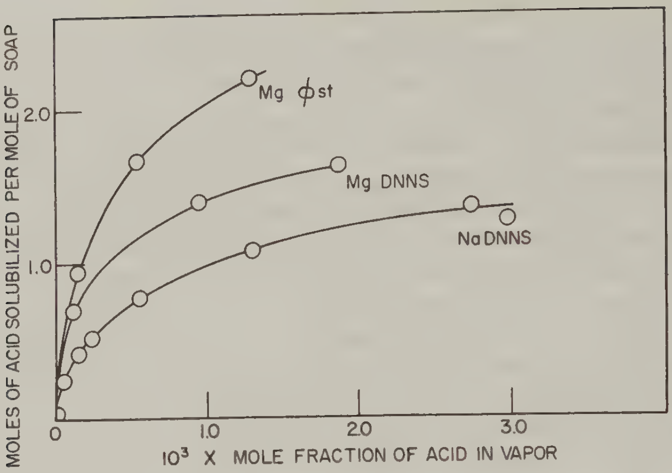

FIG. 3. Effect of acid concentration on acid held by soap.

the three lower points on this curve the acid concentration in solvent and in vapor is so low that dimerization should be negligible; hence the concentration of acid in the vapor may be taken as a useful measure of the activity of acid monomer in the system. The four lowest points fall closely on the theoretical line for the Langmuir isotherm, which confirms the inference of a specific limited bonding mechanism during the initial stage of solubilization. The initial binding of acid by the magnesium salts is not only stronger than for sodium, but a larger amount is bound per mole of salt. There are not sufficient data available, however, for a quantitative estimate of the amount coordinated.

Total acid solubilized increases with further acid addition, but the proportion entering the micelles becomes progressively smaller. The effects are shown graphically in Fig. 3, in which acid solubilized is plotted against total acid added, both quantities being expressed as moles of acid per mole of soap. The slope of this curve characterizes the distribution of the corresponding increment of acid between micelles and solvent. This slope decreases steadily with increasing concentration, but the data do not extend to concentrations high enough to show whether the micelle reaches a stable saturated state or continues to accept small increments of acid until micellar organization breaks down. In the case of NaDNNS the distribution coefficient, expressed as the ratio of mole fraction of acid in micelles to that in the benzene phase, has a value of 16000 for the first increment of acid added. This increment was 0.04 mole acid per mole of soap. The last two increments of acid, from 1.09 to 1.27 moles acid per mole of soap, show an average coefficient of 40. There is thus a 400-fold difference in partition coefficient in the two ranges. For the increment from 0.42 to 0.51 mole of acid per mole of soap, which might be taken as representative of the behavior during the first mole of acid uptake, the coefficient has a value of 800, which exceeds the value for the final increment by a factor of 20. This justifies one of the assumptions involved in the application of the Langmuir equation to the data. The final coefficient of 40, however, shows that the micelle has substantial solubilizing power for small polar molecules, even after specific coordination sites appear to have been fully occupied.

The course of the curve for magnesium phenylstearate at higher acid concentrations is distinctly different from that for the two dinonylnaphthalene sulfonate curves, the acid being more extensively solubilized by the carboxylate soap. It is apparent that the anion as well as the cation may exert selective effects on solubilization by micelles in oil.

Other qualitative information about the initial solubilization mechanism emerged from the study of the magnesium compounds. The first measurements of the acid fixed by the micelles gave erratic results, which showed a drift towards higher acid fixation as successive equilibration measurements were made on a given solution. The difficulty was traced to incomplete removal of water from the soap during freeze drying. It is unusually difficult to remove the last traces of water from the magnesium soaps, repeated lyophilization from benzene solution and drying at 85°C. under a high vacuum being required. The interference of water was confirmed by adding 2 moles of water per mole of soap to a solution of $Mg(DNNS)_2$ containing 2.9 moles of acetic acid per mole of soap. This addition reduced the acid bound by the soap from 1.6 to 1.3 moles per mole of soap. The effect of water again suggests that some specific interaction is responsible for the initial stage of solubilization in the systems studied. This stage of solubilization may then exhibit competition between polar solutes when these are held in the micelle by the same type of reactivity.

The authors are pleased to acknowledge the technical advice and the constructive discussion which Mr. Samuel Kaufman has generously given during this investigation.

REFERENCES

1. McBain, M. E. L., and Hutchinson, E., "Solubilization and Related Phenomena." Academic Press, New York, 1955.
2. Baker, H. R., Singleterry, C. R., and Solomon, E. M., *Ind. Eng. Chem.* **46**, 1035 (1954).
3. Mathews, M. B., and Hirschhorn, E., *J. Colloid Sci.* **8**, 86 (1953).
4. Honig, J. G., and Singleterry, C. R., *J. Phys. Chem.* **60**, 1108, 1114 (1956).
5. Kaufman, S., and Singleterry, C. R., *J. Colloid Sci.* **12**, 465 (1957).
6. Singleterry, C. R., and Weinberger, L. A., *J. Am. Chem. Soc.* **73**, 4574 (1951).
7. Corson, B. B., *Ind. Eng. Chem., Anal. Ed.* **10**, 646 (1938).
8. Hovorka, F., and Dreisbach, D., *J. Am. Chem. Soc.* **56**, 1664 (1934).
9. Kolthoff, I. M., and Stenger, V. A., "Volumetric Analysis," Vol. 2, p. 59. Interscience Publishers, New York, 1947.
10. Gilmont, R., *Anal. Chem.* **20**, 1109 (1948).

JOURNAL OF COLLOID SCIENCE **13**, 576–583 (1958)

THE EFFECT OF SALTS UPON STARCH GRANULE RUPTURE

Stephen S. Winter[1] **and Arthur A. Loiselle**[2]

Department of Chemistry, Northeastern University, Boston 15, Massachusetts

Received July 22, 1958

Abstract

Viscosity measurements show that salts do not affect the rate of starch granule rupture. This indicates that only the solvent plays a major role in the swelling process. The salts affect the conformations of the hydrated starch molecules in the same manner in which electrolytes affect other polyelectrolytes.

Introduction

When potato starch is suspended in water and the mixture is heated, the viscosity of the system rises rapidly to a maximum from which it slowly decreases upon further heating (1). The rising viscosity has been ascribed to the swelling of the starch granules as they absorb water until they burst, releasing individually solvated starch molecules. The viscosity maximum is reached when the granules are fully swelled, and the subsequent decrease results from the less rigid arrangement of the individual molecules released upon granule rupture (2).

The presence of salts greatly affects the behavior of the suspensions. If the starch is heated with an electrolyte solution, the viscosities of the resulting sols are far smaller than when pure water is used (3). Also, the addition of salts to fully dispersed, salt-free sols causes large decreases in the viscosity (4–6). This behavior has been explained in terms of ion-adsorption and an electroviscous effect (5, 6), or in terms of polyelectrolyte behavior (4) and dehydration of the starch molecules (3, 4).

The knowledge that potato starch contains an appreciable number of ionizable phosphate groups (7, 8) and that these readily exchange their counter-ions (4) lends support to the polyelectrolyte explanation of the potato starch sol behavior. Furthermore, the viscosity of these pastes acts in an entirely analogous manner to the behavior of polyelectrolytes established by Markovitz and Kimball (9). The role of dehydration has not been established as firmly. Nor is it known whether the added electrolyte participates in the process of granule dissolution or rupture in addition to affecting the individually dispersed starch molecules.

[1] Present address: University of Minnesota, Minneapolis, Minnesota.

[2] Present address: The Norton Company, Worcester, Massachusetts.

This report describes some experiments undertaken to determine whether the salt changes the rate of granule rupture. Further comments are also made on the polyelectrolyte behavior of potato starch and on the roles of dehydration and ion-adsorption.

Experimental Methods

Starch sols were prepared by heating a high-grade potato starch (Aroostocrat Brand) with gentle stirring in aqueous solutions over a steam cone. Pyrex beakers were used. The resulting sols were 1% in potato starch. The temperature of the system was measured at short intervals, and it was found that this simple experimental setup gave reproducible time-temperature curves. The sols reached 93° ± 1°C. after 30 minutes and remained at that temperature.

Periodically, the viscosity of the system was measured with a Brookfield Synchroelectric Viscometer (Multispeed Model LVF). Because of the pronounced shear-dependence of the viscosity of starch sols, spindle No. 1 was used throughout, and data to be compared were obtained at equal rotational velocities of the viscometer spindle. The viscosities were measured directly in the beakers over the steam cone and gave reproducible time-viscosity curves.

Transmission of light by starch sols was measured in a Beckman Model DU spectrophotometer. All reagents were standard laboratory reagents.

Results

The effect of salts upon the formation of the potato starch sols is shown in Fig. 1. The salt curve, given for a 0.1% sodium chloride solution, is

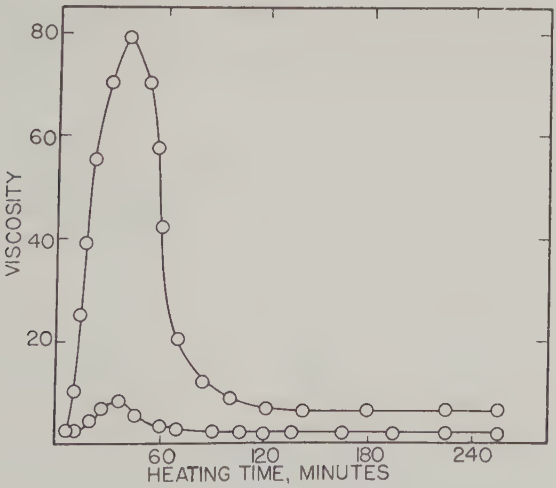

Fig. 1. The effect of salts upon the pasting curve. Upper curve, aqueous sol; lower curve, salt-containing sol.

representative also of 0.1% magnesium chloride and 0.1% ferric phosphate solutions and of 0.5% sodium chloride, all containing 1 g. of starch per 100 ml. of suspension. It can be seen that the shapes of the curves are nearly identical except for a translation of the ordinate values. Apparently, the rate of swelling and of dissolution of the starch granules is identical in salt-free and salt-containing sols, although the salt depresses the viscosity greatly. The similarity of the rates of swelling and granule rupture in the two instances is further brought out by the fact that the addition of salt to a salt-free sol at any point along the heating curve immediately drops its viscosity to that of the corresponding point on the heating curve of the sol that had contained salt from the inception of heating (Table I). Further heating then maintains the coincidence of the viscosity of the sol that had contained salt all along with that of the sol to which salt had been added at some point during or after granule swelling and/or rupture.

The effect on viscosity of the reverse process—removal of salt by dialysis—was next investigated. The salt chosen for this experiment was ferrous sulfate which can easily be analyzed. The salt-containing sample and a salt-free control were dialyzed against distilled water which was changed twice daily. The dialysis bags were shaken periodically. After 5 days, the external water failed to show ferrous ion as determined by the potassium ferrocyanide color test. The sol within the dialysis bag likewise gave no test for ferrous ion, although a light green color developed upon standing. The viscosity changes accompanying dialysis are given in Table II. In spite of the removal of nearly all the ferrous ions, the viscosity remains essentially unchanged.

Although one could assume that dialysis had removed all ferrous ions, the slowly appearing green color suggested that some of the iron had been chemically bound to the starch and slowly exchanged with the potassium ions from the ferrocyanide. An aliquot of the dialyzed solution was therefore evaporated, ignited, and the reddish-brown ash analyzed for iron.

TABLE I

Effect of the Addition of Salt to Partially Pasted Starch Sols

Pasting time (*min.*)	Temp.	Viscosity (*c.p.s.*) Before addn.	After addn.	Control[a]
10	78	9.5	4.2	4.6
20	90	112.7	10.0	8.0
40	92	149.8	14.3	13.5
60	92	95.0	8.2	7.0
80	92	22.1	3.7	2.5
100	92	18.3	3.2	2.0

[a] The control sample contained salt from the beginning of pasting.

1% starch sol, salt content—0.1%. Spindle No. 1 at 30 r.p.m.

TABLE II

Effect of Dialysis on Starch Sol Viscosity

	Viscosity (*c.p.s.*)	
	Before	After
Sol containing $FeSO_4$	7.0	8.2
Aqueous sol (control)	29.2	28.3

1% starch sols. Spindle No. 1 at 30 r.p.m.

Analysis yielded 0.0026 g. of iron per gram of dissolved starch. This small amount, 4.6×10^{-4} gram-atoms, is absorbed so strongly that dialysis failed to remove it. Yet, this small quantity of ferrous ion is sufficient to maintain the sol viscosity near its minimum value.

To determine whether this strong ion-absorption exists also in the starch granules, partially swelled salt-free and salt-containing sols were stained with iodine and examined under a microscope. The salt-free granules were spherical or ellipsoidal. The salt-containing ones, on the other hand, had highly irregular surfaces, although their mean linear dimensions were approximately equal to those of the salt-free granules. In appearance, the granules in electrolyte solutions resemble those of the various exchanged starches described by Nutting (4).

Because the small quantity of strongly absorbed ferrous ions had caused a large reduction in viscosity, the effect of minute amounts of electrolyte on the viscosity of salt-free sols was next determined. It was the purpose of these experiments to find the magnitude of the viscosity reduction when traces of salt were added and to determine the quantity of electrolyte required to reach the minimum viscosity. The desired changes were brought about by adding dilute sodium chloride and magnesium chloride solutions dropwise to 100 ml. of a starch sol. With each salt, 10 drops (1 drop = 0.05 ml.) of a 0.01 N solution were first added, and the viscosity was read after the addition of each drop. This was followed by the addition of a 0.1 N solution, 2 drops at a time, until a total of 4.5 ml. had been added. After this point, further addition of salt caused no further viscosity decrease. Even the addition of solid salt to increase its concentration 100-fold gave a change in viscosity smaller than experimental error. These data are given in Fig. 2. Not shown is a control run in which the addition of 4.5 ml. of distilled water to an equal amount of starch sol reduced its viscosity from 51.3 c.p.s. to 47.2 c.p.s.

It is apparent from the figure that salt concentrations as low as 10^{-5} N begin to affect the viscosity of the potato starch sol. Furthermore, at equivalent salt concentrations magnesium ions are nearly twice as effective in reducing the viscosity as are sodium ions despite the fact that their number in equinormal solutions is only half as great. The greater efficiency

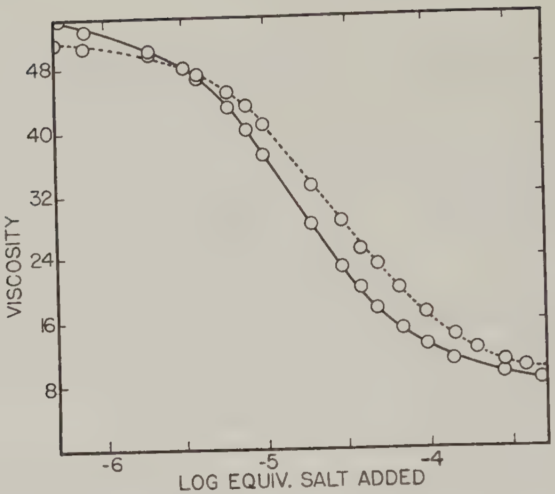

Fig. 2. The reduction of starch sol viscosity on the addition of small amounts of salt. Solid curve—magnesium chloride; broken curve—sodium chloride.

of multivalent ions in reducing the potato starch sol viscosity had already been noted by Boutaric and Chapeaux (5) and by Kruyt and Edelman (6). It is a characteristic property of polyelectrolyte solutions (9). Neither set of authors interpreted the effect in this manner, however, since polyelectrolyte behavior was very poorly understood when their researches were carried out.

Nutting (4) in his work with exchanged potato starches had noted the greater turbidity of salt-containing sols when compared to salt-free ones. Two experiments were therefore performed in an attempt to get a quantitative measure of the scattering of starch sols. Table III gives the transmission of two starch sols, one with and one without electrolyte, as a function of the wavelength. Although the transmission of light by the salt-containing sol is lower, the shapes of the transmission curves are identical for these two systems. The transmission of light for the salt-containing sol as a function of time is given in Table IV at the transmission maximum. No change in transmittance accompanies the pronounced viscosity changes in the range of 20 to 100 minutes of pasting.

Discussion

The similarity of the curves giving the starch sol viscosity as a function of pasting time in salt-free and salt-containing systems leads to the conclusion that the rate of granule swelling and rupture is not affected by the added electrolyte. Further corroboration for this view comes from the experiments which show that the viscosity of the salt-containing sol does not depend upon the time at which the salt had been added. Although the salt greatly affects the magnitude of the viscosity of the starch sol, it has

TABLE III

Transmission of Starch Sols as a Function of Wavelength

Wavelength (*millimicrons*)	% Transmission	
	Aqueous sol	Salt-containing sol
215	12.7	—
230	19.2	7.2
250	31.9	13.6
300	51.4	26.8
350	67.0	40.9
400	75.9	52.0
450	75.9	61.0
500	85.0	67.3
550	87.2	72.0
600	89.8	76.0
650	80.8	65.0
670	73.6	56.9

1% starch sol. Salt content—0.3%.

TABLE IV

Transmission of Starch Sols as a Function of Pasting Time

Pasting time (*min.*)	% Transmission	
	Aqueous sol	Salt-containing sol
20	91.5	72.8
30	91.8	74.9
40	92.2	74.8
50	92.7	75.0
60	92.1	75.1
70	92.3	75.1
80	92.3	75.2
90	91.4	75.5
100	92.0	75.5

1% starch sols. Salt content—0.3%.

no appreciable effect upon the manner in which the viscosity changes during pasting. Thus, swelling occurs by the action of the solvent only, without salt participation.

The process of granule swelling and rupture described by Bear and Samsa (10) fits these data very well. According to these authors, swelling results from the rearrangement of the individual starch molecules in the granule under the influence of small amounts of solvent that penetrate the granule sac and the successive layers of starch molecules. The inflowing solvent slightly hydrates the starch molecules. This causes rearrangements that result, through a large tangential expansion of the starch layers, in a swelling of the granules. The rearrangements also break some of the bonds that had given the stability to the granule structure. Bear and Samsa rule out increases of granule volume resulting either from hydration and dissolution of starch molecules within the granule sac or from osmotic effects.

If one accepts their explanation, one predicts that the rate of granule rupture is a function of the rate of solvent penetration only. This, in turn, should not be greatly affected by the presence of salts since moderate quantities of electrolyte will not change the solvent activity by a factor large enough to be detected by experiments such as those described here. But the salts will affect the conformations of the rearranged starch molecules. The latter effect will not set in, however, until after the granule structure has been weakened by the prior hydration. In this manner the electrolyte affects the final viscosity of the sol without participating in the process of granule swelling.

The nature of the interactions that cause the viscosity reductions still requires comment. As Nutting (4) has already pointed out and as the experiments described here confirm, the major factor is the change of bound-ion repulsions to attractions between bound and counter-ions on the addition of electrolyte (11). The attractions tend to draw the starch segments into a more tightly coiled conformation which shows a much smaller hydrodynamic volume.

The interaction between the bound and counter-ions must be considered as chemical absorption rather than as ion adsorption which previous authors (5, 6) have suggested. Nutting's (4) exchange of various counter-ions indicates a chemical reaction between the phosphate groups and the counter-ions. Moreover, the slow appearance of color on addition of potassium ferrocyanide to the dialyzed ferrous ion starch suggests a slow chemical exchange reaction

$$\text{K ferrocyanide} + \text{Fe starch} \rightleftharpoons \text{K starch} + \text{Fe ferrocyanide}$$

Hence, adsorption, which suggests physical interaction and surface effects, appears misleading.

Questions must also be raised about the contribution which dehydration makes to the reduction in the hydrodynamic volume of the starch molecules in salt solution. In particular, Nutting (4) implies that the compacting segments of the starch molecules squeeze out water of hydration from between them. In this manner he accounts for the increase in turbidity of the salt-containing starch sols.

If the water of hydration is so loosely bound to the starch molecules that simple rearrangement can dislodge it, it may be an improper use of the term hydration to suggest that the water had actually solvated the starch molecules. The released solvent would simply have been associated with the solvated starch molecules. On the other hand, if the released water had truly solvated the starch molecules, one must look for a source of chemical potential for the dehydration. This could have come from the added salt, perhaps by competition for the solvent molecules. But at the low salt concentrations at which appreciable viscosity reductions occur, it is doubtful whether a sufficient quantity of electrolyte is present to tie up an appreciable fraction of the solvent molecules, let alone to abstract them from the starch. Furthermore, competition for the solvating water molecules should lead to a salting out of the starch at higher electrolyte concentrations. These arguments raise serious doubt whether dehydration occurs to an appreciable extent when salts are added to starch sols.

It is not necessary to consider effects other than the coiling of the polyelectrolyte (starch) molecules in order to explain the viscosity behavior or the turbidity. The contraction of the molecules by the counter-ions not only changes their hydrodynamic volumes, it also changes the refractive index from point to point in the solution. In particular, it produces larger refractive index gradients near the surface boundaries of the contracted molecules. This would increase the scattering from the starch molecules and explain the higher turbidity. Furthermore, it has been shown that the addition of salts makes a solvent poorer with respect to a polyelectrolyte (12). A poorer solvent tends to increase the compaction of the starch molecules which also increases their scattering. Thus one can account for the behavior of the potato starch sols without assuming dehydration to accompany the coiling.

SUMMARY

It has been shown that salts do not appreciably affect the rate of granule swelling and rupture of potato starch sols although they greatly affect the conformations of the hydrated starch molecules. The reduction of the sol viscosity in the presence of salts is the result of the polyelectrolyte properties of potato starch. Further experiments are given to support this conclusion. It is not necessary to assume a dehydration of the starch molecules in addition to their coiling in order to explain the behavior of potato starch sols.

REFERENCES

1. KERR, R. W., "Starch," p. 118. Academic Press, New York, 1944.
2. CAESAR, G. V., *Ind. Eng. Chem.* **24,** 1432 (1932).
3. WOLFF, O., *Die Stärke* **2,** 115 (1950) .
4. NUTTING, G. C., *J. Colloid Sci.* **7,** 128 (1952).
5. BOUTARIC, A., AND CHAPEAUX, M., *Compt. rend.* **214,** 949 (1942).
6. KRUYT, H. R., AND EDELMAN, H. J., *Kolloid-Beih.* **36,** 350 (1932).
7. SAMEC, M., *Kolloid-Beih.* **4,** 132 (1912).
8. BRIGGS, D. R., AND HANIG, M., *Cereal Chem.* **23,** 277 (1946).
9. MARKOVITZ, H., AND KIMBALL, G. E., *J. Colloid Sci.* **5,** 115 (1950).
10. BEAR, R. S., AND SAMSA, E. G., *Ind. Eng. Chem.* **35,** 721 (1943).
11. WINTER, S. S., *J. Chem. Educ.* **33,** 246 (1956).
12. WINTER, S. S., AND PAPAZIAN, L. A., *J. Phys. Chem.* **61,** 1142 (1957).

JOURNAL OF COLLOID SCIENCE **13,** 584–588 (1958)

THE HEAT OF MICELLIZATION OF POTASSIUM OCTANOATE IN WATER IN THE PRESENCE OF EXCESS POTASSIUM CHLORIDE[1]

P. White[2] and G. C. Benson

The Division of Pure Chemistry, National Research Council, Ottawa

Received July 11, 1958

Abstract

Results are presented for the heat of dilution of potassium octanoate solutions containing 1.8 molal potassium chloride, and are compared with values obtained in the absence of potassium chloride. The differences in the shape of the graphs for the two systems as well as the values for the heats of micellization are discussed in terms of current micelle theory.

Introduction

Many properties of aqueous detergent solutions are markedly influenced by the presence of an added electrolyte. There is, however, very little information available about the thermochemical data for such systems.

Hutchinson and co-workers have measured heats of solution of sodium decyl sulfate (NaDS) in water (1) and in 0.1 molar NaCl solution (2). In both cases a plot of the heat of solution against concentration of the paraffin chain salt exhibited a discontinuity in the C.M.C. region. The "jump" in the curve, which was identified with the heat of micellization ΔH_M, was negative and was increased in magnitude by the presence of NaCl, but the effect of the salt was rather small.

Heats of dilution of aqueous sodium octyl sulfate (NaOS) solutions and of NaOS solutions containing NaCl (approx. 0.7 molal) have been reported by Goddard, Hoeve, and Benson (3). Plots of these data against concentration of NaOS gave smooth sigmoid-shaped curves in the C.M.C. region. Heats of micellization, estimated according to a method described by Goddard and Benson (4), were small and positive; in the presence of 0.7 molal NaCl the heat of micellization of NaOS decreased by about 50%.

In the present paper heats of dilution for solutions of potassium octanoate (K-Oct.) containing KCl (1.802 molal) are reported and the results compared with data given in reference 3 for aqueous K-Oct. solutions to which no extraneous electrolyte had been added.

---

[1] Issued as N.R.C. No. 4936.

[2] National Research Council of Canada Postdoctorate Fellow 1956–1958.

EXPERIMENTAL

Eastman White Label octanoic acid was purified by fractionation and a sample having a freezing point of 16.52°C. was used in the preparation of K-Oct. The acid was neutralized with carbonate-free potassium hydroxide (volumetric reagent grade). A slight excess (0.042 molal) of base was added to suppress hydrolysis. The potassium chloride was recrystallized three times from conductivity water, and freshly distilled conductivity water was used in making up all the solutions.

The heats of dilution were determined in an adiabatic solution calorimeter which has been described elsewhere (5). In the initial runs a stock potassium octanoate solution (1.4310 molal) made up in 1.802 molal potassium chloride as solvent was diluted into 1.802 molal aqueous potassium chloride solution and the heat evolved was measured. All solutions contained 0.042 molal potassium hydroxide in addition to the potassium chloride. The results at higher concentrations were obtained by multiple dilutions. The experimental technique for carrying out these dilutions was exactly the same as described in reference 3. All experiments were performed at 25°C.

RESULTS

Intermediate heats of dilution $\Delta H_{m' \to m}$ for aqueous K-Oct. solutions containing 1.802 molal KCl and 0.042 molal KOH are shown in Fig. 1.

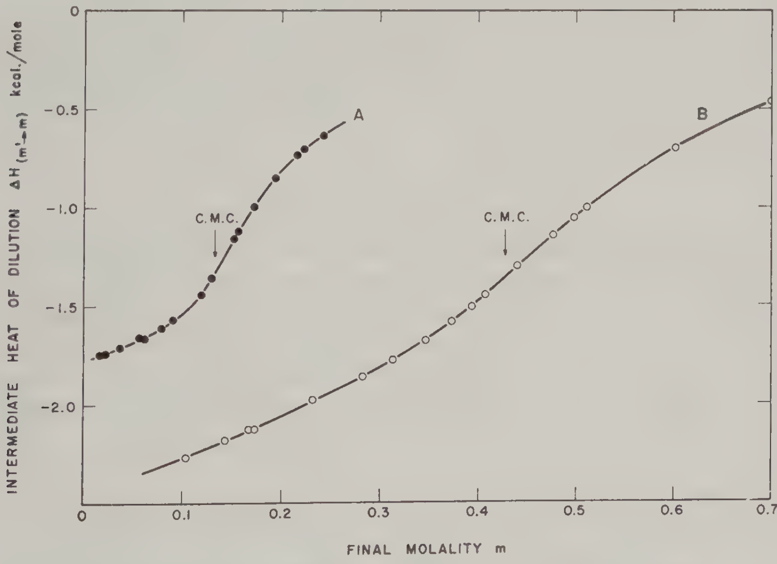

FIG. 1. Intermediate heats of dilution $\Delta H_{(m' \to m)}$ for aqueous potassium octanoate solutions at 25°C. plotted as a function of the final molality m. Curve $A - m' = 1.4310$, solvent 1.802 molal KCl and 0.042 molal KOH. Curve $B - m' = 3.1890$, solvent 0.0417 molal KOH (data from ref. 3).

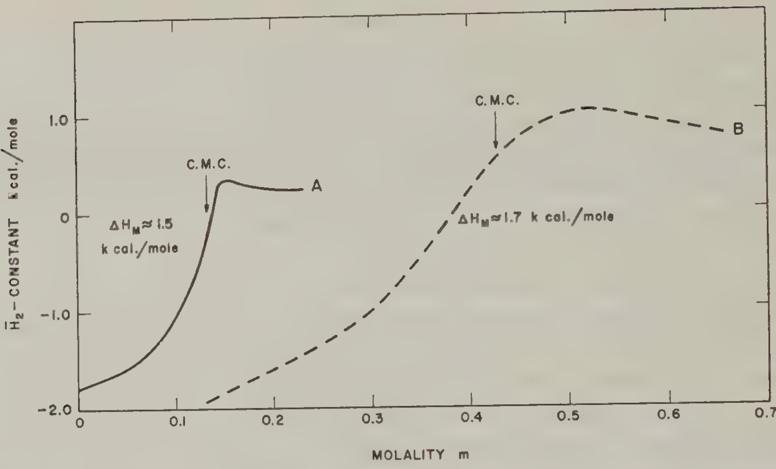

FIG. 2. Plot of the partial molal heat $\bar{H}_2$ against molality m for aqueous potassium octanoate solutions at 25°C. Curve $A - m' = 1.4310$, solvent 1.802 molal KCl and 0.042 molal KOH. Curve $B - m' = 3.1890$, solvent 0.0417 molal KOH (data from ref. 3).

The constant subtracted from the ordinate is $\bar{H}_2^\circ + \phi_{L'}$ and has a different value for the two curves.

Included in the same graph for comparison are results from reference 3 for the corresponding system without added salt. The partial molal heat content $\bar{H}_2$ (– constant) of K-Oct. calculated from the above data is plotted in Fig. 2 for both systems. It is to be noted that the value of the constant is different in the two cases. Values of the heat of micellization estimated as indicated in references 3 and 4 are also written on the graphs as well as the C.M.C. taken from Herzfeld (6).

DISCUSSION

Recently Hoeve and Benson (7) in the course of a statistical mechanical treatment of micelle formation in detergent solutions examined a number of models which have been proposed for these systems, and concluded that there is, as yet, no theory which adequately explains the properties of aqueous ionic detergent solutions. Accordingly only qualitative inferences concerning the nature and energetics of micelles can be drawn from the results displayed in Figs. 1 and 2; nevertheless several features of these graphs do appear to be significant.

The general sigmoid shape of curve A of Fig. 1 is the same as that obtained in reference 3 for several other detergent systems, and there is no sign of a discontinuity at the C.M.C. as has been reported for heats of solution of NaDS and several other detergents (1, 2, 8).

Goddard and Benson (4) have pointed out that in the case of a very simple detergent system where both single ions and micelles behave ideally, the graph of $\bar{H}_2$ against concentration should be a step function made up of two horizontal sections joined by a nearly vertical line. The "step" is located at the C.M.C. and its height is equal to ΔH_M . Implicit in the derivation of this shape are the assumptions that the distribution of micellar sizes is narrow and that the number of single ions in a micelle is rather large. Nonideal behavior of the components will cause the horizontal parts of the graph to slope; relatively large amounts of small micelles and broad distributions of micellar sizes will make the rise more gradual and round the corners.

The plots of $\bar{H}_2$ in Fig. 2 have the shape to be expected from the above considerations. The curve for K-Oct. in the presence of salt lies to the left of that without salt, indicating the decrease of the C.M.C. The value of the C.M.C. obtained from other measurements falls within the central section of each curve and, in fact, comes fairly near the point of inflection. The slopes of the initial and final portions of the curves fit in with the view of nonideal behavior and are leveled out somewhat by the added electrolyte which tends to reduce the electrostatic interactions between the charged detergent ions and micelles. The "step" in both curves of Fig. 2 corresponds to a small positive ΔH_M of micelle formation. Again this quantity is less when salt is present, probably owing to the increase in electrostatic shielding. It has also been pointed out (3) that structural effects in the solvent surrounding the single ions may play an important role in the energetics of micelle formation. It is quite possible that part of the decrease in ΔH_M, noted above, arises from an increase in the energy of the single ion state brought about by the "solvent depolymerizing" effect of the added salt (9).

It is also evident from Fig. 2 that the step becomes more abrupt when KCl is present. This is suggestive of larger micelles and a sharper size distribution. Although no quantitative information about this can be obtained from the present data, the increase in micellar size in the presence of added salt is in agreement with interpretations of light-scattering measurements (10, 11).

Acknowledgment

The authors wish to thank Mr. P. J. D'Arcy for aid in the calorimetric measurements.

References

1. Hutchinson, E., Manchester, K. E., and Winslow, L., *J. Phys. Chem.* **58**, 1124 (1954).
2. Hutchinson, E., and Winslow, L., *J. Phys. Chem.* **60**, 122 (1956).
3. Goaddard, E. D., Hoeve, C. A. J., and Benson, G. C., *J. Phys. Chem.* **61**, 593 (1957).

4. Goddard, E. D., and Benson, G. C., *Trans. Faraday Soc.* **52**, 409 (1956).
5. Benson, G. C., Goddard, E. D., and Hoeve, C. A. J., *Rev. Sci. Instr.* **27**, 725 (1956).
6. Herzfeld, S. H., *J. Phys. Chem.* **56**, 959 (1952).
7. Hoeve, C. A. J., and Benson, G. C., *J. Phys. Chem.* **61**, 1149 (1957).
8. Zettlemoyer, A. C., Schneider, C. H., and Skewis, J. D., *Proc. 2nd Intern. Congr. on Surface Activity,* **III**, 472 (1957).
9. Frank, H. S., and Evans, M. W., *J. Chem. Phys.* **13**, 507 (1945).
10. Debye, P., *Ann. N. Y. Acad. Sci.* **51**, 575 (1949).
11. Anacker, E. W., *J. Phys. Chem.* **62**, 41 (1958).

JOURNAL OF COLLOID SCIENCE **23.** 589–599 (1958)

FLOCCULATION, SUBSIDENCE AND FILTRATION OF PHOSPHATE SLIMES[1]

VI. A QUANTITATIVE THEORY OF FILTRATION OF FLOCCULATED SUSPENSIONS

Robert H. Smellie, Jr., and Victor K. La Mer

Received May 13, 1958

Department of Chemistry, Trinity College, Hartford, Connecticut, and Department of Chemistry, Columbia University, New York, New York

ABSTRACT

A quantitative theory of filtration of suspensions flocculated with polymeric flocculants is developed. The theory, based upon a simple picture of the adsorption of the flocculant combined with considerations of floc geometry and the Kozeny-Carman permeability equation, explains the variations of filtration rate with flocculant concentration observed experimentally.

A. INTRODUCTION

It has been observed that flocculating agents such as starches, gums, and synthetic polymers improve flocculation and, hence, filtration rate up to an optimum concentration of flocculant which produces the maximum in floc size and porosity of the filter cake. The decrease in the average floc size and, hence, in filtration rate for concentrations of added flocculant greater than the optimum is related to the protective and peptizing action of the flocculating agent (1, 2). Upon increasing the flocculant concentration above the optimum, the redispersed, fine particles which are now protected by the excess of flocculant clog the pores of the filters and thus decrease the filtration rate.[2]

Although the processes involved in the flocculation of slimes by polymeric flocculants are complex, it has been possible to account quantitatively for the type of filtration rate vs. concentration of flocculant curves obtained in our investigations in terms of a relatively simple theory. The mathematical development of this theory also explains the observation previously described in paper V of this series (3) which relates linearly the optimum flocculant concentration to the square of the solid content. At present the theory is somewhat oversimplified and incomplete in finer details. However, it appears to be correct in principle and is derived as follows.

---

[1] Supported by funds from Contract At(30-1)1189 between Columbia University and the U. S. Atomic Energy Commission.

[2] In previous papers of this series (2) we have described the techniques used and the results obtained in the investigations of the flocculation, subsidence, and filtration of phosphate suspensions.

B. THE ADSORPTION OF THE FLOCCULANT AS THE PRIMARY PROCESS IN THE FLOCCULATION OF SUSPENSIONS

The process of flocculation by polyfunctional polymeric flocculating agents is complex if considered as a kinetic process. Therefore, attempts to derive relationships between filtration rate and flocculating agent concentration will be extremely difficult by kinetic methods.

A simpler approach can be made on the following assumptions:

1. The flocculating agent will be distributed uniformly among the individual particles in accordance with a simple adsorption isotherm of the Langmuir type.

2. The molecules of flocculant so attached to individual slime particles will still have free, active centers which can then interact with the remaining free surfaces on other particles so that large flocs having a three-dimensional network can be formed.

It is also to be expected that there will be a certain concentration of flocculant which will give a maximum average floc size and thereby a maximum filtration rate. Protection against coagulation will occur at the higher flocculant concentrations above the optimum since the initial covering of the individual particle surfaces in process (*1*) will be so large that little or no free surface remains for interaction by process (*2*). In the latter case the situation eventually becomes one in which smaller flocs or even primary particles again constitute much of the dispersed phase.

The assumption of a simple Langmuir type of adsorption, made originally in order to avoid mathematical difficulties in the development of the filtration theory, can be justified on the basis of the experimental observations by Jellinek, Hobden, and Northey and by Jenckel and Rumbach (4) and also by recent measurements of our own on suspensions chemically similar to those described in this paper.

According to Langmuir, the fraction of the surface covered by the adsorbate (θ) is related to the equilibrium concentration or pressure of the adsorbate (P), as follows:

$$\theta = \frac{bP}{1 + bP}, \qquad [1]$$

where b is a constant.

Let P = the equilibrium concentration of polymeric flocculant in solution after the initial covering of the individual particles in process (*1*). It can be assumed that in process (*2*) the concentration P will not be changed since the interaction between the free, active centers of the attached flocculant on one particle with the free surface of another involves no further adsorption from solution.

Let P_0 = the initial concentration of added flocculant in parts per million. Then

$$P = P_0 - kw\theta, \qquad [2]$$

where $kw\theta$ = the decrease in the bulk concentration of flocculant due to adsorption, k = a constant which depends upon the specific area of the solids, and w = solid content.

In dealing with polymeric flocculants at very low initial concentrations (up to 400 p.p.m.) it is necessary and desirable to represent data in terms of the initial concentration P_0. Therefore,

$$\theta = \frac{b(P_0 - kw\theta)}{1 + b(P_0 - kw\theta)}. \qquad [3]$$

The solution of Eq. [3] leads to a quadratic in θ which becomes too cumbersome for testing the filtration data at a later stage.

Equation [3] may be rearranged to give the following:

$$\theta = \frac{bP_0}{1 + bkw(1 - \theta) + bP_0}. \qquad [4]$$

Equation [1] may also be expressed in the form

$$\frac{1}{1 - \theta} = 1 + bP$$

and by series expansion

$$\frac{1}{1 - \theta} = 1 + \theta + \theta^2 + \cdots;$$

therefore,

$$\begin{aligned} 1 + \theta + \theta^2 + \cdots &= 1 + bP \\ &= 1 + b(P_0 - kw\theta) \end{aligned}$$

and finally

$$(1 + bkw)\theta + \theta^2 + \cdots = bP_0.$$

If θ is small all terms higher than θ^2 may be dropped to obtain a useful approximation for θ

$$\therefore\ (1 + bkw)\theta + \theta^2 \cong bP_0. \qquad [5]$$

By rearranging Eq. [4] and solving for θ^2

$$\theta^2 = \frac{(1 + bkw + bP_0)\theta - bP_0}{bkw}. \qquad [5a]$$

Substituting the right-hand member of Eq. [5*a*] for θ^2 in Eq. [5]

$$\theta = \frac{P_0}{\frac{(1 + bkw)}{b} + \frac{P_0}{(1 + bkw)}}. \qquad [6]$$

Until adsorption and equilibrium concentration data became available Eq. [6] could not be tested. A method has recently been developed in our laboratories which will allow examination of the predictions of Eq. [6] with respect to the dependence on solid content.

C. FLOC SIZE IN RELATION TO ADSORPTION OF POLYMERIC FLOCCULANTS AND THE METHOD OF MIXING

The method of mixing or agitating the slime and flocculant has been shown to be a critical factor in determining the floc size with any given slime, solid content, and flocculating agent concentration (2). The studies previously reported showed that floc size reached an optimum with a particular slime, solid content, and flocculant concentration for a given number of rotations of the container. The method had been standardized for experimental purposes and close reproducibility of results established.

An optimum in flocculation indicates that a process involving destruction of flocs due to mechanical action eventually becomes more significant than the process of flocculation.

The process tending to build up flocs, which is initially very fast, should be dependent upon the amount of flocculant initially adsorbed per particle (θ) and the amount of surface still open per particle $(1 - \theta)$. The rate of formation of flocs would then depend upon the product $\theta(1 - \theta)$.

The rate of floc formation, (df/dt), may be represented as

$$\left(\frac{df}{dt}\right) = k_1 n_0^2 \theta(1 - \theta) \qquad [7]$$

in accordance with an essentially bimolecular process similar to the Smoluchowski coagulation (5) where the number of floc nuclei and the number of particles per unit volume available to add to floc nuclei are both proportional to n_0.

The probability of successfully building flocs is proportional to $\theta(1 - \theta)$. In other words, as a bimolecular process $n_0\theta$ represents the "concentrations" of active species containing flocculant, and $n_0(1 - \theta)$ represents the "concentration" of species with open surface able to react with the first species.

The disintegration of flocs should proceed at a rate which is proportional to the mass or size of flocs, and which is inversely proportional to the surface of flocs and the stabilizing or binding influence of the factor $\theta(1 - \theta)$.

Assuming for convenience that the flocs are essentially spherical, then

$$-\left(\frac{df}{dt}\right) = \text{rate of disintegration of flocs}$$

$$= \frac{k_2R^3}{R^2\theta(1 - \theta)}. \qquad [8]$$

Here R = radius of a floc, R^3, proportional to the mass of the floc, represents a factor tending to pull the floc apart due to weight, and R^2, proportional to the surface area of a floc, retards the decrease in floc size as a result of picking up particles from the surroundings. The magnitude of the factor $\theta(1 - \theta)$ will determine the stability of flocs by binding particles together by adsorption in competition with the tendency for mechanical disintegration due to the mass.

Therefore, the net rate,

$$\frac{df}{dt} = k_1n_0^2\theta(1 - \theta) - \frac{k_2R^3}{R^2\theta(1 - \theta)}. \qquad [9]$$

At the optimum in floc size, the net rate = 0. Consequently,

$$k_1n_0^2\theta(1 - \theta) = \frac{k_2R^3}{R^2\theta(1 - \theta)}$$

or the equilibrium value of floc radius,

$$R = \frac{k_1}{k_2}\cdot n_0^2\theta^2(1 - \theta)^2. \qquad [10]$$

By rearrangement of Eq. [6]

$$1 - \theta = \frac{\dfrac{1 + bkw}{b} + \dfrac{bkwP_0}{1 + bkw}}{\dfrac{1 + bkw}{b} + \dfrac{P_0}{1 + bkw}}. \qquad [11]$$

Inspection shows that the term $(bkwP_0)/(1 + bkw)$ in the numerator may be neglected compared to the constant $(1 + bkw)/b$, since upon increasing P_0, $(1 - \theta)$ approaches 0. In order for this to occur with the increasing values of P_0, $(bkwP_0)/(1 + bkw)$ must rise much more slowly than the $P_0/(1 + bkw)$ term in the denominator. With this further simplification:

$$(1 - \theta) = \frac{\dfrac{1 + bkw}{b}}{\dfrac{1 + bkw}{b} + \dfrac{P_0}{(1 + bkw)}}. \qquad [12]$$

Finally

$$\theta(1 - \theta) = \frac{\left(\frac{1 + bkw}{b}\right) P_0}{\left(\frac{1 + bkw}{b} + \frac{P_0}{1 + bkw}\right)^2}. \quad [13]$$

D. FLOC SIZE IN RELATION TO SPECIFIC SURFACE AREA OF THE FILTER CAKE AND THE FILTRATION RATE

The Kozeny-Carman equation which we have previously discussed relates the rate of filtration through a filter cake to the specific surface area of particles in the cake (3). When a slime is flocculated, the effective specific area of the filter cake is reduced to smaller values corresponding to increasing filtration rates.

The Kozeny-Carman equation predicts that the filtration rate (Q) will be inversely proportional to the square of the surface area of the particles in the cake. If the flocs are considered as essentially spherical in shape and are made up of closely packed primary particles (as usually observed under the microscope), it may be shown that the other factors in the Kozeny-Carman equation such as (ϵ), the porosity of the filter cake, and (L), the thickness of the cake, will be essentially constant. The cross section of the cake is the same in all cases since the same cylindrical funnel is used throughout for filtration. Therefore, the volume of the filter cake will be essentially constant for slimes in different degrees of flocculation. The filtration rate (Q) is then proportional to S^{-2}, where S is the surface area of particles (or flocs) in a unit volume of the filter cake for a given series of experiments using the same slimes, per cent of solids, and flocculant.

Within the limits of this picture, basic relationships among primary particle size and area, and floc size and area may be derived as follows:

Let n_0 = number of primary particles (of average radius R_0) in unit volume of slime.
n = number of primary particles in a floc of average size.

Therefore, $n \tfrac{4}{3}\pi R_0^3$ = volume of solid in unit volume of slime; n_0/n = number of flocs formed per unit volume of slime.

The volume of solid in a unit volume of slime is the same before and after flocculation. Therefore,

$$n_0 \tfrac{4}{3}\pi R_0^3 = \frac{n_0}{n} \tfrac{4}{3}\pi R^3,$$

where R is the radius of a floc which is assumed to be spherical

$$R^3 = nR_0^3$$

or

$$R = n^{1/3}R_0 .$$

The surface area per unit volume of untreated slime,

$$S_0 = n_0 4\pi R_0^2.$$

The surface area per unit volume of flocculated slime,

$$S = \frac{n_0}{n} 4\pi R^2.$$

Therefore,

$$\frac{S_0}{S} = \frac{nR_0^2}{R^2},$$

but

$$n = R^3/R_0^3$$

and

$$S_0/S = R/R_0 .$$

Since for a given series of flocculated samples with the same per cent solids,

$$Q = K/S^2$$

(when L and ϵ are constant as usually observed); then

$$Q/Q_0 = S_0^2/S^2$$

and

$$Q/Q_0 = R^2/R_0^2. \qquad [15]$$

From Eq. [10]

$$R = \frac{k_1}{k_2} \cdot n_0^2 \theta^2 (1 - \theta)^2.$$

Since n_0 is proportional to W for a given slime, then

$$R = kw^2\theta^2 (1 - \theta)^2. \qquad [16]$$

When no flocculant is present, $\theta = 0$, and R approaches 0. Actually in the untreated slime $R = R_0$, the average radius of primary particles. Therefore, Eq. [16] should be corrected. According to Eq. [15] ($Q/Q_0 = R^2/R_0^2$), and $R^2 = R_0^2$, when $Q = Q_0$. Adding unity to each side of the equation and rearranging:

$$Q - Q_0 = Q_0 \left(\frac{R^2 - R_0^2}{R_0^2} \right). \qquad [17]$$

When no flocculant is present, $R = R_0$. Therefore, it is reasonable to represent $R^2 - R_0^2$ in terms of the square of Eq. [16] as follows:

$$R^2 - R_0^2 = k^2w^4\theta^4 (1 - \theta)^4, \qquad [18]$$

and

$$Q - Q_0 = \left(\frac{Q_0}{R_0^2} \right) k^2w^4\theta^4(1 - \theta)^4. \qquad [19]$$

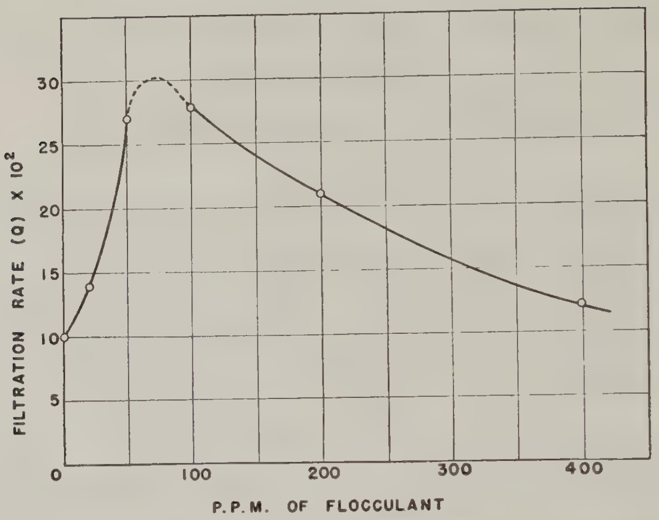

FIG. 1. Shows the variation of the "refiltration rate" in c.c. per second vs. the concentration of Lytron 886 (product of Monsanto Chemical Co.) in parts per million. Each sample contained 1000 p.p.m. of added $CaCl_2$.

Substituting for θ and $1 - \theta$ in terms of Eqs. [6] and [12] gives

$$Q - Q_0 = \frac{k' P_0^4}{\left(\frac{1 + bkw}{b} + \frac{P_0}{1 + bkw}\right)^8} \qquad [20]$$

where

$$k' = \frac{(Q/R_0^2)k^2w^4(1 + bkw)^4}{b^4}.$$

A plot of the measured filtration rate Q vs. P_0 gives a curve which goes through a maximum at the optimum in filtration rate such as shown in Fig. 1.[3] This behavior is typical for a variety of slimes and flocculants.

At the maximum, $dQ/dP_0 = 0$. Differentiating Eq. [20] and setting the derivative = 0, we get:

$$\frac{dQ}{dP_0} = 0 = k'\left[\frac{4P_0^3\left(\frac{1 + bkw}{b}\right) - \frac{4P_0^4}{1 + bkw}}{\left(\frac{1 + bkw}{b} + \frac{P_0}{1 + bkw}\right)^9}\right]$$

and $P_{0(\text{optimum})} = (1 + bkw)^2/b$, or $P_{0(\text{optimum})} = \frac{1}{b} + 2kw + bk^2w^2$.

This is essentially the form of parabolic dependence of the optimum on the square of solid content found experimentally and described in paper V (3). Letting

---

[3] The filtration rate referred to here is actually the "refiltration" rate described in paper V of this series (3).

$$\frac{1 + bkw}{bk'^{1/8}} = A$$

and

$$\frac{1}{k'^{1/8}(1 + bkw)} = B,$$

Eq. [20] becomes:

$$Q - Q_0 = \frac{P_0^4}{(A + BP_0)^8},$$

which may be rearranged into a form which is linear:

$$\frac{P_0^{1/2}}{(Q - Q_0)^{1/8}} = A + BP_0. \qquad [21]$$

Plots of $P_0^{1/2}/(Q - Q_0)^{1/8}$ vs. P_0, the parts per million of added flocculant, are found to be linear for a variety of slimes and flocculating agents when applied to our refiltration data as shown in Fig. 2.

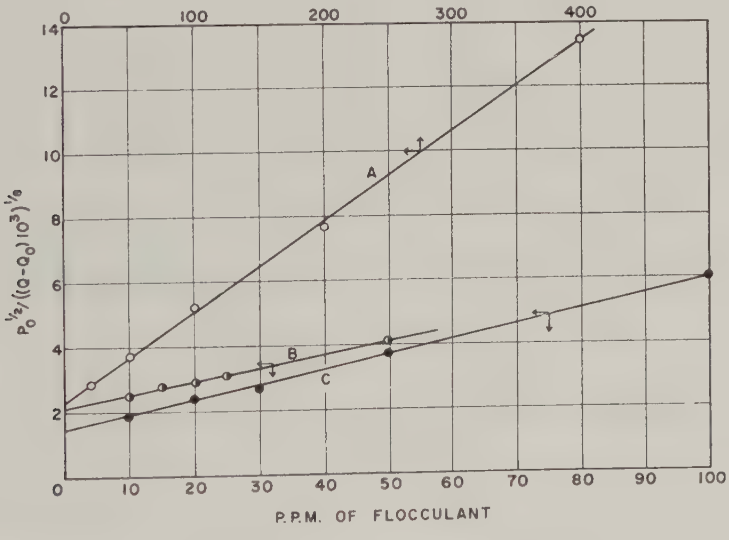

FIG. 2. Shows plots of $\dfrac{P_0^{1/2}}{[(Q - Q_0) \times 10^3]^{1/8}}$ vs. the concentration of flocculant in parts per million (P_0).

A—"Lakeview Reduced" ore slime (prepared from a uranium ore obtained from Mr. Robert G. Beverly of the National Lead Co., Grand Junction, Colorado)—5% solids with Lytron 886 as the flocculant. Each sample also contained 1000 p.p.m. of added $CaCl_2$.

B—Slime XIII (a replica of "leached zone" phosphate slime III previously described in paper II of this series)—5.5% solids, with PVM/MA as the flocculant. PVM/MA (copolymer of methyl vinyl ether and maleic anhydride) is a product of General Aniline and Film Co.

C—Slime VIII (also a replica of slime III)—5.5% solids, with Lytron 886 as the flocculant.

The ratio of the intercept A, to the slope, B, is equal to $(1 + bkw)^2/b$ or to $P_{0(\text{optimum})}$, i.e., $A/B = P_{0(\text{optimum})}$. It is thus possible to determine the value of $P_{0(\text{optimum})}$ from the intercept and slope of the above plot, where it has not been determined directly by experiment.

The particular criticism that can be made of Eq. [21] above, concerns the lack of sensitivity of the 8th root of the filtration rate. Where the data include an experimental determination or close estimate of the value of $P_{0(\text{optimum})}$, i.e., P_m, the following procedure can be used to test the validity of the function.

Since $P_{0(\text{optimum})} = A/B$, then

$$Q - Q_0 = \frac{P_0^4}{(A + BP_0)^8}$$

$$Q - Q_0 = \frac{P_0^4}{(BP_m + BP_0)^8}$$

$$= \frac{P_0^4}{B^8[P_m + P_0]^8}$$

$$\frac{P_0^4}{Q - Q_0} = B^8[P_m + P_0]^8$$

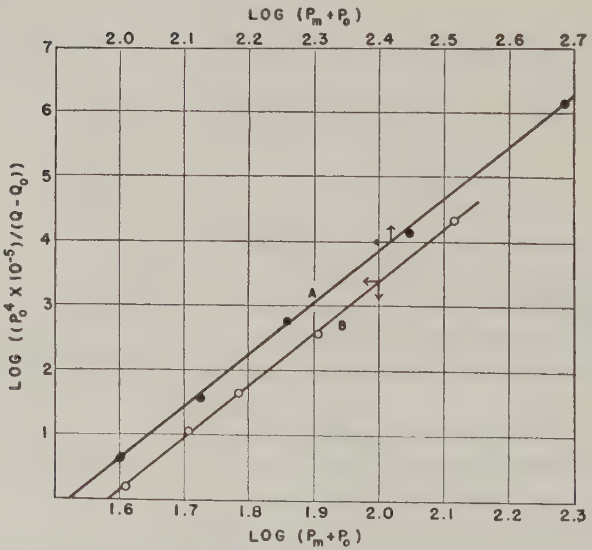

FIG. 3. Shows two sets of data from Fig. 2 plotted as

$$\log_{10}\left[\frac{P_0^4\,(10^{-5})}{(Q - Q_0)}\right] \text{ vs. } \log_{10}\left[P_m + P_0\right].$$

A—"Lakeview Reduced" ore slime. The optimum $(P_m) = 80$ p.p.m. Slope of line = 8.10.

B—Slime VIII. The optimum $(P_m) = 31$ p.p.m. Slope of line = 8.07.

and

$$\log\left[\frac{P_0^4}{Q - Q_0}\right] = 8 \log B + 8 \log [P_m + P_0].$$

Therefore a plot of $\log\left[\frac{P_0^4}{Q - Q_0}\right]$ vs. $\log\ [P_m + P_0]$ should be linear with slope = 8.

Figure 3 shows two sets of data (from Fig. 2) plotted in this way. The slopes obtained are 8.10 and 8.07, respectively. Plots of the data assuming other powers such as 4, 6, and 10 either deviate from a straight line or give incorrect slopes so that the 8th power function is well established.

From data that are now being obtained with techniques for determining the adsorption of polymers, we expect to develop the filtration theory to a higher degree of refinement.

REFERENCES

1. LA MER, V. K., AND SMELLIE, R. H., JR., *J. Colloid Sci.* **11,** 704 (1956); LA MER, V. K., AND SMELLIE, R. H., JR., *ibid.* **11,** 710 (1956); SMELLIE, R. H., JR., AND LA MER, V. K., *ibid.* **11,** 720 (1956).
2. LA MER, V. K., SMELLIE, R. H., JR., AND LEE, PUI-KUM, *J. Colloid Sci.* **12,** 230 (1957).
3. LA MER, V. K., SMELLIE, R. H., JR., AND LEE, PUI-KUM, *J. Colloid Sci.* **12,** 566 (1957).
4. JELLINEK, H. H. G., HOBDEN, J. F., AND NORTHEY, H. L., *J. Polymer Sci.* **11,** 365 (1953); *ibid.* **14,** 583 (1954); JENCKEL, E., AND RUMBACH, B., *Z. Elektrochem.* **55,** 612 (1951).
5. For a good discussion see: "Colloid Science" (edited by H. R. Kruyt), Vol. 1, p. 278. Elsevier, Houston, Texas, 1952.

JOURNAL OF COLLOID SCIENCE **13**, 600–615 (1958)

RADIOIODINE EXCHANGE BETWEEN IODOSTEARIC ACID MONOLAYERS AND SUBSTRATE IODIDE. II

W. Rabinovitch, R. F. Robertson, and S. G. Mason

The Department of Chemistry, McGill University, and the Pulp and Paper Research Institute of Canada, Montreal

Received August 15, 1958

Abstract

The kinetics of exchange of radioiodine between α-iodostearic acid spread as a unimolecular film on aqueous solutions of KI have been studied. The possible influence on the exchange rate of the film characteristics as determined by the pressure-area isotherms and their variation with pH have been studied. The effect of insoluble barium soap formation on the exchange velocity at high pH values has also been investigated. Exchange reactions and the relation between surface radioactive count rate and surface concentration of film molecules have been studied in both spread and collapsed films.

Introduction

The kinetics of halogen exchange reactions between radioactively tagged halogen derivatives of fatty acids in unimolecular films at the air/water interface and substrate halide ions were first reported in a previous publication (1). In that and the present paper, the iodine exchange between iodide ion and I^{131}-tagged α-iodostearic acid is discussed. The experimental data of the earlier work indicated a discontinuity between 14°C. and 22.5°C. in the Arrhenius plot of the (first-order) exchange rate constants. This discontinuity was assumed to be related to the type of film present during exchange as determined from the pressure-area relations of α-iodostearic acid on 0.01 *M* HCl substrates. A study of the pressure-area isotherms of this acid on (0.01 *M* HCl + 1.0 *M* KI) substrates was impossible in the earlier work. The construction of a self-compensating automatically recording vertical pull balance, however, overcame the technical difficulties involved in measuring these isotherms.

The possible influence of substrate pH on the velocity of exchange and the influence of change in pH due to air oxidation of the I^- ion during the course of exchange were not investigated in the earlier work. Van der

---

[1] Based on work conducted under Extra-Mural Grant 2031-08 of the Defence Research Board of Canada.

Straaten and Aten (2) reported a marked influence of pH on the solution exchange reaction:

$$CH_2I^{131}\,COOH + I^- \rightarrow CH_2ICOOH + I^{131-}$$

the exchange occurring ten times more rapidly in acidic than in alkaline medium. Analogous effects have been reported by La Mer and Kamner (3) leading to the conclusion that the rate at which substituents α to a carboxyl group can react with an ionic species (I^- or OH^-) may be determined by the degree of ionization of the carboxyl group. The approach of the reacting ionic group may consequently be greatly influenced by the electrostatic field of the carboxyl group.

Adam and Miller (4) have shown that the pressure-area isotherms of unimolecular films may be markedly affected by electrostatic repulsion between the head groups arising from their degree of ionization. Gaseous films may be transformed, as demonstrated by Langmuir and Schaefer (5), to coherent films by the addition of alkaline-earth cations such as Ba^{++}.

The present work had as its immediate purpose determination of the effect upon pressure-area isotherms and upon exchange velocity in 1 N iodide substrates of *(1)* various values of substrate pH, *(2)* the presence of Ba^{++} in the substrate, and *(3)* the temperature of the monolayer-substrate system. To elucidate physical features of film structure, secondary aims have been to determine exchange velocity when the monolayer was collapsed and to investigate the relationship between observed monolayer count rate and its surface concentration from the heterogeneous two-phase system to well beyond film collapse.

Experimental Part

The materials, apparatus, and method employed were essentially those of Robertson *et al.* (1), but with the following modifications:

1. *Radiochemically Tagged α-Iodostearic Acid*

A sample of α-iodostearic acid (subsequently designated as ISA), 20 mg., was taken from the stock previously prepared and dissolved in 5 ml. of absolute ethanol in a 250-ml. Erlenmeyer reaction flask. A drop of concentrated hydrochloric acid and 10 mc. of NaI^{131} in alkaline $NaHSO_3$ solution (less than 1 ml.) was added to the alcoholic solution. The acidity of the resulting solution was tested and more HCl added if necessary. After refluxing the reaction medium for 1 hour, about 25 ml. of distilled water were added to precipitate the I^{131}-tagged α-iodostearic acid. The precipitate was allowed to stand overnight to permit easier filtration. The radioactive α-iodostearic acid (designated as RISA) was then filtered on a sintered glass filter stick by suction and the precipitate was washed with 25 to 50 ml. of 0.01 N HCl in small portions to remove inorganic salts. The crystals were then dried on the filter stick by suction and the product dissolved in 10 ml. reagent grade benzene.

2. Substrate Solutions

The presence of barium ion in some substrate solutions necessitated precautions to minimize the CO_2 content and prevent precipitation of $BaCO_3$. Freshly boiled distilled water was used to prepare the substrate solutions and a nitrogen atmosphere was maintained in the air bath of the film balance.

3. Trough and Barriers

The trough 21 x 8 x ½ inches was milled from a block of stainless steel, heat treated and sprayed with several coats of Teflon, then baked to render it nonwetting. Heavy steel strips 3⁄16 x ⅝ x 10½ inches and 3⁄16 x ⅝ x 15 inches backed with foam rubber and carefully wrapped in Teflon sheet 0.003 inch thick, were used as very effective leak-proof barriers. The barriers could be moved along the trough by a motor-driven remote control.

4. Surface Balance

A Wilhemy type vertical-pull balance was adapted to permit automatic registration of film pressure on a Minneapolis-Honeywell Multi-span strip recorder. The balance is described in detail elsewhere (6). Since the glass dipping plate of this balance remained essentially stationary, increasing or decreasing surface pressures could be measured even on the concentrated salt solutions used without the problems of changing contact angle (7) or of deposition of salt on the dipping plate (1).

5. Procedures

The experimental procedures differed in several details from those previously employed (1), but were otherwise the same.

Pressure-area curves of ISA and RISA were automatically recorded at a constant rate of surface compression. This required about 5 min. instead of 2 to 3 hr. by the manual stepwise procedure previously followed. Owing to relaxation effects the π-A curves were somewhat influenced by the rate of compression, but the general shape of the curves and transition areas were unaffected (8).

The measured first-order reaction velocity constants k' were measured as before (1) by following the decrease in radioactivity using an end-window G-M counter placed about 5 mm. above the surface, but were corrected for the background count effect due to I^{131}-ions present in the substrate using correction factors calculated from theoretical considerations (9). This correction, which was previously ignored (1), yielded values of the true rate constant k which were 3 % to 15 % greater than k'.

Results

1. *Count Rate versus Surface Concentration*

In computing k it was assumed (1) that, except for the substrate contribution, the radioactive count rate is proportional to the surface concentration of tagged molecules. This assumption was tested by spreading RISA monolayers on KI-free substrates and compressing at a constant rate while simultaneously recording the count rate and the surface pressure.

In these experiments the films were spread at an initial area of 65 sq. A./molecule and were compressed at a constant rate of 3¼ sq. A./molecule/minute. In Fig. 1 the relative count rate was plotted against surface concentration for four typical experiments. In the region between 52 and 30 sq. A./molecule the plot was linear and passed through the origin, but marked deviation and irregularity occurred outside of this region. The π-A curve indicated a homogeneous coherent film in the linear region of Fig. 1. This is the region in which most of the exchange measurements were made.

The region corresponding to molecular areas greater than 52 sq. A./molecule in which the count rate varied erratically with increase in the surface concentration is the two-phase region of the film, the heterogeneity of which has previously been inferred from surface potential measurements (10). The nonlinearity below 30 sq. A./molecule, i.e., in the region of collapse, was unexpected and may have been due to an "edge" effect resulting

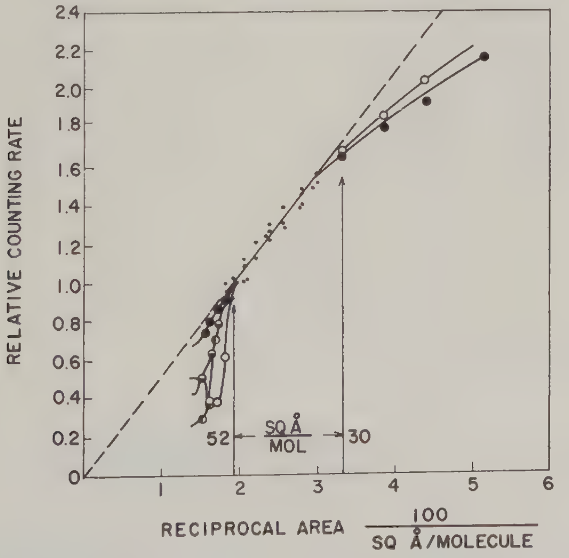

FIG. 1. Relative count rate as a function of surface concentration in monolayers of I^{131}-tagged α-iodostearic acid.

from imperfect collimation of the β-radiation entering the counter and thus unrelated to collapse. Alternatively, the decrease in surface count rate beyond collapse may also have been due to heterogeneity of the collapsed films, for which evidence is presented later. It is significant that such heterogeneity has been demonstrated with deposited films of stearic acid by electron micrography (11).

2. Pressure-Area (π-A) Isotherms and Exchange Reactions

The possible relation between electrostatic repulsion in the head groups of α-iodostearic acid films and the velocity of exchange in these films required a knowledge of the π-A (pressure-area) isotherm on acid and alkaline substrates in the presence and absence of Ba^{++} ion in the substrates. In general the experimental conditions leading to gaseous or coherent liquid films are known (4, 5). On substrates 1 N in KI as used in the exchange reactions, however, it was considered necessary to determine precisely the π-A isotherms. A standard procedure was adopted in which the initial area per molecule on spreading the film was 100 sq. A./molecule, and compression was carried out at a constant rate of 5 sq. A./molecule/minute.

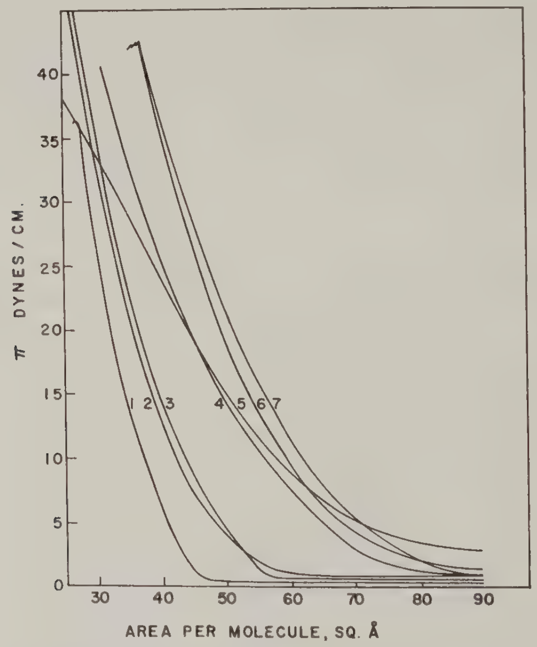

FIG. 2. Pressure-area isotherms of α-iodostearic acid on various substrates at 25°C. Curve (*1*) 0.01 N HCl; (*2*) 0.01 N NaOH + 0.0002 N $BaCl_2$; (*3*) 0.002 N $Ba(OH)_2$ + 1.0 N BaI_2 ; (*4*) 0.01 N NaOH; (*5*) 0.001 N $Ba(OH)_2$ + 1.0 N KI; (*6*) 0.01 N NaOH + 1.0 M KI; (*7*) 0.01 N NaOH + 1.0 N KI + 0.0004 N $BaCl_2$.

a. Effect of Ba^{++} *Ion.* Figure 2 shows the π-A diagram obtained using substrates 0.01 N in HCl (curve 1) and 0.01 N in NaOH (curve 4). The gaseous film on the alkaline substrate has no definite condensation area as a consequence of mutual electrostatic repulsion of the ionized carboxyl polar groups of the sodium salt. The addition of barium ion sufficient to make the 0.01 N NaOH substrate 0.0002 N in Ba^{++} caused contraction of the gaseous film as shown in curve 2. This contraction indicated a reduction of electrostatic repulsion in the head groups as the ionized acid was converted to the insoluble barium salt, as was found by Langmuir and Schaefer (5).

When the substrate solution was made 1 M in KI, however, the above change in the film characteristics upon the addition of Ba^{++} ion to an alkaline substrate did not occur. Figure 2, curves 6 and 7, are the isotherms obtained on one substrate of composition 0.01 N NaOH plus 1.0 M KI, and on another of composition 0.01 N NaOH plus 1.0 M KI plus 0.004 N $BaCl_2$, respectively. The curves are seen to be very similar. Thus the addition of Ba^{++} ion to alkaline 1 M KI substrates did not lead to a coherent film as did the addition of Ba^{++} ion to alkaline substrates containing no KI. The relatively high concentration of KI seemed, in effect, to exclude Ba^{++} ion from the surface region.

Figure 2, curve 5, shows the isotherm obtained on a substrate 1 M in KI and 0.001 N in $Ba(OH)_2$, indicating a gaseous film. On replacing the KI with 1.0 N BaI_2 (Fig. 2, curve 3) a coherent liquid film was obtained at pH 10.8. The values of the area of condensation (58 sq. A./molecule) and initial pressure were somewhat higher than those found under acid conditions. The alkaline BaI_2 substrate permitted the formation of a nonionized monolayer of barium α-iodostearate.

The first-order rate constants of the iodine exchange reactions for some of these 1 M iodide substrate solutions are given in Table I. The rate constants were determined from the slope of plots of log $c(t)$ vs. time for

TABLE I

Exchange Reaction with Various Substrates

(Temp. = 25°C.)

		Exchange reaction		Film properties
pH	Substrate	$10^4\,k$ (*min.*$^{-1}$)	Surface/pressure π (*dynes/cm.*)	Transition area (*sq. A./molecule*)
2	0.01 N HCl 1.0 M KI	26.6	5	53.0
12	0.01 N NaOH 1.0 M KI	0.8	30	None, gaseous
13	0.1 N NaOH 1.0 M KI	1.1	5	None, gaseous
10.8	0.001 N $Ba(OH)_2$ 1.0 N KI	1.5	22	None, gaseous
10.8	0.002 N $Ba(OH)_2$ 1.0 N BaI_2	2.4	5	58
		3.0	30	

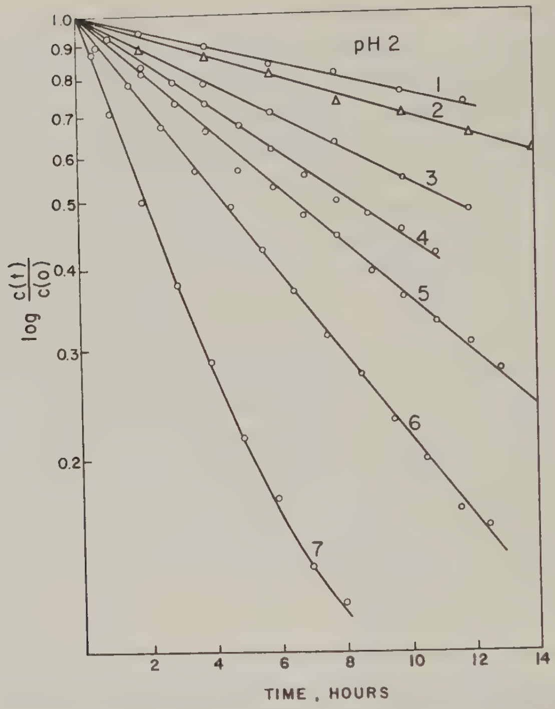

FIG. 3. Semilogarithmic plot of relative count rate against time at various temperatures at substrate pH 2. Curve (*1*) 10.5°C.; (*2*) 13.5°C.; (*3*) 15.6°C.; (*4*) 18.0°C.; (*5*) 20.3°C.; (*6*) 25.2°C.; (*7*) 35°C.

which the curves of Fig. 3 are typical. In Table I the exchange rate constants are compared with the film properties on the various substrates in this table.

b. Effect of pH. In a further attempt to relate the pH of the substrate, the resulting film characteristics, and exchange velocity, π-A isotherms and exchange rate constants were determined as functions of pH. Solutions of 1 M KI at pH's from 1.0 to 6.0 were used as substrates. The exchange reactions were carried out at a monolayer surface pressure of approximately 5 dynes/cm. unless otherwise indicated. The results of these experiments at 25°C. are summarized in Table II. A marked trend can be noticed in the velocity constants over the pH range studied, the velocity constants varying from 27×10^{-4} min.$^{-1}$ at pH 2 to 3 to 1.3×10^{-4} min.$^{-1}$ at pH 6. In Fig. 4, the π-A isotherms are given for the range of pH 1 to 12. These isotherms were determined for films of inactive α-iodostearic acid spread on phthalate-buffered substrates 1 M in KI. In conjunction with the data of Table II it seems improbable that the shape of the isotherms is intimately related to the reaction velocity, since over the pH range 2 to 5 the isotherms

TABLE II

Variation of Exchange Velocity with pH on 1.0 M KI Substrates
(Temp. = 25°C.)

pH	$10^4 k$ (*min.*$^{-1}$) (mean value)	Film properties	
		Area of first-order transition (*sq. A./molecule*)	Surface pressure π, at 100 sq. A./molecule (*dynes/cm.*)
1	11.6	56.0	0.00
2	26.6	53.2	0.03
3	27.1	53.0	0.05
4	8.7	53.0	0.10
5	2.2	55.0	0.60
6	1.3	72.0	0.50

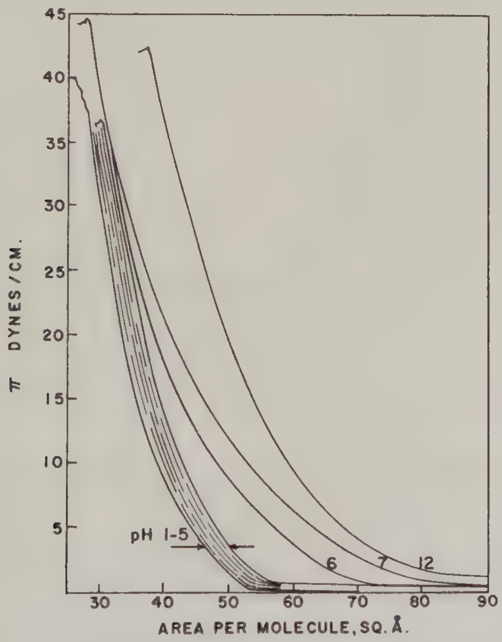

FIG. 4. Pressure-area isotherms of α-iodostearic acid at 25°C. on 1.0 M KI; substrate pH varied from 1 to 12 units.

remained essentially the same, but the reaction velocity decreased by a factor of ten with increasing pH.

An apparent discontinuity around 18°C. in the Arrhenius plot of the exchange velocity constants was previously noted (1). This was ascribed to the transition from the condensed to the expanded liquid film through the intermediate liquid film present below 18°C. A more detailed investigation of this phenomenon seemed advisable. In Fig. 5, π-A isotherms are

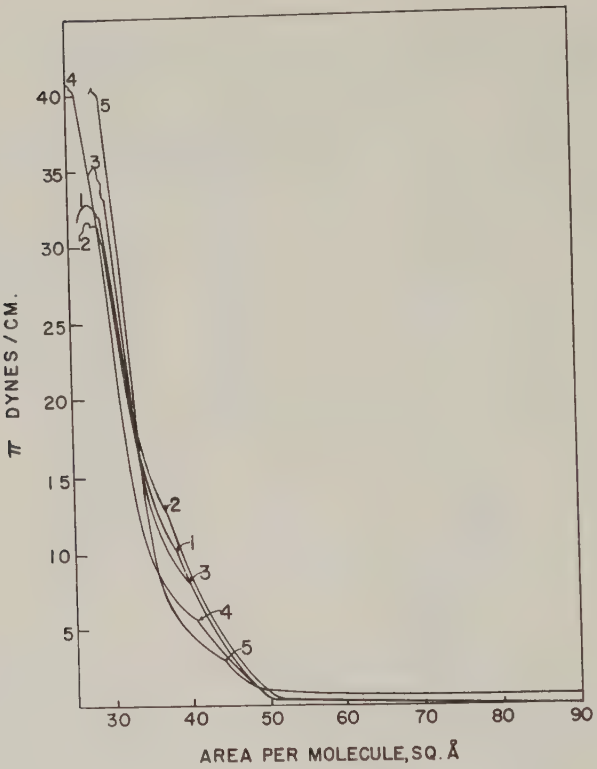

FIG. 5. Pressure-area isotherms of α-iodostearic acid on 1.0 M KI at 18°C.: the effect of pH. Curve (*1*) pH 0.4; (*2*) pH 1; (*3*) pH 2; (*4*) pH 3; (*5*) pH 4.5.

given for α-iodostearic acid monolayer on 1.0 N KI substrates over a range of pH. The corresponding plots log $c(t)/c(0)$ vs. t for the exchange reaction were all linear over the pH range investigated.

The exchange rate constants obtained from these plots and the corresponding film characteristics are given in Table III.

c. Effect of Temperature. Robertson *et al.* (1) have reported π-A isotherms for an α-iodostearic acid monolayer on 0.01 N HCl, for the temperature range 9°C. to 27.4°C. Pressure-area isotherms (Fig. 6) for the monolayer on 1 M KI, 0.01 N HCl substrates show that the liquid condensed film obtained at 9.3°C. begins to undergo expansion at 14°C. As the temperature is raised, the expansion is almost completed for the π-A isotherm at 18°C. A fully expanded film is obtained at 25°C. The area of first-order transition for this film is 53.0 sq. A./molecule, which is approximately 8 sq. A./molecule greater than the value when the substrate contains no KI (1), as can be seen in Fig. 2, curve 1.

Plots of log $c(t)/c(0)$ vs. time for exchange reactions on 0.01 N HCl + 1 M KI substrates at various temperatures are given in Fig. 3. The plots

TABLE III

Variation of Exchange Velocity with pH on 1.0 M KI Substrates
(Surface pressure = 4–5 dynes/cm.)
(Temp. = 18°C.)

pH	$10^4 k$ (*min.*$^{-1}$)	Film properties—partially expanded liquid films		
		Area of first-order transition (*sq. A./molecule*)	Surface pressure at 100 sq. Å./molecule (*dyne/cm.*)	Surface pressure at second-order transition. (*dynes/cm.*)
0.4	10.4	50.5	0.05	10.00
1.0	12.8	50.0	0.00	12.50
2.0	12.6	50.0	0.00	8.20
3.0	8.3	49.8	0.00	5.75
4.5	3.9	47.5	0.60	2.90

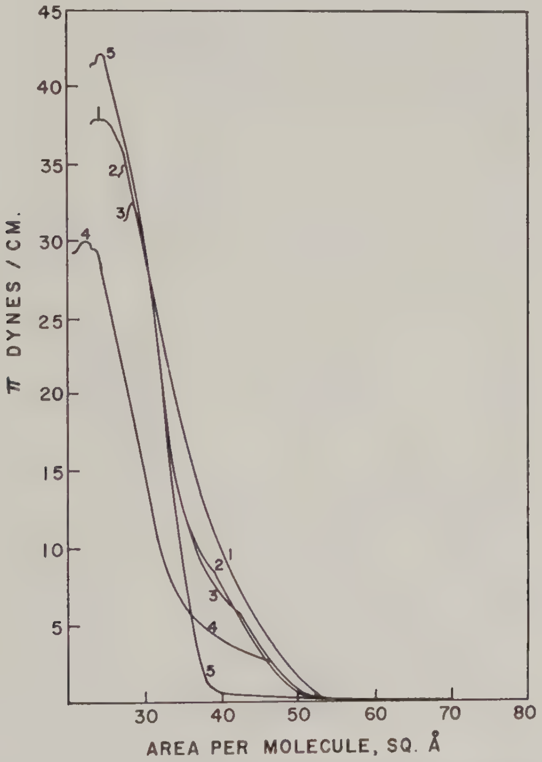

FIG. 6. Pressure-area isotherms of α-iodostearic acid on 1.0 M KI + 0.01 N HCl substrates. Curve (*1*) 24.8°C.; (*2*) 18.0°C.; (*3*) 16.2°C.; (*4*) 13.9°C.; (*5*) 9.3°C.

are substantially linear and show a trend of increasing slope, k', with increasing temperature. It is possible that the nonlinearity observed after 4 hr. at 35°C. arose because the rapid exchange reaction at this temperature had been followed to a point where the $c(t)/c(0)$ ratio was small (0.12), and consequently the diffusion-controlled contribution of substrate background counts became increasingly significant (9).

Figure 7 illustrates the temperature and pH dependency of the exchange rate constants (*cf.* Table IV) after being corrected for the natural decay of I^{131} and diffusion-controlled substrate contribution to the observed counting rate.

From both the data shown in Fig. 7 and earlier work (1), Arrhenius plots have been constructed for the pH 2 and pH 3 data (Fig. 8).

The continuous solid line of Fig. 8 corresponds to an activation energy of 16 kcal./mole, the value reported by Van der Straaten and Aten (2).

For the pH 3 plot of Fig. 8, the break shown near 25°C. (and which may not be real) may have been due to a slight change of pH, to which k has been shown (Fig. 7) to be highly sensitive.

It is possible that a series of experiments in which the Arrhenius plot was obtained at pH 4 would shift the discontinuity to a higher temperature.

d. Exchange in Collapsed Films. It is known that the rate of hydrolysis in vapor-expanded films of ethyl palmitate spread upon caustic solutions may be decreased about eight-fold by increasing compression on the film (10).

In the early work on radioiodine exchange reactions similar behavior was expected. However, by varying the surface pressure between 2 and 15 dynes/cm. (between 50 to 36 sq. A./molecule approximately), k was

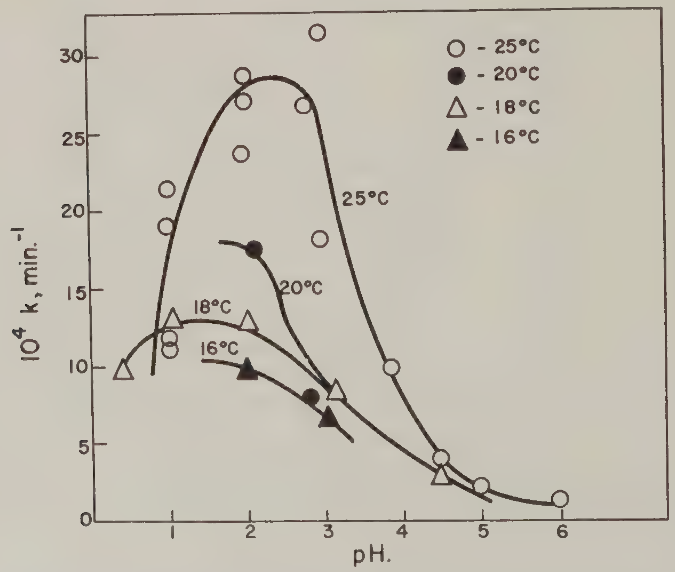

FIG. 7. Effect of pH and temperature on the exchange rate constant k, corrected for diffusion-controlled background contribution.

TABLE IV

Variation of Exchange Velocity with Temperature and pH

Temperature (°C.)	pH	Surface pressure (*dynes/cm.*)	$10^4 k$ (*min.*$^{-1}$)
35	2.2	4–5	58
	—	15	48.8[a]
	—	17	50.5[a]
25	1.0	4–5	11.8
	1.0	4–5	21.6
	1.0	4–5	11.2
	2.0	4–5	27.2
	2.0	4–5	23.6
	—	2.0	28.2[a]
	—	15.0	27.4[a]
	2.8	4–5	26.8
	3.0	4–5	31.6
	2.8	4–5	22.9
	3.9	4–5	9.9
	4.0	4–5	3.9
	5.0	4–5	2.2
	6.0	4–5	1.3
20	2.1	4–5	7.8
	2.8	4–5	17.5
18	0.4	4–5	10.0
	1.0	4–5	12.8
18	2.1	4–5	13.9
	2.2	4–5	12.6
	—	—	14.8[a]
	—	—	15.0[a]
	2.4	4–5	6.9
	2.5	4–5	6.5
	3.1	4–5	8.3
	—	15	8.2[a]
	—	15	9.8[a]
	4.5	2	3.1
	4.5	4–5	3.9
16	2.0	4–5	10.0
	2.3	4–5	5.8
	3.1	4–5	6.9
14	2.1	4–5	5.8
	—	13	7.25[a]
	—	13	7.4[a]
10	2.2	4–5	4.9
	—	8	6.1[a]
	—	8	6.1[a]

[a] Data from Robertson, Winkler, and Mason (1) in unbuffered 0.01 *N* HCl + 1.0 *M* KI.

not observed to be affected appreciably. Apparently the range of variation of area per molecule which must be covered when obtaining the conventional isotherm for ISA, i.e., 30 to 53 sq. A./molecule, cannot alter the orientation of the polar group, and hence the ability of the I atom to exchange at the interface. It was therefore considered to be of interest to investigate extremes in molecular area, i.e., films which had been compressed beyond collapse, and gaseous films.

Exchange reactions in gaseous films (on acidic substrates) are complicated by the conflicting requirements of extremely low surface concentration, i.e., high molecular area and sufficient radioactivity on the surface to give adequate count rates. A film which gives a counting rate of 10^4 c.p.m. at an area of 60 sq. A./molecule would, if homogeneously distributed on the surface, give only 10^3 c.p.m. at 600 sq. A. Several trials, in which films were spread at areas in the range 600 to 800 sq. A./molecule, consistently led to the observation of severely fluctuating count rates, indicative of film heterogeneity. It is possible that film heterogeneity would disappear at even higher molecular areas, e.g., 2500 sq. A./molecule, but an extremely high specific activity of the tagged fatty acid would be required for sufficiently high count rates. Consequently, the present study was confined to collapsed films.

Films of ISA were spread upon acidic KI substrates at 18° and 25°C., and permitted to exchange at a surface pressure of 4 dynes/cm. (i.e., 43 to 50 sq. A/molecule) while radioactive counting-rate measurements were being recorded. Subsequently the films were compressed to about ⅓ of the initial area to beyond collapse as observed by simultaneously recorded

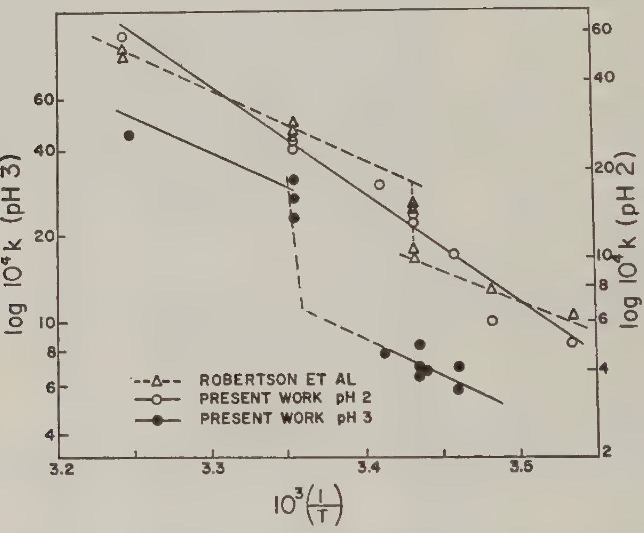

FIG. 8. Arrhenius plot of log $k \times 10^4$ for the exchange reaction on 1 M KI, 0.01 N HCl substrates.

TABLE V

Exchange Velocity in Monolayers and Collapsed Films

(Substrate 1.0 M KI)

pH	Temperature (°C.)	10^4 *k* (*min.*$^{-1}$)	Area molecule (calculated) (*sq. A./molecule*)	State of film
2	25.2	23.7	46	Monolayer
		11.8 → 2.3	14	Collapsed
1	25.0	11.8	50	Monolayer
		4.6	17	Collapsed
1	18	12.8	43	Monolayer
		4.4	15	Collapsed

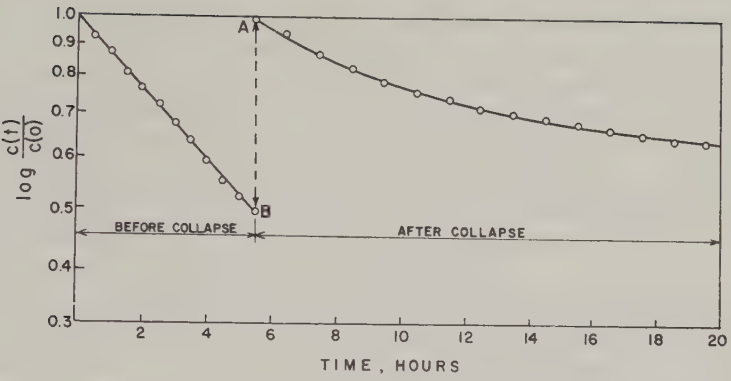

FIG. 9. Semilogarithmic plots of relative counting rate with time for the exchange reaction in a monolayer and in a collapsed film at 25°C.

surface pressure. Following film collapse the exchange reaction was followed for periods up to 14 hr. Table V compares the rates of exchange found in the monolayer and collapsed films investigated, and Fig. 9 shows the corresponding log $c(t)/c(0)$ vs. time plots for the smoothed data.

The marked reduction in the rate of iodine exchange taking place in collapsed films is set forth by the data of Table V, and the general trend of the slope of the curves before and after compression to collapse in Fig. 9. The curve after collapse is nonlinear, and k appears asymptotic to zero. During a 14-hr. interval, 10^4 k decreased from 11.8 to 2.3 min.$^{-1}$. Moreover, the counting rate of collapsed films showed sporadic irregularities of much lower frequency and greater amplitude than statistical fluctuations, indicating heterogeneity in the collapsed film.

It is concluded that collapse of the I^{131} α-iodostearic acid monolayer by reduction of the area per molecule to about 15 sq. A. results in *(1)* the immediate removal of more than half the polar groups from the substrate interface, *(2)* the formation of multilayers which are at least two molecules thick and which lie above the substrate surface, rather than below it, and *(3)* the appearance of a slow collapse process which persists spontaneously after initial compression.

DISCUSSION

When monolayers of α-iodostearic acid were spread on alkaline substrates, expansion to gaseous films occurred, and at pH 11 to 12, k dropped to values $1/8$ to $1/30$ those obtained at pH 2. Increasing concentrations of Ba^{++} ion in these alkaline substrates tended to increase k as the films became more coherent, but the constants for coherent films of barium

α-iodostearate fell far below those obtained for the free fatty acid on acidic substrates, although above those for films of the sodium salt. The π-A curves of the films of barium iodostearate on alkaline substrates were very similar to those of α-iodostearic acid on an acidic medium. Reorientation of the fatty acid molecules on the surface due to salt formation would not of itself be a sufficient explanation of the marked decrease of exchange velocity. The decrease in exchange velocity must be attributable to conditions associated with the polar groups themselves. Electrostatic repulsion of the I^- ion by the neutralized head groups does not seem likely, but a decrease in accessibility of I^- ion for the α iodine atom due to the bridges between iodostearic acid molecules arising from the insoluble salt formation with divalent barium does seem to be one possible explanation of these phenomena.

The effect of hydrogen ion concentration in the absence of Ba^{++} ion on the exchange velocity could again be attributable either to a reorientation of the monolayer molecules as a result of the increased dissociation of the carboxyl group, or to electrostatic repulsion of the iodide ion by the presence of the negatively charged carboxyl group. Both explanations are possible, but in the range of pH 1 to 5 the physical properties of the films did not indicate any marked reorientation of the film molecules, except insofar as the appearance of the liquid-intermediate film was concerned at a temperature of 18°C. The pressure at which the more condensed film appeared decreased as the pH increased, except for the inversion of pH 0.4 and 1.0 (Fig. 5). The rate constants, on the other hand, passed through a maximum of 12.8×10^{-4} min.$^{-1}$ at pH 1 and then decreased steadily to 3.9×10^{-4} min.$^{-1}$ at pH 4.5. Thus, the rate constants decreased with increased ionization of the polar end groups.

The variation in shape of the isotherms caused by the appearance of an intermediate phase as the temperature is changed at constant pH (Fig. 6) is closely paralleled at a constant temperature of 18°C. by variation of the pH (Fig. 5) for buffered 1 N KI substrates. Since the exchange rate constants were found to parallel the magnitude of the second-order transition pressure of the surface phases obtained, similar experiments at constant temperatures between 10° and 20°C. should throw further light on the film structure and the kinetic mechanism.

The pressure-area isotherms obtained on substrates 1.0 M in KI showed little difference compared with those on substrates containing 0.01 N HCl alone. The curves were slightly expanded, the beginning of the appearance of coherent film being at an area 8 sq. A./molecule larger on KI than on HCl alone.

The discontinuity or inflection in the activation energy plot could be accounted for by a pH change due to air oxidation of the iodide ion in the substrate. Certainly the change in the rate constant is within the range of changes noted in the present paper from pH variation alone. It is difficult to conceive how sufficient iodide ion could have been oxidized during the time available for exchange to account for a pH change sufficient to alter the rate constants so markedly as in the earlier work. This problem must remain open until further experimental work is completed.

The mechanism of the exchange reaction is being studied by combined radioactivity and surface potential measurements. Preliminary results show a marked parallelism between the surface potential *versus* pH curves and the k *versus* pH curves shown in Fig. 7 (12).

The present studies have been limited to α-iodostearic acid so that the film properties and exchange mechanism cannot be considered separately from the proximity of the iodine atom to the hydrophilic carboxyl group. It would be interesting to move the I atom down the chain from the α- to the β- or γ-position, or beyond, and so remove the iodine from the substrate when the molecules become oriented vertically. In such a case k would be expected to drop to zero in going from a gaseous to a nongaseous film.

ACKNOWLEDGMENT

The authors express their indebtedness to Dr. L. Yaffe for advice and assistance in radiochemical procedures.

REFERENCES

1. ROBERTSON, R. F., WINKLER, C. A., AND MASON, S. G., *Can. J. Chem.* **34**, 716 (1956).
2. VAN DER STRAATEN, H., AND ATEN, A. H. W. J., *J. Am. Chem. Soc.* **76**, 3798 (1954).
3. LA MER, V. K., AND KAMNER, M. E., *J. Am. Chem. Soc.* **53**, 2832 (1931).
4. ADAM, N. K., AND MILLER, J. G. F., *Proc. Roy. Soc.* (*London*) **A142**, 401 (1933).
5. LANGMUIR, I., AND SCHAEFER, V. J., *J. Am. Chem. Soc.* **58**, 284 (1930).
6. RABINOVITCH, W., Ph.D. Thesis, McGill University, Montreal, 1956.
7. HARKINS, W. D., AND ANDERSON, T. F., *J. Am. Chem. Soc.* **59**, 2189 (1937).
8. RABINOVITCH, W., AND MASON, S. G., *Proc. Roy. Soc.* (*London*), *Series A*. In Press 1958.
9. RABINOVITCH, W., AND MASON, S. G., *Proc. Roy. Soc.* (*London*), *Series A*. In Press 1958.
10. ALEXANDER, A. E., AND SCHULMAN, J. H., *Proc. Roy. Soc.* (*London*) **A161**, 115 (1937).
11. RIES, H. E., AND KIMBALL, W. A., *Nature* **181**, 901 (1958).
12. RAMARADHYA, J. M., Ph.D. Thesis, McGill University, Montreal, 1958.

JOURNAL OF COLLOID SCIENCE **13**, 616–618 (1958)

LETTERS TO THE EDITOR

A DEVICE FOR THE DETERMINATION OF THE RATE OF INCREASE OF SURFACTANT AT THE LIQUID-AIR INTERFACE

A device (Fig. 1) for the determination of the rate of increase of surfactant at the liquid-air interface is made up of a water bath to maintain constant temperature, a magnetic stirring motor, stirrer, and a monitoring device (Geiger Tube, gas flow tube, or scintillation crystal) mounted over the surface of the solution. The surfactant to be studied is tagged with a radioactive tracer, preferably a soft beta-emitter, and introduced into a Teflon vial in the center of the apparatus. The use of a soft beta-emitter permits monitoring to a depth of a few millimeters; this depth is determined by the energy of the radioactive isotope. A fixed volume of surfactant is used to maintain constant geometry. The solution is stirred until it has

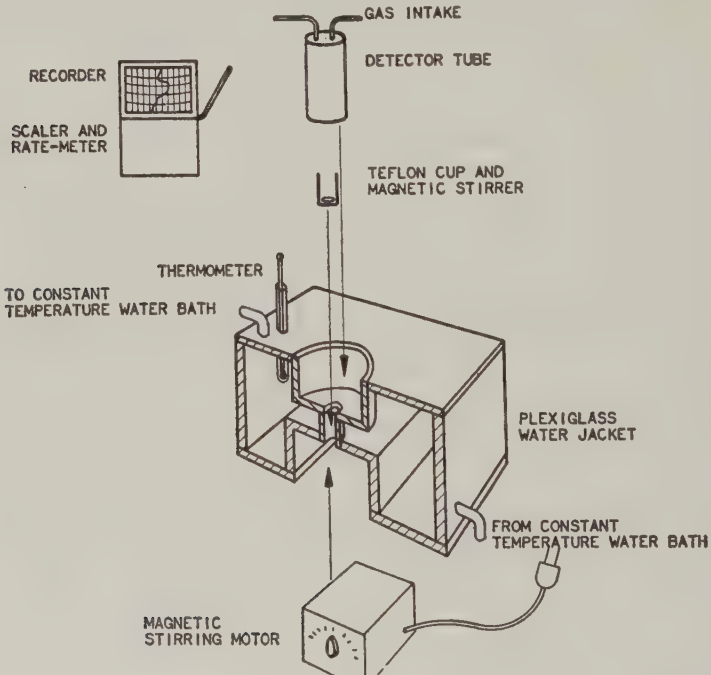

FIG. 1. Cross section of apparatus.

reached a constant, preselected temperature. Monitoring is initiated with the stirring operation to record the changes at the surface the instant the stirring is stopped. The radioactive count obtained is recorded continuously. The preparation of a standard curve to show the change in activity above a surface vs. concentration at constant geometry and temperature permits the calculation of the exact concentration at the surface at any given time.

Figure 2 shows a graph of a typical experiment, performed at 8°C., comparing the surface concentration of a colloidal solution and a molecular solution. Line *A* was obtained using a 1% S^{35} tagged sodium dodecylbenzenesulfonate solution and line *B* by using a 1% S^{35} tagged sodium sulfate solution in an identical experiment as a control. Line *A* exhibits an increase in radioactivity of the newly formed surface with time; line *B* shows no such change.

Care should be taken to stir the surfactant for a sufficient time to pass a maximum (*Y*, Fig. 2) at which point the new surface is being formed. The increase in activity from *X* to *Y* is caused by a change in geometry due to the vortex.

Experiments showed 8°C. to be the optimum temperature because both water evaporation and solute crystallization are minimized at this temperature. At higher temperatures, a mica sealed vial is recommended to avoid any changes of activity brought about by evaporation which in turn will change the geometry of the system.

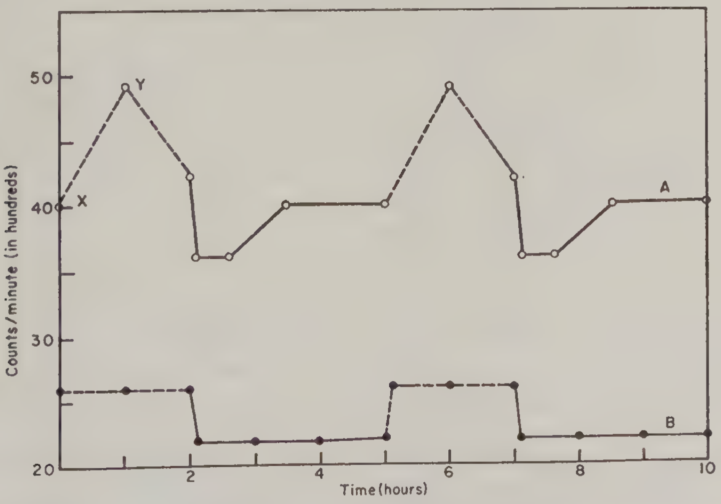

FIG. 2. Surface radioactivity vs. time at 8°C. Line *A*: 1% S^{35} tagged sodium dodecylbenzenesulfonate; Line *B*: 1% S^{35} tagged sodium sulfate. Dashed lines indicate periods of agitation.

The use of this device can be expanded to allow the calculation of changes in surface tension with time. This can be done by preparing a standard curve of surface tension vs. concentration and reading the surface tension at various concentrations from the obtained data as described above.

WERNER J. SCHWARZ
D. C. WOOD

Research Laboratories,
Whirlpool Corporation,
St. Joseph, Michigan

Received September 12, 1958

THE ROLE OF CATIONIC GROUP IN SULFATED DETERGENTS

Although the sodium salt of lauryl sulfate has been extensively studied, few data are available on the spread surface films of the morpholine, triethanolamine, and pyridine salts of lauryl sulfate. All three specimens occupy practically identical surface areas with SLS(1) (the pyridine salt alone deviates slightly from the equation probably owing to the relatively small degree of dissociation of pyridine.)

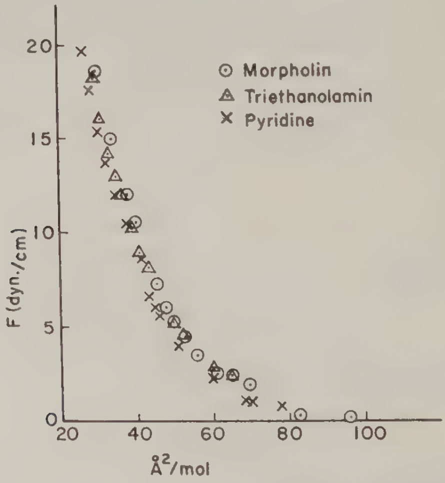

FIG. 1. Surface pressure-area diagrams (substrate 25% $(NH_4)_2SO_4$).

Critical micelle concentrations of these detergents are also identical using surface tension measured with Du Nuoy's apparatus.

The specimens were synthesized from lauryl alcohol, chlorosulfonic acid, and the corresponding organic base. The nitrogen analysis follows: morpholine Ls, found 3.90%, calculated 3.97%; triethanolamine LS, found 3.50%, calculated 3.37%; pyridine LS, found 4.08%, calculated 4.05%.

Surface pressure was measured with a surface balance of Wilhelmy type and the detergent spread from its isopropanol (40% by volume)-water solution over the substrate containing 25% ammonium sulfate.

Figure 1 shows F-A diagrams of those sulfated detergents on the same substrate. All F-A curves are approximately identical.

Figure 2 shows surface tension curves of morpholine and triethanolamine LS; they have a singular point at 0.154% and 0.20%, respectively. It is known that spread and adsorbed monolayers of SLS are of the same character (2). Pethica has shown that monolayers of SLS obey the relation $F(A - A_0) = nkT$. The curves in Fig. 1 obey this equation within graphical and experimental error. The value of A_0 is 34 A.^{2}/mole between areas of 40 A.^{2}/mole and 70 A.^{2}/mole and at 40 A.^{2}/mole A_0 decreases to 18 A^2/mole, which might correspond to the cross-sectional area of hydrocarbon chain of the detergent. These values of A_0 are in good agreement with surface areas of SLS (2–4).

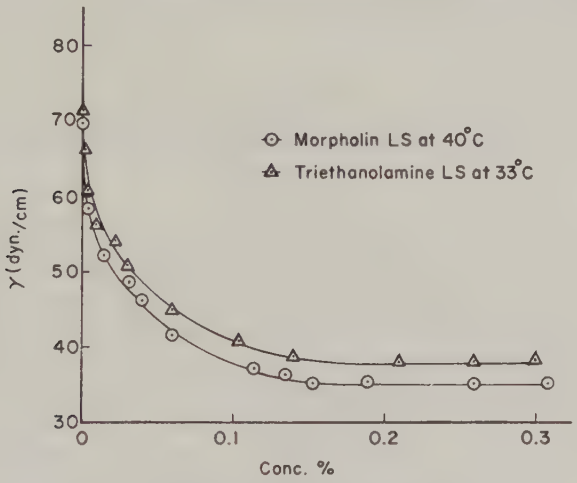

FIG. 2. Surface tension of organic LS.

The critical micelle concentration from the curves in Fig. 2 is 0.0048 mole for the triethanolamine salt and 0.0043 mole for the morpholine salt, which is excellent agreement; moreover, the CMC of SLS is about 0.007 mole (5)—a value close to but higher than that of organic LS.

These results suggest that some surface properties of univalent lauryl sulfate are not dependent greatly on the kind of cation attached to it, although bulk properties such as solubility and viscosity behavior are remarkably dependent on cationic group.

The writer expresses his thanks to Mr. Heihachi Ezaki of our company and to Prof. Ryohei Matsuura of Kyushu University for their advice and encouragement.

References

1. Kashiwagi, M., *Bull. Chem. Soc. Japan* **31,** 667 (1958).
2. Pethica, B. A., *Trans. Faraday Soc.* **50,** 413 (1954).
3. Davis, J. T., *J. Colloid Sci.* **11,** 377 (1956).
4. Nilsson, G., *J. Phys. Chem.* **61,** 1135 (1957).
5. Goette, E. K., *J. Colloid Sci.* **4,** 457 (1949).

K. Maresuke Kashiwagi

Mitsuwa Chemical Laboratory,
Marumiya Co., Ltd.,
Terajima-machi 8, Sumida-ku, Tokyo
Received October 1, 1958

FAT GLOBULES AS TRACERS FOR INTERFACE STUDIES

The amount of light transmitted by a thin layer of milk when flowing differs from that transmitted when stationary. This observation was made in the course of some turbidity studies of the fat phase in milk. A Beckman DU spectrophotometer was used in those studies at a wavelength of 1 μ in order to eliminate interference from casein turbidity. The optical path was 250 μ long. It was further observed that the difference in transmission is smaller for the total transmitted light than for its parallel component alone. The latter was measured by placing the receiving photocell at a distance of 12 cm. from the sample. Transmission increased upon stopping milk flow through the cell and reached a constant value after 10 to 20 minutes time. This is shown graphically by Curve *B* of Fig. 1.

Cell windows of various materials were tested for the same effect on light transmission. Windows of soda-lime, lead, borosilicate, 96%-silica, and fused-silica glasses, as well as of synthetic sapphire and of Plexiglas, all showed a similar effect. The difference in light transmission can be attributed to a less random distribution or spatial orientation of fat globules in a stationary layer of milk than in a flowing one.

To permit direct observation of any actual change in globule randomness, thin layers of milk were studied in a microscope using visible light. The microscope was fixed with its stage in the vertical position in order to eliminate creaming as a disturbing factor. Cells for this series of experiments were made by cementing a thin cover slip to a slide after placing a spacer of the desired thickness between them.

In homogenized milk, three-quarters of the fat globules are 2 μ in diameter or under. With a short depth of focus on the order of 5 μ obtained by using 970× magnification, those globules in *sharp* focus could be accurately counted at any chosen depth in the milk layer.

Homogenized milk diluted with four parts water was syringed into a 250 μ cell on the microscope stage and globules in one field were counted at a 5 μ depth. Counting was repeated in the same field and at the same depth periodically until an equilibrium condition was observed. The counts from two experiments of this type are shown graphically as Curve *A* of Fig. 1.

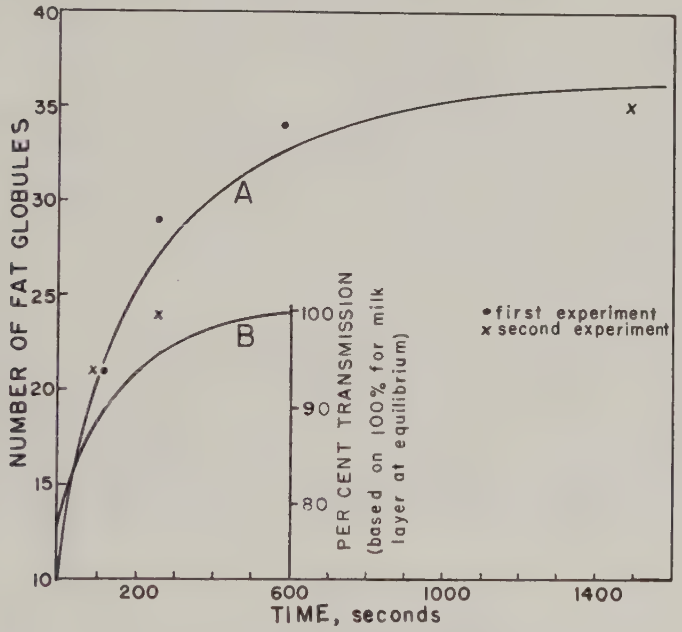

FIG. 1. Fat globule build-up near interface.

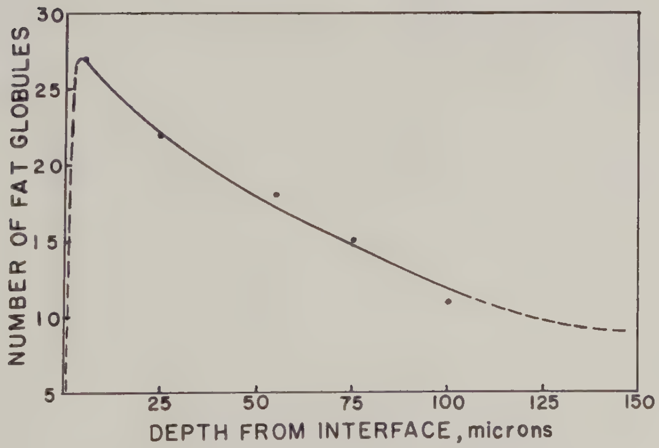

FIG. 2. Fat globule distribution at equilibrium.

Another experiment was concerned with the description of the globule distribution as related to depth in the layer *after* an equilibrium condition was obtained. Using a 500 μ cell globule-counts were made at different depths up to 100 μ 30 minutes after filling the cell. The data obtained are shown in Fig. 2. In a very thin cell of 75 μ spacing between windows no difference in counts was found through the entire depth of the layer. The globules remained randomly distributed. In none of the microscopic studies were globules seen to adhere to the window surface adjacent to the layer, as all globules showed Brownian movement. Both the fat globules and the glass surface carry a negative charge.

An observation by King (1) may be related to our findings. He observed microscopically the relative absence of fat on the undisturbed surface of milk and cream. After mechanically disturbing the surface, the rapid appearance of fat would suggest that a layer of oriented proteins carrying a negative charge repels fat globules from the surface until it is cleaved.

The tendency of fat particles to become less randomly distributed when rather thin layers down to 75 μ thickness are allowed to stand undisturbed probably influences a column of light traversing that layer so that the gross effect photometrically is a change in the relative amounts of coherent and multiple scattering produced. The concentration of the charged fat globules at equilibrium varies with the distance from the glass surface. If their charge were known quantitatively, they could be used as tracer substances for the determination and characterization of the electric potential which exists near interfaces.

REFERENCE

1. KING, N., J. Dairy Res. **22,** 328 (1955).

Research & Development Division,
National Dairy Products Corporation,
Oakdale, Long Island, New York

G. HAUGAARD
J. D. PETTINATI

Received October 1, 1958

JOURNAL OF COLLOID SCIENCE **13**, 623 (1958)

BOOK REVIEW

Rheology: Theory and Applications. Edited by F. R. Eirich. Vol. II. Academic Press Inc., New York 3, New York. 591 pages, $18.00, 1958.

Although this reviewer was a contributor to the first volume, he does not hesitate to state that this second volume, again under international authorship, continues the high level and broad coverage of its predecessor.

The topics treated may be arranged under three headings. There are three chapters on theory and emphasizing comparison of theory with experimental results on a variety of systems. Two of these are devoted to the phenomenological description of linear, viscoelastic phenomena. The interpretation by means of models of the Maxwell or Voigt type and the successful "corresponding states" relations are discussed in detail. The third summarizes essentially the application of the theory of absolute reaction rates to flow and diffusion processes, which encompasses nonlinear phemomena.

Again three chapters are concerned with experimental techniques per se. Two of these cover viscoelastic effects and the flow of fluids, including those with elastic components and large Reynolds numbers. A third deals with rheogoniometry, i.e., the measurement of angular variations in stresses, strains, and strain rates, including the region of rupture.

The other half of the book is given to specific systems or types. Organic polymers are represented by fibers, plastics, and raw elastomers, with additional specific chapters on cellulose derivatives, gelatin, and asphalts. A welcome and novel addition in a book stressing colloidal and polymeric aspects, is the inclusion of a chapter on the rheology of the earth's interior.

The by now familiar stressing of one's own contributions does not seem to be unduly exaggerated. Also, without detailed examination it is not possible to decide, but one wonders to what extent noteworthy, even if less accessible, foreign research has been omitted from consideration.

Duplication occurs, as pointed out in the Editor's introduction, in the theoretical parts and also in respect to experimental technique during the discussion of particular materials. This can not be altogether avoided. However, it makes for individual contributions which are self contained and not mere reviews of facts and research accomplishments. Consequently they invite the student (in the general sense of the word) wishing to be introduced to a particular aspect of the field as well as those active in rheological research. Since nowadays rheology covers or necessarily intrudes into a wide range of endeavors, this should include quite a broad audience.

Robert Simha, Los Angeles, Cal.

AUTHOR INDEX

A

Adams, George, 441
Alexander, A. E., 383
Allan, A. J. G., 273
Allawala, N. A., 208
Allen, P. W., 483
Allinson, P. A., 513

B

Bartok, W., 293
Bascom, W. D., 569
Benson, G. C., 584
Bhagwan, Hari, 232, 237
Bikerman, J. J., 509
Bourdillon, Jacques, 407
Boyd, G. E., 275
Brooks, C. S., 522
Brown, D. J., 286
Bulas, R., 429

C

Chanley, J. D., 565
Chatterjee, S. N., 61
Chatterji, A. C., 232, 237
Chessick, J. J., 358, 372
Child, William C., Jr., 103
Cole, Richard, 337, 348
Corbett, William J., 472
Czeczowisczka, Nina, 188

D

Dahlgren, Sven-Eric, 151
Dannhauser, Walter, 103
Debye, P., 86
Defay, Raymond, 553
Demeny, Margaret, 565
Dey, Arun K., 99
Dixon, J. K., 411

E

Evans, H. C., 537

F

Ferry, John D., 103, 459
Fujishige, Shoei, 193
Fujita, Hiroshi, 418

G

Gillespie, T., 32
Gotz, K. G., 266
Granath, Kirsti A., 328
Gundiah, S., 170

H

Harteck, Paul, 1
Haugaard, G., 620
Haydon, D. A., 159
Heckmann, K., 266
Heiman, W. J. 329, 337
Heller, Wilfried, 6
Hermans, J. J., 488, 508
Hommelen, Jacques R., 553
Hrenoff, M. K., 208
Hurd, F. Kenneth, 472

I

Ihde, Aaron J., 163

K

Kahn, Allan, 51
Kapur, S. L., 170
Kashiwagi, K. Maresuke, 618
Kishimoto, Akiro, 418
Kline, Robert J., 163
Kumins, C. A., 429

L

La Mer, V. K., 589
Lane, W. B., 348
Loiselle, Arthur A., 576

M

Mackin, J. L., 348
Mason, S. G., 179, 293, 600
Matijevic, E., 242

McCartney, E. R., 383
Mercurio, A., 197
Milburn, Richard H., 114
Miller, Carl F., 337, 348
Miller, M. L., 411
Mukherji, Anil K., 99
Murakami, K., 197

N

Nagamatsu, Kazuo, 257
Nagels, P., 140, 148
Nash, T., 134
Nawab, M. A., 179
Nielsen, Lawrence, E., 441

O

Orr, Clyde, 472
Ottewill, R. H., 242

P

Peper, Henry, 199
Pettinati, J. D., 620
Prins, W., 86
Pultz, W. W., 397

R

Rabinovitch, W., 600
Riegelman, S., 208
Robertson, R. F., 600
Ross, Sydney, 397
Ruigrok, A. B., 488
Rutgers, A. J., 140, 148
Ryke, A. M., 508

S

Schaffer, Vincent J., 3
Schwarz, Werner J., 616
Shniad, Harold, 24
Smellie, Robert H., 589
Singleterry, C. R., 569
Sobotka, Harry, 188, 565
Stern, Kurt H., 24
Strait, L. A., 208
Strasburger, H., 218
Street, Norman, 288
Strella, Stephen, 459

T

Tabibian, Richard M., 6
Takemoto, Tatsuro, 257
Tobolsky, A. V., 197
Tschoegl, N. W., 500

V

Van den Tempel, M., 125
Vaslow, F., 275

W

Wall, Robert, 441
White, P., 584
Winter, Stephen S., 576
Wood, D. C., 616

Y

Yoshitomi, Tatsuya, 257
Young, G. J., 67, 358, 372

Z

Zettlemoyer, A. C., 372

SUBJECT INDEX

A

Acetic acid, distribution between benzene and soap micelles, Bascom and Singleterry, 569
Adsorption, adsorbed monolayers at argon and nitrogen, Ross and Pultz, 397; of aliphatic compound on silica, Brooks, 522
Aerosol size, and humidity, Orr *et al.*, 472
Aurintricarboxylate, as colloidal electrolyte, Mukherji and Dey, 99

B

Bile salt solutions, gelation, Sobotka and Czeczowiczka, 188

C

Calcium sulfate, crystallization, McCartney and Alexander, 383
Clouds, turbulent evaporating, Milburn, 114
Colloidal spheres, light scattering, Tabibian and Heller, 6

D

Detergents, defoaming, Peper, 199
Destrans, solution properties of branched, Granath, 308
Diffusion, in inhomogeneous media, Stern and Shniad, 24
Drops, coalescence of liquid, Nielsen *et al.*, 441

E

Electroviscous equation, Street, 288
Emulsions, by electrical dispersion, Nawab and Mason, 179; velocity of sound in, Allinson, 513

F

Fiber swelling, and detergent adsorption, Evans, 537

G

Glass, scratch effect, Bourdillon, 407
Glycerides, dispersion, Debye and Prins, 86
Greases, nonsoap lubricating, Young and Chessick, 358; Chessick *et. al.*, 372

M

Methacrylate, poly-*n*-octyl methacrylate, Dannhauser *et al.*, 103; dilatometric and viscoelastic data on poly-*n*-alkyl methacrylates, Fujita and Kishimoto, 418; dielectric dispersion of polymers, Ferry and Strella, 459
Micellization, of potassium octanoate, White and Benson, 584
Monolayers, at oil-water interface, Haydon, 159; elastic moduli in, Tschoegl, 500; radioactive tracer studies, Sobotka *et al.*, 565
Montmorillonite, flocculation, Kahn, 51

N

Naphthalene derivatives, and cationic soap, Nash, 134

O

Obituaries, *Bonhoeffer, K. F.* (Harteck, P.), 1; *Langmuir, I.* (Schaffer, V. J.), 3
Oil globules, emulsified, Van den Tempel, 125

P

Periodic formations, Chatterji and Bhagwan, 232, 237
Phosphate slimes, filtration of flocculated suspensions, Smellie and La Mer, 589

Polyoxyethylene glycol, dielectric relaxation, RUIGROK AND HERMANS, 488
Polyvinylalcohol-water solutions, extinction angle, FUJISHIGE, 193

R

Radiation, gamma radiation from a nuclear detonation, HEIMAN, 329; nuclear detonations, MILLER *et al.*, 337, 348
Radioiodine, exchange between iodostearic acid and iodide, RABINOVITCH *et al.*, 600
Rubber, viscosity of solutions, KAPUR AND GUNDIAH, 170; swelling of rubber latex, ALLEN, 483

S

Silica, particle size in colloidal, HERMANS AND RYKE, 508
Silver halide sols, and detergents, MATIJEVIĆ AND OTTEWILL, 242
Silver iodide, double layer surrounding and electroviscosity, RUTGERS AND NAGELS, 140, 148
Soap micelles, and electrical conductivity, GÖTZ AND HECKMANN, 266
Solubility, of long-chain amines, BROWN, 286
Solubilization, and ultraviolet absorption, RIEGELMAN *et al.*, 208
Spreading, of low vapor pressure liquids, GILLESPIE, 32
Starch granule rupture, WINTER AND LOISELLE, 576
Stress relaxation, and molecular weight, TOBOLSKY *et al.*, 196
Sulfosuccinates, conductance, MILLER AND DIXON, 411
Surface tension, Wilhelmy's plate, ALLAN, 273; and Young's equation, BIKERMAN, 509; measurement, DEFAY AND HOMMELEN, 553
Surface viscosities, of films, BOYD AND VASLOW, 275; measuring, BULAS AND KUMINS, 429
Surfactant, determination of increase, SCHWARZ AND WOOD, 616
Suspensions, particle motions in sheared suspensions, BARTOK AND MASON, 293

T

Tacky adhesion, STRASBURGER, 218
Thixotropy, and flow, DAHLGREN, 151
Triethylamine and water, effect of soaps, KLINE AND IHDE, 163
Tungstic oxide, in the colloidal state, CHATTERJEE, 61

V

Viscoelasticity, of polymers, NAGAMATSU *et al.*, 257

W

Water vapor, and silica surfaces, YOUNG, 67

INDEX OF BOOK REVIEWS

EDSALL, J. T., AND WYMAN, J., Biophysical Chemistry. Volume I. Thermodynamics, Electrostatics, and the Biological Significance of the Properties of Matter (STEINHARDT, J.), 510
EIRICH, F. R. (ed.), Rheology: Theory and Applications. Vol. II (SIMHA, R.), 623
HAMANN, S. D., Physico-Chemical Effects of Pressure (HUGGETT, C.), 511
REID, C., Excited States in Chemistry and Biology (STEINHARDT, J.), 291

JOURNAL OF COLLOID SCIENCE

Editor-in-Chief
Victor K. La Mer, Columbia University, New York

Advisory Board

C. O. Beckmann
J. A. Christiansen
P. J. W. Debye
John T. Edsall
I. Fankuchen
John D. Ferry
Wilfried Heller
J. J. Hermans
John G. Kirkwood
E. C. Lingafelter
L. G. Longsworth
S. G. Mason
J. Th. G. Overbeek
R. Ruyssen
J. H. Schulman
Leo Shedlovsky
Theodore Shedlovsky
Robert Simha
R. H. Smellie
Jacinto Steinhardt
The Svedberg
Hugh S. Taylor
Arne Tiselius
Robert D. Vold
Bernard Vonnegut
Ralph W. G. Wyckoff
Bruno H. Zimm

VOLUME 13

1958

ACADEMIC PRESS INC.—PUBLISHERS
NEW YORK, N. Y.

Copyright© 1958, by Academic Press Inc,
Made in United States of America

Contents of Volume 13

Number 1, February 1958

Paul Harteck. In Memoriam: Karl Friedrich Bonhoeffer 1
Vincent J. Schaffer. In Memoriam: Irving Langmuir—Scientist ... 3
Richard M. Tabibian and Wilfried Heller. Experimental Investigations on the Light Scattering of Colloidal Spheres. III. The Specific Scattering at 90° 6
Kurt H. Stern, and Harold Shniad. Diffusion in Inhomogeneous Media. Capillary Diffusion in Beds of Glass Beads 24
T. Gillespie. The Spreading of Low Vapor Pressure Liquids in Paper 32
Allan Kahn. The Flocculation of Sodium Montmorillonite by Electrolytes 51
S. N. Chatterjee. On the Structure of Tungstic Oxide in the Colloidal State 61
G. J. Young. Interaction of Water Vapor with Silica Surfaces 67
P. Debye and W. Prins. Micellar Dispersion of α-Monoglycerides in Benzene and Chlorobenzene 86

LETTER TO THE EDITOR

Anil K. Mukherji and Arun K. Dey. Behavior of Ammonium Aurintricarboxylate as a Colloidal Electrolyte 99

Number 2, April 1958

Walter Dannhauser, William C. Child, Jr., and John D. Ferry. Dynamic Mechanical Properties of Poly-*n*-Octyl Methacrylate .. 103
Richard H. Milburn. Theory of Turbulent Evaporating Clouds ... 114
M. Van den Tempel. Distance Between Emulsified Oil Globules Upon Coalescence 125
T. Nash. The Interaction of Some Naphthalene Derivatives With a Cationic Soap Below the Critical Micelle Concentration 134
A. J. Rutgers and P. Nagels. Structure of the Double Layer Surrounding the Particles of the Sol of Silver Iodide 140
A. J. Rutgers and P. Nagels. The Electroviscous Effect in Sols of Silver Iodide 148
Sven-Eric Dahlgren. Eyring's Model of Flow Applied to Thixotropic Equilibrium 151

D. A. Haydon. Equations of State for Ionized Monolayers at the Oil-Water Interface . . . 159

Robert J. Kline and Aaron J. Ihde. The Effect of Soaps and Detergents on the Critical Solution Temperature of Triethylamine and Water . . . 163

S. L. Kapur and S. Gundiah. Anomalous Behavior of Polymer Solutions. II. Viscosity Behavior of Rubber Solutions at High Dilutions . . . 170

M. A. Nawab and S. G. Mason. The Preparation of Uniform Emulsions by Electrical Dispersion . . . 179

Harry Sobotka and Nina Czeczowiczka. The Gelation of Bile Salt Solutions . . . 188

LETTERS TO THE EDITORS

Shoei Fujishige. Anomalous Behavior of the Extinction Angle of Moderately Concentrated Polyvinylalcohol Water Solution . . . 193

A. V. Tobolsky, A. Mercurio, and K. Murakami. Molecular Weight Distribution by Stress Relaxation . . . 197

Number 3, June 1958

Henry Peper. The Defoaming of Synthetic Detergent Solutions by Soaps and Fatty Acids . . . 199

S. Riegelman, N. A. Allawala, M. K. Hrenoff, and L. A. Strait. The Ultraviolet Absorption Spectrum as a Criterion of the Type of Solubilization . . . 208

H. Strasburger. Tacky Adhesion . . . 218

A. C. Chatterji and Hari Bhagwan. Studies on Periodic Formations. I. Radial Rhythmicity . . . 232

A. C. Chatterji and Hari Bhagwan. Studies on Periodic Formations. II. Time and Distance Relationships of Periodic Precipitates . . . 237

E. Matijević and R. H. Ottewill. The Formation of Silver Halide Sols in the Presence of Cationic Detergents . . . 242

Kazuo Nagamatsu, Tatsuya Yoshitomi and Tatsuro Takemoto. On the Viscoelastic Properties of Crystalline Polymers. I. Polytetrafluoroethylene . . . 257

K. G. Götz and K. Heckmann. The Shape of Soap Micelles and other Polyions as Obtained from Anisotropy of Electrical Conductivity . . . 266

A. J. G. Allan. Wilhelmy's Plate and Young's Equation . . . 273

G. E. Boyd and F. Vaslow. Surface Viscosities of Mixed Unimolecular Films . . . 275

LETTERS TO THE EDITOR

D. J. Brown. Solubility of Long-Chain Amines in Water........ 286
Norman Street. A Simple Derivation of an Electroviscous Equation.. 288

BOOK REVIEW

Jacinto Steinhardt. Excited States in Chemistry and Biology.. 291

Number 4, August 1958

W. Bartok and S. G. Mason. Particle Motions in Sheared Suspensions. VII. Internal Circulation in Fluid Droplets (Theoretical).. 293
Kirsti A. Granath. Solution Properties of Branched Dextrans.... 308
W. J. Heiman. Variation of Gamma Radiation Rates for Different Elements Following an Underwater Nuclear Detonation...... 329
Carl F. Miller, Richard Cole, and Warren J. Heiman. Decontamination Reactions of Synthesized Fallout Debris for Nuclear Detonations. I. Nuclear Detonation in Sea Water........... 337
Carl F. Miller, Richard Cole, W. B. Lane, and J. L. Mackin. Decontamination Reactions of Synthesized Fallout Debris for Nuclear Detonations. II. Land-Surface Nuclear Detonation.... 348
G. J. Young and J. J. Chessick. Basic Factors in the Formation and Stability of Nonsoap Lubricating Greases. I. A Study of the Factors Responsible for Gel Formation......................... 358
J. J. Chessick, A. C. Zettlemoyer, and G. J. Young. Basic Factors in the Formation and Stability of Nonsoap Lubricating Greases. II. The Mechanism of Gel Formation......................... 372
E. R. McCartney and A. E. Alexander. The Effect of Additives upon the Process of Crystallization. I. Crystallization of Calcium Sulfate.. 383
Sydney Ross and W. W. Pultz. On Physical Adsorption. X. Adsorbed Monolayers of Argon and Nitrogen on Boron Nitride and on a Graded Series of Partially Graphitized Carbon Blacks.... 397

LETTER TO THE EDITOR

Jacques Bourdillon. The Glass Scratch Effect............. 407

Number 5, October 1958

M. L. Miller and J. K. Dixon. Conductance of Dialkyl Sodium Sulfosuccinate Surface-Active Agents......................... 411
Hiroshi Fujita and Akira Kishimoto. Correlation Between Dilatometric and Viscoelastic Data on a Series of Poly-*n*-Alkyl Methacrylates.................................... 418

R. Bulas and C. A. Kumins. A Modified Method for Measuring Surface Viscosity 429
Lawrence E. Nielsen, Robert Wall, and George Adams. Coalescence of Liquid Drops at Oil-Water Interfaces 441
John D. Ferry and Stephen Strella. Dielectric Dispersion in Methacrylate Polymers and Its Correlation with Mechanical Properties 459
Clyde Orr, Jr., F. Kenneth Hurd, and William J. Corbett. Aerosol Size and Relative Humidity 472
P. W. Allen. The Swelling Behavior of Natural Rubber Latex 483
A. B. Ruigrok and J. J. Hermans. Dielectric Relaxation of Polyoxyethylene Glycol (POEG) in Toluene 488
N. W. Tschoegl. Elastic Moduli in Monolayers 500

LETTERS TO THE EDITORS

J. J. Hermans and A. M. Ryke. Distribution of Particle Size in Colloidal Silica by Ultracentrifugation 508
J. J. Bikerman. A Note on Young's Equation 509

BOOK REVIEWS

Jacinto Steinhardt. Biophysical Chemistry, Volume I 510
Clayton Huggett. Physico-Chemical Effects of Pressure 511

Number 6, December 1958

P. A. Allinson. The Velocity of Sound in Emulsions 513
C. S. Brooks. Competitive Adsorption of Aliphatic Compounds and Water on Silica Surfaces 522
H. C. Evans. Fiber Swelling and Detergent Adsorption in Detergent/Textile Fiber Systems 537
Raymond Defay and Jacques R. Hommelen. I. Measurement of Dynamic Surface Tensions of Aqueous Solutions by the Oscillating Jet Method 553
Harry Sobotka, Margaret Demeny, and J. D. Chanley. Radioactive Tracer Studies of Monolayers. II. Comparison of Floating and Built-up Monolayers 565
W. D. Bascom and C. R. Singleterry. The Distribution of Acetic Acid Between Solvent and Soap Micelles in Benzene Solutions 569
Stephen S. Winter and Arthur A. Loiselle. The Effect of Salts Upon Starch Granule Rupture 576
P. White and G. C. Benson. The Heat of Micellization of Potassium Octanoate in Water in the Presence of Excess Potassium Chloride 584

ROBERT H. SMELLIE, JR., AND VICTOR K. LA MER. Flocculation, Subsidence and Filtration of Phosphate Slimes. VI. A Quantitative Theory of Filtration of Flocculated Suspensions........ 589
W. RABINOVITCH, R. F. ROBERTSON, AND S. G. MASON. Radioiodine Exchange Between Iodostearic Acid Monolayers and Substrate Iodide. II.. 600

LETTERS TO THE EDITOR

WERNER J. SCHWARZ AND D. C. WOOD. A Device for the Determination of the Rate of Increase of Surfactant at the Liquid-Air Interface.. 616
K. MARESUKE KASHIWAGI. The Role of Cationic Group in Sulfated Detergents.. 618
G. HAUGAARD AND J. D. PETTINATI. Fat Globules as Tracers for Interface Studies.. 620

Book Review

ROBERT SIMHA. Rheology: Theory and Applications. Volume II.. 623

Author Index.. 625
Subject Index.. 627
Index of Book Reviews.. 628